Investigating the spatial variability of Abrupt Cooling Events during the Lateglacial Interstadial (c. 14.7 – 12.5 ka cal BP) in Britain and Ireland using chironomids and oxygen isotopes to assess potential forcing mechanisms

Christopher Philip Francis

Centre for Quaternary Research,
Department of Geography,
School of Environmental and Life Sciences,
Royal Holloway, University of London

And

Department of Geography,
Birkbeck, University of London

Thesis submitted for the degree of Doctor of Philosophy,
Royal Holloway, University of London,
December 2021

Declaration of authorship

I, Christopher Philip Francis, hereby declare that the work presented in this thesis is entirely my own. Where I have consulted the work of others this is clearly stated.

Signed:

Date: 16.12.2021

Abstract

NW Europe will become more susceptible to abrupt cooling events (ACE) due to a reduction in the strength of the Atlantic Meridional Overturning Circulation (AMOC) caused by anthropogenic warming (IPCC, 2021). The Lateglacial Interstadial (LGIS) (~GI-1; c. 14.7-12.9 kyr ago), a relatively warm period at the end of the last glaciation, provides an excellent opportunity to study centennial-scale ACEs which are potential analogues to future ACEs. Three centennial-scale ACEs are clearly expressed in the Greenland ice core records, however, the spatial variation in magnitude of these ACEs across the British Isles and continental Europe is poorly understood due to the paucity of high-resolution well-dated records with quantified temperature reconstructions. By studying the spatial expression of ACE magnitude, potential forcing mechanisms can be assessed.

Three sites were selected to improve the spatial coverage of LGIS sites in the British Isles: Crudale Meadow (Orkney), Llangorse (Wales), and Old Buckenham Mere (East Anglia). Chironomid and oxygen-isotope analysis was conducted at a high temporal resolution (~decadal), allowing for quantitative reconstructions of past climatic temperature change, insight into seasonal temperature change and understanding of hydrological regime shifts. All three sites have robust age models based on radiocarbon dated terrestrial plant macrofossils and/or tephrochronology.

Differences in the spatiotemporal signatures in the magnitude and abruptness of the observed ACEs indicate that each ACE has a unique combination of forcing mechanisms operating at different times. The early-LGIS ACE may have primarily driven by North Sea sea-ice amplification of cooling that originated in the NW Atlantic, while the late-LGIS ACE was potentially the result of oceanic forcing from the NW and NE Atlantic. During the Mid-LGIS, numerous ACEs occurred of varying amplitude and apparent timing. This study shows the important of combining high-resolution analysis and high-precision age models in order to understand regional patterns, and potential drivers, of ACEs.

Publications and authorship contributions

Francis, C. P., Engels, S., Matthews, I. P., Palmer, A. P., Timms, R. G. O., Jourdan, A. L., and Candy, I. (2021). A multi-proxy record of abrupt cooling events during the Windermere Interstadial at Crudale Meadow, Orkney, UK. Journal of Quaternary Science, 36(3), 325–338. doi.org/10.1002/jqs.3289

Abrook, A. M., Matthews, I. P., Candy, I., Palmer, A. P., Francis, C. P., Turner, L., Brooks, S. J., Self, A. E. and Milner, A. M. (2020). Complexity and asynchrony of climatic drivers and environmental responses during the Last Glacial-Interglacial Transition (LGIT) in north-west Europe. Quaternary Science Reviews, 250, 106634. doi.org/10.1016/j.quascirev.2020.106634

Timms, R. G. O., Abrook, A. M., Matthews, I. P., Francis, C. P., Mroczkowska, A., Candy, I., Brooks S. J., Milner, A. M., and Palmer, A. P. (2021). Evidence for centennial-scale Lateglacial and early Holocene climatic complexity from Quoyloo Meadow, Orkney, Scotland. Journal of Quaternary Science, 36(3), 339–359. https://doi.org/10.1002/jqs.3282

Palmer, A., Matthews, I., MacLeod, A., Abrook, A., Akkerman, K., Blockley, S., Candy, I., Francis, C., Hoek, W., Kingston, F., Maas, D., El-Hady, S., Gulliford, R., Lincoln, P., Perez Fernandez, M., and Staff, R. (2021). The Late Quaternary sediment successions of Llangorse Lake, south Wales. *Proceedings of the Geologists' Association*, *132*(3), 284-296. doi.org/10.1016/j.pgeola.2021.01.004

Acknowledgements

First and foremost, I would like to thank my supervisors, Professor Ian Candy, Dr Stefan Engels, Dr Ian Matthews and Dr Adrian Palmer for their support, guidance, encouragement, and patience throughout my studies. This thesis would not have been possible without them. Additional thanks must go to the Geography Department technical staff at Royal Holloway who have aided in techniques to make this thesis possible and who have made my time at Royal Holloway so enjoyable: Dr Marta Perez, Mr Iñaki Valcarel, Mrs Jen Thornton, Mrs Katy Flowers, Dr Claire Mayers, and Mr Raymond Aung. I would also like to thank Dr Rupert Housley for dealing with all my finance enquires and many a conversation on how to grow the best tomatoes. Thank you is also due to Pierre Schreve for his company, conversations on Formula 1 and lessons on mammal bones while working in the palaeoecology laboratory.

Thanks is owed to Steve Brooks and Professor Oliver Heiri for sharing the Norwegian and the combined Norwegian-Swiss chironomid climate calibration datasets. In particular, I would like to express my gratitude to Steve for investing so much time teaching me all things chironomids and sparking my interest in the proxy. I am also appreciative to Dr Anne-Lise Jourdan at UCL and Dr Angela Lamb at the British Geological Survey who taught me a lot about mass spectrometry and analysed many of the isotope samples during this PhD. Acknowledgement is also owed to Steve Askew and Lucy Thatcher for their permission to core Old Buckenham Mere.

I would like to express my appreciation to past and present MSc Quaternary Science cohorts, PhD researchers and post-docs who have made the last 4.25 years a lot less lonely and a lot of fun. I would especially like to thank Dr Ashley Abrook, Dr Roseanna Mayfield, Dr Emily Wiesendanger, Jo Hornsey, Dr Rhys Timms, Dr Rachel Devine, Dr Dave Arnold, Dr Richard Clark-Wilson, Laura Boyle, Joanna Tindall, and Josh Pike. To Alice Carter-Champion, Lizzy Harvey-Hawes, Emma cooper and Shuang Zhang for the frequent pub trips. To Kitkat, the stray cat who I took in and has kept me company over the last 6 months, insisting I take frequent breaks. An extra special thank you is owed to Alice Carter-Champion for the many lockdown walks, gardening chats and much-needed personal support!

Finally, to my family, my parents Susan and Stuart, my brother Mark, and his fiancée Laura, thank you for everything (and the hours of proof reading!) over the last four years.

Abbreviations

ACE	Abrupt cooling event
BIIS	British and Irish ice sheet
BP	Before present
C-IT	Chironomid-inferred temperature
cal	calibrated
CM	Crudale Meadow
COTL-type	*Corynocera oliveri/Tanytarsus lugens*-type
DIC	Dissolved inorganic carbon
DS	Dimlington Stadial
HC	Head capsule
LGIS	Lateglacial Interstadial
LGIT	Lastglacial Interglacial transition
LL	Llangorse
LLS	Loch Lomond Stadial
m	Metres
Mag sus	Magnetic susceptibility
MAT	Mean annual temperature
OBM	Old Buckenham Mere
SIS	Scandinavian ice sheet
T_{Jul}	Mean July air temperature
THC	Thermohaline circulation
Undiff.	undifferentiated
yrs	Years

Contents

List of Figures

List of Tables

Chapter 10: Synthesising the spatial expression of ACEs and discussion of potential forcing mechanisms.

Chapter 1: Introduction

1.1 Scientific rationale

Increasing attention is focused on the impact that greenhouse gas emissions will have on rising global mean temperature and the implications it will have on populations around the world. However, the IPCC and modelling experiments also suggests that, paradoxically, northwest Europe will become more susceptible to abrupt cooling events (ACEs) due to anthropogenic global warming (IPCC, 2021; Petoukhov *et al.,* 2005; Lenton *et al*., 2008). According to the IPCC predictions, future ACEs could be triggered by changes in ocean circulation strength in the North Atlantic, namely the Atlantic Meridional Overturning Circulation (AMOC) which could play a substantial role in modifying the future climate of NW Europe (Gregory *et al*., 2005; Hawkins *et al*., 2011) through the enhanced melting of the Greenland ice cap under warmer atmospheric conditions. There is already evidence to suggest that there is anomalously weak sea convection and Atlantic overturning in the Labrador Sea over the last 150 years (Thornalley *et al.,* 2018) and is weakest for the last millennium in the wider North Atlantic (Caesar *et al.,* 2021). Arguably, ACEs could have a far greater and more significant impact on the human population than increasing global mean temperatures. The historical record shows that even very short-lived declines in temperature of only a few degrees over several years can cause significant impact on societies. For example, the Volcanic eruption of Mount Toba in 1815 caused global temperatures to decline by 0.4-0.7 °C and summer temperatures in 1816 to decline as much as 3.5 °C in NW Europe. This led to widespread famine, disease and social distress (Slothers, 1984; Schurer *et al.,* 2019).

The Lateglacial-Interglacial transition (LGIT; *c.* 11.7-14.7yrs b2k GICC05; Lowe *et al*., 2008), a period of dynamic, high-amplitude, abrupt climatic changes, make it an ideal period to further our understanding of the climate system (Hoek, 2001). The most notable ACE during the LGIT is the Lateglacial Stadial (GS-1; 12,896 - 11,703 GICC05 yrs b2k), broadly equivalent to the Loch Lomond Stadial (LLS) in Britain, the Nahanagan Stadial in Ireland, and the Younger Dryas in continental Europe (Sisson, 1967, 1974; Gray and Lowe, 1977; Mitchell and Ryan, 1997; Mangerud *et al*., 1974, 2020). The LLS has been the subject of extensive research as it is the last major ACE prior to the Holocene and is detected in a range of marine, ice core and terrestrial archives. Consequently, the LLS provides a natural laboratory to test the interactions between different components of the earths system (Lowe *et al*., 2008).

However, the largescale re-arrangement of the climate system associated with millennial-scale ACEs such as the LLS are unlikely to occur in the near future as most climate models suggest future ACEs will be shorter duration, centennial in scale, and occur against a background of warm climate conditions (Lenton *et al*., 2008). Such centennial-scale ACEs have been identified in the Greenland ice-core records during the Greenland Interstadial-1 (GI-1; 14,692 – 12,896 GICC05 yrs b2k), broadly coeval with the Lateglacial/Windermere Interstadial (LGIS) in Britain, the Woodgrange Interstadial in Ireland and the Bølling-Allerød in continental Europe, a period of prolonged warmth of near interglacial level (Gray and Lowe, 1977; Mitchell and Ryan, 1997; Mangerud *et al*., 1974). During the LGIS/GI-1 at least three centennial scale ACEs are recorded in multiple archives from Greenland, through Britain and onto the continent. However, the origin of these widespread centennial-scale ACEs and the role of different forcing mechanisms in driving them, e.g., solar activity (Adolphi *et al.,* 2014), and changes in the thermohaline conveyor (Nesje *et al.,* 2004; Thornalley *et al.,* 2011), are still widely debated (Van Raden *et al.,* 2013).

Identifying centennial-scale changes in ocean circulation from ocean core archives using proxies such as *Neogloboquadrina pachymderma*, current flow speed proxies and ^{14}C ventilation ages (e.g., Thornalley *et al.,* 2011; Figure 1.1), are problematic. This is because (i) the resolution of many oceanic cores are often very low meaning that short-term changes may be smoothed out or absent (e.g., Barker *et al*., 2019; Waelbroeck *et al*., 2019), (ii) they are analysed at a low sampling resolution and so centennial-scale changes may only be represented by one or two samples, and (iii) ocean cores are affected by chronological issues such as either spatially variable marine reservoir offsets from radiocarbon dates, which are often far larger than the duration of the centennial-scale ACEs themselves (Telesiński *et al*., 2021; Muschitiello *et al*., 2020), and/or complications in establishing tephra isochrons due to taphonomic issues (Griggs, 2015; Griggs *et al*., 2015; Abbott *et al.,* 2018).

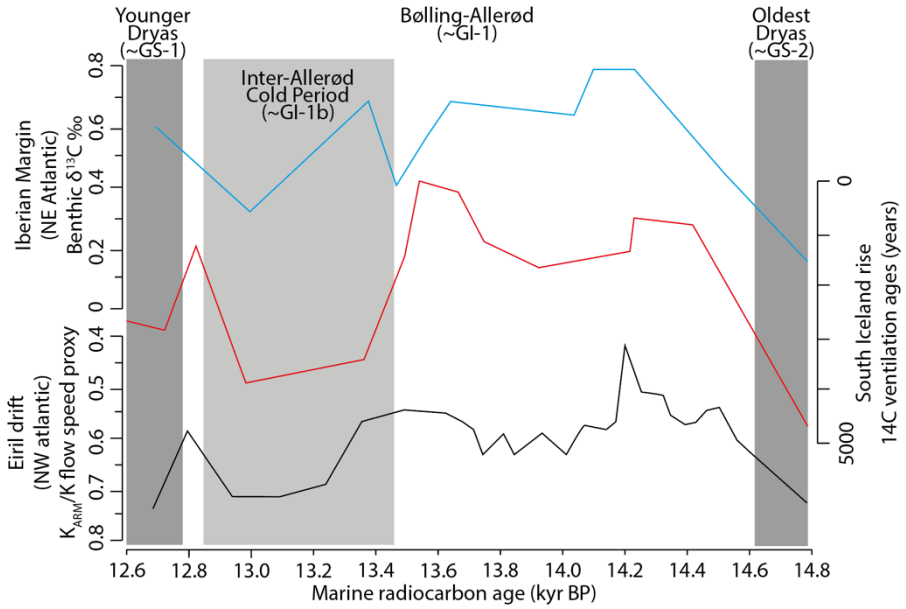

Figure 1.1, Proxies used to reconstruct ocean circulation during the Lateglacial from the North Atlantic region by Thornalley *et al*. (2011). A decline in the northward movement of warm water and an increase in cold meltwater from Greenland is inferred to have caused the Inter-Allerød cold period. However, similar changes cannot be clearly seen for other ACEs in the LGIS potentially due to low sampling resolution and/or stratigraphic resolution (after Thornalley *et al*., 2011).

An alternative way to assess the potential role of different forcing mechanisms is through the changing expression of different ACEs spatially, i.e., patterns of past climate change should display the greatest degree of cooling closest to the origin of forcing. The British Isles, which lie between the latitudes 50-60 °N, are highly sensitive to ACEs because of their reliance on the northward movement of warm water from the tropics that moderates its climate, making it an ideal study location to investigate the impacts of ocean forcing. The LGIS is often well represented in lake sediments across Britain and Ireland with relatively high sedimentation rates permitting temperature reconstructions at decadal resolution. Chironomids and oxygen-isotopes are two of the best suited proxies available to reconstruct the climatic temperature changes of these events as they have two key advantages. Firstly, they are very responsive to short-term climatic changes, and secondly, they can be applied at high-resolution, as only a small amount of sediment is needed (Brooks *et al*. 2007). This allows for detailed, but most importantly quantitative, or at least semi-quantitative, reconstructions which are vital for improving our understanding of climate dynamics and assessing potential forcing mechanisms (Vandenberghe *et al*., 1998; Heiri *et al.*, 2014).

1.2 Current limits of understanding

The LGIS is well represented in proxy-records across Europe including pollen (Walker *et al*., 1994), sedimentology (Lang *et al*., 2010), Coleopteran (Coope *et al*., 1998), macrofossils (Birks, 2001), chironomids (Brooks *et al*., 2006) and oxygen-isotopes (Candy *et al.,* 2016; van Asch *et al*., 2012a). Chironomid-inferred temperatures, which reflect mean July air temperatures (T_{Jul}), and oxygen isotopes, which can broadly reflect mean annual air temperatures (MAT; $\delta^{18}O$) display many differences in both the magnitude of ACEs and the long-term climatic trends across Europe during the LGIS that are needed to understand the associated forcing mechanisms (Brooks and Langdon, 2014; Candy *et al*., 2016). Currently, the published literature shows that both T_{Jul} and $\delta^{18}O$ records from Britain identify an ACE early in the LGIS, often correlated to GI-1d, which displays a large magnitude of cooling, close to the magnitude of change between the LGIS and the LLS, and much larger than the late-LGIS ACE, often correlated to GI-1b (Brooks *et al.,* 2016). While in Ireland and continental Europe the early-LGIS ACE (~GI-1d) often has a smaller magnitude which is closer to that of the late-LGIS ACE (~GI-1b). Similarly, there are also discrepancies in the timing of peak warmth attained during the LGIS between mainland Europe, Greenland and the British Isles (and within these regions also). The timing of peak warmth in these locations varies between the beginning, middle and end of this Interstadial (e.g., Lotter *et al*., 2012; Rasmussen *et al*., 2006; Brooks *et al*., 2012, 2016) (Figure 1.2). Further complications arise as peak warmth occurs at different times in T_{Jul} and $\delta^{18}O$ records suggesting different aspects of temperature, potentially seasonal differences, are recorded between each proxy. These spatial differences outlined here and elsewhere (e.g., Rach *et al*., 2014; Brauer *et a*l., 2008; Lane *et al*., 2013) demonstrates that the use of Greenland as a regional stratotype for the North Atlantic region may not be fully appropriate and the development of high-resolution proxy records with secure chronologies are needed from beyond Greenland to further our understanding of the climate system and forcing mechanisms. However, further description of the trends described here are limited by several factors which are outlined below.

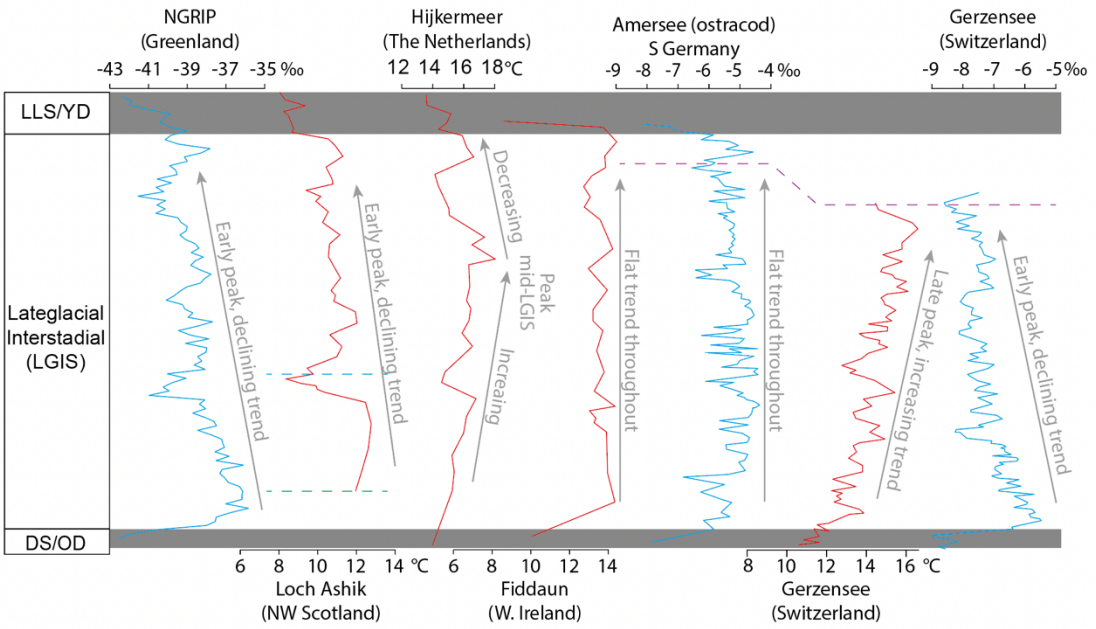

Figure 1.2, Examples of T_{Jul} and $\delta^{18}O$ records from the British Isles and Continental Europe displaying differing trends during the LGIS. Green dashed line = Borrobol Tephra, Blue dashed line = Penifiler Tephra, Purple dashed line = Laacher See Tephra.

Firstly, there is generally a low spatial density of sites that currently have T_{Jul} and $\delta^{18}O$ records (see Figure 1.3). These sites tend to be concentrated in central Scotland and the north of England with only a small number of records for the whole of Ireland (Brooks and Langdon, 2014). The density of T_{Jul} and $\delta^{18}O$ records in mainland Europe is even lower and the spatial coverage of $\delta^{18}O$ records is particularly poor being constrained largely to the Alpine region. Due to these issues, currently spatial gradients in the expression of different ACEs, which can be used to examine the magnitude of temperature change during ACEs, is limited.

Secondly, the chronological constraint on many records is relatively poor making correlations and comparisons of ACEs challenging in some instances. Scottish sites have more robust chronologies through age models with tephrochronology supplemented by radiocarbon dated terrestrial plant macrofossils. In Ireland, radiocarbon dating is the main tool used to date sequences, however, due to sparse terrestrial plant macrofossil remains, many dates are generated using either aquatic plant macrofossils or bulk material causing erroneous ages as a result of hardwater error and detrital contamination (e.g., Diefendorf *et* al., 2006; Watson *et al.,* 2010; Turner *et al.,* 2015). Most English sites have no independent chronology and rely on climatostratigraphy. Sites in mainland Europe, which do have tephra, usually only contain the Laacher See Tephra in GI-1b (Bogaard and Schmincke, 1985; Reinig *et al.,* 2021) and therefore rely on pollen stratigraphy and radiocarbon dates.

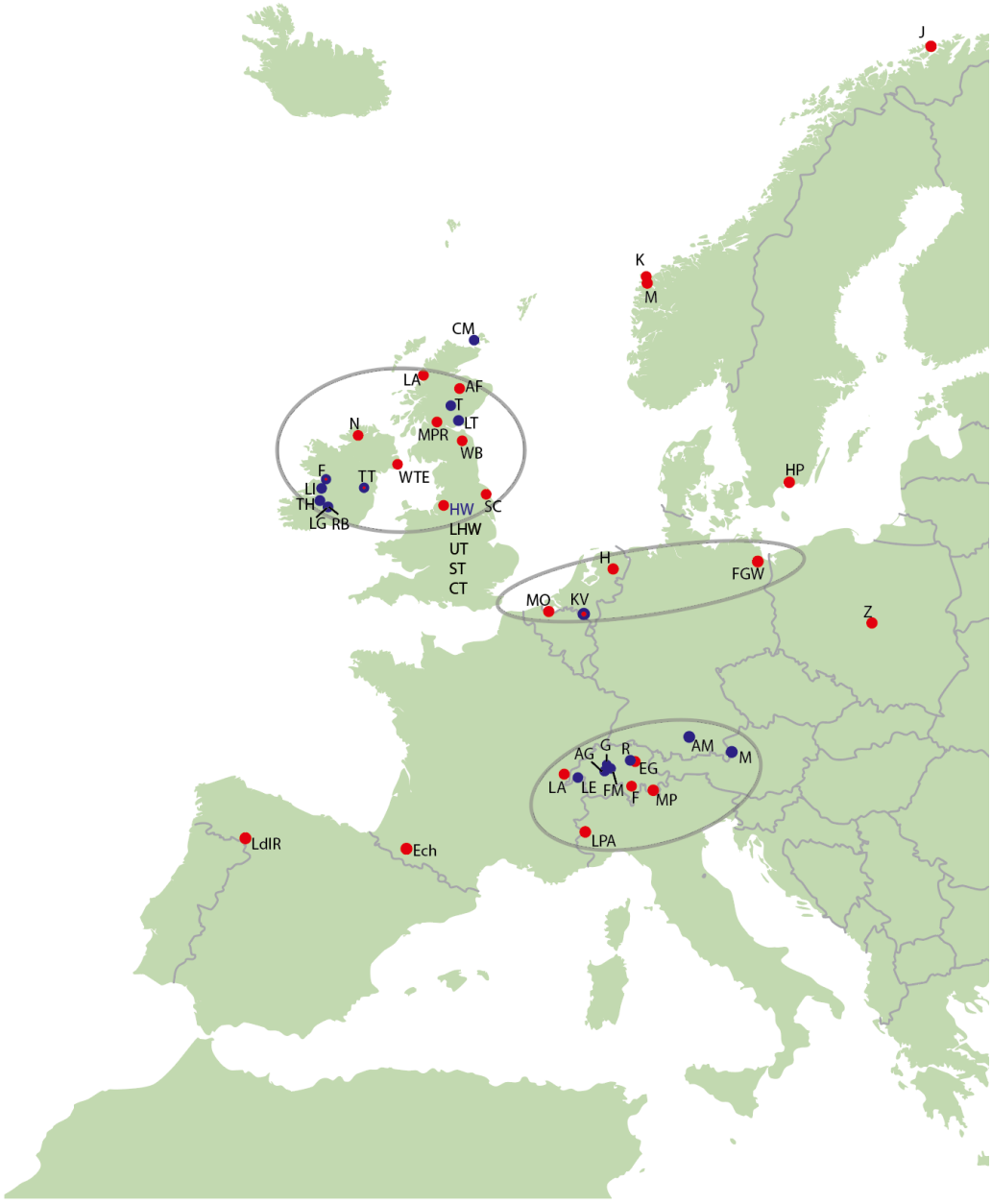

Figure 1.3, Locations of T_{Jul} and $\delta^{18}O$ records in Europe highlighting spatial clustering of sites. There are large areas of the British Isles which do not have published T_{Jul} and $\delta^{18}O$ records including northern Scotland (except Crudale; Whittington *et al.,* 2014), and southern England. In Continental Europe, there are even larger areas where there are no T_{Jul} nor $\delta^{18}O$ records including the lowland plains of France and Germany, southern Italy and Spain, and eastern Europe. A number of T_{Jul} records in continental Europe also do not cover the whole of the LGIS period, e.g., Kråkenes, Moervaart, Klein Ven and Friedländer Große Wiese. Abbreviations: AF = Abernethy Forest, AG = Aegelsee, AM = Amersee, CM = Crudale Meadow, CT = Cunswick Tarn, EG = Egelsee, F = Fiddaun, FO = Foppe, FGW = Friedländer Große Wiesse, FM = Faulenseemoos, G = Gerzensee, H = Hijkermeer, HP = Hässeldala Port, HW = Hawes Water, J = Jansvatnet, K = Kråkenes, KV = Klein Ven, LA = La Roya, L = Lac Lautrey, LA = Loch Ashik, LE = Leysin, LG = Lough Gur, LHW = Little Hawes Water, LI = Lough Inchiquin, LP = Lago Piccolo di Avigliana, LT = Lundin Tower, MO = Mondsee, MK = Myklevatnet, M = Moervaart, MP = Maloja Riegel, MPR = Muir Park Reservoir, N = Nadourcan, R = Rotsee, RB = Red Bog, SC = Star Carr, ST = Sunbiggin Tarn, T = Tirinie, TH = Tory Hill, TT = Thomastown, UT = Urswick Tarn, WB = Whitrig Bog, WTE = White Bog, Z = Żabieniec

Thirdly, many T_{Jul} and $\delta^{18}O$ records are conducted at a reasonably low sampling resolution with most sites only attaining a 50 yr resolution on average, however, some are as low as 100-250 yrs per sample. This is insufficient to properly represent the full magnitude and structure of centennial-scale abrupt events. In some instances, the resolution of the archive is the limiting factor, for example, at Fiddaun, the early LGIS ACE broadly coeval with GI-1d is only represented by a few centimetres of sediment and four chironomid samples (van Asch *et al.*, 2012a).

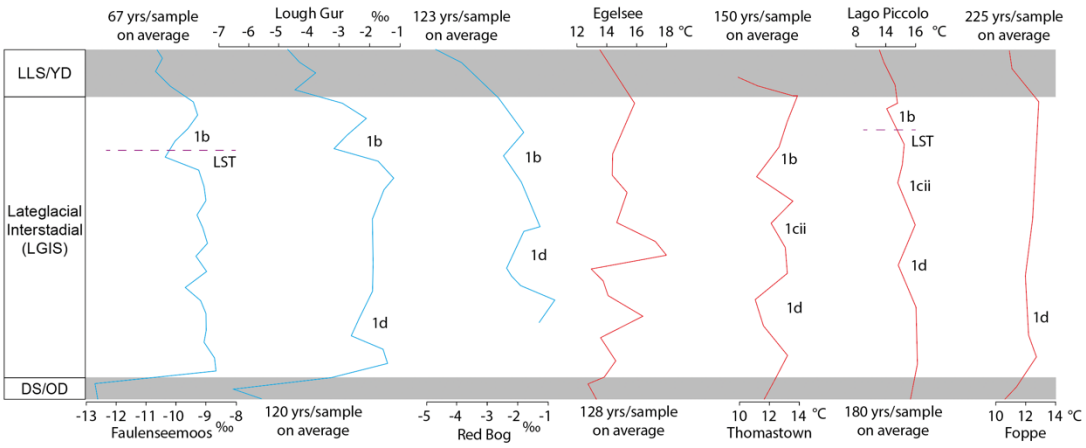

Figure 1.4, Selected T_{Jul} (red) and $\delta^{18}O$ (blue) records from the British Isles and Continental Europe which have a low sampling resolution and possibly do not adequately define the magnitude of the ACEs during the LGIS, which are marked on using GICC05 terminology. References for sites can be found in Tables 2.3 and 2.4.

1.3 Aims and Objectives

The aim of this thesis is to better understand the spatial expression of centennial-scale ACEs during the LGIS in NW Europe, allowing the potential climate forcing mechanisms which cause them to be assessed. A set of subsidiary aims have also been devised:

1) To compare patterns of climate change across the LGIS generated using two independent high-resolution proxies: chironomids and oxygen isotopes.

2) To understand how the expression of ACEs that occurred during the LGIS vary across spatial gradients in Britain and Europe.

3) To use the data generated in aims 1 and 2 to discuss the potential driving factors of climate change during LGIS ACEs

To achieve these aims the following objectives will be undertaken:

1) Review the literature and compile a database of all sites in the British Isles and continental Europe that have oxygen isotope data and chironomid-inferred temperature reconstructions for the LGIS to identify geographic areas where data is absent.

2) In regions where T_{Jul} and $\delta^{18}O$ records are absent, identify sequences which already have material available for study which are well-dated using independent dating techniques i.e., tephra and/or radiocarbon-dated terrestrial plant macrofossils.

3) Utilise any further chronological analysis (e.g., tephra analysis and radiocarbon dating) to further improve the chronological constraint of sequences already available to use in this thesis, if needed.

4) Where sequences are not already available for study in regions where T_{Jul} and $\delta^{18}O$ records are absent, search the literature to find appropriate site(s) and retrieve new sediment sequences.

5) Apply standard sedimentological techniques to better understand the new sequences retrieved for this thesis and identify the LGIS in the first instance.

6) Carry out investigations for tephra shards and terrestrial plant macrofossils for tephrochronology and radiocarbon dating to create robust independent chronologies for the new sequences.

7) Perform chironomid and oxygen isotope analysis at high resolution to reconstruct mean July air temperatures (T_{Jul}) and mean annual air temperatures (MAT), with contiguous sampling during ACEs to ensure the full magnitude of the ACEs is identified.

8) Synthesise data from the newly studied sites and integrate with existing data to analyse the spatial variations in magnitude of abrupt cooling events along altitudinal, latitudinal, and longitudinal gradients.

1.4 Thesis structure

This thesis is divided into eleven chapters including this introduction chapter. Chapter two provides an overview of high-resolution palaeotemperature records from chironomids and oxygen isotopes that are currently available for the LGIS in the British Isles and Europe for which the new records generated for this thesis will be compared to. Two of the main climates forcing mechanisms attributed to causing ACEs will also be described, namely oceanic forcing via changes in AMOC (Atlantic meridional overturning circulation) and solar variability. Chapters 3 and 4 give background information on chironomids and oxygen isotopes, respectively, including a brief history of how these proxies have been used, advantages of using them in the study of centennial-scale events and considers the range of environmental variables other than temperature which may cause issues with the temperature inferences being made. Chapter 5 outlines the criteria used to select the study sites for this thesis and details the field, laboratory and numerical methods used. The study sites selected to obtain new T_{Jul} and $\delta^{18}O$ records from are introduced in Chapter 6 giving site specific information which may cause issue with the temperature inferences made, including the local geology and topography, glacial history, lake-level changes, and vegetation changes. Previous palaeoecological and palaeoclimatic investigations, as well as chronological work will be detailed for each site. In Chapters 7, 8 and 9, the results and interpretations from the chironomid and oxygen isotope analysis is presented for each site respectively. These chapters aim to reconstruct the palaeolimnological environments and palaeoclimatic histories for the LGIS at each site. The new chironomid records presented in this thesis are integrated with other T_{Jul} and $\delta^{18}O$ records in Chapter 10, allowing the spatial expression of ACEs during the LGIs to be examined across spatial gradients (altitude, latitude, and longitude) with potential forcing mechanisms suggested. Chapter eleven summarises the major findings of this research and suggests directions for future research.

Chapter 2: High-resolution temperature records of the LGIS and potential forcing mechanisms of ACEs

Chapter overview

This chapter will introduce the key high-resolution temperature records from the circum-north Atlantic region for the LGIT. Although the focus of this PhD is on the LGIS, the preceding stadial, the Dimlington Stadial/GS-2/Oldest Dryas, and proceeding stadial, the Loch Lomond Stadial/GS-1/the Younger Dryas, will also be included as studies rarely focus on the LGIS by itself and often span all of these time periods; the Last Glacial-Interglacial transition (LGIT). This chapter is split into three sections. The first section will introduce the most widely discussed record of the LGIT, the Greenland Ice cores, which are widely considered to have the best stratigraphic resolution and chronological constraint. The second section will look at the range of temperature proxies utilised to reconstruct past climatic temperature changes in terrestrial sequences during the LGIT. A focus is then placed on the currently available T_{Jul} and $\delta^{18}O$ records for the LGIS in the British Isles and Continental Europe, with an additional brief overview of records from North America. The final section will review the key forcing mechanisms operating during the LGIT, with a particular focus on oceanic and solar forcing.

2.1 The Lateglacial in Greenland

The Greenland ice cores arguably provide the best records for the Lateglacial as they are continuous, have an independent annually resolved chronology and are the best stratigraphically resolved archives in the northern hemisphere (Rasmussen *et al*., 2006). Due to the issues with assumed synchroneity and imprecise radiocarbon dating during the LGIT (Lowe and Walker, 2000; Walker *et al*., 2001), the INTIMATE (INTegration of Ice, MArine and TErrestrial records) community has proposed that the ice-core isotopic stratigraphy from the North GRIP ice core (NGRIP) should be used a stratotype for the Northern Hemisphere. The NGRIP proxy records, along with the GRIP and GISP2 records, have been placed on a common timescale (GICC05) using multiple proxy parameters (e.g., visual stratigraphy, electrical conductivity measurements, Ca^{2}+, SO^{2}_{4}) (Rasmussen *et al*., 2006; Lowe *et* al., 2008). Not only does the NGRIP record have a robust time scale with mean counting errors (MCE) of ±186 yrs at the start of the LGIS but there are also a variety of proxies contained within the ice cores that record climate change at a sub-annual resolution (Dansgaard *et al*., 1993; Rasmussen *et al*., 2006; Steffensen *et al*., 2008). The main proxy used though are oxygen isotopes, which are widely interpreted as relative temperature change through the ratio between ^{18}O and ^{16}O. This

relationship is primarily dependent on the condensation temperature at which precipitation was formed, which is closely related to surface temperature (Schwander *et al.*, 2000), as such, more negative $\delta^{18}O$ values indicate colder conditions while more positive values reflect warmer conditions (Dansgaard, 1964). The LGIS has been annually layer counted to have a duration of 1,796 yrs and is characterised by declining temperatures throughout as inferred from the $\delta^{18}O$ record with maximum temperatures attained early in GI-1e (Table 2.1; Figure 2.1). Overprinted on this declining trend, several ACEs are present (GI-1d, GI-1cii, GI-1b), with coldest temperatures recorded during GI-1b. It should be noted that other declines in $\delta^{18}O$ do also occur within GI-1, with the most notable in GI-1e (GI-1e* in Figure 2.1) but have not been given a name in the Greenland event stratigraphy (van Raden *et al.*, 2013).

Table 2.1, The main subdivision of the Lateglacial in the GICC05 event stratigraphy (after Rasmussen *et al.*, 2014).

Greenland Event	Depth (m)	Date event commenced (GICC05 yrs B2k)	Error (MCE)	Duration (yrs)	Total Duration (yrs)	British/Irish terminology
GS-1	1526.52	12,896±4	138	1,193	1,193	Loch Lomond Stadial/ Nahanagan Stadial
GI-1a	1534.5	13,099	143	203		Windermere Interstadial/ Late Glacial Interstadial/ Woodgrange Interstadial
GI-1b	1542.1	13,311	149	212		
GI-1ci	1554.75	13,600	156	289		
GI-1cii	1557.08	13,660	158	60	1,796	
GI-1ciii	1570.5	13,954	165	294		
GI-1d	1574.8	14,075	169	121		
GI-1e	1604.64	14,692±4	186	617		
GS-2a	1669.09	17,480	330	2,788	8,208	Dimlington Stadial/ Glenavy Stadial

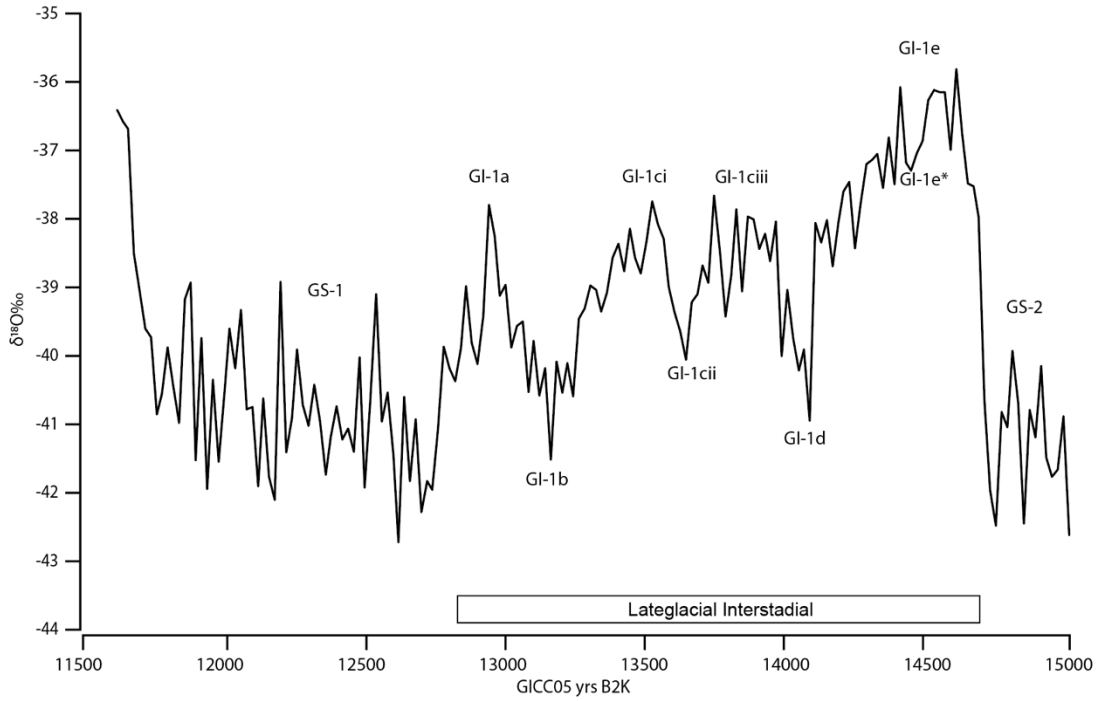

Figure 2.1, $\delta^{18}O$ record (20-year means) for the Lateglacial from the NGRIP ice core plotted against the GICC05 timescale. Greenland stadials are given the prefix GS- and Greenland interstadials GI-. Several cold oscillations punctuate the relatively warm LGIS, most notably GI-1d, GI-1cii and GI-1b (Rasmussen *et al*., 2006; 2014).

2.2 The LGIS in circum-North Atlantic terrestrial archives

Prior to the extraction of the first ice cores, evidence for a warm period (the LGIS) at the end of the last glaciation was already established. The LGIS was originally identified in palynological biozones in Scandinavia (Mangerud *et al*., 1974) and was characterised as two warm interstadials, termed the Bølling and the Allerød, separated by a cold period, the Older Dryas. Through radiocarbon dating, these broad bio-zones became the basis of chronozones (Mangerud *et al*., 1974). Subsequently, throughout the North Atlantic, a warm period containing several short-lived cold oscillations, were identified in a plethora of records. Many of these climatic events were termed using the Scandinavian terminology of Bølling, Allerød and Older Dryas. These, along with other local names have been applied to events during the LGIS (see Figure 2.2), outside of their appropriate regional area.

The issue with this framework is that it suggests that the period(s) identified were the same event and therefore synchronous (Lowe *et al*., 2008). Further confusion comes from the same name being used to describe different intervals within the LGIT, e.g., the Oldest Dryas in many regions is used to describe events broadly equivalent to GS-2 (Lotter *et al.,* 1992), however it is used to describe an event broadly equivalent to GI-1d in the Eifel region (Merkt and Müller, 1999; Litt and Stebich, 1999). Similarly, the Older Dryas could refer to events

broadly correlative with GI-1d in North America (Yu and Eicher, 1998) or GI-1cii in the Eifel region (Merkt and Müller, 1999; Litt and Stebich, 1999) and NE North America/Cariaco basin (Yu, 2007; Hughen *et al.,* 1996). This has led the INTIMATE group to suggest adopting the event stratigraphy approach using the GICC05 timescale as a stratotype for the Northern Hemisphere, with individual records initially being defined using appropriate regional terminology and independently dated, before being compared to it (Lowe *et al*., 2008). As the aim of this thesis is to compare the magnitude of events and is less concerned about the exact timing/synchronicity of events, the Greenland event names (i.e., GI-1d and GI-1b) will be used in this chapter when reviewing the available T_{Jul} and $\delta^{18}O$ records as it helps avoid confusion when drawing comparisons from many different regions around the North Atlantic. In Chapters 7, 8 and 9, where the results and interpretation are presented for each of the sites studied in this thesis, events will be inferred to as their broad age, e.g., *c.* 14.0 ka BP ACE, as the chronological constraint allows for this.

Local isotope zonation GRZi bulk	Modified Greenland terminology	Swiss Plateau, S-Germany *1)	Eifel region, N-Germany *2) *3)	N-America, Cariaco basin *4) *5)	N-America *6)	Norwegian Sea *7)	N-Atlantic *8)	Greenland *9)
13	Younger Dryas	Younger Dryas	Younger Dryas	Younger Dryas	Younger Dryas	Younger Dryas	Younger Dryas	GS-1
12	transition							
11	GI-1a							GI-1a
10	GI-1b	Gerzensee Oscillation	Gerzensee Oscillation	IACP	Killarney Oscillation	Older Dryas II	IACP II	GI-1b
9	GI-1c1		Allerød	Allerød		Allerød	Allerød	
8	GI-1c2	Allerød	Older Dryas	Older Dryas	Allerød	Older Dryas I	IACP I	GI-1c
7	GI-1c3		Bølling	Bølling				
6	GI-1d	Aegelsee Oscillation	Oldest Dryas	IBCP	Older Dryas	BCP II	Older Dryas	GI-1d
5	GI-1e1					Bølling		
4	GI-1e2	Bølling	Meiendorf	Bølling	Bølling	BCP I	Bølling	GI-1e
3	GI-1e3							
2	transition							
1	Oldest Dryas	Oldest Dryas	Pleniglacial	Oldest Dryas	Oldest Dryas	Oldest Dryas	Oldest Dryas	GS-2

Figure 2.2, Summary of terminology used to identify different events through the LGIT from the areas bordering the North Atlantic. Note how the same name has been used for different events e.g., the Older Dryas. *1: (Lotter *et al.*, 1992); *2: (Merkt and Müller, 1999); *3 (Litt and Stebich, 1999); *4 (Yu, 2007); *5 (Hughen *et al.,* 1996); *6 (Yu and Eicher, 1998); *7 (Karpuz and Jansen, 1992); *8 (Thornalley *et al.,* 2010); *9 (Lowe *et al.,* 2008). (From: van Raden *et al*., 2013).

2.2.1 Temperature proxies utilised

Temperature changes during the LGIT have been studied using a number of quantitative temperature proxy-records including those based on Coleoptera (e.g., Atkinson *et al*., 1987; Coope *et al*., 1998; Elias and Matthews, 2014), pollen (e.g., Walker *et al*., 1994; Lotter *et al*., 2012) and plant macrofossils (e.g., Isarin and Bohncke, 1999, Isarin *et al*., 1999; Birks, 2003).

Coleoptera

The Mutual Climatic Range method (MCR) is often used to obtain palaeotemperature estimates from beetles and is based on the concept that beetles live within the bounds of the climatic conditions that occur within their present geographic range (Atkinson *et al*., 1986). The modern climatic ranges of species found in a fossil assemblage can, therefore, be used to estimate the temperature regime of the time interval represented using a constructed temperature envelope that contains the climatic tolerances of all species. Such studies usually calculate T_{max}, temperature of the warmest month, T_{min}, temperature of the coldest month and T_{range}, the range between the coldest and the warmest months. Two key examples from Britain where the MCR technique has been applied continuously throughout LGIT sequences are from Gransmoor (Walker *et al.,* 1993) and Llanilid (Walker *et al.,* 2003) (Figure 2.3).

Although this method can yield reasonably accurate temperature data, large amounts of sediment are needed, often tens of cubic centimetres at least, to collect enough beetle remains (Table, 2.2c), limiting the number of samples in an MCR reconstruction due to limited material (Table, 2.2d). For examples, at Llanilid, samples covered 4-8 cm meaning centennial scale events within the LGIS are only represented by 3 datapoints, and the full magnitude of ACEs may have been reduced, or the entire ACE event missed completely. Therefore, the ability to study centennial scale ACEs with Coleopteran records is compromised by the sampling resolution at which they can be applied. It is also evident in the synthesis by Coope *et al.* (1998) that many Coleoptera records are fragmentary and not continuous throughout the LGIT at many sites. Methodologically there are several limitations of the MCR method. Firstly, the presence/abundance data used by the MCR method is very sensitive to count size (Birks *et al.,* 2012). Secondly, the MCR approach assumes a taxon has an equal probability of occurring anywhere within its climatic range which is unlikely for ecological or biogeographical reasons (Horne and Mezquita, 2008; Hengeveld, 1990; Birks *et al.,* 2012). Thirdly, it is difficult to test an MCR model with an independent test-set to ascertain the model's reliability when the two sets of variables considered, geographic distributions of taxa and broad-scale climatic variables,

show strong spatial autocorrelation meaning an independent test-set cannot be created (Beale *et al.,* 2010; Telford and Birks 2009; Birks *et al.,* 2012).

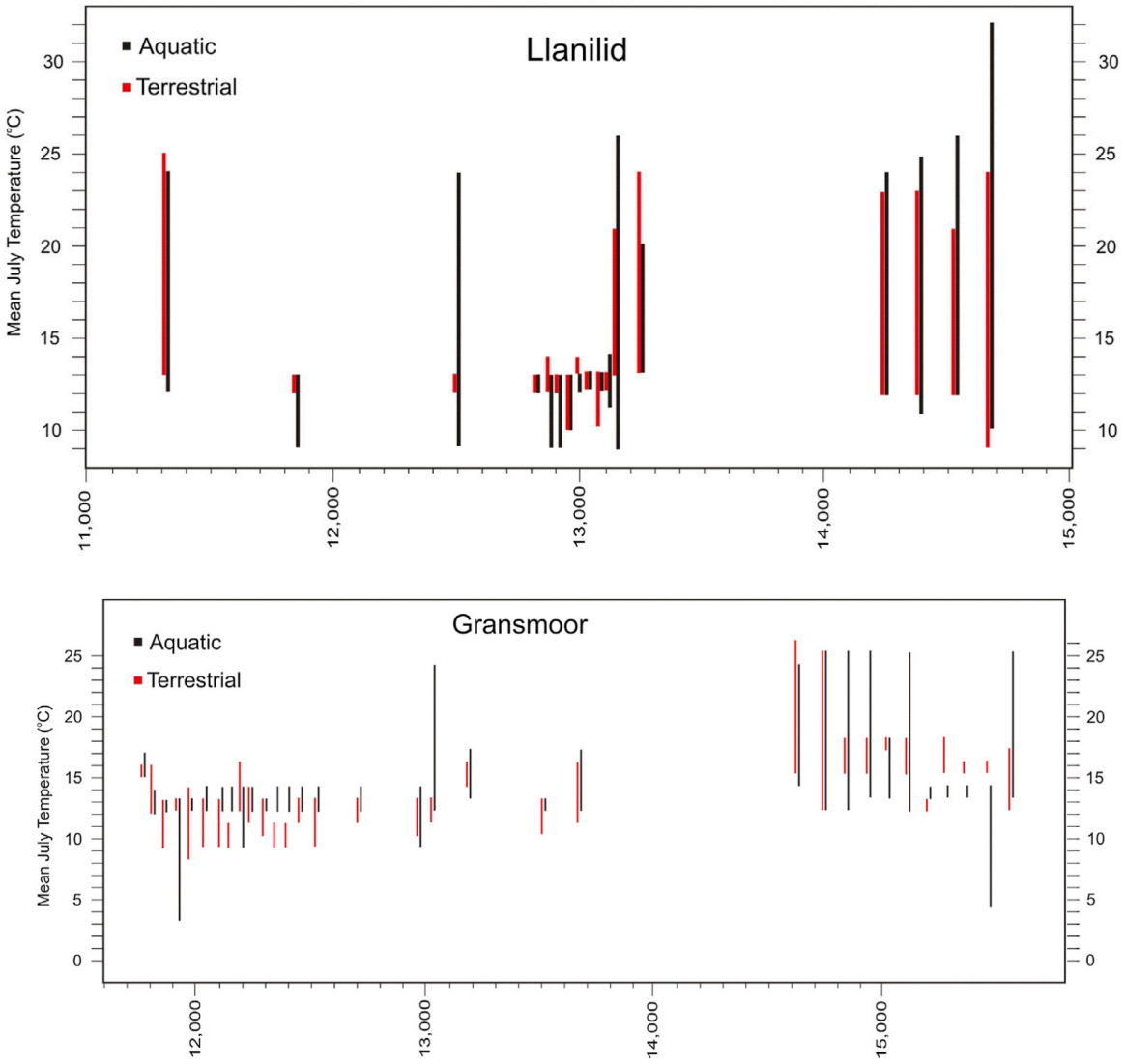

Figure 2.3, MCR mean July temperature estimates based on aquatic and terrestrial beetles for Gransmoor and Llanilid plotted against calibrated radiocarbon using Intcal09. Note the low sampling resolution is too low to pick out ACEs within the LGIS. (From Elias and Matthews, 2014).

Table 2.2, Information on MCR temperature reconstructions in the British Isles covering the LGIT (after Elias and Matthews, 2014)

a) Site	b) Age range of samples (ka cal BP)	c) Sediment volume per sample	d) Number of samples in MCR	e) Number of species used in MCR	f) Reference
St Bees, Cumbria	14.8-11.2	5 L	27	51	Coope and Jaochim (1980)
Gransmoor, Yorkshire	15.5-11.7	2 L	32	137	Walker *et al.* (1993)
Glanllynau, Gwynedd	16.5-13.5	5 L	11	117	Coope and Brophy (1972)
Llanilid, Glamorgan	14.7-11.3	2 L	16	64	Walker *et al.* (2003)

Pollen

Several techniques have been employed to estimate palaeotemperatures from pollen data including Mutual Climatic Range (MCR) (Kershaw and Nix, 1988; Fauquette *et al.,* 1998), Response Surface (Bartlein *et al.,* 1986), Artificial neural networks (Peyron *et al.,* 1998) and weighted-averaging partial least squares regression (WA-PLS; Lotter *et al.,* 2000). Temperature reconstruction based on pollen assemblages can be applied at high temporal resolution as only 1cm^3 of sediment is needed per sample (Faegri and Iversen, 1989). Another advantage is that there are thousands of records which already have pollen datasets throughout Europe (Williams *et al.,* 2018) for which statistical techniques can be readily applied to. An example of pollen-based temperature reconstructions for the LGIS is Gerzensee in which WA-PLS techniques were applied (Lotter *et al.,* 2000; 2012) (Figure 2.4). Although mean July air temperature was the parameter that was reconstructed, Lotter *et al.* (2012) suggested that the pollen temperature reconstruction may be influenced by winter temperatures because the trends of declining temperatures displayed a similar declining pattern seen in the ^{18}O of Greenland ice cores and contrasted to the increasing temperatures from chironomid-inferred temperatures.

Issues with reconstructing temperatures from pollen counts come less from the statistical methods used to derive them, but more from the vegetation itself. Firstly, there are potential vegetation lag effects due to edaphic factors and dispersal capabilities meaning the vegetation may not be in equilibrium with climate (Lotter *et al.,* 2012). Secondly, other environmental parameters may be constraining the distribution and abundance of plant taxa including

precipitation, periods of drought, wind strength, soil type, number of days below freezing. As in the example above, winter temperatures have an influence on plant distributions and can cause artefacts in summer temperature reconstructions when varying independently. Thirdly, pollen can only be identified to genus level (some instances only family), in which there can be numerous species with contrasting climatic limits (Brewer *et al.,* 2007). Finally, the lake setting can greatly affect whether it records a local or more regional climate signal (Brewer *et al.,* 2007). These issues are partially responsible for the large errors on pollen inferred temperature reconstructions of *c*. ±2 °C (e.g., Lotter *et al.,* 2012).

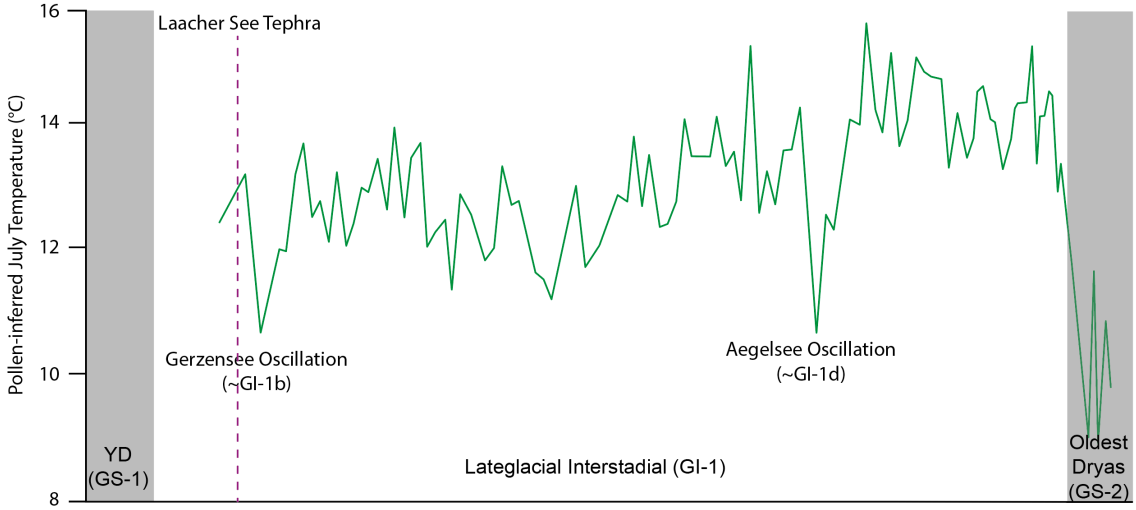

Figure 2.4, Pollen-inferred mean July air temperature reconstruction from Gerzensee, displaying a decline in temperatures throughout the LGIS and two ACEs. (After Lotter *et al*., 2012).

Plant macrofossils

Palaeotemperature estimates from plant macrofossils typically utilises the indicator species approach based on the theory that trees and plants require a minimum summer temperature (often taken from July) to flower and reproduce in a growing season (Isarin and Bohncke, 1999; Figure 2.5). Isarin and Bohncke (1999) used the minimum mean July temperature (MMJT) for a range of species (Figure 2.5a) to create temperature gradient maps for the Younger Dryas in Europe (Figure 2.5b). This technique can yield accurate quantitative data, as there is little issue with long distance transport and plants can be identified to species level, unlike pollen. However, as with pollen, a number of factors affect the distribution of plants including migrational lags, dispersal ability, soil development, landscape stability, seasonality and precipitation (Lowe and Walker, 2014). Moreover, few sequences preserve enough plant macrofossils, and preserve them contiguously throughout the sequence, to allow the

technique to be applied at high resolution. Large samples are likely to be needed limiting the resolution at which they can be applied in many sequences. Comparisons of reconstructions from plant macrofossils to other temperature proxy data as minimum temperature estimates are produced (Brooks and Birks, 2000). However, there are recent developments with the application of weighted means on assemblages (Delde and Birks, 2019).

a) Climatic indicator plant species and their Minimum Mean July Temperature (MMJT)

Species	MMJT
Betula nana	7
Calluna vulgaris	7
Caltha palustris	8
Carex acutiformis[1]	13
Carex dioica[1]	8
Carex distichia[1]	12
Cladium mariscus	13
Ceratophyllum spp.[2]	13+
Filipendula ulmaria[1]	8
Filipendula vulgaris[1]	9
Hippophaë rhamnoides	11
Juniperus communis	8
Menyanthes trifoliata[2]	8
Myriophyllum alterniflorum[2]	9
Myriophyllum spicatum[2]	10
Myriophyllum verticillatum[2]	10
Najas marina[2]	15
Nuphar lutea[2]	12
Nymphaea alba[2]	12
Nymphaea candida[2]	12
Potamogeton mucronatus[1,2]	13
Potentilla palustris[1]	8
Ranunculus subg. *Batrachium*[2]	10
Sanguisorba officinalis	9
Sanguisorba minor	12
Solanum dulcamara	13
Typha latifolia[2]	13
Urtica dioica[1]	8

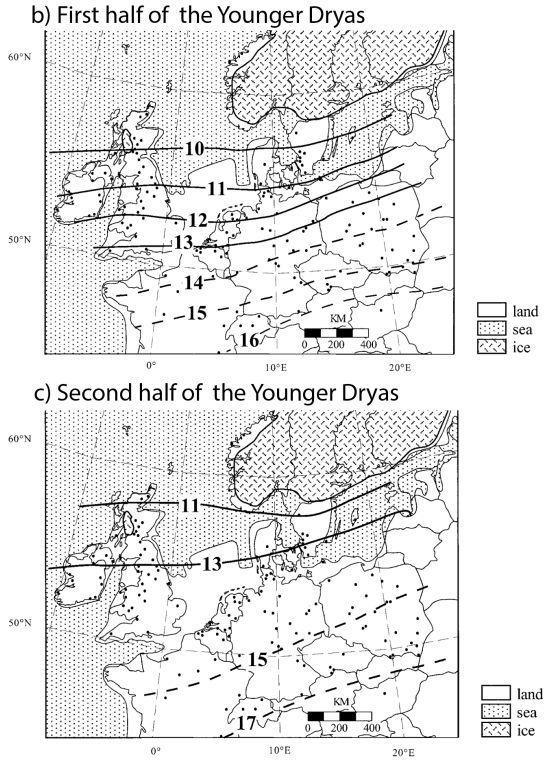

Figure 2.5, Macrofossil July temperature reconstructions of the Younger Dryas. a) A list of the main indicator species used by Isarin and Bohncke (1999) with values obtained by comparing plant distribution maps of Hultén (1950, 1958, 1964, 1971a, b) and Jalas and Suominen (1980) with mean July isotherms from the 1931-1960 interval (Wallén, 1970); b) isotherm map based on MMJT for the first half of the younger Dryas; and, c) isotherm map based on MMJT for the second half of the younger Dryas. In a) [1] = Identified by macrofossil analysis, [2] = Aquatic. (After Isarin and Bohncke, 1999).

Summary

The indicators outlined above have limitations which restrict their application to studying centennial-scale climatic changes for a range of reasons including the limited sampling resolution at which they can be applied at, lags in proxy response to climatic temperature changes and issues relating to the numerical techniques used to quantify temperatures. Chironomids and $\delta^{18}O$, however, overcome many of these issues as they are very responsive to changes in climatic temperature, can be applied at high-resolution, and provide quantitative, or at least semi-quantitative reconstructions. Therefore, Chironomids and $\delta^{18}O$ are two of the most suitable proxies available to study centennial-scale abrupt climatic temperature changes.

The advantages and issues with these proxies are explored in greater detail in Chapters 3 and 4.

2.2.2 Chironomid and oxygen isotope records

This section will give an overview of the chironomid-inferred temperature and oxygen isotope records from the circum-north Atlantic region covering the LGIS. Currently there are 35 Chironomid-inferred temperature reconstructions and 22 oxygen-isotope records published from Europe which contain samples of LGIS age (Figure 2.6). Table 2.2 and 2.3 provides details of the records for the British Isles and Continental Europe, respectively. Although the time duration of the LGIS is likely to vary between sites (Lowe *et al.,* 2008; Hoek *et al.,* 2008), the chronology at most sites is not robust enough to make such determinations. It is also acknowledged that the sedimentation rate is unlikely to be linear throughout the LGIS and would have varied independently at each site during the LGIS time interval. However, due to many sequences having few robust chronological tie points (i.e., tephra, radiocarbon dates), and a notable number of sequences reliant on stratigraphic techniques (i.e., pollen, isotope), it is difficult to provide more accurate estimates on the duration of the LGIS, and variation in sedimentation rates within. For some records, the LGIS is incomplete as sedimentation began late, e.g., Abernethy Forest (Brooks *et al*., 2012), or finished early due to infilling of the basin, e.g., Gerzensee (Lotter *et al.,* 2012) or Moervaart (van Bos *et al.,* 2017). For these sites, the duration of the LGIS was approximately calculated using the subdivisions of GI-1 in Greenland.

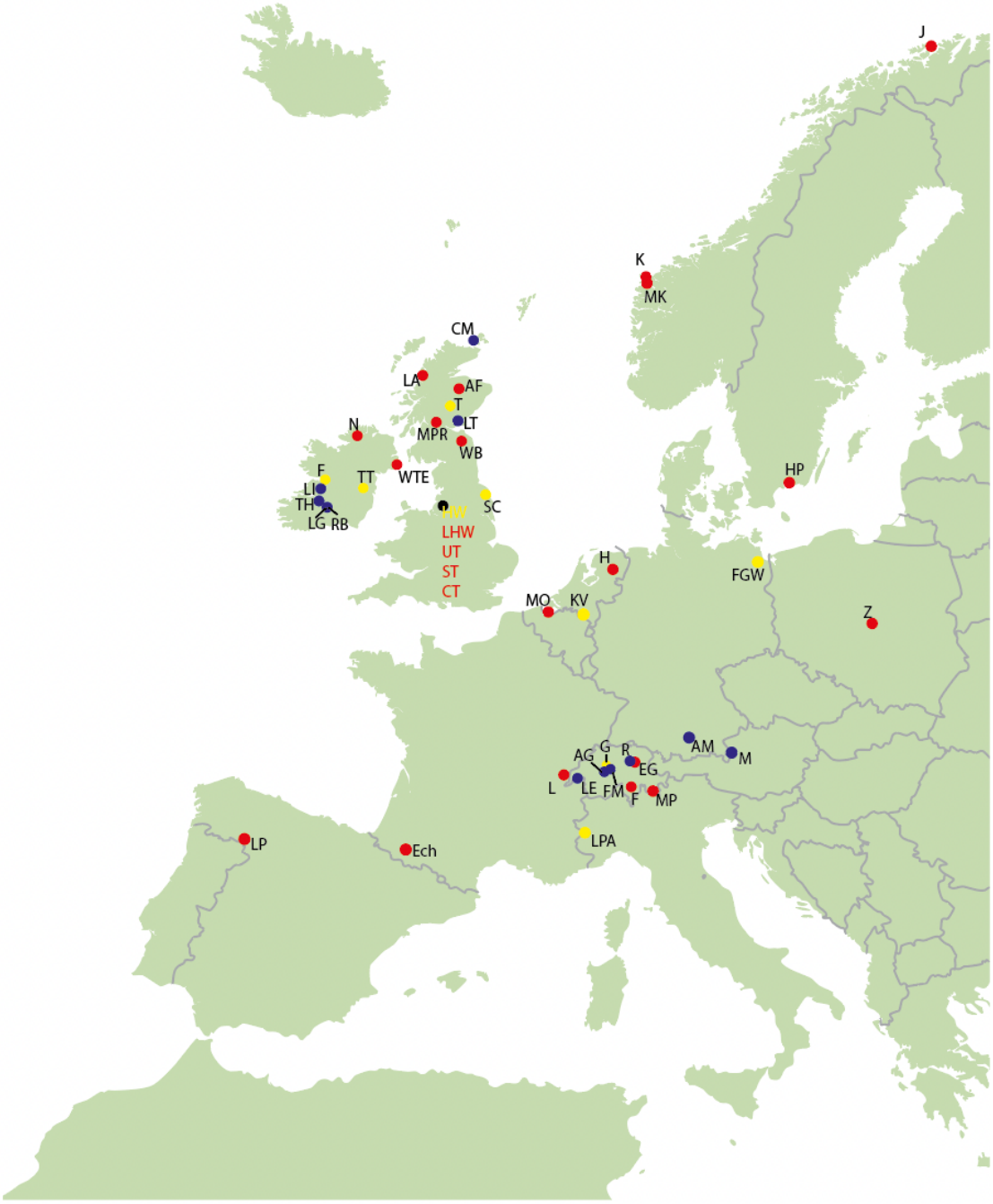

Figure 2.6, Map of sites with T_{Jul} (red circles) and $\delta^{18}O$ records (blue circles) in Europe covering the Lateglacial Interstadial. Sites denoted with a yellow circle have both T_{Jul} and $\delta^{18}O$ records. Note, for the cluster of sites in Cumbria, the abbreviation is coloured instead. Abbreviations: AF = Abernethy Forest, AG = Aegelsee, AM = Amersee, CM = Crudale Meadow, CT = Cunswick Tarn, EG = Egelsee, F = Fiddaun, FO = Foppe, FGW = Friedländer Große Wiesse, FM = Faulenseemoos, G = Gerzensee, H = Hijkermeer, HP = Hässeldala Port, HW = Hawes Water, J = Jansvatnet, K = Kråkenes, KV = Klein Ven, LA = La Roya, L = Lac Lautrey, LA = Loch Ashik, LE = Leysin, LG = Lough Gur, LHW = Little Hawes Water, LI = Lough Inchiquin, LP = Lago Piccolo di Avigliana, LT = Lundin Tower, MO = Mondsee, MK = Myklevatnet, M = Moervaart, MP = Maloja Riegel, MPR = Muir Park Reservoir, N = Nadourcan, R = Rotsee, RB = Red Bog, SC = Star Carr, ST = Sunbiggin Tarn, T = Tirinie, TH = Tory Hill, TT = Thomastown, UT = Urswick Tarn, WB = Whitrig Bog, WTE = White Bog, Z = Żabieniec. References for sites can be found in table 2.3 and 2.4.

Britain and Ireland

Currently there are 15 chironomid-inferred temperature records from the British Isles covering the LGIS (Figure 2.7; Table 2.2). There is a strong spatial bias with many T_{Jul} records located in central Scotland. Scottish LGIS sites are often temporally constrained by the presence of the

Borrobol and Penifiler Tephras and supplemented by the Vedde Ash in the LLS. These LGIS sites are sometimes also supported by radiocarbon dates e.g., Loch Ashik and Abernethy Forest (Brooks *et al.,* 2012). Outside of the Scottish sites, the chronological control on many sites is limited. The Cumbrian lake sites rely on climatostratigraphy (Lang *et al.,* 2010), however, most sites in the British Isles display a clear structure with high temperatures either attained at the start of the LGIS or stable temperatures being maintained throughout and punctuated by 2-3 well defined centennial-scale cold events. The ACE early in the LGIS, broadly equivalent to GI-1d, generally has the greatest magnitude of all the ACEs within the LGIS in Britain. However, in Ireland both the GI-1b and GI-1d oscillations are relatively muted at only 1-2 °C. Many sites have a good stratigraphic resolution with *c.* 20 yrs per cm comparable to the 20 yr averages of the $\delta^{18}O$ profiles from Greenland ice cores (Rasmussen *et al.,* 2006). Many sites take advantage of this resolution and include analyses of samples at between 1-2 cm intervals, with a greater number of samples around temperature minima. The Norwegian 157 lake training set is used for temperature inferences at most sites, many of which are dominated by clastic sediments. The exception is Thomastown Bog where $CaCO_3$ is precipitated during the LGIS. Only the T_{Jul} reconstruction from two sites use the combined Nor-Swiss calibration data set, Fiddaun (Van Asch *et al*., 2012a) and Tirinie (Abrook *et al.,* 2020 supp info). Tirinie and Quoyloo are the only two sites that used both the Norwegian and Combined Nor-Swiss calibration datasets and will be discussed more in Chapter 10. It is noted that Whitrig Bog used the old Norwegian calibration dataset of only 44 lakes (Brooks and Birks, 2000).

There are 10 $\delta^{18}O$ records from Britain and Ireland covering the Lateglacial that are typically interpreted as reflecting climatic temperature change (Table 2.3). Several of these sites also have T_{Jul} records including Tirinie (Abrook *et al*., 2020), Hawes Water (Marshall *et al.,* 2002), Fiddaun (Van Asch *et al*., 2012a), Thomastown (Turner *et al.,* 2015) and Star Carr (Blockley *et al.,* 2018). $\delta^{18}O$ records which have been completed recently (*c.* last two decades) have also taken advantage of the high stratigraphic resolution of sequences and have sampling intervals of 1-2 cm. However, older $\delta^{18}O$ records (*c.* pre-2000) have a much lower sampling resolution with an average of over 60 years per sample e.g., Lundin Tower (Whittington *et al.,* 1996), Lough Gur and Red Bog (Ahlberg *et al.,* 1996). Therefore, there are relatively fewer $\delta^{18}O$ records which have similar sampling resolution in comparison to the T_{Jul} records for the British Isles, three of which cluster on the west coast of Ireland including Loch Inchiquin (Diefendorf *et al.,* 2006, Fiddaun (Van Asch *et al.,* 2012a) and Tory Hill (O'Connell *et al.,* 1999), and two of which are for sites in northern England, Hawes Water (Marshal *et al.,* 2002) and Star Carr (Candy,

unpublished). Other $\delta^{18}O$ records are present in the Grampian Highlands, Tirinie (Candy *et al.*, 2016; Abrook *et al.*, 2020), the east coast of Ireland, Thomastown (Turner *et al.,* 2015), and the Orkney Isles, Crudale Meadow (Whittington *et al.,* 2015). The majority of $\delta^{18}O$ records have not caried out pre-treatment on samples such as sieving to remove detrital carbonate fragments, except for Tirinie (Candy *et al.,* 2016; Abrook *et al.,* 2020) and Crudale Meadow (Whittington *et al.*, 2015).

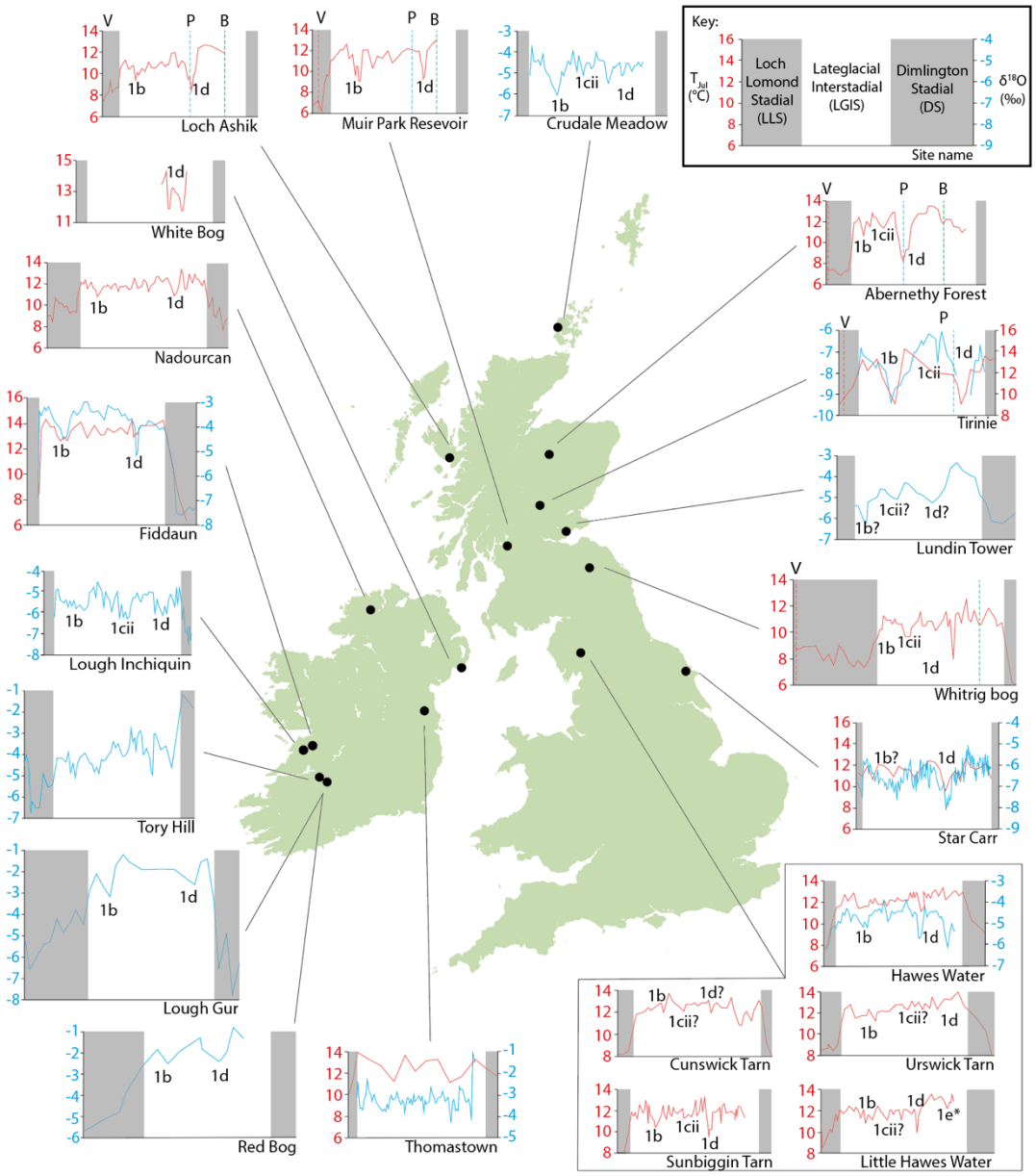

Figure 2.7, T_{Jul} (red lines) and $\delta^{18}O$ records (blue lines) covering the LGIS from the British Isles. Dashed lines represent the Vedde Ash (red), Penifiler Tephra (green) and Borrobol Tephra (blue). References for sites can be found in table 2.3.

Table 2.3, T_{Jul} and $\delta^{18}O$ records for the British Isles, arranged by latitude from North to South. Site names and location are in column (a). Column (b) notes the chronological methods used to provide age estimates for the sequences during the LGIS which range from tephrochronology, radiocarbon dating and several stratigraphic techniques. The material used for radiocarbon dating and any potential issues with these dates flagged by the authors are also noted. In column (c) an average stratigraphic resolution of the LGIS is given calculated by dividing the age duration of GI-1 in GICC05 (1796 yrs) by the stratigraphic length of sediments dated to the LGIS in each sequence and given as yrs/cm. Column (d) gives the average sampling resolution based on the duration of the LGIS in GICC05 is divided by the number of $T_{Jul}/\delta^{18}O$ data points during the LGIS (yrs/sample) and the number of data points divided in the LGIS divided by its length in a site to give an average sampling interval (cm interval). (e) gives details on the calibration dataset used or $\delta^{18}O$ sample preparation. Abbreviations for the tephra layers are as follows: B = Borrobol, P = Penifiler, V = Vedde Ash. Red shading is used for chironomid records and blue for oxygen isotope records.

a) Site and location	Chronology			c) Average LGIS Stratigraphic resolution	d) Average LGIS sample resolution	e) Calibration dataset and $\delta^{18}O$ Sample prep	Reference
	Tephra	Radiocarbon	-stratigraphy				
Quoyloo Meadow, N. Scotland	B			72 yrs/cm	257 yrs/cam	Norwegian 157, Nor-swiss 274	Timms *et al.,* 2021
Crudale Meadow, N. Scotland		3 Aquatic macrofossils (Hardwater error)	Climato-	30 yrs/cm	42 yrs/sample 1.4cm interval	Dry sieved at 63 µm	Whittington *et al.,* 2014
Abernethy Forest C. Scotland		10 Terrestrial macrofossils		16 yrs/cm	33 yrs/sample 2.1cm interval	Norwegian 157	Brooks *et al.,* 2012
Loch Ashik NW Scotland	B, P, V			18 yrs/cm	33 yrs/sample 1.8cm interval	Norwegian 157	Brooks *et al.,* 2012
Tirinie, C. Scotland	P V	1 Terrestrial macrofossils		44 yrs/cm	60 ys /sample 1.35 cm interval	Norwegian 157, Nor-swiss 274	Abrook *et al.,* 2020
					39 yrs/sample 0.9cm interval	Wet sieved 63 µm	Abrook *et al.,* 2020; Candy *et al.,* 2016
Lundin Tower, SE Scotland			Pollen-	26 yrs/cm	64 yrs/sample 2.5cm	None	Whittington *et al.,* 1996
Muir Park Reservoir S. C. Scotland	B, P, V			14 yrs/cm	33 yrs/sample 2.3 cm interval	Norwegian 157	Brooks *et al*., 2016

Table 2.3, continued (2)

a) Site and location	b) Chronology			c) Average LGIS Stratigraphic resolution	d) Average LGIS sample resolution	e) Calibration dataset and $\delta^{18}O$ Sample prep	Reference
	Tephra	Radiocarbon	-stratigraphy				
Whitrig Bog SE Scotland	B, V			19 yrs/cm	32 yrs/sample 1.6cm interval	Norwegian 44	Brooks and Birks, 2000
Lough Nadourcan NW Ireland		12 Bulk, Humic, Humin (Hard water error)		17 yrs/cm	28 yrs/sample 1.7cm interval	Norwegian 157	Watson *et al.,* 2010
Sunbiggin Tarn NW England			Climato-	18 yrs/cm	28 yrs/sample 1.6cm interval	Norwegian 157	Lang *et al*., 2010
Cunswick Tarn NW England			Climato-	37 yrs/cm	49 yrs/sample 1.3cm interval	Norwegian 157	Lang *et al.,* 2010
White Bog, N. Ireland			Pollen-	3 yrs/cm * Only GI-1d studied	9 yrs/sample 3.7 cm interval	Norwegian 157	O'Neill-Munro, 2017
Hawes water, NW England		1 Terrestrial macrofossils	Climato-	28 yrs/cm	33 yrs/sample 1.2cm interval	Norwegian 157	Lang *et al.,* 2010
					25 yrs/sample 0.9cm interval	Not stated	Marshal *et al.,* 2002
Little Hawes Water NW England			climato-	24 yrs/cm	33 yrs/sample 1.4 cm interval	Norwegian 157	Lang *et al.,* 2010
Urswick Tarn NW England			Climato-	28 yrs/cm	62 yrs/sample 2.2 cm interval	Norwegian 157	Lang *et al.,* 2010
Thomastown, E. Ireland		2 Bulk (Hardwater error)		10 yrs/cm	150 yrs/sample 15cm interval	Norwegian 157	Turner *et al.,* 2015
					26 yrs/sample 2.6cm interval	Not stated	Turner *et al.,* 2015

Table 2.3, continued (2)

a) Site and location	b) Chronology			c) Average LGIS Stratigraphic resolution	d) Average LGIS sample resolution	e) Calibration dataset and $\delta^{18}O$ Sample prep	Reference
	Tephra	Radiocarbon	stratigraphy				
Thomastown, E. Ireland		2 Bulk (Hardwater error)		10 yrs/cm	150 yrs/sample 15cm interval	Norwegian 157	Turner *et al.,* 2015
					26 yrs/sample 2.6cm interval	Not stated	Turner *et al.,* 2015
Fiddaun, W. Ireland		4 Terrestrial macrofossils		20 yrs/cm	60 yrs/sample 3cm interval	Nor-swiss 274	Van Asch *et al.,* 2012a
					25 yrs/sample 1.3cm interval	Not stated	Van Asch *et al.,* 2012a
Star Carr, N. England				8 yrs/cm	69 yrs/sample 9cm interval	Norwegian 157	Langdon (unpublished)
					12 yrs/sample 1.6cm interval	Wet sieved 63 µm	Candy (unpublished)
Loch Inchiquin, W. Ireland		2 Aquatic macrofossils (Hard water error)		25 yrs/cm	25 yrs/sample 1cm interval	Not stated	Diefendorf *et al.,* 2006
Tory Hill, W. Ireland			Isotope- Pollen-	5 yrs/cm	40 yrs/sample 8.8cm interval	Not stated	O'Connell *et al.,* 1999
Lough Gur, W. Ireland			Pollen-	45 yrs/cm	120 yrs/sample 2.7cm interval	Not stated	Ahlberg *et al*., 1997
Red Bog W. Ireland			Pollen-	13 yrs/cm	245 yrs/sample 10.6cm interval	Not stated	Ahlberg *et al.,* 1997

Continental Europe

Currently there are 17 chironomid-inferred temperature records from continental Europe with samples dating to the LGIS (Figure 2.8; Table 2.4), with a concentration of records in the alpine region, e.g., Gerzensee (Lotter *et al*., 2012), Foppe (Samartin *et al*., 2012). Four sites occur around the edge of the Scandinavian peninsula, e.g., Kråkenes (Brooks and Birks, 2001) and Jansvatnet (Birks *et al.,* 2012), and four on the lowland plains of Belgium (Moervaart; van Bos *et al.,* 2017), The Netherlands (Hijkermeer; Heiri *et al*., 2007; 2011), Germany (Friedländer Große Wiese; Van Ash *et al*., 2012) and Poland (Żabieniec; Plociennik *et al.,* 2011). Some sites in other mountain regions e.g., Ech in the French Pyrenees (Millet *et al*., 2012) and Laguna de la Roya in the Galician-Duero mountains, NW Iberia (Muñoz Sobrino *et al*., 2013).

The majority of sites in continental Europe have relatively good chronology with numerous radiocarbon dates on terrestrial plant macrofossils, e.g., Hässeldala port (Wohlfarth *et al.,* 2017), and/or the presence of tephra layers such as the Vedde Ash and Laacher See Tephra, e.g., Lago Piccolo di Avigliana (Larocque and Finsinger, 2008). Some, however, have to rely on pollen stratigraphy, e.g., Ech (Millet *et al.,* 2012) and Hijkermeer (Heiri *et al.,* 2007; 2011). Stratigraphic resolution is usually high with between 3 and 30 yrs/cm in most sites, however, there is a large range of average sampling intervals for sites from 1.5-20 cm intervals, resulting in sample resolution varying between 25 yrs/sample (Gerzensee) and 224 yrs/sample (Foppe). Therefore, the stratigraphic resolution of many sequences has not been used to their full potential.

Most sites have used a calibration dataset from their locality, i.e., the Swiss 103-lake calibration dataset has been used for reconstructions in the alpine region while the Norwegian calibration dataset has been used for Scandinavian records. In the lowland plain sites, the combined Swiss-Norwegian 274-lake calibration dataset has been applied. Unusually, the Swedish 100-lake and north American 82-lake calibration datasets were applied to the alpine site of Lago Picolo di Avigliana by Larocque and Finsinger (2008). It is also worth noting that the reconstructions from Egelsee and Ech are near the upper end of the temperature gradient for the Swiss 105 (4.98-18.41 °C) and combined Nor-Swiss (3.5-18.4 °C) calibration datasets (Heir and Lotter 2010; Heiri *et al.,* 2011).

The chironomid-inferred temperature records from continental Europe display a variety of trends throughout the LGIS, which is not surprising given that the land area it covers is much

larger than the British Isles. Many Scandinavian sites either only capture the very end of the LGIS due to ice from the Scandinavian ice sheet covering the site, e.g., Kråkenes (Brooks and Birks, 2001) and Myklevatnet (Nesje *et al*., 2014), or display supressed temperatures earlier in the LGIS due to the local cooling effect the SIS had on air temperatures, e.g., Jansvatnet (Birks *et al*., 2012) and Hässeldala port (Wohlfarth *et al.,* 2017). In the Alpine region the T_{Jul} records display an increase in temperature throughout the LGIS, e.g., Gerzensee (Lotter *et a*l., 2012) and Maloja Riegel (Ilyashuk *et al.,* 2009), potentially driven by increasing solar insolation over the LGIT (Lotter *et al.,* 2012; Ilyashuk *et al.,* 2009; Heiri and Millet, 2005). To the west and north of the Alpine region a declining trend in T_{Jul} is observed similar to that seen in the British Isles and Greenland, e.g., Laguna de La Roya (Muñoz Sobrino *et al.,* 2013), Lago Piccolo di Avigliana (Larocque & Finsinger, 2008) and Moervaart (Bos *et al.,* 2017). Others display no real discernible trend due to low sampling resolution or local processes disrupting continuous deposition at the site e.g., Klein Ven and FGW (Van Ash *et al.,* 2012b, 2013). Despite these variations in summer temperature trends throughout the LGIS, ACE punctuating the time period can still be easily discerned.

Most $\delta^{18}O$ records in continental Europe are restricted to the Alpine region. The two sites which do have a $\delta^{18}O$ record outside of the alpine region, Klein Ven and FGW, do not record a climatic signal (Van Asch *et al.,* 2012b, 2013). Many sequences with $\delta^{18}O$ records contain the LST but have few other independently dated horizons and so rely on pollen-stratigraphy to date regional pollen sequences (Hoek, 1997a, b, c) and isotope-stratigraphy to the Greenland Ice cores, GRIP and NGRIP (Alley *et al.,* 1993; Hoek and Bohncke, 2001; Rasmussen *et al.,* 2014). The exception is Rotsee which has 21 radiocarbon dates during the LGIS, thought these were published prior to the calibration curves. Sampling resolution for oxygen isotopes is generally very good with near continuous sampling at 1 cm intervals and even at 0.5 cm intervals e.g., Mondsee (Lauterbach *et al*., 2011), Gerzensee (van Raden *et al.,* 2013). $\delta^{18}O$ records in the alpine region display a declining trend throughout the LGIS, similar to Greenland and many of the $\delta^{18}O$ and T_{Jul} records from the British Isles.

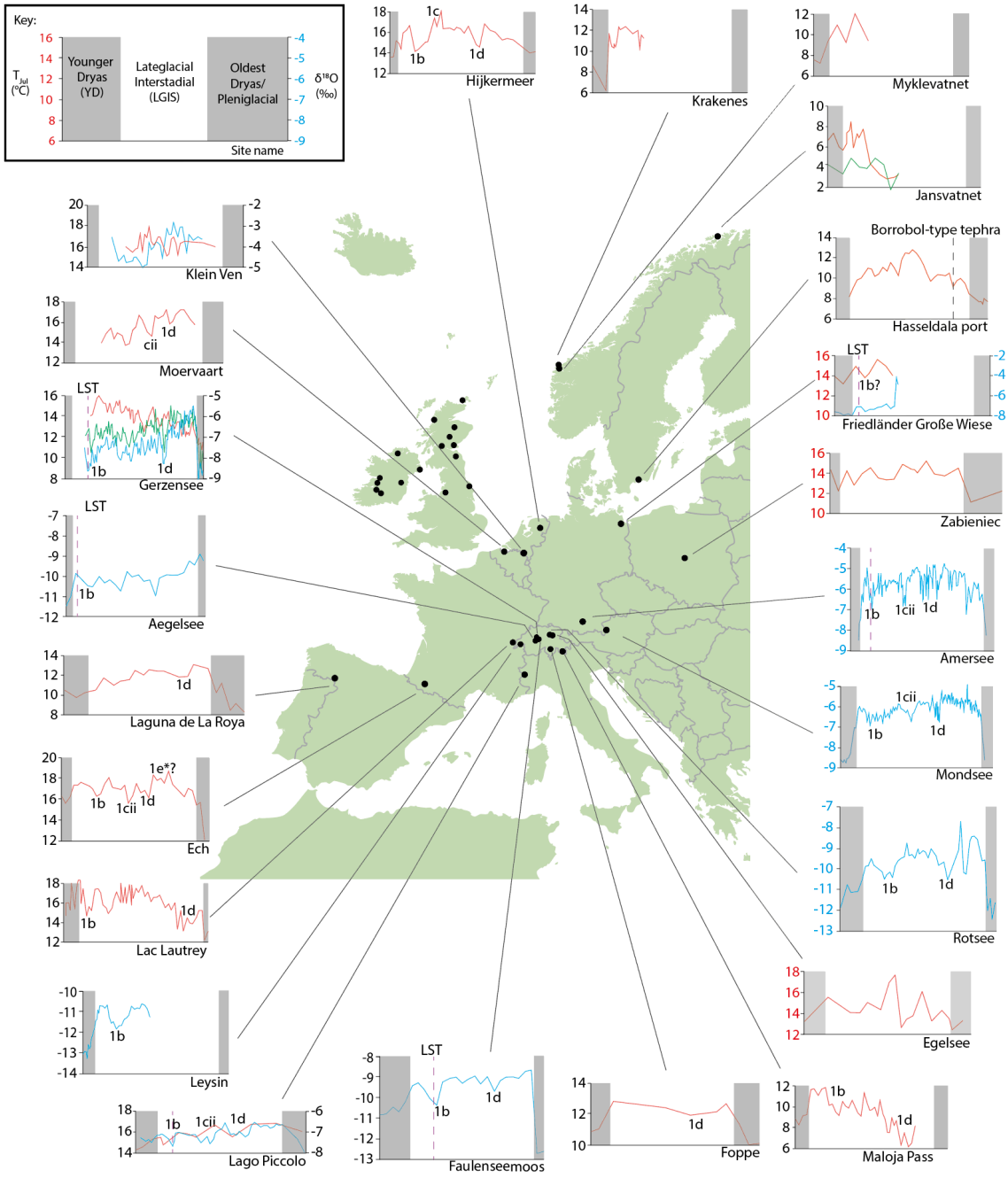

Figure 2.8, T_{Jul} and $\delta^{18}O$ records covering the LGIS from continental Europe. Blue lines = $\delta^{18}O$ record, red = T_{Jul}, green = pollen-inferred temperature. References for sites can be found in table 2.4.

Table 2.4, T_{Jul} and $\delta^{18}O$ records for continental Europe, arranged by latitude from North to South. Site names and location are in column (a). Column (b) notes the chronological methods used to provide age estimates for the sequences during the LGIS which range from tephrochronology, radiocarbon dating and several stratigraphic techniques. The material used for radiocarbon dating and any potential issues with these dates flagged by the authors are also noted. In column (c) an average stratigraphic resolution of the LGIS is given calculated by dividing the age duration of GI-1 in GICC05 (1796 yrs) by the stratigraphic length of sediments dated to the LGIS in each sequence and given as yrs/cm. Column (d) gives the average sampling resolution based on the duration of the LGIS in GICC05 is divided by the number of $T_{Jul}/\delta^{18}O$ data points during the LGIS (yrs/sample) and the number of data points divided in the LGIS divided by its length in a site to give an average sampling interval (cm interval). Column (e) gives details on the calibration dataset used or $\delta^{18}O$ sample preparation. Abbreviations for the tephra layers are as follows: LST = Laacher See Tephra, V = Vedde Ash. Red shading is used for chironomid records and blue for oxygen isotope records.

a) Site and location	b) Chronology			c) LGIS Stratigraphic resolution	d) Average sample resolution	e) Calibration dataset and $\delta^{18}O$ sample pre-treatment	refs
	Tephra	Radiocarbon	stratigraphy				
Jansvatnev, N. Norway		2 Terrestrial macrofossils		39 yrs/cm	79 yrs/sample 2 cm interval	Norwegian 157	Birks *et al.*, 2012
Kråkenes, Norway		None in LGIS	Climato-	7 yrs/cm	20 yrs/sample 3 cm interval	Norwegian 44 lakes	Brooks and Birks, 2001
Myklevatnet, W. Norway	Vedde			30 yrs/cm	59 yrs/sample 2 cm interval	Norwegian 157	Nesje *et al.,* 2014
Hässeldala port, S. Sweden	B-type	10 Terrestrial macrofossils		7 yrs/cm	31 yrs/sample 4.6 cm interval	Norwegian 157	Wohlfarth *et al.*, 2017
Friedländer Große Wiese, NE Germany	LST	2 Terrestrial macrofossils		3 yrs/cm	52 yrs/sample 16.3 cm res	Combined Nor-swiss 274	Van Asch *et al.,* 2012b
					Not climatic signal		Van Asch *et al.,* 2012b
Hijkermeer, Netherlands			Pollen-	35 yrs/cm	51 yrs/sample 1.6 cm interval	Swiss 103; Combined Nor-swiss 274	Heir *et al.,* 2011
Żabieniec, Poland		1 moss		6 yrs/cm	112 yrs/sample 19.7 cm interval	Norwegian 157, Swiss 103, Russian.	Plociennik *et al.,* 2011
Klein Ven, Netherlands		2 Terrestrial macrofossils	Pollen-	22 yrs/cm	69 yrs/sample 3.2 cm interval	Combined Nor-swiss 274	2012c
					Not climatic signal		Van Asch *et al.,* 2013

Table 2.4, continued (2)

a) Site and location	b) Chronology			c) LGIS Stratigraphic resolution	d) Average sample resolution	e) Calibration dataset and $\delta^{18}O$ sample pre-treatment	refs
	Tephra	Radiocarbon	- stratigraphy				
Moervaart, NW Belgium		4 Terrestrial macrofossils	Pollen-	11 yrs/cm	55 yrs/sample 4.7 cm interval	Swiss-Norwegian 274	Van Bos *et al.,* 2017
Amersee, Germany (Ostracod)	LST	1	Isotope-	18 yrs/cm	16 yrs/sample 0.9 cm interval	Candona sp., Fabaeformiscandona levanderi and Fabaeformis-candona tricicatricosa	Von Grafenstein *et al.,* 1999b
Mondsee, Austria (Ostracods)			Isotope-	16 yrs/cm	8 yrs/sample 0.5 cm interval	125µm wet sieved Candona neglecta and Fabaeformiscandona harmsworthi	Lauterbach *et al.,* 2011
Egelsee, Swiss Alps		5 Terrestrial macrofossils		Length of LGIS not given	128 yrs/sample X cm interval	Swiss 103	Larocque-Tobler *et al.,* 2010
Rotsee, Switzerland		21 Terrestrial macrofossils - not cal. on RL-300/305		40 yrs/cm	50 yrs/cm 1.3 cm interval On ROT05	Not stated	Lotter *et al.* 1990; Verbruggen *et al.,* 2010
Gerzensee, Switzerland GEJK core	LST		Isotope-	16 yrs/cm	25 yrs/sample 1.6 cm interval	Swiss 107	Lotter *et al.,* 2012
					14 yrs/sample 0.9 cm interval	Sieved 125 µm	Lotter *et al.,* 2012
Gerzensee, Switzerland GEM core				20 yrs/cm	10 yrs/sample 0.5cm interval	Not stated	Van Raden *et al.,* 2013
Faulenseemoos, Swiss Alps	LST		Pollen-	20 yrs/cm	67 yrs/sample 3.3 cm interval	Not stated	Eicher and Siegenthaler, 1976; Lotter *et al*., 1992

Table 2.4, continued (3)

a) Site and location	b) Chronology			c) LGIS Stratigraphic resolution	d) Average sample resolution	e) Calibration dataset and $\delta^{18}O$ sample pre-treatment	refs
	Tephra	Radiocarbon	-stratigraphy				
Aegelsee, Swiss Alps	LST		Pollen-	30 yrs/cm	72 yrs/sample 2.4 cm interval	Not stated	Wellington and Lotter, 1990; Lotter *et al.,* 1992
Lac Lautrey, France	LST	7 Wood fragments	Pollen- Isotope-	15 yrs/cm	35 yrs/sample 2.3 cm interval	Swiss 103	Heiri and Millet, 2005; Magny *et al.,* 2002; Millet *et al.,* 2003
Foppe, Switzerland		2 material not stated		45 yrs/cm	224 yrs/sample 5 cm interval	Swiss-Nor 274	Samartin *et al.,* 2012
Leysin, France	LST		Isotope-	17 yrs/cm	14 yrs/sample 0.8 cm interval	Not stated	Schwander *et al.,* 2000
Maloja Riegel, C. Swiss alps		2 Terrestrial macrofossils		30 yrs/cm	35 yrs/sample 1.2 cm interval	Swiss	Ilyashuk *et al.,* 2009
Lago Piccolo di Avigliana, Italian Alps	LST	3 Terrestrial macrofossils		Not stated	180 yrs/sample ? cm interval	Swedish 100, North American 82	Larocque and Finsinger, 2008
					45 yrs/sample ? cm interval	Not stated	Finsinger *et al.,* 2008
Ech, West Pyrenees France			Pollen-	54 yrs/cm	60 yrs/sample 1.1 cm interval	Nor-Swiss 274	Millet *et al.,* 2012
La Roya, NW Spain		6 Terrestrial macrofossils		45 yrs/cm	120 yrs/sample 2.7 cm interval	Swiss-Norwegian 274	Munoz Sobrino *et al.,* 2013

North America

Although this thesis focuses on the ACEs that occurred during the LGIS in Europe, it is worth noting climatic changes on the other side of the Atlantic in North America as climatic forcing such as AMOC affected the whole North Atlantic Regions (e.g., Thornalley *et al.,* 2011). There are very few chironomid-inferred temperature records from the east coast of North America at similar latitudes to those in Europe (40° to 70°N) (Figure 2.9). As in Scandinavia, this is because many sites were still covered by ice of the Laurentide Ice Sheet, meaning lake formation and sediment accumulation did not begin until well into the LGIS (Brooks and Birks, 2001). Although ice from the Laurentide Ice Sheet didn't extend much further north than 60 °N, there are still very few sequences with continuous lake sedimentation from the Lateglacial due to hiatuses caused by erosion of glacial meltwater and the deposition of crudely stratified sands, e.g., Lake CF8 (Axford *et al.,* 2011; Briner *et al.,* 2007). Nevertheless, the sites studied by Cwynar and Lévesque (1995) and Lévesque *et al.,* (1997) consistently display the Killarney Oscillation, an oscillation late in the LGIS that is broadly equivalent to GI-1b, which displays a large variation in magnitude from *c.* 1.7 °C in Brier Island Bog Lake to *c.* 8 °C in Pine Ridge Pond (Cwynar and Lévesque, 1995; Lévesque *et al.,* 1997). It should be noted that these reconstructed values are for water temperature (Walker *et al.,* 1991) as opposed to air-temperature commonly reconstructed in Europe. The sequences were dated using AMS radiocarbon measurements on unidentified twigs, wood fragments, spruce needles, and other terrestrial plant macrofossils (Cwynar and Levesque, 1995; Levesque *et al.,* 1993; Levesque *et al.,* 1994).

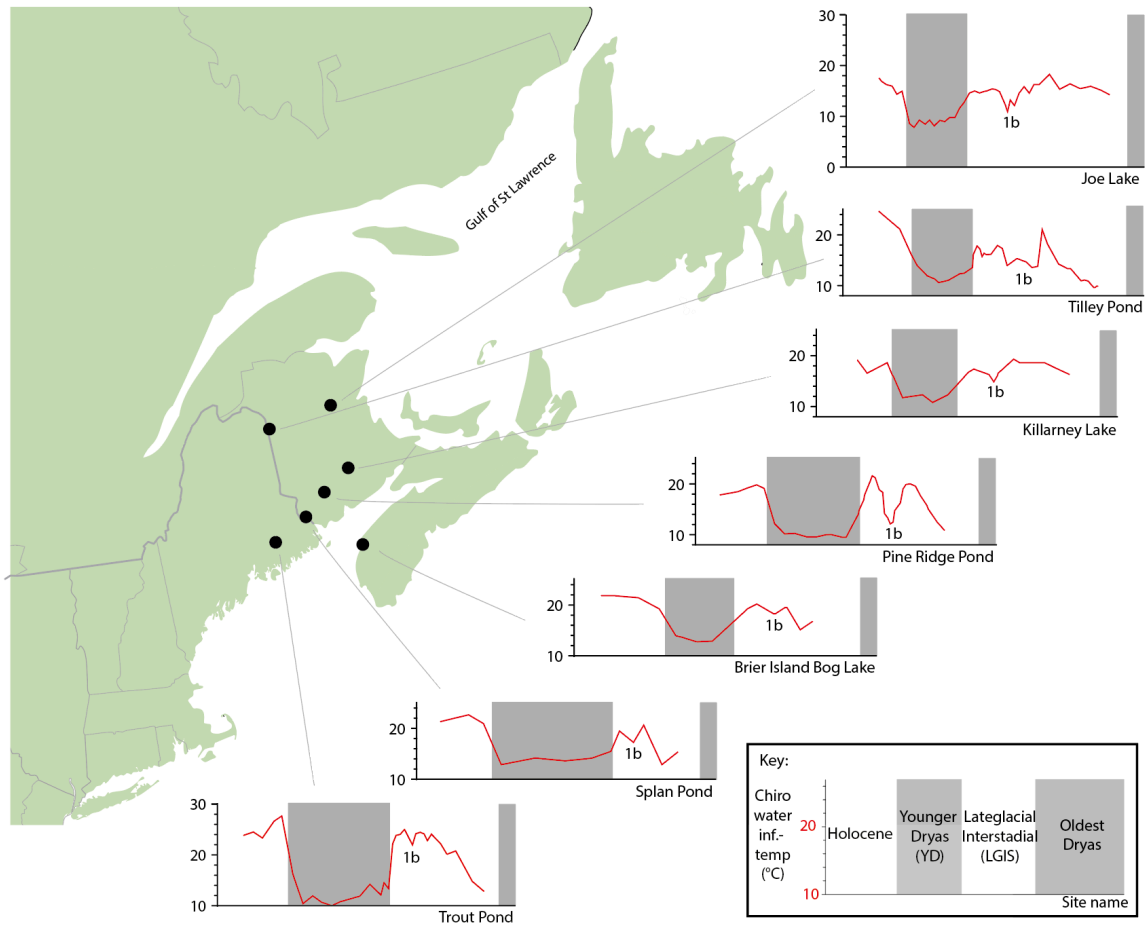

Figure 2.9, Chironomid-inferred water temperature reconstructions from sites in NE North America (After Cwynar and Lévesque, 1995; Lévesque *et al.,* 1997)

2.4 Previous compilations of chironomid records

Brooks and Langdon (2014) created temperature isotherm maps for a series of time slices throughout the LGIT and Holocene from chironomid-inferred temperature records across Europe (Figure 4.10). They noted a strong W-E gradient during the LGIS which they attributed to the influence of the thermohaline circulation, which increased the degree of warming for those regions more proximal to the North Atlantic and diminishing toward the east. Brooks and Langdon (2014) also noted the potential effect of the Scandinavian ice sheet that may have suppressed air temperatures in the vicinity of Scandinavia and eastern Europe. The impact of the Scandinavian Ice Sheet is particularly clear during GI-1 and created a strong N-S temperature gradient (Coope *et al*., 1998; Brooks and Langdon, 2014). The pattern of temperature change observed in the isotherm maps based on the chironomid inferred temperatures display similar trends with those produced by Coope *et al.,* (1998) using Coleopteran MCR estimates, although the latter were generally *c.* 2 °C higher but could be explained by differences in microenvironment and temperature estimate methodological differences (Brooks and Langdon, 2014). Nevertheless, the chironomids appear to produce spatially and temporally coherent temperature estimates, suggesting they are reliable, and that summer temperature is the main environmental variable influencing chironomid distribution and abundance (Brooks and Langdon, 2014).

Heiri *et al*. (2014) created stacked chironomid inferred temperature records for seven different regions of Europe including, north Norway, west Norway, the Baltic region, the British Isles, the Alpine region, southwestern Europe, and east and central southern Europe (Figure 4.11). The stacked records created agree well with past climate simulations from the ECHAM-4 model suggesting such atmospheric general circulation models can predict regional temperature trends in Europe (Heiri *et al.,* 2014) and also suggests temperature is the main environmental variable influencing the distribution and abundance of chironomids.

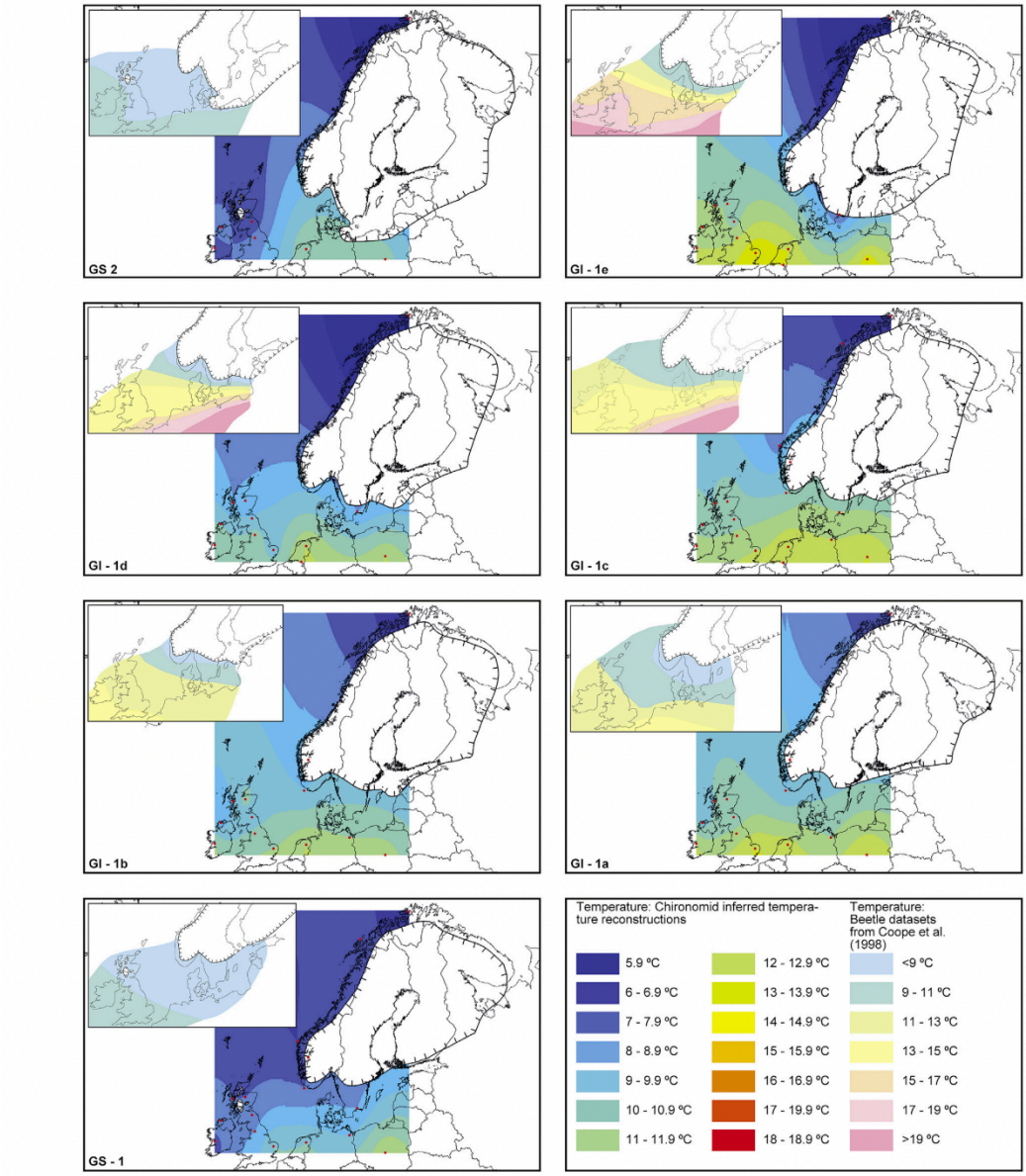

Figure 2.10, Temperature isotherm maps based on chironomid inferred temperatures changes for a series of time-slice throughout the LGIS by Brooks and Langdon (2014). In the top left-hand corner of the windows are inserts of temperature gradient maps created by Coope *et al.*, (1998) based on beetle MCR estimates.

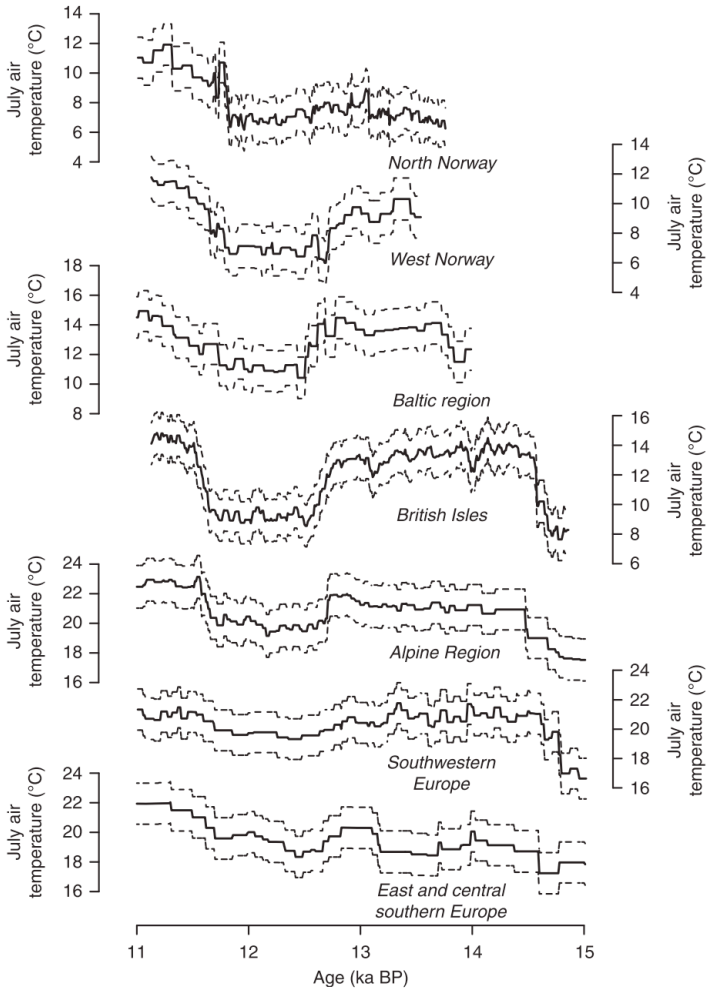

Figure 2.11, Regional stacked temperature reconstructions for different parts of Europe. Dashed lines indicate estimate error of prediction. Reconstructions are adjusted to modern sea level. (From Heiri *et al.*, 2015)

2.5 Forcing Mechanisms

Several forcing mechanisms have been proposed as drivers of climatic change during the Late-Quaternary period over varying time scales. It is widely accepted that the large-scale Glacial-Interglacial cycles that have dominated the Quaternary period, lasting on average 100,000 yrs, are controlled by variations in the earth's orbit around the sun, known as Milankovitch forcing (Hays *et al.,* 1976; Ruddiman *et al.,* 1986; EPICA community members, 2004; Masson-Delmotte *et al.,* 2005; Sun *et al.,* 2006). Solar insolation at 65 °N controlled the waxing and waning of the large continental ice sheets that grew over continents in the northern hemisphere during glacial periods (Hays *et al.*, 1976). However, the changes in summer insolation the earth received are insufficient to cause the glacial-interglacial cycles on their own and are therefore thought of as a 'pacemaker' (Hays *et al.*, 1976). In order for glaciations to occur, internal feedback mechanisms that amplify Milankovitch forcing are required (Ruddiman and McIntyre, 1981). Importantly, changes in insolation are relatively gradual and occur over longer timescales of tens of thousands of years and cannot account for the abrupt millennial to centennial-scale events that are discussed above.

The oxygen-isotope records from the Greenland ice cores (Stocker, 1999; Johnsen *et al.,* 2001, Rasmussen *et al*., 2006), and the terrestrial temperature reconstructions described above, display periodic high-magnitude abrupt events with irregular structure, occurring over shorter centennial to millennial timescales. These centennial- and millennial-scale events are too short in duration to be caused by Milankovitch forcing alone and are the result of sub-Milankovitch forcing mechanisms. Several potential mechanisms and influences have been discussed including changes in ocean circulation (Broecker *et al*., 1988; Nesje *et al*., 2004; Candy *et al*., 2016), changes in atmospheric circulation (Bakke *et al*., 2009; Brauer *et al*., 2000), changes in solar activity (Adolphi *et al*., 2014) and changes in volcanic activity (Renssen *et al*., 2015). However, the roles of these different mechanisms are still not well understood and there is no definitive consensus on which cause centennial-scale ACEs during the LGIS (Bakke *et al.,* 2009; van Raden *et al.,* 2013). Each of these forcing mechanism has a different spatial expression, in terms of the magnitude of temperature changes they produce. The impact of the forcing effects individual localities differently because their geographic influence is relatively restricted, i.e., the effects of changes in North Atlantic circulation being most strongly felt in western rather than eastern Europe. Therefore, the spatial variability in the expression of each ACE can be used to assess the influence of each potential forcing mechanism. Two of the key forcing mechanisms, ocean forcing with associated changes in atmospheric circulation, and solar variability, will now be described in more detail.

2.4.1 Ocean forcing

Abrupt climatic shifts during the LGIT are often attributed to changes in ocean forcing, specifically changes in strength of the Atlantic Meridional Overturning Circulation (AMOC) (Broecker *et al.,* 1989; Nesje *et al*., 2004; McManus *et al*., 2004; Candy *et al*., 2016). AMOC is a system of ocean currents in the north Atlantic (Broecker *et al*., 1989). It is composed of warm salty surface waters moving northwards to higher latitudes, which then releases latent heat into the atmosphere raising air temperatures. As the water cools, becomes denser and loses buoyancy and evaporation causes salinity concentrations to increase, the combined effect of which causes water to sink forming North Atlantic Deep Water (NADW) which returns to the lower latitudes as basal flow (Buckley and Marshall, 2016). The role of AMOC is pivotal in the transfer of heat from the equator to the mid and high-latitudes and the disruption or weakening of this conveyor results in abrupt climatic shifts comparable to those seen during the LGIT (Clark *et al*., 2001). Three operational modes of AMOC have been identified by Clark

et al., (2002): (i) an interglacial/interstadial mode in which there is strong AMOC and NADW formation in the Nordic seas; (ii) a stadial mode in which AMOC and NADW formation in the sub-polar Atlantic is weakened; and (iii) a glacial mode where NADW formation ceases. Freshwater perturbations have been suggested to cause shifts between different AMOC modes (Clark et al., 2001, 2002; Broecker, 2006; Thornally *et al.,* 2010) and is supported by numerous modelling studies (Gregory *et al.,* 2005; Petoukhov *et al.,* 2005; Hawkins *et al.,* 2011; Klus *et al.,* 2018) where NADW formation is reduced through the dilution of salty waters causing AMOC to shift from interstadial/interglacial mode (i) to stadial (ii) or Heinrich mode (iii). However, the source of freshwater input is disputed. Some suggest freshwater from the Laurentide ice sheet (Broecker *et al.,* 1989; Clark *et al.,* 2001) whilst others suggest Baltic sources (Muschitiello *et al.,* 2015a, b; 2019) or inputs from the northern arctic (Tarassov and Peltier, 2005).

Following the last glacial maximum at 21 ka BP (Mix *et al*., 2001), the northern hemisphere ice sheets retreated as solar insolation at 65°N increased (Denton *et al.,* 2010). As ice sheets melted, meltwater flux into the north Atlantic caused NADW formation to reduce and the shutdown of AMOC (Clark *et al.,* 2001). At 14.65 kyr cal BP, the northern hemisphere warmed abruptly as AMOC restarted and established in interglacial/interstadial mode. Further, smaller perturbations of meltwater leading to a change in AMOC mode are thought to have caused millennial scale ACEs such as GS-1/Younger Dryas/Loch Lomond Stadial and perhaps centennial scale oscillations such as GI-1d/Aegelsee Oscillation and GI-1b/Gerzensee Oscillation (Broecker *et al*., 1985; Broecker, 1989; Clark *et al*., 2001; Tarasov and Peltier, 2005; Thornally *et al*., 2010; Muschitiello *et al.,* 2019). The reduction in temperatures across Europe by the suppression of AMOC during these ACE is further intensified by positive feedback mechanisms such as greater sea-ice formation (Isarin *et al.,* 1998; Brauer *et al.,* 2008). The combined decrease in seawater salinity from melting ice sheets causing freshwater stratification in the north Atlantic and reduced AMOC strength allowed sea ice to grow (Denton *et al*., 2005, 2010). This is hypothesised to have caused the Northern Hemisphere to experience much colder winters during the millennial-scale cold events such as the Lateglacial Stadial, amplifying the abrupt climatic changes (Denton *et al*., 2005). As winter sea ice spread, the heat exchange between the ocean and atmosphere was reduced (Denton *et al.,* 2005; Bakke *et al.,* 2009) leading to more southerly displacement of the polar front) bringing colder drier conditions (Brauer *et al.,* 2008; Bakke *et al.,* 2009). Siberian-like conditions dominated in regions adjacent to the North Atlantic characterised by large changes between winter and summer temperatures (Denton *et al.,* 2010). It has also been shown that centennial-scale oscillations during the Lateglacial

coincided with phases of minimum ocean ventilation (Bjorck *et al*., 1996; Thornalley *et al.,* 2011).

2.4.2 Solar forcing

Changes in total solar irradiance linked to sunspot activity have been proposed to influence climate at a variety of time scales (Gray *et al.,* 2010; Engels and van Geel, 2012). The effects of solar variability are well known for the late Holocene where grand-solar minima caused lower temperatures in Europe through the weakening of the polar vortex and a negative North Atlantic Oscillation NAO (Mauquoy *et al.,* 2002; Martin-Puertas *et al.,* 2012). However, the effect of solar variability on climate during the LGIT is less studied than the Holocene, though likely to be just as important. For the Lateglacial period, Adolphi *et al.,* (2014) reconstructed solar variability using Cosmogenic nuclides (Beryllium-10 and Carbon-14) in ice cores, speleothems and tree rings, which vary depending on the flux of cosmogenic rays impinging on Earth's atmosphere and their interaction with the Earth's magnetic field. By de-trending the data to remove changes brought about by Milankovitch forcing and other factors that may adversely alter the abundance/production of Cosmogenic nuclides, variability in solar irradiance can be identified at centennial-timescales. Several periods of reduced solar irradiance occurred during the LGIS and could possibly relate to the ACEs that occurred within, as there is a correlation ($r^2 = 0.3$) between beryllium-10 and ice core $\delta^{18}O$ (Adolphi *et al.,* 2014). Adolphi *et al*., (2014) suggest that solar variability may have impacted European climate at the termination of the last glacial through a negative-NAO phase. During solar minima changes in the stratosphere favoured the development of cold blocking high-pressure systems over the North Atlantic therefore leading to cooler conditions.

1.6 Chapter Summary

This chapter introduced the current stratotype for the Northern hemisphere, the NGRIP $\delta^{18}O$ record, and highlighted the complex array of terminology applied, often incorrectly, to different records around the North Atlantic region. Therefore, GI-1 will be referred to as the Lateglacial Interstadial (LGIT), which encompasses the Bølling-Allerød and the Windermere Interstadial. The centennial-scale ACEs within the LGIS will be referred to by their approximate age, i.e., GI-1d as the '14.0 ka BP ACE' and GI-1b as the '13.2 ka BP ACE', as there is no terminology for such events in the British Isles and where these centennial-scale events do have terminology, it is often not consistently applied.

This chapter has explored some of the key proxies utilised to reconstruct palaeotemperature during the LGIT, including Coleopteran MCR, pollen-inferred temperatures and plant macrofossil inferences, with an assessment of their suitability to study centennial-scale ACEs. Chironomid-inferred temperatures and oxygen isotopes are the best suited records to studying such ACEs as they can be applied at high stratigraphic resolution, are responsive to abrupt changes in temperature and can provide reliable quantitative, or at least semi-quantitative, reconstructions.

The key T_{Jul} and $\delta^{18}O$ records from the British Isles, continental Europe and NE North America are also introduced, highlighting the limitations and issues with the current data available which is limiting our understanding of how the LGIS ACE are expressed spatially including i) the poor spatial spread and coverage of records; ii) the limited chronological constraint of many sequences meaning ACEs are correlated with less certainty, if at all; and, iii) the low sampling resolution employed, particularly in many continental European sites, meaning the full magnitude of ACEs may not be identified or not recorded altogether.

Finally, the two key forcing mechanisms, to which ACEs of centennial- and millennial-scale are often attributed to, changes in ocean circulation and solar variability.

Chapter 3: Chironomid literature review

Chapter overview

The first section of this chapter provides general background information about chironomids including, their life cycle and morphological features used to distinguish between sub-families and tribes and general ecological preferences that can be drawn at that taxonomic level. Key environmental parameters, which govern chironomid distribution and abundance, are briefly discussed. This section draws on the wealth of information provided by Moller pilot (2009, 2013), Vallenduuk and Moller Pillot (2013), Armitage *et al*., (1995), Walker *et a*l., (2001), Brooks (2006), Porinchu and MacDonald (2006) and Brooks *et al*., (2007).

The second section of this chapter focuses on the use of chironomids as a proxy in palaeoenvironmental studies. A brief history in the use of chironomids as a palaeoecological proxy is given with an overview of how chironomids have progressed from a qualitative trophic status indicator to a quantitative palaeo-reconstruction technique. The characteristics that make chironomids an excellent proxy, particularly for reconstructing past temperature changes, are also described. This is then followed by a summary of calibration datasets and inference models are used to create quantitative temperature inferences and evidence put forward to support the use of chironomids as a palaeotemperature proxy. The final part of this chapter discusses some of the potential problems surrounding the use of chironomids as indicators of past temperature changes.

3.1 Introduction to chironomids, chironomid ecology and palaeoecology

3.1.1 General introduction

Chironomids are two-winged flies (Insecta: Diptera) that closely resemble well-known insect families such as mosquitos and biting midges. Chironomids are often referred to as non-biting midges as the adults have reduced mouthparts (Brooks *et al.,* 2007). About 5,000 chironomid species have been identified worldwide (Cranston and Martin, 1989), though it is estimated that as many as 15,000 species of chironomids exist. However, this number should be treated with caution as only northern hemisphere fauna are relatively well known and even in these well studied areas further new species continue to be discovered (Armitage *et al.,* 1995).

Chironomids occur in a wide range of climates from the tropics to the Arctic and are one of the few insect families that can be found on all continents (Armitage *et al.,* 1995). For instance, the chironomid species *Belgica antarctica* is the largest purely continental animal living in

Antarctica (Harada *et al.,* 2014). There are few fresh or brackish waters that cannot support chironomid larvae as they can tolerate large gradients of pH, salinity, water depth, oxygen concentration, temperature, and productivity (Armitage *et al.,* 1995). Most chironomid species live in lakes, where they are usually amongst the most abundant insects but can also live in terrestrial, semi-terrestrial and lotic environments. Chironomid larvae are largely primary consumers playing an important part in aquatic ecosystems, as they are a key source of nutrient cycling and food. The larvae and emerging adults are a key food source for fish, newts, and other aquatic organisms while swallows, martins and bats frequently feast upon flying adults. The remains of the chironomid's aquatic larval stage, found in surface and deep sediments, are used to study the contemporary- and palaeo-ecology of lakes. Therefore, the larvae will be the main focus of this chapter, however, other life stages will be discussed where needed.

3.1.2 Chironomid life cycle

Chironomids are holometabolous, meaning they complete metamorphism and go through 4 life stages: egg, larva, pupa and imago/adult, with the majority of their life spent as larvae (Porinchu and MacDonald, 2006) (Figure 3.1). The life cycle begins by the deposition of an egg mass, containing 30-3000 eggs, in a hydrophilous jelly. This egg mass can be deposited directly into the water body or attached to a substrate (e.g., macrophytes, leaf litter, shoreline) at or near the water surface. The rate of egg development depends primarily on temperature but other factors including competition, pH, photoperiod, salinity, and oxygen concentration are also important (Pinder, 1995). Depending on the species, it can take a few days to a month for eggs to hatch into first instar larvae (Brooks *et al.,* 2007; Porinchu and MacDonald, 2006).

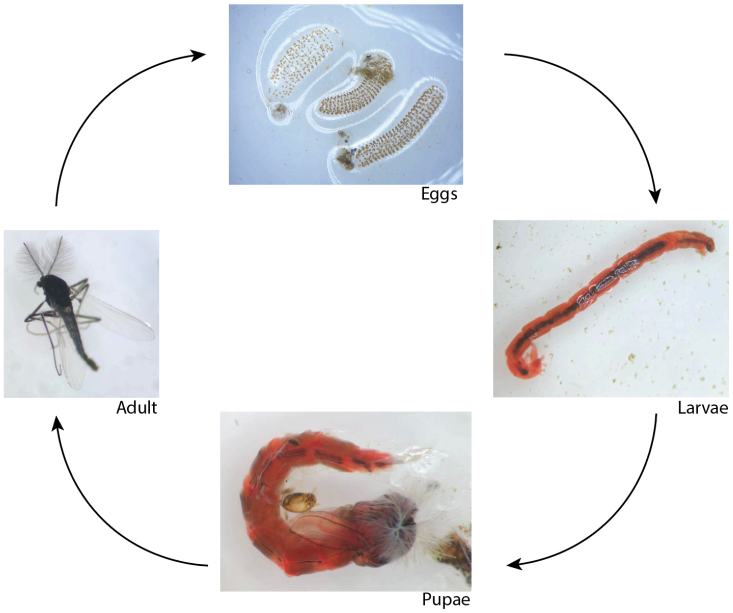

Figure 3.1, Life cycle of a chironomid (pictures taken by author).

The hatching of eggs results in first instar larvae, whose planktonic behaviour allows for their dispersal to suitable substrates (Walker, 1987). Larvae undergo ecdysis three times, shedding their exoskeleton to form the next larval stage (= 2nd to 4th instars), which become largely sedentary (Walker, 1987). The time spent at each instar becomes progressively longer, with the majority of their time being spent as 4th instars. Larvae are worm like and range in size from 2-30mm in length (Oliver and Roussel, 1983) and can range in colour with most being pale yellow, but can also be green or red. Their elongated bodies are made of soft tissue and have nine abdominal segments and three thoracic segments (Figure 3.2). The larval head capsule (HC) is heavily chitinised and morphological characteristics are further described in section 3.1.3.

Throughout the 2nd, 3rd and 4th instar stages, larvae grow exponentially in size (Walker, 1987). The development time through the larval stages is variable and dependent on temperature and food availability (Johannson, 1980). The area of the lake in which they live can also affect the development time with large species living in the profundal potentially taking one or more years to develop while small species in the littoral may produce 3-4 generations in a year (Brooks *et al.,* 2007). Some taxa, however, can take much longer or much shorter to develop. For example, two *Chironomus* species living in tundra pools in Alaska took 7 yrs to complete their larval phases (Butler, 1980; Oliver, 1968; Hershey, 1985). It is possible for larvae to survive extreme adverse conditions by temporarily arresting their growth phase through diapause in very low/sub-zero temperatures and summer drought conditions by aestivation, through building cocoons and dehydrating (Armitage *et al.,* 1995).

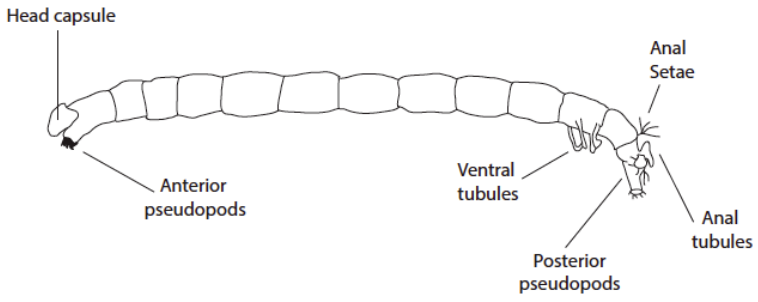

Figure 3.2, Schematic line drawing of a chironomid larvae. Chironomids poses a pair of pseudopods (false legs) on the first thoracic segment and another on the anal segment of the abdomen (Brooks *et al.,* 2007). HCs cannot be withdrawn into the body like the larvae of other Diptera families. The anal segment also possess setae as does the HC.

The subsequent pupal stage is relatively short-lived, generally only lasting 3-4 days (though occasionally known to last longer) and the larvae metamorphose into their adult form (Oliver, 1971; Brooks *et al.,* 2007). A pair of paddles at the apex of the pupal abdomen helps the pupa swim to the surface, breaking through the water surface and the imago emerges directly into the air (Brooks *et al.,* 2007). Timing of emergence is dependent on water temperature and light intensity (Kurek, 1980) causing emergence to vary between regions and species. In the Arctic and in areas where lakes are ice-covered for the majority of the year, the timing of emergence may be synchronised due to the narrow timeframe that the water surface is open. In temperate regions, emergence may occur at different times as lakes are uncovered by ice for the most part of the year. The majority of temperate species are either multivoltine (multiple emergences in a season), univoltine (one emergence in a season) or bivoltine (Two emergences in a season) (Tokeshi, 1995; Brooks *et al.,* 2007).

Male adults form aerial swarms over tall objects including trees, bushes and other landmarks (Armitage, 1995). Females enter these swarms to pair-off and mate (Porinchu and MacDonald, 2006). Species are segregated by differences in the height above ground and distance from water at which they swarm (LeSage and Harrison, 1980). Adults typically live approximately 3-4 days, up to a maximum of several weeks. During this time, most chironomids don't feed, though some individuals may take honeydew or nectar (Brooks *et al.,* 2007). Although chironomids are winged flies, dispersal is largely passive and assisted by wind (Brooks *et al.,* 2007). Flightless species, e.g., *Corynocera ambigua*, walk instead and are also wind assisted (Brooks *et al.,* 2007).

3.1.3 Taxonomy, identification, and sub-family level ecology

Chironomidae are a family of insects belonging to the superfamily Chironomidea, which occur alongside other aquatic larvae and nymphs. These include Ceratopogonidae (biting midges) and Simuliidae (buffalo gnats/black flies) along with other midge families belonging to the superfamily Cullcoidea including Culicidae (mosquitoes) and Chaoboridae (phantom midges) (Figure 3.3). Caddisflies (Insecta: Trichoptera) also frequently occur alongside chironomids.

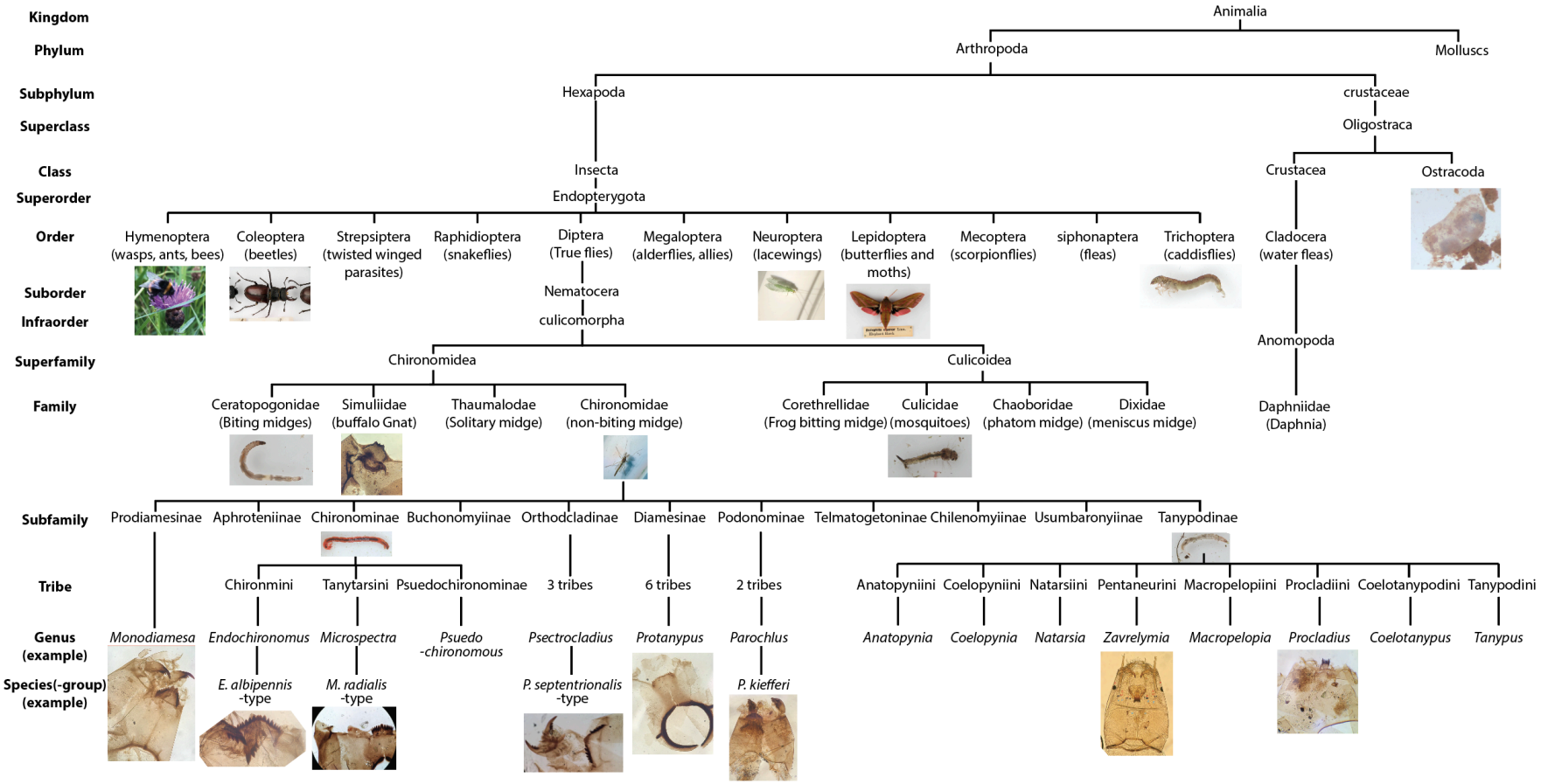

Figure 3.3, Cladogram of Chironomidae and related taxa. Along with the 6 Chironomidae subfamilies mentioned in the text, there are 5 others including Telmatogetoninae, Chilenomylinae, Buchonomylinae, Aphrotenlinae and Usumbaronylinae. Species from these subfamilies are not native to the North Atlantic region and/or are very rare with low abundance and have few species within the sub-family (Brundin 1983a, Saether 1983, Walker 1987; Andersen and Saether 1994). Telmatogentoninae are the only midge family to contain a species that lives exclusively in marine intertidal environments (Walker, 1987). (Photos taken by author).

Within the family Chironomidae, there are 11 sub-families of which only 6 are found in Northwest Europe (Brooks *et al.,* 2007). Table 3.1 outlines the morphological characteristics of the chitinised HC used to distinguish between subfamilies, which include the presence, absence, and shape of features including the ventromental plates, mentums/ligulas, and the overall look of the HC (Figure 3.4). Some very broad differences in chironomid ecology can be drawn at the subfamily- and tribal-level (Table 3.1). However, there can be considerable variation between species groups and species within each of the sub-families. These will be discussed in later chapters when necessary.

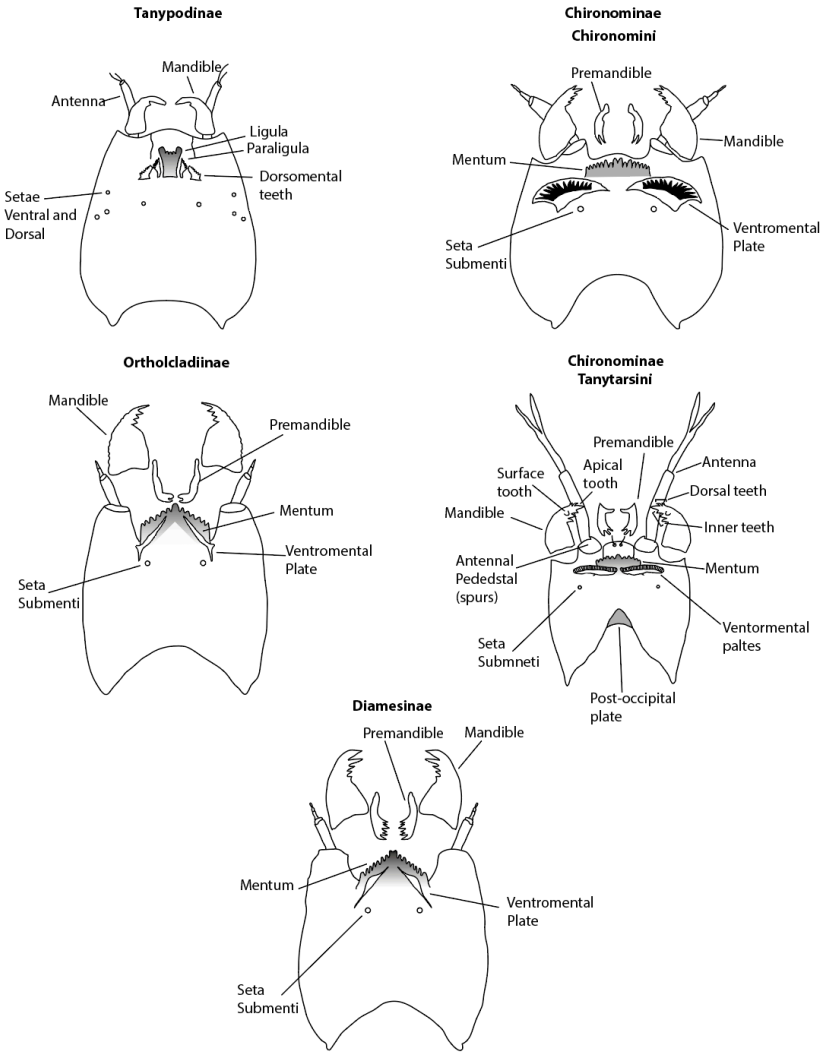

Figure 3.4, Line drawings of the different chironomid sub-families and tribes illustrating the different features to distinguish them. Note, these are generalised examples. (After Brooks *et al.,* 2007).

To identify HCs beyond sub-family level, further study of morphological features is required; in particular, the ventromental plates along with the number and grouping of teeth, their size and orientation on the mentum. Mandibles, premandible, antennae and other morphological features specific to each sub-family or tribe may also be used in larval HC identification when living specimens are collected.

Taxonomy and identification of fossil HCs

When it comes to identifying subfossil HCs, however, some of the distinguishing morphological features are often missing, damaged or obscured due to taphonomic and other processes – particularly the mandibles, premandibles and antennae (Porinchu and MacDonald, 2006). This means species-level identification is rarely achieved in fossil HC remains and so the chitinised HCs are identified to genus or morphotype/'species-type" level, which contain several species within. To date approximately 200 subfossil morphotypes have been described from the North Atlantic Region (Brooks *et al*., 2007).

Chironomini and Orthocladiinae have long had the highest taxonomic resolution of the Chironomidae sub-families, with many identified to species-type or at least genus level from early on in chironomid research, due to the clear differences in ventromental plate morphology and arrangement of teeth on the mentum. However, there have been advances in the taxonomic resolution, for example with the separation of the *Cricotopus, Corynoneura* and *Heterotrissocladius* genera (Brooks, 2006; Brooks *et al*., 2007).

Rieradevall and Brooks (2001) subdivided subfossil HC types belonging to the subfamily Tanypodinae based on the characteristic pattern of cephalic setae, allowing identification to genus level. Previously, subdivision of Tanypodinae relied on the ligula, paraligula, dorsomental teeth and mandibles, which are frequently missing in subfossils.

The taxonomic resolution of Tanytarsini has improved too. Originally, Walker *et al*. (1991) only separated this tribe into three tribes: *Stempellina, Stempellinella/Zavrelia* and sub-tribe *Tanytarsini* which included several genera but was not separated further. In the surface samples from the Swiss Alps, Lotter *et al.* (1997) identified *Cladotanytarsus, Microspectra*, *Paratanytarsus, Tanytarsus* group-*lugens, Tanytarsus* group-*chinyensis, Tanytarsus* spp. and *Tanytarsus* sp. A. Brooks and Birks (2001) increased the taxonomic resolution further to 17 different *taxa* with three morphotypes of *Microspectra* and two morphotypes of *Paratanytarsus*. Currently, the Tanytarsini subfamily is subdivided into 28 different types (Brooks *et al.,* 2007).

Sub-family	Morphological characteristic	General sub-family/tribal ecology
Orthocladiinae (Abundant)	**HC**: small to large, globular **Ventrimental plate**: less conspicuous than other sub-families, never striated, narrow, can be bulbous, triangular at apex or hardly visible. Sometimes has beard. **Mentum**: trongly arched, 4-6 lateral teeth usually.	**Feeding guilds/Food**: grazers, scrappers, deposit/collectors, a few shredders. Feeding on bacteria, fungi, detritus, diatoms, and algae. **Habitat**: amongst vegetation or on sand and gravel in streams **Climate**: across temperature gradient **Other**: intolerant of low DO and so dominates oligotrophic lakes with hard substrates
Tanypodinae (Abundant)	**HC**: large, Weakly pigmented, featureless, generally elongated with cephalic setae and sensory pores. **Ligula**: fork shape, often missing, suspended within HC, variations in shape and number of teeth **Antennal Rod**: retractable so can be within HC **Dorsomental Teeth**: Adjacent to ligula **Mandibles**: narrow, at antero-lateral margin.	**Feeding guilds/Food**: carnivorous predators. Feeding on other Chironominae and invertebrates. **Habitat**: free roaming **Climate**: typically warm, occasionally cold. **Other**: intolerant of low DO and so dominates oligotrophic lakes with hard substrates
Chironominae (Abundant)	Chironomini **HC**: large, **Ventrimental plates**: variations in fan shape, striations, and other features. Clearly visible. **Mentum**: variable number of teeth, length and grouping.	**Feeding guilds/Food**: filter feeders. **Habitat**: produces a cocoon of silk and lives in soft substrates. Profundal but can also dominate warm eutrophic lakes. **Climate**: typically warm, occasionally cold. **Other**: possesses haemoglobin so can tolerate low oxygen conditions. Can live for several months without oxygen and respire anaerobically
	Tanytarsini **HC**: small to large. **Ventrimental plates**: Sausage shape, striated, sits below mentum **Mentum**: variable number of teeth, length and grouping. **Post-occipital**: sometimes present at base of HC **Spurs and antennal pedestals**: variations in the presence/absence, length and shape of pedestals and attached spurs	**Feeding guilds/Food**: macrophytes, Periphytic algae **Habitat**: amongst vegetation, on substrate **Climate**: typically warm, occasionally cold. **Other**: possess haemoglobin but is less efficient (Walshe, 1948). Therefore, absent from low DO lakes or in smaller numbers

Table 3.1, General ecological information of the six subfamilies commonly found in Northwest Europe. Ecological preferences, though, can differ greatly within these subfamilies and are discussed in more detail in the next section, 3.1.4, and where appropriate in the individual site chapters. Adapted from Brooks *et al.,* (2007) and Walker, (1987), Moller pilot (2009, 2013), and Vallenduuk and Moller Pillot (2013)

Sub-family	Morphological characteristic	General sub-family/tribal ecology
Diamesinae (Rare)	**HC**: small to large, dark red or brown, rough edge round back of HC Ventrimental plates: Ventrimental plates narrow, long and conspicuous. **Mentums**: more than 6 lateral teeth **Premandibles**: premandible broad with more than 3 apical teeth	**Feeding guilds/Food**: predators, diatoms, detritus, **Habitat**: glacial fed streams and profundal of proglacial lakes, hard substrates. **Climate**: cold
Prodiamesinae (Rare)	**HC**: large **Ventrimental plates**: large ventrimental plates, broad at apex, no striations but has beard. **Mentum**: heavily pigmented,	**Feeding guilds/Food**: planktonic detritus, bacteria **Habitat**: streams and littoral. Sandy substrates. **Climate**: cold, Montane to polar and alpine climatic regions (Oliver, 1971).
Podonominae (Very Rare)	**HC**: mall to medium Ventrimental plates: Weakly pigmented **Mentum**: Mmany lateral teeth, weakly pigmented mentum **Mandibles**: numerous inner teeth	**Feeding guilds/Food**: detritus, diatoms, **Habitat**: lotic, cool springs and running waters. Climate: Cold, **Other**: replaces Diamesinae in southern hemisphere

Table 3.1, continued

3.1.4 key environmental influences on chironomids, their ecology and habitats.

Temperature

Numerous laboratory studies have demonstrated that temperature has a direct effect on each stage of chironomid development (Eggermont and Heiri, 2012). Egg hatching rate and survivability is heavily temperature dependant as Hilsenhoff (1966) demonstrated with *Chironomus anthricinus* eggs, which took 1.5-2 days to hatch at 22-25 °C, 14 days at 9 °C, but failed to hatch at 8 °C. The proportion of successful egg hatching can also decline with higher temperature with only 20% of *Thienemanniella vittata* hatching at 20 °C, compared to 90% of eggs at 15 °C (Williams, 1981). During the larval growth stages temperature has an effect on physiological processes (Eggermont and Heiri, 2012, Porinchu and MacDonald, 2006; Konstantinov, 1958; Anderson and Cummins, 1979. Mackay (1979) and Johansson (1980) both demonstrated a high positive correlation between larval growth rates and water temperature. This can be directly through the biogenic relationship via altered larval feeding, assimilation, and respiration rates, and also, indirectly through oxygen concentrations, quality and quantity of food (Tokeshi, 1995). The highest growth rate of larvae is associated within a temperature range, above or below this causes growth to decline (Eggermont and Heiri, 2012; Konstantinov, 1958; Dickinson and Walker, 2015). Threshold water temperatures, as opposed to cumulative degree-days, have been found to affect the timing of emergence from the pupal case

(Dickinson and Walker, 2015). Due to the effect temperature has on larval and pupal durations and emergence, temperature also affects the number of generations that can be produced per year (Eggermont and Heiri, 2012). Species, which may have several emergences in warmer climates, may only have one per year in arctic climates (Eggermont and Heiri, 2012).

Trophic status

Trophic status has long been known to affect chironomid through several means. It affects larval growth rate through food availability, quantity, and quality. The type of food present also strongly influences chironomid distribution as different chironomid genera and species specialise on different sources. Other key environmental variables such as dissolved oxygen concentrations and lake water temperature can co-vary with trophic status. Chironomini and Tanypodinae often dominate eutrophic lakes, which are often productive, oxygen poor and warm (Brooks *et al*., 2007). Oligotrophic lakes, on the other hand, are often less productive, cooler and oxygen-rich meaning they are dominated by smaller taxa dominating which are intolerant of low oxygen conditions and require less food to complete development e.g., Orthocladiinae, Tanytarsini and Diamesinae (Brooks *et al*., 2007).

Environments - Lake water depth and habitats

Habitats within lakes can exert a strong influence as to what chironomids are present and can be categorised into three broad zones: profundal, sub-littoral and littoral. The Profundal is the deepest part of the lake while the littoral is the shallow area around the edge of the lake. The sub-littoral is the intermediate area between the profundal and littoral. Typically, each zone supports its own characteristic assemblage of chironomids (Porinchu and MacDonald, 2006; Armitage *et al*., 1995) (Table 3.2). Lake depth itself does not exert a direct influence on the chironomid taxa present in each zone but a combination of abiotic and biotic factors that change with lake depth (e.g., Kurek & Cwynar 2009, Engels & Cwynar, 2011) does strongly influence within-lake distribution patterns of chironomids. Abiotic factors include wind-induced currents, light, substrate, oxygen-concentrations, and temperature (Armitage *et al*., 1995; Porinchu and MacDonald, 2006). Biotic factors also have an influence and include food (quantity and quality), competition (intra- and interspecific), habitat availability and species-specific physiological adaptation (Porinchu and MacDonald, 2006). A fourth type of habitat, the surf zone, is present at the exposed shores of lakes. This zone typically supports taxa that are more commonly encountered in rivers and streams, as wave action produces a relatively coarse stable substratum (Armitage *et al*., 1995). Changes in the dominance of taxa associated with

each of these zones can indicate changes in water depth through lake level fluctuations (Engels *et al*., 2012).

Lake zone	Feature of zone	Typical Common Taxa present
Profundal	• Potentially low oxygen conditions • Low light levels = insufficient for photosynthesis = no aquatic macrophytes • Fine sediments • Generally colder	• *Procladius and Chironomus* when low oxygen conditions prevail. • *Microspectra, Heterotrissocladius, Orthocladius consorbrinus, Tanytarsus lugens* in colder oligotrophic lakes • Taxa that possess haemoglobin or can withstand anoxia: *Chironomus, Sergentia, Procladius*
Sub-littoral	Intermediate between profundal and littoral	Intermediate between profundal and littoral
Littoral	• High light levels = Aquatic macrophytes • Large quantity of food • High oxygen conditions • Coarse sediments • Generally warm	• Orthocladiinae and Chironomini associated with macrophytes common e.g., *Psectrocladius, Cricotopus, Glyptotendipes* and *Polypedillum* • Taxa associated with streams
Surf zone	• High light levels, • Affected by wind, • High oxygen concentrations, • Coarse substrate due to wave action	• Generally, stream taxa present: • Mainly Orthocladiinae, in particular: e.g., *Eukiefferiella, Thienemanniella, Rheocricotopus, Lymnophyes, Smittia* • Chironomini adapted to macrophytes: e.g., *Parachironomous, Glyptotendipes, Polypedillum.*

Table 3.2, Features associated with each lake zone and typical associated taxa. (After Armitage *et al.,* 1995).

Although the work presented in this thesis focuses on lake sediments, it is important to briefly review taxa that live in terrestrial, semi-terrestrial and lotic environments as these can sometimes occur in lakes and provide further useful environmental information. Orthocladiinae are the only sub-family to contain taxa whose larvae live in terrestrial or semi-terrestrial habitats (e.g., *Gymnometriocnemus*) (Armitage *et al.,* 1995). These larvae can for instance live in damp leaf litter, mosses, cow dung, soil and vegetables. The presence of remains of such larvae in lakes samples can indicate erosional events (Brooks *et al.,* 2007).

A number of chironomids can occur in the flowing waters of rivers and streams, including *Diamesa, Prodiamesa, Psuedosmittia, Metriocnemus* and some *Micropsectra* species. The presence of these taxa are further controlled by water temperature, flow rate, food availability and substrate (Armitage *et al.,* 1995). Increases in their numbers in lake sediment samples can indicate a river or stream having a greater influence over the lake by increases in stream flow.

Limnophyes is sometimes a useful indicator of lake level fluctuations with higher abundance thought to occur during periods of lower lake level (Massaferro and Brooks, 2002).

Substrate morphology

The substrate morphology also exerts an influence on chironomid assemblage composition (Pinder, 1986). There is a significant correlation between substrate morphology and lake depth, as the profundal is often characterised by soft fine sediments, which are often oxygen poor and so host Chironomini, Tanytarsini and Tanypodinae (Brooks *et al.,* 2007). In contrast, the margins of lakes are characterised by coarser sediments and macrophytes offering more diverse habitats. However, chironomid larvae can utilise a variety of substrates and are not constrained to a single type (Pinder, 1980).

Dissolved oxygen

Dissolved oxygen (DO) is related to temperature and lake productivity, morphometry and length of ice cover (Porinchu and Macdonald 2006; Brooks *et al.,* 2007). Chironomini can tolerate low oxygen conditions and periods of anoxia due to their haemoglobin. Periods of anoxia are mainly an issue in the profundal of deep, thermally stratified lakes in summer or lakes with extended ice cover in the winter (Brooks *et al.,* 2007). *Chironomus* and *Procladius* often dominate the profundal of oxygen-poor lakes but are eliminated after prolonged hypoxia and so the assemblage becomes dominated by littoral and stream taxa (Brodersen and Quinlan, 2006; Quinlan and Smol, 2002, 2001a).

pH

pH changes can affect chironomids in a number of ways through the solubility of toxic heavy metals, changes in micro-organism and algae composition which form food for chironomids, alterations in metabolism, changes in predatory-prey relationships and regulation of calcium and sodium in larvae (Brooks *et al.,* 2007). *Macropelopia, Psectrocladius, Heterotanytarsus, Heterotrissocladius, Zalutschia, Chironomus, Dicrotendipes, Phaenopsectra* and *Sergentia* often dominate acidic lakes (Walker, 2007; Brooks *et al.,* 2007). However, *Prodiamesa*, *Endochironomous*, *Microspectra* and *Tanytarsus lugens*-type are acidophobic and so largely absent in acidic lakes (Johnson and Wiederholme, 1989).

Feeding strategies/guilds

The adult chironomids rarely feed, though they sometimes feed on nectar or honey dew (Walker, 1987). The larvae vary greatly in their feeding strategies, though many are detritivores (e.g., most *Psectrocladius*) or filter-feeders (e.g., *Rheotanytarsus* and *Chironomus*) (Moller Pillot, 2009, 2013; Vallenduuk and Moller Pillot, 2013). Very few actually live off living plant tissue though some mine the stems of aquatic macrophytes (e.g., some *Cricotopus, Glyptotendipes* and *Paratanytarsus*). Many Orthocladiinae and Diamesinae are largely scrappers feeding on algae growing on rocks (Walker, 1987). Tanypodinae and some genera belonging to other sub-families (e.g., *Parachironomous*, *Cryptochironomus* and *Cardocladius*) are carnivorous and preying on other aquatic larvae as well as other matter (Vallenduuk and Moller Pillot, 2013; Moller Pillot, 2009, 2013). Though, larvae are not restricted to these and can adapt to any of the six feeding strategies: deposit-feeders, filter feeders, shredders, scrapers, predators, or a mixture of these (Berg, 1995).

3.2 Chironomids as a palaeoecological proxy

3.2.1 History of chironomids as a proxy

Chironomids have long been known to be sensitive environmental indicators (Brooks, 2001). Originally, characteristic chironomid faunal assemblages were used to classify the trophic state of lakes. Thienemann (1918, 1921, 1922) tried to characterise lakes based on the dominant components of benthic fauna describing oligotrophic Tanytarsus lakes, eutrophic Chironomus lakes and humic lakes in which both *Chironomus* and *Coretha* (Chaoborus) were prominent. Brundin (1949; 1956; 1958) further refined Thienemann's classification describing several classes of stratified temperate lakes (Figure 3.5). Saether (1979) developed this further with a continuum of 15 profundal communities expressed as either Total Phosphorous/Lake Depth or Chl a/Lake Depth. These works were largely interpreted changes in chironomid assemblage composition as a response to within-lake variables, such as trophic status and water depth (Brooks, 2001; 2006). These classification systems were developed on a very small subset of lakes from temperate regions that were formed after the relatively recent deglaciation regions in North America and northwest Europe (Walker, 2007), and were never tested under different climate regimes or lakes of different origins (Walker, 2007). In these early years of chironomid research, climate was largely not considered as a major driver of chironomid assemblage change (Brooks, 2006).

I	Ultra-oligotrophic	*Heterotrissocladius subpilosus*
I/II	Oligotrophic	*Tanytarsus-Heterotrissocladius*
II	Moderately Oligotrophic	
II/III	Mesotrophic	*Stictochironomus-Sergentia*
III	Eutrophic	*Chironomus*
	a) moderately eutrophic	*C. anthricinus*
	b) Strongly eutrophic	*C. plumosus*
	c) Dystrophic	*C. tentuistylus, Zalutschia zalutschia, Chaoborus*

Figure 3.5, Lake trophic status classification by Brundin (1956) based on the presence of certain chironomid taxa.

However, from early on in chironomid research, there was evidence that changes in assemblages corresponded to climatic periods. In 1927, Gams demonstrated that *Eutanytarsus* became abundant in interstadial sediments of Lunzer Obersee, which was later replaced by *Bezzia* (Ceratopogonidae) and *Chironomus*. Andersen (1938) also demonstrated switches in the chironomid fauna of a Lateglacial Danish lake sequence between the Older Dryas, Allerød and Younger Dryas. In the 70s and 80s, Lateglacial climate change began to be explored in some qualitative detail by Wolfgang Hofmann who found similar assemblage changes through the Lateglacial period in a number of European lakes including Grosser Segeberger (Northern Germany; Hoffman, 1978), Schohsee (Hofmann, 1971), Lobsigensee (swiss plateau; Hoffmann, 1983a), Poolsee (Hofmann, 1983b) and Meerfelder Maar (Hofmann, 1984). The Lateglacial littoral sediments at Poolsee were dominated by taxa typical of cold conditions including *Heterotrissocladius, Protanypus, Sergentia coracina* and *Paracladius*. Hofmann argued that the presence of these taxa in the littoral, rather than their more native profundal, must be the result of climate instead of trophic conditions. Walker and Matthews (1987; Figure 3.6) further demonstrated the link between temperature and chironomid distribution with the decline of Heterotrissocladius, a taxon associated with cold conditions, in post-deglacial sediments as climate warmed. Several papers also pointed out that the best analogues for Lateglacial assemblages could be found in present day arctic alpine settings (Walker and Mathewes, 1987; 1989; Walker, 1991).

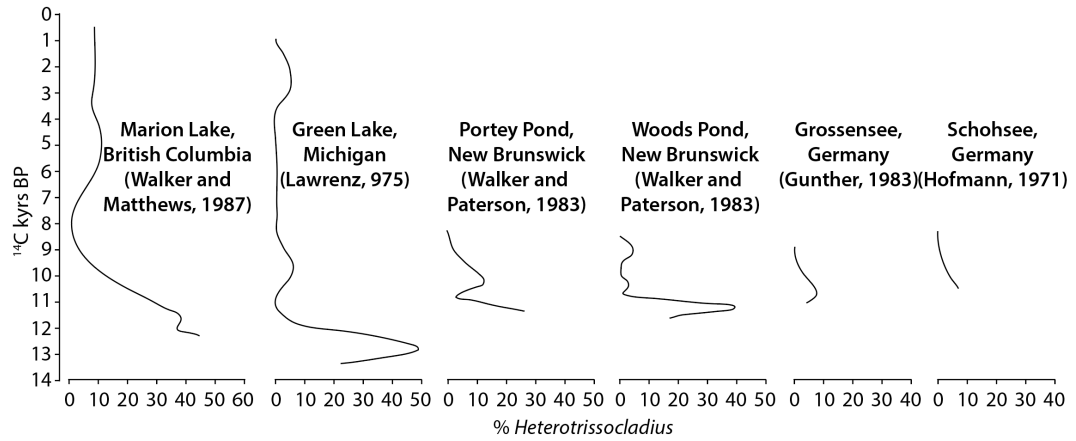

Figure 3.6, Abundance of Heterotrissocladius in 6 lakes from North America and Europe. (after Walker and Mathewes, 1978).

It wasn't until Walker and Matthews (1989) and Walker *et al.,* (1991, 1992) that temperature was statistically demonstrated as the most important variable in driving the broad-scale geographic distribution and abundance of midge taxa. The justification of this finding has grown over the last few decades from several lines of evidence including good correlation between direct comparisons of meteorological data and T_{Jul} (Larocque *et al.,* 2008), regional consistency between T_{Jul} reconstructions (Lang *et al.,* 2010) and good replication of climate model outputs (Heiri *et al.,* 2014). These are discussed in more detail in section 3.2.4. Now mean July air temperature is recognised as the single most important driving variable in chironomid distribution (Eggermont and Heiri, 2012). Temperature changes, however, cause a distinct and unique faunal response in each lake reflected by the presence of different taxa (Brooks, 2000). Therefore, chironomid biostratigraphies cannot be developed as is the case with other biological proxies e.g., pollen, making between-site comparisons and correlations challenging (Brooks, 2001). However, the development of calibration datasets has allowed the chironomid response to be quantified, facilitating inter-lake comparisons. Walker *et al.,* (1991) developed the first calibration dataset and inference model based on 24 lakes in Labrador Quebec, Eastern Canada, with 24 taxa identified. Now there are over 20 calibration dataset able to reconstruct mean July air temperature (or mean January air temperature in the southern hemisphere) from Europe (Heiri *et al.,* 2011), the Americas (Barley *et al.,* 2006), and Australasia (Woodward and Shulmeister, 2006). Chironomids have mostly been used to reconstruct Holocene and Lateglacial temperatures (e.g., Brooks *et al.,* 2016) but have also been applied further back in time to MIS3 and MIS5 (e.g., Engels *et al.,* 2008; 2010). The calibration dataset approach has also been adapted to reconstruct other environmental variables, with varying degrees of success, including nutrient status (e.g., Langdon *et al.,* 2006), Lake level changes (e.g., Cwynar

et al., 2012), salinity (e.g., Zhang *et al.,* 2007), and Dissolved oxygen (e.g., Quinlan and Smol, 2001a; 2002).

3.2.2 Advantages of using chironomids as a proxy

A number of aspects make chironomids an ideal proxy for palaeoenvironmental reconstructions. They are incredibly species rich with an estimated 5,000 species described worldwide (Cranston and martin, 1989), 1,000 of which in Europe (Lindegaard, 1997). Although the majority of larvae cannot be identified to species level, over 200 morpho-types or 'species groups' are recognised and provide ample taxonomic resolution for studying past environments. Chironomids are also very abundant, usually several hundred HCs can be obtained from small samples of only a couple of grams meaning they can be applied at a high temporal resolution, e.g., 0.5 cm intervals (Brooks and Heiri, 2013). This makes them ideal for multi-proxy studies as it allows other techniques to be undertaken on the same core. Larvae are ubiquitous and found in most lake systems providing there are organics present as a food source. The heavily chitinised HCs of the third and fourth instar larvae means they are preserved very well and can be identified to species group ('-type') level. Sometimes even species level identification can be attained (Samartin *et al.,* 2012). Finally, as chironomid larvae grow *in situ* in lake sediments there is no issue of long-distance dispersal like with pollen, therefore, local climatic conditions are reflected. The chironomids present also reflect the climate and environment at time of sedimentation (Hoffman, 1988).

Further to those features outlined in the previous paragraph, there are several other characteristics that make chironomids ideal for reconstructing abrupt temperature changes in particular. Firstly, chironomids are sensitive, as they have a rapid generation time, potentially producing up to 5 generations per year (Armitage *et al.,* 1995). The combination of short life cycles with the high dispersal capabilities of the winged adults means the assemblages can respond quickly to any changes in temperature, attaining near equilibrium (Walker *et al.,* 1989; Walker and MacDonald, 1995; Porinchu and MacDonald, 2006; Porinchu and Cwynar, 2002). Secondly, generally at least 50 taxa are present in a Lateglacial-Holocene sequence living at a wide variety of temperatures meaning assemblages are very responsive to temperature changes (Brooks *et al*., 2007). Thirdly, most chironomids are stenothermic, adapted to surviving only in a narrow range of temperatures, ideal for temperature reconstructions.

3.2.3 Quantitative temperature reconstructions from chironomids

As already discussed, the work of Hofmann, Walker and Mathewes, demonstrated that temperature is a key driver in determining chironomid assemblages and had an over-riding impact on changes in chironomid distribution and abundance between different climatic periods (Brooks and Birks, 2001). Though, due to local factors the faunal response was reflected by different taxa in each lake (Brooks, 2000; Brooks and Birks, 2001). Therefore, this inhibits the development of chironomid biostratigraphies, as with pollen and other biological proxies, meaning between-site correlations and comparisons of taxa cannot be made. However, inter-site comparisons can be made with the quantification of chironomid response in terms of temperature with the application of modern calibration data sets and transfer functions (Brooks and Birks, 2001). This approach is based on the principle of uniformitarianism in that the knowledge of the present-day conditions can be used to infer past conditions (Birks *et al.,* 2010; Juggins and Birks 2011).

Step 1: Developing a modern calibration data set

In order to quantify and infer temperature changes from a fossil chironomid record, a modern chironomid-temperature calibration dataset is needed, allowing the modern distribution patterns of chironomid taxa to be compared to modern temperatures (Brooks and Birks, 2001). This facilitates the development of a numerical model to quantify and describe these relationships, identifying the temperature optima and tolerances of each taxon, which can then be applied to a fossil dataset in order to infer past temperature changes (Brooks and Birks, 2001). This approach utilises the concept of switching the contemporary spatial slope with the temporal slope. Over the last few decades there has been a large increase in the number of calibration datasets from many regions (Porinchu and MacDonald, 2006), Table 3.3 provides and overview of these.

Area covered	Enviro. Var. reconstructed	No. of lakes	No. of Taxa	Temp range	Reference
Norway	Mean July air temp	157	131	3.5-16 °C	Brooks and Birks (unpub)
Nor-Swiss combined	Mean July air temp	274	154	3.5-18.4 °C	Heiri *et al*., (2011)
Eastern Canada	Surface water temp	39	34	6-27 °C	Walker *et al.,* (1997)
Russian combined	Mean July air temp	268	176	1.8-18.8 °C	Nazarova *et al.,* (2015)
Swedish	Mean July air temp	100	48	7-14.7 °C	Larocque *et al*., (2001)
Finland	Mean July air temp	82	110	11.3-17 °C	Luoto *et al.,* (2009a)

Table 3.3, Examples of chironomid climate calibration datasets.

Calibration datasets consist of data from a number of modern samples taken from a series of lakes, typically 30 lakes for simple systems dominated by a single strong environmental variable (Juggins and Birks, 2012), although chironomid calibration datasets usually have 100 lakes or more to accurately estimate the ecological preferences of taxa. Generally, those with a greater number of lakes have better performance statistics and therefore produce better reconstructions (Brooks, 2006). The lakes selected should span a broad range of climatic zones between different latitudes and altitudes to maximise the temperature gradient, therefore capturing the full potential abundance and distribution of taxa (Brooks, 2006). Ideally, the lakes should also be spread evenly over the temperature gradient (Birks, 1995; Brooks and Birks, 2001; Brooks, 2006). Other lake variables such as trophic status, lake depth and pH should also not vary greatly between the calibration dataset of lakes to minimise their influence on chironomid distribution and maximise the variable of interested - temperature (Brooks and Birks, 2001). The type of sedimentary environment should also be kept the same between lakes as to not influence the fossil material through taphonomic effects (Birks, 1995).

The modern samples collected from the calibration dataset lakes are mostly surface sediment samples taken from the centre so that the sample contains a fair representation of the modern chironomid assemblage of the lakes. Sediment samples are typically taken using a gravity corer to limit the disturbance of surface sediments, and the top 0.5-2 cm of sediment is taken for analysis depending on sedimentation rate (Brooks *et al*., 2007). The sample is then prepared, picked, and identified to determine the contemporary chironomid assemblage. To accompany this, 30-year averages of mean July air temperatures are gathered from nearby weather

stations and altitudinal offsets with the sampling site are corrected for using the environmental lapse rate.

The very first calibration datasets used to reconstruct past temperature changes measured surface water temperature using a single point instead (e.g., Walker *et al*., 1997). However, mean July air temperature is frequently employed now as it provides better inference model performance statistics (Brooks and Birks, 2001). This is because, (i) surface water point measurements can be subject to daily-monthly variations in temperature (Livingstone *et al.,* 1999) whereas air temperature data is available in much higher temporal resolution (Brooks, 2006; Walker and Cwynar, 2006); and (ii) water temperature only affects the larval stages whereas air temperature affects both the adult and larvae due to the strong highly linear relationship between air and water temperatures (Olander *et al.,* 1999; Livingstone and Lotter 1998; Eggermont and Heiri, 2012).

Step 2: Inference model and Transfer function

Several different statistical methods have been employed to reconstruct past temperatures, including Weighted Averaging (WA) (e.g., Levesque *et al.,* 1997) and Bayesian methods (e.g., Korhola *et al.,* 2002). WAPLS is now the most commonly used statistical method for chironomid-inferred temperature reconstruction as it usually provides superior model performance compared to the previously widely used two-way WA regression (Salonen *et al.,* 2011). WAPLS combines the attractive features of WA, allowing the modelling of unimodal responses, and Partial Least Squares (PLS), allowing the efficient extraction of components (ter Braak and Juggins, 1993; Juggins and Birks, 2012).

Firstly, WA employs regression to model the optima and tolerances of taxa to an environmental variable (i.e., temperature) in the modern calibration dataset by fitting a unimodal response curve to a taxon's abundance (Birks, 1995). A unimodal distribution resembles a taxon's real-world response to a variable, much more closely than a linear regression. WA assumes the most abundant taxa present will have optima that are close to the prevailing conditions. WA then uses calibration to reconstruct/estimate the prevailing temperature conditions the assemblage of a sample experienced by averaging the optima of all the taxa present. Taxa with greater abundance are more heavily weighted during averaging as conditions are thought to be close to their optima and are therefore given more influence when estimating the past temperature conditions.

Secondly, PLS which is a combination of regression, allowing high correlation, and, Principal Components Regression (PCR), which seeks to extract components to maximise variance. Components are selected to maximise the covariance between linear combinations or predictor values with the environmental response variables. PLS allows for the efficient extraction of 'components' from a dataset as it uses the environmental data and biological data to extract them. PLS models assume a linear response of a taxon to an environmental variable; however, the combination with WA means unimodal responses can be modelled. The first component of a WAPLS is essentially the same as a simple WA. If too many components are extracted then the model becomes 'over-fitted' to the data and starts to model intrinsic features of data (Juggins and Smol, 2011). The number of components chosen to extract is largely based on cross-validation methods such as leave-one-out jack-knifing (Birks *et al.,* 1990) or bootstrapping and associated performance statistics including the coefficient of determination (r^2), root-mean-square error of prediction (RMSEP) and maximum bias (Salonen *et al*., 2011). Usually, the 2nd or sometimes 3rd component of WAPLS selected for chironomid-inferred temperature reconstructions.

3.2.4 Justification of using chironomids to reconstruct past temperature changes

It is now largely accepted that mean July air temperature is thought to be the most important factor in controlling chironomid distribution (Brooks and Birks 2001; Eggermont and Heiri, 2012; Brooks, 2006; Heiri *et al.,* 2014). Although there was some initial scepticism by Warner and Hann, (1987) and Hann *et al.,* (1992), there is ample evidence to support the chironomid-temperature relationship to justify their use to infer past temperature changes. As seen in sections 3.1.4, laboratory experiments have demonstrated that temperature has a direct influence on every stage of the chironomid life cycle. This is corroborated by several other lines of evidence including good correspondence with meteorological data, regional consistency of T_{Jul} records and good agreement with other temperature proxy reconstructions.

Firstly, justification comes from the comparison of instrumental temperature records and T_{Jul} records. Larocque and Hall (2003) found remarkable consistency between sub-decadal chironomid-inferred temperatures from 4 Swedish lakes with temperature data between AD1999-1867. Nearly 90% of the instrumental data were within the errors of the T_{Jul} records. Larocque *et al*., (2009) demonstrated very good relationships between T_{Jul} and meteorological

temperature data from varves lake Silvaplana, Switzerland, between AD 1850-2001). Further to this, Larocque-Tobler *et al.,* (2015) also showed good correlation between T_{Jul} and meteorological temperature records at Żabińskie, Poland, since 1986 to present. Moving averages were applied at different time windows and attained r^2 values of 0.71 (annual), 0.91 (3 yrs), 0.91 (10 yrs) and 0.86 (30 yrs).

Many Lateglacial T_{Jul} sites show good regional consistency, with the vast majority of Lateglacial Interstadial records showing three cooler periods separated by two cooler periods. Lang *et al.* (2010) demonstrated remarkable regional consistency between the T_{Jul} records from 5 sites over a small geographic area in the Lake District, which are Sunbiggin Tarn, Cunswick Tarn, Little Hawes Water, Hawes water and Urswick Tarn. Slight variations between these sites were accounted for due to difference in altitude, Lake morphometry, proximity to ocean, local topography, aspect, lake depth and surface area. The temperature oscillations in the Sunbiggin Tarn T_{Jul} record are the largest in magnitude of the 5 sites due to its high altitude possibly causing species to be nearer their environmental tolerances (Lang *et al.,* 2010). The temperature oscillations in the T_{Jul} record from Urswick Tarn however are much small due to the site's proximity to the ocean (Lang *et al.,* 2010). Heiri *et al.,* (2014) created a spliced and stacked record for the seven regions of Europe which all showed very good consistency to the general circulation model, ECHAM-4. Some differences do exist though over larger geographic regions, as discussed in section 3.2.1, however, these are tentatively attributed to differences in climatic forcing and other influencing factors (Brooks *et al.*, 2016).

Remarkable consistency is also present when comparisons of T_{Jul} are made with other temperature proxies including Coleopteran MCR estimates, pollen-inferred temperatures, and oxygen-isotopes. Brooks and Langdon (2014) constructed and compared isotherm maps from chironomid-T_{Jul} and Coleopteran MCR records from Europe which showed good agreement in the spatial pattern of temperature changes throughout the Lateglacial and early Holocene, although T_{Jul} reconstructions are *c.* 2 °C lower than Beetle MCR estimates. This may be due to differences in the microclimates in which beetles and chironomids live. Recalibration of MCR though means there is no offset now (Brooks, pers. Comms.). Good correlation is also shown with oxygen isotopes, which broadly respond to temperature changes, as seen in the $\delta^{18}O$ record from Fiddaun in Ireland (Van Asch *et al.,* 2012) and the $\delta^{18}O$ record from the Greenland Ice cores (Brooks and Birks 2001; Rasmussen *et al.,* 2014).

3.2.5 Assumptions of quantitative palaeo-temperature reconstruction

There are a number of assumptions made during quantitative palaeoecological reconstructions, originally outlined by Birks (1995) and Birks *et al.,* (1990). Juggins (2013), Huntley (2012) and Velle *et al.,* (2010) have recently brought some of these areas to light again and questioned the use of biological proxies, in particular chironomids, to reconstruct past environmental variables. The chironomid community have worked hard to show that these assumptions have been carefully thought about, demonstrating that they have negligible effect on using chironomids as a palaeothermometer. These can be split into 4 broad categories: 1) reconstructing ecologically important variables, 2) taxonomic resolution, 3) employment of models, and 4) the impact of other secondary variables affecting the variable under reconstruction.

Firstly, Juggins (2013) argues that the physiological response of biological taxa to the variables under construction is poorly understood and that justification from cross-validation of models is relied upon to demonstrate their predictive power rather than showing a direct ecological effect (Juggins, 2013). He questions if it is appropriate to reconstruct the ecological variable in question. As demonstrated in sections 3.1.4 and 3.2.4, temperature has been shown to play a key role in the chironomid life cycle and is the main environmental parameter that governs the distribution of chironomid taxa, particularly during the Lateglacial Interstadial. Therefore, it is appropriate to infer past temperature changes from chironomids.

Secondly, Velle *et al.,* (2010) argue that the degree of taxonomic resolution can influence the environmental inference. In many cases fossil chironomid HCs cannot be identified to species level as the soft larval body parts and fragile HC features are frequently not preserved (Velle *et al.,* 2010). Working with the remaining limited and potentially unclear morphological features can result in Type 1 and Type 2 errors. Type 1 errors are where differences are seen between fossil HCs that do not exist as taxa are over split. This can introduce noise into the reconstruction and weaken the interpretation by misidentification of HCs. Type 2 errors are when differences between taxa are not recognised (Velle *et al.*, 2010). This will produce more conservative results with less and weaker ecological information as species are lumped together with different ecological preferences (Velle *et al*., 2010). Therefore, an optimal resolution occurs between these states. The chironomid community have worked hard to ensure that the optimal resolution is attained. As described in section 3.1.3, improvements have been made over the last few decades to improve the level of taxonomic resolution

through careful observation of morphological features and sound distinctions drawn between specimens (Porinchu and MacDonald, 2006; Brooks, 2006). Although there are still many species groups, with several different species within, further separation of these would result in Type 1 errors. It is also widely recognised that correct and consistent identification of HCs is vital for accurate chironomid temperature reconstructions (Brooks *et al.,* 2007). Particularly, consistency is needed between the site of study and the modern calibration dataset. To ensure this, a standardised taxonomic approach is employed in many studies using the same guides and keys e.g., Brooks *et al.* (2007) and Wiederholme (1980). The effect of this is visible through the improved performance on inference models (Brooks, 2006).

Thirdly, Juggins (2013) suggests that models are context sensitive and so when applied spatially/temporally they are unreliable, even if they have good predictive powers as the underlying driving factors are different from those modelled. Chironomid-inferred temperature reconstructions often carefully select the calibration dataset(s) employed in order to best match the lake and environmental characteristics or the calibration dataset with the palaeolake(s) used for the reconstruction. Numerical and statistical measures, such as the Modern Analogue Technique and the percentage of taxa absent or rare, are frequently used to assess the similarity of the assemblages present in the fossil data compared to the calibration dataset. Fossil assemblages with few taxa present, or have very different assemblages, compared to the modern calibration dataset will have less robust reconstructions as the reconstruction relies on fewer taxa (Heiri *et al.,* 2011; Nazarova *et al.,* 2011). Even so, different calibration datasets have been applied to regions outside of their native area by several studies in order to test their ability to infer past temperatures in other regions (Holmes *et al.,* 2011; Heiri *et al.,* 2011; Plociennik *et al.,* 2011; Self *et al.,* 2011; Nazarova *et al.,* 2011). These studies demonstrate that the majority of calibration data sets can be applied to other regions as they produce similar patterns of temperature changes, albeit offset by 1-2 °C. Differences that are observed can be attributed to differences in lake type, as humic/acidic lakes are very different to neutral/hardwater lakes in terms of water chemistry, intensity of biological processes and physical conditions (Heiri *et al.,* 2011). Some discrepancies can also be attributed to the differences in climate regime (Plociennik *et al*., 2011).

Finally, Juggins (2013) and Huntley (2012) argue that frequently in palaeoenvironmental reconstructions, the environmental variable under reconstruction is considered in isolation and that any other (secondary) variables are considered to have a negligible influence. As shown in

section 3.1.4, temperature is not the only environmental variables that influences chironomids as other environmental variables including dissolved oxygen (Quinlan *et al.,* 1998; Little et al., 2000), trophic status (Langdon *et al.,* 2006), macrophytes (Langdon *et al.,* 2010), pH (Brodin and Gransberg, 1993) and lake level changes (Hofmann, 1998; Korhola *et al.,* 2000) all influence chironomid presence and abundance. These may over-ride temperature as the main driver of chironomid assemblage change (Velle *et al*., 2005; Walker and Cwynar, 2006) and could also be acting as surrogate variables for temperature changes as they can confound (Velle *et al.,* 2012). However, numerous studies have shown that centennial-scale abrupt climate events are still clearly recorded in lake sequences and concur with other temperature proxy reconstructions during periods there are significant changes in secondary variables (Brooks *et al.,* 2012; Gathorne-Hardy *et al*., 2007; Lang *et al*., 2010). During the Lateglacial Interstadial, these secondary variables are particularly unlikely to have a significant effect on chironomids responding to temperature changes as temperature changes are larger than the predictive powers of the inference models and, generally, changes in lake depth, nutrient flux and soil development are minimal during this period (Brooks *et al.,* 2012). The influence of secondary variables will be discussed in detail in the results and interpretation section of each site as these are often very much site and time dependant.

3.3 Chapter Summary

The above review of how chironomids can be used to reconstruct past environmental changes can be summarised in the following points:

- Chironomids were initially used as trophic status indicators but are now commonly used to provide quantitative estimates of mean July air temperature (T_{Jul}) using WAPLS models and transfer functions.

- Temperature affects many aspects of the chironomid life cycle from the number and speed of egg hatching, larval growth rate and the timing of emergence. Temperature is therefore the main environmental variable influencing the distribution and abundance of chironomid taxa.

- Chironomids can respond quickly to temperature changes as they have high dispersal capabilities and can have numerous generations per year, making them ideal to study ACEs.

- Although chironomid respond to other environmental variables (e.g., trophic status, water depth, substrate texture and dissolved oxygen concentrations), many taxa can respond to each of these environmental variables while also responding to temperature.

- A range of statistical techniques are available (e.g., goodness-of-fit, modern analogue technique), along with qualitative ecological analysis of assemblages, allows the identification of periods where the T_{Jul} reconstruction may be less reliable due to the influence of other environmental variables.

- Several lines of evidence show that chironomids can be used to reconstruct past climatic temperature changes including (i) good correspondence between T_{Jul} and instrumental records, (ii) regional consistency in T_{Jul} records over small geographic areas, and (iii) remarkable agreement with Coleopteran MCR, pollen-inferred temperature and oxygen isotope records

Chapter 4: Stable isotopes ($\delta^{18}O$ and $\delta^{13}C$) literature review

Chapter overview

This chapter is divided into the following four sections. The first section will introduce the stable isotopes commonly used in stable isotopic analysis and the basic laws of physics which govern their fractionation in the hydrological cycle. The second section looks at the factors controlling the precipitation of calcium carbonate and how the isotopes of oxygen and carbon are incorporated into lake carbonates. The third section outlines the factors which alter the $\delta^{18}O$ of rainfall during meteorological precipitation and the recharge of lake waters as well as the within-basin modification processes, all of which have an influence on the $\delta^{18}O$ of lake waters and need to be taken into consideration when interpreting $\delta^{18}O$ records. Some examples of how oxygen isotopes have been used in palaeoclimate reconstructions and the benefits of using oxygen isotopes as a proxy are found in section 3. The final section briefly explores the environmental factors which cause changes in $\delta^{13}C$ and how $\delta^{13}C$ can be used to aid the interpretation of $\delta^{18}O$.

4.1 Introduction to oxygen and carbon isotopes

4.1.1 General Introduction

The use of stable isotopes in palaeoenvironmental research is based around the principle that isotopes of the same element (e.g., oxygen) behave in a similar manner chemically but are separated on the basis of mass by a range of environmental processes. Stable isotopes are atoms of the same element that contain the same number of protons but vary in the number of neutrons that they contain. For Oxygen, three stable isotopes exist, ^{16}O, ^{17}O and ^{18}O (Figure 4.1). Whilst ^{16}O contains 8 protons and 8 neutrons in its nucleus, ^{18}O contains 8 protons and 10 neutrons in its nucleus. This means that atoms of ^{18}O are heavier than atoms of ^{16}O and require more energy to be "moved" around the environment. The most abundant isotope of oxygen is ^{16}O and accounts for 99.76 % of all oxygen isotopes, in contrast, ^{18}O only makes up 0.2 % of all oxygen isotopes. The ratio between ^{16}O and ^{18}O is affected by a number of environmental processes, i.e., evaporation, consequently the analysis of these isotopes can be used to reconstruct palaeoenvironmental changes (e.g., Leng and Marshall, 2004; Diefendorf *et al.,* 2006; Candy *et al.,* 2015). Similarly, Carbon has two stable isotopes, Carbon-12 and Carbon-13, the ratio of which is again affected by a range of environmental processes, such as

photosynthesis. Because isotopes are of the same elements, they are chemically identical, however, the differences in mass cause a number of physical and biological processes/reactions to alter the relative proportions of isotopes (Kendall and Caldwell, 1998).

One of the main causes of fractionation between the isotopes of oxygen and carbon to occur is when the compounds in which they are part of undergoes phase changes. For example, fractionation of oxygen isotopes can occur when H_2O changes from a liquid to gas, with the isotopic ratio of the end product containing less of the heavier ^{18}O than the initial water. Similarly, the isotopic composition of carbon will change during transfer from gas to organic molecules during photosynthesis (Mook, 2006). Such fractionation is due to the mass differences between the heavier isotopes (e.g., ^{18}O and ^{13}C) and the lighter isotopes (e.g., ^{16}O and ^{12}C). The heavier isotopes have greater binding energy and require more energy to undergo phase changes (Craig, 1953). The lighter isotopes will therefore react faster than the heavier isotopes during phase changes and will therefore fractionate more easily (O'Neil, 1986). At higher temperatures, the differences between binding energies of isotope molecules are smaller and so at higher temperatures, water evaporating from a source will have an enriched $\delta^{18}O$ value, compared to water evaporating at lower temperature (Leng and Marshall, 2004).

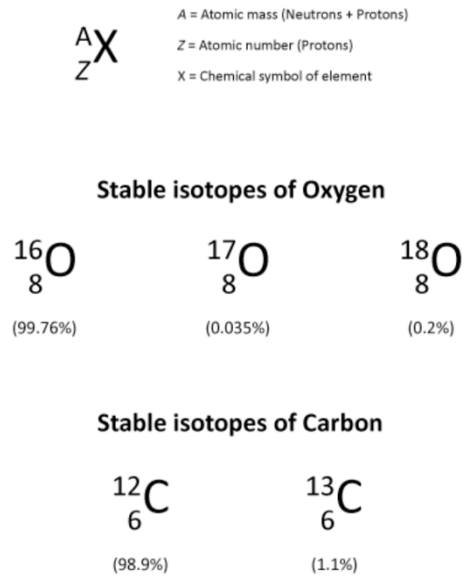

Figure 4.1, The stable isotopes of oxygen and carbon accompanied by standard nuclear notation of an element. The numbers in brackets below each isotope, is the approximate natural abundance of each isotope (after Tye, 2014)

4.1.2 Oxygen and Carbon isotope notation

This study focuses on the isotopic analysis of lacustrine carbonates. The isotopic values of such are measured using mass spectrometry with the amount of sample required determined by the amount of carbonate in the sample and the sensitivity of the equipment. Carbonate isotopic

data is reported relative to the standard VPDB (Vienna Pee Dee Belemnite (Friedman *et al.,* 1982) using the following equation:

$$\delta^{18}O = 1000 \times \left(\frac{\left(\frac{^{18}O}{^{16}O}\right)_{sample} - \left(\frac{^{18}O}{^{16}O}\right)_{standard}}{\left(\frac{^{18}O}{^{16}O}\right)_{standard}} \right)$$

When a sample is depleted in the heavier isotopes (e.g., ^{18}O or ^{13}C) relative to the standard, the δ value will be negative. If a sample is enriched in the heavier isotopes, then the δ value would be more positive. As the difference in the relative abundance between^{18}O and ^{16}O is so large, δ values are quoted in parts per thousand (per mil, ‰).

4.2 Oxygen and carbon isotopes in lacustrine carbonates

The oxygen isotopic value of any lake carbonate is controlled by two main factors; 1) the oxygen isotopic value of the lake water and 2) the temperature at which carbonate mineralisation occurs. The oxygen isotopic value of lake waters is strongly controlled by the oxygen isotopic value of rainfall which is, in mid-latitude regions such as the British Isles, strongly controlled by air temperature (Rozanski *et al.,* 1992; 1993). Consequently, an understanding of the processes by which lake waters are recharged, and the impact this may have on isotopic properties, is vital in the interpretation of such records. Less attention is paid to the carbon isotopic value of lake carbonates as this is primarily controlled by local intra-basin processes and biological activity and, consequently, has less significance for palaeoenvironmental studies. The following sections will discuss; 1) the incorporation of oxygen and carbon isotopes into lacustrine carbonates, 2) the factors that may control the isotopic composition of lake water, and 3) carbon isotopes in lacustrine carbonates.

4.2.1 calcium carbonate precipitation and the incorporation of oxygen and carbon isotopes

In lakes which precipitate calcium carbonate ($CaCO_3$), the isotopes of oxygen, derived from the oxygen in H_2O, and carbon, derived from dissolved inorganic carbon (DIC), are incorporated into the $CaCO_3$ molecule. For $CaCO_3$ to form and precipitate however, a source of Ca^{2+} ions is needed. In the atmosphere, CO_2 reacts with water to form a weak carbonic acid which can dissolve carbonate parent materials e.g., limestone bedrock or carbonate-rich tills (Equation 3) (e.g., Smith *et al.,* 1976; Dean and Fouch, 1983). The chemical weathering of the parent material causes the water that infiltrates through the soil zone, enters the aquifer and

recharges the lake basin to become enriched in calcium (Ca^{2+}) and bicarbonate ($2HCO_3^-$) ions (Equation 1) (Wetzel 1975; Horne and Goldman 1983).

$$CaCO_3 + CO_2 + H_2O \Leftrightarrow Ca^{2+} + 2HCO_3- \quad (1)$$

Equation 1 can be further divided into the following equations:

CO_2 (g) ⇔ CO_2 (l)	• Dissolved CO_2 equilibrates with atmospheric CO_2	(2)
$CO_2 + H_2O \Leftrightarrow H_2CO_3$	• Formation of weak carbonic acid	(3)
$H_2CO_3 \Leftrightarrow H+ + HCO_{3-}$	• 1st dissociation stage creating bicarbonate, pH increases	(4)
$HCO_{3-} \Leftrightarrow H+ + CO_3^{2-}$	• 2nd dissociation stage forming carbonate, pH increases	(5)
$Ca^{2+} + CO_3^{2-} \Leftrightarrow CaCO_3$	• Precipitation of calcium carbonate	(6)

For calcium carbonate to precipitate out of solution in the water column, surface waters must become supersaturated in Ca^{2+} ions, a process which is largely mediated through biological activity in mid-latitude, hard-water, open lake systems. Photosynthesis of plants and organisms removes CO_2 from the water column (Equation 2). Thompson *et al.,* (1997) and Dittrich *et al.,* (2004) postulated the role of cyanobacterial picoplankton in aiding this process. The concentration of CO_2 is also temperature dependant, as higher lake water temperatures lead to a loss of CO_2 as its solubility is reduced (Leng and Marshall, 2004). Removal of CO_2 lowers the concentration of carbonic acid in the lake water which also lowers the concentration of hydrogen ions, thus causing an increase in pH. Carbonic acid will dissociate its first hydrogen ion between pH 6-8 and the second hydrogen ion above pH 8 (Figure 4.2; Equation 4 and 5) (Wetzel, 1975; O'Sullivan, 1983; Horne and Goldman, 1994). This process increases the concentration of the calcium and carbonate ions to supersaturation point, which then combine resulting in $CaCO_3$ mineralisation and the fall out of precipitated grains from suspension (Equation 6).

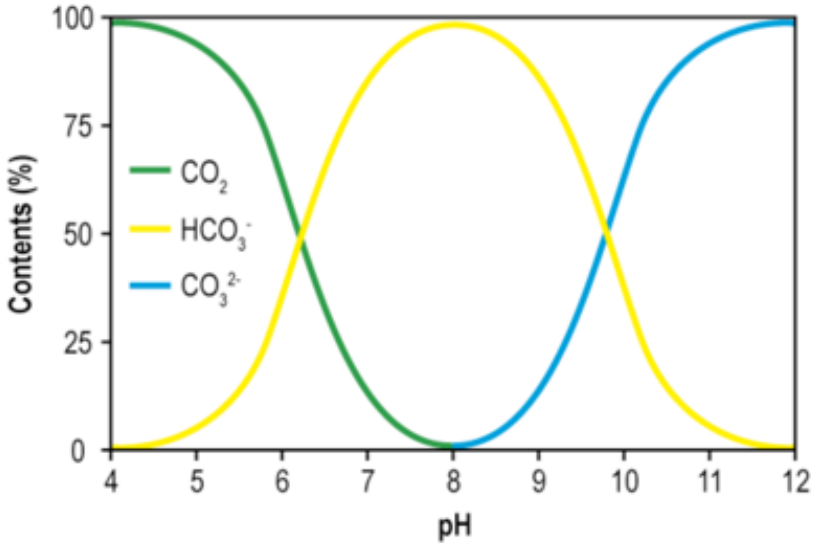

Figure 4.2, Relationship between pH and the relative proportions of inorganic carbon species of CO_2 in solution in hardwater lakes (Wetzel, 1975).

Ultimately, the precipitation of $CaCO_3$ in mid- to high-latitude lakes is thus governed by two environmental factors:

1) **Temperature** – which modulates biological activity and largely restricts $CaCO_3$ precipitation to between early spring and late autumn when higher temperatures and light levels stimulates algal growth (Bernasconi and McKenzie, 2007).
2) **Landscape stability** – clear lake waters free of suspended sediment is required for light to penetrate, allowing photosynthetic activity to occur (Bernasconi and McKenzie, 2007).

Whilst the $\delta^{18}O$ value of the resulting carbonates is controlled by the $\delta^{18}O$ value of lake waters, fractionation occurs during mineralisation and this is controlled by temperature (Leng and Marshall, 2004). This fractionation has been quantified using empirical data from laboratory and field studies resulting in its mathematical expression by Kim and O'Neil (1997) as:

$$1000\ln\alpha_{(calci^{18}Owater)} = 18.03(10^3 T°K^{-1}) - 32.42$$

The above equation has subsequen*et al.,* een re-expressed by Leng and Marshall (2004):

$$T°C = 13.8 - 4.58(\delta^{18}O_{calcite} - \delta^{18}O_{wate}{}^{18}o + 0.08(\delta^{18}O_{calcite} - \delta^{18}O_{water})^2$$

Where T is the temperature in Kelvin. This relationship means that carbonates precipitated under warmer temperatures will have more negative $\delta^{18}O$ values. In a water body of constant

$\delta^{18}O$ values, for example, for every degree of increase in water temperature, the $\delta^{18}O$ value of the carbonate decreases in the order of 0.24-0.28 ‰ (Andrews, 2006).

4.2.2 Lake Marl

In terrestrial lake settings, lake sediments containing >60 % $CaCO_3$ dry weight, are termed lake marl (Kelts and Hsu, 1978). Although lake marl is often largely composed of an inorganically precipitated carbonate, formed by the processes outlined above, the carbonate fraction from lacustrine sediments can contain $CaCO_3$ from multiple sources (Pentecost, 2009; Bernasconi and McKenzie, 2007). This can include the $CaCO_3$ rich shells of molluscs (Leng *et al.,* 2010) and valves of ostracods (Holmes, 2001; von Grafenstein *et al.,* 1999a). This is an issue for stable isotopic studies as different forms of carbonate will record $\delta^{18}O$ values differently under the same environmental conditions (due to vital offsets) and/or the carbonate may form in different seasons where the $\delta^{18}O$ of the water body could vary. Also, several different carbonate minerals can be precipitated which fractionate $\delta^{18}O$ differently. Calcite ($CaCO_3$) is most commonly produced in mid-latitude freshwater systems but as evaporation increases aragonite ($CaCO_3$) and dolomite ($CaMg(CO_3)_2$) can occur which fractionate $\delta^{18}O$ values by +0.6 ‰ and +3 ‰, respectively, compared to calcite (Leng and Marshall, 2004, Land, 1980). Finally, many carbonate-precipitating hard-water lakes occur in catchments that are at least partially composed of carbonate bedrock which could be eroded and deposited into the lake.

4.3 Environmental influences on $\delta^{18}O$ in lake waters

The use of $\delta^{18}O$ to reconstruct past climatic temperature changes is Based on three key principles. Firstly, the $\delta^{18}O$ of the precipitated calcite is formed in equilibrium with the $\delta^{18}O$ of lake water (Kim and O'Neil, 1997; Leng and Marshall, 2004). Secondly, the $\delta^{18}O$ of lake water is controlled by the $\delta^{18}O$ of water that recharges the lake, be it by direct recharge, surface runoff, rivers or groundwater, and in turn is controlled by the $\delta^{18}O$ of precipitation (Rozanski *et al.,* 1997; Darling 2004; Froehlich *et al.,* 2005). Thirdly and finally, that a positive linear relationship exists between the $\delta^{18}O$ of precipitation and local air temperature, which is commonly seen in mid-latitude temperate regions and is defined as +0.58 ‰/1 °C (Dansgaard, 1964; Rozanski *et al.,* 1992; 1993; Darling and Talbot, 2003). Therefore, under warmer temperatures, the $\delta^{18}O$ of rainfall has more positive values while more negative $\delta^{18}O$ values occur under colder temperatures. It should be noted that the isotopic fractionation that occurs during mineral precipitation and the fraction during rainfall formation occur in opposite directions, with the former causing a shift to more negative $\delta^{18}O$ values, while the latter causes a shift to more

positive $\delta^{18}O$ values. The fractionation that occurs during rainfall however is greater and overall leads to a *c.* 0.3-0.4 ‰ increase for every 1 °C increase in temperature (Leng and Marshall, 2004; Andrews, 2006).

In many temperate mid-latitude settings, such as northwest Europe, these three principles hold true, and temperature can be considered to be the primary control of the $\delta^{18}O$ of carbonates which precipitate in lake waters. However, in practice, a number of other environmental variables can alter the isotopic signal as water moves through the system (Leng and Marshall, 2004, Leng *et al.,* 2006) and these will now be discussed in turn as to how they can alter the $\delta^{18}O$ of precipitation, recharge waters and lake waters (Figure 4.3). The potential influence of detrital contamination will also be discussed.

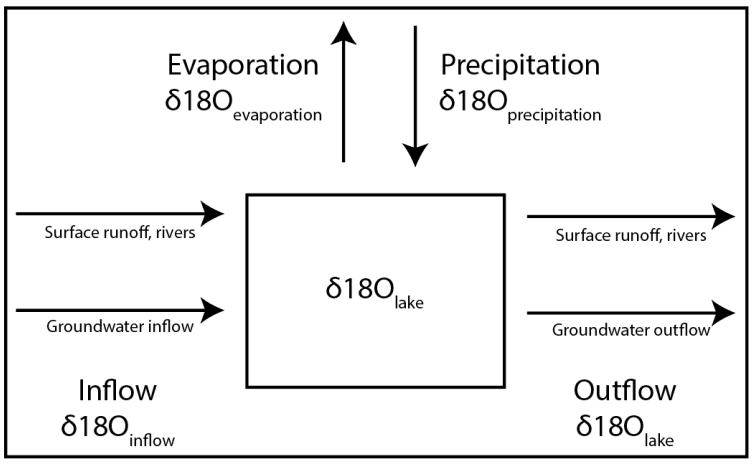

Figure 4.3, Schematic of the environmental factors that control the $\delta^{18}O$ of lake water and therefore the $\delta^{18}O$ of the $CaCO_3$ precipitate (after, Bernasconi and McKenzie, 2007).

4.3.1 $\delta^{18}O$ of precipitation

The $\delta^{18}O$ of meteoric water can be influenced by the $\delta^{18}O$ of the source water, the distance between the moisture source and the site of precipitation, the seasonality of precipitation and the amount effect. The effect each of these factors have on the $\delta^{18}O$ of rainfall will be discussed below.

$\delta^{18}O$ of source water and distance from source

The isotopic composition of precipitation will strongly reflect the isotopic composition of the source of the water, i.e., isotopic composition of the ocean water and will also be altered by the isotopic composition of any water bodies it may encounters along its pathway (McKenzie and Hollander, 1993). Over long timescales of glacial/interglacial cycles, the $\delta^{18}O$ of sea water

evolves as the ^{16}O is stored in glaciers and icecaps, causing the ocean to be enriched in ^{18}O (Shackleton and Opdyke, 1973, Darling *et al.,* 1997; Rozanski *et al.,* 1997). As the LGIS is a relatively short time period no large changes in the $\delta^{18}O$ of source water are thought to have occurred. However, changes in the thermohaline circulation, due to the influx of cold glacial meltwater into the north Atlantic, are thought to be responsible for millennial-scale abrupt cooling events such as the Loch Lomond Stadial (GS-1) during the Lateglacial (see section 2.4.1). This may produce changes in the proportion of more northerly or southerly waters in the Atlantic and this may have an impact on surface water $\delta^{18}O$ values (e.g., Muschitiello *et al.,* 2015).

Water molecules which contain the heavier oxygen isotope, ^{18}O, will be preferentially rained out from the air mass, leading to enriched rainfall falling out of a progressively depleted air mass (Talbot, 1990; Rozanski *et al.,* 2003). Therefore, as the air mass moves away from its source, it can give the appearance of cooler temperatures because the ^{18}O value of the rainfall will decline (Rozanski *et al.,* 1997; 2003). In coastal areas, the isotopic composition of the first rainfall event is closer to that of the ocean, however, as the air mass moves further away e.g., into continental Europe, the $\delta^{18}O$ of precipitation decreases by 0.002 ‰ per km (Rozanski *et al.,* 1993). As the longitudinal length of the British Isles is relatively short, the distance of the airmass from source is not thought to be a major issue in interpreting the $\delta^{18}O$ from palaeorecords.

Seasonality of precipitation

Changes in the relative contribution of rainfall from different seasons can alter the $\delta^{18}O$ of lake water and lacustrine carbonates. Temperature changes between different seasons i.e., winter and summer, can be nearly as large as those experienced during abrupt cooling events. A change in the season in which precipitation falls can therefore heavily affect the $\delta^{18}O$ of rainfall and therefore the $\delta^{18}O$ of lake water, which can give a false impression of mean annual temperature change (Candy *et al.,* 2015). Candy *et al.,* (2015) attributed a change in the seasonality of precipitation to be the cause of shifts to more negative $\delta^{18}O$ values seen in many early Holocene records from the British Isles (Figure 4.4). In this model the climate changed from being continental in nature, dominated by summer convectional rainfall enriched in ^{18}O to a more maritime climate dominated by cyclonic winter rainfall depleted in $\delta^{18}O$. If an isotopic shift is driven by such a change, then it is recording a change in the seasonality of rainfall rather than any change in temperature.

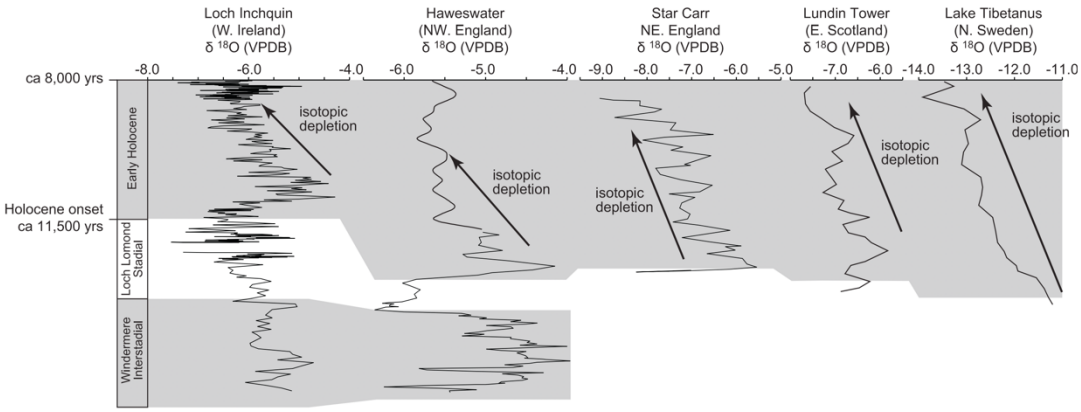

Figure 4.4, Comparison of early Holocene $\delta^{18}O$ records from Britain (Marshall et al., 2002, 2007; Whittington et al., 1996, Ireland (Diefendorf et al., 2006, 2008) and Sweden (Hammarlund et al., 2002) all displaying a consistent shift to more depleted $\delta^{18}O$ values *d*uring the early Holocene (from Candy et al., 2015).

Amount effect

The amount effect was noted by Dansgaard (1964) in which rainfall events with higher precipitation led to more negative $\delta^{18}O$ values while smaller rainfall events lead to more positive values. This is due to evaporation from the cloud base and the falling precipitation (Rozanski *et al.,* 1993). During periods of low rainfall amounts, evaporitic enrichment of precipitation is more effective though the preferential removal of ^{16}O, while during periods of high rainfall, evaporitic enrichment is less effective and leads to lower $\delta^{18}O$ values (Rozanski *et al.,* 1993). The amount effect phenomena, however, is thought to have little effect in mid-latitude temperate regions such as the British Isles and only has a significant effect in areas with exceptionally high rainfall such as in the low latitude tropics.

4.3.2 $\delta^{18}O$ of recharge waters

Precipitation can enter a lake basin and recharge lake waters through several pathways, and by varying amounts e.g., directly from precipitation, surface runoff, and from ground water (Darling *et al.,* 2003). Most lakes in the mid-latitudes derive their water from ground water, either by direct recharge through phreatic water, or by inflowing rivers and streams which are maintained by groundwater (Bernasconi and McKenzie, 2011). Therefore, an understanding of how water recharges lake basins is required as potential modification of the $\delta^{18}O$ signal can occur during the recharge process and may be of different magnitudes for different pathways. Once fallen, precipitation percolates through soils and bedrock into the underlying aquifer and ground waters (Andrews, 2006). The mixing of waters that occurs during groundwater recharge causes any seasonal variations that occur in the $\delta^{18}O$ of precipitation to be averaged out, resulting in the $\delta^{18}O$ of groundwater to be an average of the $\delta^{18}O$ of annual rainfall (Darling *et*

al., 2003; Darling, 2004; Candy *et al.,* 2011). Therefore, the $\delta^{18}O$ of recharge waters is a reflection of the mean weighted isotopic composition of rainfall, which in turn is controlled by temperature. It should be noted, however, that in these situations the $\delta^{18}O$ signal of the lake carbonates reflects "average" annual temperature even though the carbonate precipitates in the summer months.

4.3.3 $\delta^{18}O$ of lacustrine waters

A very important factor to consider when interpreting the $\delta^{18}O$ of freshwater carbonates is the hydrology of the lake basin in which they form. Two types of lakes are recognised, hydrologically 'closed' or 'open' lakes, however, these are the extremes of a continuum of hydrological types (Table 4.1; Leng and Marshall, 2004)

Basins with a closed hydrology are generally large with water that has a long residence time as they have no outflow, meaning water only exits through seepage and/or evaporation. Hydrologically closed basins have a high evaporation to precipitation ratio leading to isotopic fractionation in favour of the loss of $H_2{}^{16}O$ and therefore an increase in the $\delta^{18}O$ of the lake water. Concurrently, evaporation reduces the volume of the lake water, which reduces the solubility of CO_2 causing degassing, which also increases the $\delta^{13}C$ of DIC (Talbot, 1990; Leng and Marshall, 2004). A basin with greater evaporation than precipitation therefore leads to increases in both $\delta^{18}O$ and $\delta^{13}C$ which may cause isotopic covariance, and so can be used as an indicator of hydrological closure, although this is not a universal trend and some closed lake basins can show no evidence for isotopic co-variance (Talbot, 1990).

Basins that have an open hydrology have an inflow and outflow of water and a much shorter residence time, therefore there is less opportunity for isotopic modification by evaporation to occur. The $\delta^{18}O$ of open lake systems are therefore more likely to retain the $\delta^{18}O$ of precipitation which is primarily controlled by air temperatures (Dansgaard, 1964; Rozanski *et al.,* 1993). Open lake systems therefore generally shows weak or no co-variance at all (Talbot, 1990; Leng and Marshall, 2004). There are however two complications to this. Firstly, the size of basin needs to be considered as a lake that has a large volume of water relative to its annual recharge water flow may be affected by evaporation even though it is an open system. This may cause evaporitic modification of the $\delta^{18}O$ signal without showing evidence for isotopic co-variance. Smaller lakes with relatively high recharge rates are less likely to be affected by evaporation and, therefore, the $\delta^{18}O$ of the lake water is more likely to record that of

precipitation (Pearson and Coplen, 1978). Relatively small lakes in temperate regions that have short water residence times of less than a few years, therefore, enables them to record rapid changes in isotope composition of rainfall and, therefore, air temperature through preserving the $\delta^{18}O$ of rainfall in their waters (Leng and Marshall, 2004). Secondly, it is important to understand how regularly/rapidly a water body is recharged by groundwater and other sources as this can determine how susceptible it is to isotopic modification (Darling *et al.,* 2003).

Lake-water volume	Very small	Small-medium open lakes	Small-medium closed lakes	Large
Residence time	<1 yr ('open lake')	≥1 yr	10's yrs	100's yrs ('closed' lake)
Predominant forcing	*S, T, δp*	*T, δp*	*P/E*	*P/E*
$\delta^{18}O$ ranges through the Holocene	Often -ve values, Small range of 1-2 ‰, larger range if materials precipitated in different seasons	Often -ve values, small range of 1-2 ‰	-ve to +ve values, large swings (5 to >10 ‰)	+ve values, subdued signal homogenised by buffering of large lake volume
Examples	Lake Abisko (SWE) (Shemesh *et al.,* 2001)	Hawes Water (UK) (Marshall *et al.,* 2002) Amersee (GER) (Von Grafenstein *et al.,* 1999a, b)	Greenland lakes (Anderson and Leng 2004), Lake Tilo (ETH) (Lamb *et al.,* 2000)	Lake Turkana (KEN) (Ricketts and Anderson 1998).

Table 4.1, Summary of lake features and the resulting predominant forcing likely to be driving changes in the oxygen isotope record (After Leng and Marshall, 2004).

4.3.4 Other potential influences on $\delta^{18}O$

The inwashing and mixing of detrital carbonate with endogenic carbonate can result in the contamination of the isotopic signature as it is frequently difficult to physically or chemically separate these two end members. Detrital contamination from geological carbonate can sometimes be detected by co-variance analysis between $\delta^{13}C$ and $\delta^{18}O$, as geological carbonate was often precipitated in marine environments which typically has a different carbon and oxygen isotopic signature to that of lake carbonates. When such material washed into the lake, it does not go through the process of fractionating carbon and oxygen atoms and so geological material retains its initial signature. Samples that contain varying proportions of endogenic and geological carbonate will, therefore, express a linear relationship on a plot of $\delta^{18}O$ and $\delta^{13}C$. Another test for this is if $CaCO_3$ is not present in sediments deposited during periods of high erosion and low authigenic $CaCO_3$ production e.g., the Loch Lomond stadial. If the catchment doesn't yield carbonate when it is most susceptible to erosion then it is often considered unlikely that geological carbonate will be reworked during warmer climates when marl development is abundant, e.g., the Lateglacial Interstadial and Holocene. Detrital biological carbonate, i.e. ostracods and mollusc shells, is also an issue as the $\delta^{18}O$ of this material can

often different from that of lake marl, due to vital effects, by up to 3‰ (Keatings *et al.,* 2002). It can be difficult to remove detrital carbonate from geological and biological sources, although routinely sieving samples at 63µm can remove many allogenic and biological components as these are generally coarser than endogenic precipitated marl.

4.4 The application of oxygen isotopes in reconstructing palaeo climatic temperatures

4.4.1 Ice cores

In the early 1950's, Dansgaard investigated the stable isotopic composition of frontal precipitation over Copenhagen, Denmark, and proposed that stable isotopic analysis could be conducted on Greenland ice cores (Dansgaard, 1954). In 1961, Dansgaard studied the effect latitude has on the isotopic composition of precipitation in Greenland and the strong correlation between mean annual temperatures and isotopic values of the ice cap (Dansgaard, 1961). He used the Rayleigh condensation model to improve the understanding of the physics behind how climate information is contained within natural precipitation (Vinther and Johnsen, 2007).

Dansgaard's work ultimately laid the foundations for stable isotope analysis of deep ice cores from Greenland (Figure 4.5a & b) including cores from Camp century (Dansgaard *et al.,* 1969), DYE-3 (Dansgaard *et al.,* 1982), GRIP (Johnsen *et al.,* 1992; Dansgaard *et al.,* 1993; GRIP members, 1993), GISP2 (Grootes *et al.,* 1993; Taylor *et al.,* 1993; Meese *et al.,* 1994; Alley *et al.,* 1997), NGRIP (NGRIP members, 2004; Rasmussen *et al.,* 2008) and NEEM (NEEM community members, 2013). Similarly, deep ice cores have been retrieved from Antarctica, e.g., Vostok (Jouzel, 1987; Petit *et al.,* 1999), Dome C (EPICA members, 2005; Masson-Delmotte *et al.,* 2010) and from numerous glaciers and ice fields from around the world (e.g., Thompson *et al.,* 2002).

4.4.2 Terrestrial carbonates

Since their application in the Greenland ice cores, stable isotopes have been applied to a range of terrestrial carbonate precipitates including speleothems (Bar-Matthews *et al.,* 2010; Duan *et al.,* 2014) and freshwater carbonates (e.g. Leng and Marshall, 2004; Marshall *et al.,* 2006) as well as directly on the fossil remains of aquatic fauna including Ostracods (e.g., Holmes, 1992; Von Grafenstein *et al.,* 1999), Diatoms (e.g., Cartier *et al.,* 2019) and chironomids (e.g., Wooller *et al.,* 2004; Verbruggen *et al.,* 2010; Lombino *et al.,* 2021a, b). Some examples of $\delta^{18}O$ records covering the LGIS from lacustrine carbonate sequences in Europe are displayed in

figure 4.6, along with accompanying chironomid T_{Jul} records from the sites. The strong degree of similarity between the $\delta^{18}O$ and T_{Jul} records adds support to the argument that $\delta^{18}O$ is a reliable proxy for identifying past temperature changes. Discrepancies between $\delta^{18}O$ and T_{Jul} can be explained in part by the different aspects of temperature they record, i.e., with T_{Jul} representing changes in summer temperature and $\delta^{18}O$ as changes in mean annual temperature (MAT) (e.g., Lotter *et al.,* 2012).

Figure 4.5, Greenland δ18O records. a) location of deep ice cores in Greenland; b) δ18O records from the deep ice cores in Greenland covering the Early Holocene, last glacial and the Eemian. Numbers next to the δ18O records denote prominent interstadials (from Vinther and Johnsen, 2007).

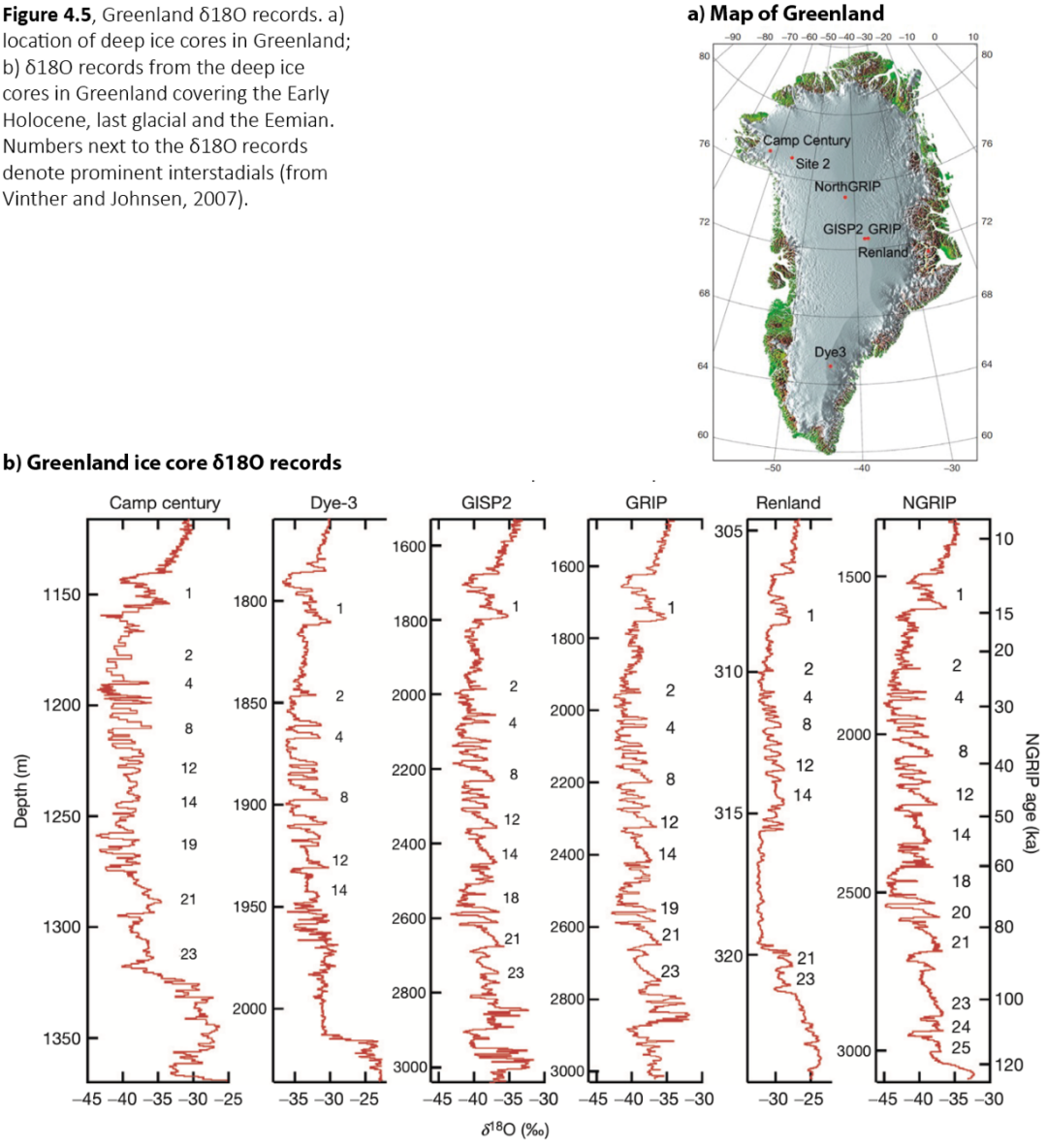

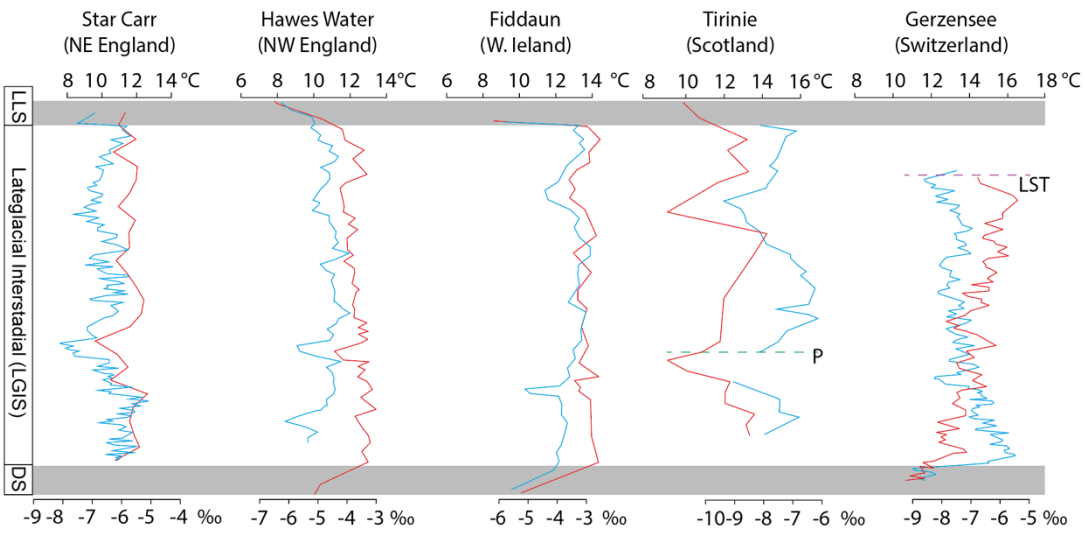

Figure 4.6, Select sites which have both T_{Jul} and $\delta^{18}O$ records covering the LGIS. References for sites can be found in Tables 2.3 and 2.4.

4.4.3 Justification of $\delta^{18}O$ as a temperature proxy

Despite the range of other factors that can modify the isotopic signal outlined in section 4.3, oxygen-isotopes from lacustrine bulk sediments offer a good broad match with isotopes curves from Greenland ice cores (Candy *et al.,* 2016), T_{Jul} reconstructions (Brooks and Birks, 2000) and Coleopteran mutual climatic range estimates (Atkinson *et al.,* 1987; Coope *et al.,* 1998). In these sequences and during these time intervals temperature is a key driver of $\delta^{18}O$ changes at every stage of isotopic fractionation in one aspect or another (Dansgaard, 1954, 1961). A large number of studies have shown that the $\delta^{18}O$ of rainfall in the mid-latitudes is strongly correlated to air temperature (Rozanski *et al.,* 1993; Andres, 2006; Candy *et al.,* 2015) and that the response of isotopes in rainfall to temperature change is rapid without any major delay (Wright, 1984). Moreover, these other environmental factors that can affect the $\delta^{18}O$ signal discussed in section 4.3, are not necessarily a 'problem' as they can reveal other dimensions of past climatic changes when used in conjunction with other proxies such as chironomids.

4.4.4 Advantages of using oxygen isotope as a proxy

There are several advantages of using the stable isotopes of oxygen to investigate the abrupt cooling events of the Lateglacial interstadial. Firstly, there is minimal lag between changes in atmospheric temperature and corresponding change in the $\delta^{18}O$ of rainfall (Candy *et al.,* 2016) as they rely on physical processes of Rayleigh distillation dictated by the laws of physics (Leng and Marshall, 2004). Many other proxies rely on biological responses and process, which can add uncertainty in the reconstruction as they over/underestimate or delay the response to the

climate parameter being reconstructed. Secondly, a strong linear relationship exists between air temperature and the isotopic composition of rainfall and provides a semi-quantitative proxy integrated within the sediment itself (Leng and Marshal, 2004). Thirdly, a very small amount of sediment is needed for stable isotope analysis meaning the technique can be applied at a high sampling resolution (i.e., 0.5cm) and can also be easily conducted in conjunction with other proxy analyses. The combination of the above three points makes oxygen isotopes an ideal proxy for studying abrupt climatic changes.

4.5 Environmental influences on $\delta^{13}C$ in lake waters

The $\delta^{13}C$ of lacustrine precipitated carbonate is controlled by the $\delta^{13}C$ of dissolved inorganic carbon ($\delta^{13}CDIC$) in lake water. This, in turn, is primarily controlled by biological and chemical processes, i.e., photosynthesis and gaseous exchange of CO_2 between lake water and the atmosphere, see Figure 4.7 (Leng and Marshall, 2004). The isotopic fractionation of $\delta^{13}C$ in dissolved inorganic carbon is only weakly temperature dependant and so has little use as a palaeotemperature proxy (Bernasconi and McKenzie, 2007; Leng and Marshall, 2004), however, understanding the processes that cause changes in $\delta^{13}C$ can aid the palaeoenvironmental interpretation of the sequence.

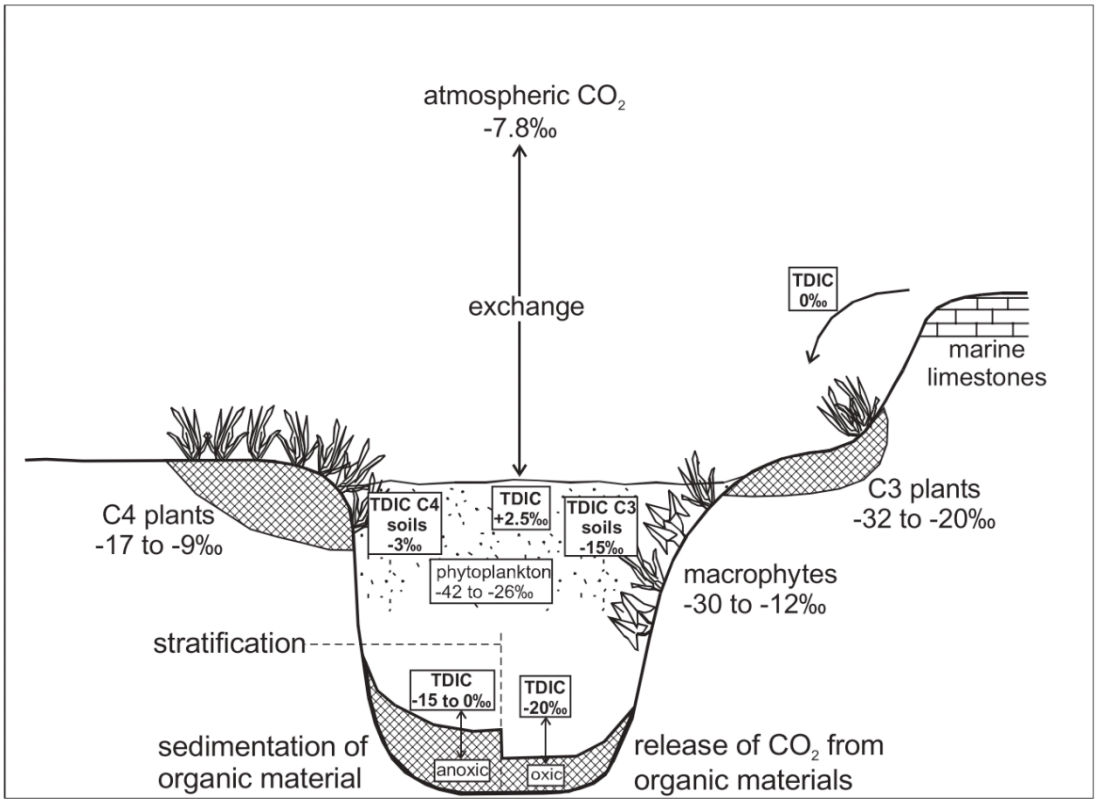

Figure 4.7, Diagram displaying the main sources of carbon for lakes with example $\delta^{13}C$ total inorganic carbon ranges (TIDC). (From Leng and Marshall, 2004).

4.5.1 Lake Catchment processes and inflowing water

The $\delta^{13}C$ of total dissolved inorganic carbon (TDIC) component of the recharge water which enters the lake is determined by the relative contributions of carbon from geological sources and carbon derived from soils and vegetation (Cerling and Quade, 1993). During periods when vegetation in the lake and catchment is low, i.e., during stadials and glacials, carbon is mainly sourced from geological carbonates and atmospheric carbon dioxide. Geological carbonates were often deposited in marine environments and have a $\delta^{13}C$ values of between -3 and +3, which is reflected in the $\delta^{13}C_{DIC}$ of groundwater when predominately derived from geological sources (Andrews *et al.,* 1997; Leng and Marshall, 2004). During warmer climates, i.e., interstadials and interglacials, the $\delta^{13}C$ value of DIC typically becomes lower as the proportion of carbon derived from geological sources declines relative to the input of soil respired CO_2 from vegetation that develops on the surrounding landscape, which is enriched in the isotopically lighter $^{16}CO_2$ (Cerling and Quade, 1993; Andrews, 2006). Photosynthesis causes significant fractionation in carbon isotopes resulting in plant material, and plant respired CO_2, having significantly more negative isotope values than atmospheric and geological carbon (Cerling and Quade, 1993; Andrews, 2006). In temperate settings such as Britain, the landscape is largely dominated by plants that utilise the C3 photosynthetic pathway which have $\delta^{13}C$ values of -24 to -30 ‰ (Cerling and Quade, 1993). The more isotopically depleted CO_2 in the soil zone will be taken up by percolating water during groundwater recharge (Andrews, 2006). As the gaseo$^{18}OCO_2$ becomes dissolved in the percolating water, fractionation of the opposite direction occurs of around +14 ‰ (Cerling and Quade, 1993), causing the overall $\delta^{13}C$ of ground water to be around -12 to -10 ‰ (Candy *et al.,* 2011). A decline in $\delta^{13}C$ is often seen in lacustrine carbonate isotope records that span climatic ameliorations, i.e., the LGIS (Figure 4.8; Candy *et al.,* 2016) and the early Holocene (Figure 10; Candy *et al.,* 2015), as the $\delta^{13}C$ of the lake water DIC becomes increasingly negative due to recolonisation of the landscape by temperate climate vegetation.

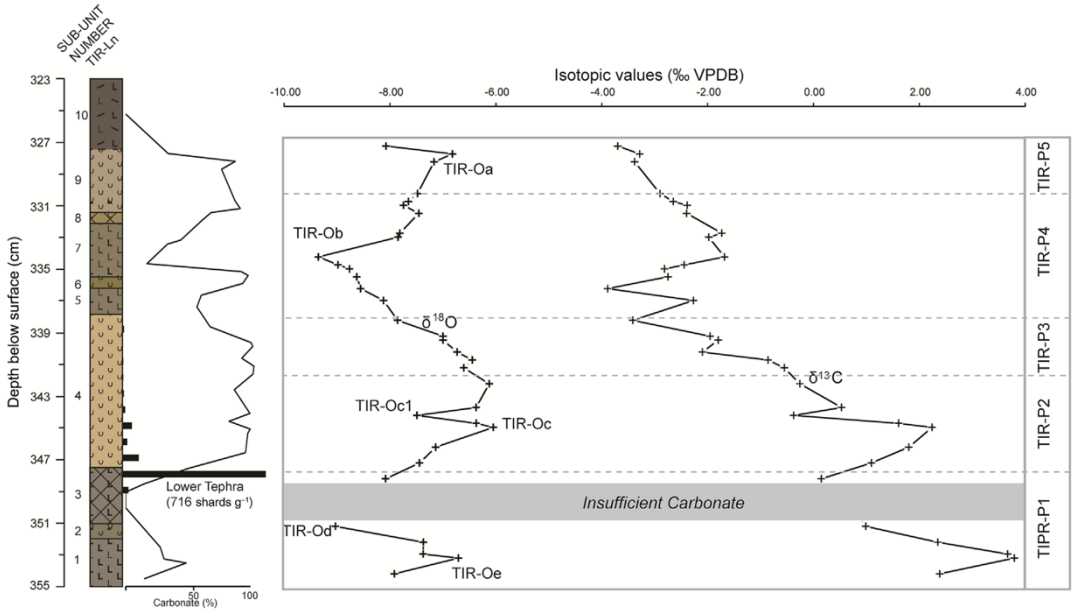

Figure 4.8, Declining trend in $\delta^{13}C$ at Tirinie during the LGIS attributed to enhanced terrestrialisation (from Candy et al., 2016).

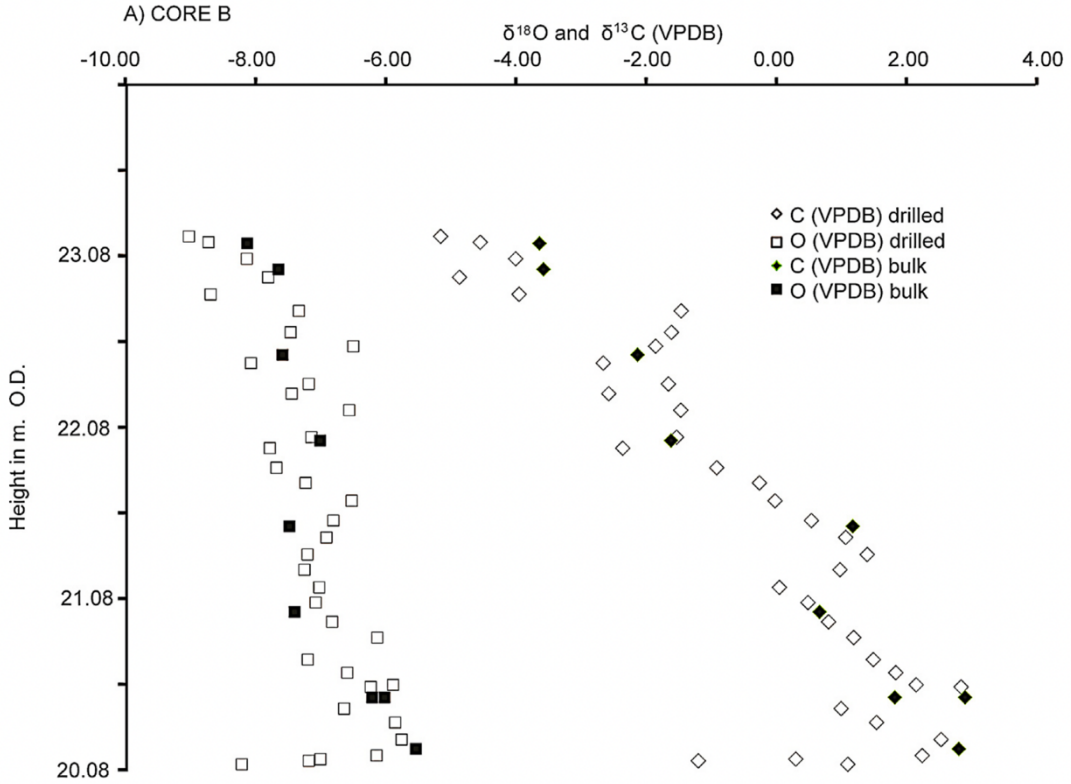

Figure 4.9, Declining trend in $\delta^{13}C$ at Star Carr during the early Holocene attributed to enhanced terrestrialisation (from Candy et al., 2015).

4.5.2 Within lake processes

When recharge water enters the lake basin, it begins to equilibrate with atmospheric CO_2 (Leng and Marshall, 2004; Usdowski and Hoefs, 1990)). The extent to which lake water DIC can equilibrate with atmospheric CO_2 depends on the residence time of the water. Waters with very short residence times, i.e., rivers, tufas and ponds/small lakes with rapid inflow and outflow, do not typically allow complete equilibration. Consequently, the $\delta^{13}C$ of carbonates formed in such environments as very similar to the $\delta^{13}C$ of the soil environment and soil carbonates (Andrews, 2006). In water bodies with long residence times complete equilibration is possible, this is typical in lakes where the rate of inflow and outflow is low relative to the size of the water body (Leng and Marshall, 2004). In a lake that has achieved equilibrium with atmospheric CO_2, which has a pre-industrial $\delta^{13}C$ value of *c.* -8 ‰, lake water $\delta^{13}C$ would be between -3 and +3 ‰ (Leng and Marshall, 2004). In closed system lakes the effect of evaporation on water body volume and CO_2 degassing may result in lake carbonate with $\delta^{13}C$ values that are much greater than this, but such processes can typically be identified by a strong degree of co-variance between $\delta^{13}C$ and $\delta^{18}O$.

4.6 Chapter Summary

The above review of how the stable isotopes of oxygen and carbon can be used as proxies for reconstructing past environments are highlighted in the following key points:

- The $\delta^{18}O$ of freshwater lacustrine carbonates in mid-latitude regions, such as the British Isles, often reflects the $\delta^{18}O$ of precipitation which is primarily controlled by temperature.

- As oxygen isotopes rely on the physical processes of Rayleigh distillation, which is dictated by the laws of physics, there is minimal lag between atmospheric temperature changes and subsequent changes in the $\delta^{18}O$ of rainfall, making $\delta^{18}O$ an ideal proxy to investigate ACEs.

- Factors other than temperature can also influence the $\delta^{18}O$ of lacustrine carbonates and need to be taken into consideration when interpreting $\delta^{18}O$ records. These include the $\delta^{18}O$ of precipitation (e.g., source water $\delta^{18}O$, seasonality of precipitation, the amount effect), the $\delta^{18}O$ of recharge waters, the $\delta^{18}O$ of lacustrine waters (e.g., lake basin hydrology) and non-precipitated carbonate components (e.g., geological carbonate, Ostracod valves, mollusc shells).

- Analysis of the co-variance between $\delta^{18}O$ and $\delta^{13}C$ can help understand the nature of the lake basin hydrology, identify periods where the lake basin hydrology may have become 'closed' with the isotopic signal affected by evaporitic enrichment, as well as potential contamination of the isotopic signal by detrital carbonate.

- Assuming the same hydrological conditions occurred in the past, $\delta^{18}O$ can be used as a semi-quantitative proxy for climatic temperature changes, though caution is needed due to the other environmental factors which could alter the $\delta^{18}O$ signal.

- In cases where oxygen isotopes records reflect changes in mean annual temperature (MAT) and are analysed in conjunction with chironomid-inferred mean July air temperatures (T_{Jul}), temperature changes in different seasons can be investigated.

- The $\delta^{13}C$ of lacustrine carbonates record a more local signal and primarily reflect changes in the catchment as well as lake productivity.

Chapter 5: Methodology

Chapter overview

This chapter will: (i) set out the criteria used to select the study sites; (ii) outline the field methods employed in the retrieval of sediment cores and construction of composite sequences; (iii) layout the laboratory methods used to analyse the different proxies around which this research is based; and (iv) outline the numerical and statistical analyses performed on the proxy data generated. A larger focus is placed on the chironomid methodology as this is the primary technique used in this study. In particular, multiple chironomid sample preparation procedures were tested and are described in detail, as standard methods proved ineffective in releasing a sufficient number of Head Capsules (HCs) in a clean identifiable state. Some techniques were undertaken by people other than the author and are duly acknowledged in an overview at the end of the chapter.

5.1 Site selection criteria

Sites were selected for inclusion in this study based on four main criteria. Firstly, that they lie beyond the current geographical range of existing LGIS chironomid/isotope records found within the British Isles. This is to increase the spatial coverage of records in order to investigate climatic gradients. Secondly, the sequences must be carbonate rich across most of the interstadial for stable isotope analysis to be carried out. Thirdly, the sequences must have experienced higher sedimentation rates to provide adequate stratigraphic resolution. Finally, the sequences must offer the potential for the construction of robust independent chronologies so that the magnitude of climatic events can be compared between localities.

Based on these criteria, three sites were selected for study including Crudale Meadow in Orkney, North Scotland, Llangorse Lake situated in the Brecon Beacons, South Wales and Old Buckenham Mere in East Anglia, SE England (Figure 5.1). A fourth site in Ireland, Tory Hill in County Limerick, was initially planned for investigation, however, due to COVID-19 related travel restrictions, fieldwork to collect new core material could not take place. A replacement Irish site, White Bog in Northern Ireland, for which sediment cores were already stored at the Department of Geography, RHUL, was subsequently selected. Unfortunately, continued restricted access to laboratories due to the COVID-19 pandemic meant the White Bog sequence could not be studied either.

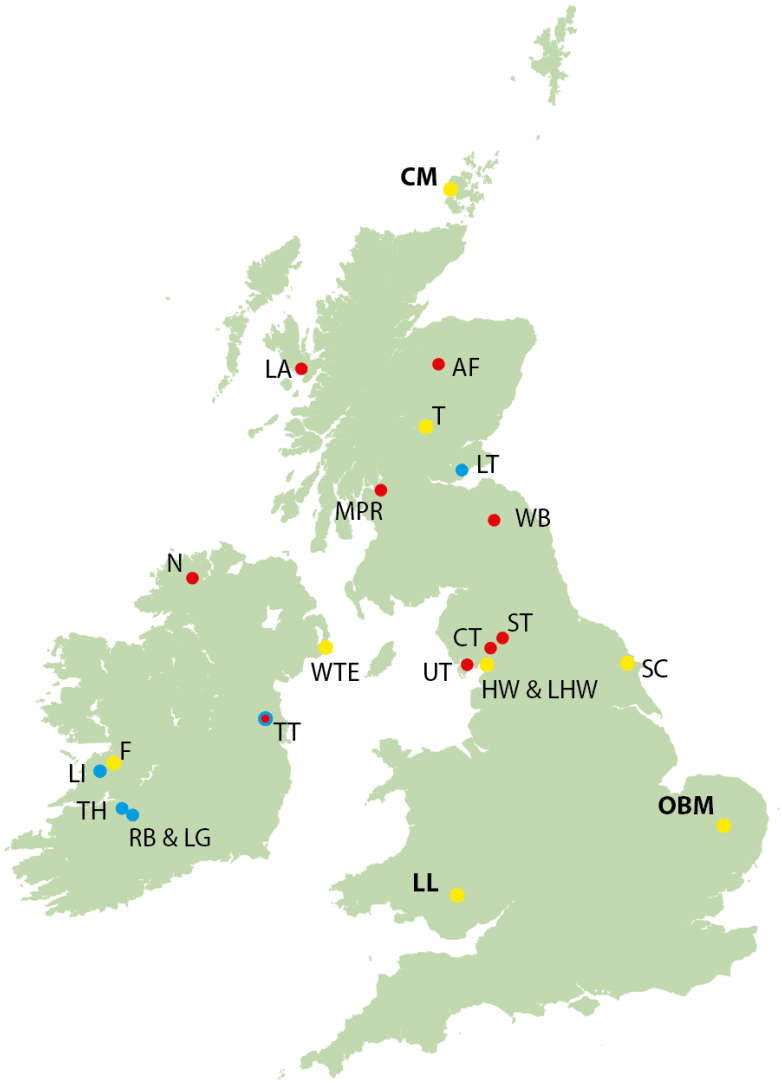

Figure 5.1, Map of sites with T_{Jul} (red circles) and $\delta^{18}O$ (blue circles) records from the British Isles. Sites which have both T_{Jul} and $\delta^{18}O$ records are represented by yellow circles. Those in bold are the selected new sites for which T_{Jul} and $\delta^{18}O$ reconstructions have been created during this PhD.

5.2 Field Methods and sequence selection

The sites of Crudale Meadow and Llangorse were cored prior to this PhD study as part of other research projects focussed on LGIT climate dynamics. The methods employed at these sites will be discussed briefly. New cores were collected from Old Buckenham Mere for this thesis and will be discussed in greater detail. All the selected study sites were cored using manual Russian corers of 50cm and 100cm in length (Jowsey, 1966). This was chosen over mechanical coring devices which can cause the sediments to become disturbed due to the intense vibrations. Cores were taken from alternating bore holes, overlapping with the previous core section, to ensure complete retrieval of continuous sediment sequences. The location of coring, bathymetry surveys and amount of core overlap varied between the study sites and are

explained in further detail below. Some sites had more than one sequence available for the study and justification of the selected sequences is also discussed.

5.2.1 Crudale Meadow

Crudale Meadow (59°00'44" N 3°19'57" W) was cored in 2016 by a team from the Centre for Quaternary Research to support Dr Rhys Timms' PhD research. No bathymetric survey was conducted at the site as the immediate objective was to retrieve a replicate core of the material recovered by Whittington *et al.* (2015). Timms *et al.* (2018), therefore cored in approximately the same location and retrieved the composite CRUM1 sequence which included sediments from the Dimlington Stadial, LGIS, LLS and Early Holocene. Other cores were recovered in an attempt to identify deeper and therefore expanded Lateglacial sequences, but the chronological work undertaken on CRUM 1 meant that this core was favoured for the continuity of the proxy work such as chironomid and isotopic analysis.

5.2.2 Llangorse

Llangorse lake (51°56'12" N 3°16'15" W) and the vicinity has been extensively cored over the past *c.* 10 yrs by members of the CQR, led by Dr Adrian Palmer, in order to further refine the timing of LGM ice retreat. The bathymetry of the extant lake and infilled lake margins are therefore well known (Palmer et al., 2021). The extant lake bathymetry was measured using a Uwitec echosounder in order to relocate the deepest parts of the basin that had been cored previously (Jones et al., 1978, 1983). It was hoped the deep-water cores would contain a continuous sequence of Lateglacial and Holocene sediments as the previous sequence retrieved from the Crannog were missing LGIS and LLS sediments (Walker *et al.,* 1993). Deep-water cores were retrieved from the central basin (LLA) and the south basin (LLAS) but were stratigraphic compressed with less than 30 cm representing the LGIS (Palmer *et al.,* 2021). The sequence selected (LLAN14) was from the shallower infilled northern basin (LLAN) and had been surveyed using Russian core depth measurements at 14 locations (Palmer *et al.,* 2021). The LLAN14 sequence was selected because the LGIS deposits were stratigraphically expanded, covering at least one metre, and would have been deposited in approximately 6 m of water depth, limiting the potential influence of bottom water anoxia on chironomid distribution and abundance. As part of the broader project, other lithological and palaeoecological analyses have been applied and geochronological investigations have focussed on radiocarbon dating and tephrochronology.

5.2.3 Old Buckenham Mere

Old Buckenham Mere (52° 29’ 18” N 1°00’59” E) was cored in April 2019 by the author with help from members of the CQR and family members. Little was known about the true depth of the basin as the site had not been studied for over half a century. The only study to investigate the basin bathymetry was by Tallantire (1953a) and their exploratory North-South transect had a large un-cored area in the central portion of the basin as it was flooded during their field campaign. This study set out to replicate the North-South transect of Tallantire (1953a) and improve the density of depth soundings for the central part of the transect using a Dutch Gouge. A second transect running East-West was also attempted but time constraints meant it was not completed. The results from our own bathymetry survey are combined with the results from Tallantire (1953a). Precise core locations were not given by Tallantire (1953a) and so our depth soundings have been incorporated using the local landscape features including the Mere itself, drainage channels and hedgerows. The deepest point of the basin was chosen to retrieve a complete sequence using the Russian corer as this had the thickest marl sediments and therefore provided the highest resolution for the LGIS possible. Two sequences, OBM-S2 and OBM-S3, were retrieved and combined to form a composite sequence for the site (OBM19). Core retrieval for OBM-S2 commenced at a depth of 7 m as the overlying Holocene sediments were not relevant to this PhD. One metre Russian cores were used down to 13.8 m, with 50 cm overlaps, however, below 1380 cm, 0.5 m Russian cores were used with overlaps of 10-20 cm. The basal metre of sediments at OBM-S2 could not be retrieved without significant contamination as the core chamber opened on ascent. A shallower coring location was therefore chosen, approximately 20 m north of OBM-S2 to retrieve the basal sediments of the sequence and named OBM-S3.

5.3 Laboratory Methods: Sedimentological techniques

5.3.1 Sediment description and imaging

In the laboratory, sediments were cleaned back using a scalpel to remove any potential contamination during core extraction. Sediments were classified using Troels-Smith (1955) for each individual core and colours were described using the Munsell Soil Colour system. The identification of stratigraphic units and sub-units were based on changes in sediment texture, colour and structure. These were used in the first instance to align the individual core sections to produce a continuous composite sequence.

Sediment cores were photographed using a Canon 600D or a Nikon D810 DSLR with a 105 mm macro lens supported by a Kaiser Copy Stand to ensure consistent frame alignment between photos and camera distance from the core. The cameras were set to manual mode and ambient light kept to a minimum, while cores were illuminated by florescent day lights mounted either side of the camera. Photos were taken with a 1cm overlap at either end and stitched together using Adobe Photoshop Creative Cloud. This provided a core archive of the pristine sediment surface before destructive analysis was undertaken.

5.3.2 Loss-on-ignition (LOI)

Loss-On-Ignition was used to give an approximation of the organic content present in the sediments for the CRUM1 sequence at 1 cm resolution as part of the tephra analysis by Timms *et al.* (2018) (Table 5.1). It is used as a proxy for landscape productivity, lake productivity and potential erosional events (Heiri *et al.,* 2001). 1 cm^3 of sediment were dried overnight at 105 °C to remove excess moisture before being combusted at 550 °C for 2 hrs to remove organic components (Heiri *et al.,* 2001). The disadvantage of this method is that such high temperatures can lead to structurally bonded water, volatile salts and inorganic carbon to be liberated causing an over-estimation of the organic content (Heiri *et al.,* 2001). However, the LOI method still has sufficient accuracy for our purposes.

Table 5.1, Loss-on-Ignition sampling strategy at Crudale Meadow.

Site	Depth	Resolution	Analyst
Crudale Meadow	595-652 cm	1 cm	Timms *et al.* (2018).

To express the Loss-on-ignition as a percentage, the following equation was used:

$$\%LOI = ([DW_{105} - AW_{550}]/DW_{105})*100$$

Where DW_{105} is the dry weight of the sediment after heating at 105 °C and AW_{550} is the ashed weight of the sample following combustion at 550 °C.

5.3.3 Total Organic Carbon (TOC)

A more accurate method of determining the organic component of sediment is using the Walkley-Black (1934) titration method. As with LOI, it can show the primary productivity of the water column, the level of soil development and plant growth within the catchment (Doyle and

Garrels, 1985). It may also reveal phases of slope erosion in the catchment (Mayle *et al.,* 1999). 0.2-0.5 g of finely crushed dried sediment was soaked in a mixture of potassium dichromate ($K_2Cr_2O_7$), sulphuric acid (H_2SO_4) and Phosphoric acid (H_3PO_4) followed by titration with a ferrous ammonium sulphate solution ($[NH_4]_2Fe[SO_4]_2{\cdot}6H_2O$). This method was applied to LLAN14 sequence at Llangorse by Palmer *et al.* (2021) with 1-2 cm resolution while the author undertook TOC measurements at OBM at 2 cm resolution (Table 5.2).

Table 5.2, Total organic carbon sampling strategy at Llangorse and Old Buckenham Mere.

Site	Depth	Resolution	Analyst
Llangorse	483-504 cm	2 cm	Palmer (2021)
	504-572 cm	1 cm	
	572-616 cm	2 cm	
	616-640 cm	1 cm	
Old Buckenham Mere	1208-1523 cm	2 cm	This Study

To present the TOC content of a sample as a percentage, the following equation was used:

$$\% \text{ TOC} = [(10 - (Vt*Mf)]*0.3*1.33/W$$

Where Vt is the volume of ferrous ammonium sulphate used during titration; Mf is the volume of ferrous ammonium sulphate solution used during titration of the blank; and W is the weight of the dried sample.

5.3.4 Calcimetry

Calcimetry was used to determine the amount of calcium carbonate ($CaCO_3$) within sediments and to give an indication of lake productivity, as precipitation of lake marl is partly the product of aquatic floral photosynthesis. Clear water is also needed for carbonate precipitation and therefore increased $CaCO_3$ levels can indicate decreased turbidity in the water column or increased stability within the catchment. $CaCO_3$content was determined using a Bascomb calcimeter (Gale and Hoare, 1991). 0.2-0.5 g of dried crushed sample was reacted with 10 % Hydrochloric Acid (HCl). The CO_2 emitted causes water displacement in the calcimeter which is directly proportional to the amount of $CaCO_3$ present in a sample. This was the primary parameter used to align sediment core sections due to its high level of precision and accuracy, as well as the presence of large identifiable changes in $CaCO_3$ throughout the sediment cores. The sampling strategy for the three study sites is displayed in Table 5.3.

Table 5.1, Calcium carbonate sampling strategy at Crudale Meadow, Llangorse and Old Buckenham Mere.

Site	Depth	Resolution	Analyst
Crudale Meadow	595-652 cm	2 cm	Timms *et al.* (2018)
	595-629 cm	1 cm	This study
	629-634 cm	0.5 cm	
	634-652 cm	1 cm	
Llangorse	483-640 cm	1 cm	Palmer (2021)
Old Buckenham Mere	1208-1523 cm	2 cm	This Study

To express the amount of $CaCO_3$ within a sample as a percentage, the following equation was used:

$$\% CaCO_3 = VpC/MT$$

Where V is the volume of carbon dioxide in cm^3 liberated during reaction with HCl; p is the barometric pressure in milligrams of mercury (mm Hg); C is a constant of 0.1605; M is the weight of the sample in grams (g); and T is the air temperature in Kelvin.

5.3.5 Magnetic susceptibility

Magnetic susceptibility is the ability of the sediments to be magnetised due to the presence of iron bearing mineral compounds (Dearing, 1999). It is frequently used as a proxy for erosion as erosive activity releases iron bearing compounds from bedrock and unconsolidated sediments. A Bartington MS2C core-scanning sensor was used with magnetic susceptibility recorded in $x10^{-5}$ SI units. Magnetic susceptibility was measured at 1 cm intervals for all records (Table 5.4) and was used to align cores during intervals of very low or absent $CaCO_3$ and LOI.

Table 5.2, Magnetic susceptibility sampling strategy for the study sites.

Site	Depth	Resolution	Analyst
Crudale Meadow	595-652 cm	1 cm	Timms (2018)
Llangorse	483-640 cm	1 cm	Palmer (2021)

Old Buckenham Mere	1200-1523 cm	1 cm	This Study

5.3.6 µ-XRF

The Old Buckenham Mere sequence was analysed using the Itrax™ Core Scanner at BOSCORF to generate a µ-XRF trace (Table 5.5). Since this was the first time that a possible LGIT sequence had been extracted from the site in 50 years, it was deemed necessary to acquire a rapid assessment of the lithological variability within the core and an initial indication of where key climatostratigraphic boundaries may exist using elemental analysis. µ-XRF core scanning data are recorded as peak area integrals and raw data normalised using kilo counts per second (kcps) to account for variations in µ-XRF intensities and reduce matrix effects (Jouve *et al.,* 2013). Selected elements were chosen to be reported (Si, Ti, Fe).

Table 5.5, µ-XRF sampling strategy for the study sites.

Site	Depth	Step-length	Count	Analyst
Old Buckenham Mere	1200-1523 cm	200 µm	30 s	This Study

5.4 Laboratory Methods: Chironomids

5.4.1 Sub-sampling strategy

A decadal-scale sampling resolution was employed in order to capture the full magnitude of abrupt temperature changes. The sub-sampling strategy for each site is displayed in Table 5.6. The sampling interval was adjusted between sites, so each sampling interval represented on average ~ 15-20 yrs. Sequences were sampled contiguously and samples were placed in Ziplock™ bags for ease of resampling with a minimum of every other sample being analysed.

Where preliminary runs of the chironomid-climate transfer function revealed notable changes in temperature, further samples were analysed to produce contiguous data points covering stratigraphic intervals of interest. Sequences were also sampled contiguously when HC concentrations were low in case samples needed to be combined to reach higher count sums. The onset of both the LGIS and the LLS were also sampled for completeness.

Table 5.6, Summary of Chironomid sampling strategy.

Site	Length of LGIS	Sampling intervals	Approx. Yrs per sample interval	Depths of analysed samples	Analyst
Crudale Meadow	50 cm	0.5 cm	*c.* 16 yrs/0.5 cm	LGIS onset: Contiguous LGIS: Every 2nd sample generally but contiguous between: 634.5 – 628 cm, 621.5 – 619 cm, 612.5 – 610 cm. LLS onset: Contiguous	This Study
Llangorse	130 cm	1 cm	*c.* 13 yrs/1 cm	LGIS onset: Contiguous LGIS: Early – contiguous, Mid – near contiguous, Late – every 2nd sample LLS onset: Contiguous (bar 2 samples)	This Study
Old Buckenham Mere	unknown	1 cm	*c.* 5 yrs/1 cm	Every 2nd sample	This Study

5.4.2 Sample preparation

Initially samples were treated using the method outlined in Brooks *et al.* (2007) with sediments disaggregated in 10 % KOH for 20 minutes at 75 °C. This, however, resulted in poor HC yields and long picking times as the marl sediment did not adequately breakdown. Therefore, several procedures using additional stages were trialled, each using the method by Brooks *et al.* (2007) as a 'base', to investigate if they released more HCs from the sediments (Figure 5.2). It should be noted that one alteration was made to the Brooks *et al.* (2007) method in which clay-rich samples were soaked in de-ionised water for 48 hrs to help reduce the strong cohesive forces between clay particles. The subsequent additional stages tested included reaction with 10 % HCl (Procedure 1), submersion in an ultrasonic bath (Procedure 2), and 'pre-picking' the sample prior to ultrasonic bath treatment (Procedure 3). The effectiveness of each procedure was judged quantitatively through the concentration of HCs attained and any compositional changes of the sample assemblages compared to the control. The effectiveness was also

determined qualitatively through the level of cleanliness/degradation of HCs, i.e., missing mandibles, tears, visibility of key identifying features. Summarised results can be found in the following section. The sample preparation procedures were tested on samples from different sediment types (marl-rich, minerogenic-rich and organic-rich) within each sequence where present, as indicated by the sedimentological analysis.

Following re-sieving, samples were transferred to a Bogorov sorting tray and chironomid HCs were handpicked using fine forceps under a Motic SMZ-168-BP stereo microscope at 25x magnification. Hydromatrix™ mounting medium was used with 8 mm diameter (#0) cover slips and identified using a binocular CX41 microscope at 400 X magnification. HCs were identified to the highest taxonomic resolution possible in accordance with Brooks *et al.* (2007), Rieradevall and Brooks (2001) and Wiederholme (1983).

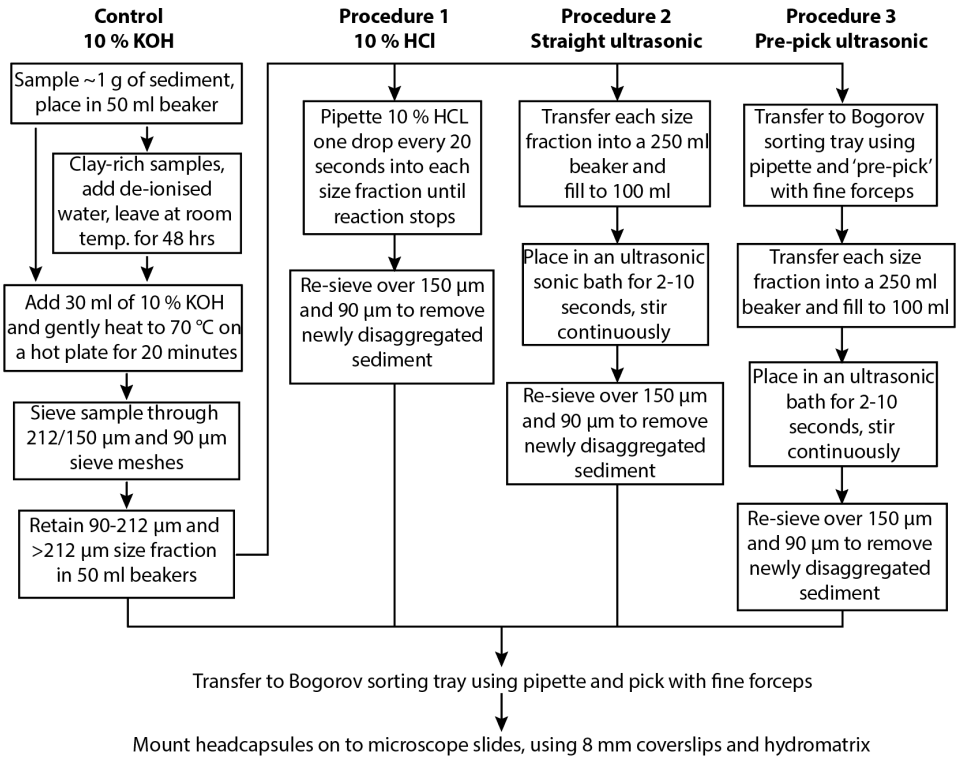

Figure 5.2, Flow chart of the different preparation procedures tested for chironomid samples.

5.4.3 Summary of sample preparation procedure test results

Below are summary tables of the preparation procedure tests conducted with taxa grouped into sub-family of tribal level classification for simplification. Raw HC counts were converted to concentrations for easier comparison between the preparation procedures.

Crudale Meadow

At Crudale Meadow, the chironomid preparation procedures were tested at two stratigraphic levels, one of which was marl-rich (616-616.5 cm; Table 5.7) and one minerogenic-rich (598-598.5 cm; Table 5.8). Due to the lack of $CaCO_3$ present in the LLS interval at Crudale Meadow, procedure 1 (HCL) was not tested. In both test samples, Procedure 3 (pre-pick ultrasonic) yielded the highest overall HC concentrations, increasing by 73 % for the minerogenic-rich sample and 33 % for the marl-rich sample. The texture of the marl was very fine and only required 3-5 seconds in the ultrasonic bath to achieve good disaggregation. Very little sediment remained in the sieves and greatly reduced picking time.

Procedure 2 (straight ultrasonic) did yield the most Tanytarsini HCs, however, this percentage increase is exacerbated by the very low numbers of Tanytarsini present. Similarly, the KOH control had the highest Orthocladiinae concentrations, though this is likely due to the sparse distribution of HCs within the sediment as a result of low Orthocladiinae concentrations overall. Procedure 3 (Pre-pick ultrasonic) was therefore selected to prepare the chironomid samples at Crudale Meadow.

Table 5.7, Crudale Meadow marl-rich sediment test sample (616-616.5 cm; $CaCO_3$ 81 %, LOI 5 %, Minerogenic 15 %). sample depth: Bold indicates the highest concentration of HCs yielded out of the tested procedures.

Procedure	Control (KOH)	Procedure 1 (HCl)		Procedure 2 (Straight Ultrasonic)		Procedure 3 (Pre-pick Ultrasonic)	
Taxon group	HC concentration	HC concentration	% change	HC concentration	% change	HC concentration	% change
Tanypodinae	24	12	-52	19	-19	**24**	**0**
Chironomini	38	8	-78	47	24	**50**	**31**
Tanytarsini	1	1	-3	**4**	**238**	1	0
Orthocladiinae	46	41	-10	49	8	**69**	**51**
Overall concentration	109	62	-43	119	10	**144**	**33**
HC Sum	100	59		130		133	
Sample Weight (g)	0.92	0.95		1.09		0.92	

Table 5.8, Crudale Meadow minerogenic-rich sediment test sample (598-598.5 cm; $CaCO_3$ 0 %, LOI 5 %, Minerogenic 95 %). Bold indicates the highest concentration of HCs yielded out of the tested procedures.

Procedure	Control (KOH)	Procedure 1 (HCl)		Procedure 2 (Straight Ultrasonic)		Procedure 3 (Pre-pick Ultrasonic)	
Taxon group	HC concentration	HC concentration	% change	HC concentration	% change	HC concentration	% change
Chironomini	2	N/A	N/A	6	263	**9**	**508**
Tanytarsini	3	N/A	N/A	14	388	**25**	**786**
Orthocladiinae	**4**	N/A	N/A	2	-58	2	-50
Diamesinae	0.0	N/A	N/A	**2**		1	
Overall concentration	22	N/A	N/A	23	8	38	73
HC Sum	20	N/A		26		35	
Sample Weight (g)	0.92	N/A		1.09		0.92	

Llangorse

At Llangorse, the chironomid preparation procedures were tested at three stratigraphic levels. Two of these levels were marl-rich (529-530 cm, Table 5.9; 552-553 cm, Table 5.10) and one minerogenic-rich (636-637 cm; Table 5.11). All three test samples yielded the highest HC concentrations using Procedure 3 (pre-pick ultrasonic), with overall concentrations increasing by 132% for 529-530 cm, 184 % for 552-553 cm and 92 % for 636-637 cm. Even after 5-8 seconds in the ultrasonic bath, there was still a notable amount of marl remaining in the sample, due to the coarse platy structure of the marl and additional time in the ultrasonic bath resulted in HC damage. This procedure meant picking time was not reduced to the same degree as the marl-rich test sample from Crudale Meadow, it was still advantageous with an increase in head capsule concentrations. It is also noted that a substantial increase in Cladocera remains following ultrasonic bath treatment was observed.

The largest decline in concentrations of 67 % was observed in the minerogenic-rich sediment sample under procedure 2 (straight ultrasonic). This is likely due to the agitation of the sharp clay particles by the ultrasonic bath (Lang, 2003) and the dominance of thick heavily chitinised HCs which are more brittle than thinner walled Orthocladiinae. Procedure 3 (Pre-pick ultrasonic) was therefore selected to prepare the chironomid samples at Llangorse.

Table 5.9, Llangorse marl-rich sediment test sample number 1 (529-530 cm; $CaCO_3$ 66 %, LOI 2 %, Minerogenic 32 %). *Pre-pick was not initially tested for this sample depth; however, the pre-pick procedure was conducted on a completely new sample. Unfortunately, no sediment remained for this sample depth and so neighbouring samples were analysed with the data presented for the level below, 530-531 cm. Bold indicates the highest concentration of HCs yielded out of the tested procedures.

Procedure	Control (KOH)	Procedure 1 (HCl)		Procedure 2 (Straight Ultrasonic)		Procedure 3* (Pre-pick Ultrasonic)	
Taxon group	HC concentration	HC concentration	% change	HC concentration	% change	HC concentration	% change
Tanypodinae	16	8	-49	16	-1	**33**	**107**
Chironomini	29	24	-18	24	-16	**65**	**126**
Tanytarsini	19	5	-77	23	20	**47**	**143**
Orthocladiinae	24	18	-25	28	15	**59**	**146**
Overall concentration	87	54	-38	90	3	**203**	**132**
HC Sum	101	54		90		231	
Sample Weight (g)	1.15	1		1		1.14	

Table 5.10, Llangorse marl-rich sediment test sample number 2 (552-553 cm; $CaCO_3$ 77 %, LOI 3 %, Minerogenic 20 %). *Pre-pick ultrasonic was not initially tested for this sample depth, however, the pre-pick procedure was conducted on a totally new sample which is included in the table above. Bold indicates the highest concentration of HCs yielded out of the tested procedures.

Procedure	Control (KOH)	Procedure 1 (HCl)		Procedure 2 (Straight Ultrasonic)		Procedure 3* (Pre-pick Ultrasonic)	
Taxon group	HC concentration	HC concentration	% change	HC concentration	% change	HC concentration	% change
Tanypodinae	14	20	40	23	58	**45**	**216**
Chironomini	6	11	78	7	12	**21**	**236**
Tanytarsini	20	8	-60	21	1	**56**	**174**
Orthocladiinae	28	22	-19	33	21	**73**	**163**
Overall concentration	68	61.	-10	83	22	**194**	**184**
HC Sum	67	68		85		198	
Sample Weight (g)	0.98	1.1		1.02		1.02	

Table 5.11, Llangorse minerogenic-rich sediment test sample (636-637 cm; CaCO3 13 %, LOI 0 %, Minerogenic 87 %). Bold indicates the highest concentration of HCs yielded out of the tested procedures.

Procedure	Control (KOH)	Procedure 1 (HCl)		Procedure 2 (Straight Ultrasonic)		Procedure 3 (Pre-pick Ultrasonic)	
Taxon group	HC concentration	HC concentration	% change	HC concentration	% change	HC concentration	% change
Chironomini	5	3.8	-24	1	-74	**9**	**86**
Tanytarsini	2.7	3.1	14	1	-52	**5**	**75**
Orthocladiinae	0.3	1.5	357	0.3	-4	**2**	**399**
Overall concentration	8.7	8.8	1	3	-67	**17**	**92**
HC Sum	13	12		5		25	
Sample Weight (g)	1.5	1.31		1.57		1.5	

Old Buckenham Mere

At Old Buckenham Mere, the chironomid preparation procedures were tested at three stratigraphic levels. One was minerogenic-rich (1390-1391 cm; Table 5.12), one marl-rich (1462-1463 cm; Table 5.13) and one organic-rich (1500-1501 cm; Table 5.14). Overall, the highest concentrations of HCs for the minerogenic-rich and organic-rich sediment test samples were produced using Procedure 3 (pre-picked ultrasonic). Unusually, the marl-rich sample yielded the best concentration using procedure 2. This could be because the sample required a much shorter time in the ultrasonic bath because the marl is very fine grained and disaggregated easily. HC concentrations were also very low and could have been highly variable spatially within the sediment. On balance, Procedure 3 (Pre-pick ultrasonic) was thought to be the most suitable and therefore selected to prepare the chironomid samples at Old Buckenham Mere.

Table 5.12, Old Buckenham Mere minerogenic-rich sediment test sample (1390-1391 cm; CaCO3 54 %, LOI 3 %, Minerogenic 43 %). Bold indicates the highest concentration of HCs yielded out of the tested procedures.

Procedure	Control (KOH)	Procedure 1 (HCl)		Procedure 2 (Straight Ultrasonic)		Procedure 3 (Pre-pick Ultrasonic)	
Taxon group	HC concentration	HC concentration	% change	HC concentration	% change	HC concentration	% change
Tanypodinae	7	5	-28	7	2	**12**	**72**
Chironomini	5	17	224	14	176	**18**	**260**
Tanytarsini	20	63	211	77	278	**73**	**258**
Orthocladiinae	4	5	26	9	130	**11**	**176**
Overall concentration	37	90	146	108	194	**115**	**213**
HC Sum	36	88		104		113	
Sample Weight (g)	0.98	0.97		0.96		0.98	

Table 5.13, Old Buckenham Mere marl-rich sediment test sample (1462-1463 cm; CaCO3 78 %, LOI 1 %, Minerogenic 21 %). Bold indicates the highest concentration of HCs yielded out of the tested procedures.

Procedure	Control (KOH)	Procedure 1 (HCl)		Procedure 2 (Straight Ultrasonic)		Procedure 3 (Pre-pick Ultrasonic)	
Taxon group	HC concentration	HC concentration	% change	HC concentration	% change	HC concentration	% change
Tanypodinae	1	1	-34	2	57	**3**	**101**
Chironomini	4	4	-9	**8**	**77**	7	62
Tanytarsini	3	8	197	**12**	**371**	5	101
Orthocladiinae	0	4		2		1	
Overall concentration	8	17	106	**24**	**198**	15	89
HC Sum	13	20		36		24	
Sample Weight (g)	1.54	1.17		1.47		1.54	

Table 5.14, Old Buckenham Mere organic-rich sediment test sample (1500-1501 cm; CaCO3 68 %, TOC 10 %, Minerogenic 22 %). Bold indicates the highest concentration of HCs yielded out of the tested procedures.

Procedure	Control (KOH)	Procedure 1 (HCl)		Procedure 2 (Straight Ultrasonic)		Procedure 3 (Pre-pick Ultrasonic)	
Taxon group	HC concentration	HC concentration	% change	HC concentration	% change	HC concentration	% change
Tanypodinae	3	2	-30	10	291	**14**	**434**
Chironomini	3	12	358	19	63	**26**	**885**
Tanytarsini	16	9	-41	50	220	**60**	**287**
Orthocladiinae	4	3	-21	10	193	**13**	**263**
Overall concentration	24	26	5.8	89	268	**113**	**363**
HC Sum	28	28		106		130	
Sample Weight (g)	1.15	1.09		1.18		1.15	

Summary

In general, procedure 1 (HCl) produced a large decline in HC concentrations compared to the control. This was most likely because the large CO_2 bubbles produced from the vigorous reaction between the HCl and $CaCO_3$ could have caused HCs to break apart. The sediment also appeared charred/burnt and stuck together. Procedure 2 (straight ultrasonic) resulted in an overall increase in HCs, though not as large as pre-pick ultrasonic, and some sub-families/tribes displayed a decline in concentrations. This meant some HCs were not released from the sediment or were destroyed. Evidence for the latter came from the presence of Chironomini fragments. Diamesinae, Prodiamesinae and large Chironomini generally have heavily chitinised HCs which are perhaps more brittle and less malleable to the bubble formation in the ultrasonic

bath. Procedure 3 (pre-pick ultrasonic) generally produced the largest increase in overall HC concentrations as well as in many of the sub-families/tribes. There are several reasons for this. Firstly, 'pre-picking' the sample prior to the ultrasonic bath allowed any clumps of sediment not disaggregated by the KOH stage to be carefully broken-down using forceps. Secondly, the larger more brittle HCs could also be removed. Thirdly, any large sharp sediment particles (e.g., pyrite, very coarse sands) that could damage the HCs could also be removed. Therefore, Procedure 3 (pre-pick ultrasonic) was chosen to prepare samples from the three sequences for consistency.

5.4.4 Head capsules preservation and taxon amalgamation

Head capsule preservation in all sequences was generally good allowing identification to a high taxonomic resolution. However, some taxa had to be combined in both the fossil samples as well as in the calibration dataset, in order to allow numerical comparisons. A common problem in all three sites was the differentiation between *Paratanytarsus austriacus*-type and *Paratanytarsus penicillatus*-type due to the low number of mandibles preserved attached to the HCs, prohibiting the differentiation of these morphotypes. Both morphotypes were combined to form *Paratanytarsus* undifferentiated in both the fossil data and in the calibration dataset. Second, *Corynocera oliveri*-type and *Tanytarsus lugens*-type were also combined, and are referred to as *COTL*-type, as they were difficult to distinguish due to the varying degree of overlap between the lateral teeth on the mentum.

5.4.5 Count sums and sample amalgamation

Minimum HC sums of 45-50 head capsules provide a reliable T_{Jul} estimate (Heiri and Lotter, 2001). However, count sums of 100 or more are recommended for palaeoecological interpretations as this provides a better representation of taxa in a population, especially when a large variety of taxa are present (Quinlan and Smol, 2001b). Therefore, count sums of 100-150 HCs were aimed for in this study (Quinlan and Smol, 2001b; Heiri and Lotter, 2001). However, several samples from different sites fell below the minimum target count sum of 50 HCs in which case neighbouring samples were combined.

For the Crudale Meadow sequence, there were initially 65 samples. Six samples did not reach the minimum count sum of 50 HCs. The lower most samples analysed at 649.5 cm (21 HCs) + 649 cm (27 HCs) and 648.5 cm (24 HCs) + 648 cm (15 HCs), were combined to form samples of 48 HCs and 39 HCs respectively. Although the resulting HC counts were below 50, resampling

to gain further HCs was not undertaken as the low taxonomic diversity meant additional HCs would not have improved estimates of community composition (cf. Quinlan and Smol, 2001b). Samples at 647 cm (48 HCs) and 597cm (48 HCs) did not reach 50 but were not combined to neighbouring samples as they also possessed low taxon diversity. This resulted in a dataset of 63 chironomid samples for the inferred temperature reconstruction and numerical analysis.

129 chironomid samples were analysed at Llangorse. Fourteen samples yielded HC counts of less than 50, not including nine samples between 613-622cm, which did not yield any HCs at all. Samples at 633 cm (18 HCs) + 634 cm (41 HCs), 636 cm (17 HCs) + 637 cm (39 HCs), and 638 cm (41 HCs) + 639 cm (19 HCs), were amalgamated to form samples of 58, 68 and 60 HCs, respectively. Samples at 622 cm (9 HCs), 612 cm (18 HCs), 608 cm (43 HCs), 593 cm (21 HCs), 592 cm (25 HCs), 587 cm (10 HCs), 586 cm (2 HCs) and 585 cm (32 HCs) were removed altogether from the inferred temperature reconstruction and numerical analysis as most of these fell well below the minimum required count sum and adjacent samples had sufficient HC counts. This resulted in a dataset of 109 fossil chironomid samples.

For the chironomid analysis at Old Buckenham Mere, 98 samples were analysed. Twelve samples yielded HC counts of less than 50. Ten of these were amalgamated with adjacent samples, to which some had sufficient HC counts of between 45- 50. This was done to ensure robust temperature reconstructions as HC concentrations were very low for this section of the sequence. The amalgamated samples are as follows: 1458 cm (56 HCs) + 1457 cm (12 HCs); 1455 cm (47 HCs) + 1454 cm (48 HCs); 1453 cm (15 HCs) + 1452 cm (56 HCs); 1451 cm (29 HCs) + 1450 cm (42 HCs); 1445 cm (28 HCs) + 1443 cm (33 HCs). This formed samples of 68, 85, 71, 71, 61 HCs, respectively. Two samples, at 1437cm (33 HCs) and 1447 cm (46 HCs) were removed and not combined with adjacent samples as the adjacent samples had sufficient HC counts of over 60 heads. This produced a dataset of 91 fossil chironomid samples for the inferred temperature reconstruction and statistical analysis.

5.5 Laboratory Methods: Oxygen and Carbon Isotopes

5.5.1 Sub-sampling strategy

Samples for stable isotope analysis ($\delta^{18}O$ and $\delta^{13}C$) were taken at 1 cm or 0.5 cm intervals (Table 5.15), with analysed samples varying from every 4th sample to contiguous sampling. In order to better understand the timings of change in both T_{Jul} and $\delta^{18}O$, the aim was to take samples for both proxies at the same stratigraphic depth. However, where $\delta^{18}O$ showed very little

variability or change, additional samples to accompany the chironomid samples were not analysed to save on costs, time and resources.

Table 5.15, *Stable I*sotope sampling strategy

Site	Sampling intervals	Depths of analysed samples	Analyst
Crudale Meadow	0.5 cm	LGIS onset: Contiguous LGIS: Every 2nd sample generally but contiguous between: 634.5 – 628 cm, 621.5 – 619 cm, 612.5 – 610 cm. LLS onset: Contiguous	This Study
Llangorse	1 cm	LGIS onset: Contiguous LGIS: Early – Every 4th sample Mid – Varied, contiguous to 4th sample Late – Every 4th sample LLS onset: Every 4th sample	Palmer *et al.,* (in prep) & This Study
Old Buckenham Mere	1 cm	Every 2nd sample	This Study

5.5.2 Sample preparation

Approximately 0.5 cm^3 of sediment was disaggregated in 5 % Sodium Hexametaphosphate ($[NaPO_3]_6$) overnight and then wet-sieved through a 63 µm nylon mesh using deionised water. This removed any ostracod and mollusc shell fragments, which are known to strongly fractionate oxygen isotopes during shell formation and can therefore adversely affect the isotopic signal of the autogenic calcite lake sediments (Candy *et al.,* 2016). The <63 µm fraction, largely autogenic calcite precipitated from the water column, was retained and reacted with 10 % hydrogen peroxide (H_2O_2) for two weeks to remove other organic material. Samples were thoroughly rinsed in deionised water using a centrifuge and left to dry.

5.5.3 Measuring isotopic values

All isotope samples from Crudale Meadow and Old Buckenham Mere were analysed at the Department of Earth Sciences at UCL. 34 isotope samples from Llangorse were analysed at UCL also. Samples were weighed using a Mettler Toledo XP6 microbalance and digested in phosphoric acid at a temperature of 90 °C to produce CO_2. A ThermoFisher Delta Plus XP mass spectrometer with a Gasbench II preparation system was used to analyse the $\delta^{18}O$ and $\delta^{13}C$ of the liberated CO_2. Three internal standards (BDH) were analysed every five samples and three

external standards (NBS-19) were analysed every machine run. The remaining 24 isotope samples from Llangorse were analysed at the Department of Earth Sciences, Royal Holloway, prior to the commence of this PhD by Professor Ian Candy and Dr Adrian Palmer. These samples were weighed out using a Cahn C-31 Microbalance and measured using a VG PRISM series 2 mass spectrometer. Internal (RHBNC-PRISM) and external (NBS-19, LSVEC) standards were run every 10 samples. All stable isotopic values are quoted with reference to Vienna Pee Dee Belemnite (VPDB).

5.6 Laboratory Methods: Chronological techniques

Good chronological control for each sequence is paramount to allow robust correlation of ACEs between sites and therefore allow comparison of event magnitude across the British Isles and continental Europe. In order to achieve robust chronologies, radiocarbon dating and tephrochronology were undertaken. The chronological work for Llangorse had been undertaken prior to the start of this PhD and so is not discussed in detail here, though a basic description can be found in section 6.2.6. The chronology for Crudale Meadow was originally undertaken by Timms *et al.* (2018), which is briefly summarised here along with details of work undertaken as part of this study to further improve the chronological constraint. As Old Buckenham Mere was a completely new site, no existing chronological work had been completed on the OBM19 sequence. The tephra analysis was undertaken by Ms Katy Flowers and radiocarbon dating by the author.

5.6.1 Crudale Meadow

This study has improved the tephra-based age-depth model constructed by Timms et al. (2018) for Crudale Meadow by the addition of a radiocarbon date from the later part of the LGIS as there are few tephra horizons found during this time period in the British Isles. The radiocarbon sample consisted of selected terrestrial plant macrofossil remains from between 614-615.5 cm which included leaves of *Dryas Octopetela, Empetrum and Betula nana* as well as *Betula nana* fruit. The sample was analysed at Queen's University, Belfast.

5.6.2 Old Buckenham Mere

Tephra

Tephra stratigraphical analysis for the Old Buckenham Mere sequence was conducted by Ms Katy Flowers. 1 cm^3 of sediment from 10 cm rangefinder scan samples were sieved between 80 and 25 µm meshes to remove sand particles (>80 µm) as well as silts and clays (<15 µm)

which can obscure tephra shards. Samples were then processed following the density separation method by Blockley *et al.* (2015). Samples were then analysed under an Olympus CX-41.

Radiocarbon

Five radiocarbon dates were obtained for Old Buckenham Mere based on terrestrial plant macrofossils. Due to the paucity of macrofossils preserved in the sequence, only one sample contained enough terrestrial macrofossil material to provide a radiocarbon age from a single stratigraphic depth (i.e., 1 cm). Therefore, the other four radiocarbon samples are composed of macrofossil material picked from stratigraphic intervals spanning 2 - 5 cm.

Samples were analysed at the Keck-Carbon cycle AME facility in California (UCIAMS) and were treated with acid-base-acid (1N HCl and 1N NaOH, 75 °C) prior to combustion. Sufficient carbon was present in four out of the five samples to provide $\delta^{13}C$ values which were measured using a Thermo Finnigan Delta Plus stable isotope ratio mass spectrometer (IRMS) with gas bench input to a precision of <0.1‰ relative to standards traceable to PDB.

5.7 Numerical Methods: Chironomids

5.7.1 Diagram construction and zonation

Percentage assemblage diagrams were drawn in C2 (version 1.7.7; Juggins, 2007) and edited in Adobe Illustrator Creative Cloud. To aid interpretation, assemblages were grouped into distinctive bio-stratigraphic units based on major changes in taxa abundance and presence. In the first instance, a broken stick model (Bennett, 1996) was used to identify the number of statistically significant zones on untransformed percentage data which were then plotted using CONISS (Constrained Incremental Sum of Squares Cluster Analysis; Grimm, 1987). Both were conducted in R (R Core Team, 2018) using vegan (Oksanen *et al.,* 2017) and rioja (Juggins, 2017) packages.

5.7.2 Calibration dataset

The 274-lake combined Swiss-Norwegian chironomid-climate calibration dataset was used, with 13 outlier lakes removed, to estimate past mean July air temperatures (T_{Jul}; Heiri *et al.,* 2011). The Swiss-Norwegian calibration dataset has several advantages over the Norwegian dataset (Brooks & Birks, *unpublished*) which is more commonly applied to British lake records (e.g., Brooks *et al.,* 2012; Brooks *et al.*, 2016). Firstly, incorporation of lakes from the Swiss

calibration dataset means the calibration dataset contains lakes with similar characteristics to that of Crudale Meadow, Llangorse and Old Buckenham Mere during the LGIS, i.e., they are alkaline carbonate lakes with similar chemistry. Secondly, the combined Swiss-Norwegian calibration dataset contains a greater number of chironomid taxa. Thirdly, the combined calibration dataset covers a longer T_{Jul} gradient of between 3.5 - 18.4 °C.

5.7.3 WA-PLS model selection

A two-component weighted averaging partial least squares (WA-PLS; ter Braak and Juggins, 1993; ter Braak *et al.,* 1993) regression model was selected for reconstruction purposes as it combines the best predictive power with a root mean squared error of prediction (RMSEP) of 1.4 °C, r^2_{jack} of 0.9 °C and maximum $bias_{jack}$ of 0.9 °C, as estimated using leave-one-out cross-validation. Sample specific errors for our reconstructed T_{Jul} values were calculated by 999 bootstrap cycles (Birks *et al.,* 1990). The chironomid percentage data was square root transformed prior to analysis to minimise variances. WA-PLS analysis was performed in C2 (Juggins, 2006).

5.7.4 Validation statistics and assessing the reconstruction

Several methods were used to assess the reliability of the chironomid-inferred reconstructions. Firstly, goodness-of-fit to temperature tests were performed by passively plotting fossil samples on the first axis of a canonical correspondence analysis (CCA) of the modern calibration dataset, using T_{jul} as the sole constraining variable. Fossil samples which had a squared residual distance value that exceeded the 90^{th} and 95^{th} percentiles of samples in the modern calibration dataset had a 'poor' or 'very poor' fit to temperature, respectively (Birks *et al.,* 1990; Telford, 2014a). CCA analysis was conducted in R using the vegan package (Oksanen et al., 2017).

Secondly, Modern Analogue Technique (MAT) analyses were performed to assess the similarity of fossil assemblages to those in the modern calibration dataset using the analogue package in R (Simpson, 2020). Squared-chord distance was used as a measure of dissimilarity, and samples were not square-root transformed prior to analysis. Fossil samples with distances to the closest modern analogue larger than the 5^{th} and 10^{th} percentile of all modern distances are treated as having 'no close' and 'no good' analogue, respectively (Birks *et al.,* 1990; Telford, 2014b).

Thirdly, the percentage of 'rare taxa' present in fossil samples were calculated as their temperature optima are less reliably modelled (Birks, 1998). A low percentage of rare taxa in

fossil samples is favourable so that the T_{Jul} estimate is based mainly on taxa that have well-modelled optima. Rare taxa were identified in the modern calibration dataset using C2 and defined as having a Hill's N2 of less than 5 (Hill, 1973; Heiri et al., 2003). The percentage abundance of rare taxa was then summed for each fossil sample in Microsoft Excel.

Finally, the total abundance of taxa 'not present' in the modern calibration dataset, but present in the fossil dataset, was calculated to give an indication as to how many HCs in a fossil sample are not included when calculating the T_{Jul} estimates. A low percentage of taxa absent is favourable (Birks, 1998).

5.8 Numerical Methods: Isotopes

Pearson Product-Momentum tests were used to investigate the correlation between $\delta^{18}O$ and $\delta^{13}C$ values were calculated for each sequence in order to highlight potential detrital contamination of the isotope signal from geological carbonate or any potential evaporitic effects on the lake water body (Leng and Marshal, 2004; Talbot, 1990). In some instances where $\delta^{18}O$ and $\delta^{13}C$ strongly covary, Spearman rank correlation coefficients were calculated for each isotopic subzone to ascertain if covariance changed through time. Low co-variance is defined as an r^2 value <0.2, moderate as an r^2 value between 0.3 to 0.7, and high co-variance as an r^2 values >0.7.

5.9 Numerical Methods: Chronology

Bayesian statistics were employed as they allow robust age models to be generated by incorporating prior information relating to the sediments. They are widely used in LGIT studies (e.g., Matthews *et al.*, 2011, Bronk Ramsey *et al.,* 2015). All age-depth models used in this thesis were produced using the *p_sequence* function in OxCal v 4.4 (Bronk Ramsey, 2009) and the IntCal20 calibration curve (Reimer *et al.,* 2020). The Poisson depositional function was implemented which states that depositional events are random and allows for variability in sedimentation rates (Bronk Ramsey, 2008). All dates are presented as $\mu \pm 2\sigma$ cal a BP and rounded to the nearest decade to align with the resolution of proxy sampling.

6. Summary of contributors to analyses

Table 5.16 below summarises all who have contributed to the data presented within this thesis.

Table 5.16, Summary table of all investigators who contributed. N/A = not analysed

	Fieldwork and coring	**S**edimentology **and** Physical parameters	Chronology	Chironomids	Isotopes	XRF
Crudale Meadow	R. Timms, I. Matthews, A. Palmer	R. Timms,	R. Timms (Tephra) **C. Francis** (Radiocarbon)	**C. Francis**	**C. Francis**	N/A
Llangorse	A. Palmer, I. Matthews, R. Timms, A. Abrook,	A. Palmer, A. Abrook,	A. Palmer I. Matthews, P. Lincoln (Radiocarbon)	**C. Francis**	**C. Francis** I. Candy A. Palmer	N/A
Old Buckenham Mere	**C. Francis,** A. Palmer, I. Matthews, S. Engels, I. Candy, J. Pike, M. Francis	**C. Francis**	K. Flowers (Tephra) **C. Francis** (Radiocarbon)	**C. Francis**	**C. Francis**	**C. Francis**

Chapter 6: Introduction to study sites

Chapter Overview

The aim of this chapter is threefold. Firstly, to introduce each of the study sites and to discuss the background conditions that characterise them (i.e., modern hydrology and climate). Secondly, to discuss local factors that may exert an influence on the proxies being studied (i.e., chironomid ecology and carbonate isotope values). These include: (i) the local geology and topography as detrital limestones may contaminate the isotope signal; (ii) the local glacial history because cold-water flux from glaciers entering a lake can cause T_{Jul} to be underestimated; (iii) lake level fluctuations as changes in water depth also exerts a control on the chironomid taxa present; and (iv) vegetation changes which can affect both $\delta^{18}O$, through catchment stability and associated inwash of detrital geological carbonate, and $\delta^{13}C$, by affecting the exchange of carbon isotopes in soils. Finally, the chapter will present the existing stratigraphy and chronology for each of these sites and discuss the issues and uncertainties that are associated with them.

6.1 Crudale Meadow, Orkney Isles, Scotland.

6.1.1 Site location and vicinity

In the northern British Isles, Crudale Meadow (59°0'57" N; 03°19'42" W) is a former lake basin situated in the west of Mainland, the largest island of the Orkney archipelago. (Figure 6.1a & 6.1b). It lies 6.1 km north of Stromness, 1.7 km inland from the west coast, at an altitude of 9 m asl. Moar (1969) named the site 'Yesnaby', although subsequent investigations by Bunting (1994), Whittington *et al.* (2015) and Timms *et al.* (2018) have referred to the site as 'Crudale Meadow'.

The infilled lake contains a valley mire with some areas of open water. The area is fed from the west by the Burn of Clovigarth, which flows from another mire Spretta Meadow, and drains eastwards through the Burn of Cruland into Loch of Stenness. The valley mire vegetation is dominated by *Phragmites australis* and *Cyperaceae*. The surrounding slopes and dryland areas are in use for rough grazing and feature a heathland mosaic with *Calluna vulgaris, Empetrum nigrum, Erica cinerea, Poaceae* spp., *Angelica* sp., *Potentilla erecta, Plantago lanceolata, Succisa pratensis, Hypericum* sp., *Rumex* sp., *Cirsium* sp. and *Senecio* sp. (Whittington *et al.,* 2015).

The Orkney archipelago currently has a cool temperate climate and experiences mean daily maximum temperatures of 6.4 °C in January, 15.9 °C in July and 8 °C annually. These relatively high temperatures at this high latitude are the result of the warming influence of the North Atlantic and Gulf Stream (Whittington *et al.,* 2015). The site does however experience high windspeeds and high exposure. Mean annual rainfall is 1038mm and mainly falls in the winter months (Data from meteorological station at Kirkwall, 21 km east of Crudale Meadow; Met Office data 1981-2010).

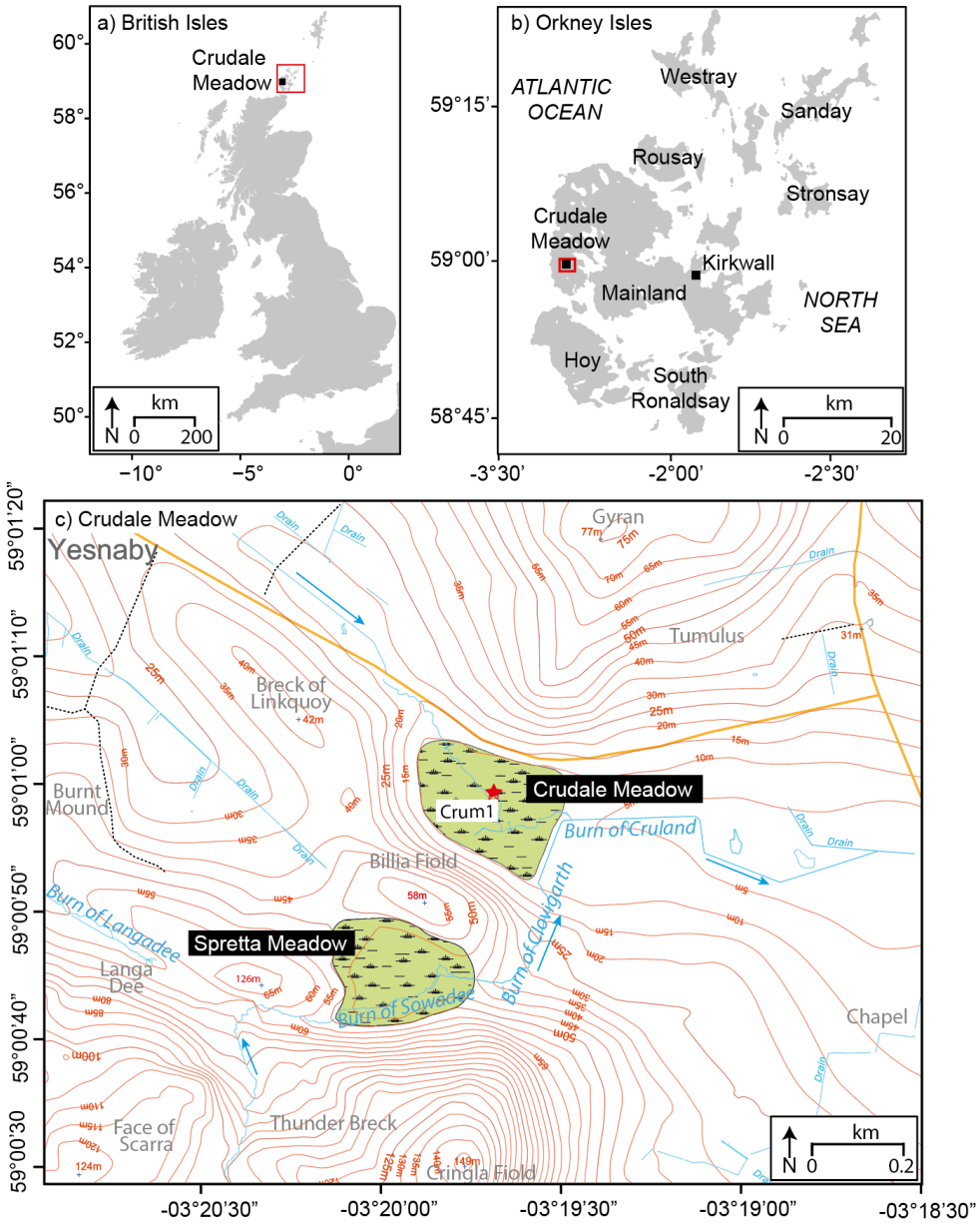

Figure 6.1, Crudale Meadow location maps. (a) A map of Britain and Ireland showing the position of the Orkney Isles marked in red; (b) map of the Orkney Isles and the position of Crudale Meadow marked in red; (c) topographic map of site showing the coring location (red star) and 5m contours. Streams and drainage channels are in in blue and roads in orange, respectively. Hiking trails denoted by black dotted lines. Data downloaded from digimap.edina.ac.uk © Crown Copyright and database rights (2020) Ordnance Survey (1000252525).

6.1.2 Geology and topography

The basal geology of the area consists of Siltstones, Mudstones and Sandstones of the Yesnaby Sandstone Group of the Lower Old Red Sandstone (Figure 6.2; Mykura, 1976). The former lake lies within a topographic depression between Devonian Qui Ayre sandstones and mid-late Devonian Upper Stromness Flagstones (Mykura, 1976). Thin Devensian tills cover the surrounding slopes (Figure 6.3) and are partially derived from the carbonate-rich dolomitic siltstones, shales and sandstones of the Middle Old Red Sandstone Lower Stromness Flags (Whittington *et al.,* 2015). The Orkney Isles are largely low lying and rarely exceed 150 m. Tumulus Gyran to the north of Crudale Meadow rises to 77 m and the Breck of Linkquoy to the west reaches 42 m (Figure 6.1c). To the south, Billia Fiold reaches 58 m while slightly further to the south, Cringla Fiold peaks at 149 m.

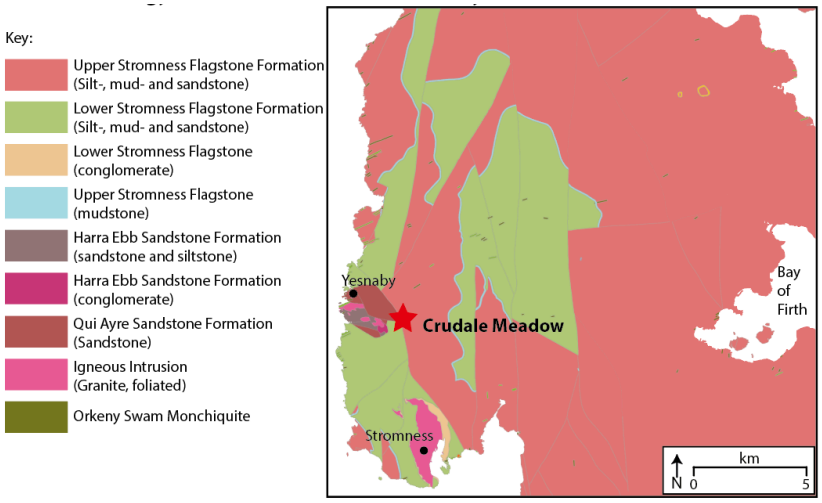

Figure 6.2, Bedrock geology of the west coast of Mainland, Orkney. Data downloaded from digimap.edina.ac.uk © Crown Copyright and database rights (2020) British Geological Survey materials © (2020).

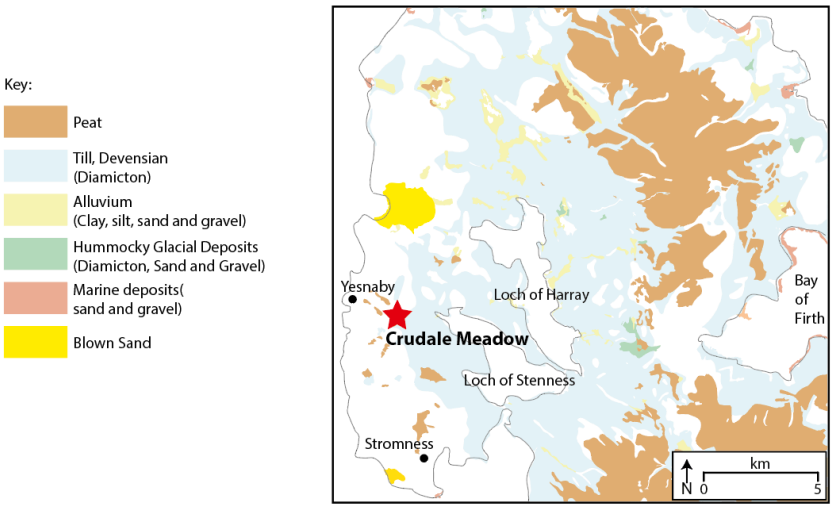

Figure 6.3, Superficial geology of the west coast of Mainland, Orkney. Data downloaded from digimap.edina.ac.uk © Crown Copyright and database rights (2020) British Geological Survey materials © (2020).

6.1.3 Glacial history

It was originally thought that during the Devensian, ice radiated from central Scotland, streamed out of the Moray, up the North Sea and subsequently across Orkney (Peach and Horne, 1880; Mykura, 1976). However, the identification of several superimposed till formations (Digger, Scara Taing and Quendal), with sharp erosive contacts, gives evidence for three separate phases of ice-flow across Orkney (Rae, 1976; Hall *et al.,* 2016). Originally, ice was considered to have traversed the archipelago earlier in the Devensian and was ice free during the LGM (Rae, 1976; Bowen *et al.,* 2002). However, it is now commonly accepted that ice inundated the northern North Sea during the LGM (Bradwell *et al.,* 2008; Ballantyne, 2010; Sejrup *et al.,* 2015; 2016) and across Orkney (Hall and Whittington, 1989). Cosmogenic dating of glacial erratics and ice-moulded bedrock suggest a final deglaciation from the Late Devensian ice sheet at ~ 15-17 ka BP (Clark *et al.,* 2012; Hughes *et al.,* 2016). The Crum1 sequence by Timms *et al.* (2018) shows 50 cm of clay/silt had accumulated in the Crudale basin prior to the onset of the LGIS inferred by the increase in $CaCO_3$ (Figure 6.5), suggesting Crudale Meadow was ice free well before the onset of the LGIS. There is some evidence for small corrie glaciation on the island of Hoy during the LLS due to the high relief (Figure 6.1b; Ballantyne *et al.,* 2007; Bickerdike *et al.,* 2016), however, evidence for glaciation during the LLS on Mainland is very limited (Whittington *et al.,* 2015). Therefore, the lack of evidence for local glaciation on Orkney during the later phases of the LGIT indicates glacial ice was unlikely to have directly impacted the invertebrate fauna and depositional environment of Crudale Meadow.

6.1.4 Lake formation and lake-level changes

The Crudale Meadow basin sits within a bedrock topographic depression formed by glacial scour of the LGM ice (Whittington *et al.,* 2015). The lake is thought to have covered an area of approximately 0.09 km^2 (Timms *et al.,* 2018) in the past and this property, allied to relatively high precipitation rates, means large changes in lake level were unlikely. Previous studies (Moar, 1969, Bunting, 1994; Whittington *et al.*, 2015) have not detected substantial lake-level changes at Crudale Meadow during the Lateglacial, although notable shallowing of the lake through the Holocene through natural sediment processes led to the basin being infilled in its present state.

6.1.5 Previous palaeoecological and palaeoclimatic investigations

Moar (1969), Bunting (1994) and Whittington *et al.* (2015; Figure 6.4) all obtained sediment sequences with consistent tripartite structure from the Crudale Meadow palaeolake. These

studies showed the islands bore a reduced floral diversity compared to the Scottish mainland during the LGIT (Moar, 1969; Bunting, 1994; Whittington *et al.,* 2015; Abrook *et al.,* 2020). The vegetation was open throughout and was dominated by herbaceous and low shrub taxa characteristic of unstable substrates (Whittington *et al.,* 2015). The high-resolution $\delta^{18}O$ record of Whittington *et al.* (2015) identified three possible climate oscillations within sediments they believed to be of LGIS age (Figure 6.4). These short-lived changes were characterised by lowered $\delta^{18}O$ values and a reduction in *Empetrum nigrum* and *Betula*, along with expansions in *Artemisia*, *Poaceae* and *Asteraceae*/*Cardueae* undifferentiated.

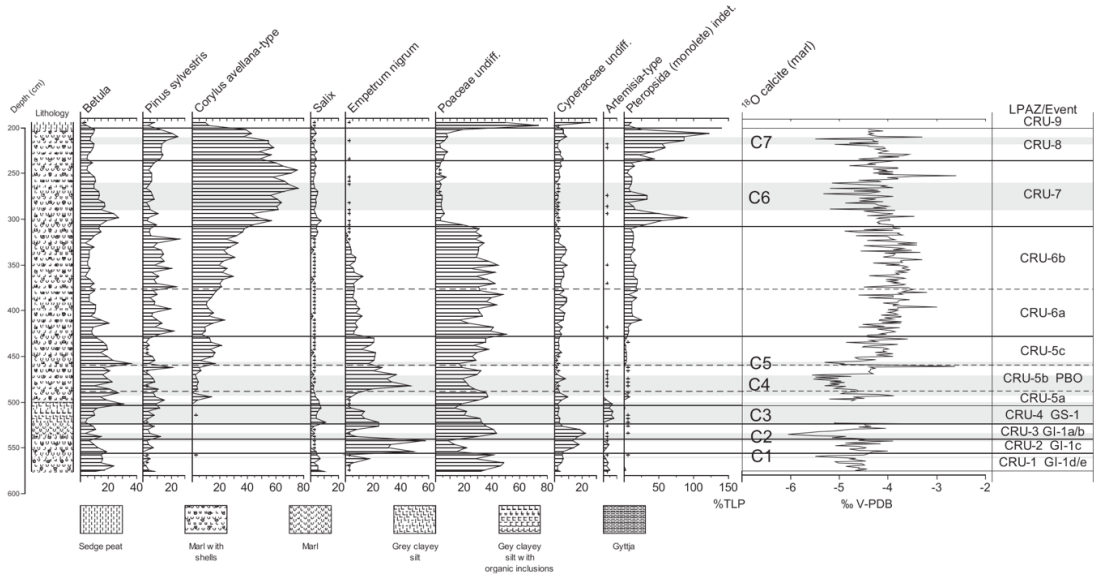

Figure 6.4, Pollen and oxygen isotope data from Whittington *et al.* (2015). Events labelled C1 and C2 were proposed as relating to GI-1b and GI-1d, respectively. (From Whittington *et al.,* 2015).

6.1.6 Chronology

Whittington *et al.* (2015) attempted to construct an independent age-model for their sequence using radiocarbon dates obtained from bulk sediments and aquatic remains, however, the yielded ages were considered too old (Whittington *et al.,* 2015). The abrupt cooling events identified in their sequence were correlated to GI-1d (C1) and GI-1b (C2) based on stratigraphic wiggle matching to regional records (Whittington *et al.,* 2015; Figure 6.4).

Timms *et al.* (2018) were able to create a robust chronology for their CRUM1 sequence through the identification and correlation with six known tephra layers (Figure 6.5). These included the Borrobol and Penifiler Tephras in the LGIS, the Vedde Ash in the LLS, and the Hässeldalen, Askja-S and Saksunarvatn tephras in the Holocene. Age estimates were generated for three other tephra layers found at 597 cm, 510 cm and 444 cm which are not correlated to known tephra horizons. The tephrochronological age-depth model presented by Timms *et al.* (2018) uses the

best age estimates available at the time for the correlated tephra layers (Bronk Ramsey, 2015) and were modelled in OxCal v 4.3 (Bronk Ramsey, 2008; Bronk Ramsey and Lee, 2013) using the IntCal13 calibration curve (Reimer *et al.,* 2013). This produced one of the best age constrained sequences in the British Isles for the Lateglacial and Early Holocene. However, to date there are no accompanying proxies to this work, other than the physical sediment parameters, that might allow a palaeoenvironmental reconstruction across this time interval to be made.

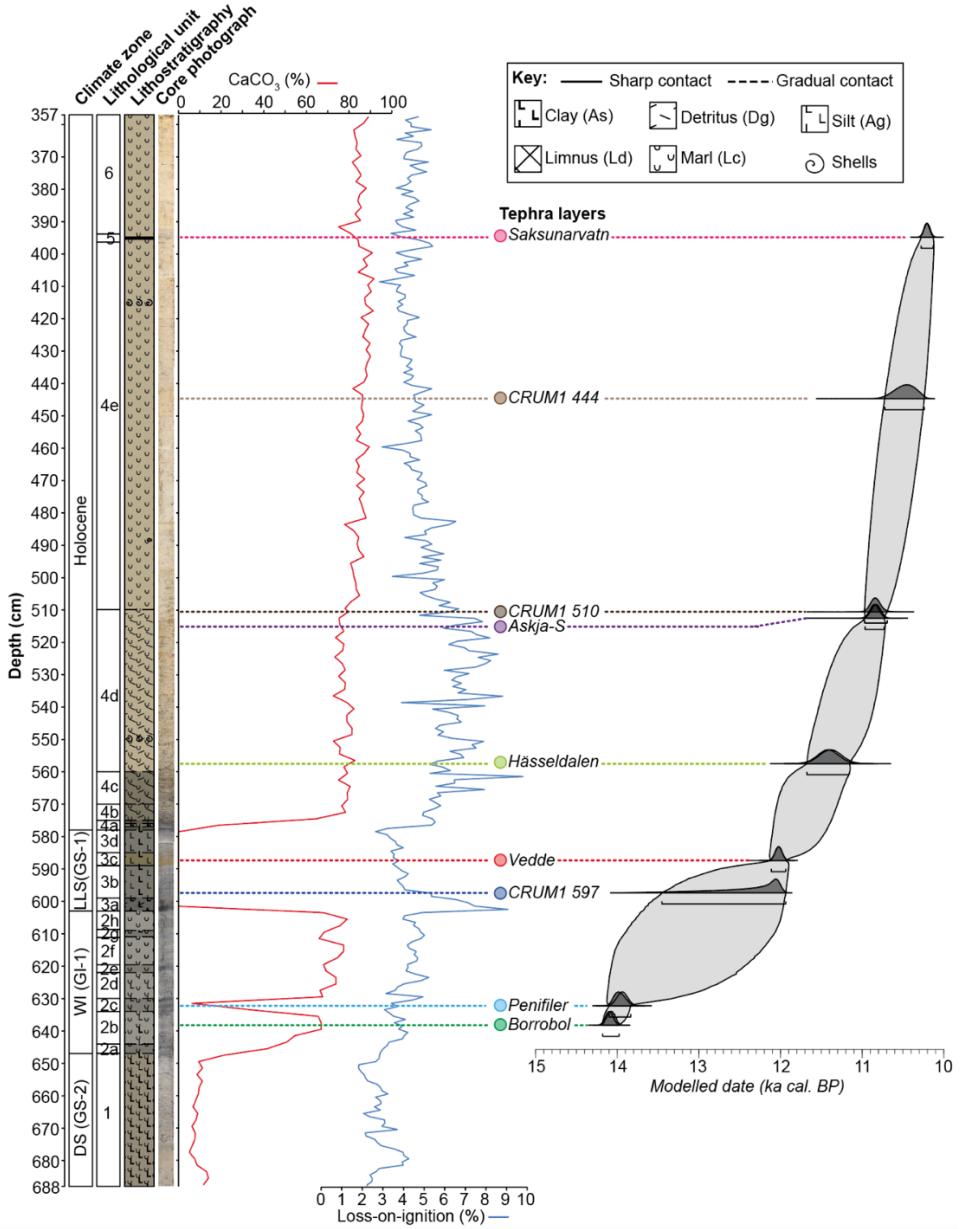

Figure 6.5, Data for the CRUM1 sequence from Timms *et al.* (2018). The broad climatostratigraphy, sedimentology and physical parameters are displayed on the left. The age depth model is on the right with the six known tephra layers used to construct the age model marked on as well as three uncorrelated tephra layers (CRUM1 597, CRUM1 510 and CRUM1 444). After Timms *et al.* (2018).

6.2 Llangorse, Brecon Beacons, South Wales

6.2.1 Site location, vicinity and the contemporary lake

Llangorse lake (Llyn Syfaddan; 51°55'50" N; 3°15'47" W) is an extant lake located on the northern flank of the Brecon Beacon escarpment, located near to the interfluve with the River Usk, with a current lake surface altitude of 153 m a.s.l. (Palmer *et al.,* 2008) (Figure 6.6a & 6.6b). The lake sits 8 km to the east of Brecon and is the largest natural body of freshwater in the southern Wales (*c.* 150 ha) (Jones *et al.,* 1985; Jones and Benson-Evans, 1974). It lies in the catchment of the River Wye, near the headwaters of the Afon Llynfi, which enters the basin from the south and drains to the north into the River Wye (Palmer *et al.,* 2008; Chambers, 1999). Smaller streams drain into the northern and eastern shorelines too including Nany Cwy, Hoel Ddu, Cwm Sogum and Cathedine (Cragg *et al.,* 1980). Bathymetry of the lake shows much of the lake is currently less than 2 m deep (Wade, 1999) (Figure 6.6c). However, two deep troughs occur in the basin both exceeding 7 m in depth, separated by a ridge at 4 m water depth (Jones *et al.,* 1985). A medieval crannog lies about 40 m from the northern shoreline in water about 1 m deep (Campbell and Lane, 1989).

South Wales currently experiences a cool temperature climate with mean daily maximum temperatures of 8.1 °C in January, 22.3 °C in July and 14.8 °C annually. Mean annual rainfall is 1076mm with an average of 121 mm falling in December and 60 mm in June. (Data from meteorological station at Usk, 40km southeast of Llangorse; Met Office data 1981-2010).

6.2.2 Geology of the area and topography

The main bedrock geology of the Brecon Beacons are Lower Devonian Old Red Sandstones, siltstones and mudstones and causes the sediments and soils to have a red colouration (Chambers, 1999) (Figure 6.7). Lake Llangorse is underlain by argillaceous rocks and sandstone of the St Maughans Formation. To the north there are silt and mudstone of the Raglan Mudstone Formation, while to the east and south Mudstones and sandstones from the Senni and Brownstones Formations dominate. Further south, a complex array of different rock types including Limestone from the Castell Coch and Dowlais Limestone Formations, South Wales Coal Formations and the Grey Grit Formation are interspersed between the Sand-, silt- and mudstones of the Twrch Sandstone Formation, Cwymyniscoy mudstone formation and Garns Caws Sandstone Formation. The Quaternary deposits immediately around Lake Llangorse consists of glaciolacustrine silts and clays and Devensian diamicton (British Geological Survey 2003; Palmer *et al.,* 2008) (Figure 6.8). The Usk Valley to the south exhibits a complex array of

alluvium, glaciofluvial and alluvial fan deposits. Peat and Devensian Till cover much of the surrounding landscape, particularly at higher altitudes, which has a mainly upland character (Chambers, 1999). The lake is situated in a basin with land to the west rising to over 380 m asl, whilst to the east the relief is steeper and rises to 515 m asl (Mynydd Llangorse) and 609 m asl (Mynydd Troed), both separated by a col at *c.* 350 m asl at the head of Cwm Sorgum (Humpage, 2007). To the south, elevation increases to 391m asl at Yr Allt which divides Llynfi basin and the River Usk (Chambers, 1999; Palmer *et al.,* 2021) although there are two cols at 190 m (Pennorth and Bwlch) on the southern borders of the basin and the watershed between the Wye and Usk (Figure 6.6).

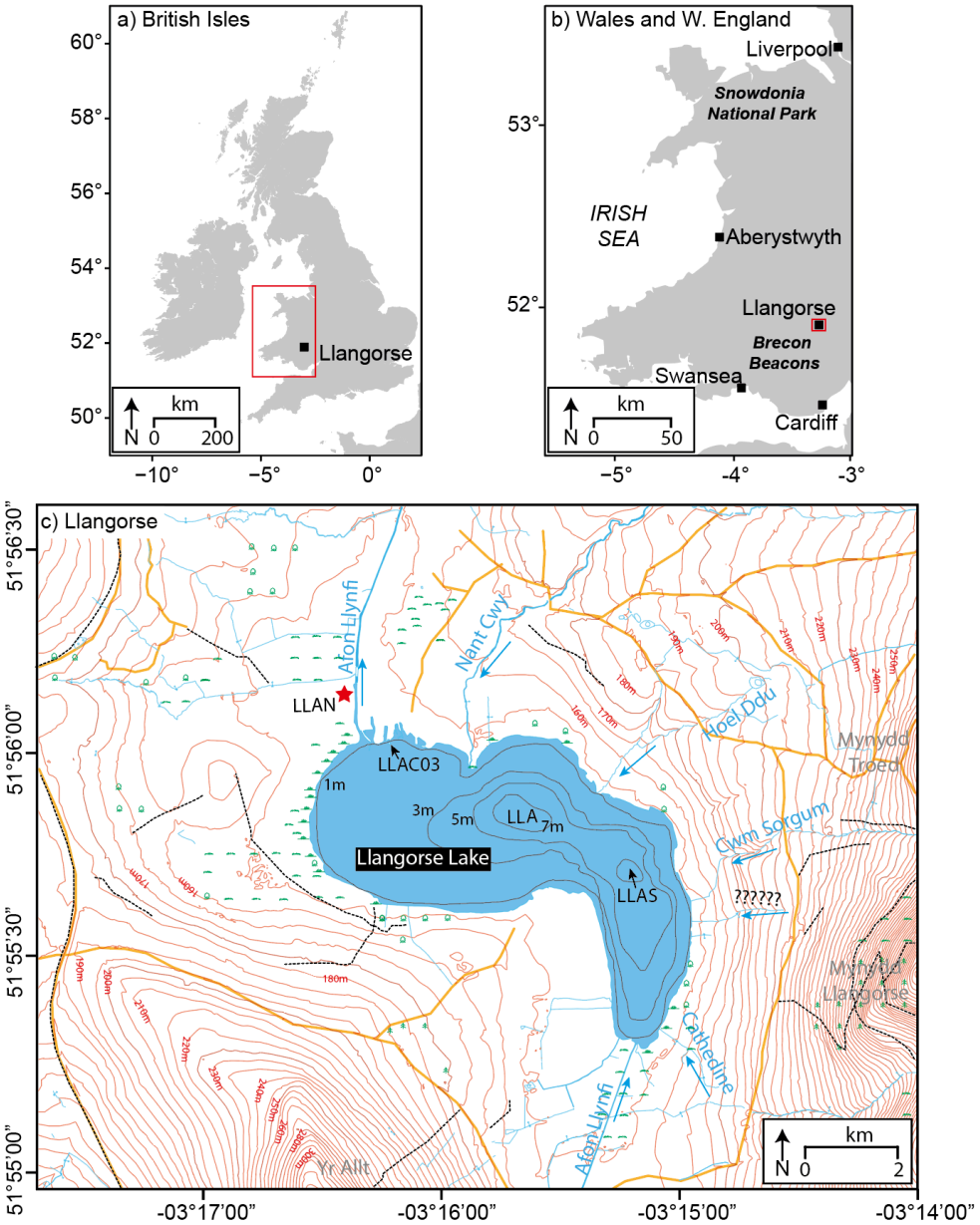

Figure 6.6, Location maps for Llangorse. (a) A map of Britain and Ireland showing the location of Wales marked in red; (b) map of Wales and the location of Llangorse Lake marked in red; (c) topographic map of site showing the

coring location (red star) and 5m contours. Streams and drainage channels are in in blue and roads in orange, respectively. Hiking trails are denoted by dotted black line. A number of sequences have been retrieved from the Llangorse basin by Palmer *et al.,* and are denoted on the map as follows: LLAN = Llangorse North basin sequence, LLAC03 = Llangorse Crannog sequence from Palmer *et al.* (2008), LLA = Llangorse central basin sequences, and LLAS = Llangorse southern basin sequence. Data downloaded from digimap.edina.ac.uk © Crown Copyright and database rights (2020) Ordnance Survey (1000252525).

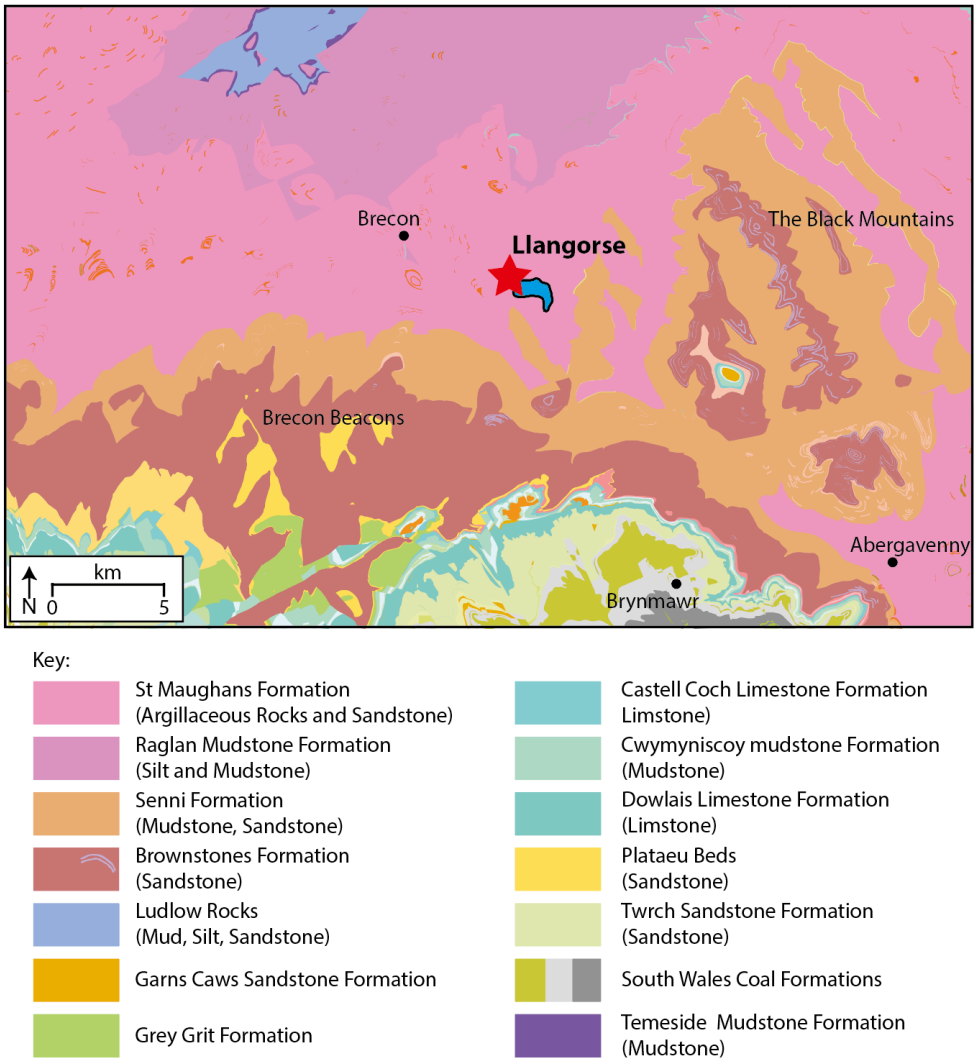

Figure 6.7, Bedrock geology of the Brecon Beacons, South Wales. Data downloaded from digimap.edina.ac.uk © Crown Copyright and database rights (2020) British Geological Survey materials © (2020).

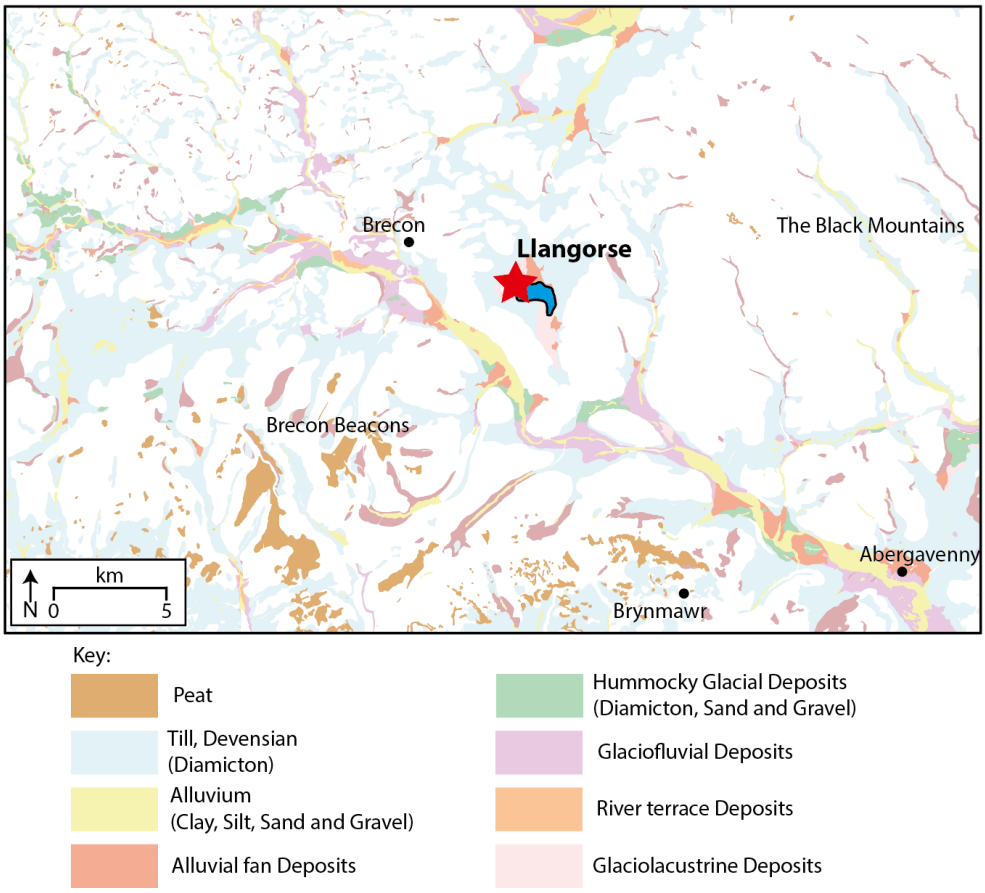

Figure 6.8, Superficial geology of the Brecon Beacons, South Wales. Data downloaded from digimap.edina.ac.uk © Crown Copyright and database rights (2020) British Geological Survey materials © (2020).

6.2.3 Glacial history

It is widely accepted that the Brecon Beacons were covered in ice during the LGM (Clark *et al.,* 2018). Ice from the Brecon Beacons flowed down the Usk Valley, merged with ice from mid-Wales reaching its maximum extent in the Abergavenny area forming part of the south-eastern sector of the Welsh Ice Cap (Jansson and Glasser, 2008; Palmer *et al.,* 2020). Computer modelling simulations suggest ice began to retreat from the area at around 23.55 ka BP (Patton *et al.,* 2013). Previously, two theoretical models of ice retreat from the last deglaciation were put forward by Lewis (1970) and Humpage (2007) based on geomorphological evidence. Lewis (1970) suggested the dominance of ice from mid-Wales pushing south from the Wye Valley into the Llynffi basin and then into the Usk Valley prior to the development of an Usk Valley glacier. The mid-Welsh Ice mass then retreated north, and the ice sourced from the Brecon Beacons separated into two valley glacier lobes near Bwlch with one in the Usk Valley and the other within the Wye catchment (Lewis 1970). Lewis (1970) identified a series of four moraine ridges representing ice still stands during retreat of the mid-Wales ice mass. Humpage (2007) put forward a different model suggesting that based on the presence of material sourced from

the Usk Valley in the Llynfi basin and the formation of dead-ice topography in the Llynfi basin, early retreat of the Welsh Ice cap, through the Wye Valley, may have allowed the easterly advance of local ice lobes within the Usk Valley (Humpage, 2007). The retreating ice described in these models may be responsible for the contemporary basin bathymetry. The shallow ridge running NE-SW between LLA and LLAS (Figure 6.6c) could represent subaqueous ice-contact fans or moraine ridges that formed at the retreating ice margin (Palmer *et al.,* 2021) and another area of high ground in the vicinity of LLAC03 could have a similar origin (Palmer *et al.,* 2021). Following the retreat of the LGM ice, paraglacial activity led to rock instability and landslides, leading to colluvial and alluvial redistribution of sediments (Shakesby *et al.,* 2007).

During the LLS, conditions were sufficiently severe in the higher mountains of the Brecon Beacons (above 600 m) for small glaciers and snow beds to form cwms as indicated by the presence of short depositional ridges and striated clasts (Evans 2007; Shakesby *et al.,* 2007, Bickerdike *et al.,* 2018). Biostratigraphic pollen studies provide further evidence for LLS glaciation. Sites with pollen assemblages that reflect WI and LLS vegetation occur outside of stadial glacier limits e.g. Traith Mawr (Walker 1982) and Waen Ddu Bog (Coleman and Parker, 2007). Sites inside glacier limits however only display assemblages associated with Holocene vegetation, e.g. Craig-y-Fro (Walker, 2007a) and Craig Cerrig-gleisiad (Walker, 2007b) due to the glacial erosion of earlier LGIS deposits. Despite the proximity of Llangorse to the Brecon Beacons, there is no evidence of active cwm glaciers in the Llangorse catchment during the LLS and the landscape would have been dominated by periglacial activity (Chambers, 1999).

6.2.4 Lake formation and lake-level change

Both models of glacial retreat (Lewis, 1970; Humpage, 2007) propose the formation of a large proglacial lake called Glacial Lake Llangorse, 6 km long by 3 km wide, with a lake surface elevation of 190 m asl, approximately 50-60 m in water depth (Palmer *et al.,* 2007; 2021). The presence of shorelines on either side of the Llynfi Basin and the glaciolacustrine deposits in the cores means there is no doubt that a proglacial lake existed (Walker *et al.,* 1993; Palmer *et al.,* 2008) and extended as far south as Blaenllynfi (Barclay *et al.,* 2005; Palmer *et al.,* 2008). The maximum elevation of the proglacial lake is thought to be 37 m above present day due to cols present at Pennorth and Bwlch and shorelines at approximately 190 m asl (Lewis 1970). Investigation into the annually laminated clastic sediments from the base of the Crannog core (LLAC03) revealed the lake existed in an ice contact configuration for a minimum of 75 yrs (Palmer *et al.,* 2008). Lake level fell as the ice dam failed following the northward ice retreat.

Water drainage was diverted northward through the Afon Llynfi and into the River Wye (Lewis *et al.,* 1970; Palmer *et al.,* 2008; 2021). Around the time of the lake-level fall, the dominant source of sedimentation switched from the retreating northward glacier to subaerial streams from the southern part of the catchment (Palmer *et al.,* 2020). The lake then became ice distal for a minimum of 515 yrs (Palmer *et al.,* 2008), however, this is under further investigation with new deep-water cores (LLA and LLAS) retrieved from the centre of the basin (Palmer *et al.,* 2021).

Further investigation into lake-level changes, throughout the LGIT and the early Holocene, has been undertaken by Palmer *et al.* (2021), through an extensive core survey of the basin (Figure 6.9). During the latter part of the Dimlington Stadial and the LGIS, the lake is inferred to have a minimum level of between 153-153.5 m asl, similar to the present day (Palmer *et al.,* 2020). This is reconstructed from the presence of marl in the northern basin at 151.5 m asl which requires water depths of 1.5-2 m to form (Murphy and Wilkinson, 1980; Palmer *et al.,* 2020). A lake-level fall of 1.5-3.5 m to 151-152 m asl is thought to have occurred either near the end of the WI and/or during the very early phases of the LLS, possibly driven by hydrological changes affecting the local water table. Evidence for this comes from the absence of WI marl sediments in LLAC03 at the Crannog caused by subaerial stream erosion of the exposed WI sediments as water level fell; the eroded marl has been found as intraclasts in the deep-water cores (LLA14 and LLAS14). However, lake-water levels could not have fallen below 148.54 m as complete WI deposits exist at LLAn14 at this altitude. During the Holocene, and potentially prior to the Holocene onset, the lake level rose to 152-154 m asl, which is similar to current lake levels.

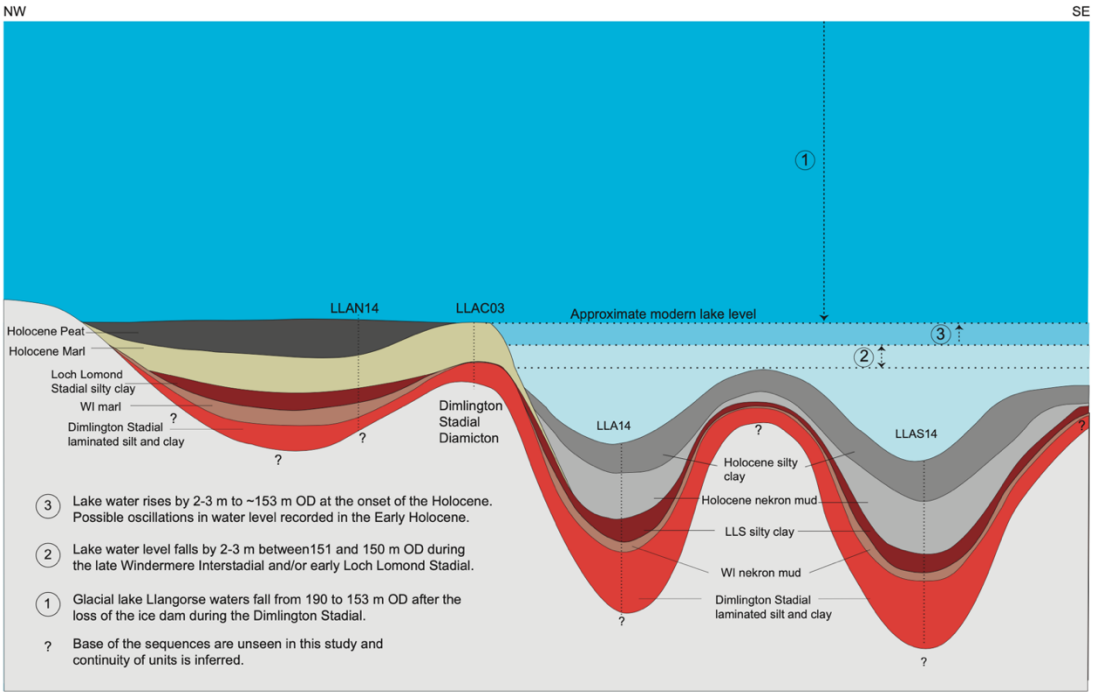

Figure 6.9, Lake-level changes at Llangorse. From Palmer *et al.,* (2021)

6.2.5 Previous palaeoecological and palaeoclimatic investigations

Until recently, previous palaeoecological work has largely focused on sediment from the Holocene. Walker *et al.* (1993) undertook a palaeoecological investigation of the site using pollen, molluscs, and ostracods on the LLAC03 core (Figure 6.7c) taken from the Crannog, just south of the northern shoreline. Due to the lake-level changes described above, the LLAC03 sequence did not contain sediments of WI age, and so efforts focused on the Holocene Marl. Walker *et al.,* (1993) demonstrated during the first 2000 yrs of the Holocene, there was rapid expansion of *Juniperus*, *Betula* and *Pinus*. Changes in sedimentation rate are also present following the elm decline and over the last 1800 yrs due to human impact on the catchment. Walker *et al.,* (1993) also described evidence for several lake-level changes as well as a short-lived climatic event inferred from a decline in *Juniperus* during in early Holocene. Jones *et al.* (1985) had also previously postulated human modification of the surrounding landscape during the mid-Holocene. Investigations by Chambers (1985; 1999) indicated that during the Mid-Holocene the surrounding land was dominated by woodland, with a closed canopy, on stable soils.

Recently, Abrook (2018) undertook a high-resolution palynological investigation using a core from the northern basin, LLAN14, which contained a complete Lateglacial sequence (Figure 6.10). The early WI (LlaP-1 & -2) was characterised by open-habitat herbaceous vegetation

dominated by *Poaceae, Artemisia, Rumex* and *Salix* (Dwarf) with some long-distance transportation of *Pinus sylvestris*. During LLaP-3a (14.0-13.8 ka BP), *Betula* declines, and arctic/alpine affiliated taxa increase (e.g., *Artemisia, Poaceae, Cyperaceae, Asteraceae, Compositae*) suggesting a brief decline in temperatures and a shift to more arid conditions. An extensive *Juniperus* scrub then establishes in LLaP-3b, although open grass land still prevailed, suggesting climatic amelioration (Lowe and Walker, 1986). In the Mid-WI (LLaP-4) open *Betula* woodland developed suggesting mature soils and temperatures of at least 12 °C (Birks 1994; van Dinter and Birks, 1996). The prevalence of *Filipendula* also suggests climatic warmth (Walker *et al.,* 1993b) and moist conditions with nutrient rich soil (Birks and Matthews 1978). During LLaP-5, a vegetation revertence to a more open and diverse habitat is observed, with a decrease in *Betula* and increases in *Pinus, Salix, Cyperaceae, Artemisia, Helianthemum, Rumex* and *Thalictrum. Filipendula* is still present suggesting the climate is not arid, unlike the previous revertence in LLaP-3a, and also suggests summer temperatures did not fall below 8-9 °C (Hormata, 1995). *Betula* woodland returned in the following zone, LLaP-6. During the LLS, LlaP-7, *Betula* woodland was replaced by *Betula nana* and a plethora of low-lying arctic-alpine herbaceous vegetation. The taxa present indicates an open exposed landscape (*Caryophyllaceae, Compositae, Thalictrum, Selaginella selaginoides*; Whittington *et al.,* 2015), disturbed soils (*Artemisia and Rumex*; Barney and DiTommaso, 2002), exposed soils (*Salix*; Walker, 1975; Beerling *et al.,* 1993) and possibly lower lake levels (*Cyperaceae*). Vegetation responded to the climatic amelioration of the early Holocene with succession of Juniper scrub (LLaP-8), *Betula-Juniperus* woodland scrub (LLaP-9), *Betula* woodland (LLaP-10) and *Corylus* woodland (LLaP-11).

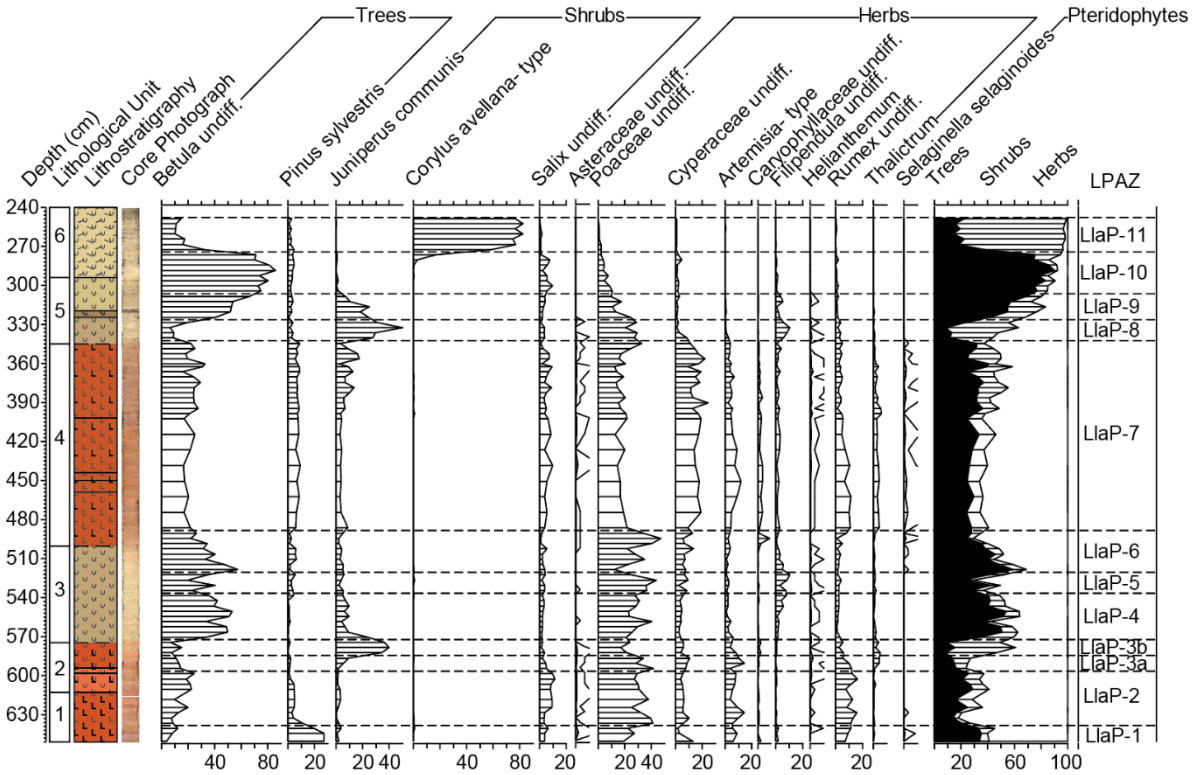

Figure 6.10, Selected pollen from the LLAN14 sequence covering the Lateglacial and Early Holocene. After Abrook (2018).

6.2.6 Chronology

Attempts to date the sequences from the aforementioned studies have been made using a variety of techniques. Jones *et al.* (1978) radiocarbon dated the Mid- and Late-Holocene in two cores using bulk samples. Walker *et al.* (1993) created a provisional chronology for the LLAC03 sequence, using the radiocarbon dates from Jones *et al.* (1993), along with several age determinations of comparable biostratigraphic horizons on other sites in south wales. These included Llanilid (Walker and Harkness, 1990), Waun-Fignen-Felen (Smith and Cloutman, 1988), Cefn Gwernffrwd (Chambers, 1982) and other sites in the Welsh Borderland (Beales, 1980) and west Wales (Hibbert and Switsur, 1976).

The best dated sequence for Llangorse is LLAN14 (Abrook, 2018; Palmer *et al.,* 2021; unpublished) in which 26 radiocarbon dates were obtained across the whole sequence and 15 were related to immediately before, during and after the LGIS. Key information related to the dates, including the uncalibrated ^{14}C age, $\delta^{13}C$ values, calibrated age ranges and the terrestrial plant macrofossils analysed are given in Table 6.1. Samples were analysed at Scottish Universities Environmental Research Centre (SUERC-) and the Keck-CCAMA Group in Irvine California (UCIAMS-). Bayesian statistics were employed as they allow robust age models to be

generated by incorporating prior information relating to the sediments. The age-depth model, which unfortunately cannot be presented within this thesis, was produced using the *p_sequence* function in OxCal v 4.4 (Bronk Ramsey, 2009) and the IntCal20 calibration curve (Reimer *et al.,* 2020). The Poisson depositional function was implemented which states that depositional events are random and allows for variability in sedimentation rates (Bronk Ramsey, 2008). The age-model errors were calculated using the 95 % confidence interval. Dates are presented as μ ± 2σ cal a BP and rounded to the nearest decade.

Table 6.1, Radiocarbon dates obtained from the LLAN14 sequence in the LGIS. For all samples from the LGIS, except 2, there was insufficient sample remained for $\delta^{13}C$ analysis.

Publication Code	Sample identifier	Conventional ^{14}C Age (1 sig)	$\delta^{13}C$	95.4% cal. BP range	Sampled material
UCIAMS-229595	LLAN14 480-484	10525 ± 40		12554 (12678-12472)	*Betula* fruits and bud scale; Silene/Lychnis seed; *Ericaceous* leaf; *Carex* seed; *Poaceae* seed; leaf and wood fragments undiff.
UCIAMS-229596	LLAN14 488-492	10960 ± 90		12901 (13075-12752)	*Betula* leaf fragments and bud scale; *Empetrum* leaf; *Juncus* seed; *Rumex* acetosa seed; *Poaceae* seed; charred wood fragments; woody fragments undiff.
UCIAMS-210603	LLAN 14 501-502	11125 ± 35		13044 (13111-12925)	*Betula* twig and leaf fragments; *Saxifraga aizoides* seeds.
UCIAMS-210597	LLAN 14 508-511	11420 ± 35		13283 (13404-13178)	*Asteraceae* seed; *Betula* fruits, *l*eaf fragments and twig; *Saxifraga aizoides* seed.
UCIAMS-225393	LLAN 14 515-516	10940 ± 100		12891 (13076-12891)	*Betula* fruits and bud scale; leaf fragments undiff.
UCIAMS-225395	LLAN 14 525-526	11240 ± 70		13154 (13307-13010)	*Betula* fruits, catkin, and leaf fragments.
UCIAMS-210602	LLAN-14 534-535	11390 ± 40		13257 (13334-13171)	*Betula* fruits, leaf fragments and twig.
UCIAMS-22597	LLAN 14 535-538	8735 ± 30		9697 (9889-9552)	*Betula* leaf fragments, bud scale and fruits; Salix bud scale; *Poaceae* seed; *Carex* seed; twigs and leaf undiff.
SUERC-81797	LLAN 14 548-549	11619 ± 45	-28.1	13483 (13353-13589)	*Betula* fruits, twigs, catkin scale and bark.
SUERC-82300	LLAN 14 565-566	12306 ± 47	-27.8	14331 (14810 – 14083)	*Betula* fruits, leaf fragments and catkin scale; *Taraxacum* seed; twig undiff.
UCIAMS-229599	LLAN 14 573-574	11810 ± 70		13668 (13505 – 13796)	*Betula* fruits and bud scale; *Poaceae* seed; *Ranunculaceae* seed

Table 6.1, (continued)

Publication Code	Sample identifier	Conventional ^{14}C Age (1 sig)	δ^{13}C	95.4% cal. BP range	Sampled material
UCIAMS-225396	LLAN 14 582-584	12180 ± 35		14085 (14185 – 13886)	*Betula* fruits and leaf fragments; *Rumex acetosella* seed.
UCIAMS-229600	LLAN 14 590-591	12300 ± 70		14360 (14828 – 14060)	*Betula* leaf fragments
UCIAMS-225397	LLAN 14 606-610	12545± 45		14854 (15115 – 1452)	*Betula* fruits and catkin scale; *Dryas octopetala* leaves; leaf fragments undiff.
UCIAMS-210598	LLAN 14 610-614	12750 ± 80		15216 (15498 – 14977)	*Betula* fruit, bud scale and leaf fragments; Ericaceous leaf fragment

6.3 Old Buckenham Fen, Norfolk, East Anglia

6.3.1 Site location and vicinity

Old Buckenham Fen (52°29'19" N; 01°01'03" W;) is a former lake basin situated in central East Anglia, southeast Britain (Figure 6.12a & 6.12b), currently covered with fenland measuring 1.5 x 0.6 km (Figure 6.12c). It is located 2.5 km south of Attleborough, 47 km inland from the east coast and lies at an altitude of 28 m asl. The site was overlaid by peat, which was cut away for fuel in the mid-late 1800's (Tallantire, 1956). The current Mere is a man-made feature, dug in the late 1800's to form a private fish-lake. The area is covered by a network of drainage channels although many are now overgrown and infilled. The main drain is a straightened river channel, just north of the current mere, constrained by the main dyke of the fen running from the NE and flows to the west. Due to the limited extent of the headwater and shallow nature of the valley, much of the water comes from subterranean springs. The site currently has SSSI status.

The current fen vegetation is dominated by Sword sedge (*Cladium mariscus*) and also *Phragmites communis, Typha latifolia, Schoenus nigricans, Carex, Molinia coeulea* and *Chara* (Tallantire, 1956). A rich associate flora, which varies depending on ground level, includes *Epipactis, Vicia cracca* and *Parnassia palustris* (Tallantire, 1953a). The southwest end of the site is being colonised by *Betula-Salix* scrub.

East Anglia currently has a cool temperate climate and experiences mean daily maximum temperatures of 6.7 °C in January, 21.9 °C in July and 13.9 °C annually. Mean annual rainfall of

662 mm and is evenly distributed throughout the year with 56 mm falling in January and 58 mm in July on average. Data from meteorological station at Morley St Botolph, 10 km north of Old Buckenham Mere; Met Office data 1981-2010.

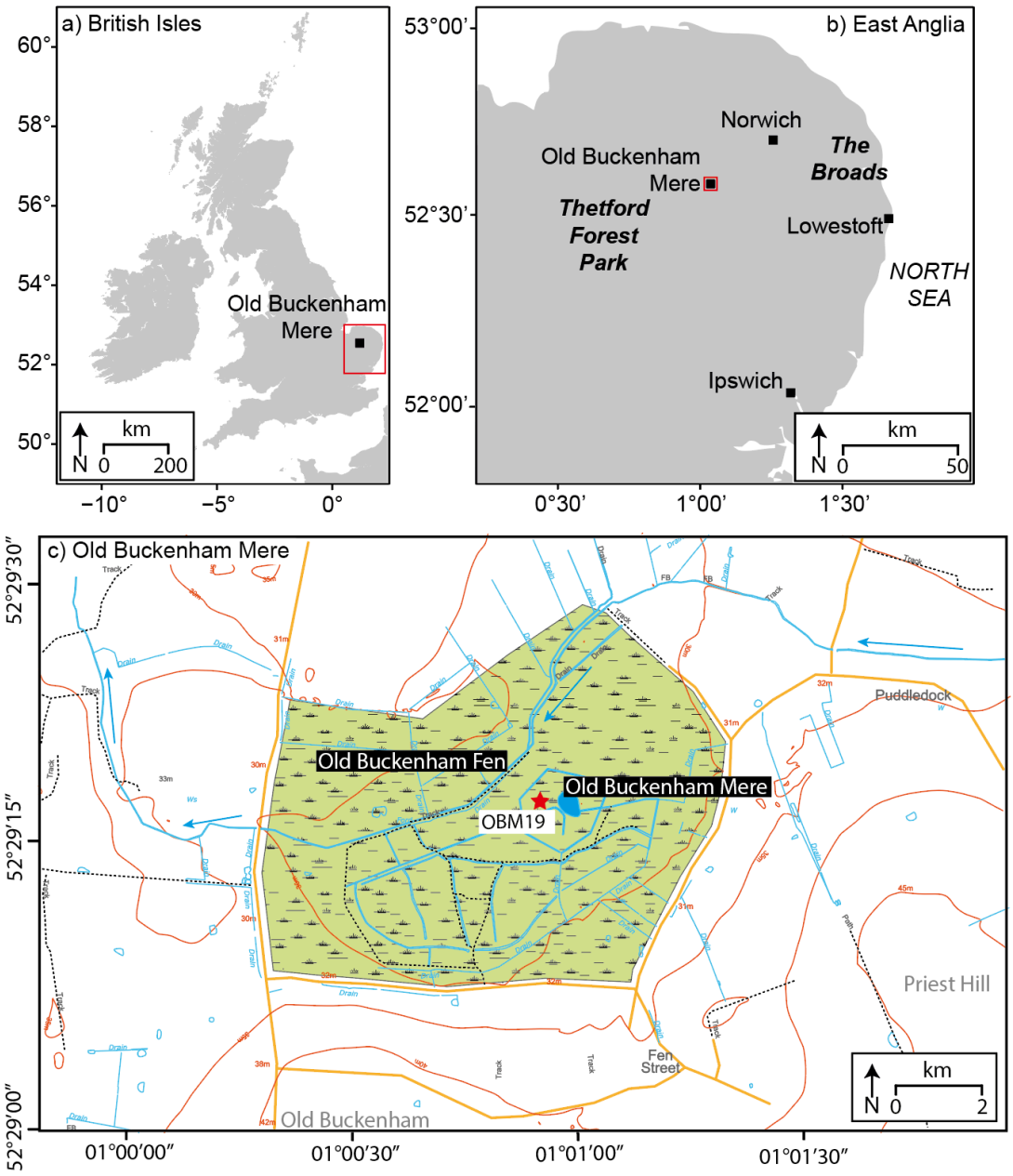

Figure 6.11, Location maps for Old Buckenham Mere. (a) A map of Britain and Ireland showing the location of East Anglia marked in red; (b) map of East Anglia and the location of Old Buckenham Mere marked in red; (c) topographic map of site showing the coring location (red star) and 5 m contours. Streams and drainage channels are in in blue and roads in orange, respectively. Walking trails denoted by dotted black line. Data downloaded from digimap.edina.ac.uk © Crown Copyright and database rights (2020) Ordnance Survey (1000252525).

6.3.2 Geology and topography

The main bedrock formations surrounding Old Buckenham Mere belong to the White Chalk subgroup deposited 66 to 100 million years ago in warm chalk seas (Figure 6.12). An array of chalk formations make up this subgroup including the Lewes Nodular, Seaford, Newham, Culver and Portsmouth Chalk Formations. There are also localised areas of Quaternary crag deposits including the Norwich Crag Formation to the east-south-east of the site. Immediately surrounding and underlaying the site, the superficial deposits are from the carbonate-rich Lowestoft and Happisburgh glaciogenic formations which are composed of clay, silt, sand and gravel (Figure 6.13). To the north, east and south of the fen, superficial deposits are dominated by diamicton of the Lowestoft Formation. To the west, a complex mosaic of superficial deposits occurs composed of aeolian coversands and riverine sediments including Croxton Sands and Gravels, Banham clays and silts, and Lodge Farm silts and clays. There is also a network of river terrace deposits, composed of sediment from palaeo-glaciofluvial processes, which have subsequently been incised by contemporary rivers, depositing alluvial sediment. The lake is situated in a shallow valley where topography undulates between 28 and 50 m asl (Figure 6.12c).

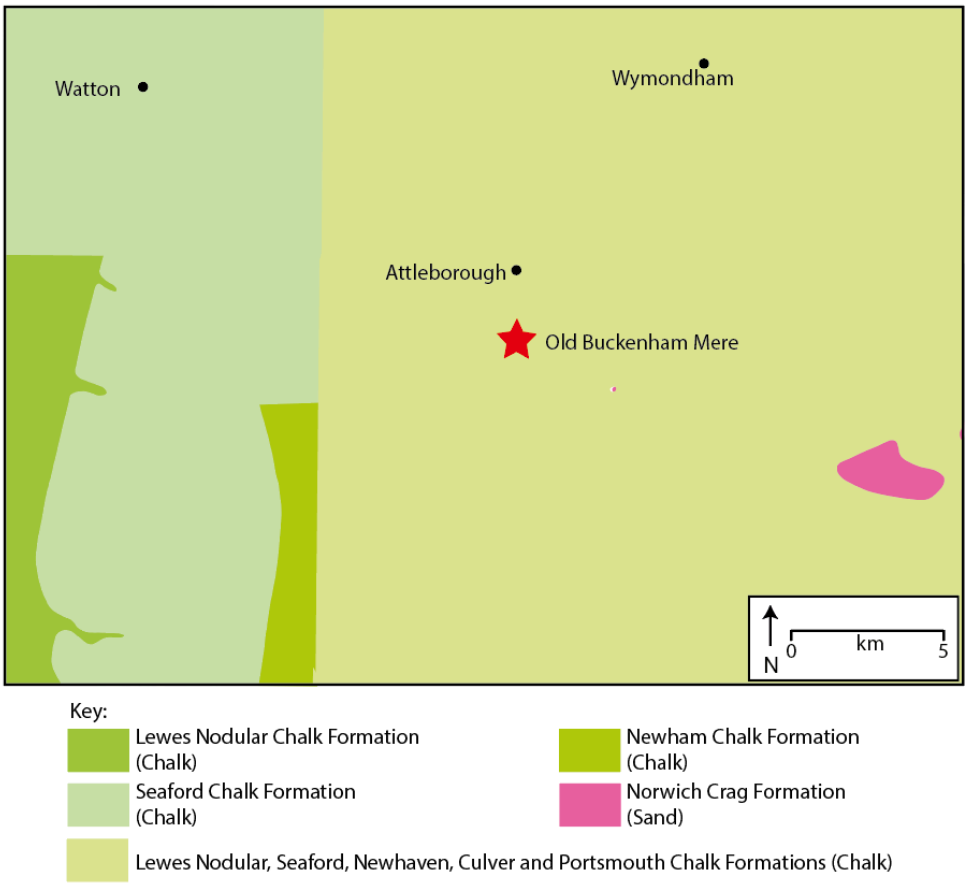

Figure 6.12, Bedrock geology in the vicinity of Old Buckenham Mere, East Anglia. Data downloaded from digimap.edina.ac.uk © Crown Copyright and database rights (2020) British Geological Survey materials © (2020).

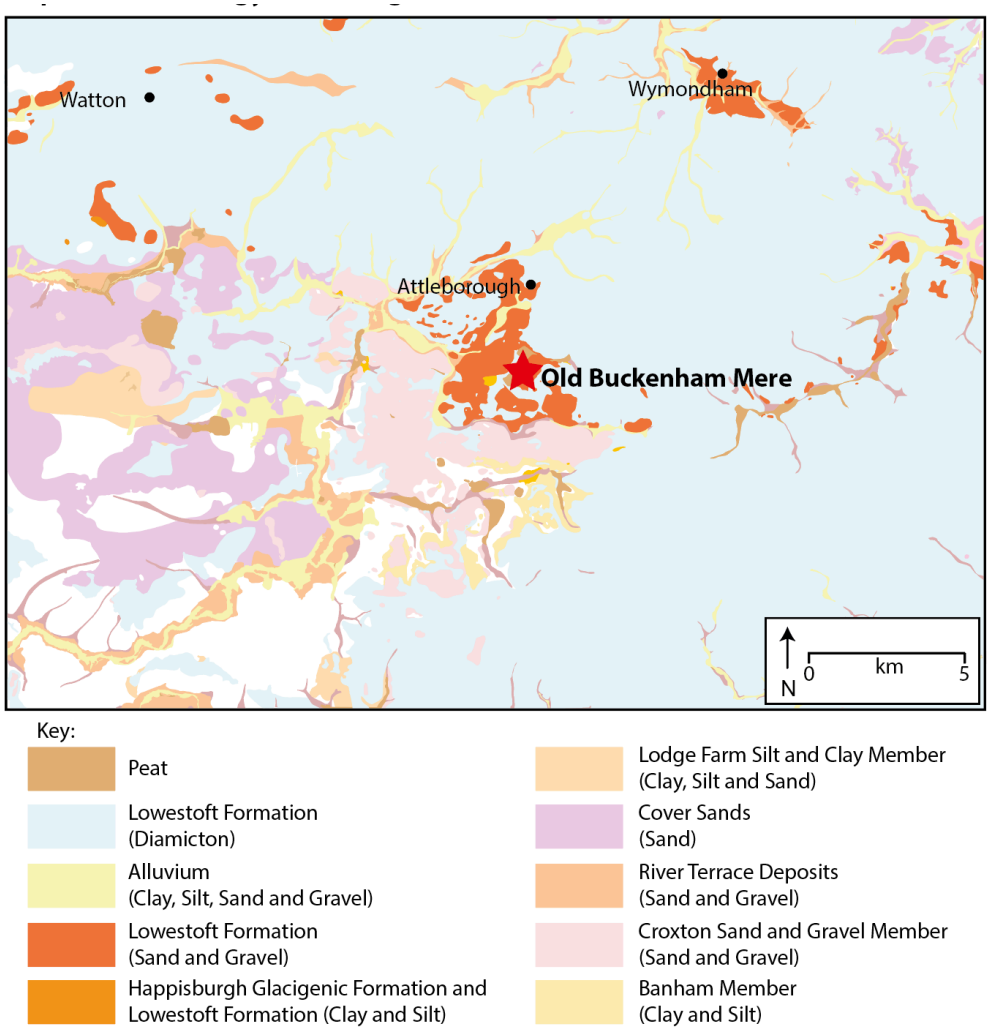

Figure 6.13, Superficial geology in the vicinity of Old Buckenham Mere, East Anglia. Data downloaded from digimap.edina.ac.uk © Crown Copyright and database rights (2020) British Geological Survey materials © (2020).

6.3.3 Glacial history

The locality of Old Buckenham Mere was last glaciated during the Anglian (Mitchell *et al.,* 1973; Perrin *et al.,* 1979), correlated to MIS12 (Lee *et al.,* 2004), and which is considered the most extensive glaciation to have affected eastern England during the Quaternary. There is some evidence for the glaciation of East Anglia during subsequent cold stages, MIS 10 and MIS 6 (Hamblin *et al.,* 2005), however, the age of these deposits is still debated (Rose, 2009). During the most recent glaciation, MIS-2/GS-2, the British and Irish Ice Sheet impinged on the northern edge of East Anglia from the North Sea around 21.5 - 20 ka BP (Hughes *et al.,* 2016; Evans *et al.,* 2019), though glacial ice did not venture far onto land in East Anglia. However, it did create an ice dam, blocking the drainage of river systems and glacial meltwater into the North Sea (Gibbard *et al.*, 2018; Clark *et al.,* 2018). This led to the creation of proglacial Lake Sparks and

Lake Fenland (Gibbard *et al.,* 2018), for which Old Buckenham Mere may have been on the south-eastern margin (Figure 6.14). During the Devensian, intense periglacial activity occurred causing the localised deposition of cover sands (Gibbard *et al.,* 2018).

6.3.4 Lake formation and lake-level changes

It is thought that the palaeolake at Old Buckenham Mere formed in a 'thermo-cirque', a periglacial thermokarst depression formed during the Devensian (West, 1991). This is contrary to the majority of LGIT sequences in Britain, where sediments accumulated in depressions caused by dead ice as the LGM Devensian ice retreated (Walker and Lowe, 2017). Thermokarsts would have initially started out as thaw lakes with the accumulation of surface water from springs and melting ground ice along pre-existing minor lines of drainage (West, 1991). Through the action of periglacial processes operating under glacial climates, substantial depressions in the land surface form primarily through the thawing of the ice-rich sediments causing thermokarsts (West, 1991). Other process can also aid the formation including thermo-abrasion, the thermal and mechanical energy of water, and thermo-denudation - the thermal energy of the air and solar radiation acting on the surrounding exposed slopes. Collectively these processes cause back-wearing, leading to an increase in thermokarst size. West (1991) suggests these features eventually form a flat bottom, however, due to the relative resistance of the surrounding glacial deposits to periglacial back wearing processes at OBM, the former lake retained a V shape (Boreham and Horne 1999). Many lakes around East Anglia are formed by the processes described above including Sea Mere (Hunt and Birks, 1982), Hockham Mere (Bennett, 1983) and Grunty Fen (West, 1991).

There is no published information specifically on potential palaeo-lake level changes at Old Buckenham Mere during the Devensian. However, the location is thought to be part of the nebulous Glacial Lake Fenland which has a proposed lake-level of 30 m a.s.l. (Clark *et al.,* 2018) (Figure 6.14a). Plotting the 17 ka BP maximum ice limit for the BIIS on the model land surface topography, it gives a plausible ice limit to permit the formation of a glacial lake at OBM (Hughes *et al.,* 2016) (Figure, 6.14b). There is some evidence for a shoreline at 30 m a.s.l in the fields to the north (Palmer, *pers. comms.*) and south and southwest (Matthews, *pers. comms.*) of OBM. When the glacial lake drained due to the retreat of the BIIS at the end of the last glacial, a smaller body of water forms with a lake level of 28.5 m a.s.l., although the route for such drainage is not clear based on modern imagery (Matthews, pers. comms.). It is currently

unclear when this change in lake level happened and if any subsequent lake level changes occurred.

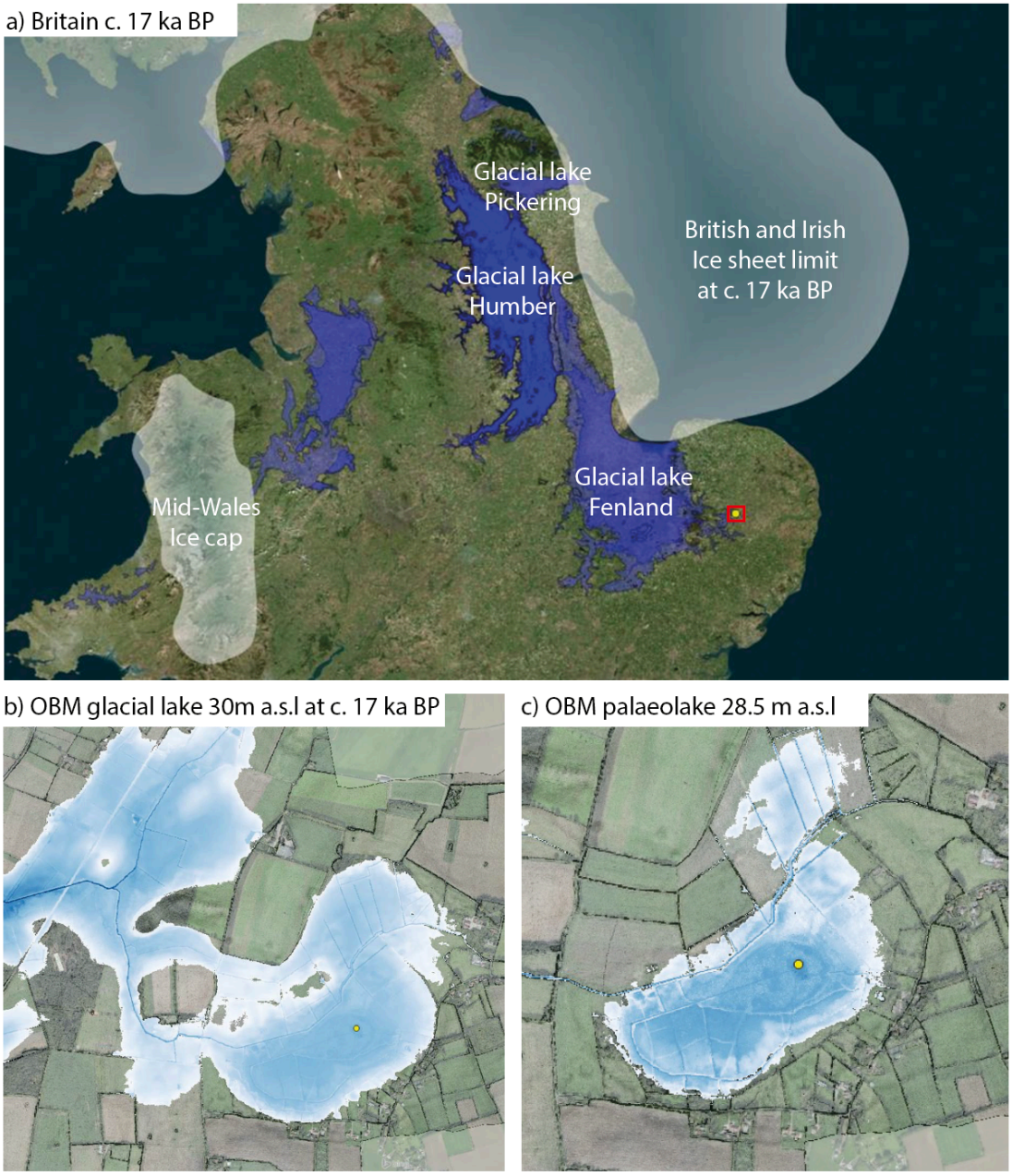

Figure 6.14, BIIS limits and the glacial lakes of Britain at *c.* 17ka BP. a) Devensian ice limit of the British and Irish Ice Sheet at *c.* 17 ka BP (Hughes *et al.,* 2016) and the proposed 30 m proglacial lake level for Glacial lakes Pickering, Humber and Fenland. b) a close up of Old Buckenham Mere with the proposed 30 m lake level at *c.* 17 ka BP. c) lake level of OBM when the BIIS retreated and glacial lakes drain which was *c.* 28.5 m a.s.l. (b) and (c) are denoted by the red square in (a). Yellow dot denotes the coring location in all diagrams. (Source: Dr Ian Matthews).

6.3.5 Previous palaeoecological and palaeoclimatic investigations

Previous palaeoecological and palaeoclimatic investigations at Old Buckenham Mere have been very limited with the only studies conducted by Tallantire (1953a) and Godwin (1968).

Tallantire (1953a) focused on the stratigraphy of the basin (Figure 6.15) and some sparse macrofossil finds (Figure 6.15; Table 6.2). Tallantire (1953a) undertook a borehole survey of the site using a Hiller peat borer along a north-south transect just to the west of the man-made mere. The saturated ground at the site meant the central portion of the transect could not be cored and there was incomplete retrieval of sediments from several boreholes. Nevertheless, their deepest core suggested at least 14 m of lake sediments was present at the site. The bottom of the sequences contained a poorly sorted diamicton containing a clayey silt matrix with chalk granules, termed a 'chalk porridge'. Tallantire noted this has also been found at the base of other East Anglian lakes e.g., Hockham Mere (Godwin and Tallantire 1951). Tallantire (1953a) attributed the 'chalk porridge' to either a glacial outwash material or a derivative of chalky boulder clay (or till). The overlying units of 'basal calcareous lake mud', 'clay mud' (laminated structure) and 'lower calcareous mud' were tentatively correlated to the Lateglacial. The presence of several hybrid tree birch fruits (*B. nana* x *pubescens*) in the basal calcareous lake muds also suggested a Late-glacial age based on their co-occurrence in dated sequences from neighbouring sites. The subsequent layers of lake chalk, lake marl/shell mud and the upper calcareous lake muds were attributed to the post-glacial climate optimum (Holocene).

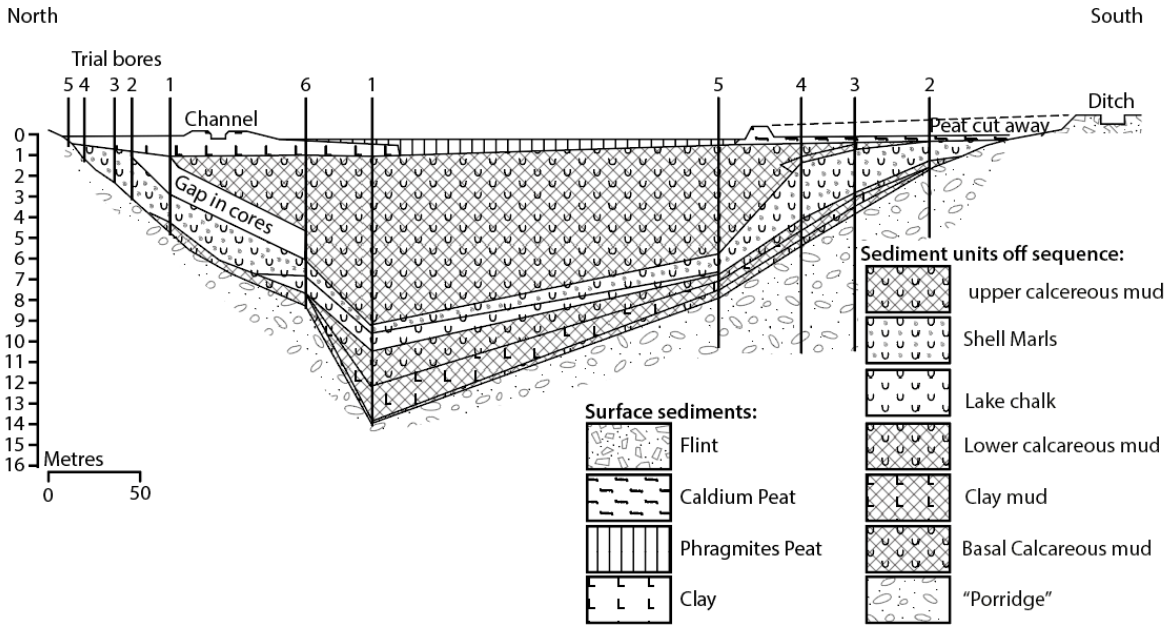

Figure 6.15, Bathymetry of Old Buckenham Mere. After Tallantire (1953a).

Table 6.2, Plant macrofossil results for Old Buckenham Mere. (After Tallantire, 1953a).

Species/type remains:	Deposit Material	Upper calc. mud	Shell marl	Lake chalk	Lower calc mud & Clay mud	Basal Calc. mud
Ceratophyllum demersum	Fruit	2	1			
Myriophyllum spicatum	Fruit	1				
Naias marina	Fruit	1	3			
Nuphar luteum	Fruit	5	1			
Potamogeton spp.	Fruit stone	1				
P. praelongus	Fruit stone	7				
P. natans	Fruit stone	5				
P. densus	Fruit stone	1				
P. pusillus group	Fruit stone	3				
Scripus lacustris	Fruit	3				
Carex spp.	Fruit	1				
C. aquatilis group.	Fruit					1
Cladium mariscus	Rhizome		+			
Calluna vulgaris	Twig				2	
Alnus glutinosa	Wood	++				
Salix spp.	Wood	+		+		+
Betula pubescens	Fruit					2
B. pubescens x nana	Fruit				1	2
B. pubescens x nana	Cone scale					1
Drepanocladus spp.	Leaves				+	+
Sphagnum spp.	Leaves	+				
Chara spp.	Oospores		++	+		

Godwin (1968) revisited the site for palynological analysis and retrieved two sequences, again with some possible gaps in the stratigraphy, but generally corresponding well with Tallantire's (1953a) stratigraphy. The basal 50 cm of Borehole 1 and the basal 1 m of Borehole 2 (Figure 6.16), had a characteristic Lateglacial fauna assemblage dominated by *Betula* (*nana* type),

Pinus, Graminae and *Cyperaceae, Artemisia, Rumex* and *Ranunculus*. Vegetation was open in nature with the presence of *Helianthemum, Armeria, Thalictrum, Plantago, Filipendula, selaginella* and *Lycopodium selago*. Godwin (1968) noted the lack of clear changes in vegetation usually seen in Lateglacial pollen assemblages and the absence of alternating minerogenic and organic deposits in the stratigraphy.

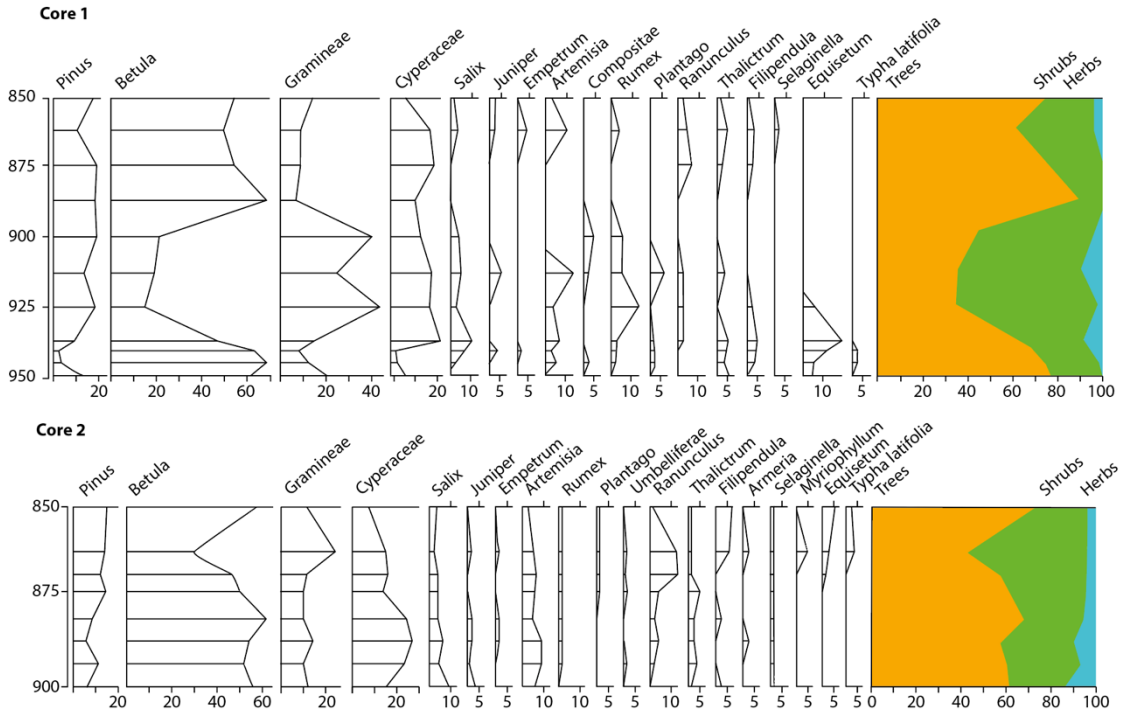

Figure 6.16, Pollen data for two basal cores from Old Buckenham Mere. After Godwin (1968)

6.4 Chapter Summary

This chapter introduced the study sites selected for this thesis, providing information on parameters which need to be considered when interpreting the T_{Jul} and $\delta^{18}O$ records produced by this thesis. Information on previous palaeoecological and palaeoclimatic interpretations were outlined along with any previous chronological work completed on the sites.

Crudale Meadow in the Orkney Isles of Scotland is an infilled palaeolake. The carbonate-rich tills surrounding the site may potentially be a source for detrital geological carbonate which could affect the $\delta^{18}O$ signal. The lake deglaciated several kyrs before the start of the LGIS and the evidence for the formation of glaciers during the LLS is very limited, strongly suggesting glacial meltwater did not enter the palaeolake during the LGIS. The small size of the lake means

significant lake level changes were unlikely to have occurred during the LGIS. The landscape was largely open with vegetation largely dominated by herbaceous and low shrub taxa, characteristic of unstable substrates, potentially meaning erosion of the surrounding hillslope during more adverse climatic periods. The CRUM1 sequence has one of the best age-models for the LGIT and early Holocene, based on tephrochronology, in NW Europe.

Llangorse is an extant lake in south Wales with an infilled basin to the north. The superficial and bedrock formations are largely composed of minerogenic clays, silts, sand, and grit, although some geological limestone is present in the catchment and could be a source for detrital contamination. There is some evidence for potential lowering of lake levels at the end of the LGIS or start of the LLS based on sediment-stratigraphy. Ice from the mid-Wales ice cap during the LGM stopped just north of the current lake and created an ice-dammed lake. However, ice retreated several kyrs prior to the start of the LGM and there is no evidence of active Cwm glaciers in the Llangorse catchment during the LLS, meaning glacial meltwater would not have affected Llangorse during the LGIS. The majority of palaeoecological and palaeoclimatic work was conducted in the Holocene but a more recent study has shown that during the early part of the LGIS, habitat was open and largely composed of arctic-alpine affiliated taxa, while the mid- and late-LGIS was more closed with prevalent *Betula* woodland. There is evidence for two reverences to more open habitat during the LGIS. The LLAN14 sequence has one of the highest number of radiocarbon dates with 15 immediately before, during and after the LGIS, firmly dating the sequence.

Old Buckenham Mere is an infilled palaeolake in SE Britain. The surrounding carbonate-rich tills could provide a source of detrital geological carbonate although they are likely heavily weathered due to their age (>400 kyrs old). OBM was part of the Fenland glacial lake system and experienced a drop in lake level of *c.* 1.5 m when ice from the BIIS retreated at *c.* 17 ka BP. It is currently not known if further lake level changes occurred after 17ka BP. Palaeoecological and palaeoclimatic investigations are limited for the site as it was last studied over 50 yrs ago, though plant macrofossil and pollen assemblages of the basal sediments indicate the presence of plant taxa usually associated with the Lateglacial. There is currently no detailed chronology for the site and current age estimation of Lateglacial age is based on biostratigraphy outlined above.

Chapter 7: Crudale Meadow results and interpretation

Chapter overview

This chapter will present the sedimentology, stratigraphy and tephrochronology of the CRUM1 sequence produced by Timms *et al.,* (2018) alongside the radiocarbon, chironomid, oxygen isotope data generated for this study. The environmental influences on both the chironomid assemblages and $\delta^{18}O$ record will be discussed and used as the basis for environmental/climatic reconstruction. Crudale Meadow is particularly important in understanding the spatial expression of ACEs across the British Isles because there are currently no other published high-temporal resolution quantified palaeoclimate records for the northern most regions of the British Isles, and so the current N-S transect of sites only goes as far north as Loch Ashik and Abernethy Forest, some 200 km further south of Crudale Meadow.

7.1. Sedimentology

The cores that make up the CRUM1 sequence are presented in Figure 7.1. Dr Timms completed the core sedimentology and the sedimentary physical parameters ($CaCO_3$, LOI, Mag Sus) to align the individual core sections and form the CRUM 1 composite sequence (Figure 7.2a). The CRUM1 composite sequence is 6.88 metres in length and is broadly composed of two marl rich phases of sedimentation, representing the LGIS (CM-L2) and the Holocene (CM-L4 to CM-L7), alternating with two clastic dominated phases of sedimentation representing the DS (CM-L1) and LLS (CM-L3). The physical parameters of the sediments deposited during the LGIS, as well as during the end of the DS and the beginning of the LLS, are shown in greater detail in Figure 7.2b and detailed sedimentological descriptions are provided in Table 7.1.

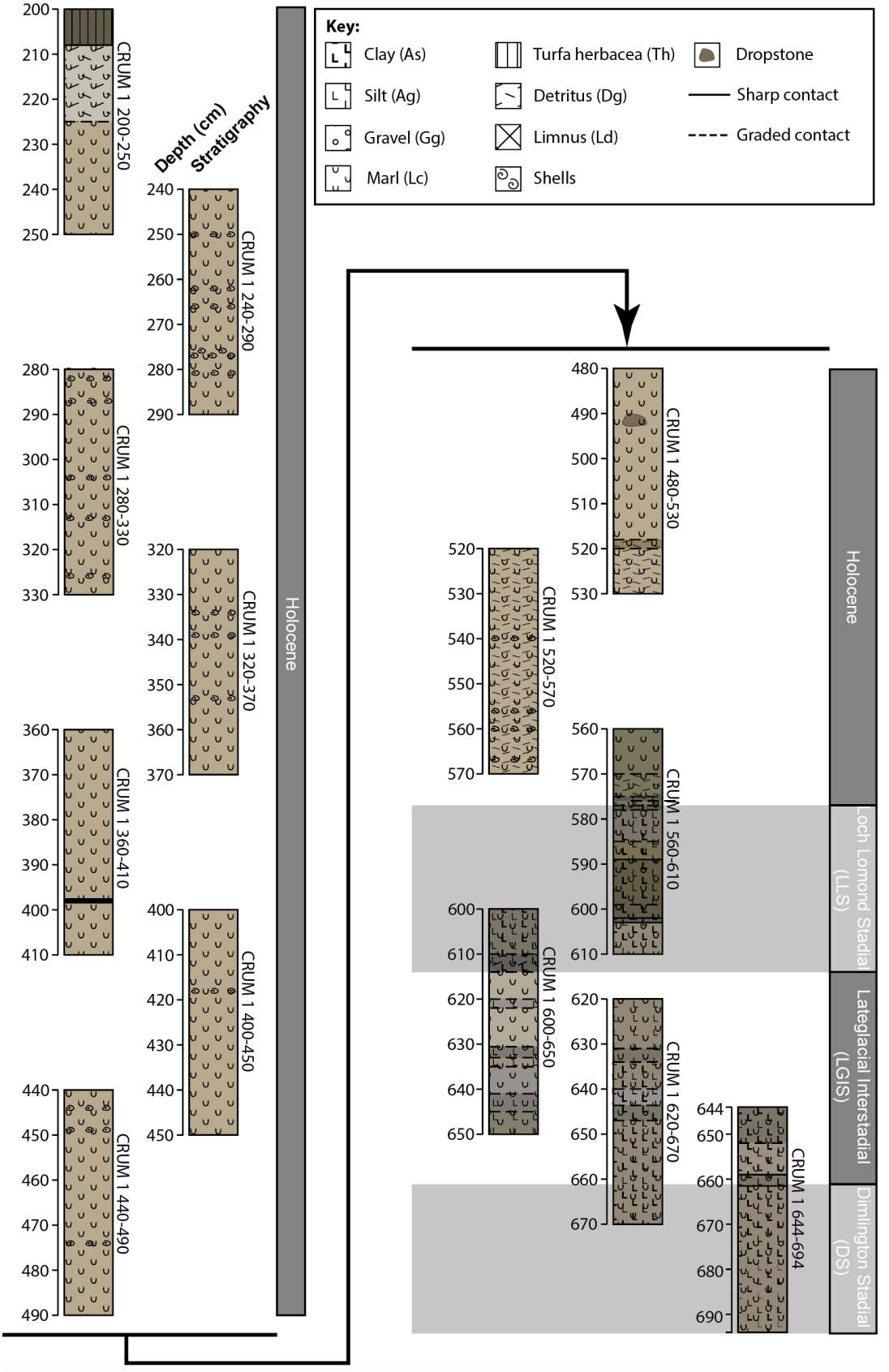

Figure 7.1, Sedimentology and stratigraphy of individual Russian core sections that make up the CRUM1 sequence (Timms *et al.*, 2018). Swatches relate to the Troels-Smith classification scheme and colours reflect the Munsell colour system.

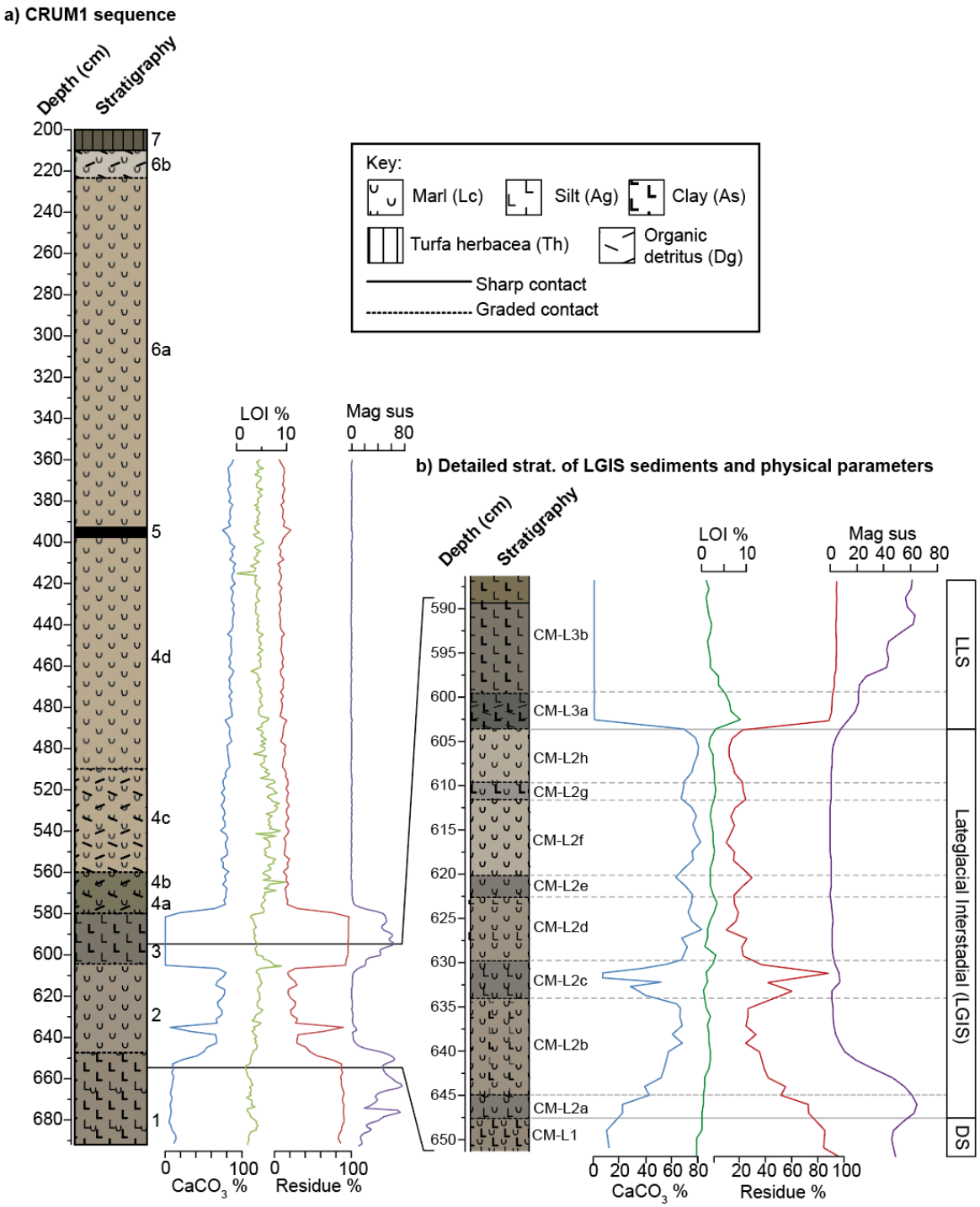

Figure 7.2, Sedimentology and stratigraphy of the CRUM1 sequence. **a**) Simplified lithostratigraphy and physical parameters of the CRUM1 sequence at Crudale Meadow, spanning the Lateglacial and Early Holocene; **b**) detailed lithostratigraphy and physical parameters of the LGIS and early LLS showing proportions (%) of calcium carbonate ($CaCO_3$), organic (Loss-on-Ignition) and minerogenic by difference (Residue) components completed by (Timms *et al.,* 2018). Lithostratigraphic zones are labelled CM-L*n* and colours are from the Munsell colour system.

Table 7.1 Lithostratigraphic units for the Lateglacial from the CRUM1 sequence.

Unit	Depth (cm)	General description	Troels-smith	Munsell colour
CM-L3b	599-357	Silty-clay	As2 Ag2	5Y 4/1 dark grey
CM-L3a	602-599	Silty-clay with organic detritus	As2 Ag1 Dg1	2.5Y 3/1 very dark grey
CM-L2h	609-602	Marl	Lc4	5Y 5/1 grey
CM-L2g	611-609	Silty-clay Marl	Lc2 Ag1 As1	5Y 4/1 dark grey
CM-L2f	620-611	Marl	Lc4	5Y 5/1 grey
CM-L2e	622-620	Silty-marl	Lc2 Ag2	2.5Y 4/1 dark grey
CM-L2d	630-622	Silty-marl	Lc2 Ag2	5Y 5/1 grey
CM-L2c	634-630	Silty-clay marl	Ag2 As1 Lc1	5Y 4/1 dark grey
CM-L2b	645-634	Silty-clay marl	Lc2 Ag1, As1	5Y 5/1 grey
CM-L2a	648-645	Silty-marl	Ag2 Lc2	5Y 4/1 dark grey
CM-L1	688-648	Silty-clay, some carbonate	Ag2 As1 Lc1	5Yr 4/1 dark grey

CM-L1 (688-648 cm) is predominantly composed of silty-clay (90 %) with a small amount of $CaCO_3$ (10 %). The minerogenic component has high magnetic susceptibility values of up to 91 $x10^{-5}$ SI units, the highest within the whole sequence. LOI displays some of the lowest values for the sequence being between 2-4 %.

Within the marl sediments of CM-L2 (648-602 cm) there is large variability in the proportion of $CaCO_3$ and minerogenic material, as well as sediment colour, leading to the subdivision of CM-L2 into eight subunits (see Figure 7.2b and Table 7.1). $CaCO_3$ increases during CM-L2a & -L2b (648-634 cm) from 10 to 67 % which is matched by declines in minerogenic sediment content along with declines in magnetic susceptibility from 63 to 1 $x10^{-5}$ SI units. During CM-L2c (634-630 cm) a strong decline in $CaCO_3$ content occurs from 67 % to 8 % and minerogenic material increases from 30 to 90 %. Magnetic susceptibility also increases to 7 $x10^{-5}$ SI units. In the following sub-units (CM-L2d to -L2h; 630-602 cm) $CaCO_3$ varies between 75 to 90 % and magnetic susceptibility remains low, 0 to 2 $x10^{-5}$ SI units. However, small declines in $CaCO_3$ occur during CM-L2e (622-620 cm) and CM-L2g (611-609 cm) with values reaching 60 and 65 %, respectively, and are accompanied by corresponding increases in minerogenic material. Although minerogenic sediment content increases during CM-L2e and CM-L2g to c. 30 %, magnetic susceptibility does not show a discernible increase. Throughout all of CM-L2, LOI gradually increases from 3 to 5 %.

LL-L3a (602-599 cm) exhibits a large decline in $CaCO_3$ to 0 % and minerogenic sediment content increases to 95 % at this stage. At the start of the zone, LOI abruptly increases to 9 % before declining to 5 %. Many fragments of moss and herbaceous material were observed during sampling. Very low

values of $CaCO_3$ combined with high levels of minerogenic sediment content continues into LL-3b, though LOI decreases to 4 % and organic macro-remains are more degraded. Units LL-L4, -L5, -L6 & -L7 (599-357 cm) are not discussed further as these are of Holocene age and therefore beyond the scope of this thesis.

7.2 Chronology

The initial age-depth model for the CRUM1 sequence was constructed by Timms *et al.* (2018) based on the occurrence of thirteen tephra layers, of which six could be correlated to known eruptions. This study has added an AMS radiocarbon date in the latter part of the LGIS. The radiocarbon sample consisted of hand-picked terrestrial plant macrofossil remains from between 614-615.5 cm including leaves of *Dryas octopetala*, *Empetrum,* and *Betula nana* along with fruits of *Betula nana*. The radiocarbon sample yielded an uncalibrated age of 11,626 ±53 ^{14}C a BP, and a calibrated modelled age of 13,491±134 cal a BP using OxCal version 4.4.2 (Bronk Ramsey, 2008, 2009) (Table 7.2). The inclusion of the radiocarbon date in the age model has reduced the age error estimate for the latter half of the LGIS by more than 50 %, from *c.* 630 – 610 cm. The age estimates for the Borrobol, Penifiler and Vedde Ash tephra layers have also been updated using the remodelled data utilising the new IntCal20 curve, although the changes in the age estimates are minimal at *c.* ±25 yrs (Table 7.2). The new age-depth model for the CRUM1 sequence is constructed in OxCal using a P-sequence and is presented in Figure 7.3. The age-model errors were calculated using the 95 % confidence interval.

Table 7.2, Chronological markers used in the construction in the age-depth model for the Lateglacial part of the CRUM1 sequence.

Dated horizons	Strat depth (cm)	Material	Radiocarbon age (μ ±1 σ ^{14}C yrs)	Original Calibration using IntCal13 (μ ± 2σ Cal a BP) (Bronk Ramsey *et al.,* 2015)	Recalibrated IntCal20 age (μ ± 2σ Cal a BP)
Vedde Ash	587	Tephra	N/A	12,023 ±86	11,997 ±80
UBA42543	614-615.5	Terrestrial plant macrofossils	11,626 ±53	N/A	13,491 ±134
Penifiler Tephra	632	Tephra	N/A	13,939 ±132	14,024 ±154
Borrobol Tephra	638	Tephra	N/A	14,098 ±94	14,107 ±116

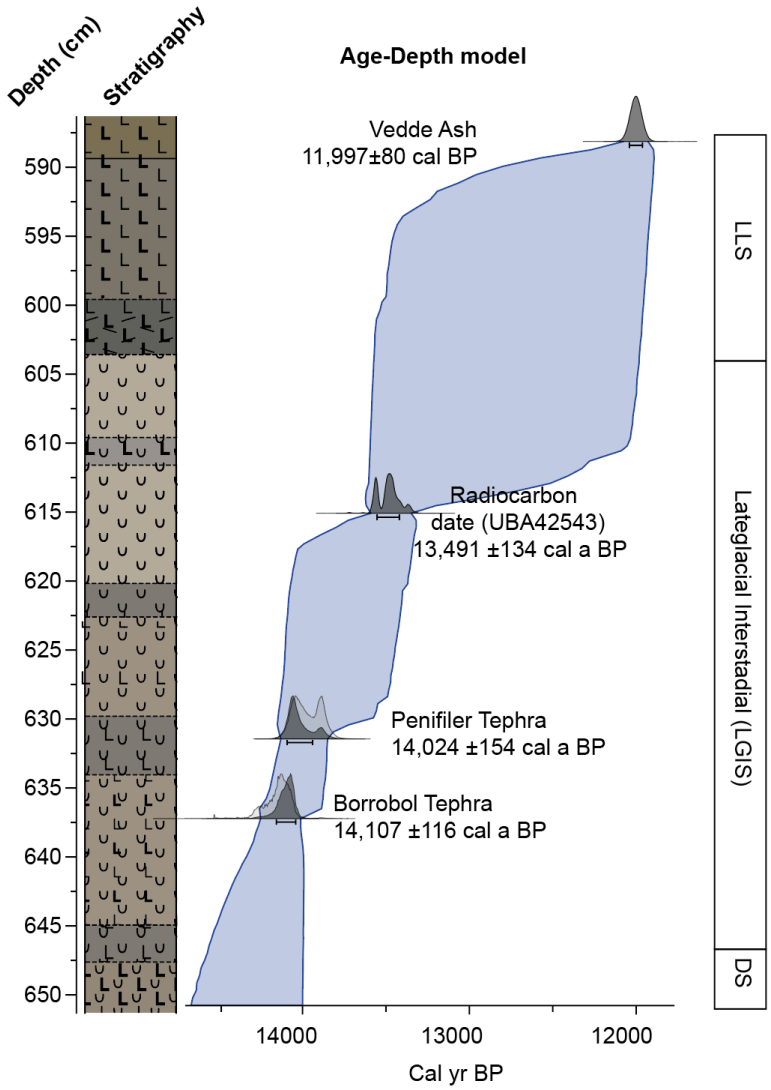

Figure 7.3, The new updated age model for the Lateglacial section of the CRUM1 sequence.

7.3 Chironomids

7.3.1 assemblages

In total 51 different chironomid taxa were identified in the 63 samples analysed, with assemblages displaying considerable variation down-core (Figure 7.4). A broken stick model identified six significant assemblage zones which are denoted as CM-C*n*. Head capsule concentrations are generally greater than 110 HCs/gram throughout the sequence, except in CM-C1 and CM-C6. The main changes in assemblage composition will now be described for each chironomid zone.

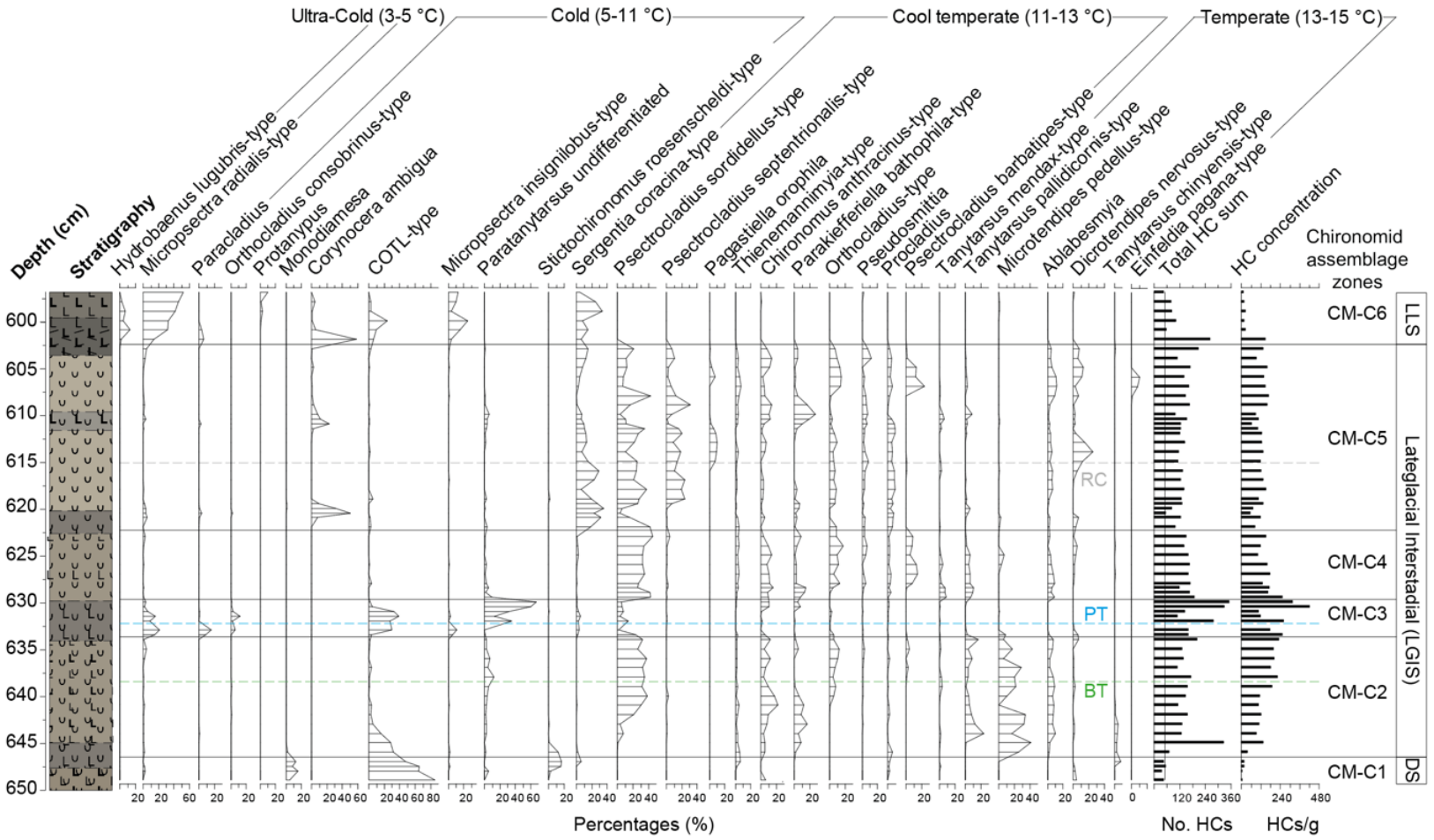

Figure 7.4, Percentage abundance diagram of selected chironomid taxa present in the LGIS sediments at Crudale Meadow alongside the CRUM1 sequence stratigraphy. Chironomid assemblage zones (CM-Cn) are marked on the right. Taxa are arranged by their T_{Jul} optima in the modern calibration dataset (Heiri *et al.,* 2011) as calculated using a Weighted-Averaging model with coolest optima on the left and warmest optima on the right. Head capsules concentrations (HCs/gram) and total head capsule counts are displayed on the right.

CM-C1: composite depth: 650-646.5 cm

CM-C1 is dominated by *COTL*-type which declines from 85 to 65 % throughout the zone. *Monodiamesa* is the second most abundant taxon consistently present forming on average 8 % of the assemblages. In the latter part of the zone, *Stictochironomus* and *Tanytarsus chinyensis*-type occur at 16 % and 8 % abundance, respectively. HC concentrations are very low throughout CM-C1 but do increase from 1 to 20 HCs/gram.

CM-C2: composite depth: 646.5 - 633.75 cm

In CM-C2, a higher number of taxa are present. *M. pedellus*-type abruptly increases and becomes the most abundant taxa forming 41 % of the assemblages at the start of the zone, though abundances decline throughout to 6 % by the end of the assemblage zone. The assemblages of the remainder of the zone are largely composed of *Psectrocladius sordidellus*-type at 30-40 %. *COTL*-type continues to decline from 31 to 3 % by 641 cm and remains low for the rest of CM-C2. HC concentrations increase throughout CM-C2 from 40 to 237 HCs/gram.

CM-C3: composite depth: 633.75 – 629.75 cm

The faunal assemblage of CM-C3 exhibits a dramatic change from the previous zone with *Paratanytarsus* undifferentiated now being the most abundant taxon, forming up to 67 % of the assemblage. *COTL*-type, *Micropsectra radialis*-type and *Paracladius* increase in abundance to 49 %, 22 % and 16 %, respectively. *Ablabesmyia*, *Orthocladius*, *T. pallidicornis*-type, and *M. pedellus*-type all largely disappear. *P. sordidellus*-type continues to be present at lower abundances around 6 %. *C anthracinus*-type and *P. bathophila*-type reappear before the end of the zone. HC concentrations are highly variable and range from 110 to 426 HCs/gram, the highest for the LGIS at Crudale Meadow.

CM-C4: composite depth: 629.75 - 622.5 cm

P. sordidellus-type again becomes the most abundant taxon comprising on average 35 % of the assemblage. *C. anthracinus*-type, *Orthocladius*-type and *Ablabesmyia* also increase again to 10 %, 9 % and 4 % on average. *Psectrocladius barbatipes*-type shows its first large increase to 7 %. *M. pedellus*-type is largely absent in CM-C4. *Pseudosmittia* is continuously present at 3 %. HC concentrations remain relatively constant at 150 HCs/gram.

CM-C5: composite depth: 622.5 - 602.5 cm

Between 622 and 619 cm, *Corynocera ambigua* peaks at 31 %. *M. radialis*-type, *Paracladius* and *Paratanytarsus* undifferentiated also briefly reappear in low abundances. *D. nervosus*-type,

Ablabesmyia and *Orthocladius*-type disappear while *P. sordidellus*-type and *C. anthracinus*-type decline to 1 % and 4 %, respectively. *S. coracina*-type increases to 35 %. *Pseudosmittia* is intermittently present with abundances of 0 – 4 %. HC concentrations also decline to around 56 HCs/gram.

From 619 to 612 cm, *P. sordidellus*-type and *D. nervosus*-type are the most abundant taxa present, increasing to 37 and 25 %, respectively. *Ablabesmyia, Orthocladius* and *Pagastiella orophila* also increase to 7, 8 and 10 %, respectively. *Psectrocladius septentrionalis*-type appears and increases to 24 %. *Pseudosmittia* is continuously present and peaks at 8 %. HC concentrations increase to around 154 HCs/gram.

C. ambigua peaks again between 612 and 608cm, reaching 23 %, along with *M. radialis*-type, *Paracladius* and *Paratanytarsus* undifferentiated also reappear in low abundances. *P. bathophila*-type also increases to 27 %. *D. nervosus*-type and *Orthocladius*-type briefly disappear again. *Ablabesmyia* and *P. sordidellus*-type decline to 1 and 4 %, respectively. *Pseudosmittia* is continuously present and peaks at 7 %. HC concentrations also decline to around 68 HCs/gram.

Between 608 and 603 cm, *P. sordidellus* and *P. septentrionalis*-type both initially increase to 43 and 31 %, respectively, but decline to 8 and 1 %, before recovering slightly. *Orthocladius*-type, *Ablabesmyia* and *D. nervosus*-type increase again to 15, 11 and 13 %, respectively. *Einfeldia Pagana*-type makes up 10 % and *P. barbatipes*-type constitutes 16 % of the assemblage. *Pseudosmittia* is initially present but briefly disappears, then followed by a peak of 11 % at the end of the zone. HC concentrations increase to around 171 HCs/gram.

CM-C6: composite depth: 602.5 – 595 cm

The composition of chironomid assemblages almost completely changes in CM-C6 with *M. radialis*-type becoming the most abundant taxon, increasing from 5 to 50 %. *C. ambigua* is briefly present in high abundance at the start of the zone, peaking at 58 %. Other taxa present in low abundances include *Hydrobaenus lugubris*-type, *Micropsectra insignilobus*-type and *Protanypus*. *S. coracina*-type is the only taxon to continue its presence from CM-C5.

7.3.2 Chironomid temperature inference

The chironomid-inferred mean July air temperatures record (T_{Jul}) is presented with sample specific errors marked on which range from 1.4 °C to 1.5 °C (Figure 7.5a). A large increase in T_{Jul} occurs from 8 °C in CM-C1 to 12.2 °C early on in CM-C2. Throughout the LGIS (CM-C2 to -C5) T_{Jul} has a relatively flat

trend throughout with T_{Jul} *c.* 12 °C, however, three notable declines in T_{Jul} occur during the LGIS. The first begins at the end of CM-C2, where T_{Jul} initially declines by 0.4 °C, followed by a stronger decline of 5.4 °C with T_{Jul} decreasing to 7 °C in CM-C3, but recovers to 12.7 °C at the start of CM-C4. Another decline occurs early in CM-C5 with minimum temperatures of 7.3 °C achieved at 620.5 cm, a fall of 3.9°C. Later in CM-C5, a final decline in T_{Jul} is present with a minimum temperature of 10.2 °C achieved at 609cm, a fall of 1.2 °C. As the LGIS ends and the LLS begins (CM-C5/CM-C6), T_{Jul} declines to 6.1 °C. One other feature to note in the T_{Jul} record is a decline in T_{Jul} during CM-C2 of very small magnitude (*c.* 0.8 °C) at 641 cm.

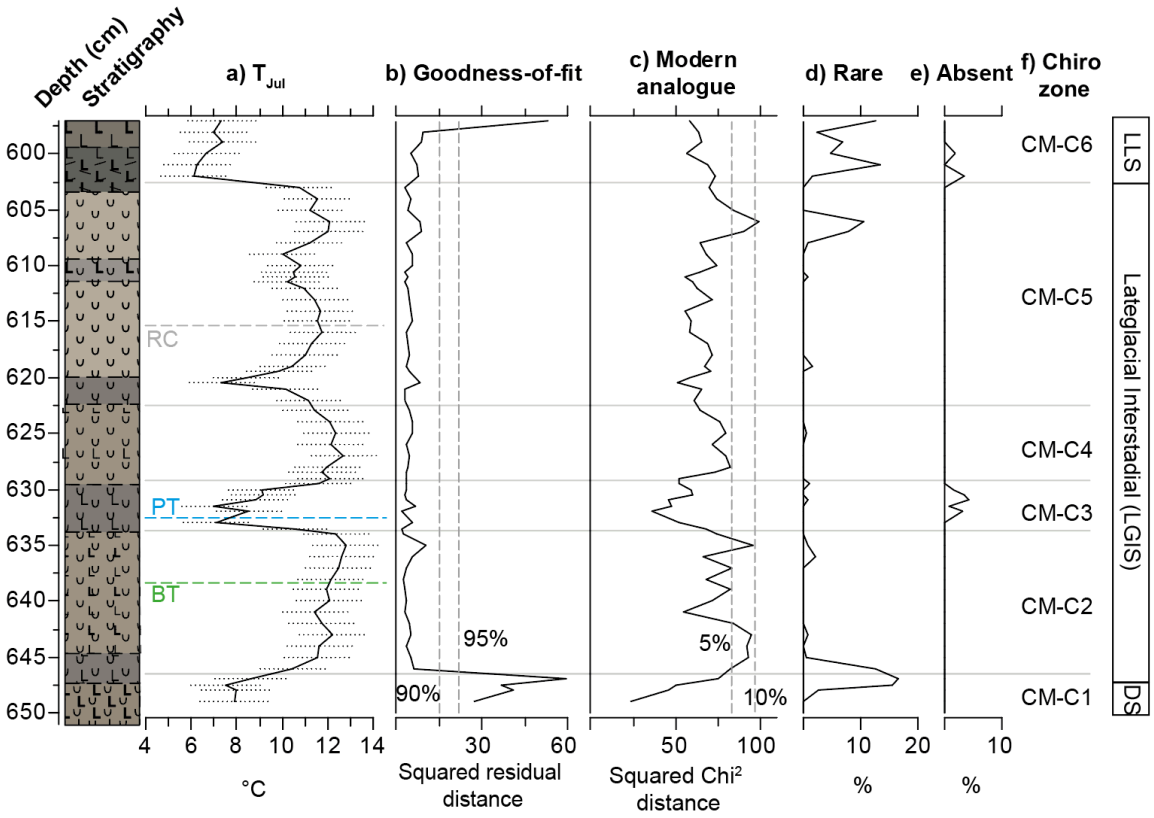

Figure 7.5, Chironomid numerical data presented alongside the stratigraphy of the CRUM1 sequence on the left and broad time periods indicated on the right. **a**) Chironomid-inferred mean July air temperature estimates (T_{Jul}) with sample specific error bars; **b**) Goodness-of-fit of the fossil assemblages to temperature, with dashed lines representing the 90th and 95th percentile of squared residual distance of modern samples to the first axis of a CCA; **c**) Distance of the fossil sample to the nearest modern analogue with dashed lines showing the 5th and 10th percentile of the Chi^2 distances of all samples in the modern calibration dataset; **d**) Abundance of fossil taxa present in the down core record which are rare in the modern calibration dataset, defined by Hill's N2 <5; **e**) Abundance of fossil taxa not present in the modern calibration dataset; **f**) Chironomid assemblage zones from Figure 7.3.

All samples of LGIS age have a good fit-to-temperature (Figure 7.5b) suggesting factors other than temperature (e.g., lake level, trophic status) had little influence on the T_{Jul} reconstruction. Samples in the DS (CM-C1) and LLS (CM-C6) generally have a 'very poor' fit-to-temperature, suggesting factors other than temperature may have influenced the chironomid assemblage. Fossil assemblages generally compare well to those in the modern calibration dataset with 55 samples having good modern analogues (Figure 7.5c). Although, seven samples had 'poor' modern analogues, only one sample had 'very poor' analogues in the modern calibration dataset which was at 606 cm and had a squared chi^2 of 99.26, just above the 10 % cut-off of 97.61. WA-PLS can however still perform very well in non-analogue situations (Birks, 1998).

Most taxa that present in the LGIS sediments at Crudale Meadow are well represented in the modern calibration dataset (Figure 7.5d & 7.5e). Taxa that are rare in the modern dataset (i.e., Hills N2 <5) remain very low throughout most of the LGIS reaching a maximum of 2.2 % and are therefore unlikely to adversely influence the reconstruction. Two samples, at 606 cm and 607 cm, reach 10.5 % and 7.8 % respectively, due to the presence of *Einfeldia pagana*-type which has a Hill's N2 of 1.73 in the modern calibration dataset. A weighted averaging model estimated *E. pagana*-type to have a T_{Jul} optimum of 13.7 °C, similar to the optima of other taxa occurring in these samples and its occurrence in the fossil record is therefore not expected to cause issue with the temperature inferences. The only fossil taxon not present in the modern calibration dataset is *Propsilocerus lacustris*-type, but this taxon does not exceed 4.1 % in the 5 samples in which it occurs during CM-C3. To conclude, the mean July air temperature reconstruction from the chironomids is robust for samples from the LGIS but is less robust for samples from the DS and LLS.

7.4 Stable Isotopes

The isotopic record for the LGIS at Crudale Meadow has been divided into seven isotopic zones, denoted as CM-O*n* (Figure 7.6a). When $\delta^{18}O$ and $\delta^{13}C$ are compared for the whole of the LGIS, there is a low level of co-variance ($r^2 = 0.04$; Figure 7.6b). For much of the LGIS the $\delta^{18}O$ values oscillate around an average of -4.6 ‰ and remain reasonably stable ($1\sigma = 0.3$ ‰), however, several declines in $\delta^{18}O$ do occur. $\delta^{13}C$ on the other hand shows greater variability ($1\sigma = 0.8$ ‰). Changes in $\delta^{18}O$ and $\delta^{13}C$ are described further in the following paragraphs.

CM-O1: composite depth 650 – 645.75 cm

Very high $\delta^{18}O$ values of *c.* -2 ‰ occur in CM-O1, 2.5 ‰ higher than any other values in the dataset. In contrast, $\delta^{13}C$ values are around 0 ‰, some of the lowest seen in the LGIS at Crudale.

CM-O2: composite depth 645.75 – 634.25 cm

$\delta^{18}O$ displays a steady and gradual decline from -4.2‰ to -4.8‰ across this zone. $\delta^{13}C$ increases from 0.7 ‰ to 2.7 ‰ at 639 cm, the highest carbonate isotope value of the sequence, and remains at around 2 ‰ for the remainder of the zone.

CM-O3: composite depth 634.25 – 629.75 cm

A large decline in $\delta^{18}O$ occurs during CM-O3 with values falling from -4.6 ‰ to -5.6 ‰ at 632 cm, an isotopic shift to more negative values of 1 ‰. Within this isotopic decline there is a single anomalously high $\delta^{18}O$ value of -4.2‰ at 633 cm and at the same time an anomalously low value occurs in $\delta^{13}C$ of -0.9 ‰. $\delta^{13}C$ is usually *c.* 1 ‰ during CM-O3.

CM-O4: composite depth 629.75 – 619.75 cm

CM-O4 exhibits some complex changes in the isotope values of both $\delta^{18}O$ and $\delta^{13}C$ and has therefore been further divided into 4 subzones. In CM-O4a, $\delta^{18}O$ and $\delta^{13}C$ initially decline from high values and level off, from -4 to -4.6 ‰ and 2.6 ‰ to 1.5 ‰, respectively. In CM-O4b, $\delta^{18}O$ declines 0.4 ‰ to -5 ‰ and $\delta^{13}C$ decline 0.5 ‰ before increasing again to -4.5 ‰ ($\delta^{18}O$) and 1.7‰ ($\delta^{13}C$) in CM-O4c. In the final subzone, CM-O4d, another isotopic oscillation occurs with $\delta^{18}O$ decreasing 0.7 ‰ to -5.3 ‰ and $\delta^{13}C$ to 0.5 ‰.

CM-O5: composite depth 619.75 – 611.5 cm

$\delta^{18}O$ remains relatively stable throughout CM-O5 at *c.* -4.5 ‰, but $\delta^{13}C$ shows a steady decrease from 1.1 ‰ to 0.3 ‰.

CM-O6: composite depth 611.5 – 608.5 cm

An oscillation to more negative $\delta^{18}O$ values of 0.5 ‰ to -5.1 ‰ occurs during CM-O6. $\delta^{13}C$ declines throughout from 0.3 ‰ to 0 ‰ and displays a small oscillation to more negative values of -0.2 ‰.

CM-O7: composite depth 608.5 – 602.5 cm

$\delta^{18}O$ remains stable around -5 ‰ and $\delta^{13}C$ declines further to -0.5 ‰.

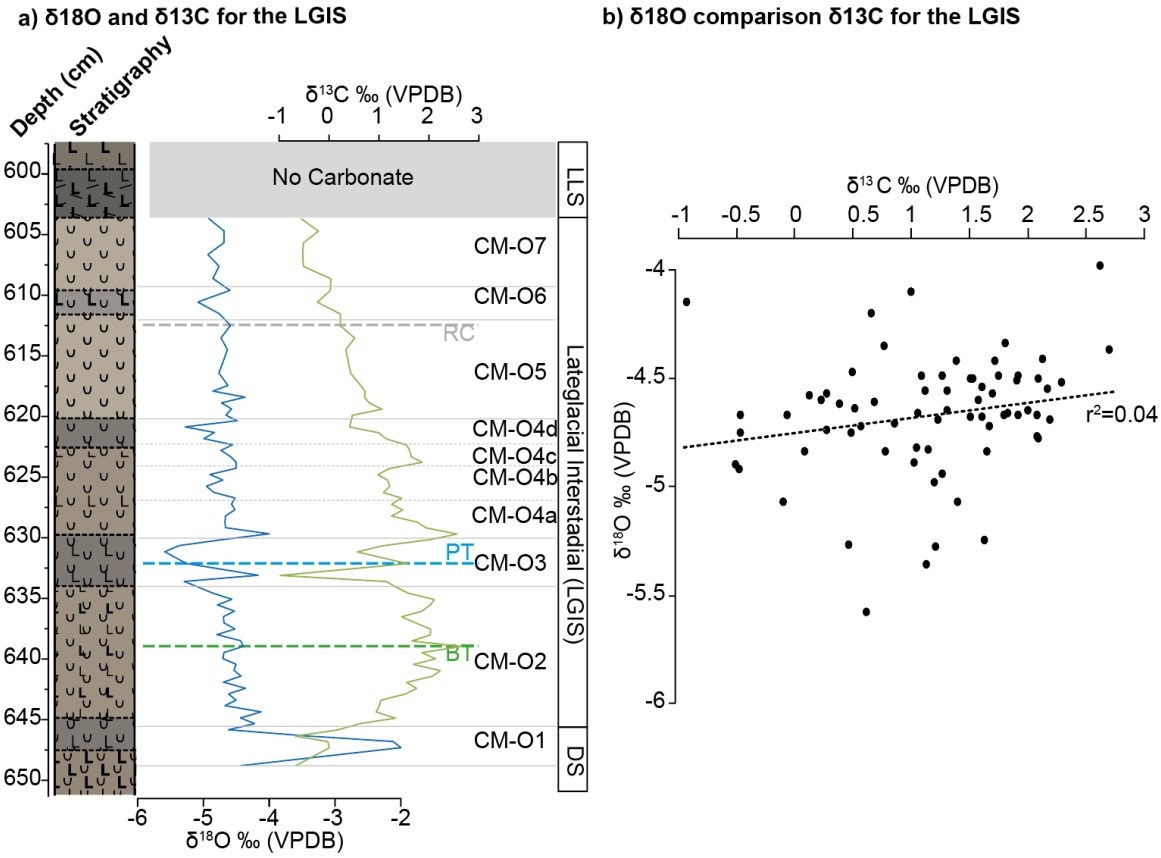

Figure 7.6, $\delta^{18}O$ and $\delta^{13}C$ records. **a**) $\delta^{18}O$ and $\delta^{13}C$ values for the LGIS. **b**) Bi-plot of $\delta^{18}O$ and $\delta^{13}C$ values showing a correlation coefficient of 0.04. Samples from CM-O1 have been removed from the biplot as it is highly likely they were affected by detrital contamination.

7.5 Palaeoenvironmental and palaeoclimatic interpretation

This section will explore the environmental and climatic history of Crudale Meadow during the Lateglacial Interstadial using the proxy data presented within this chapter. The sequence will be interpreted in chronological order starting with the oldest sediments first with a summary given in figure 7.7. Unfortunately, there is no pollen data available for the CRUM1 sequence to accompany the chironomid and isotope records to aid interpretation. Pollen data is available for a sequence studied by Whittington *et al.* (2015) and is drawn upon where appropriate. However, the limited chronological control on the Whittington *et al.* (2015) sequence and the coarse sampling resolution applied means direct comparison to our CRUM1 sequence at a centennial-scale is not possible. Pollen data is also available for neighbouring Quoyloo Meadow from Abrook *et al.* (2020). Quoyloo Meadow is located 6 km directly north of Crudale Meadow and has a very similar catchment relief and, consequently, should therefore experience similar terrestrial vegetation changes as Crudale Meadow. However, potential lake shallowing in the latter half of the LGIS at Quoyloo Meadow means the aquatic vegetation at Quoyloo is unlikely to be representative of aquatic vegetation at Crudale Meadow. The later part of the

LGIS at Quoyloo Meadow is also stratigraphically compressed, meaning centennial-scale comparison cannot be made and only broad comparisons for the LGIS interval are possible.

A range of environmental variables could potentially have had an influence on chironomid assemblages. For each time interval the main driver(s) of assemblage change will be considered and the reliability of the T_{Jul} reconstruction will be discussed. Environmental variables discussed include 1) summer-air temperatures, 2) lake water trophic status, 3) macrophyte presence/abundance/type, 4) lake water oxygenation, and 5) substrate texture and turbidity. Lake depth can also affect chironomid presence/abundance, however, the chironomid assemblages show no notable changes in the water depth and therefore lake level can be discerned. Most taxa present at Crudale Meadow are characteristic of intermediate water depths in a lacustrine environment suggesting a moderately deep lake was present throughout the LGIS, greater than 2 m in depth but less than 7 m (cf. Engels and Cwynar, 2011).

Palaeoenvironmental significance of the oxygen isotope record

Before an interpretation of the $\delta^{18}O$ record is presented, several factors that may drive the isotopic signal need to be considered for the sequences. Many $\delta^{18}O$ records from the British Isles that span the LGIT are interpreted as reflecting prevailing air temperatures, supported by the good correspondence that exists between chironomid-based T_{Jul} estimates and $\delta^{18}O$ values (e.g., van Asch *et al.,* 2012; Abrook *et al.,* 2020). At Crudale Meadow, there is overall good agreement between both proxies. For example, the three major declines in T_{Jul} are matched by well-defined decreases in $\delta^{18}O$ values. Furthermore, the low co-variance between $\delta^{18}O$ and $\delta^{13}C$ suggesting evaporitic enrichment of the lake waters did not exert a strong influence on the $\delta^{18}O$ (Talbot, 1990). The $\delta^{13}C$ of lake environments is typically between -3 and +3 ‰ in an open system (Talbot, 1990) and the values of -0.9 to +2.7 ‰ observed for the Crudale Meadow record fall within this range. This suggests that the former lake was an open system and therefore not greatly affected by evaporitic enrichment. Moreover, lake waters that have been subjected to evaporitic enrichment do not usually preserve temperature trends clearly within the $\delta^{18}O$ record. This is because the $\delta^{18}O$ of the lake water may be increased due to evaporation prior to carbonate precipitation, disrupting the relationship between air temperature and lake water $\delta^{18}O$ (Leng and Marshall, 2004). This is not the case at Crudale Meadow as several abrupt cooling events can be clearly seen and occur at similar times as those observed in the T_{Jul} record.

Detrital contamination from geological carbonate or limestone is also unlikely to be an issue at Crudale Meadow. Firstly, because there is low co-variance between $\delta^{18}O$ and $\delta^{13}C$, implying no mixing had

occurred between authigenic and detrital carbonate that have different isotopic end members (Talbot, 1990; Candy *et al.,* 2016). Secondly, during cold periods where it is too cold for authigenic carbonate to be precipitated and where erosion of the landscape is likely to be at its highest, e.g., the LLS, there is minimal carbonate preserved in the lake sediments (Candy *et al.,* 2016). This indicates that the in-washing of detrital carbonate into the lake basin was negligible even when the catchment was at its most susceptible to erosion and reworking. Thirdly, the majority of the LGIS at Crudale Meadow is dominated by high percentages of authigenic carbonate (>65 %) and so any effect of detrital contamination is likely to be heavily diluted by authigenic material and it will therefore not have an impact on the $\delta^{18}O$ value. However, in parts of the sequence where authigenic carbonate is low, i.e., CM-O1 and CM-O3, the presence of any inwashed limestone could potentially strongly influence the $\delta^{18}O$ and $\delta^{13}C$ value. Contributions of inwashed carbonate will be discussed in the following sections.

It is important to note that although lake carbonates precipitate primarily in the late spring/early summer their $\delta^{18}O$ values are strongly controlled by the $\delta^{18}O$ of lake water that frequently reflects the averaged "annual" climatic conditions (Candy *et al.,* 2016; Blockley *et al.,* 2018). This is because the $\delta^{18}O$ of lake water is controlled by the $\delta^{18}O$ of groundwater that is, in itself, a homogenisation of the $\delta^{18}O$ of annual rainfall. It is often argued that the $\delta^{18}O$ of rainfall is strongly controlled by air temperature, therefore, the $\delta^{18}O$ of lake carbonates is more strongly controlled by the mean annual temperature rather than simply by the summer temperature. Chironomids, in contrast, typically record mean T_{Jul}. If an ACE occurred which, for example, caused a major decline in winter temperatures but had little effect on summer temperatures it is, therefore, likely that a response will be seen in $\delta^{18}O$ values but not in chironomid T_{Jul}. In the CRUM1 sequence it is, therefore, possible that shifts in $\delta^{18}O$ that are not associated with shifts in chironomid T_{Jul} record changes in winter, but not summer, temperatures.

7.5.1 End of DS: pre-14,180 ±300 cal a BP (Depth 650-646.25 cm)

CM-L1, CM-C1, CM-O1

Cold stenothermic taxa dominate CM-C1 (e.g., *Monodiamesa,*) suggesting cold conditions prevailed at the end of the Dimlington stadial. T_{Jul} values were *c.* 8 °C, however, the goodness-of-fit statistics display a very poor fit-to-temperature indicating other factors (e.g., trophic status, oxygenation) may have influenced the chironomid assemblages. Although the absolute temperature estimates need to be treated with caution, the low $CaCO_3$ values, high proportion of minerogenic sediment content and the dominance of cold stenothermic chironomid taxa suggests a cold environment.

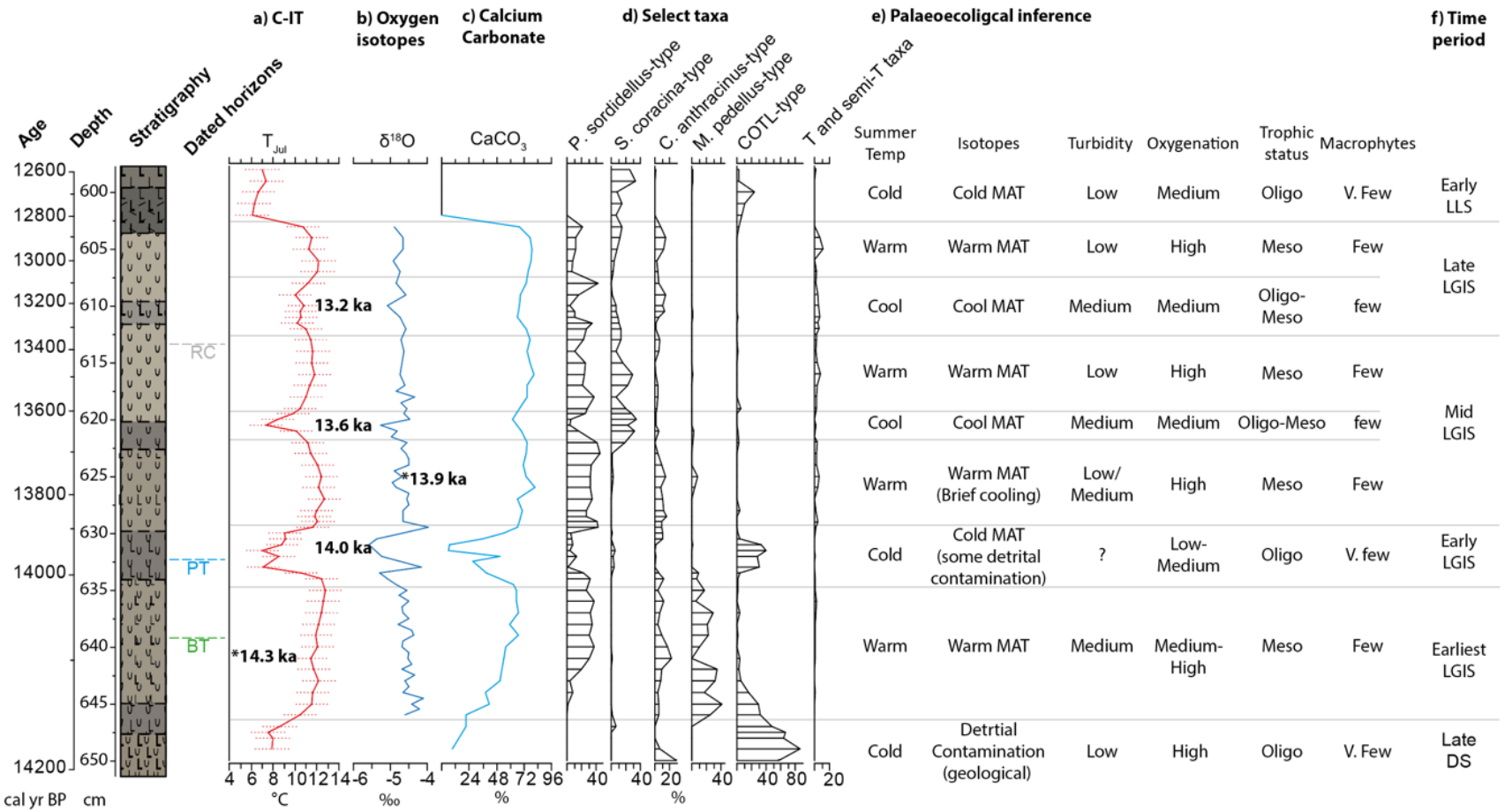

Figure 7.7, Summary figure of data from Crudale Meadow. **a**) Chironomid-inferred mean July air temperatures (T_{Jul}); **b**) Oxygen isotopes; **c)** Calcium carbonate; **d**) selected chironomid taxa; **e**) qualitative ecological inferences; **f**) broad time period.

The dominance of *COTL*-type, *Monodiamesa* and *S. rosenschoeldi*-type suggests the lake was oligotrophic (Brundin, 1949; Saether, 1979; Brodin, 1986) during CM-C1. *Monodiamesa* and *S. rosenschoeldi*-type also both have high oxygen demand indicating the lake waters were well oxygenated (Moller Pillot, 2013; Brundin, 1949). *Monodiamesa* primarily feeds on detritus and bacteria (Brundin, 1956; Brodin, 1986), and *S. rosenschoeldi*-type is a deposit feeder consuming organic detritus (Moller Pillot, 2009). The high abundance of detrital feeders and the absence of taxa usually dependant on macrophytes for habitat and food, indicates that the lake was largely devoid of vegetation during the Dimlington Stadial.

The $\delta^{18}O$ values of approximately -2 ‰ (not displayed in Figure 7.7) are uniquely high for the CRUM1 sequence and are much higher than values seen in other $\delta^{18}O$ records covering the LGIS from the British Isles e.g., Hawes Water (Marshall *et al.,* 2002), Loch Inchiquin (Diefendorf *et al.,* 2006), Fiddaun (Van Asch *et al.,* 2012), Tirinie (Candy *et al.,* 2016) and Star Carr (Candy, unpublished). Summer temperatures were likely below the threshold required for $CaCO_3$ to precipitate from the water column (10 °C, Kelts and Hsu, 1976) meaning the small amount of $CaCO_3$ present may not have been precipitated from the water column. The $\delta^{18}O$ values of marine carbonates and limestones are frequently higher than those of lacustrine precipitated carbonates and the effect of detrital contamination from such geological carbonate can cause the $\delta^{18}O$ of the lacustrine records to be artificially increased (Candy *et al.,* 2015). The surrounding carbonaceous tills could provide a source for detrital geological carbonate, which in turn was sourced from seabed scour as ice streams of the BIIS during the last glacial advanced northwards from mainland Scotland (Hall and Whittington 1989; See section 6.1.3). Such sediments could be easily eroded during cold climates due to lack of vegetation cover. Therefore, the peak of -2 ‰ in $\delta^{18}O$ is very unlikely to have been related to a large increase in MAT but instead the result of contamination from geological carbonate.

7.5.2 *Earliest-LGIS: 14,180 ±300 to 14,060 ±160 cal a BP (Depth 646.25 - 634.75 cm)*

CM-L2a & -L2b, CM-C2, CM-O2

T_{Jul} displays a large increase to 12.2 °C by 14,150 ±240 cal a BP as cold indicating taxa decline, and cool-temperate and temperate indicating taxa increase (e.g., *P. sordidellus*-type). $CaCO_3$ also increases suggesting increased biologically productivity in the lake due to warmer lake waters and/or an increase in landscape stability through greater vegetation cover, reducing the inwash of allogenic sediment to the basin (Verrechia, 2007; Palmer *et al.,* 2015; Whittington *et al.,* 2015). $CaCO_3$ shows a more gradual increase however and peaks later at 14,120 ±160 cal a BP. As $CaCO_3$ precipitation is a function of

climatic warmth and catchment stability (Candy *et al.,* 2016), it is likely that the catchment took longer to stabilise as vegetation colonisation is delayed by slow dispersal and edaphic factors (Walker *et al.,* 1994). This could be the case as high abundances of chironomid taxa accustomed to coarse substrates, e.g., *M. pedellus*-type (Hofmann, 1984), suggests the lake waters are still turbid. The early peak in magnetic susceptibility also suggests inwash of sediment, particularly iron rich minerals, due to increased chemical weathering. *M. pedellus*-type declines throughout the earliest-LGIS whilst $CaCO_3$ gradually increases, and magnetic susceptibility continuously declines suggesting further increases in landscape stability and reduction in lake water turbidity. A small decline of 0.8 °C is of note in the T_{Jul} record with minimum values achieved at 14,130 ±200 cal a BP (641 cm).

Declines in *S. rosenschoeldi*-type are usually seen in lakes under increased nutrient influx, which can cause a reduction in oxygen availability (Moller Pillot, 2009). This process may explain the decline of the taxon in Crudale Meadow. However, the presence of taxa that prefer well oxygenated water, e.g., *M. pedellus*-type and *P. sordidellus*-type, both of which occur abundantly when lake waters continuously have oxygenation saturation of over 50 % and are absent in low oxygen saturation conditions (Moller Pillot, 2009; 2013), suggests lake waters are still well oxygenated. *S. rosenschoeldi*-type has a higher oxygen demand than *M. pedellus*-type and so may be more sensitive to smaller inputs of nutrients and therefore changes in oxygen saturation (Moller Pillot, 2009). There is very little evidence for oxygenating macrophytes, e.g., *Myriophyllum*, at Crudale Meadow during the LGIS (Whittington *et al.,* 2015), however, oxygenation of the lake water may be assisted by algal communities. *Pediastrum* was not counted in Whittington *et al.* (2015), however, *Pediastrum* occurs in high abundances in neighbouring Quoyloo Meadow throughout the LGIS (Abrook *et al.,* 2020). A threshold in nutrient status was potentially crossed at 14,150 ±240 cal a BP (643 cm) with a large change in the chironomid assemblages from taxa which prefer oligotrophic conditions (e.g., *T. chinyensis*-type Brodin, 1986) to taxa with a mesotrophic preference e.g., *P. sordidellus*-type (Moller Pillot, 2013).

Ablabesmyia and *P. sordidellus*-type usually live and feed amongst macrophytes, suggesting well-developed vegetation within the lake (Brodersen *et al.,* 2001; Langdon *et al.,* 2010). However, both taxa can also live on lake bottoms (Vallenduuk & Moller Pillot, 2007; Reiss, 1968) and feed on a variety of detritus and filamentous algae (Armitage, 1968; Moller Pillot, 2013). *P. sordidellus*-type occurs in high abundance, while *Ablabesmyia,* has continuous low abundances. The low abundance of *Ablabesmyia* could be due to the sparse distribution of vegetation within the lake (Whittington *et al.,* 2015), which is needed for their developing pupae to hide amongst (Vallenduuk & Moller Pillot, 2007). The pupae of Orthocladiinae, along with Chironomini and Tanytarsini, develop within their larval tubes (e.g. Marziali

& Rossaro, 2006) and so are much less dependent on vegetation for development. A lack of other live aquatic faunal prey (e.g., Oligochaeta and Cladocera) can also slow the development of Tanypodinae larvae, and often lead to incomplete development, when they only receive detritus (Vallenduuk & Moller Pillot, 2007).

7.5.3 *Early-LGIS: 14,060 ±160 to 13,940 ±300 cal a BP (Depth 634.75 - 629.25 cm)*

CM-L2c, CM-C3, CM-O3

An ACE occurs in the early-LGIS between 14,060 ±160 to 13,940 ±300 cal a BP, with cool-temperate and temperate indicating taxa displaying a marked decline (e.g., *P. sordidellus*-type; *T. pallidicornis*-type) and some disappear (e.g., *Ablabesmyia*), while ultracold and cold indicating taxa increase (e.g., *M. radialis*-type, *COTL*-type). Both T_{Jul} and $\delta^{18}O$ start to decline at 14,020 ±140 cal a BP, however, the rate of temperature change displayed in both proxies is different. Initially, T_{jul} only shows a very minor decline with mean summer temperatures falling by 0.4 °C, which is well within the errors of the WA-PLS model, whereas $\delta^{18}O$ displays a much more substantial decline of 0.6 ‰ over the same interval. T_{Jul} only starts to show a stronger decline at 14,000±140 cal a BP, with temperatures declining by a further 5.4 °C to 7 °C, while $\delta^{18}O$ declines a further 0.4‰. The large decline in T_{Jul} of 5.4 °C occurs *c.* 20 years (i.e., 1 cm depth) after the substantial decline in $\delta^{18}O$. Several factors could explain the apparent lag in T_{Jul} to $\delta^{18}O$. Firstly, although chironomids are thought to respond almost instantaneously to air temperature changes (Brooks *et al.,* 2007), there is still likely to be a slight lag. Many palaeoecological proxies display a lag in response to changes in environmental variables due to migration delay as well as physiological and metabolic processes of organisms buffering against environmental change (Słowiński *et al.,* 2017). Secondly, the initial decline in temperature may not have been large enough for species specific thresholds to be crossed and therefore may produce a more muted T_{Jul} estimate of temperature decline. Thirdly, indirect drivers of assemblage change, that are still strongly correlated to temperatures, may slightly lag temperature changes e.g. trophic status (Juggins, 2013).

A notable change in sediment type occurred between 14,060 ±160 to 13,940 ±300 cal a BP (Depth 634.75 - 629.25 cm*)* with a large reduction in $CaCO_3$ and an increase in minerogenic content, suggesting a return of unproductive lake waters caused by either colder lake waters and/or an increase in lake water turbidity. Taxa accustomed to coarse substrates, e.g., *M. pedellus*-type (Hofmann, 1984), decline and become largely absent, as lake waters were likely too cold for *M. pedellus*-type to survive.

It should be noted that $\delta^{18}O$ may not record the full magnitude of MAT change. The isotopic value at 14,040 ±160 cal a BP (633 cm) of -4.15 ‰ appears anomalously high and occurs when minimum values in T_{Jul} were first attained (*c.* 7 °C), which may mean the sample was affected by detrital contamination as vegetation cover reduces and landscape erosion increased. The low percentages of $CaCO_3$ during this time interval means any detrital contamination from geological carbonate would have a large effect on the $\delta^{18}O$ signal. At present, it appears that minimum $\delta^{18}O$ values, and therefore MAT, occurred at 14,000 ±240 cal a BP, *c.* 40 years after minimum T_{Jul} values were first attained. However, it is possible that minimum $\delta^{18}O$ values did occur at 14,040 ±160 cal a BP (633 cm), the same time as T_{Jul}, but were obscured due to detrital contamination. This would have consequences for the timing of when minimum temperatures are reached in both proxies. Unfortunately, more data would be needed to further explore this observation.

At 14,010 ±200 cal a BP, T_{Jul} increases from 7 °C to 8.8 °C by 14,000 ±240 cal a BP as the ultra-cold and cold indicating taxa decline (e.g. *M. radialis*-type) and cool-temperate indicating taxa increase (e.g. *C. anthracinus*-type). The rise in temperature pauses for *c.* 40 years between 14,000 ±240 and 13960 ±280 cal a BP as T_{Jul} hovers around *c.* 9 °C. Following this, T_{Jul} increases further to 12.1 °C at 13,930 ±340 cal a BP as other cool-temperate and temperate taxa increase (e.g. *P. sordidellus*-type). In contrast, $\delta^{18}O$ displays a continuous increase from -5.6 to -4 ‰.

Oligotrophic indicating taxa such as *M. radialis*-type, (Walker *et al.,* 1991) increase while eutrophic indicating taxa, e.g., *Ablabesmyia* (Vallenduuk and Moller Pillot, 2007), decline and become largely absent, suggesting a return to unproductive oligotrophic lake conditions. The high abundance of *Paratanytarsus* undifferentiated may suggest aquatic macrophytes are present within the lake (Brooks *et al.,* 2007), however, a well vegetated lake seems unlikely given the shift to more oligotrophic conditions, the dominance of taxa which are detritus feeders (e.g., *Paracladius*, Moller Pillot, 2013) and previously sparse aquatic vegetation under more favourable growing conditions. *Paratanytarsus* (*austriacus*-type) has been observed to increase following the removal of macrophytes as it utilises periphytic algae (e.g., diatoms) as a food source instead (Tarkiwska-Kukuryk & Toporowska, 2021). *P. sordidellus*-type is potentially able to persist as it can live on detritus and still complete its life cycle (Reiss, 1968; Zelentsov, 1980; Moller Pillot, 2013). Taxa requiring well oxygenated conditions disappear (e.g. *Orthocladius*-type; Moller Pillot, 2013) potentially as oxygenating algae decline which is seen at Quoyloo Meadow with a decline in *Pediastrum* (Abrook, 2019).

7.5.4 Mid-LGIS: 13,940 ±300 – 13,350 ±570 cal a BP (Depth 629.25 – 612.75 cm)

CM-L2d, -L2e & -L2f; CM-C4 & first half of CM-C5; CM-O4a, -O4b, -O4c, -O4d, & CM-O5.

Between 13,940 ±300 and 13,710 ±420 cal a BP (629.25 – 621.75 cm), T_{Jul} is relatively stable at *c.* 12 °C due to the presence of cool temperate and temperate indicating taxa (e.g., *P. barbatipes*-type). $\delta^{18}O$ on the other hand displays a brief oscillation to more negative values by 0.4 ‰ between 13,850 ±400 and 13,770 ±400 cal a BP which has no corresponding decline in T_{Jul}. Several possibilities may explain this discrepancy. Firstly, summer temperatures did decline but there was no response in the chironomids, either because the change in summer temperatures was not large enough to impact on chironomid ecology and/or ecological thresholds were not crossed. Secondly, winter temperatures may have declined, but no corresponding decline occurred in T_{Jul}, i.e., an increase in seasonality. Finally, factors other than temperature may have influenced the $\delta^{18}O$ signal e.g., a change in moisture source (Rozanski *et al.,* 1992; 1993).

P. sordidellus-type re-appeared in high abundance, joined by *P. barbatipes*-type, both of which feed on algae and are mostly found in oligo-mesotrophic conditions. *Ablabesmyia* and *Thienemannimyia* also return, which usually occur in oligo-eutrophic and oligotrophic conditions receptively, but only in low abundances, suggesting vegetation within the lake is still sparse as their pupae require vegetation to hide in while developing (Vallenduuk & Moller Pillot, 2007). The oligotrophic indicating taxon, *Orthocladius*-type, also re-appears and its requirement for well oxygenated water suggests high level of dissolved oxygen within the lake (Moller Pillot, 2013). However, *S. coracina*-type and *C. anthracinus*-type, which live primarily in the profundal of lakes, can cope with less well oxygenated water and so the profundal may have experienced temporary diurnal low dissolved oxygen concentrations. Therefore, between 13,940 ±300 and 13,700 ±420 cal a BP (629.25 - 621.75 cm), the lake at Crudale Meadow was likely to have well oxygenated littoral waters, oligo-mesotrophic nutrient status with sparse vegetation but relatively abundant algae.

Between 13,710 ±420 – 13,620 ±380 cal a BP (621.75 – 619.25 cm) another ACE occurs with T_{Jul} falling to 7.3 °C, a decline of 3.8 °C. Temperate indicating taxa disappear (e.g., *D. nervosus*-type) and most cool-temperate indicating taxa decline (e.g. *P. sordidellus*-type,) while cold indicating taxa increase (e.g., *Paracladius*) and the ultra-cold indicating taxon *M. radialis*-type also reappears in low abundances. This mid-LGIS ACE is also expressed in the $\delta^{18}O$ with a decline of 0.7 ‰. Both T_{Jul} and $\delta^{18}O$ appear to begin declining at the same time at 13,710 ±210 cal a BP and reach minimum values synchronously at 13,670±400 cal a BP, with respect to the sampling resolution employed.

During the mid-LGIS ACE, the oligo-mesotrophic indicating taxon, *S. coracina*-type, and the oligotrophic indicating taxon *C. ambigua* formed a discrete peak (Johnson 1989; Saether 1979; Brooks *et al.,* 2007). The decline in algae eating *P. sordidellus*-type and *P. barbatipes*-type, and the increase in *C. ambigua* which is often associated with charophytes (Brodersen & Lindegaard, 1999b), may suggest a change in lake vegetation composition with a decline in algal abundance and an increase in charophytes. Detritivores such as *S. coracina*-type (Walshe, 1951) and, *Paracladius* (Moller Pillot, 2013) also increase in abundance. Oxygenation of the lake water may have subsequently declined as the high oxygen demanding *Orthocladius*-type disappears and taxa which can tolerate poorly oxygenated lake water increase e.g. *S. coracina*-type (Brundin, 1949). Overall, between 13,700 ±420 and 13,620 ±380 cal a BP, vegetation and algae within the lake decline meaning detritus became the main food source for chironomids and there was a shift to oligotrophic well oxygenated conditions.

Following the mid-LGIS ACE, T_{Jul} values are *c.* 11.4 °C from 13,620 ±380 to 13,350 ±600 cal a BP (619.25 – 612.5 cm), slightly lower than the start of the mid-LGIS which is possibly due to the absence of the cool-temperate taxon *P. barbatipes*-type. At Quoyloo Meadow, *Pediastrum* increased and a similar increase in algal communities in Crudale Meadow may have been responsible for the increase in abundance of *P. sordidellus*-type and *P. septentrionalis*-type.

D. nervosus-type is often associated with macrophytes (Brodersen *et al.,* 2001), living in mines in *Potamogeton* stems (Urban, 1975). The pollen data from Whittington *et al.* (2015) displays no evidence for *Potamogeton* at Crudale Meadow during the LGIS, although there are sporadic occurrences in Quoyloo Meadow. However, the potential changes in lake level at Quoyloo Meadow during this time may affect the distribution of some aquatic macrophytes. Instead, *D. nervosus*-type can also occur in high densities on stones (Brodersen *et al.,* 1998) feeding on detritus, algae, bacteria, and dead chironomid pupae (Lenz, 1954). *Pagastiella orophila* also occurs and primarily feeds on diatom and some degenerated blue-green algae (Armitage, 1968) and lives on open bottoms in the littoral zone of lakes (Brundin, 1949). The presence of *P. orophila* and *D. nervosus*-type, along with the detritus eating *S. coracina*-type (Walshe, 1951), suggests lake vegetation was still very sparse. The taxa present have a range of trophic preference. *P. sordidellus*-type and *P. septentrionalis*-type largely occur in meso-eutrophic conditions (Moller Pillot, 2013). *S. coracina*-type and *P. orophila* are typical of oligo-mesotrophic (Johnson 1989; Saether 1979) and oligotrophic conditions (Orendt, 1993; Saether, 1979), respectively. Meanwhile, *D. nervosus*-type is largely eurytopic in terms of trophic status and occurs in oligo- to eutrophic waters (Brodin, 1986). The overall trophic status of the lake is therefore likely to be

mesotrophic. *Orthocladius*-type requires well oxygenated lake waters (Moller Pillot, 2013) and so high levels of dissolved oxygen were likely to have been present in the littoral at least.

The decline in $\delta^{13}C$ values throughout the mid-LGIS may indicate a more stable catchment. An increase in terrestrial vegetation cover would result in a greater contribution of plant-respired CO_2 to the soil zone which could then subsequently be incorporated into the vadose and aquifer waters (Talbot, 1990; Andrews, 2006; Candy *et al.,* 2012). Plant-respired CO_2 is relatively depleted in ^{13}C (Cerling and Quade, 1993) and so causes a progressive decline in the $\delta^{13}C$ value of groundwater DIC as the density and coverage of vegetation increase (Candy *et al.,* 2016). *M. pedellus*-type which is often found in coarse substrates (Hofmann, 1984) and therefore in lakes with high turbidity and inwash of allogenic material, largely disappears suggesting a more stable catchment. The low but persistent presence of *Psuedosmittia* throughout the Mid-LGIS, which are usually associated with macrophytes in the littoral and splash zones of lakes (Cranston *et al.,* 1983; Brodin, 1986), may suggest the development of some littoral vegetation around the lake. However, some species of *Psuedosmittia* are semi-terrestrial and its presence may alternatively indicate the erosion of unstable soils (Brooks and Heiri, 2013). Vegetation within the lake may still be relatively scarce as Tanypodinae continue to remain low in abundance which require vegetation for pupae to hide (Vallenduuk & Moller Pillot, 2007).

7.5.5 Late-LGIS: 13,370 ±520 – 12,830 ±1040 cal a BP (Depth 612.75-602.5cm)

CM-L2g & L2h; Latter half od CM-C5, CM-O6 & -O7

An ACE occurs in the late-LGIS between 13,370 ±520 and 13,110 ±910 cal a BP (612.5 – 607.5 cm) with temperatures declining 1.2 °C from 11.4 to 10.2 °C. Cold indicating taxa reappear (e.g., *M. radialis*-type,) along with declines in most cool-temperate indicating taxa (e.g., *P. sordidellus*-type). An oscillation to more negative $\delta^{18}O$ values of 0.5 ‰ also occurs suggesting a decline in MAT also. The declines in mean July air temperature and MAT appears to be synchronous with respect to the sampling resolution, with declines beginning in both proxies at 13,300 ±300 cal a BP. Minimum values are however attained first in the $\delta^{18}O$ record at 13,210±380 cal a BP but later in T_{Jul} at 13,160±410 cal a BP.

Minor increases in oligotrophic indicating taxa occur, e.g., *M. radialis*-type (Brooks *et al.,* 2007), while taxa adapted to mesotrophic conditions decline e.g., *P. sordidellus*-type (Bituški, 2000; Orendt 1993). Therefore, the lake potentially became more oligo-mesotrophic. Although taxa which feed on algae decline, e.g., *P. sordidellus*-type (Moller Pillot, 2013), a decline in algae cannot be confirmed from the pollen data as *Pediastrum* was not counted by Whittington *et al.,* (2015) and the lake at Quoyloo

Meadow may have become very shallow during the late-LGIS and so may not be representative of Crudale Meadow during the Late-LGIS. However, the peak in *C. ambigua* abundance, may suggest a change in the vegetation composition of the lake. *C. ambigua*, also thrives in cold and unstable environments (Brooks *et al.,* 2007), so alternatively its presence could suggest an increase in turbidity, concurrent with the decline in $CaCO_3$ values and increase in allochthonous material. *Procladius* and *Ablabesmyia* decline, potentially as there is less vegetation around the lake for the pupae to hide and develop (Vallenduuk & Moller Pillot, 2007). Several Orthocladiinae (e.g., *P. sordidellus*-type) need well oxygenated water, and their decline could suggest poorer oxygenation of water, potentially due to increased decomposition of organic matter. *C. anthracinus*-type, which can cope with low oxygen conditions for small periods of time, increases, suggesting the lake was less well oxygenated. However, it is unclear why *S. coracina*-type decreases when it can also tolerate low oxygen conditions (Brundin, 1949). Surprisingly, *P. bathophila*-type increases, even though many other taxa with similar temperature optima decline and could be explained by changes in other environmental variables (e.g., substrate). *P. bathophila*-type prefers sandy-muddy bottoms (Arts, 2000) and the increase in clay during CM-L2g may allow it to increase in abundance.

From 13,110 ±910 to 12,830 ±1040 cal a BP (Depth 607.5 - 602.5 cm), T_{Jul} recovers and increases to 12.1 °C by 13,010 ±980 cal a BP. Temperate indicating taxa increase (e.g., *Ablabesmyia*) while ultra-cold and cold indicating taxa become largely absent. $CaCO_3$ increased again suggesting a final return of warm productive lake waters and a stable catchment experiencing low erosion for the remainder of the LGIS.

The taxa present have a range of trophic preferences. *P. sordidellus*-type and *P. septentrionalis*-type largely occur in meso-eutrophic conditions, while *S. coracina*-type and *P. barbatipes*-type occur in oligotrophic conditions (Orendt, 1993; Saether, 1979; Moller Pillot, 2013). The overall trophic status of the lake is therefore likely to be mesotrophic, however, *E. pagana*-type is common in eutrophic conditions (Moller Pillot, 2009) and so the lake could have had a higher trophic status than previous mesotrophic periods. Taxa which feed on detritus, algae and other aquatic organisms reappeared, e.g., *D. nervosus*-type (Lenz, 1954) and are now joined by *E. pagana*-type which also feeds on organic detritus (Moller Pillot, 2009). Therefore, vegetation within the lake is not likely to be abundant. *Orthocladius*-type requires well oxygenated lake waters (Moller Pillot, 2013) and so high levels of dissolved oxygen were likely to have been present, in the littoral zone at least. $\delta^{13}C$ values continued to decline further probably as a response to the further development of vegetation and soils on the catchment slopes developed further.

7.5.6 Start of LLS: 12,830 ±1040 – 12,429 ±980 cal a BP (602.5 - 595 cm)

CM-L3a, CM-C6,

T_{Jul} displays a large decline with T_{Jul} falling from 11.6 °C to 6.1 °C at the onset of the LLS, a decline of 5 °C. This decrease is the result of a distinct change in the chironomid assemblages as all cool temperate and temperate indicating taxa disappear, except for *S. coracina*-type. Instead, ultra-cold and cold indicating taxa (e.g., *H. lugubris*-type, *M. radialis*-type and *M. insignilobus*-type) dominate the chironomid assemblages. A return to cold unproductive lake waters is indicated by the termination of $CaCO_3$ precipitation and the increase in inwashed minerogenic sediment. As no $CaCO_3$ was precipitated during the LLS, no assessment on MAT can be made.

The very high abundance of *M. radialis*-type, which occurs in cold arctic/alpine lakes with very poor nutrient conditions, may even suggest lake waters becoming ultra-oligotrophic during the LLS (Brodin, 1986). The taxa present are largely detritivores, e.g., *H. lugubris*-type (Moller Pillot, 2013), or are carnivores, e.g., *Protanypus* (Brundin, 1949), suggesting very little vegetation was present within the lake. Numerous fragments of moss and herbaceous plant remains were found at 12,800 ±1040 cal a BP (602 cm), indicating the breakdown of landscape vegetation, resulting in the erosion of unstable catchment slopes causing sediments to be dominated by allogenic material. *C. ambigua*, which thrives in cold and unstable conditions (Brooks *et al.,* 2007), forms a discrete peak also suggesting a transitional environment. The absence of other taxa which are accustomed to coarse substrates and early colonization after significant environmental change, e.g., *M. pedellus*-type (Hofmann, 1984; Brodersen and Lindegaard, 1999a), is likely due to lake waters being too cold for them to survive. Oxygen-conditions of the lake waters is hard to reconstruct as the oxygen demands of Tanytarsini morphotypes, which dominate the assemblages, are not well known. Generally, Tanytarsini do possess some haemoglobin and so can cope with short periods of anoxia (Brooks *et al.,* 2007) suggesting the lake waters may have experienced low oxygen conditions. However, lake water oxygenation may have been higher at the very start of the LLS as *Paracladius* requires well oxygenated water with saturation over 50 % day and night (Moller Pillot, 2013).

7.6 Chapter summary

This chapter explored the palaeolimnological and palaeoclimatological development at Crudale Meadow during the LGIS using the chironomid and oxygen isotope data generated in this study. The following points summarise the key findings:

- Changes in the chironomid assemblages are largely driven by mean summer temperature (T_{Jul}) during the LGIS. Oxygen isotopes are suggested to reflect mean annual temperature changes (MAT).

- The T_{Jul} and $\delta^{18}O$ records display relatively flat trends with three ACEs recorded in both proxies punctuating during the LGIS.

- The largest ACE in terms of magnitude at Crudale Meadow occurs between 14,060 ±160 to 13,940 ±300 cal a BP, which has the strongest expression of any ACE in both proxies and is characterised by approximately 5.8 °C worth of cooling in mean July air temperature and a large decline in MAT with a 1 ‰ fall in $\delta^{18}O$.

- The second largest ACE in terms of magnitude occurs in the mid-LGIS from 13,710 ±420 to 13,620 ±380 cal a BP with T_{Jul} declining to 7.3 ± 1.4 °C, a decline of 3.8 °C, and is also accompanied by a large decline in $\delta^{18}O$ of 0.7 ‰.

- The final ACE occurs in the late-LGIS between 13,370 ±520 and 13,110 ±910 cal a BP and has the smallest magnitude of all the LGIS ACE with T_{Jul} declining by 1.2 °C and small decline in $\delta^{18}O$ of 0.5 ‰.

- Two other potential ACEs occur but are only recorded in T_{Jul} or $\delta^{18}O$, not both. A 0.8°C decline occurs in T_{Jul} in the very early LGIS with minimum values occurring at 14,130 ±200 cal a BP. A shift to more negative $\delta^{18}O$ values occurs in the mid-LGIS between 13,850 ±400 and 13,770 ±400 cal a BP which has no corresponding decline in T_{Jul}.

Chapter 8: Llangorse results and interpretation

Chapter overview

The purpose of this chapter is to present the sedimentology and stratigraphy for the LLAN14 sequence from Llangorse along with the chironomid and oxygen isotope proxy data generated by this study. The environmental influences on both the chironomid assemblages and oxygen isotopes will be discussed and used as the basis for environmental/climatic reconstruction. Llangorse is particularly important in understanding the spatial expression of ACEs across the British Isles because southern Britain is largely devoid of quantified palaeoclimate records with a high temporal resolution, and so the current N-S transect of sites only goes as far south as the Cumbrian lake sites (Lang *et al.,* 2010; Marshall *et al.,* 2002) and Star Carr (Blockley *et al.,* 2018; Abrook, 2018) in Northern England, over 200 km away.

8.1 Sedimentology and stratigraphy

The sedimentology and physical parameters for the LLAN14 sequence (51°56'09" N 3°16'25" W) used in this study were produced by Palmer *et al.* (2021), which are restated here focusing on the sediments attributed to the LGIS. The NW infilled basin of Llangorse is where the LLAN14 sequence was cored by members of the Centre for Quaternary Research, Royal Holloway, University of London in 2014. (Figure 8.1). Key marker horizons and sedimentological physical parameters ($CaCO_3$, LOI, Mag Sus) were used to align the individual core section to form the LLAN14 composite sequence (Figure 8.2a). The LLAN14 composite sequence is 7.35 m in length and is broadly composed of two marl-rich phases of sedimentation, representing the LGIS (LL-L2 to LL-L5) and the Holocene (LL-L8 to LL-L10), alternating with two clastic dominated phases of sedimentation representing the Dimlington (LL-L1) and Loch Lomond Stadials (LL-6 & 7) (Figure 8.2a). The physical parameters of sediments representing the very end of the Dimlington, the LGIS and the onset of the LLS are shown in greater detail in Figure 8.2b and detailed sedimentological descriptions presented in Table 8.1. The stratigraphy of this sequence is described below from the base upwards.

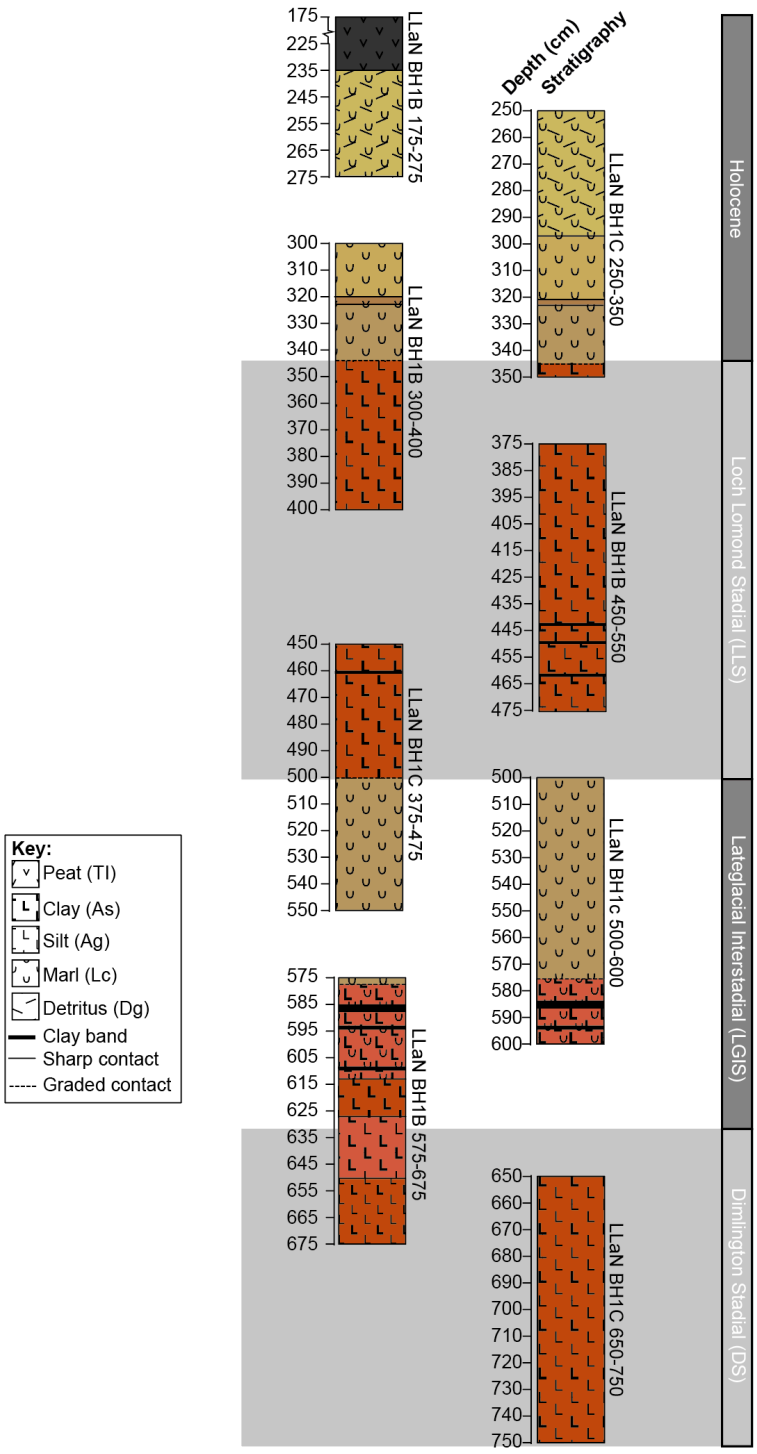

Figure 8.1, Sedimentology and stratigraphy of individual cores which make up the composite sequence LLAN14. (After Abrook, 2018)

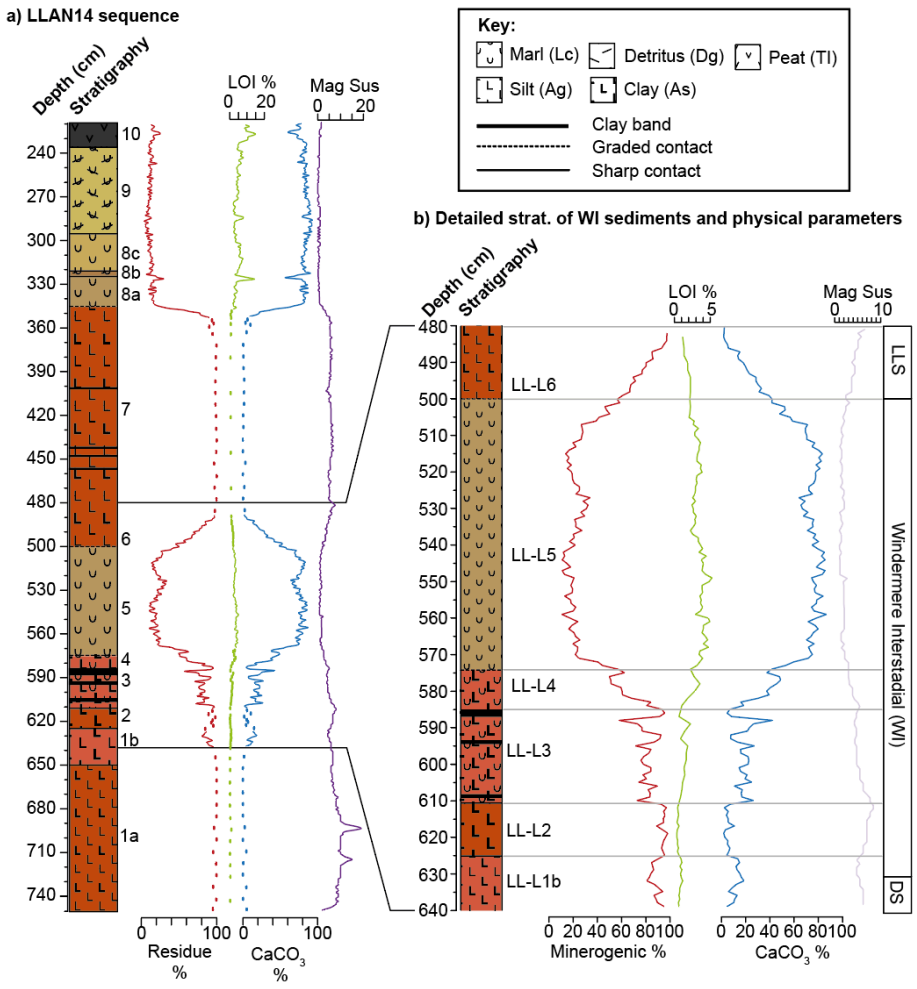

Figure 8.2, Sedimentology and stratigraphy of the LLAN14 sequence (Palmer *et al.* 2021). **a**) Simplified lithostratigraphy and physical parameters of the LLAN14 sequence at Llangorse, spanning the Lateglacial and Early Holocene; **b**) detailed lithostratigraphy and physical parameters of the WI showing proportions (%) of calcium carbonate ($CaCO_3$), organic (Loss-on-Ignition) and minerogenic components. Lithostratigraphic zones are labelled LL-L*n* and stratigraphic log colours are from the Munsell colour system

Table 8.1, Lithostratigraphic units for the LGIS from the LLAN14 sequence (After Abrook, 2018).

Unit	Depth (cm)	Troels-Smith	Classification	Munsell colour
LL-L6	500-487	Ag3, As1	Silty clay	2.5Y 4/3 Reddish Brown
LL-L5	574-500	$Lc^4$3, As1, Dg+	Marl	2.5Y 5/2 Greyish Brown
LL-L4	584-574	Lc^{42}, As2, Dg+	Clay Marl	2.5Y 5/2 Greyish Brown
LL-L3	611-584	As3, $Lc^4$1	Clay Marl	2.5YR 4/2 Weak Red
LL-L2	625-611	As4	Clay	2.5YR 4/3 Reddish Brown
LL-L1b	650-625	As3, Ag1, Lc^4+	Clay silt	2.5YR 4/2 Weak Red
LL-L1a	750-650	Ag3, As1	Silty clay	2.5YR 4/3 Reddish Brown

LL-L1 (750-622 cm) is predominantly composed of silts and clays (80-90 %). LL-L1a (750 – 650 cm) has a higher proportion of silt, while LL-L1b (650-622 cm) has a higher proportion of clay. $CaCO_3$ % content in LL-L1 is low (4-10 %) and is indiscriminately diffused in the matrix. The % $CaCO_3$ content increases towards the end of LL-L1b to *c.* 15 % and here carbonate is occasionally distributed as thin (<0.2 mm) laminae of marl. LOI is less than 2 % throughout. The minerogenic component has relatively high magnetic susceptibility values (19 $x10^{-5}$ SI units), though these decline to *c.* 5 $x10^{-5}$ SI units by the end of LL-L1b. In LL-L2 (622-611 cm), clay dominates forming 90-95 % of the sediments and $CaCO_3$ reduces to *c*. 4 %. Magnetic susceptibility increases from 6 to 8 $x10^{-5}$ SI units.

LL-L3(611-584 cm) is composed of silty marl with values of *c.* 18 % for $CaCO_3$ and *c*. 81 % for minerogenic content, however, the proportion of these is highly variable, especially towards the end of the zone. Several bands of clay occur between 609-608 cm, 594-592 cm, and 588-585 cm, and have very low $CaCO_3$ with values of 16, 7 and 4 %, respectively. Throughout LL-L3 magnetic susceptibility falls from 8 $x10^{-5}$ SI units to 4 $x10^{-5}$ SI units. LOI is low throughout, only constituting *c.* 1 %.

During LL-L4 (584-574 cm) $CaCO_3$ increases from 16 to 75 %, with a concurrent decline in minerogenic content from 84 to 22 %. However, a brief decline in $CaCO_3$ occurs at 575 cm from 48 to 38 %, accompanied by an increase in minerogenic sediment. LOI increases to 4 % throughout the zone. Magnetic susceptibility declines throughout the zone from 4 $x10^{-5}$ SI units to 1.8 $x10^{-5}$ SI units.

$CaCO_3$ forms the largest sediment component in LL-L5 (574-500 cm), comprising 75 % of the sediments on average, with maxima of up to 87 %. Minerogenic sediment contributes 20 % on average and is as low as 10 % in some instances. In the latter part of the zone there is a short-lived decline in carbonate values to 64 %, centred on 527 cm, and an increase in minerogenic sediment to 33 %. Magnetic susceptibility declines further and reaches a minimum for the sequence of 0.75 $x10^{-5}$ SI units, with values averaging 1.3 $x10^{-5}$ SI units for LL-L5. LOI forms 3 % of the sediment on average.

$CaCO_3$ declines from 75 % to 15 % throughout LL-L6 (500-487 cm) with corresponding increases in minerogenic content from 22 % to 85 %. LOI declines from 3 to 1 %. Magnetic susceptibility increases again from 1.15 $x10^{-5}$ SI units to 4 $x10^{-5}$ SI units. Units LL-L7, 8, 9 and 10 (487-220 cm) are of Loch Lomond Stadial and Holocene age and are not discussed as it beyond the scope of this thesis.

8.2 Chironomids

8.2.1 Chironomid assemblages

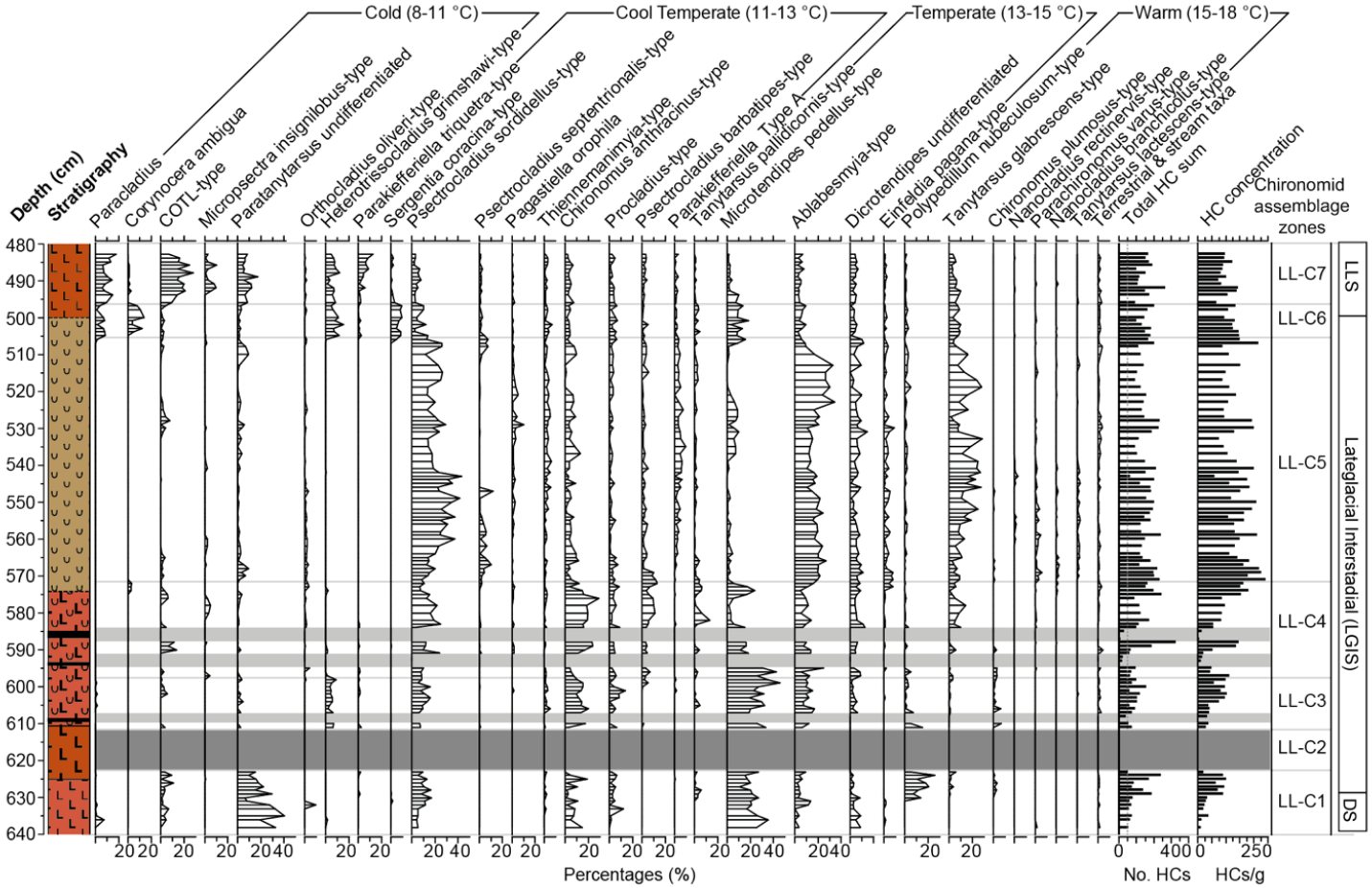

Figure 8.3, Percentage abundance diagram of selected chironomid taxa present in the LGIS sediments at Llangorse alongside the LLAN14 stratigraphy. Chironomid assemblage zones (LL-Cn) are marked on the right. Taxa are arranged by their T_{Jul} optima in the modern calibration dataset (Heiri *et al.,* 2011) as calculated using a Weighted-Averaging model. Taxa with coolest optima are on the left and warmest on the right. Head capsule concentrations (HCs/gram) and total head capsules counts are displayed on the right. Dark grey area denotes samples where no head capsules were present. The light grey zones denote where samples have been removed from the percentage-abundance curves due to very low head capsule counts.

In total, 73 different chironomid taxa were identified in the 109 fossil samples analysed, with assemblages displaying considerable variation down-core (Figure 8.3). A broken stick model suggested six significant assemblage zones, though the author has added an extra zone between 623-612 cm, a period where chironomid HCs were largely absent. Chironomid assemblage zones are denoted as LL-C*n*.

LL-C1: composite depth 640-623 cm

The most abundant taxa in LL-C1 are *Paratanytarsus* undifferentiated and *Microtendipes pedellus*-type, each contributing *c.* 20 % of the fossil assemblages. *Dicrotendipes*, *Psectrocladius sordidellus*-type, *Chironomus anthracinus*-type, *Procladius* and *COTL*-type occur in low percentages. *Polypedillum nubeculosum*-type is present in the latter part of the zone, increasing to around 20 %. HC concentrations increased from 13 HCs/gram to 102 HCs/gram throughout LL-C1.

LL-C2: composite depth 623-612 cm

A key feature of this zone is the low concentration of HCs. Only samples at 622 and 612 cm yielded any head capsules, 9 and 18 respectively, with concentrations of less than 8HCs/gram. The intervening samples yielded no HCs at all.

LL-C3: composite depth 612-598 cm

M. pedellus-type is the most abundant taxon in LL-C3, forming *c.* 30% of the assemblages. *P. sordidellus*-type, *Ablabesmyia* and *C. anthracinus*-type increase to *c*. 9 %, 11 % and 14 %, respectively. *Heterotrissocladius grimshawi*-type forms 5 % of the assemblages on average. HC concentrations are 66 HCs/gram on average and generally range between 32 to 105 HCs/gram.

LL-C4: composite depth 598-572 cm

M. pedellus-type declines throughout LL-C4 from *c.* 30 % to 2 % by 578cm, followed by a brief increase again to 25 % at 574 cm, before declining to only a few percent by the end of LL-C4. *C. anthracinus*-type increases to 20 % by 590 cm and remains around this abundance for most of the zone before a decline to 5 % starts at 576 cm.

Several taxa show low abundance in the first half of zone LL-C4 but higher abundances in the latter half of the zone. These include *P. sordidellus*-type (10 % compared to *c*. 20 %), *Psectrocladius barbatipes*-type (4 % compared to *c.* 10%) and *T. glabrescens*-type (2 % compared to *c*. 10 %). Some taxa also briefly appear in low abundances at the end of LL-C4 including *Corynocera ambigua* (3 %

between 572-575 cm), *Micropsectra insignilobus*-type (5 % at 578 cm) and *COTL*-type (14 % at 590 and 6 % at 576 cm).

HC concentrations are on average 80 HCs/gram but are highly variable and generally range from 22 to 182 HCs/gram. Two periods of particularly low HC concentrations occur between 588-585 cm, with an average of only 8 HCs/gram, and 594-592 cm, which has only 15 HCs/gram on average.

LL-C5: composite depth 572-506 cm

The three most abundant taxa in LL-C5 are *P. sordidellus-type, Ablabesmyia* and *T. glabrescens*-type. *P. sordidellus*-type increases from 8 % at the start of the zone to 37 % by 560 cm. Between 559 and 543 cm the percentage of *P. sordidellus*-type remains high and oscillates between 20 and 40 %. Following this, from 542 to 508 cm, *P. sordidellus-type* oscillates at lower percentages, between 13 and 25 %. *Ablabesmyia* abundances fluctuate around 20% throughout LL-C5, though they increase to *c.* 30 % between 523 – 513 cm, and then decline to 6 %. *T. glabrescens*-type gradually increases from 5 % at the start of zone LL-C5 to 28 % by 530cm. Following this, *T. glabrescens* declines to 1 % at 527cm, increases back to 28 % at 519cm and then finally declines to 4 % at the end of the zone.

Despite the dominance of *P. sordidellus*-type, *Ablabesmyia* and *T. glabrescens*-type, there is a large array of other taxa consistently present in low percentages throughout LL-C5 including *Thienemannimyia* and *Einfeldia pagana*-type (2-6 % abundance). *Nanocladius branchicolus*-type, *Nanocladius rectinervis*-type and *Tanytarsus lactescens*-type are only consistently present during the first half of LL-C5, each reaching *c.* 3 %, but are largely absent for the latter half of LL-C5. *P. septentrionalis*-type is also present in the first half of LL-C5 and reaches higher percentages of up to 12 %.

A brief appearance of *COTL*-type, otherwise absent throughout much of LL-C5, should be noted between 531 and 523 cm with a peak of 8 % centred at 528 cm. Similarly, *M. pedellus*-type and *Pagastiella orophila* usually compose 1-3 % of the assemblages in LL-C5, except between 537 and 521 where they increase to *c*. 7 % and 10 %, respectively. HC concentrations are high throughout LL-C5, on average 133 HCs/gram, with a range of 62-242 HCs/gram.

LL-C6: composite depth 506-497cm

Ablabesmyia, T. glabrescens-type and *P. sordidellus*-type remain low throughout at *c*. 6 %, 8 % and 8%, respectively. *M. pedellus*-type increases to *c*. 11 % and *H. grimshawi*-type reappears and reaches c. 9 %. *C. ambigua* reaches its highest abundance at 12 %. *Paracladius* and *Sergentia coracina*-type are consistently present and both increase to *c*. 7 %. *Parakieferiella triquetra*-type and *COTL*-type also appear but at low abundances only.

LL-C7: composite depth 497-483cm

In the final zone, LL-C7, *C. ambigua* and *S. coracina*-type decline and *COTL*-type, *Paracladius* and *M. insignilobus*-type increase to *c*. 25 %, 15 % and 10 %, respectively. *H. grimshawi*-type continues to be present at *c.* 10%. A number of taxa that were abundant in previous chironomid assemblage zones continue to be present but only at around c 3-5 % each e.g., *Tanytarsus glabrescens*-type, and *M. pedellus*-type.

8.2.3 Temperature reconstruction and reliability estimates

The chironomid-inferred mean July air temperature record from Llangorse is presented in Figure 8.4a. There is a large increase from 9.6 °C to 13.7 °C during LL-C1. The trend in T_{Jul} throughout LL-C3 and LL-C4 is consistent at *c*. 13°C. During LL-C5 there is a general increase in temperatures from 13.8 °C to 15.4 °C between 572 and 540 cm, followed by a gradual decline from 15.4 °C to 12°C between 540 and 505 cm. The declining trend in T_{Jul} continues throughout LL-C6 and LL-C7 to 10.2 °C. Superimposed upon these trends are several declines in T_{Jul} worthy of note. A small decline of 1.3°C is present in LL-C3. During LL-C4, two small declines in T_{Jul} of 1.3 and 1.5 °C occur between 595-585 cm and 580-572 cm, respectively. In the first half of LL-C5, a decline of 2 °C is present between 552 – 545 cm, with T_{Jul} falling to 13.4 °C. In the latter half of LL-C5, T_{Jul} declines again between 539 and 531 cm with T_{Jul} declining by 2.5 °C. Sample specific errors range from 1.4 °C to 1.6 °C.

The majority of chironomid samples have good fit-to-temperature and modern analogue equivalents (Figure 8.4b and 8.4c). Out of the 109 chironomids samples, only one has a 'very poor' fit-to-temperatures (543 cm), and 6 have a 'poor' fit-to-temperature (636, 611, 545, 542, 519 and 517 cm). All of these, except the sample at 636 cm, are from the LGIS. Similarly, the fossil assemblages compare well with those in the modern calibration dataset with no samples having 'very poor' analogues and only eight having 'poor' analogues (610, 601, 546, 533, 494, 486, 485 and 484 cm). All of these except for 486, 485 and 484 cm, occur in the LGIS. The majority of taxa present in the LGIS at Llangorse are well represented in the modern calibration dataset (Figure 8.4d and Figure 8.4e). Taxa that are rare in

the modern dataset (i.e., Hill's N2<5) generally remain below 10% and do not form a significant proportion of the assemblages. The only 'rare' taxon is *Einfeldia pagana*-type. The three taxa that are not present in the modern-day calibration dataset but that occurred in the sediment sequence were *Constempellina-Thienemanniola, Trissocladius and Psilopserus,* which do not collectively exceed 2 % in the 6 samples in which they are present.

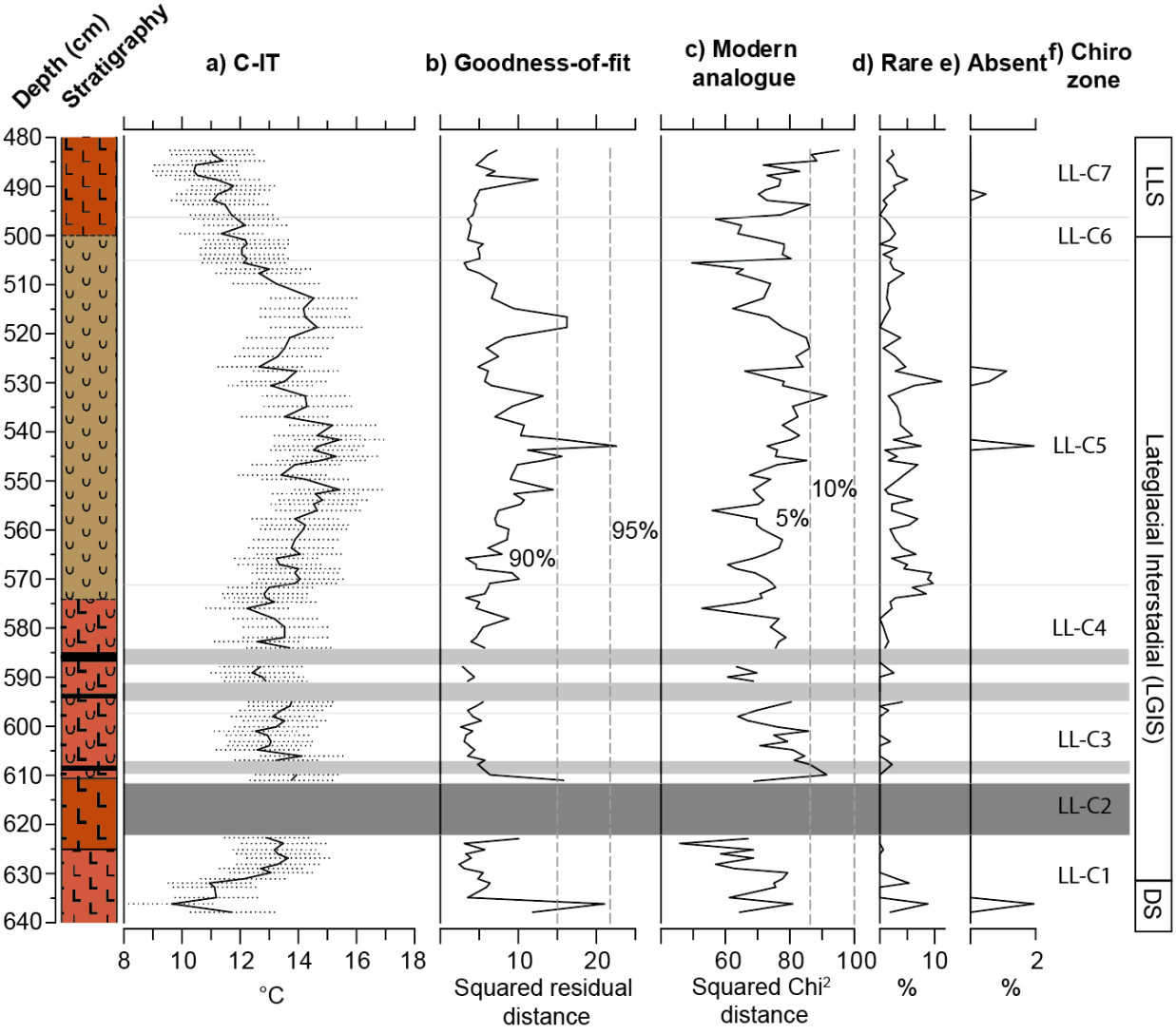

Figure 8.4, Chironomid numerical data. a) Chironomid-inferred mean July air temperature estimates (T_{Jul}) with sample specific error bars; b) Goodness-of-fit of the fossil assemblages to temperature, with dashed lines representing the 90th and 95th percentile of squared residual distance of modern samples to the first axis of a CCA; c) Nearest modern analogue with dashed lines showing the 5th and 10th percentile of the Chi^2 distances of all samples in the modern calibration dataset; d) Abundance of fossil taxa present in the down core record which are rare in the modern calibration dataset, defined by Hill's N2 <5; e) Fossil taxa not present in the modern calibration dataset; f) Chironomid assemblage zones from Figure 8.3. Dark grey area denotes samples where no head capsules were present. The light grey zones denotes where samples have been removed due to very low head capsule counts.

8.3 Stable isotopes

The isotopic record for the LGIS at Llangorse has been divided into three isotopic zones, denoted as LL-O*n* (Figure 8.5a). The broad trends in both $\delta^{18}O$ and $\delta^{13}C$ are very similar and both display large shifts in isotopic values. When $\delta^{18}O$ and $\delta^{13}C$ are compared for the whole of the LGIS, there is a moderate degree of co-variance ($r^2 = 0.59$; Figure 8.5b). To determine if a moderate degree of co-variance holds during different parts of LGIS, regression analyses were also performed for each isotopic zone (Figure 8.5c).

LL-O1: composite depth 640-582 cm

LL-O1 is characterised by a trend to more positive $\delta^{18}O$ values from *c.* -8.5 ‰ to *c.* -5 ‰. Large oscillations in $\delta^{18}O$ occur along this general trend and are in the order of 4 ‰. Minimum values occur at 597cm and 587 cm with $\delta^{18}O$ reaching -9.36 ‰ and -8.21 ‰, respectively. $\delta^{13}C$ on the other hand displays a relative flat trend throughout LL-O1, though large oscillations in the order of 8 ‰ are present and largely coincide with $\delta^{18}O$ minima. Co-variance between $\delta^{18}O$ and $\delta^{13}C$ is moderate ($r^2 = 0.45$).

LL-O2: composite depth 582-538 cm

Throughout LL-O2 there is a declining trend in $\delta^{18}O$ values from *c.* -6 ‰ to -7 ‰. $\delta^{13}C$ also displays a declining trend from 0.8 ‰ to -0.6 ‰. Co-variance between $\delta^{18}O$ and $\delta^{13}C$ is moderate ($r^2 = 0.63$).

LL-O3: composite depth 538-483 cm

Overall, the trend in $\delta^{18}O$ increases throughout LL-O3, with values increasing from *c.* -7 to -5.4 ‰. Similarly, $\delta^{13}C$ increases throughout from -3.2 ‰ to -1.1 ‰. Co-variance between $\delta^{18}O$ and $\delta^{13}C$ is very high ($r^2 = 0.79$).

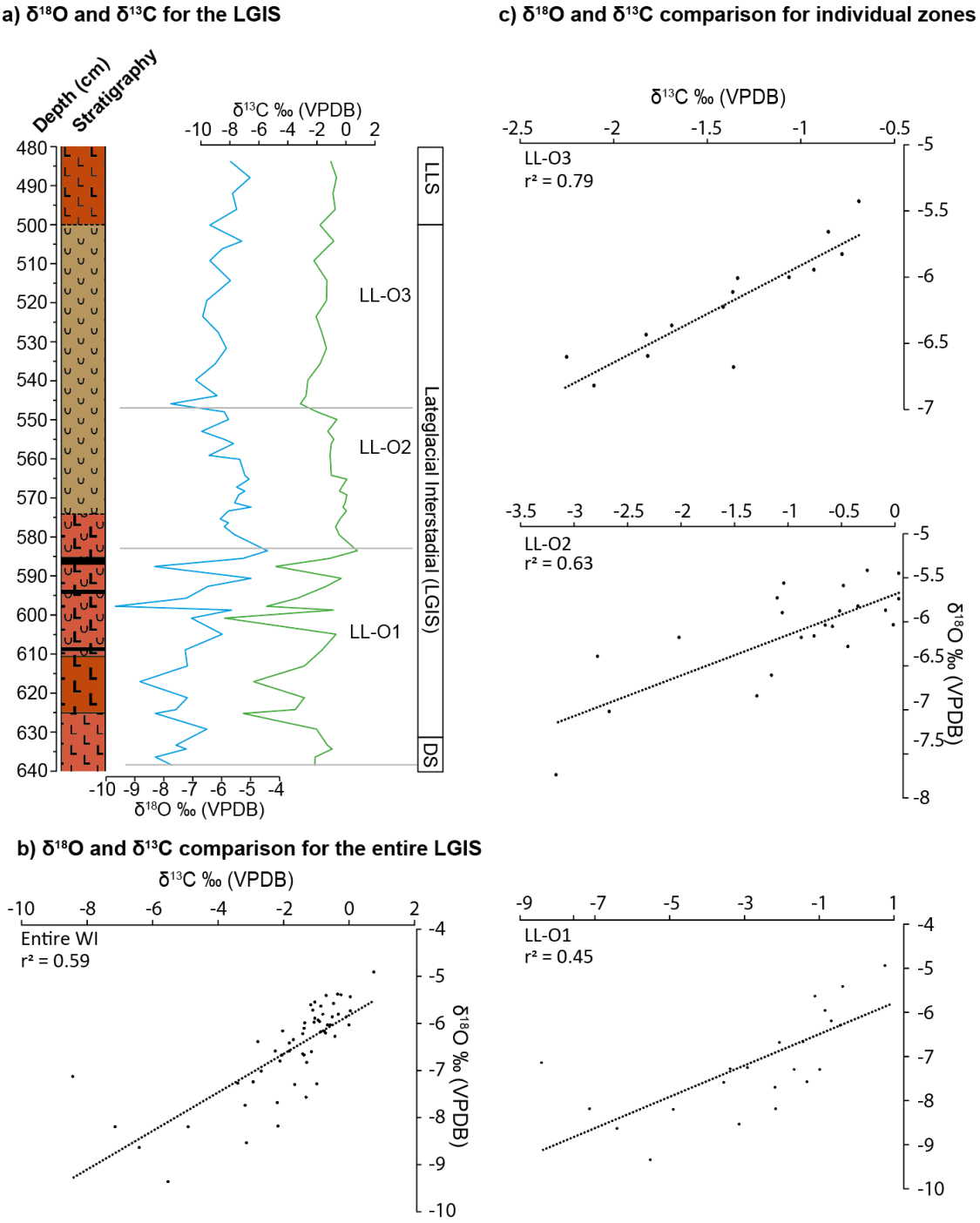

Figure 8.5, Stable isotope data for Llangorse. **a**) Stable isotope data ($\delta^{18}O$ and $\delta^{13}C$) for the LGIS with zones denoted as LL-On. **b**) Comparison of $\delta^{18}O_{carbonate}$ and $\delta^{13}C_{carbonate}$ values for the entire LGIS. **c**) Comparison of $\delta^{18}O_{carbonate}$ and $\delta^{13}C_{carbonate}$ values for different isotopic zones.

8.4 Palaeoenvironmental and palaeoclimatic interpretation

This section will explore the environmental and climatic history of Llangorse lake during the LGIS using the proxy data presented within this chapter along with the pollen data generated by Abrook (2018) prior to the start of this PhD project. The chronology presented in this section is generated from a series

of radiocarbon dates used within a Bayesian age model and the sequence will be interpreted in chronological succession (Figure 8.6).

A range of environmental variables could potentially have an influence on chironomid assemblages. For each time interval the main driver(s) of assemblage change will be considered and the reliability of the T_{Jul} reconstruction will be discussed. Such factors include 1) summer air temperatures, 2) lake water trophic status, 3) macrophyte presence/abundance/type, 4) lake water oxygenation, and 5) substrate texture and turbidity. Lake depth can also affect chironomid presence/abundance, however, no notable changes in the water depth and therefore lake level can be discerned from the chironomid assemblages. Most taxa present at Llangorse are characteristic of intermediate water depths in a lacustrine environment suggesting a moderately deep lake in the northern basin, no greater than 7 m deep but greater than 2 metres in depth, was present throughout the LGIS (cf. Engels and Cwynar, 2011).

Palaeoenvironmental significance of the oxygen isotope record

Before a climatic interpretation of MAT from the $\delta^{18}O$ record can be made, several factors need to be considered for the sequence. In many LGIT sequences from the British Isles the $\delta^{18}O$ record is interpreted as being a function of prevailing air temperatures (See chapter 4) and is often supported by the fact that there is a close correspondence between chironomid derived T_{Jul} estimates and $\delta^{18}O$ values (i.e., van Asch *et al.,* 2012; Abrook *et al.,* 2020; Blockley *et al.,* 2018). In the Llangorse sequence, however, this does not appear to be the case for the most part. Except for the transition from the Dimlington to the earliest- LGIS, where both $\delta^{18}O$ values and T_{Jul} estimates increase, these two proxies typically trend in opposite directions. This is perhaps most clearly seen in the mid- LGIS where chironomid T_{Jul} estimates increase whilst $\delta^{18}O$ values decline. Conversely, in the late-LGIS chironomid T_{Jul} estimates decrease whilst $\delta^{18}O$ values rise.

As a result of these patterns a different interpretation needs to be proposed to explain the $\delta^{18}O$ trends seen in much of the Llangorse sequence. Candy *et al.* (2016) provides a discussion of many of the potential drivers of $\delta^{18}O$ values in Lateglacial sequences. Firstly, a change in winter temperatures could impact $\delta^{18}O$ values but not T_{Jul} estimates. Secondly, a shift in the seasonality of rainfall could cause an increase or decrease in the $\delta^{18}O$ value of the lake waters depending on whether summer or winter rainfall became more dominant. Thirdly, geological carbonate can be eroded and transported into the lake basin, causing alteration to the climatic signal recorded in $\delta^{18}O$. Finally, changes in the hydrology of the lake basin resulting in higher or lower amounts of evaporation could cause the $\delta^{18}O$ value of the

lake water to increase or decrease regardless of temperature trends. When considering explanations for changes observed in palaeoenvironmental $\delta^{18}O$ records it is important to note that during the interstadial at Llangorse there is a moderate to strong degree of co-variance between $\delta^{18}O$ and $\delta^{13}C$ values throughout the sequence. Isotopic co-variance is most common in lake carbonates due to either detrital contamination from reworked limestone or evaporative modification of the lake waters. Therefore, it is likely that the changes in the $\delta^{18}O$ record at Llangorse are either a result of evaporitic enrichment of the lake water and/or the effects of detrital contamination. In some parts of the sequence where co-variance is lower, changes in MAT could also influence the isotopic signal. These factors will be discussed in the subsequent subsections.

8.4.1 Transition from the DS to LGIS: 15,500 ±180 – 15,280 ±180 cal a BP (Depth 640-623cm)

LL-C1; LL-L1b; start of LL-O1

A diverse mix of chironomid taxa with a wide range of temperature optima occur during the transition from the Dimlington into the LGIS, between 15,500 ±180 – 15,280 ±180 cal a BP (640-623 cm). The most abundant taxon is the cold indicating *Paratanytarsus* undifferentiated and occurs alongside other cold and cool-temperate indicating taxa, e.g., *COTL*-type and *P. sordidellus*-type. In the latter part of LL-C1 *Paratanytarsus* declines and the warm indicating *P. nubeculosum*-type increases, resulting in T_{Jul} increasing from 9.6 °C to 13.7 °C. However, *M. pedellus*-type which is temperate indicating occurs throughout LL-C1 at *c*. 20 % abundance. Although the Goodness-of-fit analysis suggests factors other than temperature did not affect the chironomids, other secondary variables may also be exerting a strong force on the chironomid assemblage. *M. pedellus*-type also prefers coarse substrates and unstable turbid conditions (Brooks 1997), potentially allowing it to occur in conditions well below their thermal optima.

The taxa present in the first half of LL-C1 below 630 cm generally indicate relatively nutrient poor conditions e.g., *M. pedellus*-type (Steenbergen, 1993; Brodersen *et al.,* 1998), *Procladius* (Vallenduuk & Moller Pillot, 2007) and *COTL*-type (Brooks *et al.,* 2007; Brundin, 1956; Brodin, 1986). *P. nubeculosum*-type often occurs with inwash of nutrients and appears in abundances of up to 20 % in the latter part of LL-C1 suggesting the inwash of nutrient-rich minerogenic sediment (Brundin, 1949; Saether, 1979). Head capsule abundance also increases in the latter half of LL-C1 from 13 to 102 HCs/gram suggesting an increase in lake productivity, as chironomid biomass is linked to food availability (e.g., Tokeshi, 1986).

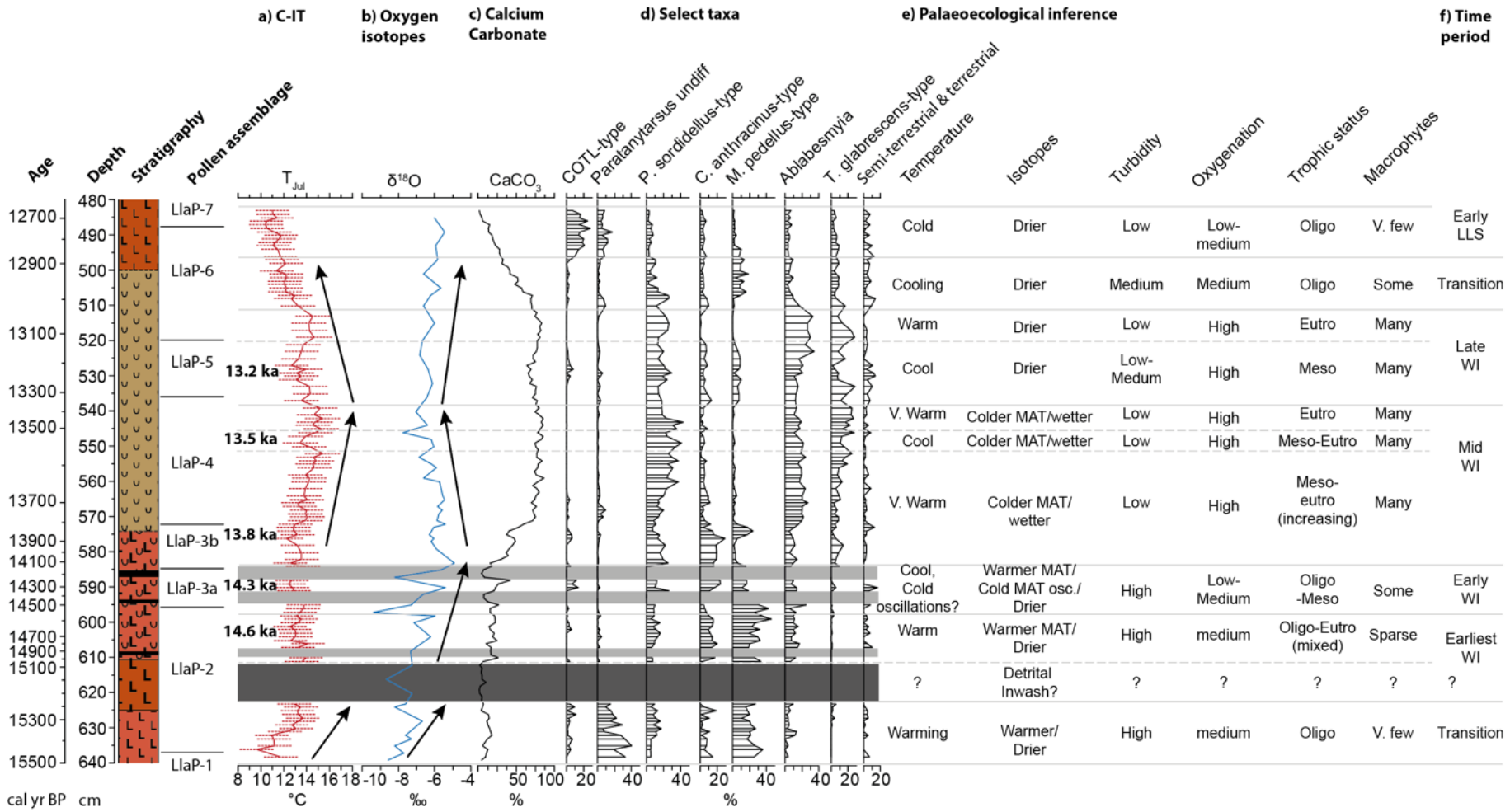

Figure 8.6, Summary figure of data from Llangorse. **a**) Chironomid-inferred mean July air temperatures (T_{Jul}); **b**) Oxygen isotopes; **c**) Calcium carbonate; **d**) select taxa; **e**) qualitative ecological inferences; **f**) broad time period. Dark grey area denotes samples where no head capsules were present. The light grey zones denotes where samples have been removed due to very low head capsule counts. Pollen assemblage zones are from Abrook (2018).

Many taxa present in LL-C1 are tolerant of low oxygen conditions and feed on detritus, bacteria, or other invertebrates e.g., *C. anthracinus*-type (Johnson 1986; Walshe, 1951), *P. nubeculosum*-type (Titmus and Badcock, 1981), *Dicrotendipes* (Steenbergen, 1993; Lenz, 1958) and *Procladius* (Heiri and Lotter, 2003; Vallenduuk & Moller Pillot, 2007). However, *M. pedellus*-type requires relatively well oxygenated water (Steenbergen, 1993) and lake waters must therefore have been reasonably well oxygenated, potentially facilitated by the presence of *Pediastrum* (Abrook, 2018). It could be that the littoral zone of the lake was well oxygenated but the profundal zone was not. The low percentages of LOI and the low percentage abundance of aquatic pollen, in particular the absence of *Myriophyllum,* suggests vegetation within the lake was sparse (Abrook, 2018). Although taxa which are often associated with macrophytes form a notable part of the assemblages collectively, they can also occur in low abundances individually living on or in minerogenic substrates, e.g., *P. sordidellus*-type (Brodersen *et al.,* 2001; Reiss, 1968), *Dicrotendipes* (Brodersen *et al.,* 2001; Moller Pillot, 2009) and *Ablabesmyia* (Brodersen *et al.,* 2011; Vallenduuk & Moller Pillot, 2007).

During the transition from the Dimlington Stadial into the very early LGIS, there is an increase in $\delta^{18}O$ from -8.6 ‰ to -6 ‰. There is a moderate degree of co-variance between $\delta^{18}O$ and $\delta^{13}C$ (LL-01; r^2 = 0.45) suggesting detrital contamination and/or isotopic modification of the lake waters. The sediment of LL-L1b is largely composed of minerogenic clays and silts with very low $CaCO_3$ values of <20 % and so any detrital contamination would have a large impact on the isotopic signal. The T_{Jul} record suggests that summer temperatures are above the required level for $CaCO_3$ to form (> *c.* 10 °C; Kelts and Hsu, 1978) and so other factors must be limiting $CaCO_3$ precipitation in the lake. There could potentially be a lack of dissolved carbonate ions in the lake water to precipitate. There is very little limestone present in the Llangorse catchment, restricted to the Castell Coch Limestone and Dowlais Limestone formations (cf. section 6.2.2) which sit high up in the hills surrounding Llangorse. It could be that soil and bedrock at higher altitude are still frozen in permafrost, prohibiting the percolation of water and subsequent enrichment in calcium, reducing the concentration of Ca^{2+} ions in the lake water. There is also a high percentage of taxa accustomed to coarse substrates and early colonization after significant environmental change, e.g., *M. pedellus*-type (up to 40 %) and *C. anthracinus*-type (up to 20 %) (Hofmann, 1984; Brooks, 1997) suggest a high level of turbidity within the lake and the potential inwash of detrital carbonate. The pollen also indicates disturbed soils during LLaP-1 and LLaP-2, as suggested by

the presence of *Artemisia* and *Rumex*, however both plant taxa are also characteristic of arid conditions (Barney and DiTommaso, 2002; Walker 1975; Beerling 1993). The increase in $\delta^{18}O$ of 2.6 ‰ does however also coincide with the large increase in T_{Jul} of 4.1 °C suggesting $\delta^{18}O$ may reflect MAT in this part of the record. Therefore, the increase of 2.6 ‰ in $\delta^{18}O$ is cautiously interpreted as reflecting an increase in mean annual temperature, however, evaporitic enrichment of the lake waters and detrital contamination cannot be ruled out.

8.4.2 Earliest-LGIS: 15,270 ±180 – 14,550 ±170 *cal a BP (Depth 623-598 cm)*

LL-C2, LL-C3; LL-L2, LL-L3; Middle of LL-O1

In the earliest-LGIS, between 15,270 ±180 - 15,040 ±160 cal a BP (623-612 cm), a change in the predominant grain size occurs in LL-L2 from clay-silt to clay, with low amounts of $CaCO_3$ (<6 %) and organic material (<0.4 %). There is no evidence for Cwn glacier activity in the Llangorse catchment during the LGIS (Chambers, 1999; cf. section 6.2.3) and LGM ice retreated well before the start of the LGIS (Palmer *et al.,* 2008). Therefore, it is unlikely that the clay-rich sediment of LL-L2 originated from an increase in glacial activity. More likely, the clay was reworked from glacial till deposits in the catchment which was washed into the lake and/or long winters where the lake froze over, allowing the clay to fall out of suspension. The age model for the LLAN14 sequence indicates this phase of clay sedimentation lasted *c*. 200 yrs; however, the error estimates are large (180 yrs at 2σ), meaning unit LL-L2 could have been deposited in a single event or over *c*. 560 yrs. The lack of chironomid head capsules in the LL2 sediments indicates high sedimentation rates (cf. Brooks *et al.,* 2007; Pinder, 1980) and T_{Jul} has similar values either side of LL-L2, *c*. 13.5 °C, suggesting that the unit was deposited over a very short period. Due to the lack of chironomid HCs present, it is not possible to comment on summer temperature changes during the earliest LGIS. The very low $CaCO_3$ values in LL-L2 means that even a small amount of detrital contamination could greatly alter the isotopic signal. A small decline in T_{Jul} of 1.3 °C is of note in the earliest- LGIS with minimum values achieved at 14,630 ±180 cal a BP.

Several cold indicating taxa continue to persist in low abundances during the earliest- LGIS between 15,040 ±160 – 14,460 ±170 cal a BP (612-594 cm) including *Paracladius*, *COTL*-type and *Paratanytarsus* undifferentiated and T_{Jul} average around 13 °C. Both cool temperate (e.g., *C.*

anthracinus-type) and temperate taxa (e.g., *M. pedellus*-type, *Ablabesmyia*) increase in abundance, as well as cold-indicating taxa such as *H. grimshawi*-type, albeit in low abundances.

H. grimshawi-type (Brundin, 1956; Saether, 1979; Brodin 1986; Walker and MacDonald 1995) and *Procladius* (Brodin and Gransberg, 1993) are indicative of low nutrient levels, while the increase in *P. sordidellus*-type suggests more mesotrophic conditions (Moller Pillot, 2013). Some eutrophic indicating taxa are also present in low abundances e.g., *C. plumosus*-type (Saether, 1979) and *P. nubeculosum*-type (Brundin 1949; Saether 1979; Lindegaard and Jonsson 1983). The lake is therefore most likely in a transition period from low to high nutrient conditions, with conditions allowing oligotrophic taxa to persist. Productivity is still relatively low, with low but highly variable HC concentrations. Vegetation within the lake potentially increased slightly, indicated by increases in *Ablabesmyia* to 15 % (Brodersen *et al.,* 2011). However, vegetation is likely to have been still rather sparse as LOI remains low (<3 %) and the assemblages are still largely dominated by detritus feeders e.g., *H. grimshawi*-type (Moog, 1995). Oxygenation of the lake water also likely improved further as *H. grimshawi*-type, which requires well oxygenated conditions (Moller Pillot, 2013), was present in high abundances.

Clay continues to form the main sediment component, however, $CaCO_3$ precipitation increases, contributing *c*. 19 % of the sediment on average. Taxa adapted to coarse substrates and unstable conditions continue to be present in high abundance, e.g., *M. pedellus*-type and *C. anthracinus*-type (Hofmann, 1984; Brodersen and Lindegaard, 1999a). Continued turbidity is likely to be the main cause of the low $CaCO_3$ precipitation as T_{Jul} values are above 10 °C and the vegetation cover of the surrounding slopes remains open, with pollen spectra dominated by taxa indicative of disturbed bare soils e.g., *Artemisia and Rumex* (Abrook, 2018).

8.4.3 Early -LGIS: 14,550 ±170 – *14,100 ±90 cal a BP (Depth 598-584 cm)*

LL-C4; end of LL-L3; end of LL-O1

During the early-LGIS (14,550 ±170 – 14,100 ±90 cal a BP) a small decline in T_{Jul} occurs with a magnitude of 1.4 °C. declining from 13.7 to 12.3 °C and can most likely be attributed to the increase in the cold-indicating *COTL*-type. Two clay-rich layers also occur at *c.* 14,450 ±170 cal a BP (594-592 cm) and *c*. 14,180 ±100 cal a BP (588-585cm), either side of the T_{Jul} minimum and contain very

few HCs meaning reliable T_{Jul} estimates cannot be made. Similar processes which formed the clay layer between 623-612 cm are invoked, in which clay from previous episodes of glacial activity was washed into the lake, and/or extended periods of lake ice cover allowed the clay to fall out of suspension. The increase in *COTL*-type suggests the lake may have become slightly more oligotrophic during the 14.4 ka BP ACE.

Co-variance between $\delta^{18}O$ and $\delta^{13}C$ continues to be moderate (LL-O1; $r^2 = 0.45$) suggesting the isotopic signal may be affected by evaporitic enrichment of the lake waters and/or detrital contaminations. An increase in aridity is also suggested by the pollen data which show a return to colder and more arid conditions, with a decline in *Betula* and the return of colder artic-alpine affiliated vegetation (e.g. *Artemisia, Poaceae, Cyperaceae, Asteraceae*) during LLaP-3a (Abrook, 2018). Around the same time, two large isotopic shifts in $\delta^{18}O$ (*c*. 4‰) to more negative values occur, with minimum values attained at 14,540 ±170 cal a BP (597 cm; -9.4‰) and 14,200 ±110 cal a BP (587 cm; -8.1‰). These minimum values could reflect declines in MAT. The $\delta^{18}O$ signal is also susceptible to detrital contamination during the early-LGIS as $CaCO_3$ is generally low, around 10–20 %. Sample depths which contained a sufficient number of HCs indicate that T_{Jul} was above 10 °C and the continued high abundance of M. pedellus-type, which is accustomed to coarse substrates (Hofmann, 1984), and *C. anthracinus*-type, which often occurs after significant environmental change (Brooks *et al.,* 2007) suggests catchment instability is the main controlling factor on $CaCO_3$ production. $CaCO_3$ is particularly low during the two clay-rich layers of sediment and broadly coincide with the isotopic lows in $\delta^{18}O$ at 594-592cm (*c*. 9 %) and 588-585cm (*c*. 2 %). Very few HCs were preserved in the clay meaning reliable T_{Jul} estimates cannot be made but the sedimentology may suggest colder periods. Isotopic values of the Castell Coch Limestone and Dowlais limestone formations are not available. However, $\delta^{18}O$ and $\delta^{13}C$ data of carboniferous limestone ranges from -14 to -1.9 ‰ and -12 to +3.54 ‰, respectively (Searl, 1989; Leslie *et al.,* 1992, Brasier *et al.,* 2014) and therefore overlaps with the isotopic values observed in LL-O1b. It should also be noted that the deposition of $CaCO_3$ is not uniform, with thin laminae of near pure marl sporadically occurring in LL-L1b, potentially causing certain years or even seasons to be more strongly recorded in the $\delta^{18}O$ signal. Therefore, the $\delta^{18}O$ signal is complex, potentially recording increasing aridity and two potential short-lived declines in MAT, but this could be an artefact of detrital contamination. If the decline in $\delta^{18}O$ at 14,540 ±170 cal a BP (597 cm) does represent a cooling in MAT, as this precedes the cooling in T_{Jul} at 14,500±170 cal a BP (595 cm).

8.4.4 Mid-LGIS: 14,100 ±90 ±100 - 13,340 ±60 cal a BP (composite depth 584-538cm)

Latter half of LL-C4, First half of LL-C5; LL-L4, First half of LL-L5; LL-O2, first half of LL-O3

The initial warming at the start of the Mid-LGIS coincides with the spread of the *Juniperus* scrub in LLaP-3a (Abrook, 2018), suggesting climatic amelioration (Lowe and Walker, 1986). Subsequently throughout the Mid-LGIS T_{Jul} increases from 13.8 °C to 15.4 °C, the highest mean July air temperatures of the LGIS at Llangorse. The high T_{Jul} values for the LGIS at Llangorse are associated with the high abundance of cool-temperate, temperate, and warm-indicating taxa (e.g., *P. sordidellus*-type, *Ablabesmyia* and *T. glabrescens*-type), forming 20-40 % of the assemblages. Other warm adapted taxa are also consistently present in their highest abundance for the sequence, albeit at only 1-5 %, e.g., *Nanocladius rectinervis*-type, *Nanocladius branchicolus*-type, and *P. varus*-type. Sediment composition undergoes a distinct change with marl becoming the dominant sediment component as $CaCO_3$ increases from 20% to 75%. Although the warmer summer temperatures may have helped increase $CaCO_3$ precipitation, improved catchment stability is likely to have been the main cause as the *Juniperus* scrub helps stabilise the soils in the catchment (Abrook, 2018). *M. pedellus*-type, which is accustomed to coarse substrates (Hofmann, 1984) declines at this time, suggesting a reduction in lake water turbidity allowing more light penetration and therefore photosynthesis to occur, facilitating $CaCO_3$ precipitation. It should be noted that two T_{Jul} samples in the Mid- LGIS has a 'poor' fit-to-temperature and one has a 'very poor' fit suggesting factors other than temperature may have affected the chironomid assemblages. However, the temperature reconstructions for these samples are in line with other neighbouring reconstructed T_{Jul} estimates and so are thought to be reliable. The reconstructed T_{Jul} temperatures also agree well with the pollen data displaying the presence of open birch woodland, which requires temperatures of at least 12 °C (Birks 1994; van Dinter and Birks, 1996; Abrook, 2018). Two notable declines in T_{Jul} occur during the mid-LGIS and will be discussed in the following paragraph.

The first mid-LGIS decline in T_{Jul} occurs between 13,930 ±100 – 13,730 ±110 cal a BP (579-571 cm) with T_{Jul} declining from 13.7 to 12.2 °C, a magnitude of 1.5 °C. This decline in T_{Jul} is associated with the brief re-occurrences of cold adapted taxa (e.g., *C. ambigua*, *COTL*-type and *H. grimshawi*-type) in low abundances along with small declines in cool-temperate, temperate, and warm indicating taxa (e.g., *P. barbatipes*-type, *Ablabesmyia* and *T. glabrescens*-type). A slight decline of 10 % in

$CaCO_3$ occurring at *c.* 13,870 ±110 (575 cm) may have been caused by an increase in catchment instability as the Juniper scrub declines. The peak in *M. pedellus*-type may reflect a return of more unstable and better oxygenated conditions (Brooks *et al.,* 2007; Steenbergen, 1993). This temperature decline broadly aligns with the decline in Juniper scrub and the expansion of birch woodland. A second decline in T_{Jul} occurs between 13,520 ±70 – 13,410 ±60 cal a BP (552-545 cm), where T_{Jul} declines from 15.4 °C to 13.4 °C, a decline of 2°C. Unlike the previous ACE, there is no re-occurrence of cold indicating taxa, however, there is a small increase in the cool-temperate indicating *P. septentrionalis*-type and a decline in the warm indicating *T. glabrescens*-type.

Eutrophic indicating taxa e.g. *P. sordidellus*-type (Bituški, 2000; Orendt 1993) and *T. glabrescens*-type (Brodin 1986; Uutala 1986, Bilyj and Davies, 1989), increase throughout the Mid-LGIS to their highest abundances of the LGIS suggesting trophic status has peaked. Other taxa indicating high nutrient levels include *E. pagana*-type (Kansanen 1985; Saether, 1979) and *Nanocladius,* which can live sporadically in moderately eutrophic lakes (Moller Pillot, 2013; Cranston *et al.,* 1983). The lake is not hypereutrophic though as *P. sordidellus*-type cannot tolerate such conditions (Moller Pillot, 2013). High LOI values and chironomid HC concentrations suggests a productive lake during the mid-LGIS (Tokeshi, 1986). The pollen data shows aquatic vegetation is well developed with high abundance of *Myriophyllum*, *Potamogeton* and other aquatic macrophytes (Abrook, 2018). This is also reflected in the chironomid assemblages where *P. sordidellus*-type and *Ablabesmyia* (Brodersen *et al.,* 2011) occur in high abundance. Algal communities may also have developed, as both *P. septentrionalis*-type and *E. pagana*-type appear and are known to occur in association with filamentous algae (Moller Pillot, 2013) and blue-green algae (Cannings & Scudder, 1978; Saether, 1979), respectively. The pollen data also shows an increase in *Pediastrum* during the mid-LGIS (Abrook, 2018). The increase in oxygenating aquatic flora also allows the increase in $CaCO_3$ precipitation and helps sustain chironomid taxa with high oxygen demands, e.g., *Nanocladius* (Moller Pillot, 2013). *P. varus*-type, which feeds on the snail *Physa fontinalis* (Guibé, 1942), suggests a diverse range of aquatic fauna was living in the lake. During the c. 13.8 ka BP ACE, the brief appearance of *COTL*-type and *C. ambigua*, and decline in *P. sordidellus*-type and *Ablabesmyia*, could point towards slightly more oligotrophic conditions, though the lake largely remained mesotrophic (Brooks, *et al.,* 2007; Moller Pillot, 2013; Vallenduuk and Moller Pillot, 2007).

$\delta^{18}O$ declines throughout the mid-LGIS (-5.4 to -6‰). $\delta^{18}O$ and $\delta^{13}C$ are moderately correlated (r^2 = 0.63) suggesting $\delta^{18}O$ may be influenced by changes in the balance between precipitation and evaporation as well as mean annual temperatures. The pollen data also indicates a stable landscape that would produce minimal allogenic input due to the development of birch woodland (Abrook, 2018). *M. pedellus*-type and *C. anthracinus*-type, which are accustomed to coarse substrates and early colonization after significant environmental change (Hofmann, 1984; Brooks, 1997), decline further throughout the Mid-LGIS, to less than 5 %, suggesting catchment stability continues to improve. Semi-terrestrial and stream taxa occur at very low levels, generally <0.5 %, their lowest levels for the LGIS, also suggesting stability within the catchment. If there were any detrital contamination, it would probably have had little, if any, influence on the $\delta^{18}O$ signal as any reworked geological carbonate present would be heavily diluted by the high level of precipitated $CaCO_3$ (75-80 %). It is therefore likely that a change in the balance between precipitation and evaporation may have occurred with the climate becoming more humid and wetter. This concurs with the pollen data as *Filipendula* is prevalent which requires warm moist conditions (Abrook, 2018).

8.4.5 Late-LGIS: 13,340 ±60 - *13,030 ±50 cal a BP (Depth 538-512 cm)*
Latter part of LL-C5; Latter half of LL-L5; Middle of LL-O3

During the late-LGIS there is an ACE of 2.5 °C in T_{Jul} from 15.2 °C to 12.7 °C between 13,340 ±60 – 13,110 ±50 cal a BP (538-520 cm) which is largely driven by the large decline in the warm indicating taxon *T. glabrescens*-type from 28% to 1%. Other warm indicating taxa also disappear from the lake including *N. branchicolus*-type, *N. rectinervis*-type and *T. lactescens*-type. The cold adapted taxon *COTL*-type appears in low abundance. $CaCO_3$ does display a minor decline between 13,340 ±60 – 13,110 ±50 cal a BP (538-520 cm) to 64 %. A slight shift to more unstable turbid conditions is indicated by small increases in *M. pedellus*-type, which is accustomed to coarse substrates (Hofmann, 1984), and *C. anthracinus*-type, which often occurs after significant environmental change (Brooks *et al.,* 2007), to 10 % each (Hofmann, 1984; Brodersen and Lindegaard, 1999a; Brooks, 1997). The pollen data also supports the interpretation of increased instability as vegetation once again becomes more open with a decrease in birch woodland and a range of taxa typical of disturbed bare soils including *Artemisia* and *Rumex* (Abrook, 2018). However, marl still forms the largest sediment component, suggesting climate remains warm and catchment

conditions stable. Trophic status of the lake potentially declined slightly as indicated by an increase in oligotrophic indicating taxa such as *P. orophila* (Kansanen 1985; Brodin and Gransberg, 1993), *M. pedellus*-type (Steenbergen, 1993; Brodersen *et al.,* 1998) and *COTL*-type (Brooks *et al.,* 2007; Brundin, 1956; Brodin, 1986). However, the lake is likely to be meso-eutrophic, as *P. sordidellus*-type and *Ablabesmyia* both still occur in abundance (Moller Pillot, 2013; Orendt, 1993). The large decline in *T. glabrescens*-type may relate to a change in the lake vegetation composition. The pollen data shows that *Nuphar* becomes largely absent and *Myriophyllum* declines but *Pediastrum* and *Potamogeton* increase (Abrook, 2018). *Ablabesmyia* and *P. sordidellus*-type, which usually live amongst plants, can also live on detritus and filamentous algae (Armitage, 1968; Zelentsov 1980) and therefore may be better able to adapt to changes in habitat and food sources. Lake waters probably remain well oxygenated as taxa which require well oxygenated water are still present in abundance e.g., *M. pedellus*-type (Steenbergen, 1993), *Ablabesmyia* (Vallenduuk &Moller Pillot, 2007) and *P. sordidellus*-type (Moller Pillot, 2013).

The abrupt cooling of 2.5 °C is followed by an increase in T_{Jul} to *c.* 14.2 °C between 13,110 ±50 - 13,030 ±50 cal a BP (520-512 cm) driven by increases in temperate and warm indicating taxa (e.g., *Ablabesmyia* and *T. glabrescens*-type). Other warm indicating taxa, *P. varus*-type and *T. lactescens*-type, briefly re-appear in low abundances. Warm stable lake water conditions return causing a final increase in $CaCO_3$. Both *C. anthracinus*-type and *M. pedellus*-type decline to only a few percent as an increase in birch woodland helps stabilise the landscape (Abrook, 2018). Macrophytes flourish, lake water oxygenation increases, and trophic status returns to eutrophic levels, as eutrophic indicating taxa (e.g., *T. glabrescens*-type and *Ablabesmyia*) increase to their highest abundances for the LGIS, reaching 25 and 35 % respectively. The aquatic pollen in LLaP-6 displays an increase in *Nuphar*, *Myriophyllum* and *Pediastrum* (Abrook, 2018).

$\delta^{18}O$ and $\delta^{13}C$ display a strong degree of co-variance during LL-O3 ($r^2 = 0.79$). The effect of detrital contamination is likely to be minimal as $CaCO_3$ generally remains high throughout the late-LGIS (65-83%) and would dilute any signal from geological carbonate. Therefore, the more likely cause of the high co-variance is an increase in aridity, causing the lake waters to become increasingly enriched in ^{18}O isotope due to the preferential loss of the lighter ^{16}O isotope. $\delta^{18}O$ values displays a general increasing trend throughout the late-LGIS from -7 ‰ to -5.4 ‰ and contrasts with T_{Jul}

which shows an overall decline from its mid-LGIS peak of 15.3 °C to 14.2 °C by the end of the late-LGIS.

When taking the general trends in both T_{Jul} and $\delta^{18}O$ into account, the climate is interpreted as becoming colder and drier throughout the Late-LGIS. Palmer *et al.* (2021) suggested a fall in lake level occurred during the Late-LGIS or early LLS (see section 6.2.4) and a shift to drier conditions may cause such a change. There is limited evidence for a fall in lake level in the chironomid assemblages, although, the rise in *Ablabesmyia* may be due to an increase in the littoral area caused by a fall in lake level (Brooks *et al.,* 2007). Massaferro and Brooks (2002) also suggested that a notable increase in *Limnophyes* may occur as lake level falls, but semi-terrestrial and terrestrial taxa only increase to 3.5 %. However, a minor fall in lake level of about 150 cm is unlikely to cause a significant response in a chironomid assemblage (Brooks and Heiri, 2013). Although climate is inferred to have become increasingly arid throughout the late-LGIS, *Filipendula* and *Cyperaceae*, which require relatively moist conditions, increase (Abrook, 2018). Such increases in plants characteristic of moist conditions are seen during the Allerød-Younger Dryas transition at Meerfelder Maar and were proposed to have resulted from a fall in lake level, which lead to what was previously the littoral becoming exposed, providing an ideal substrate high in nutrients, organics and moisture (Engels *et al.,* 2016).

8.4.6 Transition from the LGIS to the early-LLS: 13,030 ±50 – 12,670 ±70 cal a BP (Depth 512-483 cm)

LL-C6, LL-C7; LL-L6; latter half of LL-O3

During the transition from the LGIS to the LLS, 13,030 ±50 to 12,890 ±50 cal a BP (512 – 497 cm), T_{Jul} declines from 14.5 °C to 11.1 °C, as cold indicating taxa (e.g., *Paracladius*, *H. grimshawi*-type) and cool temperate taxa (e.g. *S. coracina*-type) re-appear while temperate and warm indicating taxa (e.g., *P. sordidellus*-type, *Ablabesmyia* and *T. glabrescens*-type) decline to only few percent. Several oligotrophic-indicating taxa increase in abundance, including *S. coracina*-type (Pinder and Reiss, 1983; Kansanen, 1985), *H. grimshawi*-type (Brodin 1986; Walker and MacDonald, 1995) and *P. triquetra*-type (Walker and MacDonald 1995) suggesting trophic status probably shifted from eutrophic to oligotrophic conditions. The pollen assemblages show that *Myriophyllum*, *Nuphar* and *Potamogeton* largely disappear (Abrook, 2018). The decline in aquatic vegetation is also apparent

in the chironomids as taxa largely dependent on macrophytes for habitat and food e.g., *T. glabrescens*-type, *Ablabesmyia* and *P. sordidellus*-type (Brooks *et al.,* 2007) decline. Detritus feeders increase e.g., *Paracladius* (Moller Pillot, 2013), *H. grimshawi*-type (Moog, 1995) and *S. coracina*-type (Walshe, 1951) indicating a shift in the main food source from aquatic macrophytes to organic detritus. The presence of *Paracladius* also indicates that the lake bottom is silty with little or no vegetation (Reiss 1968; Zinchenko, 2002). It is possible that charophytes were present as there are relatively high numbers of *C. ambigua* (Brodersen and Lindegaard 1999b). Lake waters continue to be well oxygenated as required by *H. grimshawi*-type (Moller Pillot, 2013) and *M. pedellus*-type (Steenbergen, 1993).

T_{Jul} declines further to 10 °C during the early LLS as cold-indicating taxa increase including e.g., COTL-type, *M. insignilobus*-type and *Paratanytarsus* undifferentiated. The lake becomes increasingly oligotrophic, and is well oxygenated, as indicated by the presence of e.g. *H. grimshawi*-type (Saether 1979), *COTL*-type (Brundin 1956; Brodin 1986) and *P. triquetra*-type (Walker and Matthews, 1989; Walker and MacDonald 1995). Taxa usually associated with macrophytes continue to be present in low abundances suggesting they may live on or in minerogenic substrates, e.g., *P. sordidellus*-type (Brodersen *et al.,* 2001; Reiss, 1968), *Dicrotendipes* (Brodersen *et al.,* 2001; Moller Pillot, 2009) and *Ablabesmyia* (Brodersen *et al.,* 2011; Vallenduuk & Moller Pillot, 2007).

$\delta^{18}O$ and $\delta^{13}C$ continue to exhibit strong co-variance (LL-O3; $r^2 = 0.79$) during the transition out of the LGIS and into the early LLS, suggesting the climate continues to be arid causing modification of the isotopic signal through evaporitic enrichment of the lake water. Detrital contamination may also play an increasing role as $CaCO_3$ declines from 80 % to only 2 %. The pollen assemblages display an increase in taxa indicative of an exposed landscape (*Caryophyllaceae*, *Asteraceae*, *Thalictrum*, *Selaginella selaginoides*; Whittington *et al.,* 2015) and disturbed soils (*Artemisia* and *Rumex*; Barney and DiTommaso, 2002). The increase in low-lying arctic-alpine herbaceous vegetation, as well as *Betula nana*, replacing birch woodland point towards an increasingly unstable landscape prone to erosion. Taxa accustomed to coarse substrates and colonization after significant environmental change, e.g., *M. pedellus*-type and *C. anthracinus*-type (Hofmann, 1984; Brooks, 1997) increase during the transition out the LGIS suggesting turbidity increases within the lake and the potential inwash of detrital carbonate. The lack of $CaCO_3$ production during the early LLS is likely to be the result of a continuation of turbid lake waters, and therefore lack of light penetration for

photosynthesis, as well as summer temperatures being near the threshold for marl formation to occur (*c.* > 10 °C; Kelts and Hsu, 1979). Overall, the climate is inferred as becoming colder and more arid as the LGIS transitions into the LLS.

8.5 Chapter summary

This chapter explored the palaeolimnological and palaeoclimatological development at Llangorse during the LGIS and early LLS. Using the chironomid and oxygen isotope data generated in this study, along with pollen data generated by Abrook (2018), I conclude that:

- Changes in the chironomid assemblages are largely driven by mean summer temperature (T_{Jul}), while the oxygen isotopes are responding to changes in the balance between precipitation/evaporation as well as mean annual temperature changes (MAT).

- A small-amplitude decline in mean summer temperatures occurs in the early-LGIS at *c.* 14.3 ka cal BP (*c.* 1.3 °C). The event is clearly expressed in the pollen record with a shift to arctic-alpine affiliated vegetation (Abrook, 2018). The oxygen isotope record potentially show two cold oscillations at *c.* 14.5ka cal BP and 14.2 ka cal BP, superimposed on a general rise in MAT. However, these isotopic shifts may be modified by changes in the precipitation/evaporation balance and detrital contamination from geological carbonate. Another ACE of small amplitude even earlier in the earliest-LGIS at 14.6 ka cal BP with a cooling of 1.3 °C.

- The chironomids display a trend to warmer summer temperatures throughout the mid-LGIS reaching 15.4 °C while the decline in oxygen isotope record may reflect a decline in MAT and/or a shift to wetter conditions. Two notable declines in T_{Jul} occur. One at 13.8 ka cal BP (*c.* 1.5 °C) and aligns with a decline in *Juniperus* and increase in *Betula* woodland. Another ACE occurs at 13.5 ka cal BP with T_{Jul} declining by 2 °C.

- During the late-LGIS, an ACE is evident in mean summer air temperatures of 2.5 °C between 13.2 ka cal BP. The chironomids also show a trend to colder mean summer temperatures throughout the late-LGIS while the oxygen isotopes display a trend to drier, more arid conditions.

Chapter 9: Old Buckenham Mere results and interpretation

Chapter overview

The purpose of this chapter is to present the sedimentology and stratigraphy for the new composite OBM19 sequence with the accompanying µ-XRF, chironomid and oxygen isotope data generated for this study. The environmental influences on both the chironomid assemblages and oxygen isotopes will be discussed and used as the basis for environmental/climatic reconstruction whilst these proxies, along with µ-XRF data which will provide detail on the limnological processes operating during the accumulation of this sequence.

Sites in East Anglia are particularly important in understanding the spatial expression of ACEs across the British Isles because southern Britain is largely devoid of high-temporal resolution quantified palaeoclimate records, and so the current N-S transect of sites only goes as far south as the Cumbrian lake sites (Lang *et al.,* 2010; Marshall *et al.,* 2002) and Star Carr (Blockley *et al.,* 2018; Abrook, 2018) in Northern England, over 200 km away. The only chironomid record covering the Lateglacial and early Holocene in the southeast of Britain is from Quidenham (Jeffers *et al.,* 2011), 2 km southwest of OBM. However, the sequence from Quidenham has very limited chronological constraint and a very noisy T_{Jul} reconstruction rather than the usual structure seen in LGIT sequences suggesting environmental variables other than temperature may have driven changes in the chironomid assemblages. Unfortunately, the radiocarbon-based age-model for the sequence retrieved from Old Buckenham Mere suggests only the end of the LGIS is covered and therefore no centennial-scale ACEs are recorded. Old Buckenham Mere does however provide a very stratigraphically expanded Loch Lomond Stadial and Holocene deposits. Although OBM does not contribute to our understanding of the spatial expression of centennial scale ACE during the LGIS, it does provide contribute to our understanding of centennial-scale changes within the Loch Lomond Stadial for which there are no quantified palaeoclimate records in southeast Britain either.

9.1. Sedimentology and µ-XRF

Old Buckenham Mere (52°29'18" N; 01°01'02" E) was cored for this PhD project in April 2019, during a field campaign led by Christopher Francis (author) with assistance from supervisors and

other members of the CQR. Our bathymetry survey agreed well with that of Tallantire (1953a), replicating many of their depth measurements along the NNW-SSE transect (Figure 9.1 and 9.2). The base of the sequence is defined by the presence of a "porridge", described by Tallantire (1953a) as consisting of gravel sized chalk clasts supported by a calcareous clayey sandy matrix. Tallantire (1953a) previously thought that the deepest point of the basin occurred near the northern end of the transect, at a depth of 13.5 m, however, we discovered it to be approximately 50 m further south, at a depth of 15.6 m. Nevertheless, the lakebed displayed a steeper gradient to the north of the deepest point, while the gradient was much shallower to the south. The new WSW-ENE transect was not completed due to time constraints, however, it showed that the western portion of the palaeolake had a relatively flat lakebed with a depth of approximately 6 m.

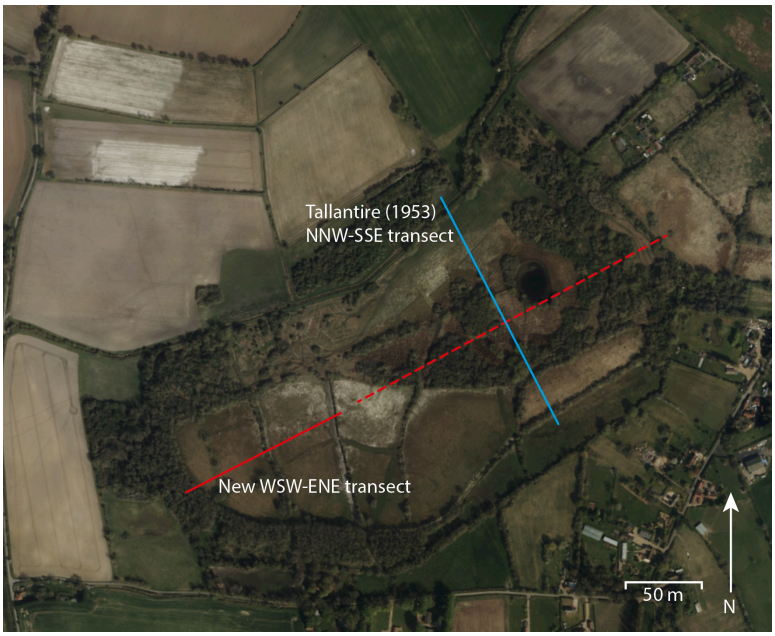

Figure 9.1, Aerial photo of Old Buckenham Fen and Mere with the NNW-SSE transect initially investigated by Tallantire (1953a) denoted by the blue line. The new WSW-ENE transect is marked in red, with the completed section denoted by the solid line and the incomplete section by the dashed line. Aerial photo Source: Digimap.

Cores retrieved during our coring campaign are displayed in Figure 9.3. As this thesis is focusing on the WI, core retrieval began at 7 m depth as the peat sediments, thought to have formed in the Holocene (Tallantire, 1953a) were not relevant to this study. However, the Holocene peat infill went to a greater depth than we originally estimated and so cores retrieved between 7 and 12 m depth were not incorporated into the composite sequence presented below, as they are not relevant to the thesis' main research question (figure 9.4).

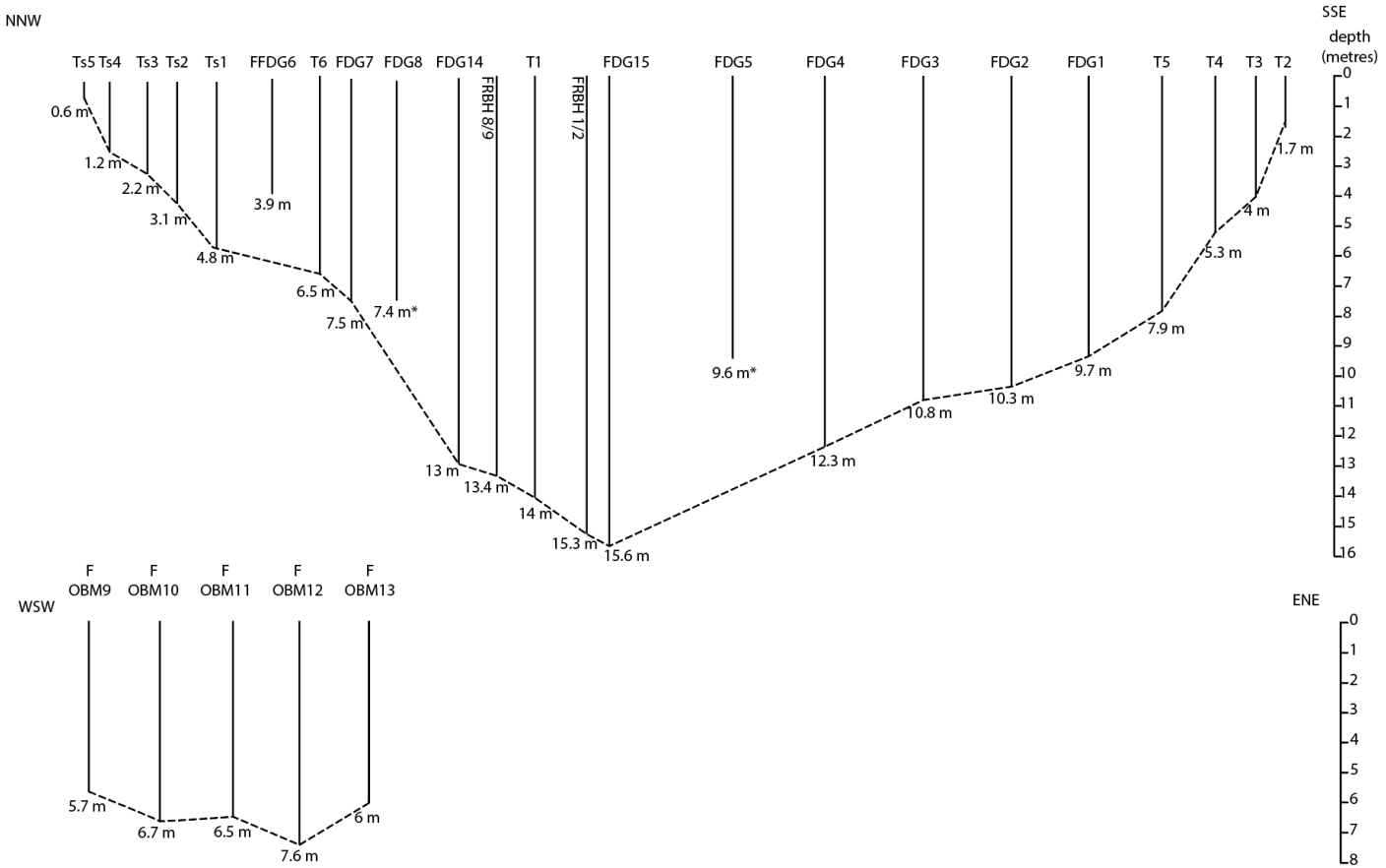

Figure 9.2, Bathymetry of the palaeolake at Old Buckenham Mere for the NNW-SSE transect in the top panel and WSW-ENE in the bottom panel. The depths presented are where the "porridge" began which line the basin. Ts*n* = trial bores by Tallantire (1953a), T*n* = deep boreholes by Tallantire (1953a), FDG*n* = Dutch gouge depth measurements by this study, and FRBH*n*/*n* = depth measurements from the Russian core boreholes taken by this study. *denotes if the depth measurement was not bottomed out.

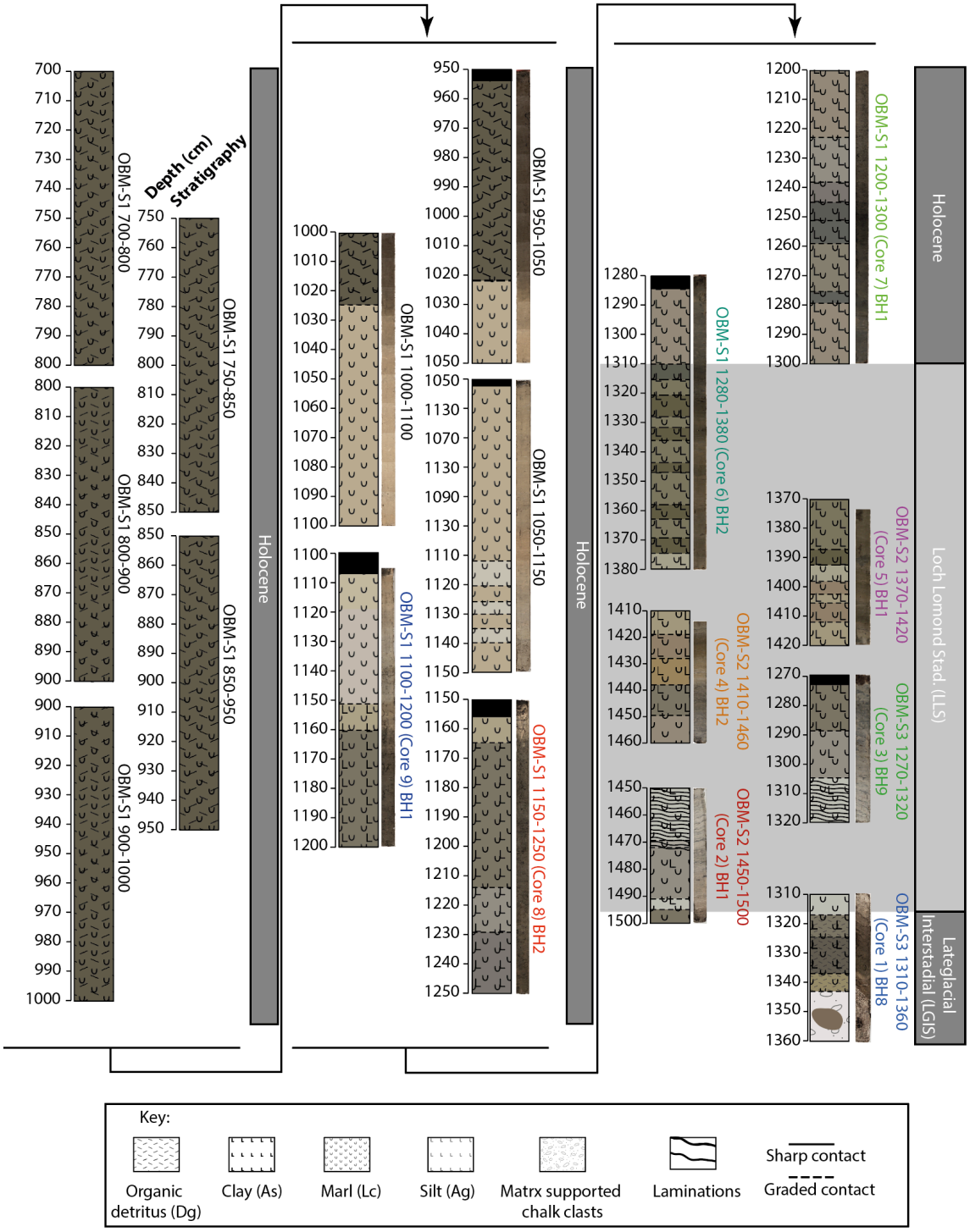

Figure 9.3, Cores forming the composite sequence, OBM19. Cores are approximately aligned by stratigraphic depth.

The sediment of OBM-L1 (1523-1508 cm) consists of chalk clasts which are granule to small pebbles in size accompanied by a matrix composed of calcareous sandy-clay giving the sediment a light grey colour. This is reflected in the physical parameters which show the sediment to be composed of 60 % $CaCO_3$ and 40 % minerogenic material (Figure 9.4). The sediments of OBM-L1 have low magnetic susceptibility with values of -0.2 to 0.7 $x10^{-5}$ SI units only. Organic material is also very sparse with TOC less than 4 %, however, a lens of organic material occurs between 1521-1517 cm and contained fragments of *Bryophytes* (moss), wood fragments and the seeds of *Betula* spp., *Cyperaceae*, *Potamogeton* and *Alnus,* along with many unidentifiable organic remains. The organic lens was not continuous throughout the core section, however, it did extend at least two thirds through the width of the core.

The sediments in OBM-L2 (1508-1482 cm) become much finer as silt becomes the main particle size. $CaCO_3$ initially increases to 80 % and the minerogenic component declines to 10 %, however, by 1493 cm $CaCO_3$ declines to 56 % while TOC and the minerogenic component increase to 14 % and 30 %, respectively.

The sediments of OBM-L3 (1482-1458 cm) are composed of silt and marl. $CaCO_3$ recovers to 80 %, the highest value observed for the composite sequence, as the minerogenic component declines to 18 % and TOC declines to less than 2 %. The sediment is grey in colour and has a mottled appearance. Magnetic susceptibility displays a small peak towards the end of the zone of 32 $x10^{-5}$ SI units.

Sediments in OBM-L4 (1458-1436 cm) display numerous rhythmic laminations alternating between layers of marl with clay and silt, which are light grey in colour, with layers composed of organic detritus, clay and fine sand. Despite the presence of organic fragments, TOC is very low, often <1 %. $CaCO_3$ is high throughout unit OBM-L4, though displays a gradual decline throughout from 77 to 68 % and minerogenic increase from 22 to 31%. Magnetic susceptibility also remains around 24 $x10^{-5}$ SI units on average, though it peaks to 32 $x10^{-5}$ SI units at 1439 cm.

In OBM-L5 (1436-1390 cm), the sediment is homogenous, and laminations no longer occur. $CaCO_3$ continues to decline to 64 % and the minerogenic component continues to increase reaching 30

%. A large peak in magnetic susceptibility occurs, reaching 56 $x10^{-5}$ SI units in the latter part of the zone. TOC increases slightly to around 2 %.

An abrupt increase in the minerogenic component occurs at the start of OBM-L6 (1390-1302 cm), initially increasing to 50%, followed by a small decline to 40 % by 1383 cm, then a gradual increase to 57 % by the end of the zone. Similarly, $CaCO_3$ shows an inverse pattern to the minerogenic component, with an initial decline to 48 %, followed by a small increase to 60 %, then a gradual decline to 38 %. TOC steadily increases from 2 to 4 % throughout. Magnetic susceptibility remains at approximately 5 $x10^{-5}$ SI units throughout.

$CaCO_3$ displays a marked increase to 65 % in OBM-L7 (1302-1260 cm) and remains relatively stable throughout the zone. The minerogenic component is around 30 % for most of the zone, and inverse to $CaCO_3$ curve. LOI shows a steady increase from 5% to 8%. Magnetic susceptibility displays a small gradually increases throughout OBM-L7 from 2 to 4 $x10^{-5}$ SI units.

In OBM-L8 (1260-1223 cm), $CaCO_3$ displays an initial decline from 64 % to 48 % but then briefly increases to 62 % at 1251 cm, coinciding with an increase in TOC to 10 %. Following this, $CaCO_3$ shows a larger decline to 32 %. $CaCO_3$ then gradually increases to 60 % and TOC decreases to 3 %. Magnetic susceptibility decreases slightly to *c.* 3.5 $x10^{-5}$ SI units.

CaCO3 continues to increase in OBM-L9 (1223-1200 cm) to *c.* 70 % and the minerogenic component decreases to *c*. 30 %. TOC remains at around 4 %. Magnetic susceptibility increases slightly to 5.3 $x10^{-5}$ SI units.

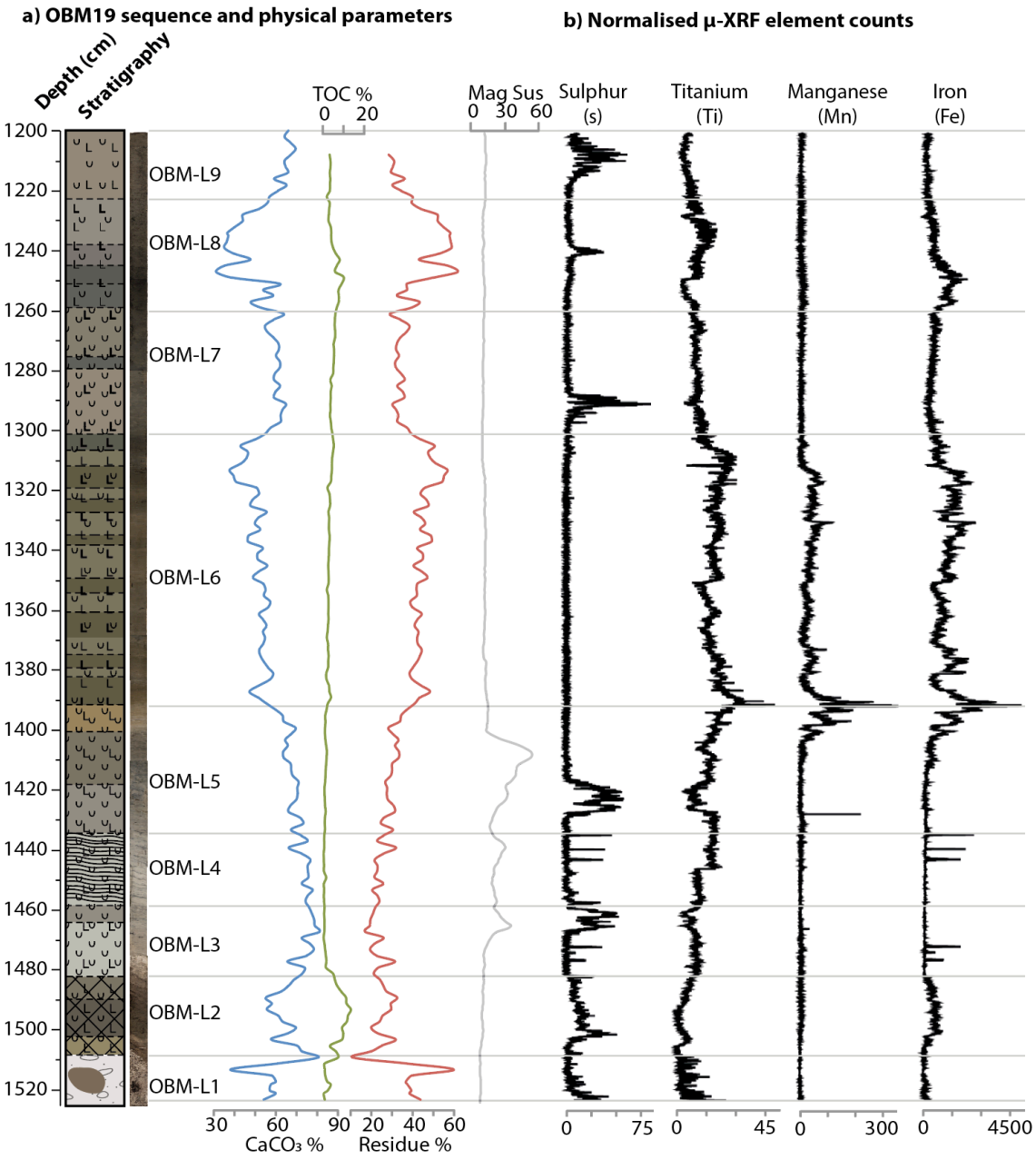

Figure 9.4, Sedimentology and stratigraphy of the OBM19 sequence. **a**) Simplified lithostratigraphy and physical parameters of the OBM19 sequence at Old Buckenham Mere showing proportions (%) of calcium carbonate ($CaCO_3$), organic (Total organic carbon; TOC) and minerogenic by difference (residue) components; **b**) normalised XRF counts for selected elements. Lithostratigraphic units are labelled OBM-Ln and colours follow the Munsell colour system.

Unit	Depth (cm)	General description	Troels-smith	Munsell colours	Geochemical stratigraphy
OBM-L9	1225-1200	Marl with silt and clay	Lc3 Ag1 As+ Dh+	5Y 4/1 dark grey	Low Ti, Mn, Fe; Peak S at 1208 cm
OBM-L8	1260-1225	Silty and clay with marl and organic detritus	Lc1 As1 Ag1 Dh1	2.5Y 3/1 very dark grey	Low High Ti, Mn; Peak S at 1243 cm; Peak Fe at 1250 cm;
OBM-L7	1302-1260	Marl with silt and some organic detritus	Lc3 As1 Dh++	5Y 5/1 grey	Low Ti, Mn, Fe; Peak S 1292 cm
OBM-L6	1396-1302	Marl with silt and clay, and organic detritus	Lc2 Ag1 As1 Dh+	5Y 4/1 dark grey	High Ti, Mn, Fe; Low S
OBM-L5	1432-1396	Marl with silt	Lc3 Ag1	5Y 5/1 grey	Low Mn, Fe but peak at end of zone; Ti increases throughout; Peak S 1430-1420 cm
OBM-L4	1473-1432	Laminations of marl with clay and silt alternating with layers of organic detritus, clay and fine sand.	Lc3 As1 Ag++ Ga+ Dh+	2.5Y 4/1 dark grey	Low Ti, Mn, Fe, S; 3 brief peaks in S and Fe in latter half
OBM-L3	1482-1473	Marl with silt and some clay	Lc3 Ag1 As+	5Y 5/1 Grey, mottled	Low Ti, Mn, Fe Peak S 1470-1460 cm 3 brief peaks in S and Fe in first half
OBM-L2	1510-1482	Silty marl with some organic detritus	Lc2 Ag2 Dh++	10YR 5/3 brown	Low Ti, Mn; Fe slightly raised S peak at 1500 cm
OBM-L1	1523-1510	Granule/small pebble sized chalk clasts, supported by a calcareous sandy-clay matrix.	Ag2 Gg1 As1 Dh+	10YR 7/1 light grey	Low S, Mn, Fe; Declining S.

Table 9.1, Lithostratigraphic units of the OBM19 sequence.

9.2 Chronology

The five radiocarbon dates attained for the OBM19 sequence are presented in Table 2. Four out of the five samples follow stratigraphic ordering with ages become increasingly older with depth. The upper most radiocarbon date (1239-1236cm) appears to be erroneously old. This could potentially be due to the inclusion of *Cyperaceae* seeds which may have been affected by hardwater error, although the low $\delta^{13}C$ value of -27.8 ‰ does not support this, or the incorporation of older material due to reworking. Radiocarbon samples at 1239-1236, 1373-1236 and 1518-1514 cm all have $\delta^{13}C$ values consistent with terrestrial plant macrofossil remains (Deines, 1980). The sample at 1504-1501 cm however has a relatively high $\delta^{13}C$ value of -18.6 ‰ and may suggest contamination from algae or lichens (Deines, 1980). However, the radiocarbon age provided by this sample is consistent with those neighbouring and has been included in the age/depth-model. It should also be noted that not enough carbon remained in sample 1492-1488cm after ^{14}C analysis to provide a $\delta^{13}C$ value.

The age-depth model was produced in OxCal v4.4.2 (Bronk Ramsey, 2008; 2009) using a *P_Sequence* function and the IntCal20 calibration curve (Reimer *et al.,* 2020). The age-depth plot is displayed in Figure 9.5. The age-model errors were calculated using the 95 % confidence interval. The resulting age model for the OBM19 sequence suggests that the sequence is slightly younger than previously thought, with only the very end of the WI present at the base of the sequence in OBM-L2. The sediments in OBM-L3 through to OBM-L6 were deposited during the LLS. Although the upper most radiocarbon date is erroneously old, the subsequent increase in $CaCO_3$ during OBM-L7 after the LLS suggests a Holocene age. Due to the erroneously old date at the top of the studied sequences, the age-depth model over-estimates the age of the sediments above 1370 cm. Therefore, the sedimentation rate in the latter half of the LLS may have been much higher than in the first half.

Table 9.2, AMS radiocarbon dates for the OBM19 sequence, normalised for isotope fractionation and calculated according to Stuiver and Polach (1977). Samples were analysed at the Keck-Carbon cycle AME facility in California.

Strat depth (cm)	Lab. Code	Material	Carbon Weight (mg)	$\delta^{13}C$ (‰)	Radiocarbon age (1 σ)	Modelled Calibrated IntCal20 age (2 σ)
1239-1236	UCIAMS-248794	Apiaceae, Cyperaceae and *Betula* seeds	0.24	-27.8	11,075 ±30	11, 861 ± 242
1373-1372	UCIAMS-248791	Twig undiff.	unknown	-29.3	10,350 ±25	12,316 ±222
1492-1488	UCIAMS-248793	*Betula* and Cyperaceae seeds. Unidentifiable leaf fragments. Charred plant remains. Undifferentiated bud	0.11	unknown	10,815 ±40	12,761 ±168
1504-1501	UCIAMS-248795	*Betula* seeds Unidentifiable leaf fragments. Charred plant remains. Undifferentiated bud	0.3	-18.6	10,960 ±25	12,898 ±392
1518-1514	UCIAMS-248792	*Betula* seeds, *Betula* female catkin scale.	0.3	-28.1	11,700±30	13,326 ±770

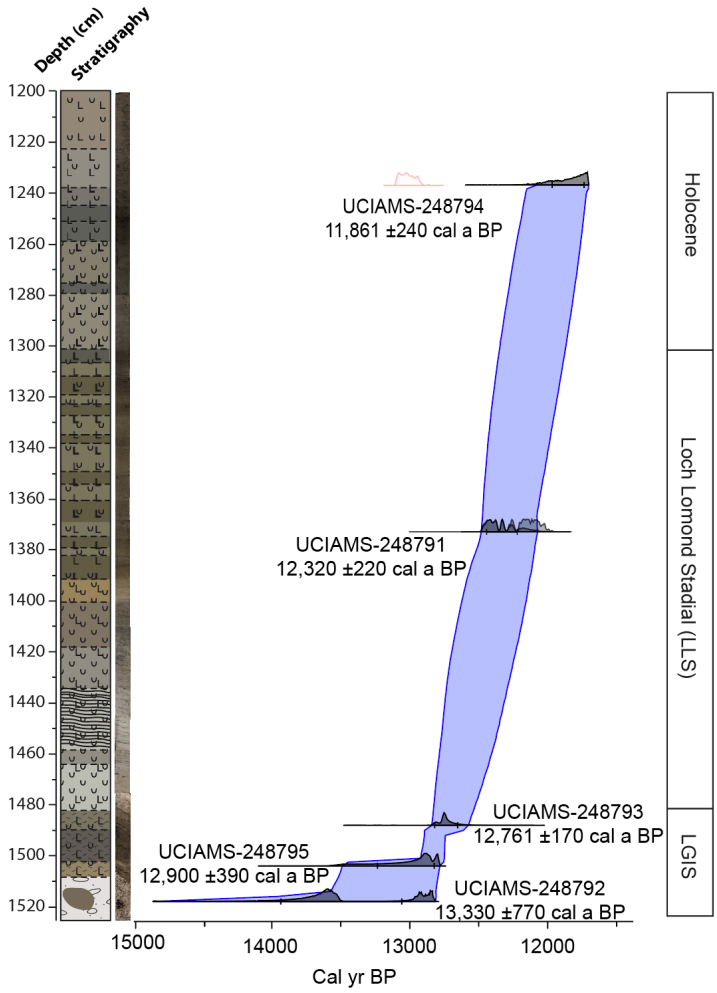

Figure 9.5, Age-depth model for Old Buckenham Mere based on 5 radiocarbon dates.

9.3 Chironomids

9.3.1 Assemblages

In total 91 different chironomid taxa were identified in the 96 samples analysed. A broken stick model identified six statistically significant assemblage zones which are denoted at OBM-C*n*. HC concentrations were generally high throughout the majority of the sequence, except in the latter half of OBM-C2 and OBM-C3 (Figure 9.5). A range of taxa which usually occur in semi-terrestrial and terrestrial settings were found throughout the OBM19 sequence including *Parametriocnemus-Paraphaenocladius*, *Psuedosmittia*, *Psuedorthocladius*, *Limnophyes*, *Metriocnemus eurynotus*-type and *fuscipes*-type and *Smittia,* all of which are summarised in the "(semi-)terrestrial" curve in Figure 9.5. The main changes in assemblage composition will now be described for each chironomid zone.

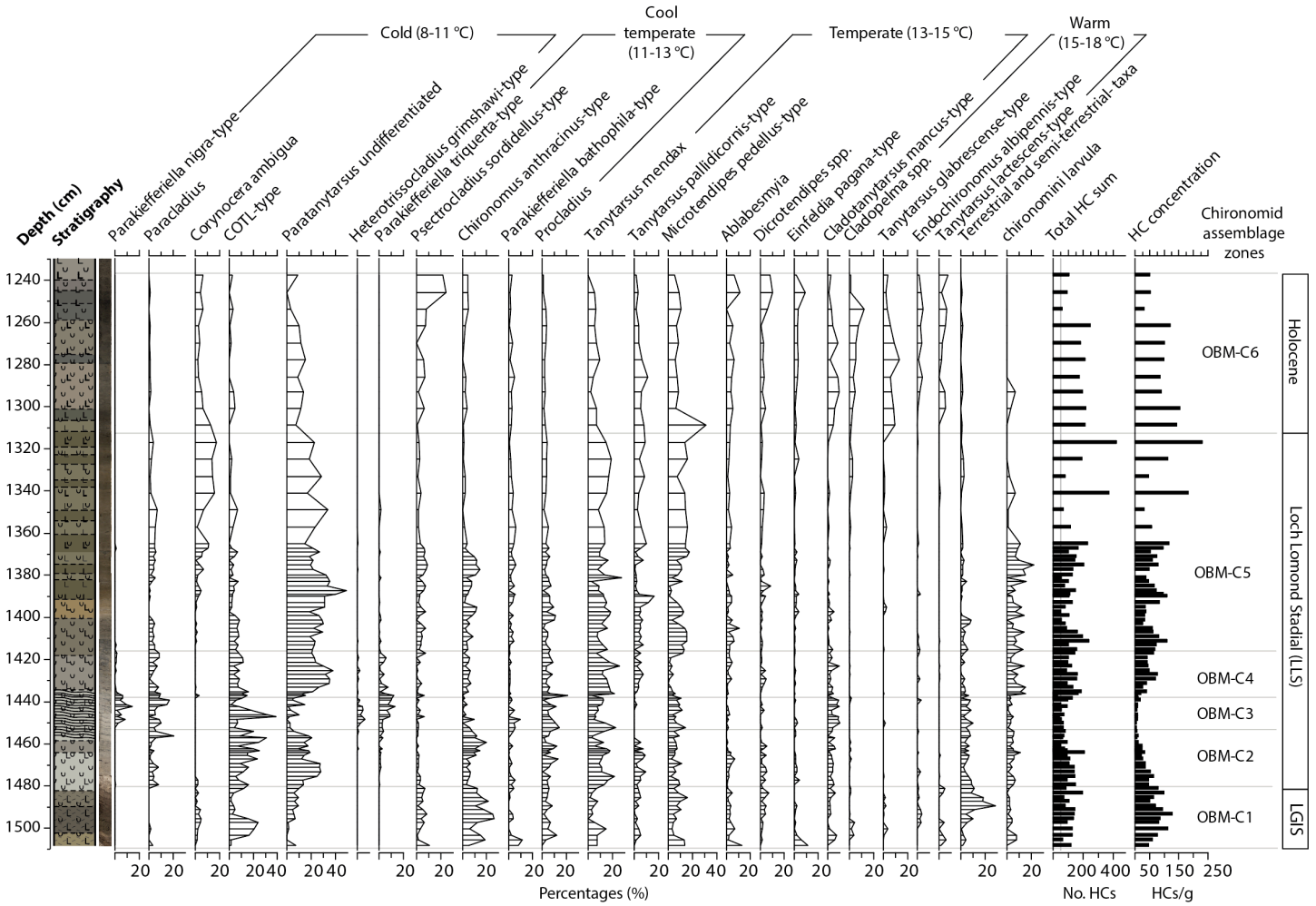

Figure 9.6, Percentage abundance diagram of selected chironomid taxa present in the OBM19 sequence presented alongside the sediment stratigraphy on the left. Chironomid assemblage zones (OBM-Cn) are marked on the right. Taxa are arranged by their T_{Jul} optima in the modern calibration dataset (Heiri *et al.,* 2011) calculated using a Weighted-Averaging model. Taxa with coolest optima are on the left and warmest on the right. HC concentrations (HCs/gram) and total HC counts are displayed on the right.

OBM-C1: composite depth 1509-1480 cm

The most abundant taxa in OBM-C1 are *COTL*-type and *Chironomus anthracinus*-type, forming up to 25 % of the chironomid assemblages. *COTL*-type peaks in the first half of the zone, though it decreases to only a few percent in the latter half. In the latter half of OBM-C1, *C. anthracinus*-type, *Paratanytarsus* undifferentiated and (semi-)terrestrial taxa increase to 26, 9 and 28 %, respectively. A number of other taxa are consistently present in low abundance of 1-10 % including *P. sordidellus*-type, *Procladius, T. mendax*-type, *M. pedellus*-type, *Ablabesmyia* and *Cladopelma* spp.

OBM-C2: composite depth 1480-1453 cm

COTL-type, *Paratanytarsus* undifferentiated and *Tanytarsus mendax*-type all increase (to 31, 28 and 22 %, respectively) and are the most abundant taxa in OBM-C2. *Paracladius* appears at the start of the zone and is consistently present at 4 %. (semi-)terrestrial taxa are also continuously present at *c.* 6 % throughout. HC concentrations decline throughout the zone from 48 HCs/gram to just 8 HCs/gram.

OBM-C3: composite depth 1453-1437 cm

Paratanytarsus undifferentiated and *COTL*-type both decline to 6 %, though *COTL*-type displays a peak in the centre of the zone to 32 %. *C. anthracinus*-type also declines to 2 %. *Parakiefferiella nigra*-type, *Heterotrissocladius grimshawi*-type and *Parakiefferiella triquetra*-type, which were either absent or present in only very low abundances in the previous zone, increase to 14, 13 and 7 %, respectively. (Semi-)terrestrial taxa declines to *c*. 7 %. HC concentrations are very low throughout the zone, on average 10 HCs/gram.

OBM-C4: composite depth 1437-1416 cm

Paratanytarsus undifferentiated once again increases and becomes the abundant taxon, increasing to 38 %. *T. mendax*-type, *COTL*-type and *C. anthracinus*-type also increases to 16, 9 and 4 %, respectively. *P. nigra*-type, *H. grimshawi*-type and *P. triquetra*-type all decline to less than 5 %. *M. pedellus*-type also declines to 2 %. (semi-)terrestrial taxa declines to less than 3 %. There is a marked increase in the number of Chironomini larvula HCs from an average of 3 per sample in the previous zone to 9 per sample in OBM-C4. HC concentrations increase to an average of 50 HCs/gram.

OBM-C5: composite depth 1416-1305 cm

Paratanytarsus and *T. mendax*-type continue to be the most abundant taxa and on average comprise 26 % and 13 % of the assemblages, respectively. Both *C. anthracinus*-type and *P. sordidellus*-type display high abundance in the first half of OBM-C5, up to 15 and 8 % respectively, but form less than 4 % of the assemblages in the latter half of the zone. *C. ambigua* displays the opposite trend with abundances rarely exceeding 4 % in the first half of OBM-C5 but increases to 18 % in the latter half. *COTL*-type declines throughout from 8 % to 2 %. (Semi-)terrestrial taxa are only present at 1-2 % apart from 1404-1400 cm where they form 8 % of the assemblages. On average 10 Chironomini larvula HCs/sample are present in the first half of the zone but largely disappear in the latter half of the zone. HC concentrations are 75 HC/gram on average, though samples late in the zone display abundances as high as 233 HCs/gram.

OBM-C6: composite depth 1305-1237 cm

Several taxa continue their presence in similar abundance to the previous zone including *COTL*-type, *C. anthracinus*-type, *P. bathophila*-type, *Procladius, E. pagana*-type, comprising 2-3 % of the assemblages. *Paratanytarsus, T. mendax*-type and *C. ambigua* decline to 9, 5 and 4 % of the assemblages respectively. *Ablabesmyia, C. mancus*-type, *Dicrotendipes* and *P. sordidellus*-type increase to approximately 5 % of the assemblages. *E. albipennis*-type, T. *pallidicornis*-type and *T. lactescens*-type were all largely absent in the previous zone but increase in OBM-C6 to between 3 and 5 %.

9.3.2 Chironomid temperature inference

The chironomid inferred mean July air temperature record (T_{Jul}) from Old Buckenham Mere is presented in Figure 9.7a. During OBM-C1, T_{Jul} values are generally around 13 °C but momentarily increase to 14.5 °C at the end of the zone. The sample specific errors range from 1.4 to 1.5 °C, both in zone OBM-C1 as well as throughout the remainder of the record. T_{Jul} then displays a marked fall in OBM-C2 to *c.* 11.4 °C and continues at around 11.2 °C in OBM-C3. T_{Jul} displays a large increase at the start of OBM-C4 to 13 °C, but then sharply declines to 10.2 °C at 1425 cm, a magnitude of 2.8 °C. T_{Jul} recovers to 12.8 °C at the start of CM-C5. During OBM-C5 several declines in T_{Jul} occur. The first of which is between 1411-1393 cm with T_{Jul} exhibiting a decline to 10.9 °C, a magnitude of 1.9 °C, before recovering to 13.1 °C. Another larger decline follows with T_{Jul} falling to 9.8 °C at

1381 cm, a fall of 3.3 °C. The remainder of OBM-C5 displays a trend to warmer T_{Jul} values of 12.8 °C by the end of the zone. T_{Jul} continues to increase into OBM-C6, reaching 15.5 °C at 1270 cm.

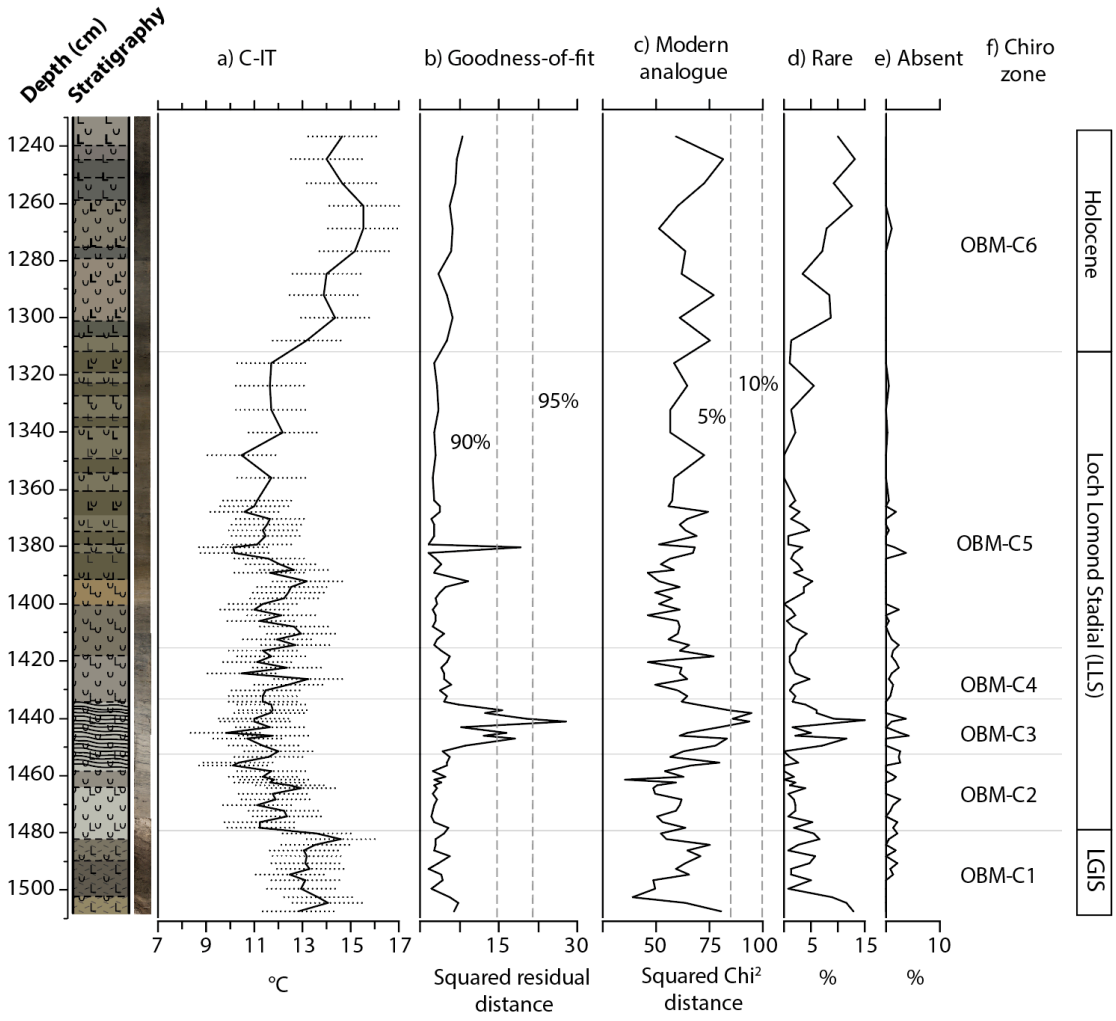

Figure 9.7, Chironomid numerical data presented alongside the lithostratigraphy of OBM19 on the left and broad time periods on the right. **a**) Chironomid-inferred mean July air temperature estimates (T_{Jul}) with sample specific error bars; **b**) Goodness-of-fit of the fossil assemblages to temperature, with dashed lines representing the 90th and 95th percentile of squared residual distance of modern samples to the first axis of a CCA; **c**) Nearest modern analogue with dashed lines showing the 5th and 10th percentile of the Chi^2 distances of all samples in the modern calibration dataset; **d**) Abundance of fossil taxa present in the down core record which are rare in the modern calibration dataset, defined by Hill's N2 <5; **e**) Fossil taxa not present in the modern calibration dataset; **f**) Chironomid assemblage zones from Figure 9.3.

The majority of chironomid samples have a good fit-to-temperature (Figure 9.6b). Out of the 91 chironomid samples analysed only one had a "very poor" fit to temperature (1442 cm) and five had a "poor" fit-to-temperature (1448, 1446, 1441, 1438 and 1381 cm). All of these, except for the

sample at 1381 cm occurred in OBM-C3. The fossil chironomid assemblages also compare well to assemblages in the modern calibration dataset (Figure 9.6c) with only three samples having a "poor" fit-to-temperature (1442, 1441 and 1439 cm), all of which are in OBM-C3. Taxa which are considered rare in the modern calibration data set (i.e. Hills N2 <5) generally occur in low abundances (<5 %) in OBM-C2, -C4 and C5. However, the abundance of rare taxa reaches higher percentages at the very start of OBM-C1 (13 %), throughout OBM-C3 (11 %) and OBM-C6 (13 %). The most abundant "Rare taxa" present in the sequence are *Einfeldia pagana*-type in OBM-C1 and OBM-C6, and *Parakiefferiella nigra*-type in OBM-C3. *Tanytarsus lactescens*-type, *Nanocladius rectinervis*-type, *Metriocnemus eurynotus*-type and *Metriocnemus fuscipes*-type also contribute in small abundances. The abundance of taxa absent in the modern calibration dataset does not exceed 4.2 % and include *Constempellina-Thienemanniola*, *Metriocnemus terrester*-type, *Propsilocerus lacustris*-type and *Trissocladius*.

9.4 Stable Isotopes

The isotope record for the OBM19 sequence is presented in Figure 9.8a and has been split into four isotopic zones, denoted as OBM-On. When comparing $\delta^{18}O$ and $\delta^{13}C$ for the sequence as a whole, there is no covariance (r^2 = 0.0038) (Figure 9.8b), however, when $\delta^{18}O$ and $\delta^{13}C$ are compared for each isotopic zone the degree of co-variance is highly variable (Figure 9.8c).

OBM-O1: composite depth 1509-1468 cm

Both $\delta^{18}O$ and $\delta^{13}C$ exhibit large shifts in isotopic values from -2.3 ‰ to -6.7 ‰ and 2 ‰ to -2.9 ‰, respectively. Both recover by the end of the zone. Co-variance between $\delta^{18}O$ and $\delta^{13}C$ for this zone is very high with an r^2 of 0.96.

OBM-O2: composite depth 1468-1438 cm

Throughout OBM-O2, $\delta^{18}O$ and $\delta^{13}C$ are relatively flat at 2.3 ‰ and -2.4 ‰, respectively, with only some minor variability in $\delta^{18}O$ in the order of 0.3 ‰. Co-variance between $\delta^{18}O$ and $\delta^{13}C$ for this zone is slightly lower than previous, with an r^2 of 0.56.

OBM-O3: composite depth 1438-1394 cm

During OBM-O3, two oscillations in $\delta^{18}O$ occur to more negative values while $\delta^{13}C$ values remain constant at around 2.4 ‰. Between 1438-1416 cm, $\delta^{18}O$ declines to -3.4 ‰, a decline of 1 ‰,

before partially recovering to -2.7 ‰. Another decline subsequently occurs between 1416-1394 cm, with $\delta^{18}O$ declining 1.3 ‰ from -2.7 ‰ to -4 ‰, followed by an increase to -2.5 ‰. When regression analysis is conducted on the whole of OBM-O3 it shows an r^2 value of 0.35.

OBM-O4: composite depth 1394-1324 cm

This unit sees a large decline in $\delta^{18}O$ from -2.5 ‰ in OBM-O3, to -4.9 ‰, a decrease of 2.4 ‰. Throughout OBM-O4 there is a slightly increasing trend of around 0.5 ‰ in $\delta^{18}O$, though there are several oscillations on this trend with some variations up to 1 ‰. $\delta^{13}C$ displays most variability during OBM-O4, with variations in the order of 0.5 ‰. A large increase in $\delta^{18}O$ values should be noted near the start of OBM-O4 with values increasing from -5.6 to -3.1 ‰ at 1381 cm but then declining back to -5.3‰ by 1375 cm. A small peak in $\delta^{13}C$ of 3‰ occurs at 1377 cm. There is no co-variance between $\delta^{13}C$ and $\delta^{18}O$ within zone OBM-O4.

9.5 Pollen

Preliminary pollen analysis was undertaken for the OBM19 sequence by Manvinder Dari for her undergraduate dissertation with results presented in Figure 9.9. The pollen assemblage diagram has not been zoned due to low count sums, i.e., 150 pollen grains per sample), and numerous identifications have not yet been checked. However, the broad changes in abundance should still stand, particularly for the most abundant taxa which are easily distinguishable, e.g., *Betula, Pinus, Cyperaceae.* Some key things to note in the pollen assemblages are: 1) the high abundance of *Cyperaceae* throughout the entire OBM19 sequence; 2) the increase in *Betula* between 1410 and 1340 cm to approximately 40 % from a previous abundance of 5 %; 3) the high abundance of *Pediastrum* between 1390 and 1260 cm.

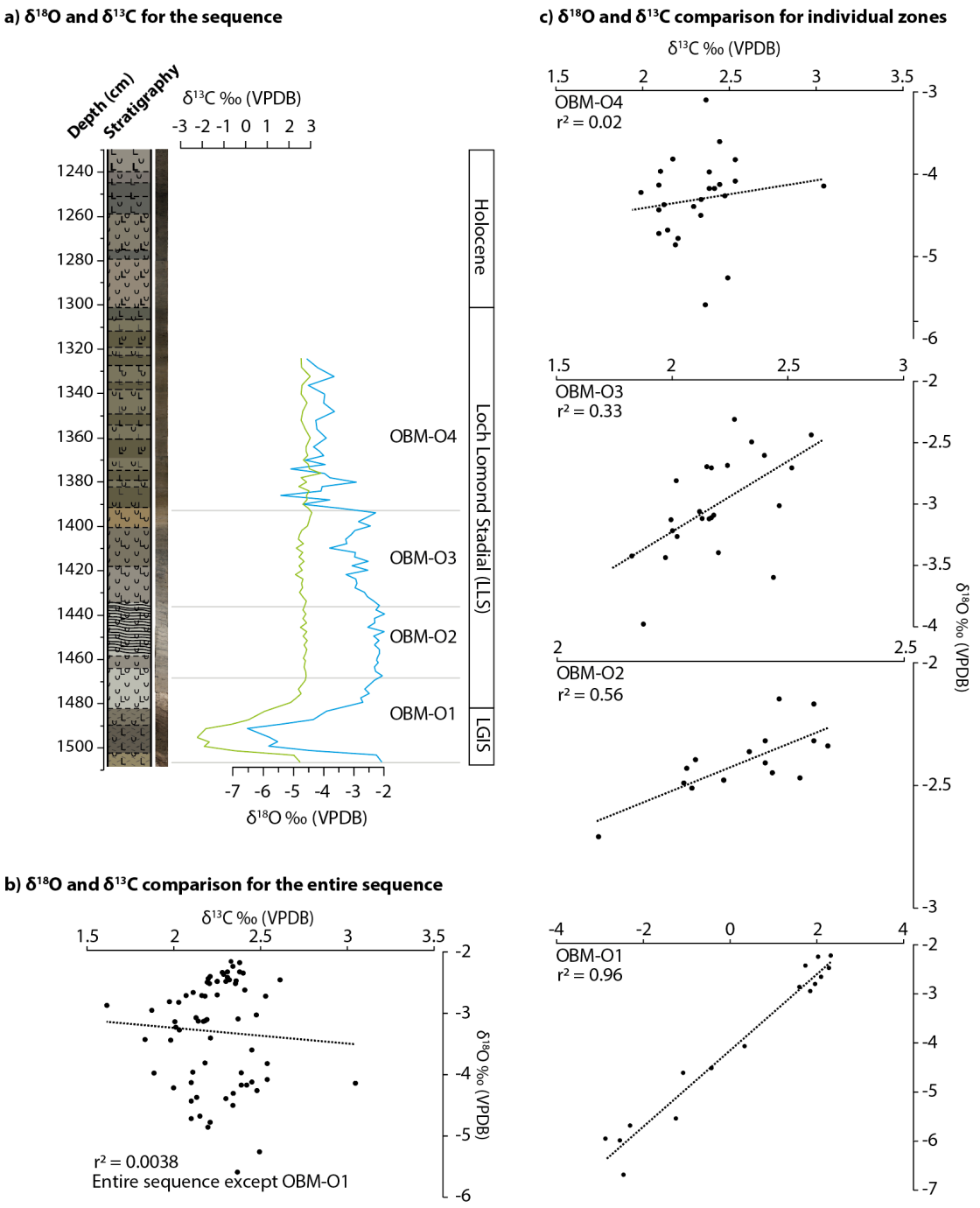

Figure 9.8, Stable isotope data for Old Buckenham Mere presented alongside the lithostratigraphy of OBM19 on the left and broad time periods on the right. **a**) Stable isotope data for the OBM19 sequence with zones denoted as LL-On. $\delta^{18}O$ is represented by the blue line and $\delta^{13}C$ by the green line; **b**) Comparison of $\delta^{18}O$ and $\delta^{13}C$ values for the entire sequence except OBM-O1; **c**) Comparison of $\delta^{18}O$ and $\delta^{13}C$ values for each isotopic zone

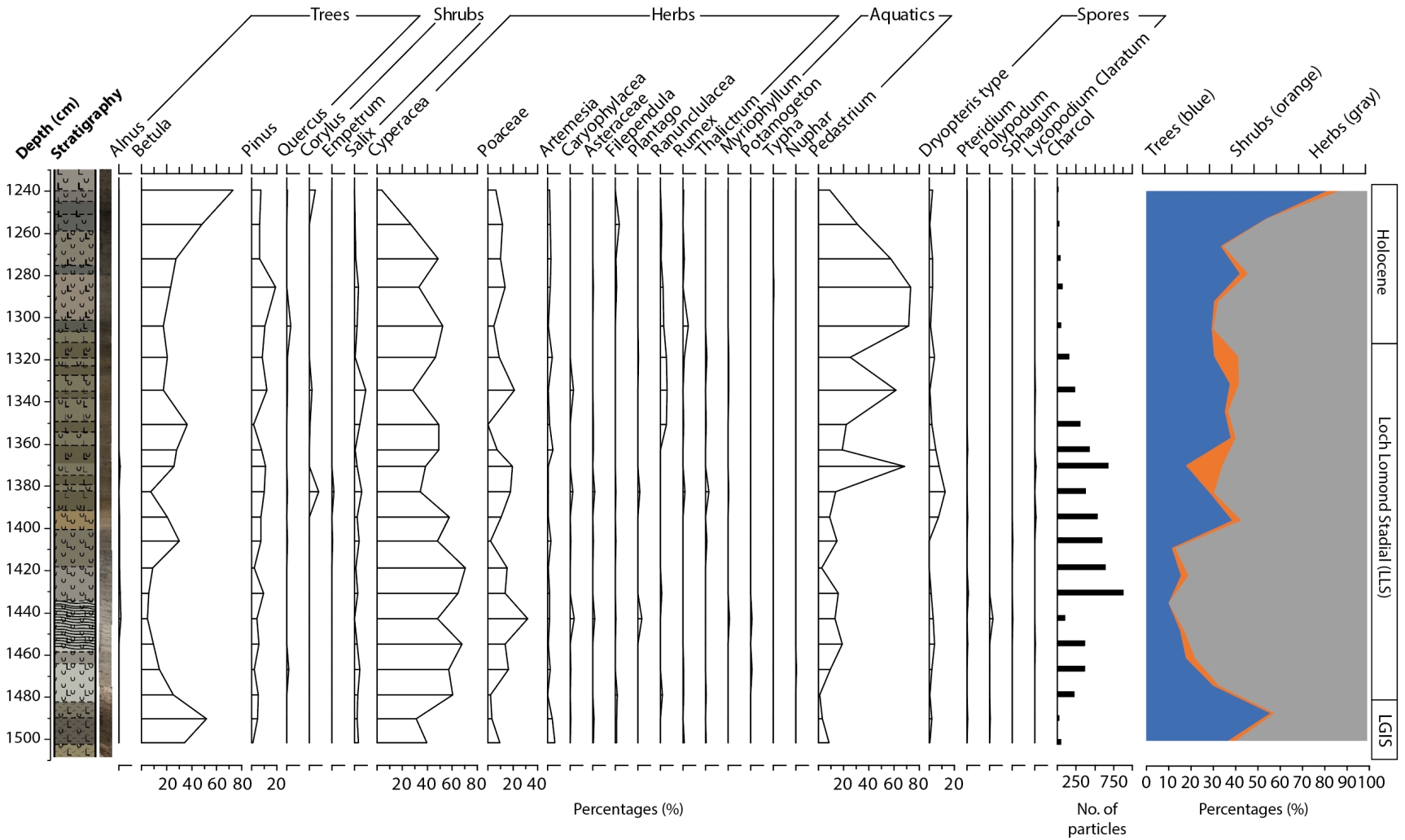

Figure 9.9, Pollen assemblage data for the OBM19 sequence.

9.6 Palaeoenvironmental and palaeoclimatic interpretation

This section will explore the environmental and climatic history of Old Buckenham Mere using the proxy data presented within this chapter. The sequence will be interpreted in chronological order and a summary is given in figure 9.10. The radiocarbon chronology of the sequence shows very clearly that rather than representing a full LGIT sequence, OBM records the transition from the end of the Windermere Interstadial onwards, through the Loch Lomond Stadial and into the Early Holocene. Although this means that much of the data generated here is outside of the scope of the project, the fact that so few records of this time period exist in this region of Britain means that its significance is discussed below.

A range of environmental variables which have an influence of chironomid assemblages. For each time interval the main driver(s) of assemblage change will be considered and the reliability of the T_{Jul} reconstruction will be discussed. Such factors include 1) summer air temperatures, 2) lake trophic status, 3) aquatic macrophyte presence/abundance/type, 4) lake water oxygenation, and 5) substrate texture and turbidity. In contrast to Llangorse and Crudale Meadow, lake depth does appear to have changed at Old Buckenham Mere during the Lateglacial which seems to have influenced the chironomid assemblages and will be discussed in the following subsections where appropriate.

Palaeoenvironmental significance of the oxygen isotope record

Many $\delta^{18}O$ records covering the Lateglacial Interstadial in the British Isles are often interpreted as being a function of prevailing air temperature. This is due to the temperature fractionation effect during precipitation formation outlined in Chapter 4 and that there is often close correspondence between chironomid derived T_{Jul} estimates and $\delta^{18}O$ values (i.e., van Asch *et al.,* 2013; Abrook *et al.,* 2020; Blockley *et al.,* 2018). However, $CaCO_3$ is rarely precipitated during the LLS in the British Isles as temperatures are often too cold. Only Hawes Water (Marshall *et al.,* 2002) and Loch Inchiquin (Diefendorf *et al.,* 2006) precipitated $CaCO_3$ during the LLS and so there are very few $\delta^{18}O$ records to compare with T_{Jul} estimates. A further complicating matter is that there is a disparity in the trends observed in T_{Jul} during the LLS with some displaying a colder latter half (e.g., Loch Ashik; Brooks *et al.,* 2012), a warmer latter half (Abernethy Forest; Brooks *et al.,* 2012) or flat temperature trend through put the LLS (e.g., Muir Park Reservoir; Brooks *et al.,* 2016). These discrepancies could reflect the spatial variations in climate during the LLS. For OBM at least, there is no correlation

between $\delta^{18}O$ and T_{Jul} (r^2 = 0.02). When considering explanations-other-than-temperature for changes in $\delta^{18}O$ it is important to note that during the end of the WI and early LLS at Old Buckenham Mere there is a moderate to strong degree of co-variance between $\delta^{18}O$ and $\delta^{13}C$ values. Isotopic co-variance is most common in lake carbonates because of either detrital contamination from reworked limestone or evaporative modification of the lake waters. Detrital contamination is not thought to be an issue at OBM as the surrounding calcareous rich tills are heavily weathered and so the stable isotopes are unlikely to retain their chemical bonds from their geological past. Therefore, it is likely that the changes in the $\delta^{18}O$ record at Old Buckenham Mere are a combination of evaporitic enrichment of the lake water and changes in MAT. The variable degree of co-variance and unique trends observed in the $\delta^{18}O$ record at OBM make the interpretation of the $\delta^{18}O$ signal difficult and so several explanations are explored below for each time interval.

9.6.1 End of LGIS: *(c. 13,500 ±880 – 12,700 ±180 cal a BP) (composite depth 1524-1482 cm)* OBM-L1; OBM-L2; OBM-C1; OBM-O1

The lower most sediment unit of the OBM19 sequence (OBM-L1; 1524-1510 cm) consists of chalk clasts, granule to small pebble in size, supported by a calcareous sandy-silt matrix. The lithological composition and bimodal nature of the deposit suggests the sediment is reworked from the carbonaceous-rich Lowestoft and Happisburgh glaciogenic formations, which surround and underly the site (See section 6.3.2). The relatively poorly sorted nature of the sediments also suggests they were deposited by mass movement processes. Although the sediments in OBM-L1 are largely devoid of organic material, there is a lens of well-preserved organic remains between 1521-1517 cm. This organic lens was not continuous throughout the sample depth and appeared 'out of place' with the surrounding sediment. It also contained an abundance of terrestrial plant macrofossils including, wood, twigs, moss and seeds of *Cyperaceae, Potamogeton, Alnus* and *Betula*. When the *Betula* seeds were radiocarbon dated, they produced a calibrated radiocarbon age of 13,330 ±770 cal a BP. This suggests that a water body which could support Cyperaceae and *Potamogeton*, surrounded by *Betula* and *Alnus* were present. It is therefore thought that the organic lens was not formed in situ and was instead transported from the littoral of a water body.

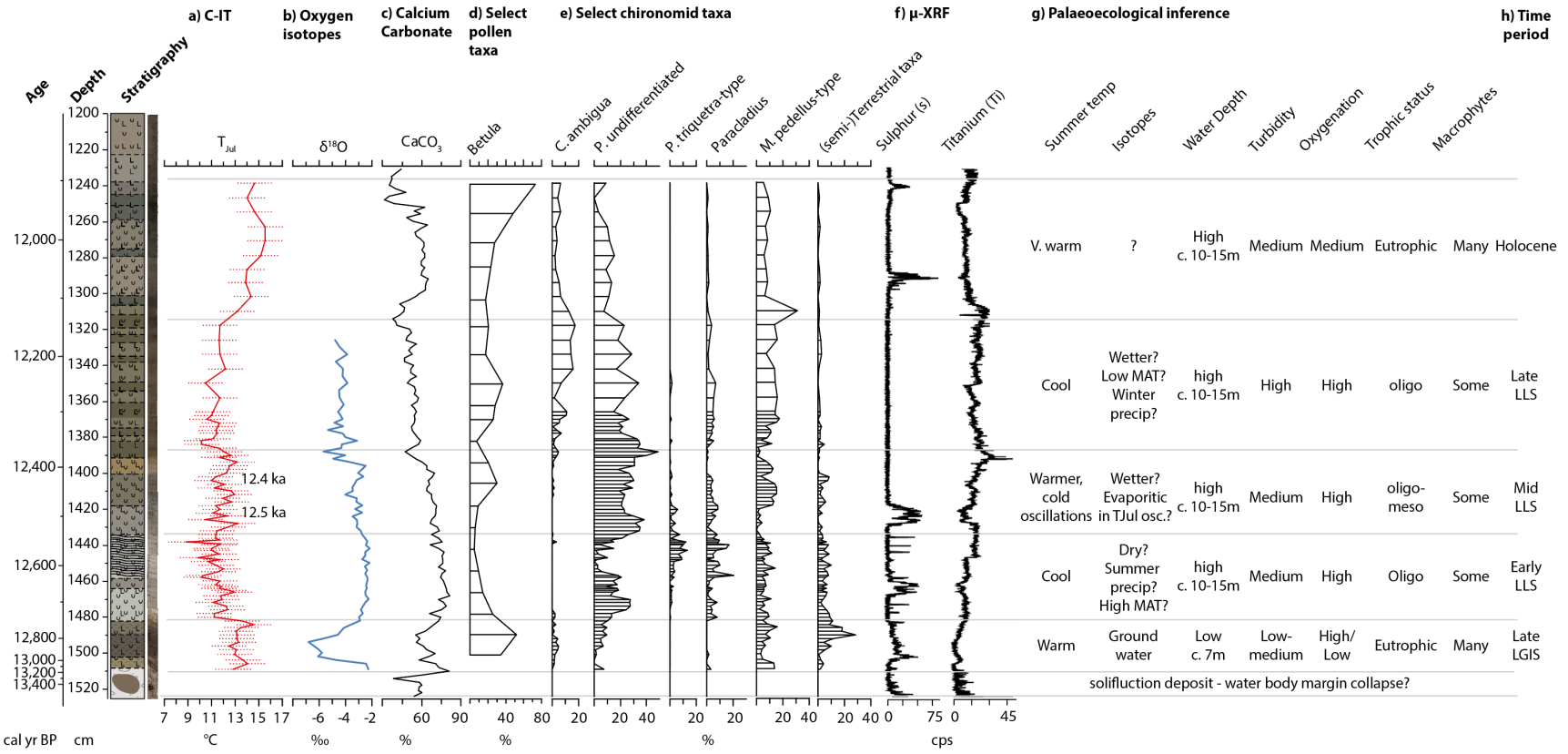

Figure 9.10, Summary figure of data from Old Buckenham Mere presented alongside the lithostratigraphy and ages of the OBM19 on the left. **a**) Chironomid-inferred mean July air temperatures (T_{Jul}); **b**) Oxygen isotopes; **c**) Calcium carbonate; **d**) select pollen taxa; **e**) percentage abundance of selected chironomid taxa; **f**) µ-XRF; **g**) palaeoecological inferences based on the chironomid assemblages; **h**) broad time period.

Between 13,100 ±480 and 12,700 ±180 cal a BP, the chironomid assemblages are largely composed of cool-temperate and temperate indicating taxa e.g., *C. anthracinus*-type, *T. mendax*-type and *M. pedellus*-type, producing T_{Jul} estimates of *c.* 13 °C, although T_{Jul} does reach 14.5 °C at the very end of the WI. All chironomid samples have a 'good' fit-to-temperature and good analogue in the modern calibration dataset. The basal sample at 1508 cm has a high percentage of rare taxa, up to 13 %, due to the presence of *E. pagana*-type, however, the temperature optima of this taxon is 13.7 °C in the modern calibration dataset is also broadly consistent with the other taxa present.

The majority of other chironomid taxa present in OBM-C1 live amongst macrophytes in the littoral of well-oxygenated meso-eutrophic lakes e.g., *Cladopelma* (Walker *et al.,* 1991; Saether, 1979; Brodin 1986), *E. albipennis*-type (Pinder and Reiss 1983; Brodin 1986), *T. lactescens*-type (Brooks *et al.,* 2007) and T. *glabrescens*-type (Brodin, 1986). In contrast there are relativly few profundal dwelling taxa, except for *COTL*-type which usually occurs in the profundal of cold oligotrophic lakes (Brundin 1956; Brodin 1986). However, *COTL*-type can also live in the profundal of warm eutrophic lakes *c.* 7 m deep (cf. Engels and Cwynar, 2011). The assemblages also have a high abundance (up to 24 %) of chironomid genera which contain species that mainly live in (semi-)terrestrial settings e.g., *Parametriocnemus-Paraphaenocladius* (Cranston *et al.,* 1983; Moog, 1995), *Psuedosmittia* (Cranston *et al.,* 1983; Strenzke, 1950), *Pseudorthocladius* (Strenzke, 1950; Saether and Sublte, 1983), Limnophyes (Kansanen, 1985), *M. eurynotus*-type and *M. fuscipes*-type (Cranston *et al.,* 1982; Brodin 1986) and *Smittia* (Cranston *et al.,* 1983). The high abundance of littoral and (semi-)terrestrial dwelling taxa, as well as the presence of the profundal dwelling *COTL*-type suggests a water body which is moderately deep (*c.* 7 m) but has a relatively large littoral area compared to the volume of the water body. It is possible that the water level was high enough to fill the deeper central portion of the basin (Figure 9.2), and spill onto the ledges producing a large littoral area.

The stable isotope records exhibit strongly negative values, -7 ‰ for δ^{18}Oand -3 ‰ in δ^{13}C, which also display a high degree of co-variances ($r^2 = 0.96$). Such strong negative values in δ^{18}O and δ^{13}C are greater than those seen in many lacustrine isotope records from the LGIT in Britain (e.g., Fiddaun, Hawes Water, Loch Inchiquin; Van Asch *et al.,* 2012; Marshal *et al.,* 2002; Diefendorf *et al.,* 2006) and are more commonly seen in riverine carbonate deposits (Andrews, 2006) or small-medium sized closed-basin lake systems (Leng and Marshall, 2004). The current mere and streams at Old Buckenham Mere are largely fed by underground springs (see section 6.3) due to the limited extent of the headwater and shallow nature of the valleys. Springs may have also fed the palaeo water body at Old Buckenham Mere and may explain the strong negatively δ^{13}C values. A large through flow of water, constantly

replenishing the water body with water from the aquifer, enriched in $^{12}CO_2$, would have a more negative $\delta^{13}C$ value (Andrews, 2006). Constant replenishment from the aquifer would also mean there is less time for $^{12}CO_2$ to be preferentially degassed as the water body has less time to equilibrate with the atmosphere, which would result in a shift to more positive $\delta^{13}C$ values (Andrews, 2006). If the water is largely sourced from the underlying aquifer, then the $\delta^{18}O$ values are likely to reflect the $\delta^{18}O$ of groundwater and not the prevailing climate. $\delta^{18}O$ values of -7 ‰ is broadly in line with the modern $\delta^{18}O$ of groundwater for east Anglia (Darling *et al.,* 2003)

9.6.2 Early-LLS: *12,700 ±180 -12,550 ±220 cal a BP (Composite depth 1482-1437 cm)* OBM-L3 & -L4; OBM-C2 & -C3; OBM-O2

During the early LLS, 12,700 ±180 -12,550 ±220 cal a BP, T_{Jul} becomes noticeably cooler with values falling by *c.* 3.1 °C to *c*. 11.4 °C as temperate and warm indicating taxa (e.g., *T. pallidicornis*-type, *T. lactescens*-type) become largely absent while cold and cool-temperate indicating taxa (e.g., *Paracladius, P. triquetra*-type) increase to their highest abundance of the sequence. Chironomid samples in OBM-C2 have a 'good' fit-to-temperature, however, most samples in OBM-C3 display a 'poor' or 'very poor' fit-to-temperature suggesting environmental variables other than temperature may be affecting the chironomid assemblages.

The appearance of *Paracladius* and the increase in COTL-type in OBM-C2, which are typical of oligotrophic conditions (Moller Pillot, 2013) suggests the lake trophic status changes from meso-eutrophic to more oligotrophic conditions. In OBM-C3, there is however a change in the composition of oligotrophic indicating taxa as COTL-type declines while other oligotrophic indicating taxa increase including *P. nigra*-type (Walker *et al.,* 1992), *P. triquetra*-type and *H. grimshawi*-type (Brooks *et al.,* 2007), coinciding with the occurrence of fine laminations in the stratigraphy. The processes forming such fine laminations are uncertain. Anoxic conditions are not thought to be a contributing factor as taxa which require well-oxygenated conditions increase, e.g., *H. grimshawi*-type; *Paracladius* (Moller Pillot, 2013). One possibility may be that the laminations are produced by nival snow melt (e.g., Cockburn and lameroux, 2007). The presence of *P. nigra*-type may tentatively lend weight to the nival snow melt argument as it occurs in cold barren arctic/alpine oligotrophic lakes (Walker, *et al.,* 1992). Thin section analysis is however required to identify the nature of these sediments with more certainty. *P. nigra*-type is also rare in the combined Nor-swiss calibration dataset, causing the percentage of 'rare' taxa to increase to 15 % and may in part cause the fit-to-temperature statistics for OBM-C3 to display 'poor' and 'very poor' values. Inwash of cold glacial meltwater has been inferred to be the cause of poor

fit-to-temperature statistics (e.g., Brooks *et al.,* 2012) and cold water from snowpack melt could have a similar effect.

$\delta^{13}C$ values during the early LLS are consistently between 2.1 and 2.4 ‰, within the typical range of lacustrine systems (-3 ‰ to +3 ‰) (Talbot, 1990). This suggests that water levels increase and now form a relatively large body of water with a residence time long enough for $^{12}CO_2$ to equilibrate with the atmosphere (Leng and Marshall, 2004; Candy *et al.,* 2016). The unstable nature of the surrounding tills may have resulted in the outflow becoming blocked, causing lake levels to rise. The consistency in $\delta^{13}C$ values during OBM-O2 suggests there is little change in the size of the water body during the LLS and the balance of inflow/outflow remained stable. Increased water depth is also indicated by the chironomid assemblages which display a greater proportion of profundal dwelling taxa compared to littoral dwelling taxa. *Paracladius* is the first such taxon to appear which is exclusively a profundal taxon (Brooks *et al.,* 2007). (Semi-)terrestrial dwelling taxa display a marked decline to 2 % and some littoral dwelling taxa also virtually disappear e.g., *T. lactescens*-type, *E. albipennis*-type; *P. sordidellus*-type (Brooks *et al.,* 2007). This could be due to the decline in summer temperatures as littoral and semi-(terrestrial) taxa generally have higher temperature optima but could also be caused by an increase in lake level, concurring with the isotope interpretation. An increase in lake level may also explain the high degree of co-variance between $\delta^{13}C$ and $\delta^{18}O$ ($r^2 = 0.56$) as an increase in lake depth would result in an increase in the residence time of lake water which could therefore be modified by evaporitic processes under an arid climate (Leng and Marshall, 2004). T_{Jul} values suggests lake waters are warm enough for authigenic $CaCO_3$ to precipitate and if any detrital contamination did occur the effect on the isotopic signal would be minimal as it would be diluted by the high percentage of authigenic $CaCO_3$.

9.6.3 Mid-LLS: *12,550 ±220 – 12,370 ±230 cal a BP (composite depth: 1437-1386 cm)* OBM-L5; OBM-C4 & -C5a; OBM-O3

During the mid-LLS T_{Jul} increases slightly by 1.6 °C to *c.* 13 °C largely due to an overall decline in the coldest indicating taxa (e.g., *P. nigra*-type and *Paracladius*). Another cold-indicating taxon with a higher temperature optimum than the aforementioned taxa, *Paratanytarsus*, increases along with temperate indicating taxa, *M. pedellus*-type and *Ablabesmyia* and cool temperate indicating taxon *P. sordidellus*-type. Two oscillations to cooler temperatures occur, with minimum T_{Jul} values at 12,500 ±220 cal a BP (1425 cm) (10.2 °C) and 12,420 ±240 cal a BP (1403 cm) (10.9 °C), declines of 2.9 °C and 1.9 °C, respectively, and are largely caused by small increase in the cold indicating taxon *Paracladius* accompanied by declines in *Paratanytarsus* and the temperate indicating taxon *M. pedellus*-type. *Paratanytarsus* undifferentiated remains at reduced abundance during the warm interlude separating the two cold oscillations when the temperate indicating taxon *M. pedellus*-type increases along with (semi-)terrestrial taxa, the latter of which generally has a high temperature optimum.

$\delta^{13}C$ values continue to be stable at *c.* 2 ‰ suggesting the size of the lake remains largely unchanged from the early LLS. In contrast, $\delta^{18}O$ values display oscillations with a magnitude of *c*. 2 ‰ with less negative values occurring during the T_{Jul} declines. During OBM-C3 co-variance between $\delta^{18}O$ and $\delta^{13}C$ is low with an r^2 value of 0.3, suggesting evaporitic enrichment of the lake waters and detrital contamination had little effect on the isotopic signal. Therefore, this suggests that $\delta^{18}O$ may be reflecting mean annual temperatures, however, the inverse relationship between T_{Jul} and $\delta^{18}O$ values would imply a complex relationship between winter temperature and summer temperature variations, i.e., that seasonality signals changed with a warming in winter temperatures, which would impact isotopes alone, being greater than a warming in summer temperatures, which would impact both chironomids and isotopes. Whilst co-variance is often used to indicate evaporation it can be a crude measure of this process and it is possible that increases in evaporation could occur even when r^2 values are low. If "wetness" does control the $\delta^{18}O$ signal here, then the sequence would record the occurrence of cold (declining T_{Jul}) and dry (increasing $\delta^{18}O$) events. Such a proposal is possible but difficult to prove.

The inability to differentiate between the *Paratanytarsus* morphotypes, the most abundant chironomid genus in the mid-LLS, does hinder the interpretation of trophic status as *P. austriacus*-type occurs in oligotrophic conditions, while *P. penicillatus*-type occurs under slightly more nutrient rich, mesotrophic conditions (Brooks *et al.,* 2007). However, the continued presence of oligotrophic indicating taxa, (e.g., *Paracladius*, Moller Pillot, 2013) and taxa frequently found in mesotrophic conditions (e.g., *M. pedellus*-

type, *P. sordidellus*-type and *Ablabesmyia*; Moller Pillot, 2009, 2013; Orendt, 1993) suggests the lake is largely oligo-mesotrophic. *Paratanytarsus*, *Ablabesmyia* and *P. sordidellus*-type are often associated with macrophytes (Buskens, 1987; Brodersen *et al.,* 2001, 2011; Langdon *et al.,* 2010) and may suggest a well vegetated lake. The pollen data however suggests aquatic vegetation is rather sparse within the lake during the mid-LLS. The high abundance of *Paratanytarsus* may be explained by its ability to thrive on periphytic algae (e.g., diatoms) as a food source instead (Tarkiwska-Kukuryk & Toporowska, 2021). The pollen data shows abundant *Pediastrum* within the lake. Both *Ablabesmyia* and *P. sordidellus*-type can also live on lake bottoms (Vallenduuk & Moller Pillot, 2007; Reiss, 1968) and feed on a variety of detritus and filamentous algae (Armitage, 1968; Moller Pillot, 2013). The presence of *Paracladius*, which often occurs on silty lake bottoms with little or no vegetation (Reiss 1968; Zinchenko, 2002) may indicate sparse vegetation. Lake waters continue to be well oxygenated throughout the water column as good oxygenation is required by the profundal dwelling *H. grimshawi*-type (Moller Pillot, 2013) and the littoral dwelling *M. pedellus*-type (Steenbergen, 1993).

9.6.4 Late Loch Lomond Stadial: 12,370 ±230 – 12,130 ±240 cal a BP (composite depth 1386-1312 cm)

OBM-L6; OBM-C5b & -C5c; OBM-O4

At the start of the Late-LLS, T_{Jul} initially declines to 9.9 °C is most likely attributed to the increase in cold-indicating taxa (e.g., *Paracladius* and *C. ambigua*), large declines in cool-temperate indicating taxa (e.g., *C. anthracinus*-type, *P. sordidellus*-type and *Procladius*), and limited change in the abundance of other cool-temperate and temperate indicating taxa which continue their presence at similar abundances from the mid-LLS (e.g., *T. mendax*-type, *T. pallidicornis*-type, *Ablabesmyia, Dicrotendipes*). Although T_{Jul} is largely at or above the 10°C minimum needed for authigenic $CaCO_3$ to precipitate (Kelts and Hsu, 1976), a decline in $CaCO_3$ is observed and could be explained by two possible reasons. Firstly, it could simply be that $CaCO_3$ production did not change and that $CaCO_3$ was 'diluted' by the inwashed minerogenic sediment as the µ-XRF data displays a large increase in elements associated with minerogenic inwash (e.g., Mn, Fe, Ti). Secondly, the inwashed minerogenic sediment may cause lake waters to become opaque, decreasing light penetration and biological photosynthetic uptake of CO_2 needed to create supersaturation of carbonate ions (Kelts and Hsu, 1978). Chironomid taxa also suggest an increase in turbidity within the lake. *C. anthracinus*-type, which often occurs in abundance after significant environmental change (Brooks et al 2007), initially increases. Although it later declines, it is replaced by other taxa accustomed to coarse substrates and turbid conditions e.g., *M. pedellus*-type (Hofmann, 1984) and *C. ambigua*, which thrives in cold unstable conditions also increases (Brooks *et al.,* 2007).

The trophic status is inferred to continue to be oligo-meso trophic in nature based on the continued presence of oligotrophic indicating taxa, (e.g., *Paracladius*; Moller Pillot, 2013) and taxa frequently found in meso-trophic conditions (e.g., *M. pedellus*-type, *P. sordidellus*-type and *Ablabesmyia*; Moller Pillot, 2009, 2013; Orendt, 1993). The pollen data suggests vegetation within the lake remains sparse and chironomids seem to also suggest this. The detritus feeder *Paracladius* shows a small increase potentially as the inwash of detritus increases as seen in the µ-XRF elemental data (e.g., Fe, Mn, Ti; Jouve *et al.,* 2013) and the increase in TOC from 2 to 6 %. Very fine degraded organic detritus is present throughout the LLS suggesting a reduction in vegetation cover and an increase in landscape instability. It is possible though that charophytes were present, as suggested by the high abundance of *C. ambigua* (Brodersen and Lindegaard, 1999b). Lake waters continue to be well oxygenated throughout the water column as good oxygenation is required by the profundal dwelling *Paracladius* (Moller Pillot, 2013) and the littoral dwelling *M. pedellus*-type (Steenbergen, 1993).

$\delta^{13}C$ and $\delta^{18}O$ display low co-variance in the late-LLS (r^2 0.02) suggesting evaporitic enrichment of the lake water is unlikely to be driving these signals. Low co-variance also suggests detrital contamination did not alter the isotopic signal either, even though the µ-XRF data displays an increase in elements which are often associated with detrital input (e.g., Ti, Fe, Mn) (Jouve *et al.,* 2013). Moreover, detrital contamination from geological carbonate usually causes $\delta^{18}O$ values to increase, opposite to what is seen here.

The $\delta^{18}O$ record during the mid-LLS could therefore be representing a number of different environmental aspects. Firstly, a change in the hydrological balance of the lake to a more open system with limited isotopic modification of the lake waters due to a shift in the balance between evaporation and precipitation as they decline and increase, respectively. An increase in precipitation also agrees with the increase in detrital inwash, however, the $\delta^{13}C$ remains constant throughout the entire LLS, suggesting there was little change in the lake size nor hydrological balance of the lake. It could be that $\delta^{13}C$ was buffered by well-developed vegetation and soils throughout the entire LLS. Higher precipitation could also lead to the increase in µ-XRF detrital elements (Ti, Fe, Mn). Secondly, there could be a change in MAT. During the transition from the mid- to late-LLS, the shift in $\delta^{18}O$ from -2 to -6 ‰ occurs slightly before the decline in T_{Jul} suggesting MAT, and therefore winter temperatures, may have started to decline prior to summer temperatures. Colder winter temperatures could also lead to greater inwash of material through physical weathering processes aided by a decreased vegetation cover. µ-XRF detrital elements (Ti, Fe, Mn) all display peaks during the decline in $\delta^{18}O$ while T_{Jul} is still

relatively high. Thirdly, there may be a change in the seasonality of precipitation with a greater proportion of the rainfall falling in the colder winter month, and less in the warmer summer month (Candy *et al.,* 2016). Finally, a change in moisture source cannot be discounted with rainfall coming from wetter rather than drier regions. It could possibly be a combination of the scenarios described above. Other proxy data such as lipid biomarkers would help characterise the changes in precipitation, and by extension temperature, proposed here.

9.6.5 Early Holocene: 12,130 ±240 – 11,870 ±500 cal a BP (composite depth 1312 – 1238 cm)

OBM-L7, -L8 & -L9; OBM-C6

During the early Holocene, T_{Jul} undergoes a large increase from 11.3 °C to 15.5 °C as warm indicating taxa markedly increase, e.g., *Cladopelma*, *T. glabrescens*-type and *T. lactescens*-type. Taxa at the upper end of the temperate category also increase (e.g., *Ablabesmyia, Dicrotendipes, C. mancus*-type) while those at the lower end generally decrease (e.g., *T. mendax*-type and *M. pedellus*-type). Most cool-temperate taxa continue in low abundances, however, *P. sordidellus*-type increases. Cold indicting taxa are largely absent or decline to very low abundances (e.g., *Paracladius, C. ambigua*). Two declines in T_{Jul} are evident during the Early Holocene with minima occurring at 1290 and 1245 cm of 0.5 °C and 1.7 °C, respectively and may relate to the abrupt cooling events of the Early Holocene, i.e., the Pre-boreal Oscillation, 9.3 or 8.2 ka events. However, the radiocarbon date at 1236-1239 cm appears far too old and prohibits any tentative correlations to known events. The low sampling resolution may also mean the full magnitude of these events may not be captured. Moreover, discussion of early Holocene abrupt cooling events in any further detail is beyond the scope of this thesis. The data presented here does however show promise for the OBM19 sequence to be a key site for reconstructing temperature changes for the early Holocene ACEs, which are usually not represented in many T_{Jul} records from the British Isles and is therefore worthy of further study.

During the Early Holocene, many eutrophic indicating taxa increase in abundance, e.g., *E. Pagana*-type (Kansanen 1985; Saether, 1979), *E. albipennis*-type (Saether, 1979), *Cladopelma* (Steenberg 1993) and *T. glabrescens*-type (Brodin 1986; Uutala 1986, Bilyj and Davies, 1989), suggesting the lake became more eutrophic and productive. It is not clear if macrophytes increased in abundance as the aquatic pollen suggest the lake is still rather sparsely vegetated. Many chironomid taxa present often live or feed on plant macrophytes, e.g., *E. albipennis*-type, *Dicrotendipes* and *P. sordidellus*-type increase, but they can also feed on algae and detritus (Brodersen *et al.,* 2001; Moller Pillot, 2009, 2013). Algal communities may develop, as both *P. sordidellus*-type and *E. pagana*-type, increase and occur in

association with filamentous algae (Moller Pillot, 2013), and blue-green algae (Cannings & Scudder, 1978; Saether, 1979), respectively. Pediastrum remains abundant in the lake and *C. ambigua*, which often occurs with charophytes (Brodersen and Lindegaard, 1999b), suggests charophytes may be present. *Cladopelma*, which is a profundal taxa often feeding on organic silts (Moller Pillot, 2009; Lenz 1960a), potentially replacing *Paracladius* which is common throughout the LLS.

9.7 Chapter summary

This chapter explored the palaeolimnological and palaeoclimatological development at Old Buckenham Mere during the Lateglacial and early Holocene. The OBM19 sediment sequence contains sediment deposited during the very end of the WI interstadial; the entire LLS which is represented by 1.8 metres of sediment producing an average stratigraphic resolution of 5 yrs/cm; and the early Holocene. The following points summarise the key findings:

- During the final part of the WI (*c.* 13,500 ±880 – 12,700 ±180 cal a BP), the palaeolake was relatively shallow, c. 7 metres deep, with an extensive littoral area and small volume, rapidly recharged by groundwater. T_{Jul} estimates suggest mean July air temperatures were *c*. 13-15 °C.

- Relatively cool summer temperatures occur in the early-LLS (12,700 ±180 -12,550 ±220 cal a BP) of 11 °C. Lake productivity is relatively low, though high enough for authigenic $CaCO_3$ to precipitate. The hydrology of the lake is largely closed, and the climate is dry causing lake waters to be altered by evaporitic enrichment.

- Summer temperatures increase during the mid-LLS (12,700 ±220 – 12,370 ±230 cal a BP), with T_{Jul} rising to *c*. 13 °C, however, two ACEs occurs in T_{Jul} at 12,500 ±110 cal a BP and 12,420 ±120 cal a BP, with magnitudes of 2.8 and 1.9 °C, respectively. $\delta^{18}O$ and $\delta^{13}C$ display lower covariance and lower $\delta^{18}O$ values could be due to wetter conditions, lower MAT, or a shift in the proportion of precipitation to the winter months. However, $\delta^{18}O$ increases during the T_{Jul} cold oscillations and may potentially caused by reduced seasonality (higher MAT) or increased aridity during the ACEs.

- During the Late-LLS (12,370 ±230 – 12,130 ±240 cal a BP), summer temperatures turn cooler again to 9.9 °C but then increases throughout to 12.8 °C. Lower $\delta^{18}O$ may reflect wetter conditions, lower MAT and greater proportion of winter precipitation.

- Summer temperatures increase in the Early Holocene to 15.5 °C. Two ACE occur in the order of 1-2 °C magnitude.

Chapter 10: Synthesis the spatial variations in the magnitude of ACEs during the LGIS and discussion of potential forcing mechanisms

Chapter overview

In this chapter, the new high-resolution records generated for this thesis from Crudale Meadow, Llangorse and Old Buckenham Mere, are integrated and compared to other chironomid and oxygen isotope records from the British Isles and continental Europe. Firstly, the broad trends in T_{Jul} and $\delta^{18}O$ will be briefly examined and the forcing mechanisms attributed to these. Then attention will turn towards the ACEs within the LGIS. In order for comparison of ACE magnitude across geographic regions to be as robust as possible, a set of criteria is defined to help select sites which have sufficient sampling resolution to define the ACEs of the LGIS as well as a robust chronological framework that allows accurate correlation of ACEs between sites. The ACEs of the LGIS will be examined in turn. For the early-LGIS ACE at *c*. 14.0ka BP (~GI-1d/Aegelsee Oscillation/Older Dryas) and the late-LGIS *c*. 13.2 ka BP ACE (~GI-1b/Gerzensee Oscillations/Killarney Oscillation), the magnitude of these ACEs in T_{Jul} and $\delta^{18}O$ will be compared against spatial gradients for (i) The British Isles, (ii) Continental Europe, and (iii) The British Isles and continental Europe combined. Based on the spatial expression of these events and evidence from the published literature, potential forcing mechanism will be proposed. Records of the mid-LGIS ACE at *c*. 13.6 ka BP (~GI-1cii) will also be examined to determine its presence and structure in T_{Jul} and $\delta^{18}O$ records. Finally, the findings from Old Buckenham Mere will be discussed in conjunction with other stadial records briefly, focusing on the centennial-scale climatic changes during the mid-LLS (~GS-1/Younger Dryas).

10.1 General temperature trends of the LGIS

While discussing the potential forcing mechanisms operating during each ACEs of the LGIS, it is also important to note the different millennial-scale temperature trends throughout the LGIS (Figure 10.1). The majority of T_{Jul} and $\delta^{18}O$ records along the western edge and more northerly locations in Europe, including those in the British Isles and the Iberian Peninsula (e.g., Laguna de la Roya), display an abrupt increase in temperatures at the start of the LGIS which then either have a relatively stable trend or decline throughout the LGIS (Figure 10.1a; Moreno *et al.,* 2014). High values are also observed in the Greenland ice core $\delta^{18}O$ records (Rasmussen *et al.,* 2014). Abrupt increases in temperature at the start of the LGIS have been attributed to the sudden restart of the THC, bringing warm water to higher latitudes, evidence for which is seen in reduced ocean ventilation ages at the South Iceland Rise and

increased benthic $\delta^{13}C$ at the Iberian Margin (Thornalley *et al.,* 2011). Moreno *et al.* (2014) noted that in more southerly locations of continental Europe, temperature records display a gradual warming trend throughout the LGIS (Moreno *et al.,* 2014), however, there is greater complexity than this. Some T_{Jul} records in southern Europe do display a general increase in T_{Jul} throughout the LGIS (e.g. Gerzensee, Lotter *et al.,* 2012; Maloja Pass, Ilyashuk *et al.,* 2009) but $\delta^{18}O$ records display an abrupt increase and either display a relatively flat trend (e.g., Amersee, von Grafenstein *et al.,* 1999b; Faulenseemoos, Lotter *et al.,* 1992) or an early peak which then declines throughout the LGIS (e.g., Gerzensee, Lotter *et al.,* 2012; Rotsee, Verbruggen *et al.,* 2010) (Figure 10.1b).

Moreno *et al.,* (2014) summarised work from modelling experiments (e.g., Renssen and Isarin, 2001; Renssen and Bogaart, 2003) and suggested the differing trends seen between north and south Europe reflects spatial changes in seasonality and storm track location. The northward shift in the Atlantic sea-ice margin at 14.7 ka BP led to the northward relocation of the Atlantic storm tracks causing a more abrupt and marked temperature change in northerly European records (Moreno *et al.,* 2014). This caused daily temperature variability to reduce by 50 %, with the greatest temperature increase occurring in the winter months, and a substantial decrease in storm activity (Rennssen and Bogaart, 2003; Moreno *et al.,* 2014). More southern European records, however, were located south of the winter sea-ice margin (at *c.* 45 °N) throughout GS-2a and so did not experience an abrupt change (Renssen and Isarin, 2001; Moreno *et al.,* 2014). Although this offers an explanation as to why some records display a gradual increase, while others display an abrupt increase in temperature, it does not explain the patterns observed during the LGIS (Moreno *et al.,* 2014). Lotter *et al.,* (2012) attributed the rise in T_{Jul} values throughout the LGIS at Gerzensee to increasing summer insolation and the decline in $\delta^{18}O$ to a decline in winter insolation. The T_{Jul} record from Llangorse, which has peak T_{Jul} values occurring in the mid-LGIS, is different from many other T_{Jul} records in the British Isles that show a relatively flat trend throughout the LGIS, e.g., Crudale Meadow (T_{Jul} and $\delta^{18}O$). It could be that, because of the southerly location of Llangorse in the British Isles, the site displays both characteristics of gradual warming in the early-LGIS, similar to records in southern Europe, but then the gradual decline on the latter part of the LGIS, more akin to records in northern Europe.

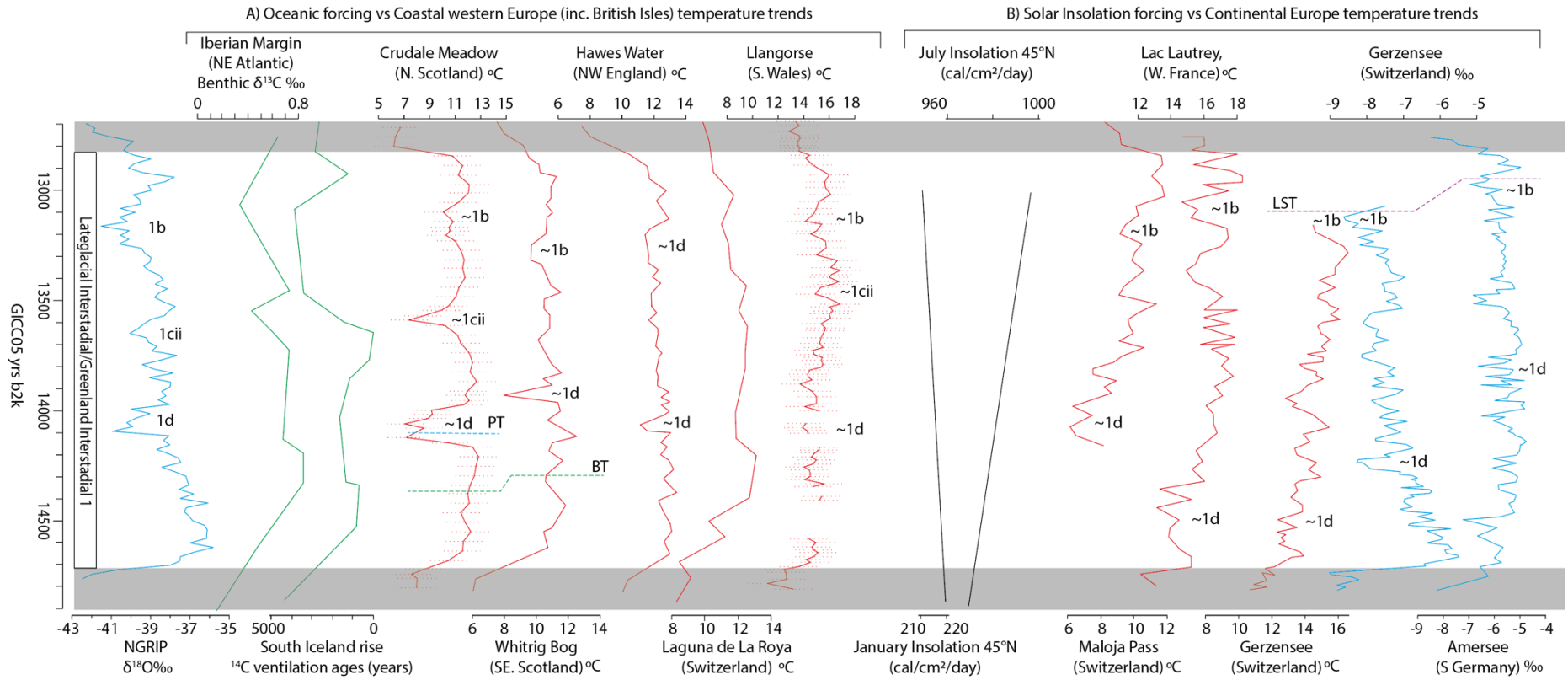

Figure 10.1, Trends in T_{Jul} and $\delta^{18}O$ for the LGIS compared to proposed forcing mechanisms. A) Comparison between oceanic forcing proxies (Thornalley *et al.,* 2011) and LGIS temperature trends displayed in T_{Jul} records of western Europe, including the British Isles. B) Comparison between calculated solar insolation values (Laskar *et al.,* 1993; Lotter *et al.,* 2012) and trends displayed in T_{Jul} and $\delta^{18}O$ records from continental Europe. Note: the NGRIP $\delta^{18}O$ and solar insolation curves are plotted against the GICC05 timescale; Oceanic proxies, T_{Jul} and lacustrine $\delta^{18}O$ records are plotted by depth from each individual record with the period denoted as the LGIS broadly aligned to the Lateglacial Interstadial. References for sites can be found in Tabless 10.1, 10.2, 10.3 and 10.4.

10.2 Centennial scale ACEs within the LGIS

10.2.1 Defining ACEs in proxy records

In order to make meaningful comparisons of ACE magnitude between sites, it is important to understand how the events have been defined in individual proxy records. Broadly, two different approaches have been used to define the magnitude of ACEs and are displayed on the $\delta^{18}O$ record from NGRIP in Figure 10.2 as an example. One approach is to use the difference between the minimum values achieved during the ACE and the highest value preceding the ACE in a proxy record and will be referred to as the 'min/max approach'. This has often been done when the record has a "spikey" character with minima and maxima defined by single data points rather than periods of stable values, and there is no clear shoulders to the event, e.g., Tirinie $\delta^{18}O$ (Candy *et al.,* 2016). A second approach is to use the difference between a high value from the shoulder of the event, immediately prior to an abrupt decline in the proxy instead, and will be referred to as the 'shoulder approach'. The shoulder approach has been used in records which have more stable periods of warm/cooler conditions separated by an abrupt shift, such as in very high resolution lacustrine $\delta^{18}O$ records, which have clear shoulders to the event, e.g., Mondsee $\delta^{18}O$ (Lauterbach *et al.,* 2011). The issue with the shoulder approach is that many T_{Jul} and $\delta^{18}O$ records from lacustrine sequences do not display such stable trends, potentially due to low sampling resolution or highly variable sedimentation rates meaning the shoulders of the ACE are not clearly expressed (Figure 10.3). Another issue with the shoulder approach is that can also lead to subjectivity in defining the start of an ACE when there is no clear shoulder to the ACE, or potentially multiple shoulder to choose from. Therefore, the min/max approach is considered favourable when defining the LGIS ACEs in T_{Jul} and $\delta^{18}O$ as it provides a more 'clear cut' definition with less subjectivity introduced. The author has therefore re-examined the magnitude of ACE in T_{Jul} and $\delta^{18}O$ from records located in the British Isles and continental Europe to ensure consistency between records. Although the ACEs in the Greenland ice core $\delta^{18}O$ records are statistically defined, the definition of events in GICC05 is closest to that of the shoulder approach and are therefore re-examined using the min/max approach in the following sections for consistency between records.

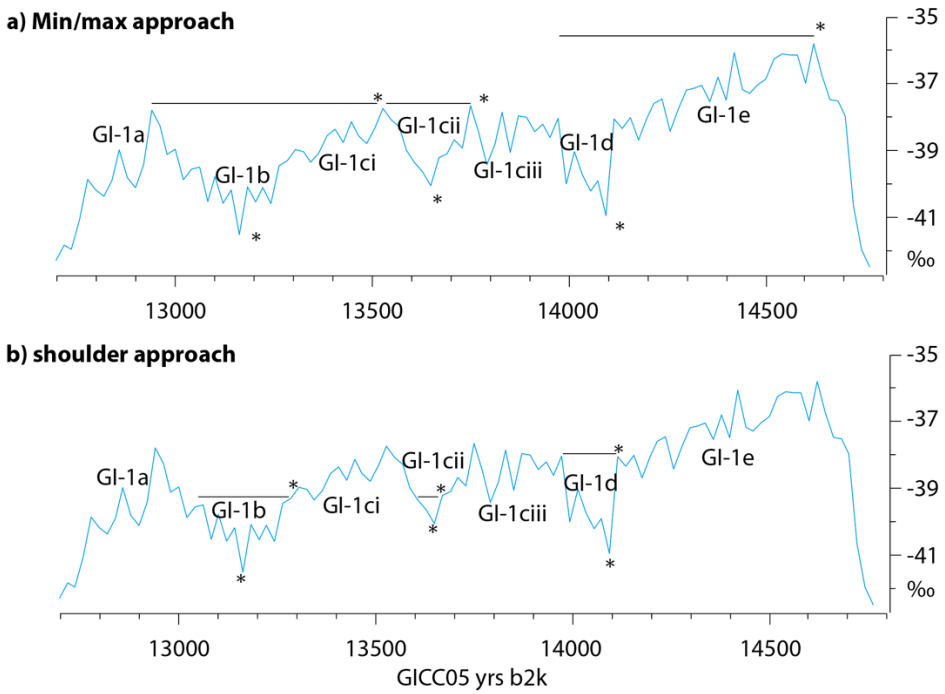

Figure 10.2, Approaches to defining an ACEs, exemplified on the $\delta^{18}O$ record from NGRIP. **a**) the min/max approach where the highest value prior to an ACE is used. **b**) the shoulder approach where the highest value occurring on the shoulder of an event is used and is immediately prior to an abrupt decline. The minimum/maximum values are defined by asterisks and black lines denote the duration of the ACEs.

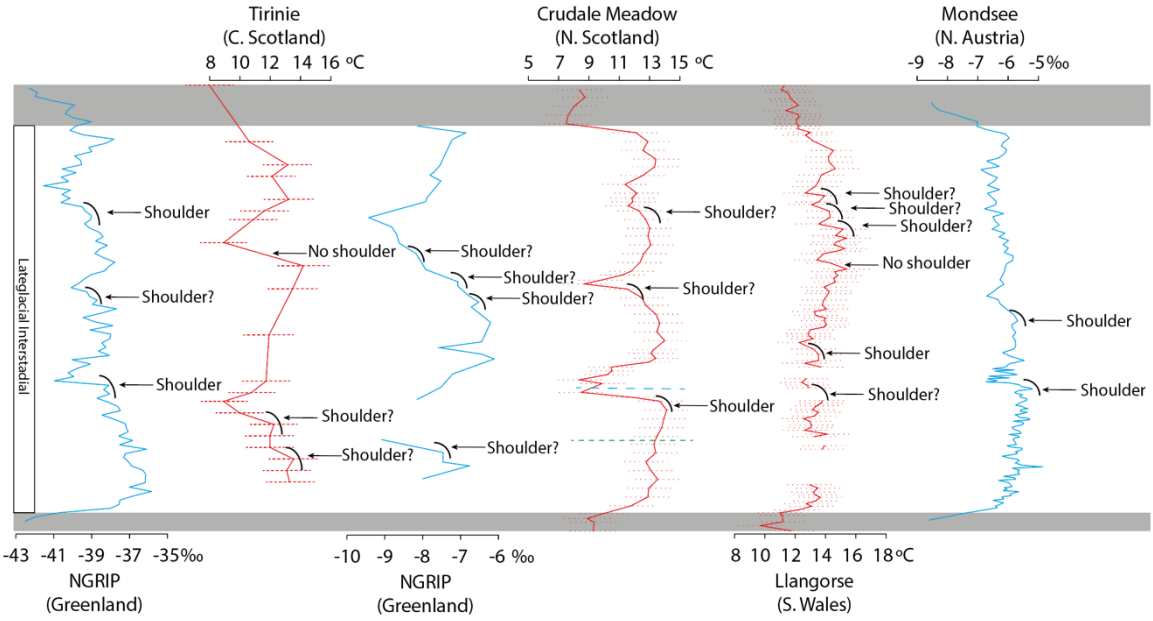

Figure 10.3, Defining ACEs in terrestrial and ice core records. Selected records displaying the issues with identifying the 'shoulder' of an ACE. Some ACEs in records do not have a clearly defined shoulder of an event while others may have multiple options. Therefore, the difference between the maximum values prior to an event and the minimum values during the event are used as this is less subjective.

10.2.2 Site selection criteria

To investigate the spatial expression of the LGIS ACEs, the new T_{Jul} and $\delta^{18}O$ records presented here need to be integrated with other available records to provide a more complete spatial coverage. To select the most appropriate records for comparison, a set of criteria has been developed.

The first criterion is concentrated on the resolution of proxy records and whether a record has a sampling resolution comparable to that of the Greenland ice cores which use a 20 yr average for the $\delta^{18}O$ records (Rasmussen *et al.,* 2006). Sufficient proxy resolution is defined as a record having fewer than 30 yr sampling resolution on average for the LGIS. If a record has more than 30 yrs/sample on average but has sufficient sampling resolution for the ACEs individually, then those records are deemed acceptable. This means that the *c.* 14.0ka event would need to be defined by ≥4 samples, and the *c*. 13.2 ka event ≥8 samples, to give a sampling resolution of *c*. 25 yrs/sample during the ACEs.

The second criterion is concentrated on the identification and dating of ACEs in records and is used to determine whether the records allow robust comparisons between sites. Ideally, each record would have robust chronologies, but this has not been possible in many cases for a variety of reasons including an absence of terrestrial plant macrofossils for radiocarbon dating (e.g., Lundin Tower; Whittington *et al.,* 1996) and/or few, if any, tephra shards present. Even for records which do have well-dated horizons, they are often few in number and/or concentrated during certain periods of the LGIS. For example, many Scottish records contain the Borrobol and Penifiler tephras constraining the early LGIS, however, the latter part of the LGIS often has no chronological constraint e.g., Loch Ashik (Brooks *et al.,* 2012) and Muir Park Reservoir (Brooks *et al.,* 2016). As long as the ACEs at *c*. 14.0 ka and 13.2 ka can be identified using a combination of robustly dated horizons and/or a clear stratigraphy of events for climatostratigraphy then this is deemed sufficient for the purposes of this thesis, as only the event magnitude is being compared and not the difference in the exact timing of event onset and when minimum temperatures were achieved. There are however occasions where the correlation of ACEs is uncertain, and these will be discussed in the following subsections where needed.

The third criterion is based on the appropriate selection of a chironomid climate calibration dataset to reconstruct mean July air temperatures. The appropriateness of a calibration dataset is based on the proximity to the site where reconstruction is being made and on whether the type/chemistry of the lakes within the calibration dataset is similar to the inferred lake environment during the time interval under consideration. Therefore, for example, T_{Jul} reconstructions from lakes which are close to the Swiss alps and are alkaline/marl-dominated, should use the Swiss Calibration dataset. T_{Jul}

reconstructions from lakes which are close to Norway and are acidic/circum-neutral should use the Norwegian calibration dataset. Sites in between these geographic regions should use the combined Norwegian-Swiss calibration datasets. Ideally, for sequences in which carbonate is abundant, the combined calibration dataset should be used as the lakes of the Norwegian calibration dataset only contains lakes with acidic or circum neutral waters.

The majority of T_{Jul} and $\delta^{18}O$ records in the British Isles pass the proxy sampling resolution and chronology resolution criteria outlined above (Table 10.1). The exceptions to this are the isotope records of Red Bog and Lough Gur (Ahlberg *et al.,* 1993) and Tory Hill (O'Connell *et al.,* 1999) which have very low sampling resolution and limited chronological constraint. The T_{Jul} record from Thomastown bog (Turner *et al.,* 2015) is also not included in the regional comparisons as it has a very low sampling resolution of 150 yrs/sample. Although the 14.0 ka BP event at Thomastown bog does have four chironomid samples defining it, it spans 30 cm of sediment in which the true minima/maxima of temperatures could have been missed. Quoyloo Meadow (T_{Jul}) is also not included as it has a very low sampling resolution of 256/yrs sample and a stratigraphically compressed LGIS.

Table 10.1, T_{Jul} records from the British Isles. A tick denotes the record passes the criteria outlined above and a cross denotes it has failed. If a record fails one of these criteria, then it is not included in later comparisons of ACE magnitude and highlighted in grey. If an individual event does not meet the minimum number of minimum number of samples to adequately define it then it is not included in comparisons and also highlighted in grey.

Site and abbreviation	sufficient proxy sampling resolution?	Sufficient chronological data	Appropriate calibration dataset used?	ACE magnitude		Refence
				14.0 ka BP ~GI-1d	13.2 ka BP ~GI-1b	
Quoyloo Meadow	X	✓	✓	(3 samples)	Not Expressed	Timms *et al.,* 2021
Crudale Meadow (CM)	✓	✓	✓	5.4 °C	1 °C	Francis *et al.,* 2021; this thesis
Abernethy Forest (AF)	✓	✓	✓	5.5 °C	2.8 °C	Brooks *et al.,* 2012
Loch Ashik (LA)	✓	✓	✓	4.4 °C	2 °C	Brooks *et al.,* 2012
Tirinie (TR)	✓	✓	✓	4.3 °C	4.5 °C	Abrook *et al.,* 2020
Muir Park Reservoir (MPR)	✓	✓	✓	3.5 °C	3.5 °C	Brooks *et al.,* 2016
Whitrig Bog (WB)	✓	✓	✓	4.5 °C	2.2 °C	Brooks and Birks, 2000
Nadourcan (N)	✓	✓	✓	2 °C	1.2 °C	Watson *et al.,* 2010
Sunbiggin Tarn (ST)	✓	✓	✓	3.5 °C	1.6 °C	Lang *et al.,* 2010
Cunswick Tarn (CT)	✓	✓	✓	2 °C	0. 9 °C	Lang *et al.,* 2010
White bog (W)	✓	✓	✓	2.5 °C	Not analysed	O'Neill-Munro, 2017
Urswick Tarn (UT)	✓*	✓	✓	(3 samples)	1.6 °C	Lang *et al.,* 2010

Hawes Water (HW)	✓	✓	✓	2	0.8 °C	Lang *et al.,* 2010
Little Hawes Water (LHW)	✓	✓	✓	3.5 °C	1.2 °C	Lang *et al.,* 2010
Star Carr (SC)	✓	✓	✓	3 °C	(5 samples)	Langdon (unpublished))
Thomastown	X	✓	✓	(4 samples)		Turner *et al.,* 2015
Fiddaun (FI)	✓	✓	✓	1 °C	1.5 °C	Van Asch *et al.,* 2012a
Llangorse (LL)	✓	✓	✓	2 °C	2.4 °C	Palmer *et al.,* in prep; This Study

Table 10.2, $\delta^{18}O$ records from the British Isles. A tick denotes the record passes the criteria outlined above and a cross denotes it has failed. If a record fails one of these criteria, then it is not included in later comparisons of ACE magnitude and highlighted in grey. If an individual event does not meet the minimum number of minimum number of samples to adequately define it then it is not included in comparisons and also highlighted in grey.

Site	sufficient proxy sampling resolution?	Sufficient chronological data	Evaporitic modification or detrital contaminatio n?	ACE magnitude		Refence
				14.0 ka BP ~GI-1d	13.2 ka BP ~GI-1b	
Crudale Meadow (CM)	✓	✓	No	1 ‰	0.5 ‰	Francis *et al.,* 2021; this thesis
Tirinie (TR)	✓	✓	No	2.3 ‰	2.5 ‰	Abrook *et al.,* 2020; Candy *et al.,* 2016
Lundin Tower (LT)	✓	✓	No	2 ‰	(4 samples)	Whittington *et al.,* 1996
White bog	✓	X	Yes			O'Neill-Munro (2017)
Hawes Water (HW)	✓	✓	No	1.5 ‰	0.9 ‰	Marshal *et al.,* 2002
Star Carr ((SC)	✓	✓	No	3 ‰	2 ‰	Candy (unpublished)
Thomastown (TT)	✓	✓	No	1.2 ‰	1 ‰	Turner *et al.,* 2015
Fiddaun (FI)	✓	✓	No	1.4 ‰	1.36 ‰	Van Asch *et al.,* 2012a
Inchiquin (IN)	✓	✓	No	1.3 ‰	0.93 ‰	Diefendorf *et al.,* 2006
Tory Hill	X	X	No			O'Connell *et al.,* 1999
Lough Gur	X	X	No			Ahlberg *et al.,* 1997
Red Bog	X	X	No			Ahlberg *et al.,* 1997

Many T_{Jul} and $\delta^{18}O$ records from continental Europe do not pass the criteria outlined above (Table 10.2). Although many T_{Jul} and $\delta^{18}O$ records from continental Europe have relatively good chronological constraints due to the presence of the Laacher See Tephra (Reinig *et al.,* (2021) and the availability of numerous radiocarbon dates e.g., Egelsee (Larocque-Tobler *et al.,* 2010) and Lago Piccolo di Avigliana (Finsinger *et al.,* 2008), many records have low sampling resolution and too few samples to define the ACEs e.g., Lago piccolo (179yrs/sample), La Roya (120 yrs/sample), Foppe (225yrs/sample) and Żabieniec (112yrs/sample). Low sampling resolution also means the structure of the LGIS in T_{Jul} and $\delta^{18}O$ is less clear making the identification of ACEs less certain. Therefore, such sites are omitted as well, e.g.,

Klein Ven (Van Asch *et al.,* 2013) and Foppe (Samartin *et al.,* 2012). Sites in which ACEs are not recorded due to the presence of the SIS either prohibiting lacustrine sedimentation (e.g., Kråkenes; Brooks and Birks, 2001) or supressing temperatures (e.g., Jansvatnet and Hässeldala Port; Birks *et al.,* 2012; Wohlfarth *et al.,* 2017) are also omitted. Some sites in continental Europe did not meet the sampling resolution criteria outlined above but were included, including Ech (Millet *et al.,* 2012), Laguna de la Roya (Munzo-Sobrino *et al.,* 2013) and Maloja Riegel (Ilyashuk *et al.,* 2009) because they have a robust chronological framework, and only just fall below the minimum number of samples defined above.

Table 10.3, T_{Jul} records from continental Europe. A tick denotes the record passes the criteria outlined above and a cross denotes it has failed. If a record fails one of these criteria, then it is not included in later comparisons of ACE magnitude and highlighted in grey. If an individual event does not meet the minimum number of minimum number of samples to adequately define it then it is not included in comparisons and highlighted in grey.

Site	High resolution temperature proxy	Sufficient chronological data	Appropriate calibration dataset used?	ACEs expressed		reference
				14.0 ka BP ~GI-1d	13.2 ka BP ~GI-1b	
Jansvatnet (J)	✓*	✓	✓	Not covered	2.3 °C	Birks *et al.,* 2012
Kråkenes			✓	Not covered	Not covered	Brooks and Birks, 2001
Myklevatnet	X	X	✓	Not expressed?	(3 samples)	Nesje *et al.,* 2014
Hässeldala port	✓	✓	✓	Not expressed	Not expressed	Wohlfarth *et al.,* 2017
Friedlander Grosse Wiesse	X	✓	✓	Not covered	(3 samples)	Van Asch *et al.,* 2012b
Hijkermeer (H)	✓	✓	✓	2.1 °C	1.5 °C	Heir *et al.,* 2011
Żabieniec	X	X	✓	Low res	Low res	Plociennik *et al.,* 2011
Klein Ven	X	X	✓	Low res	Low res	van Asch *et al.,* 2013
Moervaart (M)	✓	✓	✓	1.1 °C	Not covered	van Bos *et al.,* 2017
Egelsee	X	✓	X	Low res	Low res	Larocque-Tobler *et al.,* 2010
Gerzensee (G)	✓	✓	✓	Not expressed	2 °C	Lotter *et al.,* 2012
Lac Lautrey (L)	✓	✓	✓	0.8 °C	1.8 °C	Heiri and Millet, 2005
Foppe	X	✓	✓	Low res	Low res	Samartin *et al.,* 2012
Maloja Pass (MR)	✓	✓	✓	2.1 °C	1.4 °C (6 samples)	Ilyashuk *et al.,* 2009
Lago Piccolo di Avigliana	✓	✓	✓	(3 samples)	(3 samples)	Larocque and Finsinger, 2008
Ech (EC)	✓	✓	✓	2.5 °C	2 °C (7 samples)	Millet *et al.,* 2012
Laguna de la Roya (LR)	✓*	✓	✓	1. 1 °C (4 samples)	1.5 °C (5 samples)	Munoz Sobrino *et al.,* 2013

Table 10.4, $\delta^{18}O$ records from continental Europe. A tick denotes the record passes the criteria outlined above and a cross denotes it has failed. If a record fails one of these criteria, then it is not included in later comparisons of ACE magnitude and highlighted in grey. If an individual event does not meet the minimum number of minimum number of samples to adequately define it then it is not included in comparisons and highlighted in grey.

Site	High resolution temperature proxy	Sufficient chronological data	Evaporitic modification or detrital contamination?	ACEs expressed		reference
				14.0 ka BP ~GI-1d	13.2 ka BP ~GI-1b	
Friedlander Grosse Wiese	X	X	Yes			Van Asch *et al.,* 2012b
Klein Ven	X	X	Yes			Van Asch *et al.,* 2013
Amersee (AM)	✓	✓	No	1.8 ‰	1.5 ‰	Von Grafenstein *et al.,* 1999b
Mondsee (MO)	✓	✓	No	2 ‰	1 ‰	Lauterbach *et al.,* 2011
Rotsee (RT)	✓	✓	No	2 ‰	1.8 ‰	Verbruggen *et al.,* 2010
Gerzensee (G)	✓	✓	No	2 ‰	0.8 ‰	Lotter *et al.,* 2012
Faulenseemoos	✓	✓	No	0.7 ‰ (4 samples)	1.4 ‰	Eicher and Siegenthaler, 1976; Lotter *et al.,* 1992
Aegelsee (Core AE-3)	✓	✓	No	0.7 ‰ (3 samples)	0.7 ‰ (4 samples)	Wellington and Lotter, 1990; Lotter *et al.,* 1992
Leysin (LE)	✓	✓	No	Not analysed?	1.1 ‰	Schwander *et al.,* 2000
Lago Piccolo di Avigliana (LP)	X	✓	No	0.9 ‰	(4 samples)	Finsinger *et al.,* 2008

10.3 The early-LGIS

The most notable ACE of the Early LGIS is the event at *c.* 14.0 ka BP ACE, broadly coeval with GI-1d in Greenland, which has a duration of 121 years and has a magnitude of 2.8 ‰ in NGRIP (Figure 10.4). However, using the expanded definition of an ACE outlined in Section 10.1, which would include the maximum $\delta^{18}O$ value in GI-1e, the event has a duration of *c.* 420 years and *c*. 5 ‰ in NGRIP.

It should also be noted that other smaller declines in $\delta^{18}O$ occur during the very early LGIS (~GI-1e). Van Raden *et al.,* (2013) identified an event during the very early LGIS from the Gerzensee stacked $\delta^{18}O$ record, calling it GI-1eii, and drew comparison to the Bølling cold period 1 (BCP1) in the Norwegian sea (Karpuz and Jansen, 1992). Several small declines in the order of *c*. 1 ‰ are displayed in the Greenland ice cores during GI-1e but are not designated a name in the GICC05 timescale. A small decline in T_{Jul} of *c.* 1 °C can be seen very early on in the LGIs in a notable number of T_{Jul} and $\delta^{18}O$ records from the British Isles and continental Europe, delineated by occurring at the same time as the deposition of the Borrobol tephra at *c.* 14.14 ka cal BP (See Figure 10.5). Although the magnitude of this very early LGIS ACE is very

small and close to the sample specific errors of the WA-PLS models, its presence in numerous records suggests it may be an actual climatic event. Not all records register a very early ACE, but this could be due to low sampling resolution, low sedimentation rate or chironomid ecological thresholds were not crossed at specific sites. Chronological constraint is often poor in the very early LGIS in lacustrine sequences from NW Europe, inhibiting any correlation with the small oscillations seen in Greenland during GI-1e. Nevertheless, it is important to highlight these declines in temperature seen in T_{Jul} and $\delta^{18}O$ records as they could be easily mis-correlated with other ACEs such as the *c.* 14.0 ka BP ACE when chronological constraint is limited.

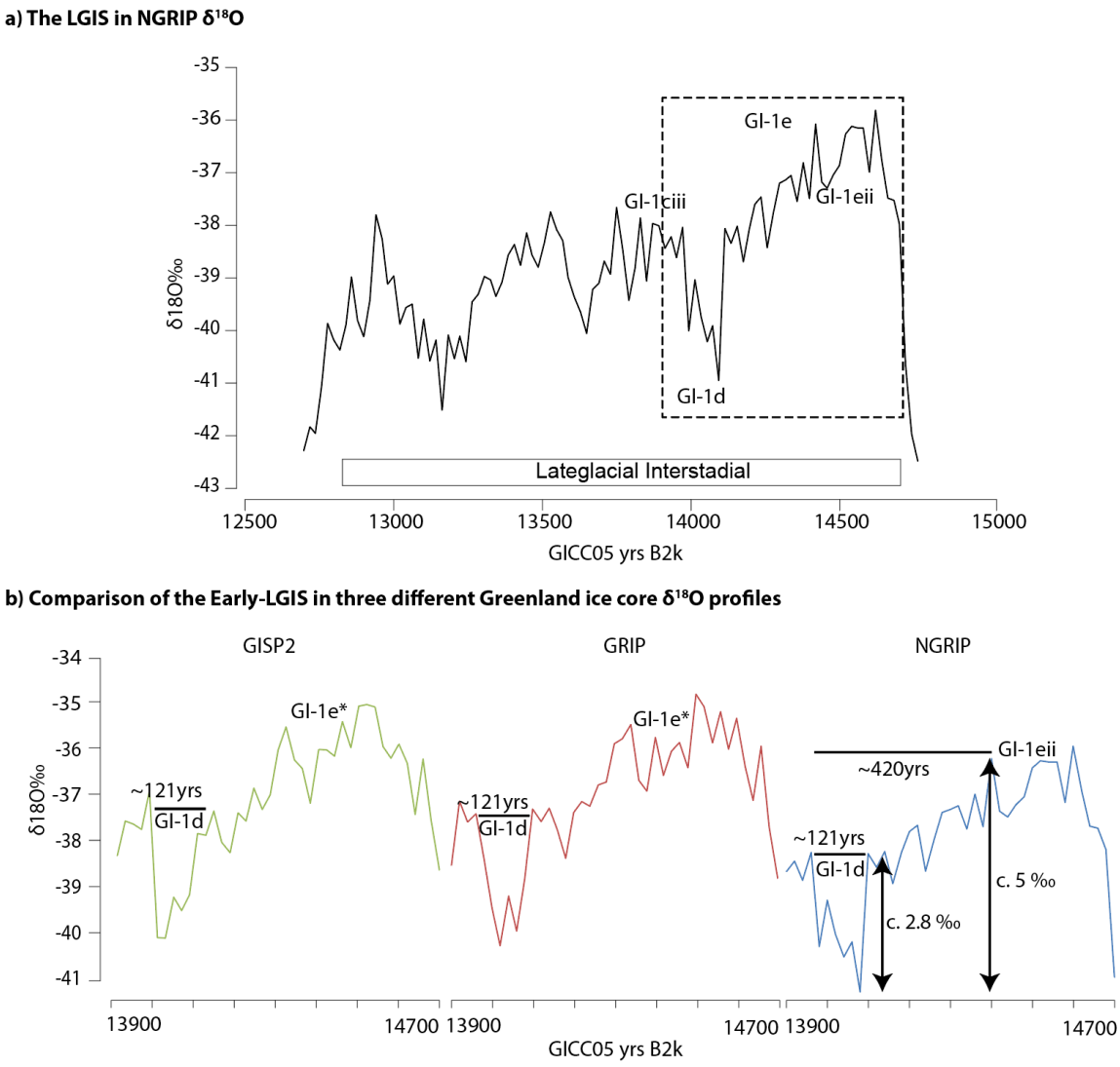

Figure 10.4, Comparison of the early LGIS (*c.* 14.7-13.9 GICC05 kyrs b2k) in Greenland ice cores. **a**) NGRIP $\delta^{18}O$ plotted against the GICC05 timescale with event names marked on. The isotope record encompassed by the dotted line is expanded in (b) for each of the three Greenland ice cores. **b**) $\delta^{18}O$ record for the Early LGIS from GISP2, GRIP and NGRIP. NGRIP has a comparison of event magnitude/duration as defined in GICC05 with that defined by the expanded definition used in this thesis.

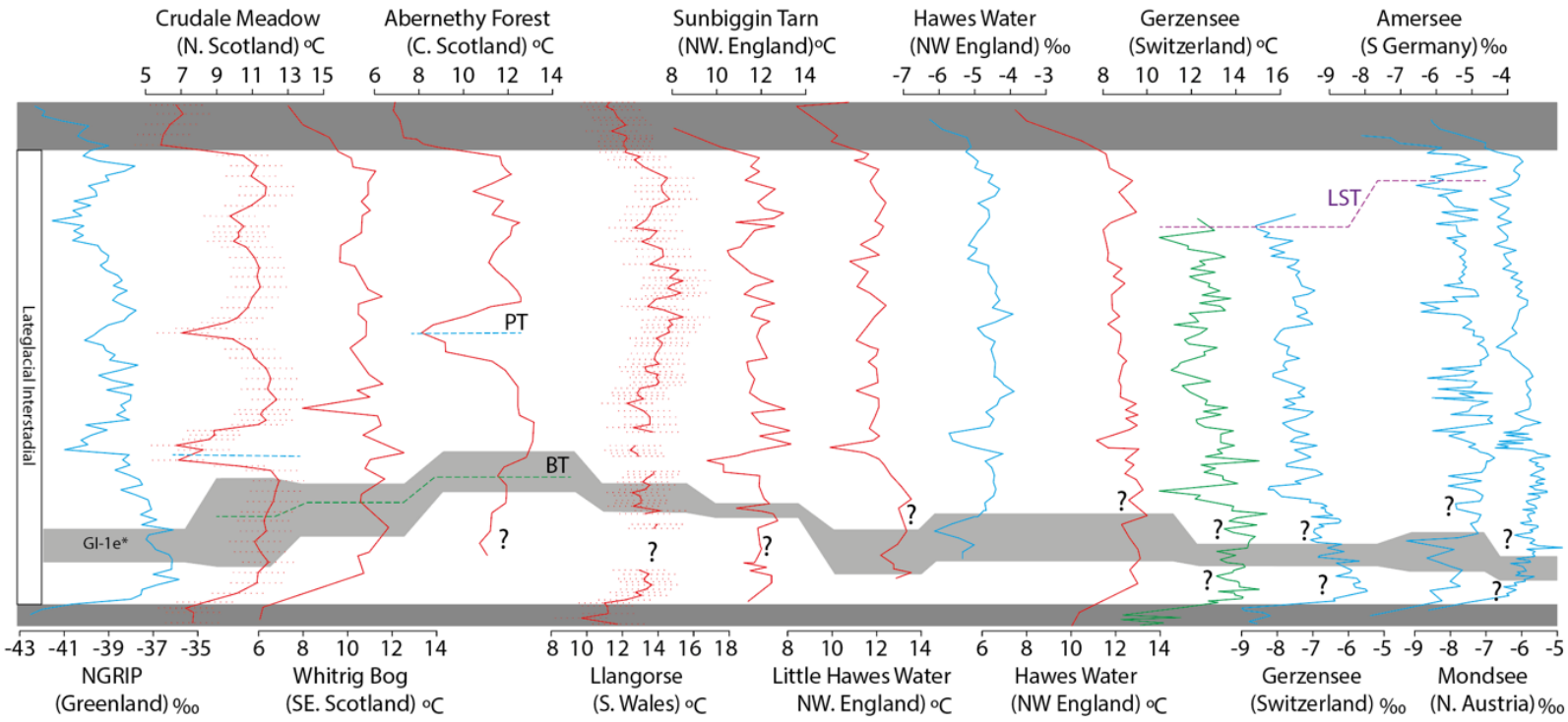

Figure 10.5, Potential expression of a very early LGIS ACE in T_{Jul} and $\delta^{18}O$ records from the British Isles and Continental Europe. Light Grey shading denotes a suggested correlation of a very Early LGIS ACE and question marks denote other declines during the very early LGIS. Limited chronological control however prohibits the definitive correlations. Dashed green line = Borrobol Tephra, dashed blue line = Penifiler Tephra, dashed purple line = Laacher See Tephra.

10.3.1 Identifying the c. 14.0 ka BP ACE event

Identifying the early-LGIS ACE which occurs at *c.* 14.0 ka BP is relatively easy in the Scottish records due to its relatively large magnitude (*c.* 3-5 °C), the occurrence of the Penifiler tephra during the abrupt decline, and the Borrobol tephra preceding the abrupt decline (e.g., Brooks *et al.,* 2012; 2016). Both tephra layers are found at Crudale Meadow allowing robust identification of the 14.0 ka BP ACE. Further south and west in the British Isles, the *c*. 14.0 ka BP event is less well constrained chronologically as the Borrobol and Penifiler tephras are rarely found. Many Irish sites rely on radiocarbon dated bulk carbonate samples (e.g., Thomastown; Turner *et al.,* 2015) or aquatic macrofossil samples (e.g., Inchiquin; Diefendorf *et al.,* 2006) resulting in hardwater error causing erroneously old age estimates. The exception is Fiddaun, on the west coast of Ireland, which has 3 radiocarbon dates on terrestrial plant macrofossils bracketing the early-LGIS ACE to 13.9-14.3 ka cal BP. However, the Irish records with erroneous radiocarbon age estimates, along with records in Northern England which have no chronology (Lang *et al,* 2010), do have a clear climatostratigraphy in which an early ACE can be identified. The records from Fiddaun, along with Llangorse, have the best chronological constraint on the 14.0 ka BP ACE outside of Scotland due to the application of radiocarbon dating on terrestrial plant macrofossils (Van Asch *et al.,* 2012a; Palmer *et al.,* in prep).

Unfortunately, the Borrobol and Penifiler tephras have not been found in many LGIS sequences in continental Europe and so the identification of the early-LGIS event must rely on other means. Borrobol-type tephras have been discovered in Scandinavia at Hässeldala Port (Wohlfarth *et al.,* 2015) and Körslättamossen (Larsson *et al.,* 2021), however further differentiation has not been possible. The 14.0 ka BP ACE has been robustly dated using independent dating means at Moervaart where the event is bracketed by 2 radiocarbon dates on terrestrial plant macrofossils which suggest an age of between 14.2 – 13.7 ka BP. The radiocarbon chronologies at Maloja Riegel and Laguna del la Roya date the early-LGIS ACE to *c.* 13.9 and *c*. 14.0 ka BP, respectively. The early LGIS ACE is dated to 14.6-15.5 ka BP in Ech, however, bulk samples were used for radiocarbon dating and are suggested to have had an aging effect (Millet *et al.,* 2012). The high-resolution isotope records from Amersee, Mondsee and Gerzensee have allowed broad correlation of the early LGIS ACE with Greenland based on isotope and climatostratigraphy (Hoek and Bohncke, 2001). The remaining records in Europe are accompanied by pollen data which has allowed them to be wiggle matched to regional pollen zones (Hoek, 1997a, b, c) providing very broad age constraint on the early LGIS ACE at *c*. 14.0 ka BP.

10.3.2 Structure of the 14.0 ka BP ACE

In NGRIP, there is a gradual decline in $\delta^{18}O$ values of 2 ‰ occurs throughout GI-1e (14.6-14.1 GICC05 kyrs B2k) following the early peak in $\delta^{18}O$. An abrupt decline in $\delta^{18}O$ of 3 ‰ then occurs during GI-1d between 14.1-13.96 GICC05 kyrs b2k. During GI-1d a brief increase in $\delta^{18}O$ occurs of *c.* 2 ‰. A similar pattern of temperature change can be observed in some T_{Jul} and $\delta^{18}O$ records from the British Isles and continental Europe with a "W" structure within the abrupt decline (e.g., Lough Inchiquin ($\delta^{18}O$), Star Carr (T_{Jul} and $\delta^{18}O$), Crudale Meadow (T_{Jul}), Amersee ($\delta^{18}O$), Mondsee ($\delta^{18}O$) (Figure 10.6). There is however a slight difference in the gradual trend prior to the abrupt decline with many T_{Jul} and $\delta^{18}O$ records showing increasing values rather than declining values as seen in NGRIP $\delta^{18}O$. It should be noted that the changes in T_{Jul} which make up the "W" structure described here are within the errors of the WA-PLS models. However, as the "W" structure is seen in multiple T_{Jul} records and in $\delta^{18}O$ across a large geographic area, it suggests that this is an actual response to temperature change. Some records however do no display a "W" structure during the 14 ka BP ACE (e.g., Abernethy Forest, Muir Park Reservoir), though this could be due to low stratigraphic resolution and the relatively coarse sampling resolution of 1cm averaging out subtle changes in T_{Jul}.

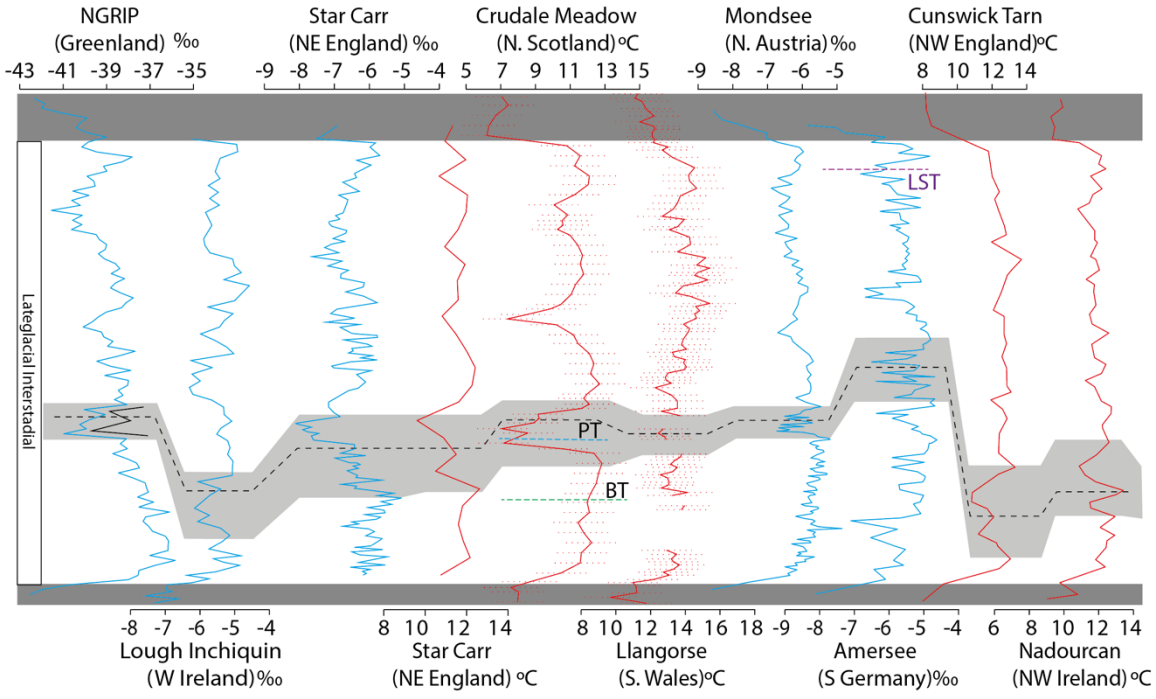

Figure 10.6, Comparison of the structure of the *c.* 14.0 ka BP ACE in sites from the British Isles and Continental Europe. The light grey shaded area denotes the abrupt decline of the event. The dotted line marks the brief increase in $\delta^{18}O$ and T_{Jul} values during the event. Dashed green line = Borrobol Tephra, dashed blue line = Penifiler Tephra, dashed purple line = Laacher See Tephra.

10.3.3 Magnitude of the c. 14.0 ka BP ACE

Chironomid-Inferred mean July air temperatures (T_{Jul})

In the British Isles, more northerly sites (56-59 °N) experience a great magnitude of cooling during the 14.0 ka BP ACE, with an amplitude of at 5.4 °C at Crudale Meadow 4.4 °C, at Loch Ashik (Brooks *et al.,* 2011) and 3.5 °C at Muir Park Reservoir (Brooks et al., 2016). Sites to the south experience a much smaller magnitude of cooling of only a few degrees centigrade, e.g., 2 °C, 2 °C and 1 °C at Llangorse, Hawes Water (Lang *et al.,* 2010) and Fiddaun (Van Asch *et al.,* 2012a), respectively. The magnitude of T_{Jul} change during the *c.* 14.0 ka BP ACE has a strong relationship with latitude with an r^2 of 0.76 (Figure 10.7a). When the magnitude of the ACE is compared to longitude, there is a moderate degree of correlation with sites further west, e.g., Fiddaun and Nadourcan, only experiencing 1-2 °C of cooling while those further east experience greater, but more variable, declines in temperature of between 2 - 5.6 °C. The larger range of magnitudes further east is likely due to the greater coverage of sites latitudinally for which there is a strong correlation with event magnitude. There appears to be little correlation between the magnitude of the *c.* 14.0 ka BP event and altitude (r^2 = 0.13). Overall, the magnitude of the 14.0 ka BP ACE is most strongly felt in the NE and decreases to the SW in the British Isles (Figure 10.8).

When the magnitude of the *c*. 14.0 ka BP ACE is compared to latitude, longitude, and altitude for continental Europe on its own, there appear to be no clear trends (Figure 10.7b). This may be due to the paucity of records which have the chronological precision and sampling resolution to accurately record the event in continental Europe meaning. However, when the data from the British Isles and the continental sites are combined, trends in the data become clearer (Figure 10.7c). The correlation between event magnitude and latitude is still strong (r^2 = 0.76) with sites below 55 °N, mainly from continental Europe, having minimal expression of generally 1-2 °C, and those above 55 °N have a magnitude greater than 2 °C. When magnitude is compared to longitude, correlation is also rather weak (r^2 = 0.27), but it can be discerned that the magnitude increases from *c*. 1 °C to 6 °C between 10 °W and 2 °W, and then declines further east to only being 1-2 °C between 4 °E to 10 °E. It is noted that there is a large gap in records between 0 °E and 4 °E in which more sites are needed to confirm this trend.

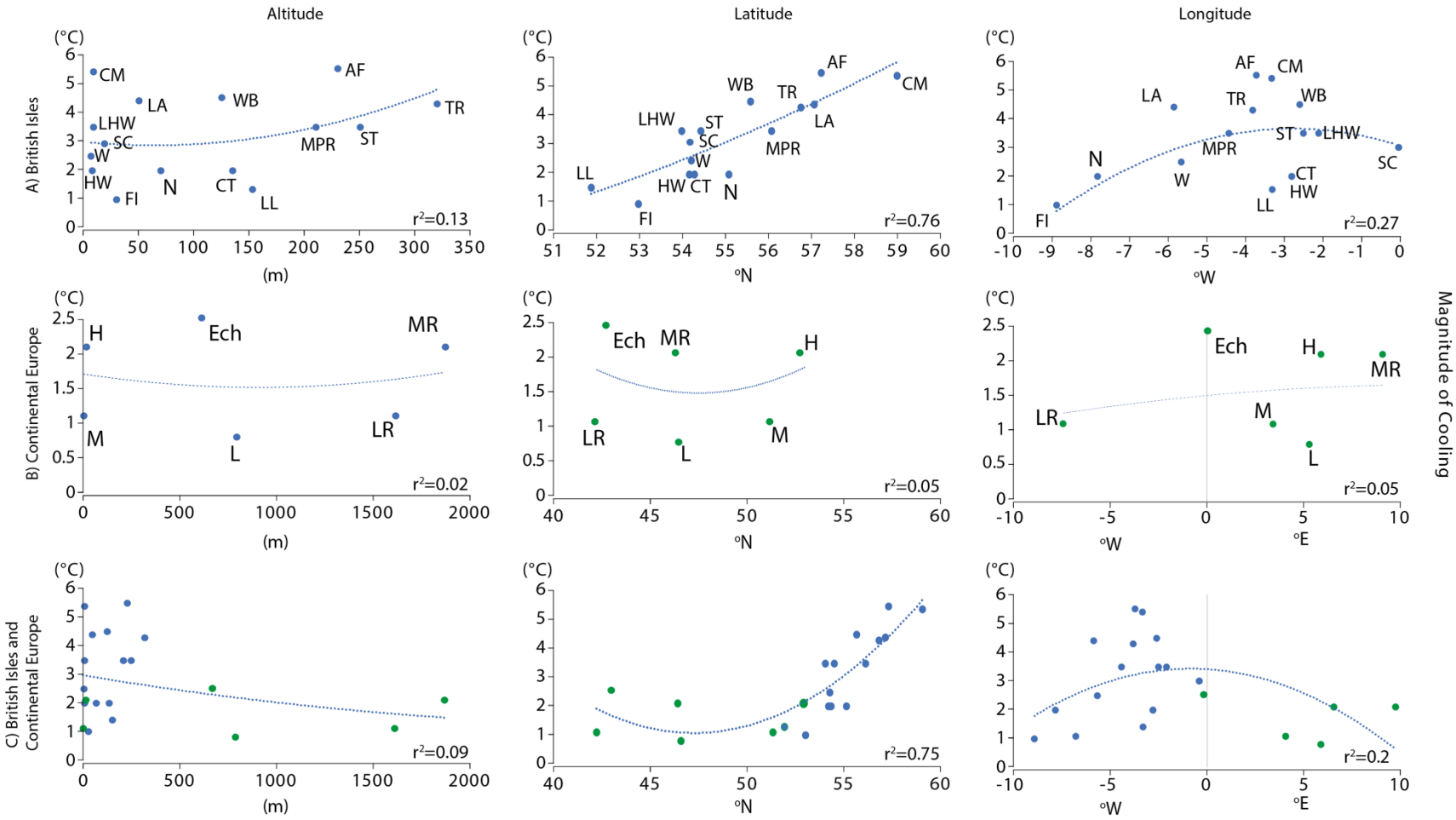

Figure 10.7, Magnitude of cooling for the *c.* 14.0 ka BP ACE in T_{Jul} compared to altitude, latitude and longitude from the (**a**) British Isles, (**b**) Continental Europe, and (**c**) the British Isles and continental Europe combined with blue circles denoting sites from the British Isles and green circles denoting sites from Continental Europe.

Figure 10.8, Magnitude of the 14.0 ka cal BP ACE in the British Isles represented by proportional circles displaying greater magnitude in the NE, which declines further south and west.

Oxygen isotopes and Mean Annual Temperature ($\delta^{18}O$/MAT)

There is strong correlation between the magnitude of the *c.* 14.0 ka BP event in $\delta^{18}O$ and altitude (r^2 = 0.88) with the largest magnitudes recorded at higher altitudes (Figure 10.9a) when analysing the records from the British Isles in isolation. However, the regression is strongly influenced by clustering in the sites with Lundin Tower and Tirinie situated at 247 and 320 m a.s.l, respectively, while five other sites lay 0-50 m a.s.l. More sites are needed between 50-350 m a.s.l to confirm this trend. Magnitude in $\delta^{18}O$ also displays a strong correlation when compared to latitude (r^2 = 0.73) with larger declines in $\delta^{18}O$ at 56-57 °N and smaller declines to the south and north. There appears to be no correlation between event magnitude and longitude.

There appears to be little correlation between the magnitude of the *c.* 14.0 ka BP ACE in $\delta^{18}O$ and Altitude, latitude, and longitude (Figure 10.9b) when analysing the records from continental Europe in

isolation. This is potentialy due to the restricted spread of sites along the spatial gradients as they are concentrated in the Alpine region occurring within 200 metres altitudinally, 3 degrees latitudinally and 3 degrees longitudinally of each other. This displays the need for more $\delta^{18}O$ records from continental Europe, however, there are relatively few $CaCO_3$ precipitating basins outside of the alpine region and those that have been studied are affected by detrital contamination (e.g., FGW, Klein Ven; Van Ash *et al.,* 2012b, c). One potential way of reconstructing $\delta^{18}O$ in basins where authigenic precipitated carbonates are not present, is by obtaining $\delta^{18}O$ values from chironomid head capsule chitin (e.g., Wooller *et al.,* (2004); Verbruggen *et al.,* (2010; 2011); Lombino (2021a, b).

When the magnitude in $\delta^{18}O$ for the *c.* 14.0 ka BP ACE is compared with the British Isles and continental Europe combined, there appears to be little corelation with Altitude and Longitude (Figure 10.9c). However, Lago Piccolo and Faulenseemoos are potential outliers and reduce the correlation coefficient. If the data points from these two records are removed, then there does appear to be a greater decline in $\delta^{18}O$ at higher altitudes, *c.* 2‰ above 250 metres, and *c*. 1-1.5 ‰ below 50 metres, suggesting amplification of the cooling with greater altitude (Pepin *et al.,* 2015). When the magnitude in $\delta^{18}O$ is compared to latitude, a polynomial curve has much greater fit than a linear or unimodal regression line, with greater magnitude occurring at *c*. 47and 57 °N, and lower magnitude at *c*. 45, 53 and 60 °N. More records are needed to further confirm this trend as it is currently influenced by several clusters of data points.

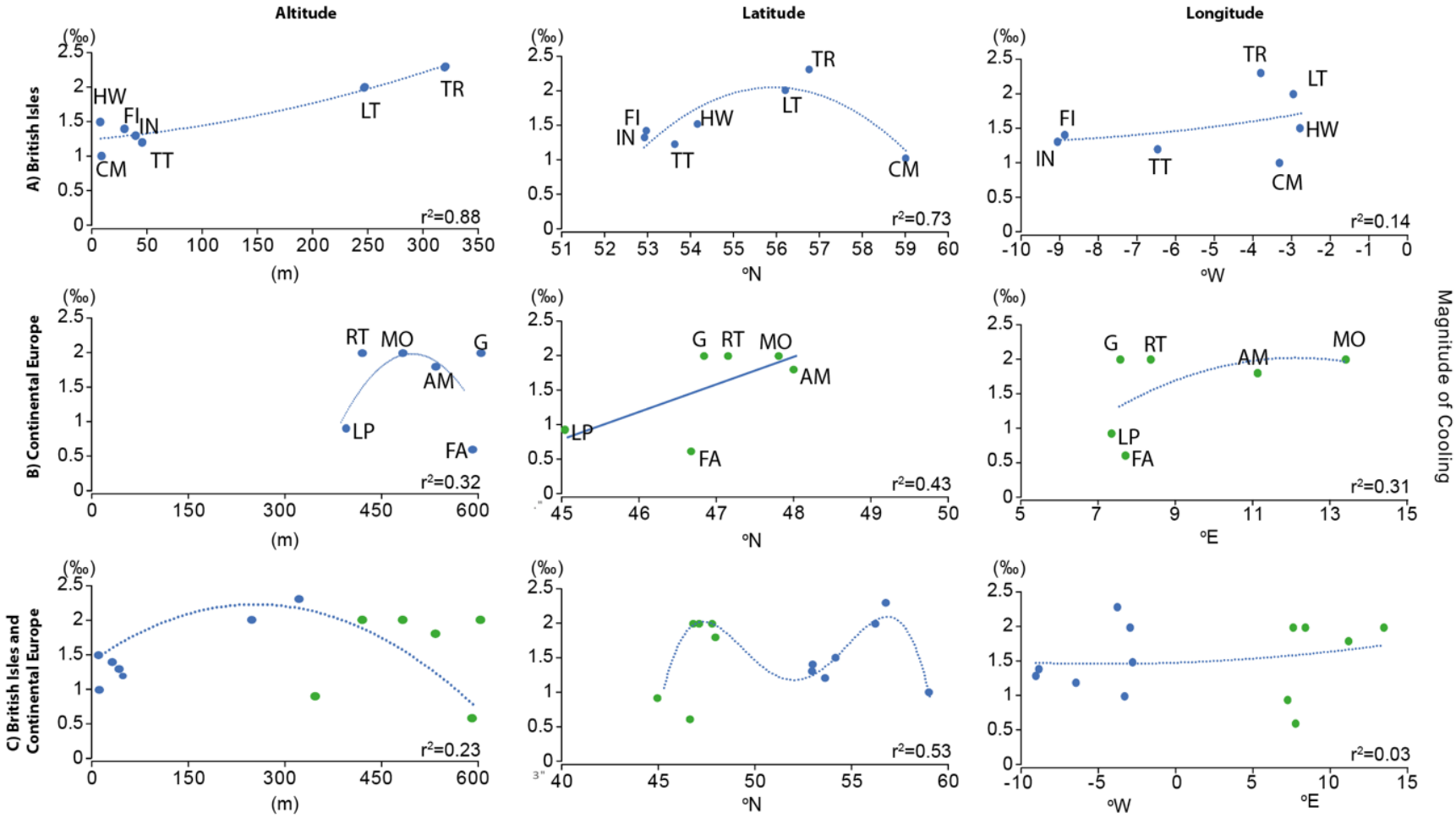

Figure 10.9, Magnitude of cooling for the *c.* 14.0 ka BP ACE in $\delta^{18}O$ compared to Altitude, Latitude and longitude from (A) the British Isles, (B) Continental Europe, and (C) the British Isles and continental Europe combined with blue circles denoting sites from the British Isles and green circles denoting sites from Continental Europe.

10.3.4 Forcing mechanisms of the c. 14.0 ka BP ACE

Oceanic forcing

The ACEs during the LGIS have often been attributed to disruption of the thermohaline circulation by meltwater discharge from one of the continental ice sheets (Clark et al., 2001; Nesje et al., 2004; Donnelly et al., 2005). In the NE Atlantic, there is limited evidence for a meltwater pulse occurring at *c.* 14.0 ka BP. This may be due to the stratigraphic resolution of oceanic cores meaning any signal of a meltwater event is smoothed out and/or the low sampling resolution may not have picked out the event. It is still however possible that a meltwater pulse did occur in the NE Atlantic, in the Nordic Seas, as proposed for the YD (Muschitiello *et al.,* 2015a, b; 2019). There is, however, evidence for a meltwater pulse from the NW Atlantic with a decline in sea surface temperatures and a decline in the $\delta^{18}O$ of seawater (Figure 10.10) (Obbink *et al.,* 2010). The spatial expression of the cooling in T_{Jul} records described here suggests that there was a strong oceanic forcing which had greatest impact in the NE of the British Isles, around the northern and eastern margins of Scotland in the North Sea. As there is a lack of evidence for a meltwater event in the NE Atlantic it is suggested that a reduction in AMOC occurred in the North Atlantic, potentially due to meltwater from the Laurentide ice sheet. As a result, the whole North Atlantic cools and allows extensive persistent sea ice formation in the North/Nordic seas, in effect causing NE Britain to have a more continental climate, magnifying the cooling, and subject to the extension of polar air masses (Li *et al.,* 2010; Dokken *et al.,* 2013; Singh *et al.,* 2014). Although this mechanism largely occurs in the winter months, it would also impact summer temperatures as persistent sea ice would lead to shorter colder summers. The relative warmth of the North Atlantic and oceanic nature of Ireland, along with the predominance of westerly winds, may have helped limit the expression of cooling in Britain to Scotland and Northern England. Changes in extent of sea ice in the North Sea, due to changes in meltwater flux from the Laurentide ice sheet in the NW Atlantic, may cause oscillations within event.

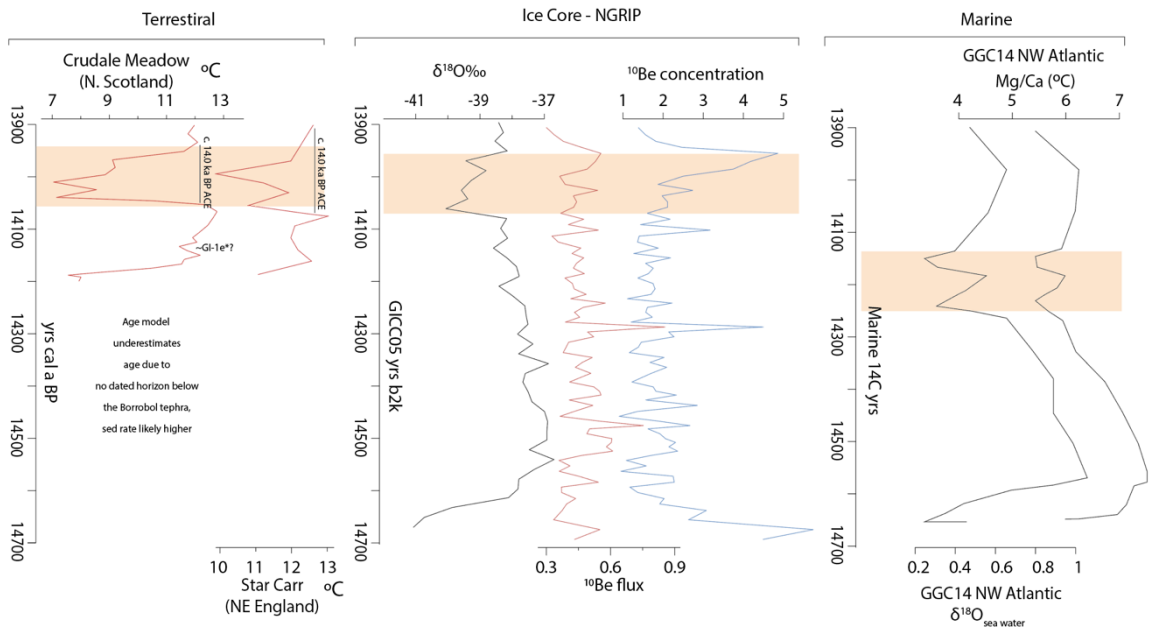

Figure 10.10, Changes seen in T_{Jul} records for the c. 14.0 ka BP ACE and climate forcing proxies, including ^{10}Be record from NGRIP and ocean circulation proxies. NGRIP data from Rasmussen *et al.* (2014). ^{10}Be data from Adolphi *et al.* (2014). Marine proxy data from Obbink *et al.* (2014) with the 14.0 ka BP ACE appearing to occur earlier in the marine proxies due to the marine radiocarbon reservoir offset.

Solar forcing

Although the large magnitude of decline in T_{Jul} and $\delta^{18}O$ for the *c.* 14.0 ka BP ACE is most likely driven by oceanic forcing (see above), it is possible that solar forcing may have had an influence on temperature changes as well (Figure 10.10). Adolphi *et al.,* (2014) inferred changes in solar activity using the cosmogenic nuclide ^{10}Be recorded in NGRIP. A large increase in ^{10}Be is also observed at the end of the *c*. 14.0 ka BP event potentially contributing to the abrupt rise in temperature at the end of the event.

10.4 The mid-LGIS

A clear mid-LGIS ACE is seen in the Greenland ice cores, termed GI-1cii, and has often been correlated to declines in $\delta^{18}O$ and T_{Jul} during the mid-LGIS (Figure 10.11). However, T_{Jul} and $\delta^{18}O$ records covering the mid-LGIS often have low sampling resolution and limited chronological constraint. This is because the mid-LGIS ACE is commonly thought as having (i) a short duration of *c.*60yrs, too short to be recorded in enough detail stratigraphically in terrestrial lake sequences, and (ii) a small magnitude of 1°C, close to the predictive powers of the WAPLS models. Therefore, efforts have been concentrated on identifying and defining the *c*. 14.0 ka BP and 13.2 ka BP ACEs instead.

The notion that GI-1cii is an event of short duration and magnitude may come from its expression in the GRIP and GISP2 records where it has a duration of *c*. 60 yrs and a magnitude of 2‰ and 1.5‰, respectively. However, in the NGRIP $\delta^{18}O$ record the GI-1cii event has a much larger expression of 2.3 ‰ and a duration of *c.* 220yrs. It should also be noted that other declines in $\delta^{18}O$ in Greenland occur during the mid-LGIS, most notably three are seen during GI-1ciii. In NGRIP these date to 13.78, 13.84 and 13.94 GICC05 kyrs B2k and have magnitudes of *c*. 1.3 ‰, 1 ‰ and 0.6 ‰ respectively, which are marked with an asterisk (*) in Figure 10.11. Although these events in GI-1ciii are of short duration and unlikely to be represented in many $\delta^{18}O$ and T_{Jul} of terrestrial lake sequences, sequences which have a very high sedimentation rate during the mid-LGIS may record them which could result in miscorrelation between ACEs of the Mid-LGIS. Erroneous correlations could also be made with the Early-LGIS ACE at *c*. 14.0 ka BP when only a small magnitude is expressed. For example, at Cunswick Tarn, a small event of 1 °C is correlated to GI-1d/*c*.14.0 ka BP ACE but may actually relate to a mid-LGIS temperature decline. Potential expression and correlation of these events in high-resolution T_{Jul} and $\delta^{18}O$ records are highlighted in Figure 10.12.

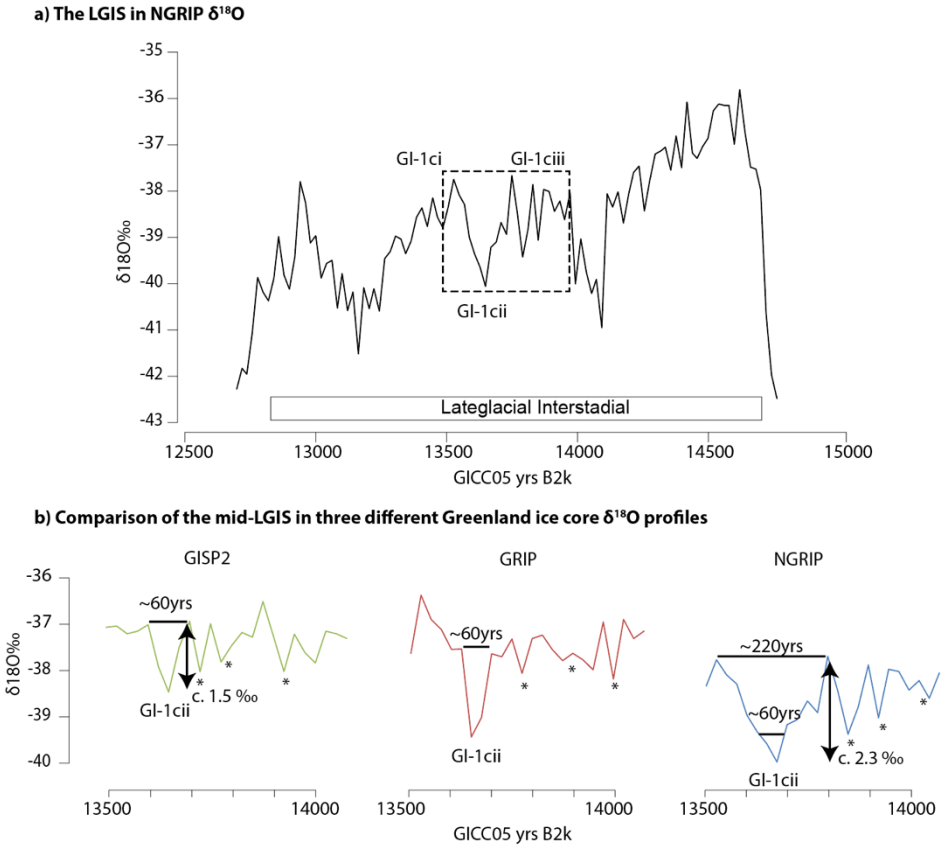

Figure 10.11, Comparison of the mid-LGIS (*c.* 14.7-13.9 GICC05 kyrs b2k) in Greenland $\delta^{18}O$ records. A) $\delta^{18}O$ from NGRIP, b) comparison of the structure of GI-1cii in GISP2, GRIP and NGRIP (Rasmussen *et al.,* 2014).

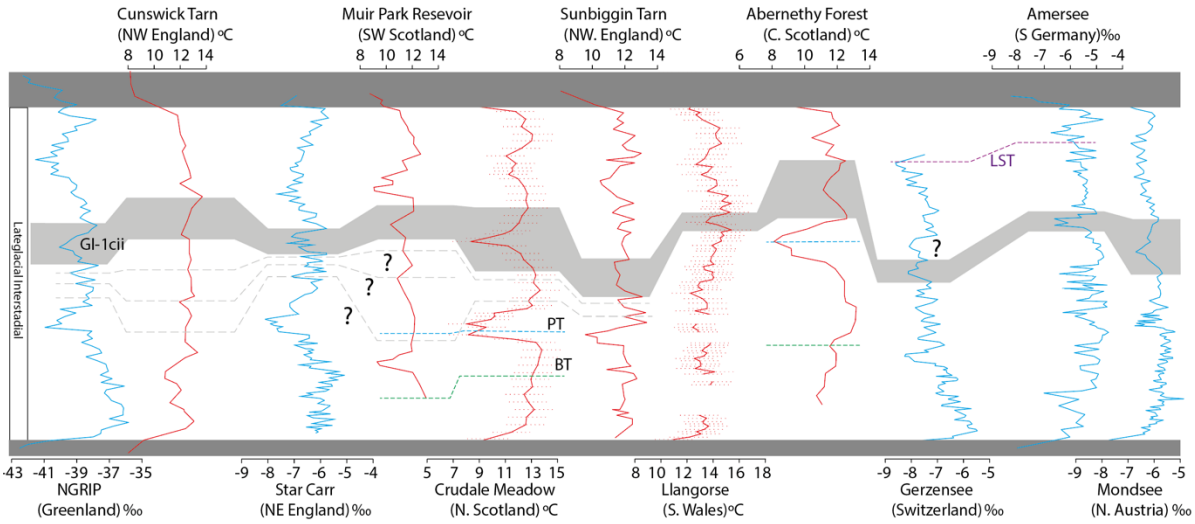

Figure 10.12, Mid-LGIS ACEs in T_{Jul} and lacustrine $\delta^{18}O$ records which are often correlated to GI-1cii, denoted by the light grey shading. Dash grey lines and question marks note the potential occurrence of other temperature declines during the Mid-LGIS. Dashed green line = Borrobol Tephra, dashed blue line = Penifiler Tephra, dashed purple line = Laacher See Tephra.

Details on the number of temperature declines recorded in T_{Jul} and $\delta^{18}O$ from the British Isles are given in tables 10.5 and 10.6, respectively, and Continental Europe, in Tables 10.7 and 10.8, respectively. The mid-LGIS is defined as occurring between the end of the 14.0 ka BP ACE and the start of the 13.2 ka BP ACE. Due to the issues surrounding chronological uncertainties, as multiple declines in temperature occur, and potentially low sampling resolution which may not adequately characterise the temperature changes during the mid-LGIS, comparisons between event magnitude with altitude, longitude and latitude cannot be made. The clearest expression of a mid-LGIS ACE with good chronological constraint comes from Llangorse where a decline of 2 °C in T_{Jul} occurs at *c.* 13.5 ka BP, and Crudale Meadow, where a 3.9 °C decline in T_{Jul} and a 0.7 ‰ decline occurs in $\delta^{18}O$ at *c.* 13.6 ka BP. Both of which are within dating errors of each other. A clear well-dated mid-LGIS ACE is also present in the Abernethy Forest T_{Jul} record showing 2.3°C cooling at 13.6 ka BP, similar in magnitude to the 13.2 ka BP ACE expressed in the same record. The occurrence of a Mid-LGIS event at Crudale Meadow, Llangorse and Abernethy Forest at *c.* 13.6 ka BP suggests this is the same event and coeval with GI-1cii in Greenland. Moreover, the *c.*13.6 ka BP ACE in these records at least, appears to be a significant event. A number of other sites identify a mid-LGIS ACE and suggest a broad correlation to GI-1cii, however, the events are often defined by few data points, the sequences lack chronological constraint and many also exhibit other cold declines in the mid-LGIS, e.g., the Cumbrian lakes (Lang *et al.,* 2010), Muir Park Reservoir (Brooks *et al.,* 2016), Nadourcan (Watson *et al.,* 2010) and Inchiquin (Diefendorf *et al.,* 2006).

Mid-LGIS ACEs in many T_{Jul} records from continental Europe are not as easily observed as in Britain and Ireland due to the low sampling resolution employed at many sites, or for $\delta^{18}O$, due to other influences

other-than-temperature on the $\delta^{18}O$ signal. However, the records with high sampling resolution do display variability during the mid-LGIS which may relate to the GI-1cii event and the other temperature declines during the Mid-LGIS but more definitive correlation is precluded due to the reliance on climatostratigraphy, e.g., Gerzensee ($\delta^{18}O$ and T_{Jul}), Amersee ($\delta^{18}O$) and Mondsee ($\delta^{18}O$). More precise age estimates allow the dating of mid-LGIS ACEs at Moervaart (T_{Jul}) and Lago Piccolo di Avigliana (T_{Jul} and $\delta^{18}O$) to 13.7 and 13.4 ka BP, respectively, though few data points represent the events in the T_{Jul} records.

Table 10.5, ACEs and declines in temperature observed during the mid-LGIS in T_{Jul} records from the British Isles. **Bold** font indicates an event attributed to GI-1cii in Greenland in their original publication. When numerous oscillations in T_{Jul} or $\delta^{18}O$ defined by only 3 data point occur, this is described as 'variability'.

Site	No. mid-LGIs ACEs	No. of samples defining event	Chronological control. and Age estimate	Magnitude of ACE(s)	Refence
Quoyloo Meadow	No	low res			Timms *et al.,* 2021
Crudale Meadow	Yes (1)	**14**	**13.6 ka BP**	**3.9°C**	Francis *et al.,* 2021; this thesis
Abernethy Forest	Yes (1)	**12**	**13.6ka BP**	**2.3°C**	Brooks *et al.,* 2012
Loch Ashik	Possibly				Brooks *et al.,* 2012
Tirinie	No	low res			Abrook *et al.,* 2020
Muir Park Reservoir	Yes (2)	5 5	climatostratigraphy	2°C 1.5°C	Brooks *et al.,* 2016
Whitrig Bog	Yes (1)	**8**	**climatostratigraphy**	**1.6°C**	Brooks and Birks, 2000
Nadourcan	variability				Watson *et al.,* 2010
Sunbiggin Tarn	Yes (2) And variability after events – start of 1b?	**7** 4	climatostratigraphy	**1.7°C** 1.9°C	Lang *et al.,* 2010
Cunswick Tarn	3	**7** 4 4	climatostratigraphy	**0.6°C** 1°C 1°C	Lang *et al.,* 2010
White bog	Not Analysed				O'Neill-Munro, 2017
Urswick Tarn	Yes (1), Variability before	**4**	climatostratigraphy	**0.7°C**	Lang *et al.,* 2010
Hawes Water	Yes (1)	**3**	climatostratigraphy	**0.5°C**	Lang *et al.,* 2010
Little Hawes Water	Yes (3)	4 **4** 3	climatostratigraphy	1°C **0.4°C** 1°C	Lang *et al.,* 2010
Star Carr	Yes (1)	5	climatostratigraphy	1.7°C	Abrook (2019); Blockley *et al.,* 2018
Thomastown	Yes (1)	**3**	climatostratigraphy	**1.8°C**	Turner *et al.,* 2015
Fiddaun	Yes (1)	6	climatostratigraphy	1°C	Van Asch *et al.,* 2012a
Llangorse	Yes (1)	**6**	**13.5 ka BP**	**2°C**	Palmer *et al.,* in prep; This Study

Table 10.6, ACEs and declines in temperature observed during the mid-LGIS in $\delta^{18}O$ records from the British Isles. **Bold** font indicates an event attributed to GI-1cii in Greenland in their original publication. When numerous oscillations in T_{Jul} or $\delta^{18}O$ defined by only 3 data point occur, this is described as 'variability'.

Site	No. mid-LGIs ACEs	No. of samples defining event	Chronological control. and Age estimate	Magnitude of ACE(s)	Refence
Crudale Meadow	Yes (2)	**5** 6	**13.6 ka BP** 13.8ka BP	**0.7‰** 0.4‰	Francis *et al.,* 2021; this thesis
Tirinie	Yes (1)	**5**	**13.7 ka BP**	**1.5‰**	Abrook *et al.,* 2020; Candy *et al.,* 2016
Lundin tower	Yes (1)	5	climatostratigraphy	0.8‰	Whittington *et al.,* 1996
Hawes Water	Yes (1)	**9**	climatostratigraphy	**1‰**	Marshal *et al.,* 2002
Star Carr	Yes (3)	9 8 5	climatostratigraphy	1.5‰ 1.3‰ 1‰	Abrook (2019); Blockley *et al.,* 2018
Thomastown	Variability				Turner *et al.,* 2015
Fiddaun	Yes	**6**	Climatostratigraphy	**0.7‰**	Van Asch *et al.,* 2012a
Inchiquin	Yes (4) plus variability after	5 7 **11** 5	climatostratigraphy	0.8‰ 1‰ **1.3‰** 0.5‰	Diefendorf *et al.,* 2006
Tory Hill	variability				O'Connell *et al.,* 1999
Lough Gur	No	low res			Ahlberg *et al.,* 1997
Red Bog	No	low res			Ahlberg *et al.,* 1997

Table 10.7, ACEs and declines in temperature observed during the mid-LGIS in $\delta^{18}O$ records from continental Europe. **Bold** font indicates an event attributed to GI-1cii in Greenland in their original publication. When numerous oscillations in T_{Jul} or $\delta^{18}O$ defined by only 3 data points or fewer occur, this is described as 'variability'.

Site	No. mid-LGIs ACEs	No. of samples defining event	Chronological control. and Age estimate	Magnitude of ACE(s)	Refence
Jansvatnet	N/A				Birks *et al.,* 2012
Kråkenes	N/A				Brooks and Birks, 2001
Myklevatnet	N/A				Nesje *et al.,* 2014
Hässeldala port	variability				Wohlfarth *et al.,* 2017
Friedlander Grosse Wiesse		Low res			Van Asch *et al.,* 2012b
Hijkermeer		Low res			Heir *et al.,* 2011
Żabieniec		Low res			Plociennik *et al.,* 2011
Klein Ven		Low res			Van Asch *et al.,* 2013
Moervaart	Yes (1)	**5**	**13.7 ka BP**	**2°C**	Van Bos *et al.,* 2017
Egelsee		Low res			Larocque-Tobler *et al.,* 2010
Gerzensee	variability	**10**	climatostratigraphy	**3°C**	Lotter *et al.,* 2012
Lac Lautrey	variability				Heiri and Millet, 2005
Foppe		Low res			Samartin *et al.,* 2012
Maloja Pass	Yes (1)	**3**	climatostratigraphy	**0.5°C**	Ilyashuk *et al.,* 2009
Lago Piccolo di Avigliana	Yes(1)	**3**	**13.4 ka BP**	**0.8°C**	Finsinger *et al.,* 2008
Ech	Yes (2)	4 **4**	climatostratigraphy	0.5°C **2°C**	Millet *et al.,* 2012
Laguna de la Roya	Variability				Munoz Sobrino *et al.,* 2013

Table 10.8, ACEs and declines in temperature observed during the mid-LGIS in $\delta^{18}O$ records from continental Europe. **Bold** font indicates an event attributed to GI-1cii in Greenland in their original publication. When numerous oscillations in T_{Jul} or $\delta^{18}O$ defined by only 3 data points or fewer occur, this is described as 'variability'.

Site	No. mid-LGIs ACEs	No. of samples defining event	Chronological control. and Age estimate	Magnitude of ACE(s)	Refence
Amersee	Yes (1) Variability also	>14	climatostratigraphy	2‰	Von Grafenstein *et al.,* 1999b
Mondsee	Yes (1) variability also	>14	climatostratigraphy	1‰	Lauterbach *et al.,* 2011
Rotsee	Variability	Low res			Verbruggen *et al.,* 2010
Gerzensee	Yes (many) Too many to mention	**5**	climatostratigraphy	**2‰**	Lotter *et al.,* 2012
Faulenseemoos	Yes (2)	4 3	climatostratigraphy	0.3‰ 0.4‰	Eicher and Siegenthaler, 1976; Lotter *et al.,* 1992
Aegelsee (Core AE-3)	Variability	Low res			Wellington and Lotter, 1999; Lotter *et al.,* 1992
Leysin	Not analysed				Schwander *et al.,* 2000
Lago Piccolo di Avigliana	Yes (1)	**>10**	**13.4 ka BP**	**1‰**	Larocque and Finsinger, 2008

10.5 Late-LGIS ACE

A large ACE occurs during the latter part of the LGIS in the Greenland ice cores, termed GI-1b, with a duration of *c*. 212 years in the GICC05 timescale and a magnitude of *c.* 2 ‰ in NGRIP (Figure 10.13). However, using the expanded definition of an ACE outline in section 10.1, which would include the preceding warm period of GI-1ci, and part of the proceeding GI-1a, the event duration becomes much longer at *c*. 580 years and the magnitude greater at *c*. 3.5‰ (Figure 10.13).

10.5.1 Identifying the c. 13.2 ka BP ACE

Identifying the ACE that occurs late in the LGIS in the British Isles is less certain than the early LGIS ACE at *c.* 14.0 ka BP as there are no dated tephra horizons found in association with the event. The Crudale Meadow and Llangorse proxy records provide an age estimate for the Late LGIS ACE of 13.5-13.0 ka BP and 13.4-13.1 ka BP, respectively, with minimum T_{Jul} and $\delta^{18}O$ values occurring at *c.* 13.2 ka BP. The chronology from Fiddaun, based on four radiocarbon dates, suggests an age of 12.8-13.3 ka BP for the late-LGIS ACE. Similarly, the model from Tirinie, constructed using the Vedde Ash, Penifiler tephra and a radiocarbon date near the end of the LGIS, gives an age estimate of 13.5-13.1 ka BP for the event. Llangorse, Crudale Meadow, Fiddaun and Tirinie have the best chronological constraint for the latter part of the LGIS in the British Isles and suggests minimum temperatures occurred at *c.* 13.2 ka BP for the Late-LGIS ACE and will thus be referred to as such. It should be noted though that some sites do provide a slightly different age estimate for when minimum temperatures occurred during the Late-

LGIS ACE e.g., Abernethy Forest (13.5 ka BP) and at Loch Ashik (13.7 ka BP), though these older ages are attributed to fewer dated horizons late in the LGIS (Brooks *et al.,* 2012). For sites which lack chronological constraint in the latter part of the LGIS either due to few dated stratigraphic layers, e.g., the Cumbrian lake sites (Lang *et al.,* 2010), Whitrig Bog (Brooks and Birks, 2000), Muir Park Reservoir (Brooks *et al.,* 2016), or have radiocarbon dates affected by hardwater error, e.g. Lough Inchiquin (Diefendorf *et al.,* 2006) and Nadourcan (Watson *et al.,* 2010), an event late in the Late-LGIS can still be identified due to the clear structure of events allowing climatostratigraphy to be used. Therefore, the events identified in the Late-LGIS here are considered broadly coeval for the purpose of this thesis. As stated in section 10.2, ideally radiocarbon dating and tephrochronology should be applied to confirm these ACEs all relate to the same event, but we can be reasonably confident given the event at 13.2 ka BP is the last event of the LGIS, the clear structure of temperature change in the LGIS with remarkable similarity to $\delta^{18}O$ in the Greenland ice cores (Rasmussen *et al.,* 2006; 2014).

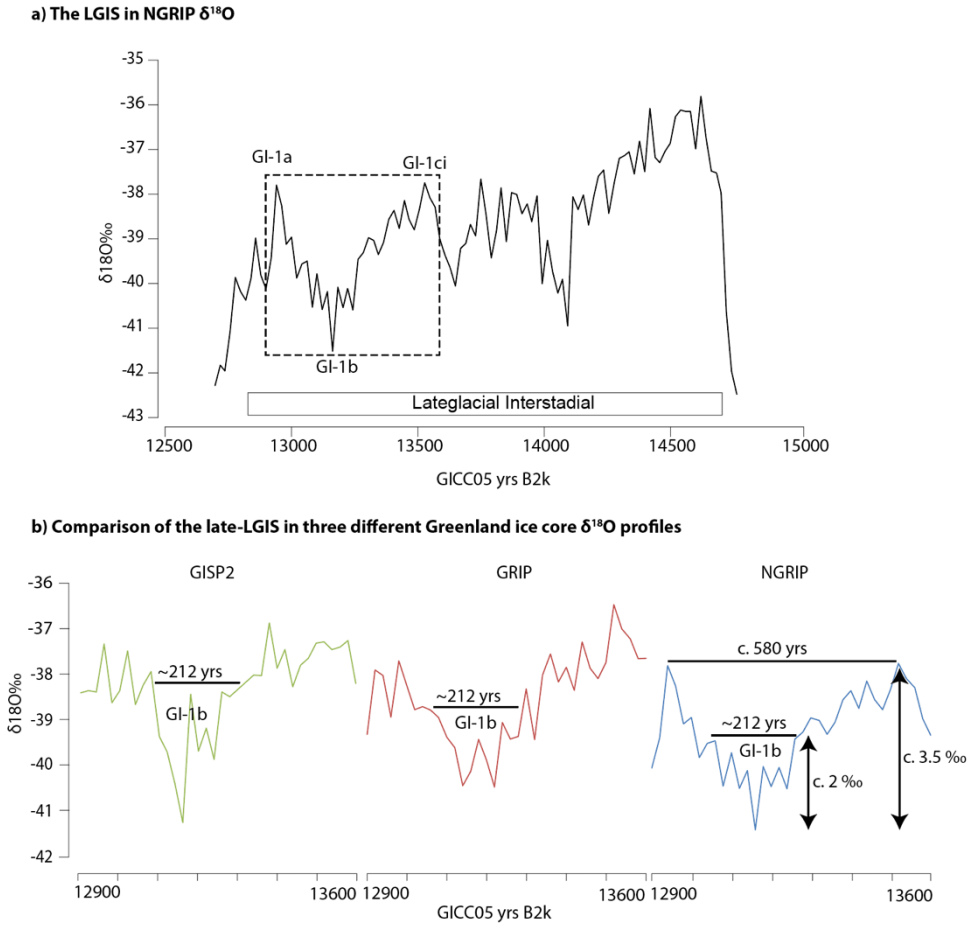

Figure 10.13, Comparison of the late-LGIS ACE (*c.* 13.6 – 12.95 GICC05 kyrs b2k) in Greenland ice cores. **a**) NGRIP $\delta^{18}O$ plotted against the GICC05 timescale with event names marked on. The isotope record encompassed by the dotted line is expanded in (B) for each of the three Greenland ice cores. **b**) $\delta^{18}O$ record for the Early LGIS from GISP2, GRIP and NGRIP. NGRIP has a comparison of event magnitude/duration as defined in GICC05 with that defined by the expanded definition used in this thesis.

For sites situated in continental Europe, the identification of the Late-LGIS ACE can be made with greater certainty due to the widespread distribution of the Laacher See Tephra which is positioned just after minimum values in T_{Jul} and $\delta^{18}O$ are attained (e.g., Amersee, Faulenseemoos, Gerzensee). The last ACE of the LGIS at Jansvatnet is bracketed by two radiocarbon dates, giving an age estimate of 13.24-13.48 ka cal BP for the event. In Ech, a radiocarbon date with an age of 12.89 – 13.39 ka cal BP conducted on charcoal occurs immediately after the last ACE in the T_{Jul} record, suggesting it broadly correlates to the *c*. 13.2 ka BP ACE. Hijkermeer, Mondsee and Leysin, all rely on pollen- and isotope-stratigraphy to date the LGIS ACE at *c*. 13.2 ka, but their temperature proxy records all exhibit a clear structure of events in the LGIS meaning miscorrelation of the final LGIS ACE is unlikely.

Due to the retreat of the Laurentide ice sheet, exposing topographic hollows for lake sedimentation to occur, the expression of the late-LGIS ACE can also be studied in NE North America. It should be noted that these records were some of the first quantified chironomid temperature estimates to be produced, using less sophisticated Weighted Averaging models, relatively coarse taxonomic resolution, and modern single point water temperature measurements in the calibration datasets (Brooks *et al.,* 2007). As a result, temperature estimates for the North American sites may not be as refined as more recently completed T_{Jul} records from Europe. Nevertheless, the magnitude of events is unlikely to be drastically differen. The Killarney oscillation, broadly coeval to GI-1b and the 13.2 ka BP event, was identified in seven sequences (Figure 10.19). The N. American sequences are also relatively well dated with several AMS radiocarbon dates on terrestrial plant macrofossils and broadly date the Killarney oscillation to *c.* 13.2 ka BP.

10.5.2 Structure of the c. 13.2 ka BP ACE

The structure of the *c.* 13.2 ka ACE observed in NGRIP is such that, $\delta^{18}O$ undergoes a gradual decline in GI-1ci (*c.* 13.5 – 13.25 GICC05 kyrs b2k) from peak values of *c.* - 38‰ to -39.5‰ upon which variability is observed in the $\delta^{18}O$ values (Figure 10.13). At the start of GI-1b (13,311 ±149 GICC05 yrs b2k), there is an abrupt decline in $\delta^{18}O$ of *c*. 2‰ with minimum values achieved at *c*. 13.2 ka BP. A gradual increase in $\delta^{18}O$ occurs with highest values attained during GI-1a at *c.* 12.9 GICC05 kyrs b2k. In lacustrine sequences which are stratigraphically expanded during the Late-LGIS ACE a similar pattern of change can be seen in the T_{Jul} and $\delta^{18}O$ records, e.g., Llangorse (T_{Jul}), Hawes Water ($\delta^{18}O$), Abernethy Forest (T_{Jul}), Whitrig Bog (T_{Jul}), Nadourcan (T_{Jul}), Fiddaun ($\delta^{18}O$ & T_{Jul}) and Inchiquin ($\delta^{18}O$) (Figure 10.15). Although these smaller scale changes in T_{Jul} are within the errors of the WAPSL models, their occurrence in numerous T_{Jul} records and in $\delta^{18}O$ records suggests they reflect climatic temperature changes. The structure described above can also be seen in temperature records from continental Europe (Figure

10.14), e.g., Gerzensee ($\delta^{18}O$), Amersee ($\delta^{18}O$) and Mondsee ($\delta^{18}O$). However, some records display only a brief pause on the decline in temperatures e.g., Hijkermeer (T_{Jul}) and Gerzensee (pollen). This could be down to rapid changes/slowdown in sedimentation rate while temperatures decline for the *c.* 13.2 ka BP ACE.

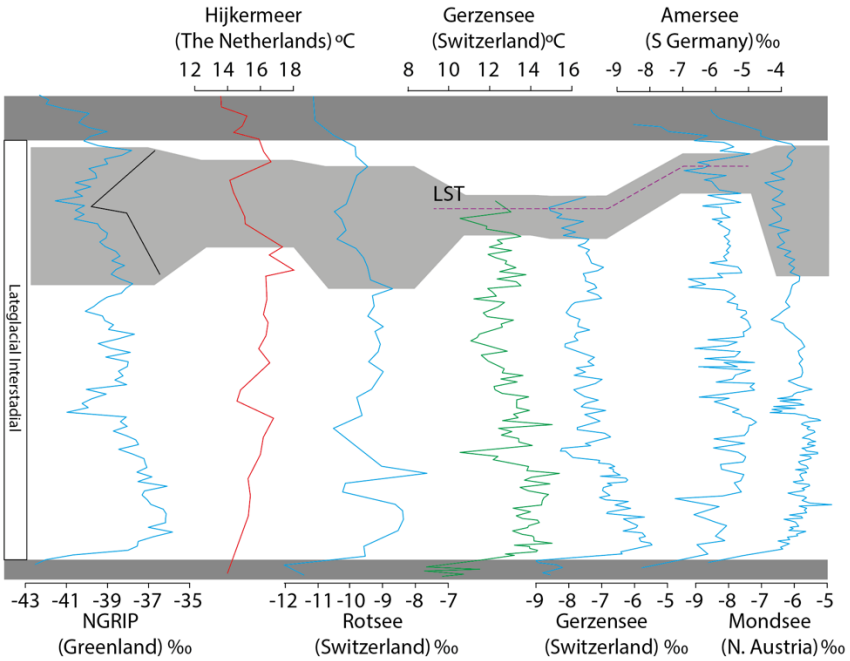

Figure 10.14, Comparison of the structure of the *c.* 13.2 ka BP ACE in T_{Ju} (red)$_I$, $\delta^{18}O$ (blue) and pollen inferred temperature (green) records from continental Europe. The light grey shading denotes the Late-LGIS ACE. Purple dashed line = Laacher See Tephra.

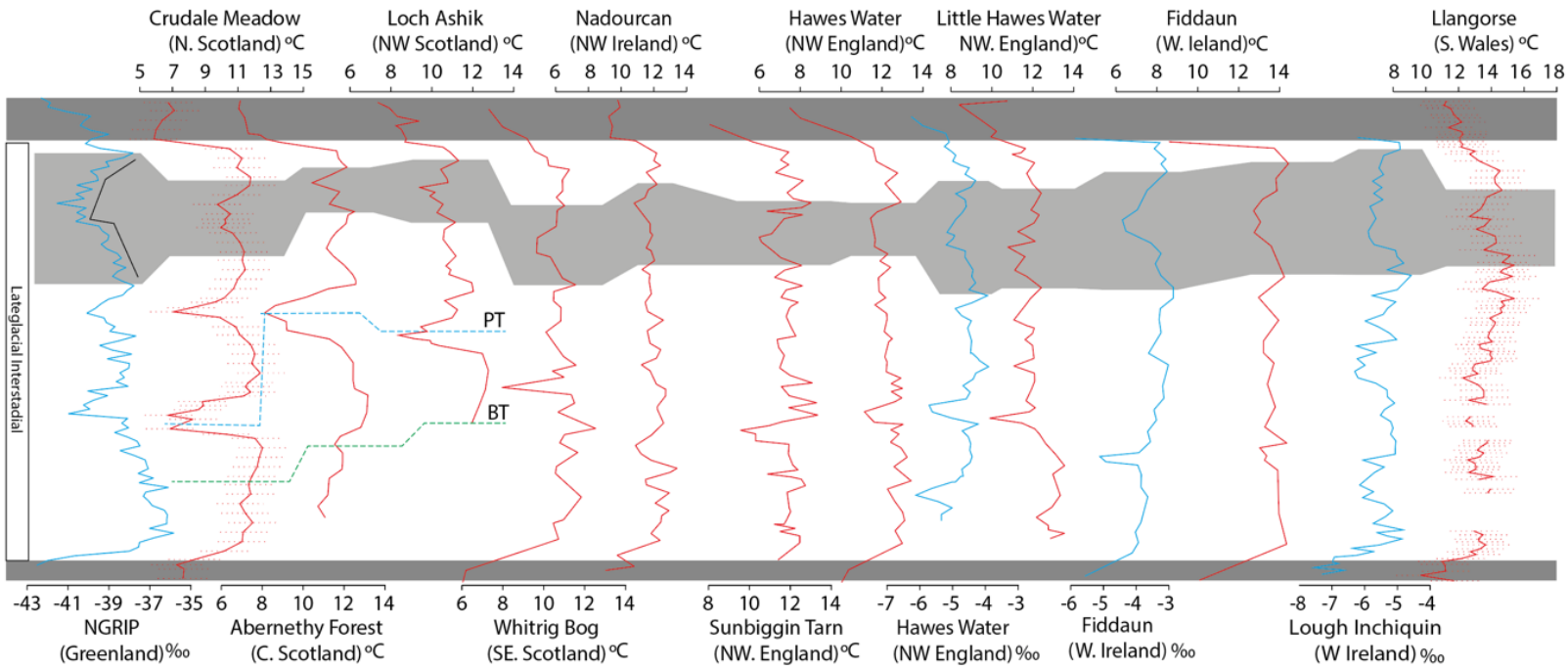

Figure 10.15, Comparison of the structure of the *c*. 13.2 ka BP ACE in T_{Jul} (red) and $\delta^{18}O$ (blue) records from the British Isles. The light grey shading denotes the Late-LGIS ACE. Blue dashed line = Penifiler tephra, Green dashed line = Borrobol tephra.

10.5.3 Magnitude of the c. 13.2 ka BP ACE

Chironomid-Inferred mean July air temperatures (T_{Jul})

In sites from Britain and Ireland, there is a strong correlation between the magnitude of the *c*.13.2 ka BP ACE and altitude (r^2 = 0.65) with sites at higher elevation experiencing a larger decline in T_{Jul} of up to 5 °C (Figure 10.16a). In continental Europe, the magnitude of T_{Jul} appears to be rather constant at *c*. 1.5 to 2 °C no matter on the altitude of the site (Figure 10.16b). Both Jansvatnet and Hijkermeer are situated at a similar altitude, however the magnitude of change at Jansvatnet is much greater and could be due to its more northerly location. When both regions are plotted together there appears to be very little relationship between the magnitude of the 13.2 ka BP ACE and altitude (Figure 10.16c). However, the T_{Jul} records from Jansvatnet, Hijkermeer and Ech agree well with T_{Jul} record from sites in the British Isles, potentially due to their more westerly and maritime locations in continental Europe.

The relationship between the magnitude of the *c*. 13.2 ka BP ACE with latitude is complex in Britain and Ireland. Magnitude decreases from 51 to 53 °N, then increases between 53 °N and 57 °N, and thereafter declines at 59 °N. However, there are few sites at the end of this trend line and the results are strongly influenced by the Crudale Meadow and Llangorse results. More data points are needed at the upper and lower latitudes of Britain to affirm the spatial trends currently observed. Sites in continental Europe display little correlation between the magnitude of the *c*. 13.2 ka ACE and latitude as the correlation is heavily influenced by Jansvatnet at 70 °N where the ACE may have been magnified or buffered by the presence of the SIS. It is likely to be difficult to produce more records covering the Late-LGIS in Scandinavia due to the persistence of the SIS. No correlation is observed when both regions are plotted together.

For Britain and Ireland, there is some corelation between the magnitude of the *c*. 13.2 ka BP ACE and longitude with sites experiencing greatest magnitude of cooling at *c*. 4 °W, and lower magnitudes to the west and east. It is hard to comment upon the relationship between the *c*. 13.2 ka BP ACE and longitude from sites in continental Europe as there is a cluster of sites between 5 and 10 °E which have large differences in altitude in the alpine region with Laguna de la Royal and Jansvatnet sitting far away at the extremes. There is also a lack of correlation when the British Isles and continental European sites are plotted together and may be due to the vast spatial differences within these regions.

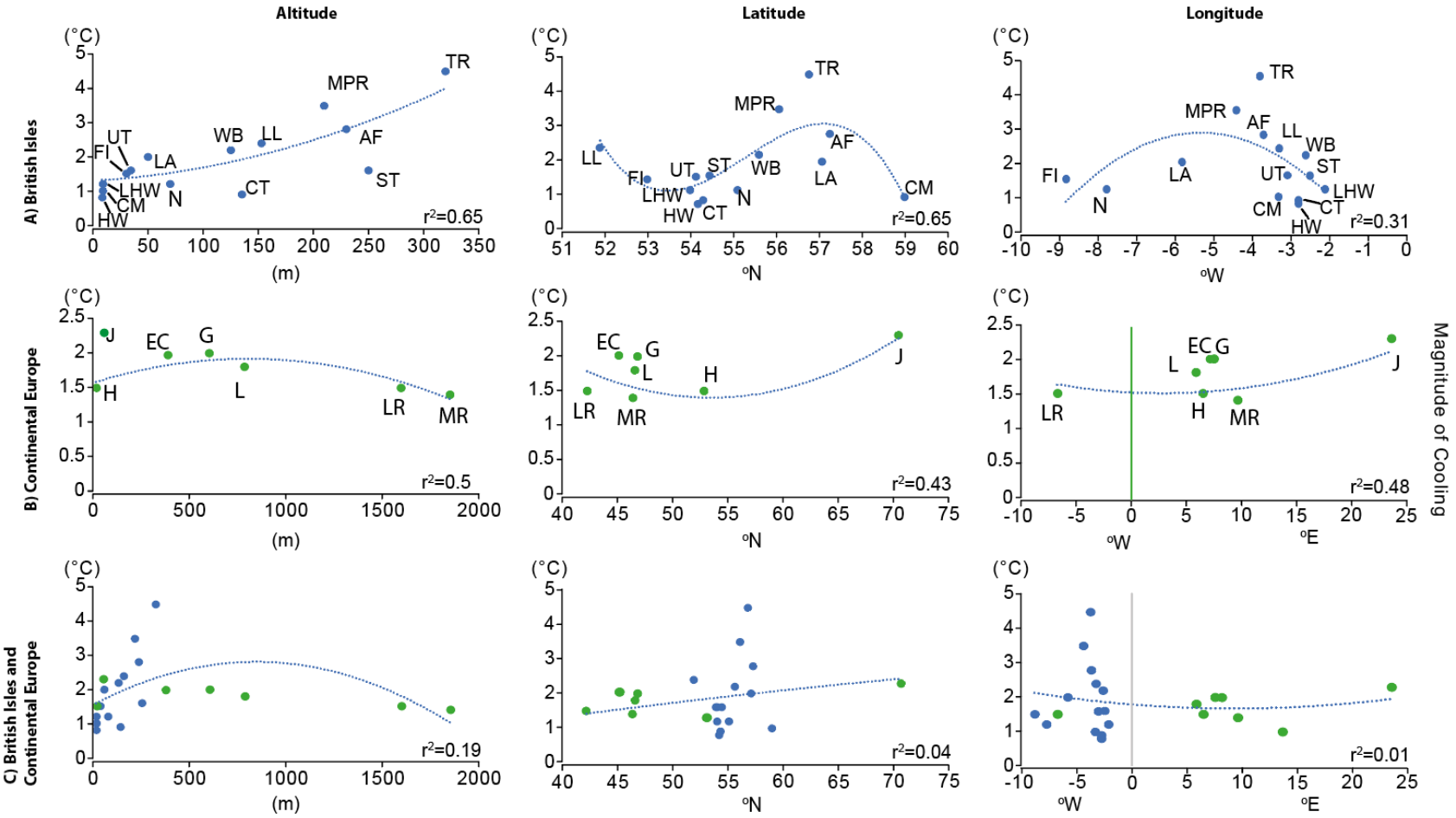

Figure 10.16, Magnitude of cooling for the *c.* 13.2 ka BP ACE in T_{Jul} compared to Altitude, Latitude and longitude from (A) the British Isles, (B) Continental Europe, and (C) the British Isles and continental Europe combined with blue circles denoting sites from the British Isles and green circles denoting sites from Continental Europe.

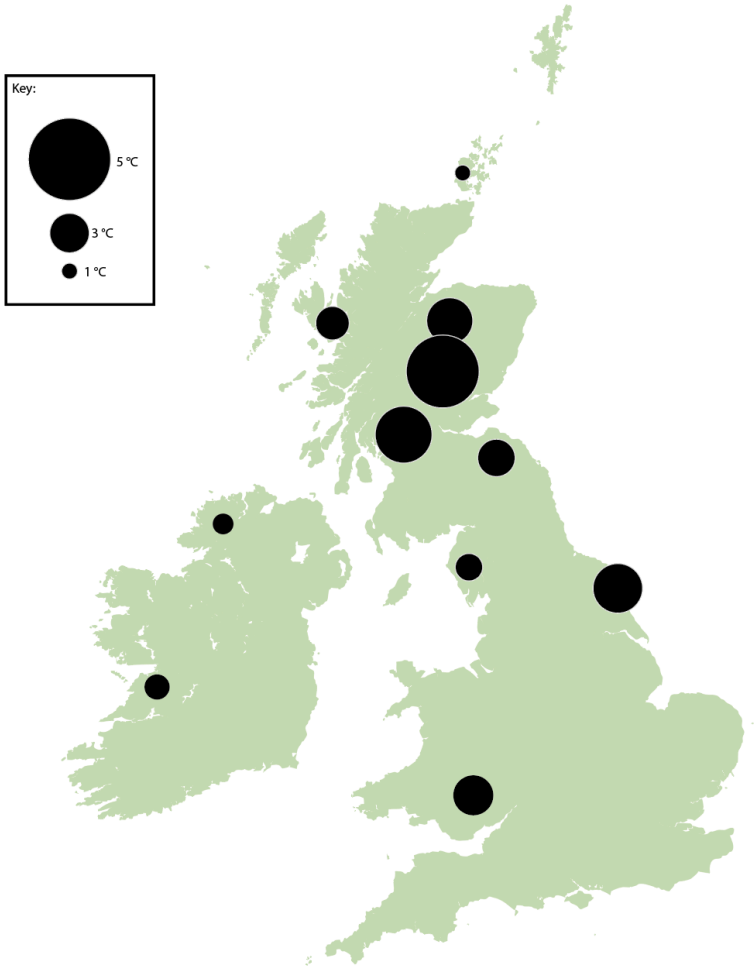

Figure 10.17, Magnitude of change for the 13.2 ka BP ACE in T_{Jul} in the British Isles. Generally, sites which lie at a higher altitude record a larger decline in temperatures.

Oxygen isotopes and Mean Annual Temperature ($\delta^{18}O$/MAT)

When comparing the magnitude of the *c.* 13.2 ka BP ACE in $\delta^{18}O$ with altitude, longitude and latitude, there generally appears to be very little correlation (Figure 10.18). Although the r^2 value is high (0.89) when event magnitude is compared to the altitude in the British Isles, this trend does seem to be exaggerated by the large magnitude exhibited at Tirinie. The cluster of sites below 50m a.s.l does show a hint of increasing magnitude with altitude, but this is a very narrow altitudinal range. More sites are needed between the altitudes of 50 and 300 m a.s.l to confirm if this trend is real. Similarly, for latitude there seems to be high values at *c.* 57 °N and low values either side, the r^2 value is 0.49, but only two sites define the trend above 55 °N.

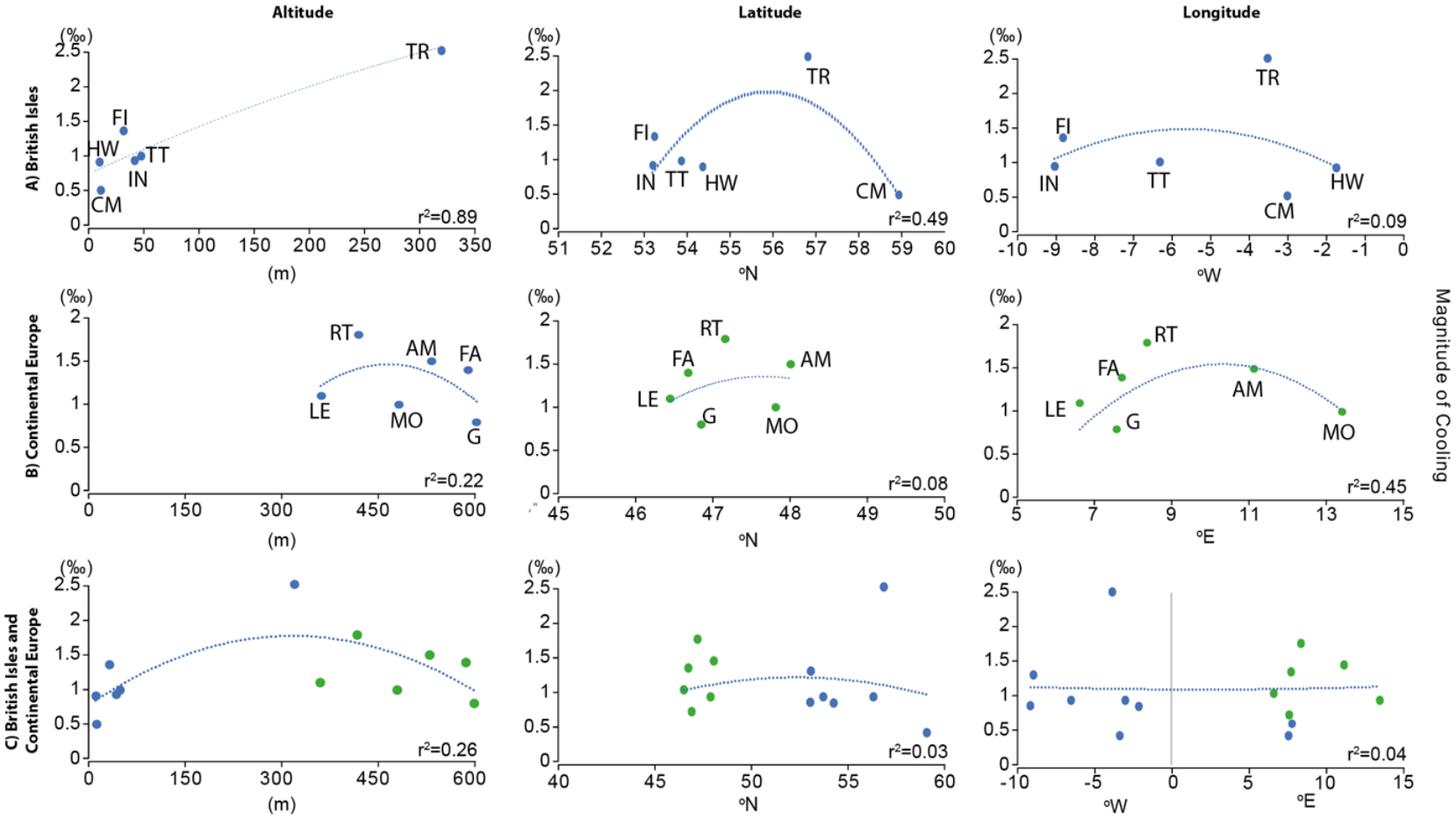

Figure 10.18, Magnitude of cooling for the *c.* 13.2 ka BP ACE in $\delta^{18}O$ compared to Altitude, Latitude and longitude from the (A) British Isles, (B) Continental Europe, and (C) the British Isles and continental Europe combined with blue circles denoting sites from the British Isles and green circles denoting sites from Continental Europe.

On the other side of the North Atlantic, the chironomid-inferred water-temperature records covering the Killarney oscillation (KO) generally display a trend of increasing magnitude the closer they are located to the Gulf of St. Lawrence (Figure 10.19) (Cwynar and Levesque, 1995; Levesque *et al.,* 1997). Some sites do not conform neatly to this trend e.g., Brier Island Bog Lake, which seems to display a slightly smaller magnitude of cooling than one would expect in relation to its proximity to the Gulf of St Lawrence. This may be explained by the coastal location of the site where the magnitude of temperature changes may be attenuated by warmth from the ocean. Other explanations for the slight discrepancies between sites may be due to the coarse taxonomic resolution used and site-specific factors such as aspect, lake size and lake depth. All sites seem to have a reasonably good sampling resolution with *c.* 10 – 20 samples defining the Killarney oscillation, except for Trout Lake which only has 5 samples defining the KO. Nevertheless, sites located further away from the Gulf of St Lawrence display a cooling of *c*. 3.5 °C while those closer show a much large cooling of *c*. 7-8 °C.

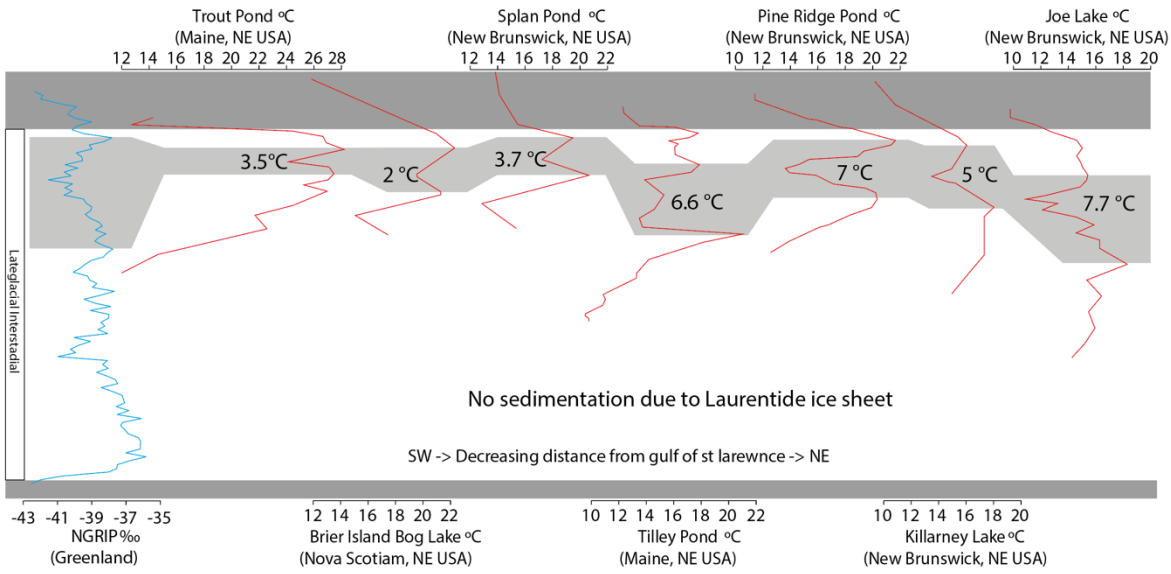

Figure 10.19, Comparison of chironomid inferred water temperature records from NE North America. Sites are broadly arranged from SW to NE with sites on the right closer to the Gulf of St. Lawrence and those on the left further away.

10.5.4 Forcing mechanisms of the c. 13.2 ka BP ACE

Oceanic forcing

Meltwater pulses from the Laurentide ice sheet have been postulated for causing the Inter Allerød cold period (IACP) which is broadly coeval to the *c.* 13.2 ka BP ACE and GI-1b (e.g., Clark *et al.,* 1996; Donnelley *et al.,* 2005). Donnelly *et al.,* (2005) suggested a meltwater pulse from the Laurentide ice sheet flowing into Hudson Bay, reducing thermohaline circulation, may have caused the IACP based on evidence form ocean cores. Thornalley *et al.,* (2005) also suggested a meltwater pulse mechanism for the IACP based on evidence from marine cores in the North Atlantic signaling a reduction in the

northerly transport of warm waters in the N. Atlantic for *c.* 300 yrs (Figure 10.20c). The south Atlantic rise shows an increase in ^{14}C ventilation ages, Eirik drift in the NW Atlantic displays an increase in flow speed, and the Iberian margin displays a reduced benthic $\delta^{13}C$ ‰. The NW and NE Atlantic both displayed a reduction in ocean convection, however, a greater reduction in convection is inferred to have occurred in the NE Atlantic suggesting a larger meltwater pulse originating from the NE Atlantic.

There may be some evidence for the impact of meltwater forcing in Britain and Ireland as the magnitude expressed in T_{Jul} does increase from *c*. 1°C to *c*. 4°C between 53 and 58 °N, though this is less clear than the latitudinal trend observed in the T_{Jul} records for the *c.* 14.0 ka BP ACE. Also, the small magnitude for the 13.2 ka BP ACE in Crudale Meadow suggests this trend does not continue above 58 °N, however, this observation is based on only one data point. Stronger evidence suggesting a meltwater pulse as the driving mechanism comes from the chironomid reconstructed temperatures in NE North America where a decline of *c*. 5-8 °C is observed, far greater than any records in Europe during the 13.2 ka BP ACE. The magnitude of the ACE also increases with greater proximity to the Gulf of St Lawrence suggesting a potential meltwater route. The passage of meltwater through the Gulf of St Lawrence has also been suggested for the millennial-scale ACE the Younger Dryas/GS-1. It is possible that meltwater did also flow into the N. Atlantic via Hudson Bay as well but there are no chironomid records in the vicinity to investigate this area.

Solar forcing

There is also evidence for a solar forcing mechanism operating around the time of the *c*. 13.2 ka BP ACE which may have been responsible for some of the more subtle changes in temperature imprinted on the overall structure of the event in T_{Jul} and $\delta^{18}O$ (Figure 10.20 a and b). Adolphi *et al.,* (2014) describe how modern observations show that during periods of reduced solar activity high pressure blocking systems occur to the south of Greenland and enhanced meridional atmospheric circulation (Woolings *et al.,* 2010), similar to a positive phase of the North Atlantic Oscillation (NAO) which can occur at centennial scales (Moffa-Sanchez *et al.,* 2014). This therefore suggests there may be greater expression in winter temps (Adolphi *et al.,* 2014). However, longer winters would result in shorter summers and few growing degree days for chironomid larvae, potentially causing summer temperatures and T_{Jul} to decline as well. Between 13.45-13.2 ka cal BP lower ^{10}Be concentrations are observed in the Greenland ice core records signalling a reduction in solar activity (Adolphi *et al.,* 2014). This interval roughly coincides with the gradual decline in T_{Jul} and $\delta^{18}O$ seen at the start of the *c.*13.2 ka BP ACE. Another period of low solar activity also occurs slightly later in the event at *c*. 13.1 ka BP at a similar time to when minimum $\delta^{18}O$ values are achieved. Solar forcing is often felt strongest in the centre of

landmasses, away from the modulating effect of warmth from the oceans. This may explain why events closer to the centre of the British Isles experience a larger decline in T_{Jul} during the 13.2 ka BP ACE. Though it could also be simply due to the amplification of temperature change with greater altitude, for which, sites in central Scotland generally lie at a higher altitude (Pepin *et al.,* 2015).

It is therefore proposed that meltwater from the Laurentide ice sheet in the west Atlantic via the Gulf of St. Lawrence, and meltwater in the NE Atlantic although to a lesser extent, primarily caused the abrupt decline in temperatures at between *c.* 13.2 and 13.0 kyrs BP. It is possible that the meltwater from N. America impacted the climate of Europe, propagated though the westerly winds. Solar forcing may be responsible for some of the subtle changes in temperature during the abrupt decline in temperatures between *c.* 13.2 and 13.0 kyrs BP and may also be responsible for some of the variability overserved during the gradual decline prior at *c*. 13.55 – 13.2 kyrs BP. The complex and often unclear relationships between the magnitude of the *c*. 13.2 ka BP ACE and altitude, latitude and longitude may be due to the expression of solar forcing, meltwater from the NE Atlantic and meltwater from America imprinting over each other.

10.6 Old Buckenham mere: the fortunate surprise

10.6.1 The search for a LGIS site in SE Britain

As became evident in Chapter 9 (Old Buckenham Mere results and interpretation), only sediments from the very end of the LGIS were found in the OBM19 sequence and so the magnitude of LGIS ACEs could not be investigated for SE Britain. It is also possible, that the rest of the LGIS may be present below the recovered OBM19 sequence due to the presence of the organic lens in the calcareous-rich diamicton at the base and were just inaccessible using manual coring equipment. Ground penetrating radar could help resolve the stratigraphy of the site further and give indication as to whether more lacustrine sediments are present below the calcareous-rich diamicton.

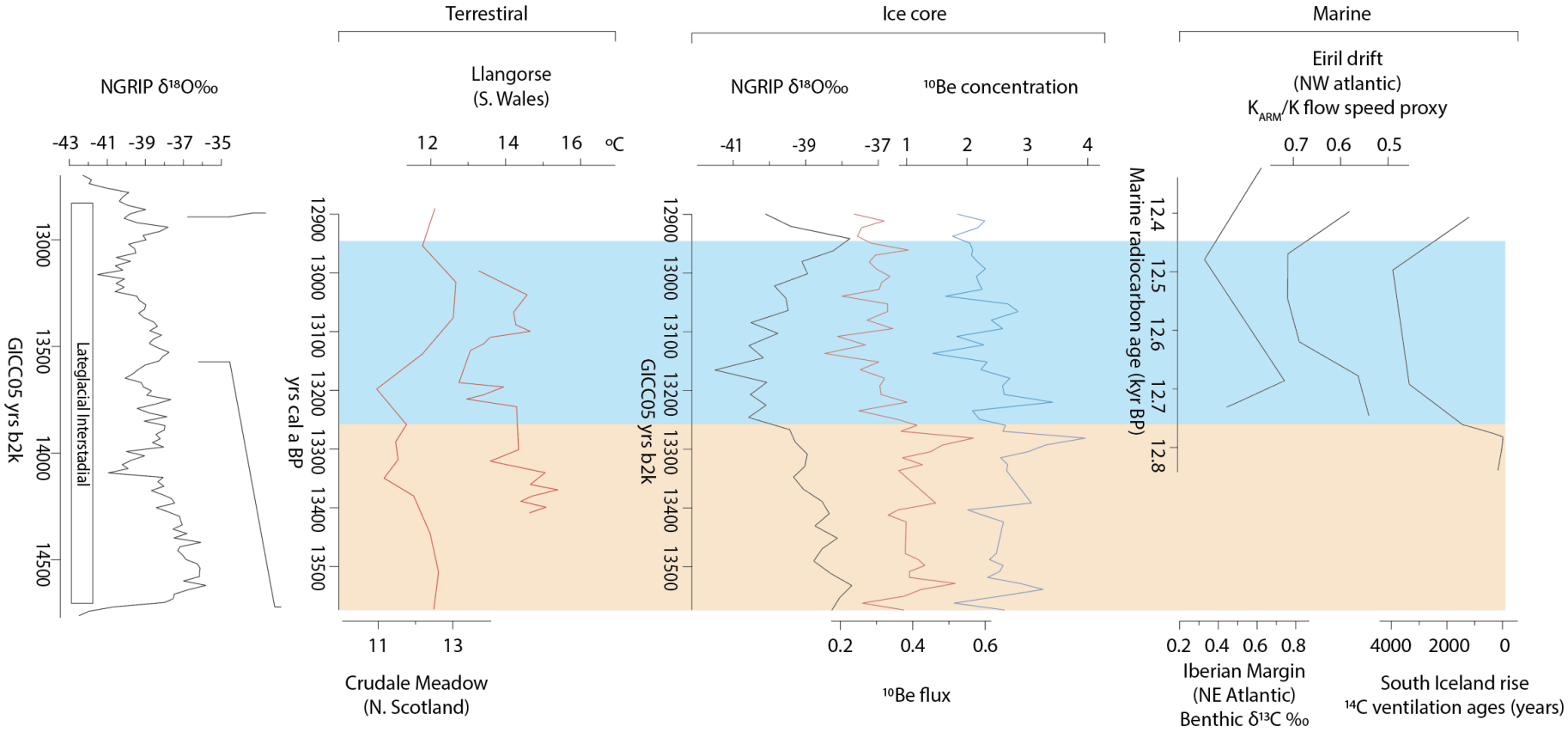

Figure 10.20, Comparison of changes in T_{Jul} records from Crudale Meadow and Llangorse during the 132 ka BP ACE with proxies for solar activity (10Be; Adolphi *et al.,* 2014) and ocean circulation proxies (Thornalley *et al.,* 2011).

There are several other possible sites which could potentially contain LGIS sediments based on pollen biostratigraphy including: Sea Mere (90 cm at 18 metre deep; Hunt and Birks, 1982), Hockham Mere (at least 60 cm at 11 metres depth; Godwin and Tallantire, 1951; Bennett 1983), Old Decoy (Godwin 1940) and Lopham Little (Tallantire, 1953b) (Figure 10.21). Despite the large area of East Anglia there are relatively few lake basins which extend beyond the start of the Holocene. This contrasts with the numerous sequences which cover the LGIT in Scotland due to repeated glaciations creating topographic hollows in bedrock and glacial till (Walker and Lowe, 2017). In SE Britain, ice sheets during glaciations did not make significant landfall so far south and only impinged on the northern coast of East Anglia with basin formation largely relying on the action of periglacial geomorphic processes and melting of ground ice features at the end of the Last Glacial (See section 6.3.4).

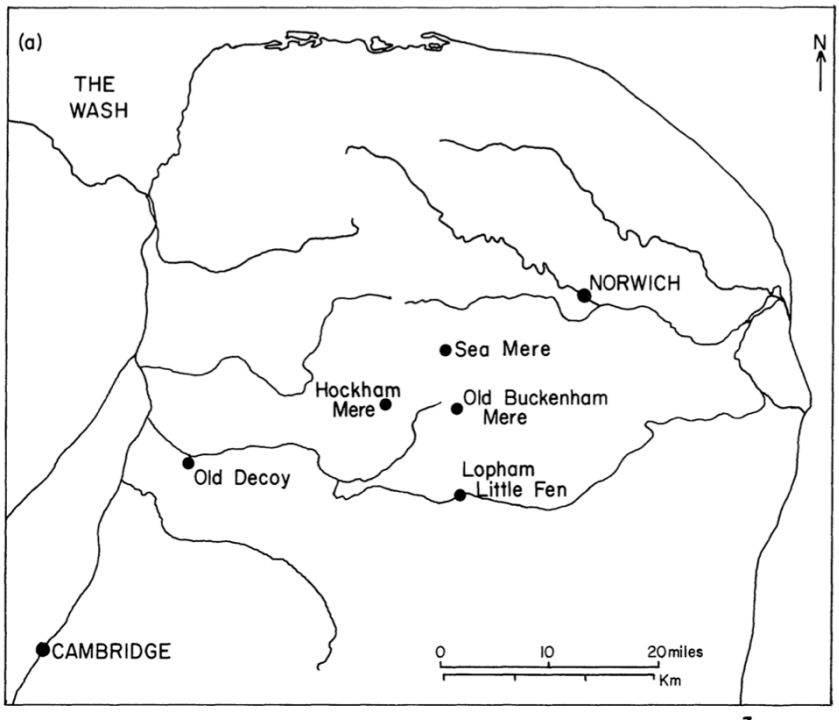

Figure 10.21, map of other potential records covering the LGIS in East Anglia. (from Hunt and Birks, 1982)

10.6.2 GS-1 and the Early Holocene

Although the lack of LGIS representation in the OBM19 sequence meant the site did not contribute to the aims of this thesis, it does however provide an extremely high-resolution record of the Loch Lomond Stadial with an average sedimentation rate of *c.* 5-10 yrs/cm on average, which to my knowledge is the highest stratigraphic resolution of any record covering the LLS in the British Isles. The decadal-scale resolution T_{Jul} record displays many centennial-scale changes in temperature not seen in other T_{Jul} records. This is potentially due to (i) the low stratigraphic resolution of records during the LLS means these centennial-scale changes in temperature are averaged out, particularly when a coarse sampling resolution is employed; (ii) the low concentrations of head capsules during the LLS meaning samples

are often combined with neighbouring samples (e.g. Muir Park Reservoir; Brooks *et al.,* 2016), and; (iii) temperatures in the LLS in Scotland and northern Britain are at the lower end of the calibration data sets' temperature gradients, where there are relatively few taxa and therefore chironomid assemblages are typically less sensitive to temperature changes.

The T_{Jul} reconstruction for the LLS at OBM bears remarkable similarity with the $\delta^{18}O$ record from NGRIP, both of which display a tripartite structure (Figure 10.22), both of which displays an initial large decline in the early-LLS, an brief increase in values during the mid-LLS during which two centennial scale ACEs can be observed, and finally in the late-LLS, another decline in values before increasing into the Holocene. Structure within the LLS/YD has been observed in two other key records from Europe: Kråkenes in Norway and Meer Felder Maar in Germany. A mid-YD shift to increased varve thickness and Ti µ-XRF counts from Meerfelder Maar, c. 120 yrs prior to the increased Ti µ-XRF counts from Kråkenes, indicating a times transgressive shift (Lane *et al.,* 2013). Such precision in the differences in timing of the shift between each site is due to the robust chronologies they possess and the presence of the Vedde Ash. This was interpreted as a times transgressive northward shift in the polar front mid-YD, allowing westerly winds to prevail at *c.* 50 °N over southern Britain and central Europe belt (Lane *et al.,* 2013). Unfortunately, the Vedde Ash was not found in the rangefinder tephra sampling at Old Buckenham Mere, although this will be re-examined at 1 cm intervals. The precision of the radiocarbon chronology at Old Buckenham Mere as it stands suggests the change seen between the mid- and late-LLS, occurs around the same time as the mid-YD shift in Meer Felder Maar and Kråkenes.

The age model at OBM suggests the Holocene started at 12,050 cal a BP, much earlier than many records. However, this is because the upper most date was rejected as it was too old and so the age model extrapolated using the sedimentation rate from the first half of the LLS. Sedimentation rate is likely to have been higher in the latter part of the LLS as the $\delta^{18}O$ suggests a shift to wetter conditions. There is also a notable change in sediment texture with more organic detritus present suggesting greater in washing of material.

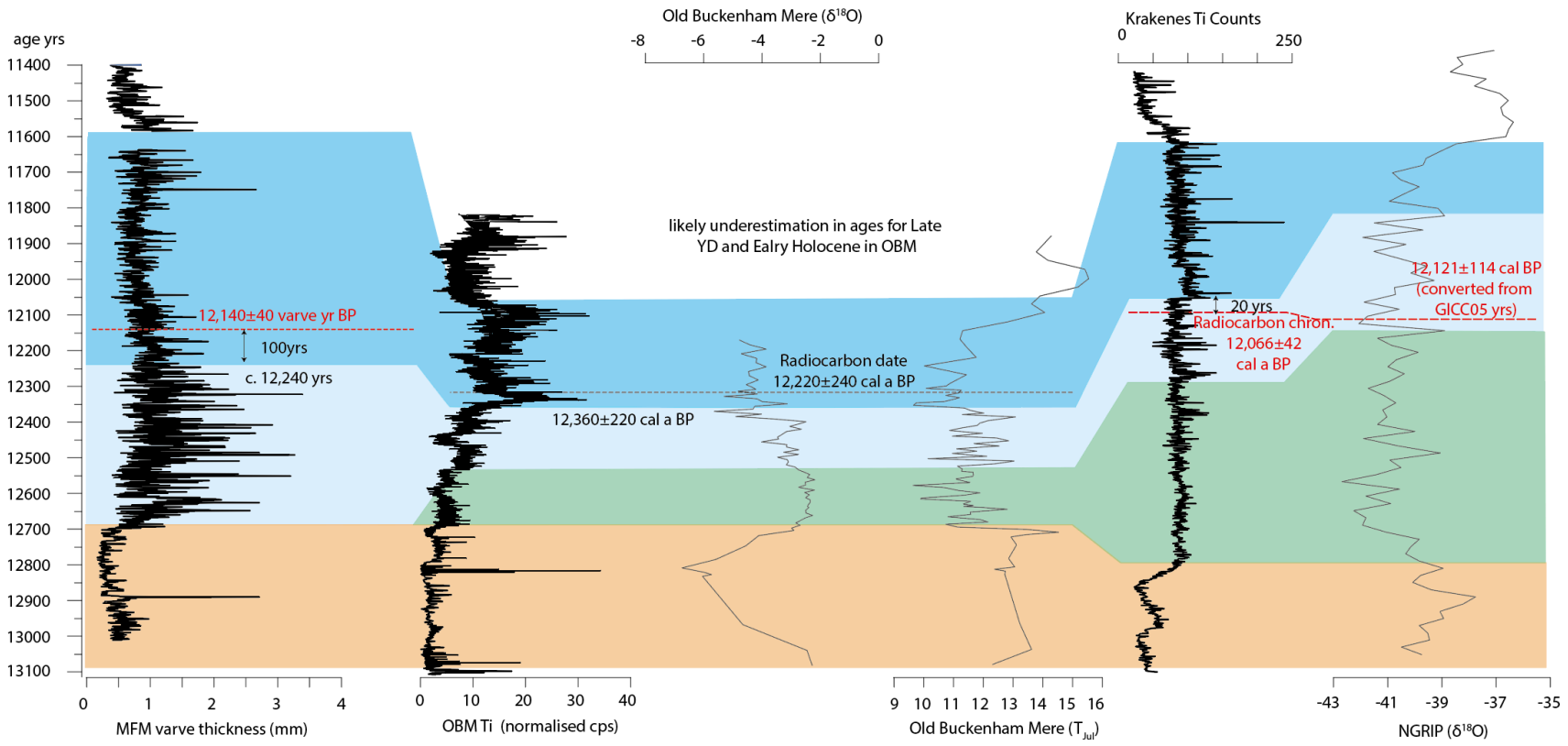

Figure 10.22, comparison between records from Old Buckenham Mere (T_{Jul}, Ti and $\delta^{18}O$) with records from Meerfelder Marr (varve thickness and Ti counts), Kråkenes (Ti counts) and NGRIP ($\delta^{18}O$) (After Lane *et al.,* 2013).

10.7 Chapter summary

- The definition of ACEs event varies greatly between different records, from statistical techniques applied to Greenland, while a similar 'shoulder' approach is used in some high-resolution terrestrial T_{Jul} and $\delta^{18}O$ records, but some used a 'min/max' approach when sampling resolution was lower. ACEs in all the records discussed here were redefined using the 'min/max' approach to ensure consistency between records.

- The spatial variations in the magnitude of temperature change during ACEs are better defined in the British Isles due to the greater number of records, more records with higher sampling resolution allowing more accurate representation of ACE magnitude and clearer definition of the pattern of temperature changes allowing ACEs to be identified when chronological constraint is limited.

- Extreme care should be taken when correlation of ACEs is reliant on climatostratigraphy due to limited chronological constraint, especially as other declines in temperature are present in the LGIS other than the three most routinely identified at *c.* 14.0, 13.6 and 13.2 ka BP.

- For the *c*. 14.0 ka BP ACE, there is evidence for a meltwater pulse in the NW Atlantic by the Laurentide Ice sheet, but limited evidence for meltwater flux into the NE Atlantic. It is suggested that the Laurentide ice sheet meltwater led to reduced advection of warm salty water from the tropics, cooling the whole North Atlantic region. This allowed the expansion of sea ice in the North Sea, magnifying the cooling in NE Britain. The variability in temperatures during the ACE may be due to changes in the evolution of the meltwater flux during its release and/or changes in solar variability. The final warming, terminating the event, may be aided by the increase in solar activity

- Correlation and comparison of the magnitude for the 13.6 ka BP event is limited due to low sampling resolution and limited chronological constraint for the mid-LGIS in many sequences, compounded with the occurrence of other temperature declines during the Mid-LGIS.

- Meltwater forcing from the Laurentide ice sheet via the Gulf of St. Lawrence, and to a lesser degree meltwater from the NE Atlantic, is proposed to have caused the abrupt

decline in temperatures at *c*. 13.2 ka BP ACE (~GI-1b). Variations in temperature during the abrupt decline (~GI-1b) and during the more gradual decline prior (~GI-1ci) may be due to changes in solar activity. Reduced solar activity may have played a role in achieving the minimum temperatures of this event.

- A tripartite structure is observed in the T_{Jul} and Ti records from Old Buckenham Mere with T_{Jul} values of c. 11°C between 12.7 - 12.55 kyr BP, temperatures increase to c. 13°C between 12.55 -12.38 kyr BP in which two centennial scale ACEs occur with cooling in the order of 2°C, followed by another decline in temperatures to 10 °C which then gradually rise into the early Holocene. The transition between the mid- and late-LLS at Old Buckenham Mere broadly coincides with the mid-YD shifts described in Meer Felder Maar varve thickness/Ti µ-XRF counts and Krakenes Ti µ-XRF counts.

Chapter 11: Conclusions

11.1 Key findings

The review of previously published T_{Jul} and $\delta^{18}O$ records covering the LGIS (Chapter 2) highlighted several issues with the data we currently have available. These limits were identified as including: i) the low spatial density of sites with large areas where no T_{Jul} or $\delta^{18}O$ records for the LGIS exist, e.g., the southern and northern reaches of the British Isles; ii) the limited chronological constraint of many records, which hinders the robust correlation and comparison of ACE magnitude across geographic regions; and iii) the variable sampling resolution employed between records ranging from 250 to 15 yrs per sample, limiting the comparability of ACEs contained within sediment records. Combined, these factors, restrict our knowledge of how the magnitude of ACEs during the LGIS varied spatially, and by extension limits out understanding of the forcing mechanisms which caused them. Through the application of a high-resolution dual proxy approach, this study has improved our understanding of how the magnitude of ACEs varies across multiple spatial gradients (latitude, longitude, and altitude) during the LGIS. This thesis has produced three of the highest temporal resolution T_{Jul} and $\delta^{18}O$ records from the British Isles, covering the LGIS at Crudale Meadow and Llangorse with *c.* 15-20 yrs/sample, and the LLS at Old Buckenham Mere with *c.* 10 yrs/sample. The main findings of this thesis are summarised below.

General trend in LGIS temperatures

The palaeotemperature proxy records from northern Europe generally display an abrupt increase at the start of the LGIS and then either decline or display a relatively steady trend throughout (Moreno *et al.,* 2014), the latter of which is observed in both the T_{Jul} and $\delta^{18}O$ records from Crudale Meadow. Palaeotemperature proxy records from southern Europe, however, display a gradual increase throughout the LGIS due to the gradual increase in summer solar insolation. This controlling factor on southern European sites is possibly driven by their location at latitudes beyond the maximum extent of the N. Atlantic Sea ice during GS-2 and so were relatively unaffected by the disintegration of N. Atlantic sea-ice at the start of the LGIS (Moreno *et al.,* 2014). The T_{Jul} record from Llangorse, which shares characteristics of both northern and southern European records as peak temperatures occur mid-LGIS, suggests summer temperatures in southern Britain may have been influenced by both factors.

The Early-LGIS ACE c. 14.0ka BP (~GI-1d)

The results presented in this dissertation show the largest cooling during the early-LGIS ACE at *c.* 14.0 ka BP (~GI-1d) was experienced in N and NE Scotland with the T_{Jul} record from Crudale Meadow displaying a decline of 5.8 °C and $\delta^{18}O$ a decline of 1 ‰. In Ireland and southern Britain, the 14.0 ka ACE had a very small magnitude, with Llangorse displaying a decline of only 1.3 °C. The spatial expression and abruptness of the *c*. 14.0 ka BP ACE suggests a forcing mechanism of oceanic origin. There is limited evidence for a meltwater event in the NE Atlantic, however, there is evidence for meltwater from the Laurentide ice sheet into the NW Atlantic during this time (Obbink *et al.,* 2014). It is possible that, this meltwater release led to reduced advection of warm salty water from the tropics, cooling the whole North Atlantic region, which may have facilitated the expansion of sea ice in the North Sea, magnifying the cooling in NE Britain. The variability in temperatures during the ACE may be sensitive to changes in the evolution of the meltwater flux during its release and/or changes in solar variability. The final warming, terminating the event, may be aided by the increase in solar activity.

The Mid-LGIS ACE c. 13.6ka BP (~GI-1cii)

At Crudale Meadow, the ACE with the second largest magnitude occurred in the mid-LGIS at *c.* 13.6 ka BP with decline of 3.8 °C and 0.7 ‰. Similarly, at Llangorse, the mid-LGIS ACE also has the second largest cooling in the LGIS with a decline of *c.* 2 °C at 13.5 ka BP. Due to the limited chronological constraint and precision in many other T_{Jul} and $\delta^{18}O$ records, a regional synthesis and comparison to spatial gradients cannot be robustly applied. This is also hindered by the fact that the mid-LGIS is often sampled at lower resolutions than the rest of the LGIS as the GI-1cii event (with which it is often equated) is thought to be insignificant and therefore overlooked. The data presented here can show this event to be of at least the same magnitude as other ACEs during this period and detectable in records from locations other than Greenland. The implications of this are discussed below.

The Late-LGIS ACE c. 13.2ka BP (~GI-1b)

The late-LGIS ACE at Llangorse has the largest decline of all the ACEs during the LGIS with a decline of 2.5 °C at *c.* 13.2 ka BP. At Crudale Meadow however, the late-LGIS ACE has the smallest magnitude of the LGIS ACEs with declines of 1.2 °C and 0.5 ‰. Additionally, at some sites (e.g., Loch Ashik and Abernethy Forest) there appears to be a longer-term declining temperature trend with short-lived abrupt changes imprinted upon it. When the magnitudes for the 13.2 ka BP ACE from Llangorse and Crudale Meadow are incorporated into the synthesis of other T_{Jul} and $\delta^{18}O$ records from Britain and Continental Europe, the spatial pattern of

magnitude for the late-LGIS ACE (~GI-1b) is more complex than the early-LGIS ACE. This additional complexity suggests there may be two or more spatially variable forcing mechanisms operating at the same time, overprinting signals on each other. Meltwater may have fed into the NW as well as the NE Atlantic, causing the more abrupt decline during the mid-LGIS (~GI-1b), while at the same time changes in solar activity may be responsible for climatic variability on the more gradual decline (GI-1cii) preceding the more abrupt decline (~GI-1b).

Other LGIS ACEs and the use of Greenland as a Northern Hemisphere stratotype

The three centennial-scale ACEs most commonly identified in proxy records are recorded in the T_{Jul} and $\delta^{18}O$ records at Crudale Meadow and the T_{Jul} record from Llangorse, however, there are also several other ACEs, or at least notable declines in temperature, that occur during the LGIS. At Crudale Meadow, a 0.8 °C decline is present in T_{Jul} at *c.* 14.1 ka BP and a shift of 0.5 ‰ to more negative $\delta^{18}O$ values occurred at 13.7 ka BP. Both events were only expressed in one proxy. Two other ACEs also occur in the T_{Jul} record at Llangorse, one of which is during the earliest-LGIS at *c.* 14.6 ka BP (*c.* 1.3 °C decline), and the other during the mid-LGIS at 13.8 ka BP (*c.* 1.5 °C decline), both of which have similar magnitudes to the ACEs at 14.0 ka BP and 13.5 ka BP, respectively. The variable spatial expression of ACE magnitude described above, and the evidence for other ACEs/declines in T_{Jul} and $\delta^{18}O$ records from the North Atlantic region e.g. Blockley et al. (2018) and Timms et al. (2021) shows the Greenland ice-core event stratigraphy does not contain a complete record of abrupt climatic variability for Europe as a whole. Therefore, solely utilising the $\delta^{18}O$ record from Greenland as a stratotype for delimiting the number of ACEs in the LGIS is not advisable. This approach alone fails to robustly capture the palaeoclimatic variability around the North Atlantic region during the LGIS and demonstrates a need to develop multiple regional palaeotemperature stratotypes and comparable chronological resolutions.

The Loch Lomond Stadial in high-resolution

The T_{Jul} record from Old Buckenham Mere provides the highest resolution quantified temperature reconstruction for the LLS from the British Isles, and potentially continental Europe, with on average 10 yrs/sample. A tripartite structure is evident with T_{Jul} values of *c.* 11°C between *c.* 12.7 - 12.6 kyr BP, temperature increase to *c.* 13 °C between *c.* 12.6 -12.4 ka BP in which two centennial-scale ACEs occur with cooling in the order of 2 °C, followed by another decline in temperatures to an average of 10 °C until the termination of the LLS into the Early Holocene. The temporal pattern of changes in the T_{Jul} record bears remarkable similarity

to the $\delta^{18}O$ record of NGRIP but suggests that existing bipartite models for climatic conditions during this period are too simplistic.

11.2 Wider significance

This study demonstrates the importance of studying the ACEs of the LGIS as they are potentially analogous to possible future ACEs triggered by anthropogenic global warming with respect to their duration and magnitude. In particular, it has been demonstrated that the magnitude of temperature change can be exceptionally large over relatively short spatial distances, i.e., a few hundred metres in altitude or several degrees of latitude/longitude, which would have significant environmental responses at a very local level. This fine detail may be particularly challenging to reproduce in numerical simulations. Also, when utilising palaeoclimatic models, validating these regional stratotypes such as Greenland, will produce an averaged viewpoint without representing the full spectrum of climatic variability.

In particular, this work has implications for modelling of future ACEs as many model simulations try to recreate an ACE using only once forcing mechanism (e.g., Gregory *et al.,* 2005; Hawkins *et al.*, 2011), where in fact multiple forcing mechanisms are likely to be operating including variations in AMOC strength, solar variability as well several modifying factors such as sea-ice expansion. The strength of the study of this time period is that each of the ACEs of the LGIS appear to have a different combination of these forcing mechanisms and modifying factors which affect the onset, duration and termination of ACEs. Effectively this means that the LGIS ACEs provide examples of the range of different climatic perturbations that may occur under a variety of forcing and baseline conditions. Finally, this work supports the growing body of evidence that suggests that the impact that these ACEs have is spatially variable and future ACEs may, therefore, have a greater impact in some regions and less in others.

11.3 Future research and recommendations

This research has highlighted that more research is needed to better understand the spatial expression of ACEs across Europe. Whilst the new sites presented within this thesis go some way to fill in some of the spatial gaps in the northern and southern reaches of the British Isles, there are still significant gaps across the European continent, particularly the lowland plains across Northern France and Germany, eastern Europe and southern Europe. Although the density of T_{Jul} and $\delta^{18}O$ records in the British Isles is relatively high compared to continental

Europe, the complex spatial expression of LGIS ACE magnitude requires a greater spatial density of sites, particularly in southern England and Ireland.

This thesis also highlights the need for increased sampling resolution to better resolve the magnitude of temperature change. Many records, particularly those from the European continent, have low sampling resolution of less than 40 yrs/per sample which is inadequate when reconstructing ACEs which are centennial in scale. Ideally, chronological investigations should be undertaken first to determine the yrs/cm for a sequence, and variations within a sequence, and then apply a sampling interval which would give *c*. 20 yrs/sample. If possible, sampling could even be conducted at fewer than 10 yrs/sample resolution if the stratigraphic resolution and HC concentrations allow, and then more robust regression approaches could be taken in order to account for sample-specific noise and short-term weather phenomena, although the amount of work required to achieve this would be substantial. Samples should also be taken from the same sequence as the offsets in the timing of shifts observed between the proxy records may occur over very short intervals of time, such as over a few cms, which may be lost with uncertainties when combining/comparing multiple datasets conducted on different sequences. Another benefit of having higher-resolution records is that break points could be statistically identified using, e.g., piecewise linear regression, to reduce subjectivity in defining ACEs.

More robust chronologies are also of paramount importance, particularly using radiocarbon and tephrochronology, as there are more ACEs/declines in temperature than the three main events in the GICC05 stratigraphy, GI-1d, GI-1cii and GI-1b, for which events in terrestrial T_{Jul} and $\delta^{18}O$ records are frequently correlated to. Particularly during the early- and mid-LGIS there is notable climatic variability with declines in T_{Jul} and $\delta^{18}O$ that could easily be mis-correlated between records. It is therefore recommended that more robust age models are created, utilising radiocarbon dated terrestrial plant macrofossils and tephrochronology, rather than relying on climato-, isotope- and pollen-stratigraphy (Brauer *et al.,* 2014; Mangerud *et al.,* 2020).

Finally, this study shows the importance of using multiple proxies to further our understanding of palaeoclimatic change. As is evident in the palaeotemperature proxies from Crudale Meadow, using only one temperature proxy may not record all the ACEs the site experienced and so several temperature reconstructions using different techniques are required. The combination of T_{Jul} and $\delta^{18}O$, when $\delta^{18}O$ records MAT, allows seasonal temperature changes to

be explored. Even when the $\delta^{18}O$ record also reflects changes in lake hydrological balance rather than solely MAT, changes in the balance of precipitation and evaporation can be inferred, such as the LGIS at Llangorse. The addition of other proxies would further improve our understanding of the climate system, including the use of compound specific deuterium isotopic biomarkers (δD) to reconstruct changes in precipitation and resolve drivers of the $\delta^{18}O$ record. Other palaeoecological proxies such as pollen would also be beneficial to further our understanding of the terrestrial impact future centennial-scale ACEs could have and how this will affect the human populations.

References

Abbott, P. M., Griggs, A. J., Bourne, A. J., et al. (2018). Tracing marine cryptotephras in the North Atlantic during the last glacial period: Improving the North Atlantic marine tephrostratigraphic framework. Quaternary Science Reviews, 189, 169–186. doi.org/10.1016/j.quascirev.2018.03.023

Abrook, A. M. (2018). Environmental responses to abrupt climate change during the Last Glacial-Interglacial Transition (ca 16-8 cal. Ka BP): delineating climatic drivers and landscape responses during millennial- and centennial-scale climatic variability. Phd thesis (unpublished).

Abrook, A. M., Matthews, I. P., Candy, I., et al. (2020). Complexity and asynchrony of climatic drivers and environmental responses during the Last Glacial-Interglacial Transition (LGIT) in north-west Europe. Quaternary Science Reviews, 250, 106634. doi.org/10.1016/j.quascirev.2020.106634

Abrook, A. M., Matthews, I. P., Milner, A. M., et al. (2019). Environmental variability in response to abrupt climatic change during the Last Glacial-Interglacial Transition (16-8 cal ka BP): Evidence from Mainland, Orkney. Scottish Journal of Geology, 56(1), 30–46. doi.org/10.1144/sjg2019-006

Adolphi, F., Muscheler, R., Svensson, A., et al. (2014). Persistent link between solar activity and Greenland climate during the Last Glacial Maximum. Nature Geoscience, 7, 662. http://dx.doi.org/10.1038/ngeo2225

Alhberg, K., Almgren, E, Wright, H. E. Jr., et al. (1996). Oxygen-isotope record of Late-Glacial climate change in western Ireland. Boreas, 25, 257-267.

Alley, R. B., Mayewski, P. A., Sowers, et al. (1997). Holocene climatic instability: A prominent, widespread event 8200 yr ago. Geology, 25(6), 483–486.

Alley, R., Meese, D., Shuman, C. et al. (1993). Abrupt increase in Greenland snow accumulation at the end of the Younger Dryas event. Nature, 362, 527–529. doi.org/10.1038/362527a0

Andersen, T. and Sæther, O. A. (1994). Usambaromyia nigrala gen. n., sp. n., and Usambaromyiinae, a new subfamily among the Chironomidae (Diptera). Aquatic Insects, 16, 21–29.

Anderson, N. H. and Cummins, K. W. (1979). Influences of diet on the life histories of aquatic insects. Journal of the Fisheries Board of Canada, 36, 335–342.

Anderson, N. J., and Leng, M. J. (2004). Increased aridity during the early Holocene in West Greenland inferred from stable isotopes in laminated-lake sediments. Quaternary Science Reviews, 23(7), 841-849. doi:10.1016/j.quascirev.2003.06.013.

Andrews, J. E. (2006). Palaeoclimatic records from stable isotopes in riverine tufas: synthesis and review. Earth Science Reviews, 75(1-4), 85-104.

Andrews, J. E., Riding, R. And Dennis, P. F. (1997). The stable isotope record of environmental and climatic signals in modern terrestrial microbial carbonate from Europe, Palaeogeography, Palaeoclimatology, Palaeoecology, Vol. 129, 171-.-189

Armitage, P. D. (1968). Some notes on the food of the chironomid larvae of a shallow woodland lake in South Finland. - Annales Zoologici Fennici, 5, 6-13.

Armitage, P., Cranston, P. S., and Pinder, L. C. V. (eds) (1995). The Chironomidae: the biology and ecology of non-biting midges. Chapman and Hall, London.

Arts, G.H.P. (2000). Natuurlijke levensgemeenschappen van de Nederlandse binnenwateren. 13, Vennen. – Rapport EC-LNVAS-13. Wageningen. 1-80.

Atkinson, T.C., Briffa, K.R., and Coope, G.R. (1987). Seasonal temperatures in Britain during the past 22,000 years, reconstructed using beetle remains. Nature, 325(6105), 587-592.

Axford, Y., Briner, J. P., Francis, et al. (2011). Chironomids record terrestrial temperature changes throughout Arctic interglacials of the past 200,000 yr, 8, 1–13. doi.org/10.1130/B30329.1

Bakke, J., Lie, O., Heegaard, E., et al. (2009). Rapid oceanic and atmospheric changes during the Younger Dryas cold period. Nature Geoscience, 2(3), 202–205. doi.org/10.1038/ngeo439

Ballantyne, C. K. (2010). Extent and deglacial chronology of the last British-Irish Ice Sheet: Implications of exposure dating using cosmogenic isotopes. Journal of Quaternary Science, 25(4), 515–534. doi.org/10.1002/jqs.1310

Ballantyne, C. K., Hall, A. M., Phillips, W., et al (2007). Age and significance of former low-altitude corrie glaciers on Hoy, Orkney Islands. Scottish Journal of Geology, 43, 107-114. doi.org/10.1144/sjg43020107

Bar-Matthews, M., Ayalon, A., Kaufman, A., et al. (1999). The Eastern Mediterranean paleoclimate as a reflection of region events: Soreq Cave, Israel. Earth and Planetary Science Letters, 166, 85–95. doi.org/10.1016/S0012-821X(98)00275-1

Bar-Matthews, M., Marean, C. W., Jacobs, Z., et al. (2010). A high resolution and continuous isotopic speleothem record of paleoclimate and paleoenvironment from 90 to 53 ka from Pinnacle Point on the south coast of South Africa. Quaternary Science Reviews, 29(17–18), 2131–2145. doi.org/10.1016/j.quascirev.2010.05.009

Barley, E., Walker, M., Kurek, et al. (2006). A northwest North American training set: Distribution of freshwater midges in relation to air temperature and lake depth. Journal of Paleolimnology, 36(3), 295-314.

Bartlein, P.J., Prentice, I.C., and Webb, T. (1986). Climatic response surfaces from pollen data for some eastern North American taxa. Journal of Biogeography 13: 35–57.

Beale., C. M., Lennon, J. J., Yearsley, J. M., et al. (2010). Regression analysis of spatial data. Ecology Letters, 13, 246-64.

Beales, P. W. (1980). The late Devensian and Flandrian vegetational history of Cross Mere, Shropshire, new phytologist 85, 133-161.

Beerling, D. J., Chaloner, W. G., Huntley, et al. (1993). Stomatal density responds to the glacial cycle of environmental change. Proceedings of the Royal Society series B: Biological Sciences, 251(1331), 133-138.

Benn, D. I. (2021). Evidence for glacier surging within the Loch Lomond Stadial West Highland Icefield, with particular reference to the Laire-Treig lobe, Glen Spean. In Palmer. A. P., Lowe, J. J., Matthews, I. P. (eds.), The Quaternary of the West Grampian Highlands: Field Guide, Quaternary Research Association, London, 139-147.

Bennett, K. D. (1983). Devensian Late-Glacial and Flandrian vegetation history at Hockham Mere, Norfolk, England. New Phytologist, 95(3), 457-487.

Bennett, K. D. (1996). Determination of the number of zones in a biostratigraphical sequence. New Phytologist, 132(1), 155–170. doi.org/10.1111/j.1469-8137.1996.tb04521.x

Berg, M. B. (1995). Larvae food and feeding behaviour. In: Armitage P. D., Cranston, P. S. and Pinder, L. C. S., (eds), The Chironomidae. The biology and ecology of non-biting midges. Chapman and Hall, London, 136-138.

Bernasconi, S. M. And McKenzie, J. A. (2007). Lake Sediments, In: Elias, S (Ed), Encyclopaedia Of Quaternary Science, Elsevier, Amsterdam, 351-359

Bickerdike, H. L., Evans, D. J. A., Ó Cofaigh, C. O., et al. (2016). The glacial geomorphology of the Loch Lomond Stadial in Britain: a map and geographic information system resource of published evidence. Journal of Maps, 12:5, 1178-1186. Doi:10.1080/ 17445647.2016.1145149.

Bickerdike, H. L., Evans, D. J. A., Stokes, C. R., et al. (2018). The glacial geomorphology of the Loch Lomond (Younger Dryas) Stadial in Britain: a review. Journal of Quaternary Science, 33, 1-54.

Bilyj, B. and Davies, I. J., (1989). Descriptions and ecological notes on seven new species of Cladotanytarsus (Chironomidae: Diptera) collected from an experimentally acidified lake. Canadian journal of zoology, 67, 948 – 962.

Birks, H. H. (1994). Late-glacial vegetational ecotones and climatic patterns in Western Norway. Vegetation History and Archaeobotany, 3(2), 107-119.

Birks, H. H. (2003). The importance of plant macrofossils in the reconstruction of Lateglacial vegetation and climate: Examples from Scotland, western Norway, and Minnesota, USA. Quaternary Science Reviews, 22(5–7), 453–473. doi.org/10.1016/S0277-3791(02)00248-2

Birks, H. H. and Matthewes, R. W. (1978). Studies in the vegetational history of Scotland. New Phytologist, 80(2), 455-484.

Birks, H. H., Jones, V. J., Brooks, S. J., et al. (2012). From cold to cool in northernmost Norway: Lateglacial and early Holocene multi-proxy environmental and climate reconstructions from Jansvatnet, Hammerfest. Quaternary Science Reviews, 33, 100–120. doi.org/10.1016/j.quascirev.2011.11.013

Birks, H. J. B. (1998). Numerical tools in palaeolimnology—progress, potentialities, and problems. Journal of Paleolimnology 20, 307–332.

Birks, H. J. B. (2011). Strengths and Weaknesses of Quantitative Climate Reconstructions Based on Late-Quaternary Biological Proxies. The Open Ecology Journal, 3(1), 68–110. doi.org/10.2174/1874213001003020068

Birks, H. J. B., Line, J. M., Juggins, S., et al. (1990). Diatoms and pH reconstruction. Philosophical Transactions of the Royal Society of London B, 327, 263-278.

Bitušik P. (2000). Priručka na určovanie lariev pakomarov (Diptera:Chironomidae) Slovenska. Časť I. Buconomyinae, Diamesinae, Prodiamesinae a Orthocladiinae. Technical university in Zvolen. Faculty of ecology and environment, 1-133.

Björck, S., Kromer, B., Johnsen, S., et al. (1996). Synchronized terrestrial-atmospheric deglacial records around the North Atlantic. Science, 274(5290), 1155-1160.

Blockley, S., Candy, I., Matthews, I., et al. (2018). The resilience of postglacial hunter-gatherers to abrupt climate change. Nature Ecology and Evolution, 2(5), 810–818. doi.org/10.1038/s41559-018-

0508-4

Boreham, S., and Horne, D. C. (1999). The role of thermokarst and solution in the formation of Quidenham Mere, Norfolk, compared with some other Breckland meres. Quaternary Research Association, Quaternary Newsletter, 87, 16-27.

Bos, J. A., De Smedt, P., Demiddele, H., et al. (2017). Multiple oscillations during the Lateglacial as recorded in a multi-proxy, high-resolution record of the Moervaart palaeolake (NW Belgium). Quaternary Science Reviews, 162, 26-41.

Bowen, D. Q., Phillips, F.M., McCabe, A.M., et al. (2002). New data for the Last Glacial Maximum in Great Britain and Ireland. Quaternary Science Reviews, 21(1–3), 89–101.

Bradwell, T., Stoker, M. S., Golledge, N. R., et al. (2008). The northern sector of the last British Ice Sheet: Maximum extent and demise. Earth-Science Reviews, 88(3–4), 207–226.

Brasier, A. T., Morris, J. L., and Hillier, R. D. (2014). Carbon isotopic evidence for organic matter oxidation in soils of the Old Red Sandstone (Silurian to Devonian, South Wales, UK). Journal of the Geological Society, 171, 621-634.

Brauer, A., Endres, C., Günter, C., et al. (1999). High resolution sediment and vegetation responses to Younger Dryas climate change in varved lake sediments from Meerfelder Maar, Germany. Quaternary Science Reviews, 18(3), 321-329.

Brauer, A., Haug, G. H., Dulski, P., et al. (2008). An abrupt wind shift in western Europe at the onset of the Younger Dryas cold period. Nature Geoscience, 1(8), 520-523.

Brauer, A., Haug, G. H., Dulski, P., et al. (2008). An abrupt wind shift in western Europe at the onset of the Younger Dryas cold period. Nature Geoscience, 1(8), 520–523. doi.org/10.1038/ngeo263

Brauer, A., Litt, T., Negendank, J.F., et al. (2001). Lateglacial varve chronology and biostratigraphy of lakes Holzmaar and Meerfelder Maar, Germany. Boreas, 30(1), 83-88.

Brauer, A., Mingram, J., Frank, U. et al., (2000). Abrupt environmental oscillations during the Early Weichselian recorded at Lago Grande di Monticchio, southern Italy. Quaternary international, 73/74, 79-90.

Brewer, S., Guiot, J., and Barboni, D. (2007). Pollen data as climate proxies. In: Elias, S (Ed), Encyclopaedia Of Quaternary Science, Elsevier, Amsterdam, 2597-2508.

Briner, J. P., Axford, Y., Forman, S. L., et al. (2007). Multiple generations of interglacial lake sediment preserved beneath the Laurentide Ice Sheet. Geology, 35, 887–890, doi: 10.1130/ G23812A.1

Brodersen, K. P., and Lindegaard, C. (1999a). Classification, assessment and trophic reconstruction of Danish lakes using chironomids.Freshwater Biology, 42(1), 143-157.

Brodersen, K. P., and Lindegaard, C. (1999b). Mass occurrence and sporadic distribution of Corynocera ambigua Zetterstedt (Diptera , Chironomidae) in Danish lakes. Neo- and palaeolimnological records, (1984), 41–52.

Brodersen, K. P., and Quinlan, R. (2006). Midges as paleoindicators of lake productivity, eutrophication and hypolimnetic oxygen. Quaternary Science Reviews, 25, 1995–2012.

Brodersen, K. P., Dall, P. C., and Lindegaard, C. (1998). The fauna in the upper stony littoral of Danish lakes: Macroinvertebrates as trophic indicators. Freshwater Biology, 39(3), 577–592. doi.org/10.1046/j.1365-2427.1998.00298.x

Brodersen, K. P., Odgaard, B. V., Vestergaard, O., et al. (2001). Chironomid stratigraphy in the shallow and eutrophic Lake Søbygaard, Denmark: Chironomid-macrophyte co-occurrence. Freshwater Biology, 46(2), 253–267. doi.org/10.1046/j.1365-2427.2001.00652.x

Brodin, Y-W, Gransberg, M. (1993). Responses of insects, especially Chironomidae (Diptera), and mites to 130 years of acidification in a Scottish lake. Hydrobiologia, 250(3), 201-212.

Brodin, Y-W., and Gransberg, M. (1993). Responses of insects, especially Chironomidae (Diptera), and mites to 130 years of acidification in a Scottish lake. Hydrobiologia 250, 201–212.

Brodin, Y. W. (1986). The postglacial history of Lake Flarken, Southern Sweden, interpreted from subfossil insect remains. Hydrobiology, 71(3), 371-432.

Broecker, W. S. (2006). Abrupt climate change revisited. Global and Planetary Change, 54(3-4), 211-215.

Broecker, W. S., and Denton., G. H. (1989). The role of ocean-atmosphere reorganization in glacial cycles. Geochimica et Cosmochimica Acta, 53, 2465–2501. doi.org/10.1016/0016-7037(89)90123-3

Broecker, W. S., Andree, M., Bonani, G., et al. (1988). Comparison between radiocarbon ages obtained on coexisting planktonic foraminifera. Paleoceanography, 3(6), 647-657, doi.org/10.1029/PA003i006p00647

Broecker, W.S., Kennett, J.P., Flower, B.P., et al. (1989). Routing of meltwater from the Laurentide Ice Sheet during the Younger Dryas cold episode. Nature, 341(6240), 318-321.

Broecker, W.S., Peteet, D.M., and Rind, D. (1985). Does the ocean–atmosphere system have more than one stable mode of operation?. Nature, 315(6014), 21-26.

Bronk Ramsey, C. (2008). Deposition models for chronological records. Quaternary Science Reviews, 27(1), 42-60.

Bronk Ramsey, C. (2009). Bayesian analysis of radiocarbon dates. Radiocarbon, 51(1), 337-360.

Bronk Ramsey, C., Albert, P.G., Blockley, S. P. E., et al. (2015). Improved age estimates for key Late Quaternary European tephra horizons in the RESET lattice. Quaternary Science Reviews, 118, 18-32.

Bronk Ramsey, C., and Lee, S. (2013). Recent and planned developments of the program OxCal. Radiocarbon, 55(2-3), 720-730.

Brooks, S. J. (2006). Fossil midges (Diptera: Chironomidae) as palaeoclimatic indicators for the Eurasian region. Quaternary Science Reviews, 25, 1894–1910.

Brooks, S. J. (1997). The response of Chironomidae (Insecta: Diptera) assemblages to late-glacial climatic change in Kråkenes Lake, western Norway. Quaternary Proceedings 5, 49–58

Brooks, S. J., and Birks, H. J. B. (2000a). Chironomid-inferred Late-Glacial air temperatures at Whitrig Bog, south east Scotland. Journal of Quaternary Science, 15(8), 759-764.

Brooks, S. J., and Birks, H. J. B. (2000b). Chironomid-inferred Late-Glacial and early Holocene mean

July air temperatures for Kråkenes Lake, western Norway. Journal of Paleolimnology, 23(1), 77-89.

Brooks, S. J., and Birks, H. J. B. (2001). Chironomid-inferred air temperatures from Lateglacial and Holocene sites in north-west Europe: progress and problems. Quaternary Science Reviews 20, 1723–1741.

Brooks, S. J., and Heiri, O. (2013). Response of chironomid assemblages to environmental change during the early Late-glacial at Gerzensee, Switzerland. Palaeogeography, Palaeoclimatology, Palaeoecology, 391, 90–98. doi.org/10.1016/j.palaeo.2012.10.022

Brooks, S. J., and Langdon, P. G. (2014). Summer temperature gradients in northwest Europe during the Lateglacial to early Holocene transition (15-8 ka BP) inferred from chironomid assemblages. Quaternary International, 341, 80–90. doi.org/10.1016/j.quaint.2014.01.034

Brooks, S. J., Axford, Y., Heiri, O., et al. (2012). Chironomids can be reliable proxies for Holocene temperatures. A comment on Velle et al., 2010. The Holocene, 22, 1482-1494.

Brooks, S. J., Birks, H. J. B., (2001). Chironomid-inferred air temperatures from Late-glacial and Holocene sites in Northwest Europe: progress and problems. Quaternary Science Reviews, 20, 1723-1741.

Brooks, S. J., Davies, K. L., Mather, K. A., et al. (2016). Chironomid-inferred summer temperatures for the Last Glacial–Interglacial Transition from a lake sediment sequence in Muir Park Reservoir, west central Scotland. Journal of Quaternary Science, 31(3), 214-224.

Brooks, S. J., Langdon, P. G., and Heiri, O. (2007). The identification and use of Palaearctic Chironomidae larvae in palaeoecology. QRA Technical guide No. 10, Quaternary Research Association, London.

Brooks, S. J., Matthews, I. P., Birks, H. H., et al. (2012). High resolution Lateglacial and early-Holocene summer air temperature records from Scotland inferred from chironomid assemblages. Quaternary Science Reviews, 41, 67-82.

Brundin, L. (1949). Chironomiden and andere Bodentiere der südschwedischen Urgebirgs- seen. Report of the Institute of Freshwater Research, Drottningholm 30, 1–914.

Brundin, L. (1956). Die bodenfaunistischen Seetypen und ihre Anwendbarkeit auf die Südhalbkugel. Zugleich eine Theorie der produktionsbiologis chen Bedeutung der glazialen Erosion. Report of the Institute of Freshwater Research, Drottningholm 37, 186–235.

Brundin, L. (1958). The bottom faunistical lake type system and its application to the southern hemisphere. Moreover a theory of glacial erosion as a factor of productivity in lakes and oceans. Verhandlungen der Internationalen Vereinigung für Theoretische und Angewandte Limnologie 13, 288–97.

Brundin, L. (1983). Chilenomyia paradoxa gen. n. and Chilenomyiinae, a new subfamily amongst the Chironomidae. Entomologica Scandinavica, 14, 33–45.

Buckley, M. W., and Marshall, J. (2016). Observations, inferences, and mechanisms of the Atlantic Meridional Overturning Circulation: A review. Reviews of Geophysics, 54(1), 5-63.

Bunting, M. J. (1994). Vegetation history of Orkney, Scotland; pollen records from two small basins in west Mainland. New Phytologist, 128(4), 771-792.

Buskens, R. F. M. (1987). The chironomid assemblages in shallow lentic waters differing in acidity,

buffering capacity and trophic level in the Netherlands. Entomologica Scandinavica supplement 29, 217-224.

Butler, M. G. (1980). Emergence phenologies of some arctic Alaskan Chironomidae, In Murray, D.A., editor, Chironomidae. Ecology, systematics, cytology and physiology. New York, Pergamon Press, 307–314.

Caesar, L., McCarthy, G. D., Thornalley, D. J. R., et al. (2021). Current Atlantic Meridional Overturning Circulation weakest in last millennium. Nature Geoscience, 14(3), 118–120. doi.org/10.1038/s41561-021-00699-z

Campbell, E., and Lane, A. (1989). Llangorse: a 10th-century royal crannog in Wales. Antiquity, 63(1866), 675–681. doi.org/10.1017/S0003598X0007681X

Candy, I., Abrook, A., Elliot, F., et al. (2016). Oxygen isotopic evidence for high-magnitude, abrupt climatic events during the Lateglacial Interstadial in north-west Europe: analysis of a lacustrine sequence from the site of Tirinie, Scottish Highlands. Journal of Quaternary Science, 31(6), 607–621. doi.org/10.1002/jqs.2884

Candy, I., Adamson, K., Gallant, C. E., et al. (2012). Oxygen and carbon isotopic composition of Quaternary meteoric carbonates from western and southern Europe: Their role in palaoenvironmental reconstruction. Palaeogeography, Palaeoclimatology, Palaeoecology. 326-328, 1-11.

Candy, I., Farry, A., Darvill, C. M., et al. (2015). The evolution of Palaeolake Flixton and the environmental context of Star Carr: An oxygen and carbon isotopic record of environmental change for the early Holocene. Proceedings of the Geologists Association, 126(1), 60-71.

Cannings, R. A., and Scudder, G. E. E., (1978). The littoral Chironomidae (Diptera) of saline lakes in central British Columbia. Canadian Journal of Zoology. 56(5): 1144-1155. doi.org/10.1139/z78-158.

Cartier, R., Sylvestre, F., Paillès, C., et al., (2019) Diatom-oxygen isotope record from high-altitude lake petit (2200m a.s.l.) in the Mediterranean Alps: shedding light on a climatic pulse at 4.2 ka. Climate Past, 15, 253–263. doi.org/10.5194/cp-15-253-2019

Cerling, T. E., and Quade, J. (1993). Stable Carbon and Oxygen Isotopes in Soil Carbonate. In: Swart, P. K., Lohmann, K. C., McKenzie, J., et al. (Eds.). Climate Change in Continental Isotopic Records, Washington DC: American Geophysical Union, 217-231.

Chambers, F. M. (1982). Environmental history of Cefn Gwernffrwd, near Rhandirmwyn, mid-wales. New Phytologist, 92, 607-615.

Chambers, F. M. (1985). Flandrian environmental history of the Llynfi catchment, South Wales. Ecologia Mediterranea, 11, 73–80.

Chambers, F. M. (1999). The Quaternary history of Llangorse Lake: implications for conservation. Aquatic Conservation: Marine and Freshwater Ecosystems, 9(4), 343–359.

Clark, C. D., Ely, J. C., Greenwood, S. L., et al. (2018). BRITICE Glacial Map, version 2: a map and GIS database of glacial landforms of the last British–Irish Ice Sheet. Boreas, 47(1), 11-18. doi.org/10.1111/bor.12273

Clark, C. D., Hughes, A. L. C., and Greenwood, S. L. (2012). Pattern and timing of retreat of the last British-Irish Ice Sheet. Quaternary Science Reviews, 44, 112–146.

Clark, I. and Fritz, P. (1997). Environmental Isotopes. In: Hydrogeology, Lewis publishers, New York.

Clark, P. U. (2003). Abrupt climate change. Atlantic, 415(508), 863–869.

Clark, P. U., Marshall, S. J., Clarke, G. K. C., et al. (2001). Freshwater forcing of abrupt climate change during the last deglaciation. Science, 293, 283–287.

Clark, P. U., Pisias, N. G., Stocker, T. F., et al. (2002). The role of the thermohaline circulation in abrupt climate change. Nature, 415(6874), 863-869.

Cockburn, J. M. H., and Lamoureux, S. F. (2007). Century-scale variability in late-summer rainfall events recorded over seven centuries in subannually laminated lacustrine sediments, White Pass, British Columbia. Quaternary Research, 67(2), 193–203. doi.org/10.1016/j.yqres.2006.10.003

Coleman, C. G., Parker, A. G. (2007). WaenDdu bog. In: Carr, S. J., Coleman, C. G., Humpage, A. J., et al. (Eds.), Quaternary of the Brecon Beacons: field guide. Quaternary Research Association, London, UK, 197–200.

Coope, G. R., Lemdahl, G., Lowe, J. J., et al. (1998). Temperature gradients in northern Europe during the last glacial-Holocene transition (14-9 ^{14}C kyr BP) interpreted from Coleopteran assemblages. Journal of Quaternary Science, 13, 419–433.

Coope, G. R., and Jaochim, M. J. (1980). Lateglacial environmental changes interpreted from fossil Coleoptera from St. Bees, Cumbria, NW England. In: Lowe, J. J., Gray, J. M., and Robinson, J. E. (eds.). Studies in the Lateglacial of North-West Europe. Pergamon, Oxford, 55-68.

Coope, G. R., and Brophy, J. A. (1972). Late Glacial environmental changes indicated by a Coleopteran succession from North Wales. Boreas, 1, 97-142.

Cragg, B. A., Fry, J. C., Bacchus, Z. et al. (1980). The aquatic vegetation of Llangorse Lake, Wales. Aquatic Botany, 8, 187–196.

Craig, H. (1953). The Geochemistry of the stable carbon isotopes. Geochimica Et Cosmochimica Acta, 3, 53-92.

Craig, H. (1961). Isotopic variations in meteoric waters. Science, 133(3465), 1702- 1703.

Cranston, P. S. (1982). A Key to the Larvae of the British Orthocladiinae (Chironomidae). Freshwater Biological Association: Ambleside.

Cranston, P. S. and Martin, J. (1989). Family Chironomidae. In: Catalog of the Diptera of the Australasian and Oceanian regions. N.L. Evenhuis (eds.) Bishop Museum Press, Honolulu and E.J. Brill, Leiden, 252-274. http://hbs.bishopmuseum.org/aocat/chiro.html

Cranston, P. S., Oliver, D. R., Saether, O. A. (1983). The larvae of Ortocladiinae (Diptera, Chironomidae) of the Holarctic region - Keys and diagnoses. In: Wiederholm T (ed.). Chironomidae of the Holartic region - Keys and diagnoses. Part 1. Larvae. Entomologica Scandinavica, Supplement 19.

Cwynar, L. C., and Levesque, A. J. (1995). Chironomid evidence for late-glacial climatic reversals in Maine. Quaternary Research, 43(3), 405–413. doi.org/10.1006/qres.1995.1046

Cwynar, L. C., Levesque, A. J., Mayle, F. E., et al. (1994). Wisconsinan Late-glacial environmental change in New Brunswick: A regional synthesis. Journal of Quaternary Science, 9(2), 161–164. doi.org/10.1002/jqs.3390090211.

Cwynar, L. C., Rees, A. B. H., Pedersen, C. R., et al. (2012). Depth distribution of chironomids and an evaluation of site-specific and regional lake-depth inference models from the southern Yukon: a good model gone bad. Journal of Paleolimnology, 48, 517-533.

Dannsgaard, W. (1961). The isotopic composition of natural waters with special reference to the Greenland ice cap. Medd. Groeland, 165(2), 120

Dansgaard, W. (1954). The ^{18}O-abundance in fresh water. Geochimica et Cosmochimica Acta, 6(5-6), 241-260.

Dansgaard, W. (1964). Stable isotopes in precipitation. Tellus, 16(4), 436-468.

Dansgaard, W., Clausen, H. B., Gundestrup, N. (1982). A New Greenland Deep Ice Core, Science, 218(4579), 1273-1277.

Dansgaard, W., Johnsen S. J., Møller, J., et al. (1969). One thousand centuries of climatic record from camp century on the Greenland Ice sheet. Science, 166(3903), 377-381.

Dansgaard, W., Johnsen, S.J., Clausen, H.B., et al. (1993). Evidence for general instability of past climate from a 250-kyr ice- core record. Nature, 364(6434), 218-220.

Darling, W. G. (2004). Hydrological factors in the interpretation of stable isotopic proxy data present and past: a European perspective. Quaternary Science Reviews, 23(7-8), 743-770.

Darling, W. G., Bath, A. H., Talbot, J. C. (2003). The O and H stable isotopic composition of fresh waters in the British Isles. 2. Surface waters and groundwater. Hydrology and Earth System Sciences, 7, 183–195.

Darling, W. G., Talbot, J. C. (2003). The O and H stable isotope composition of freshwaters in the British Isles. 1. Rainfall. Hydrology and Earth System Sciences, 7, 163–181.

Dean, W. E., and Fouch, T. D. (1983). Lacustrine carbonates. In: Scholle, P. A., Bedout, D. G. and Moore, G. H. (Eds). Carbonate Depositional Environments. American Association of Petroleum Geologists, 33, 98–130.

Dearing, J. A. (1999). Environmental Magnetic Susceptibility Using the Bartington MS2 System.

Deines, P. (1980). The isotopic composition of reduced organic carbon. In: Fritz, P., and Fontes, J. Ch. (eds.) Handbook of Environmental Isotope Geochemistry, Vol. 1 Elsevier, New York, 329-406.

Denton, G. H., Alley, R. B., Comer, G. C., et al. (2005). The role of seasonality in abrupt climate change. Quaternary Science Reviews, 24(10–11), 1159–1182. doi.org/10.1016/j.quascirev.2004.12.002

Denton, G.H., Anderson, R.F., Toggweiler, J.R., et al. (2010). The last glacial termination. Science, 328(5986), 1652-1656.

Diefendorf, A. F., Patterson, W. P., Holmden, C., et al. (2008). Carbon isotopes of marl and lake sediment organic matter reflect terrestrial landscape change during the late Glacial and early Holocene (16,800 to 5,540 cal yr BP): a multiproxy study of lacustrine sediments at Lough Inchiquin, western Ireland. Journal of Paleolimnology, 39(1), 101-115.

Diefendorf, A. F., Patterson, W. P., Mullins, H. T., et al. (2006). Evidence for high-frequency late Glacial to mid-Holocene (16,800 to 5500 cal yr BP) climate variability from oxygen isotope values of Lough Inchiquin, Ireland. Quaternary Research, 65(1), 78-86.

Dittrich, M., Kurz, P., and Wehrli, B. (2004). The role of auto- trophic picocyanobacteria in calcite precipitation in an oligo- trophic lake. Geomicrobiology Journal, 21, 45–53.

Dokken, T. M., Nisancioglu, K. H., Li, C., et al. (2013). Dansgaard-Oeschger cycles: interactions between ocean and sea ice intrinsic to the Nordic seas. Paleoceanography 28, 491–502.

Donnelly, J. P., Driscoll, N. W., Uchupi, E., et al. (2005). Catastrophic meltwater discharge down the Hudson Valley: A potential trigger for the Intra-Allerød cold period. Geology, 33(2), 89–92. doi.org/10.1130/G21043.1

Duan, F., Liu, D., Cheng, H., et al. (2014). A high-resolution monsoon record of millennial-scale oscillations during Late MIS 3 from Wulu Cave, south-west China. Journal of Quaternary Science, 29(1), 83–90. doi.org/10.1002/jqs.2681

Eggermont, H., and Heiri, O. (2012). The chironomid-temperature relationship: expression in nature and palaeoenvironmental implications. Biological Reviews, 87, 430–456.

Eicher, U., and Siegenthaler, U. (1976). Palynological and oxygen isotope investigations on Late-Glacial sediment cores from Swiss lakes. Boreas, 5, 109–117.

Elias, S. A., and Matthews, I. P. (2014). A comparison of reconstructions based on aquatic and terrestrial beetle assemblages: Late Glacial-Early Holocene temperature reconstructions for the British Isles. Quaternary International, 341, 69-79.

Engels, S., and Brauer, A., Buddelmeijer, N., et al. (2016). Subdecadal-scale vegetation responses to a previously unknown late-Allerød climate fluctuation and Younger Dryas cooling at Lake Meerfelder Maar (Germany). Journal of Quaternary Science 31(7), 741-752.

Engels, S., and Cwynar, L. C. (2011). Changes in fossil chironomid remains along a depth gradient: evidence for common faunal threshold within lakes. Hydrobiologia, 665, 15–38.

Engels, S., and van Geel, B. (2012). The effects of changing solar activity on climate contributions from palaeoclimatology. Journal of Space Weather and Space Climate, 2, A09. doi.org/10.1051/swsc/2012009.

Engels, S., Cwynar, L. C., Shuman, B. N., et al. (2012). Chironomid-based water depth reconstructions: an independent evaluation of site-specific and local inference models. Journal of Paleolimnology, 48, 693-709.

Engels, S., Self, A. E., Luoto, T. P., et al. (2014). A comparison of three Eurasian chironomid-climate calibration datasets on a W-E continentality gradient and the implications for quantitative temperature reconstructions. Journal of Palaeolimnology, 51(4), 529-547.

EPICA Community Members (2004). Eight glacial cycles from an Antarctic ice core. Nature, 429, 623-628.

Evans, D. J. A. (2007). Glacial Landsystems. In: Knight, P. G., Glacier Science and Environmental Change (2nd ed.). Elsevier. doi.org/10.1002/9780470750636.

Evans, D. J. A., Roberts, D. H., Bateman, M. D., et al. (2019). A chronology for North Sea Lobe advance and recession on the Lincolnshire and Norfolk coasts during MIS 2 and 6. Proceedings of the Geologists Association 130 (5), 523-540

F. Ruddiman, W., and McIntyre, A. (1981). The North Atlantic Ocean during the last deglaciation. Palaeogeography, Palaeoclimatology, Palaeoecology, 35, 145–214. doi.org/10.1016/0031-0182(81)90097-3

Faegri, K., and Iversen, J. (1989). Textbook of Pollen Analysis, 4th Edition. Chichester: John Wiley and Sons

Fauquette, S., Guiot, J., and Suc J-P. (1998). A method for climatic reconstruction of the Mediterranean Pliocene using pollen data. Palaeogeography, Palaeoclimatology, Palaeoecology, 144, 183-201.

Fauquette, S., Guiot, J., and Suc, J-P. (1998). A method for climatic reconstruction of the Mediterranean Pliocene using pollen data. Palaeogeography, Palaeoclimatology, Palaeoecology 144, 183–201.

Felde, V. A., and Birks, H. H. (2019). Using species attributes to characterise Lateglacial and early Holocene environments at Kråkenes, western Norway. Journal of vegetation science, 30(6), 1228-1238.

Finsinger, W., and Tinner, W. (2006). Holocene vegetation and land-use changes in response to climatic changes in the forelands of the southwestern Alps, Italy. Journal of Quaternary Science, 21(3), 243–258. doi.org/10.1002/jqs.971

Finsinger, W., Belis, C., Blockley, S. P. E., et al. (2008). Temporal patterns in lacustrine stable isotopes as evidence for climate change during the late glacial in the Southern European Alps. Journal of Paleolimnology, 40(3), 885–895. doi.org/10.1007/s10933-008-9205-7

Finsinger, W., Tinner, W., van der Knaap, W. O., *et al.* (2006). The expansion of hazel (Corylus avellana L.) in the southern Alps: A key for understanding its early Holocene history in europe? Quaternary Science Reviews, 25, 612-631.

Francis, C. P., Engels, S., Matthews, I. P., et al. (2021). A multi-proxy record of abrupt cooling events during the Windermere Interstadial at Crudale Meadow, Orkney, UK. Journal of Quaternary Science, 36(3), 325–338. doi.org/10.1002/jqs.3289

Freidman, I., ONeil, J. R., and Cebula, G. (1982). Two new carbonate stable isotope standards. Geostandard Newsletter 6, 11-12.

Gale, S. J., Hoare, P. G. (1991). Quaternary Sediments. Belhaven/Halstead: London/New York.

Gathorne-Hardy F. J., Lawson, I. T., Church, M. J., et al. (2007). The Chironomidae of Grothusvatn, Sandoy, Faroe Islands: climatic and lake-phosphorus reconstructions, and the impact of human settlement. The Holocene, 17(8), 1259-1264.

Gathorne-Hardy, F. J., Erlendsson, E., Langdon, P. G., et al. (2009). Lake sediment evidence for late Holocene climate change and landscape erosion in western Iceland. Journal of Paleolimnology, 42(3), 413–426. doi.org/10.1007/s10933-008-9285-4.

Gibbard, P. L., West, R. G., and Hughes, P. D. (2018). Pleistocene glaciation of Fenland, England, and its implications for evolution of the region. Royal Society open science. 5:170736.170736 doi.org/10.1098/rsos.170736.

Godwin, H. (1940). Studies of the post-glacial history of British vegetation-III. Fenland pollen diagrams-IV. Post-glacial changes of relative land-and sea-level in the English Fenland. Philosophical Transactions of the Royal Society of London. Series B, Biological Sciences, 230(570), 239-303.

Godwin, H. (1968). The development of quaternary palynology in the British Isles. Review of palaeobotany and palynology, 6(1), 9-20.

Godwin, H., and Tallantire, P. A. (1951). Studies in the post-glacial history of British vegetation. XII. Hockham Mere, Norfolk. Journal of Ecology, 39, 285-307.

Gray, J. M., Lowe, J. J. (1977). The Scottish Lateglacial environment: a synthesis. In: Gray, J. M., Lowe, J. J. (Eds.), Studies in the Scottish Lateglacial Environment. Pergamon, Oxford, 163-181.

Gray, L. J., Beer, J., Geller, M., et al. (2010). Solar influence on climate. Reviews of Geophysics, **48(4)**, 1-53. doi:10.1029/2009RG000282.

Gregory, J. M., Dixon, K. W., Stouffer, R. J., et al. (2005). A model intercomparison of changes in the Atlantic thermohaline circulation in response to increasing atmospheric CO2 concentration. Geophysical Research Letters, 32(12), 1–5. doi.org/10.1029/2005GL023209

Griggs, A. J. (2015). Constraining Rapid Climatic Transitions in the North Atlantic using Tephrochronology Adam James Griggs. Phd thesis, unpublished.

Griggs, A. J., Davies, S. M., Davies, Abbott, P. M. et al., (2015). Visualising tephra deposits and sedimentary processes in the marine environment: The potential of X-ray microtomography. Geochemistry, Geophysics, Geosystems, 16(12), 4329–4343. doi.org/10.1002/2015GC006073

Grimm, E. C. (1987). CONISS: A fortran 77 program for stratigraphically constrained cluster analysis by the method of incremental sum of squares. Computers and Geosciences, 13(1), 13–35.

Grootes, P. M., Stuiver, M., White, J. W. C., et al. (1993). Comparison of oxygen isotope records from the GISP2 and GRIP Greenland ice cores. Nature, 366, 552-554.

Guibé, J. (1942). Chironomes parasites de mollusqyues gastropods. Chironomous varus lymnaeid Guibé espèce jointive de Chironomous varus varus Goetgh. Bulletin biologique de la France et de la Belgique, 76, 283-297.

Gunther, J. (1983). Development of Grossensee (Holstein, Germany): variations in trophic status from the analysis of subfossil microfauna. Hydrobiologia, 103, 231-234.

Hall, A. M., and Riding, J.B. (2016). The last glaciation in Caithness, Scotland: revised till stratigraphy and ice-flow paths indicate multiple ice flow phases. Scottish journal of geology, 52, 77-89. doi.org/10.1144/sjg2016-001.

Hall, A. M., and Whittington, G. (1989). Late Devensian glaciation of southern Caithness. Scottish Journal of Geology, 25(3), 307-324. doi:10.1144/sjg25030307.

Hamblin, R. J. O., Moorlock, B. S P., Rose, J. (2005). Revised pre-Devensian glacial stratigraphy in Norfolk, England, based on mapping and till provenance. Geoloogie en Mijnbouw, 84(2), 77-85. DOI:10.1017/S0016774600022976.

Harada, E., Lee, R., Denlinger, E., et al. (2014). Life history traits of adults and embryos of the Antarctic midge Belgica antarctica. Polar Biology, 37(8), 1213-1217.

Hawkins, E., Smith, R. S., Allison, L. C., et al. (2011). Bistability of the Atlantic overturning circulation in a global climate model and links to ocean freshwater transport. Geophysical Research Letters, 38(10), 1–6. doi.org/10.1029/2011GL047208

Hays, J. D., Imbrie, J., and Shackleton, N. J. (1976). Variations in the Earths orbit: Pacemaker of the Ice Ages. Science, 194, 1121–1132.

Heiri, O., and Lotter, A. F. (2001). Effect of low count sums on quantitative environmental reconstructions: An example using subfossil chironomids. Journal of Paleolimnology, 26, 343-350. doi.org/10.1023/A:1017568913302

Heiri, O., and Lotter, A. F. (2010). How does taxonomic resolution affect chironomid-based temperature reconstruction? Journal of Paleolimnology 44, 589-601.

Heiri, O., and Millet, L. (2005). Reconstruction of late glacial summer temperatures from chironomid assemblages in Lac Lautrey (Jura, France). Journal of Quaternary Science 20, 33-44.

Heiri, O., Brooks, S. J., Birks, H. J.B., et al. (2011). A 274-lake calibration data-set and inference model for chironomid-based summer air temperature reconstruction in Europe. Quaternary Science Reviews, 30, 3445-3456.

Heiri, O., Brooks, S. J., Renssen, H., et al. (2014). Validation of climate model-inferred regional temperature change for late-glacial Europe. Nature Communications, 5, 1–7. doi.org/10.1038/ncomms5914

Heiri, O., Cremer, H., Engels, S., et al. (2007). Lateglacial summer temperatures in the Northwest European lowlands: a chironomid record from Hijkermeer, the Netherlands. Quaternary Science Reviews 26, 2420-2437

Heiri, O., Lotter, F., Hausmann, S., et al. (2003). A chironomid-based Holocene summer air temperature reconstruction from the Swiss Alps. The Holocene, 4, 477–484.

Heiri, O., Schilder, J., van Hardenbroek, M. (2012) Stable isotopic analysis of fossil chironomids as an approach to environmental reconstruction: state of development and future challenges. Fauna norvegica, 31, 7-18.

Hengeveld, R. (1990). Dynamic Biogeography. Cambridge University Press, Cambridge.

Hershey, A. E. (1985). Littoral chironomid communities in an arctic Alaskan lake. Holarctic Ecology, 42, 483-487.

Hibbert, F. A., and Switsur, V. R. (1976). Radiocarbon dating of Flandrian pollen zones in England and Wales, new phytologist, 77, 793-807.

Hill, M.O. (1973). Diversity and evenness: a unifying notation and its consequences. Ecology 54, 427–432.

Hilsenhoff, W. L. (1966). The biology of Chironomus plumosus in lake Winnebago, Wisconsin. Annals of the entomoligcal society of America, 59, 465-473.

Hoek, W. Z. (1997b). Palaeogeography of Lateglacial vegetations: aspects of Lateglacial and Early Holocene vegetation, abiotic landscape and climate in The Netherlands. Netherlands Geographical Studies 230.

Hoek, W. Z. (1997c). Atlas to Palaeogeography of Lateglacial vegetation: maps of Lateglacial and Early Holocene landscape and vegetation in The Netherlands, with an extensive review of available palynological data. Netherlands Geographical Studies, 231.

Hoek, W. Z., and Bohncke, S. J. P. (2001). Oxygen-isotope wiggle matching as a tool for synchronising ice-core and terrestrial records over Termination 1. Quaternary Science Reviews, 20, 1251-1264.

Hoek, W. Z., Yu, Z. C., and Lowe, J. J. (2008). INTegration of Ice-core, MArine, and TErrestrial records (INTIMATE): refining the record of the Last Glacial-Interglacial Transition. Quaternary Science Reviews, 27(1–2), 1–5. doi.org/10.1016/j.quascirev.2007.11.020

Hoek, W.Z. (1997a). Late-glacial and early Holocene climatic events and chronology of vegetation development in the Netherlands. Vegetation History and Archaeobotany, 6(4), 197-213.

Hofmann, W. (1971). Die postglaziale Entwicklung der Chironomiden-und Chaoborus-Fauna (Dipt.) des Schohsees. Archiv fur Hydrobiologie, 40, 1–74

Hofmann, W. (1978). Analysis of animal microfossils from the Großer Segeberger See (F.R.G.). Archiv für Hydrobiologie, 82, 316–46.

Hofmann, W. (1983). Stratigraphy of Cladocera and Chironomidae in a core from a shallow North German lake. Hydrobiologia, 103, 235–239

Hofmann, W. (1983). Stratigraphy of subfossil Chironomidae and Ceratopogonidae (Insecta: Diptera) in late glacial littoral sediments from Lobsigensee (Swiss Plateau). Studies in the late Quaternary of Lobsigensee 4. Revue de paleobioogie, 2, 205-209.

Hofmann, W. (1984). Stratigraphie subfossiler Cladocera (Crustacea) und Chironomidae (Diptera) in zwei Sedimentprofilen des Meerfelder Maares (Eifel). Courier Forschungsinstitut Senckenberg, 65, 67-80.

Holmes J. A. (2001). Ostracoda. In: Smol J. P., Birks H. J. B., Last W. M. (eds) Tracking Environmental Change Using Lake Sediments. Developments in Paleoenvironmental Research, vol 4. Springer, Dordrecht. doi.org/10.1007/0-306-47671-1_7

Holmes, J. A. (1992). Nonmarine ostracods as Quaternary palaeoenvironmental indicators. Progress in Physical Geography: Earth and Environment, 16(4), 405–431. doi.org/10.1177/030913339201600402

Holmes, N., Langdon, P. G., Caseldine, C., et al. (2011). Merging chironomid training sets: Implications for palaeoclimate reconstructions. Quaternary Science Reviews, 30(19–20), 2793–2804. doi.org/10.1016/j.quascirev.2011.06.013

Horne, A. J., and Goldman, C. R. (1983). Limnology. McGraw, Hill Book Co, New York

Horne, D. J., and Mezquita, F. (2008). Palaeoclimatic applications of large databases: developing and testing methods of palaeotemperature reconstructions using non-marine ostracods. Senckenbergiana Lethaea, 88, 93-112

Hughen, K. A., Overpeck, J. T., Peterson, L. C., et al. (1996). Rapid climate changes in the tropical Atlantic region during the last deglaciation. Nature 380 (6569), 51–54.

Hughes, A. L. C., Gyllencreutz, R., Lohne, Ø. S., et al. (2016). The last Eurasian ice sheets – a chronological database and time-slice reconstruction, DATED-1. Boreas, 45, 1–45. doi.org/10.1111/bor.12142

Hughes, A. L. C., Gyllencreutz, R., Lohne, Ø. S., et al. (2016). The last Eurasian ice sheets - a chronological database and time-slice reconstruction, DATED-1. Boreas, 45(1), 1–45. doi.org/10.1111/bor.12142

Hultén, E. (1950). Atlas of the Distribution of Vascular Plants in NW Europe. Generalstabens Litografiska Anstalts Förlag, Stockholm.

Hultén, E. (1958). The amphi-atlantic plants and their phytogeographical connections. Kungl. Svenska Vetenskapsakademiens Handligar 4 (7/1).

Hultén, E. (1964). The circumpolar plants (vascular cryptograms, conifers, monocotyledons). Kungl. Svenska Vetenskapsakademiens Handlingar 4 (8/ 5).

Hultén, E. (1971a). The circumpolar plants II (Dicotyledons). Kungl. Svenska Vetenskapsakademiens Handlingar 4 (13/1).

Hultén, E. (1971b). Atlas of the Distribution of Vascular Plants in North- western Europe. Generalstabens Litografiska Anstalts Förlag, Stockholm

Humpage, A. J. (2007). Llangorse lake and the Llynfi basin: geomorphological setting and glacial history. In: Carr, S. J., Coleman, C. G., Humpage, A. J., et al. (Eds.). The Quaternary of the Brecon Beacons: Field Guide, London: Quaternary Research Association, 216–219.

Hunt, T. G. and Birks, H. J. B. (1982). Devensian late-glacial vegetational history at Sea Mere, Norfolk. Journal of Biogeography, 9(3), 517-538. doi.org/10.1111/j.1469-8137.1983.tb03512.x

Hunt, T. G., and Birks, H. J. B. (1982). Devensian late-glacial vegetational history of Sea Mere, Norfolk. Journal of Biogeography, 9, 517-538. doi.org/10.2307/2844618

Huntley, B., (2012). Reconstructing palaeoclimates from biological proxies: some often overlooked sources of uncertainty. Quaternary Science Reviews, 31, 1-16. doi.org/10.1016/j.quascirev.2011.11.006

Huntley, B., and Birks, H.J.B. (1983). An atlas of past and present pollen maps for Europe: 0-13000 years ago, p. 667. Cambridge University Press 1982 in files so change to 83

Ilyashuk, B., Gobet, E., Heiri, O., et al. (2009). Lateglacial environmental and climatic changes at the Maloja Pass, Central Swiss Alps , as recorded by chironomids and pollen. Quaternary Science Reviews, 28(13–14), 1340–1353. doi.org/10.1016/j.quascirev.2009.01.007

IPCC. (2021). Climate Change 2021: The physical Science Basis. Contributions of working group 1 to the sixth Assessment Report of the Intergovernmental Panel on climate Change. Cambridge University Press.

Isarin, R. F., and Bohncke, S. J. (1999). Mean July temperatures during the Younger Dryas in northwestern and central Europe as inferred from climate indicator plant species. Quaternary Research, 51(2), 158-173.

Isarin, R. F., Renssen, H., and Vandenberghe, J. (1998). The impact of the North Atlantic Ocean on the Younger Dryas climate in northwestern and central Europe. Journal of Quaternary Science, 13(5), 447-453.

Jalas, J., and Suominen, J. (Eds.)(1980). Atlas Florae Europaeae: Distribution of vascular plants in Europe (5 volunes). Helsinki.

Jansson, K. N., and Glasser, N. F. (2008). Modification of peripheral mountain ranges by former ice sheets: The Brecon Beacons, Southern UK. Geomorphology, 97(1–2), 178–189.

Jeffers, E. S., Bonsall, M. B., Brooks, S. J., et al. (2011). Abrupt environmental changes drive shifts in tree-grass interaction outcomes. Journal of Ecology, 99(4), 1063–1070. doi.org/10.1111/j.1365-2745.2011.01816.x

Johannsson, O. E. (1980). Energy dynamics of the eutrophic chironomid Chironomus plumosus f. semireductus from the Bay of Quinte, Lake Ontario. Canadian Journal of Fisheries and Aquatic Sciences, 37, 1254–65. DOI:10.1139/f80-161

Johnsen, S. J., Clausen, H. B., Dansgaard, W., et al. (1992). Irregular glacial interstadials recorded in a new Greenland ice core. Nature, 359, 311-313. doi.org/10.1038/359311a0

Johnsen, S. J., Dahl-Jensen, D., Gundestrup, N., et al. (2001). Oxygen isotope and palaeotemperature records from six Greenland ice-core stations: Camp Century, Dye-3, GRIP, GISP2, Renland and NorthGRIP. Journal of Quaternary Science, 16(4), 299–307. doi.org/10.1002/jqs.622

Johnsen, S. J., Dansgaard, W., White, J. W. C. (1989). The origin of Arctic precipitation under present and glacial conditions. Tellus, 41B, 452–468. doi.org/10.1111/j.1600-0889.1989.tb00321.x

Johnson, R. K., Wiederholm, T. (1989). classification and ordination of profundal macroinvertebrate communities in nutrient poor, oligotrophic lakes in relation to environmental data. Freshwater Biology, 21, 375-386. doi.org/10.1111/j.1365-2427.1989.tb01370.x

Jones, R., and Benson-Evans, K. (1974). Nutrient and phytoplankton studies of Llangorse Lake, a eutrophic lake in the Brecon Beacons National Park, Wales. Field Studies, 4, 61 -75.

Jones, R., Benson-Evans, K., Chambers, F.M., et al. (1978). Biological and chemical studies of sediments from Llangorse Lake, Wales. Verhandlungen - Internationale Vereinigung fur Theoretische und Angewandte Limnologie 20 (1), 642–648.

Jones, R., Benson-Evans, K., and Chambers, F.M. (1985). Human influence upon sedimentation in Llangorse Lake, Wales. Earth Surface Processes and Landforms, 10(3), 227–235. doi.org/10.1002/esp.3290100305

Jones, R.T., Marshall, J.D., Crowley, S.F., et al. (2002). A high resolution, multiproxy Late-glacial record of climate change and intrasystem responses in northwest England. Journal of Quaternary Science, 17(4), 329-340.

Jouve, G., Francus, P., Lamoureux, S., et al. (2013). Microsedimentological characterization using image analysis and μ-XRF as indicators of sedimentary processes and climate changes during Lateglacial at Laguna Potrok Aike, Santa Cruz, Argentina. Quaternary Science Reviews, 71, 191–204. doi.org/10.1016/j.quascirev.2012.06.003

Jouzel, J., Lorius, C., Petit, J.R., et al. (1987). Vostok ice core: a continuous isotope temperature record over the last climatic cycle (160,000 years). Nature, 329(6138), 403-408.

Jowsey, P. C. (1966). An improved peat sampler. New Phytologist, 65, 245-248.

Juggins, S. (2013). Quantitative reconstructions in paleolimnology: new paradigm or sick science? Quaternary Science Reviews, 64, 20-32.

Juggins, S. (2016). C2 Version 1.7.7. Software for ecological and palaeoecological data analysis and visualisation. Newcastle upon Tyne: Newcastle University. [Software]

Juggins, S. (2017). Rioja: Analysis of Quaternary Science Data, R package Version 0.9-15.1. [Software] (http://cran.r-project.org/package=rioja).

Juggins, S., and Birks, H. J. B., (2012). Quantitative environmental reconstructions from biological data. In: Birks, H. J. B., Lotter, A. F., Juggins, S., et al. (ed.) Tracking Environmental Change using Lake Sediments: Data Handling and Statistical Techniques. Dordrecht: Springer, 431-494.

Kansanen, P. H. (1985). Assessment of pollution history from recent sediments in Lake Vanajavesi, Southern Finland. 2. Changes in the Chironomidae, Chaoboridae and Ceratopogonidae (Diptera) fauna. Annales Zoologici Fennici, 22(1), 57-90.

Karpuz, N. K., and Jansen, E. (1992). A high-resolution diatom record of the last deglaciation from the SE Norwegian sea, documentation of rapid climatic changes. Paleoceanography, 7, 499–520. doi.org/10.1029/92PA01651

Kearney, R., Albert, P. G., Staff, R. A., et al. (2018). Ultra-distal fine ash occurrences of the Icelandic Askja-S Plinian eruption deposits in Southern Carpathian lakes: New age constraints on a continental scale tephrostratigraphic marker. Quaternary Science Reviews, 188, 174-182. DOI:10.1016/j.quascirev.2018.03.035.

Keatings, K. W., Heaton, T. H. E., Holmes, J. A. (2002). Carbon and oxygen isotope fractionation in non-marine ostracods: results from a natural culture environment. Geochimica et Cosmochimica Acta 66(10), 1701–1711. doi.org/10.1016/S0016-7037(01)00894-8

Kelts, K., and Hsü, K. J. (1978). Freshwater carbonate sedimentation. In: Lerman, A. (Ed). Lakes: Chemistry, Geology, Physics, New York: Springer, 295-323.

Kendall, C., and Caldwell, E. A. (1998). Fundamentals of Isotope Geochemistry. In: Kendall, C., and McDonnell, J. J. (eds.), Isotope Tracers in Catchment Hydrology, Elsevier, 839.

Kershaw, A. P., and Nix, H. A. (1988). Quantitative paleoclimatic estimates from pollen data using bioclimatic profiles of extant taxa. Journal of Biogeography, 15, 589–602. doi.org/10.2307/2845438

Konstantinov, A. S. (1958). Influence of temperature on the rate of development and growth of chironomids. Doklady Akadamii Nauk SSR (Soviet Socialist Republic), 120, 1362–65.

Korhola, A., Olander, H., Blom, T. (2000). Cladoceran and chironomid assemblages as quantitative indicators of water depth in subarctic Fennoscandian lakes. Journal of Paleolimnology, 24, 43–54. doi.org/10.1023/A:1008165732542

Kureck, A. (1979). Two circadian eclosion times in Chironomus thummi; (Diptera), alternately selected with different temperatures. Oecologia (Berlin), 40, 311–23.

Kurek, A. (1980). Circadian eclosion rhythm in chironomus thummi; ecological adjustment to different temperature levels and the role of temperature cycles in chironomidae. In: Murray, D. A. (ed.) Chironomidae. Ecology, systematics, cytology and physiology. New York, Pergamon Press, 73-80.

Kurek, J., and Cwynar, L. C. (2009). The potential of site-specific and local chironomid-based inference models for reconstructing past lake-level. Journal of Paleolimnology, 42, 37–50. DOI:10.1007/s10933-008-9246-y

Lamb, A. L., Leng, M. J., Lamb, H. F., Umer, M. (2000). A 9000-year oxygen and carbon isotope record of hydrological change in a small Ethiopian crater lake. The Holocene 10, 167–177.

Lamentowicz, M., Balwierz, Z., Forysiak, J., et al. (2009). Multiproxy study of anthropogenic and climatic changes in the last two millennia from a small mire in central Poland. Hydrobiologia, 631, 213–230.

Land, L. S. (1980). The isotopic and trace element geochemistry of dolomite: the state of the art. In: Zenger, D. H., Dunham, J. B., Ethington, R. L. (eds.), Concepts and Models of Dolomitisation, SEPM Special Publication, 28, 87–110.

Lane, C. S., Brauer, A., Blockley, S. P. E. et al. (2013). Volcanic ash reveals time-transgressive abrupt climate change during the Younger Dryas. Geology, 41(12), 1251-1254. doi.org/10.1130/G34867.1

Lang, B., Bedford, A. P., Richardson, N. et al. (2003). The use of ultrasound in the preparation of carbonate and clay sediments for chironomid analysis. Journal of Paleolimnology 30(4), 451–60. DOI:10.1023/B:JOPL.0000007307.09971.19

Lang, B., Brooks, S.J., Bedford, A. et al. (2010). Regional consistency in Late-Glacial chironomid-inferred temperatures from five sites in north-west England. Quaternary Science Reviews, 29(13), 1528-1538. doi.org/10.1016/j.quascirev.2009.02.023

Langdon, P. G., Holmes, N., and Caseldine, C. J. (2008). Environmental controls on modern chironomid faunas from NW Iceland and implications for reconstructing climate change. Journal of Paleolimnology, 40(1), 273–293. doi.org/10.1007/s10933-007-9157-3

Langdon, P. G., Ruiz, Z., Brodersen, K. P. et al. (2006). Assessing lake eutrophication using chironomids: Understanding the nature of community response in different lake types. Freshwater Biology, 51(3), 562–577. doi.org/10.1111/j.1365-2427.2005.01500.x

Langdon, P. G., Ruiz, Z., Wynne, S. et al. (2010). Ecological influences on larval chironomid communities in shallow lakes: Implications for palaeolimnological interpretations. Freshwater Biology, 55(3), 531–545. doi.org/10.1111/j.1365-2427.2009.02345.x

Larocque-Tobler, I., and Heiri, O. (2010). Late Glacial and Holocene temperature changes at Egelsee, Switzerland , reconstructed using subfossil chironomids, 649–666. doi.org/10.1007/s10933-009-9358-z

Larocque-Tobler, I., Filipiak, J., Tylmann, W., et al. (2015) Comparison between chironomid-inferred mean-august temperature from varved Lake Zabinskie (Poland) and instrumental data since 1896AD. Quaternary Science Review, 11, 35-50.

Larocque, I. (2001). How many chironomid head capsules are enough? A statistical approach to determine sample size for palaeoclimatic reconstructions, 172, 133–142.

Larocque, I., and Finsinger, W. (2008). Late-glacial chironomid-based temperature reconstructions for Lago Piccolo di Avigliana in the southwestern Alps (Italy). Palaeogeography, Palaeoclimatology, Palaeoecology, 257(1–2), 207–223. doi.org/10.1016/j.palaeo.2007.10.021

Larocque, I., Grosjean, M., Heiri, O., et al. (2009). Comparison between chironomid inferred July temperatures and meteorological data AD 1850–2001 from varved Lake Silvaplana, Switzerland. Journal of Paleolimnology, 41, 329–342.

Larocque, I., Hall, R. I., (2003). Chironomids as quantitative indicators of mean July air temperature: validation by comparison with century-long meteorological records from northern Sweden. Journal of Paleolimnology, 29, 475-493.

Larsson, S. A., and Wastegård, S. (2021). A high-resolution Lateglacial-Early Holocene tephrostratigraphy from southernmost Sweden with comments on the Borrobol-Penifiler tephra complex. Quaternary Geochronology, 67, 101239.

Laskar, J., F. Jouzel, and F. Boudin (1993). Orbital, precessional, and insolation quantities for the Earth from −20 Myr to +10 Myr, Astronomy and Astrophysics., 270, 522–533.

Lauterbach, S., Brauer, A., Andersen, N., et al. (2011). Environmental responses to Lateglacial climatic fluctuations recorded in the sediments of pre-Alpine Lake Mondsee (northeastern Alps). Journal of Quaternary Science, 26, 253-267.

Lawrenz, R.W., (1975). The developmental paleoecology of Green Lake, Antrim County, Michigan. MSc Thesis, unpublished.

Lee, J. R., Rose, J., Hamblin, R. J. O., et al. (2004). Dating the earliest lowland glaciation of eastern England: a pre-MIS 12 early Middle Pleistocene Happisburgh glaciation. Quaternary Sciences Reviews 23, 1551-1566

Leng, M. J., and Marshall, J. D. (2004). Palaeoclimate interpretation of stable isotope data from lake sediment archives. Quaternary Science Reviews, 23(7-8), 811-831.

Leng, M. J., Baneschi, I., Zanchetta, G., et al. (2010). Late Quaternary palaeoenvironmental reconstruction from Lakes Ohrid and Prespa (Macedonia/Albania border) using stable isotopes.4 Biogeosciences, 7, 3109–3122. doi.org/10.5194/bg-7-3109-2010

Leng, M. J., Lamb, A. L., Heaton, T. H. E., et al. (2006). isotopes in lake sediments. In: Leng M.J. (eds) Isotopes in Palaeoenvironmental Research. Developments in Paleoenvironmental Research, vol 10. Springer, Dordrecht. doi.org/10.1007/1-4020-2504-1_0

Lenton, T. M., Held, H., Kriegler, E., et al. (2008). Tipping elements in the Earth's climate system. Proceedings of the National Academy of Sciences of the United States of America, 105(6), 1786–1793. doi.org/10.1073/pnas.0705414105

Lenz, F. (1954). Beitrag zur Kenntnis det Ernährungsweise der Tendipedidenlarven. Zoologischer Anzeiger, 153, 197-204

LeSage, L., Harrison, A. D. (1980). The biology of Cricotopus (Chironomidae: Orthocladiinae) in an algal enriched stream: 1. Normal Biology. Archiv fur hydrobiology supplement, 57, 375-418.

Leslie, A.B., Tucker, M.E., and Spiro, B. (1992). A sedimentological and stable isotopic study of travertines and associated sediments within Upper Triassic lacustrine limestones, South Wales, UK. Sedimentology, 39(4), 613-629.

Levesque, A. J., Cwynar, L. C., and Walker, I. R. (1994). A multiproxy investigation of late-glacial climate and vegetation change at pine ridge pond, southwest new brunswick, canada. Quaternary Research. doi.org/10.1006/qres.1994.1082

Levesque, A. J., Cwynar, L. C., and Walker, I. R. (1997). Exceptionally steep north-south gradients in lake temperatures during the Last Deglaciation. Nature, 385, 423-426. doi.org/10.1038/385423a0

Levesque, A. J., Mayle, F. E., Walker, I. R., et al. (1993). The Amphi-Atlantic Oscilation: A proposed late-glacial climatic event. Quanterary Sciences Reviews, 12(8), 629-643. Doi.org/10.1016/0277-3791(93)90004-6

Lewis, C. A. (1970). The Upper Wye and Usk Regions. In: Lewis, C.A. (Ed.). The Glaciations of Wales and Adjoining Regions, London: Longman, 147–173.

Li, C., Battisti, D. S. and Bitz, C. M. (2010). Can North Atlantic sea ice anomalies account for Dansgaard-Oeschger climate signals? J. Clim. 23, 5457–5475.

Lind, E. W., Lilja, C., Wastegård, S., et al. (2016). Revisiting the Borrobol Tephra. Boreas 45, 629–643.

Lindegaard, C. (1997). Diptera Chironomidae, non-biting midges. In A. N. Nilsson (ed.), Aquatic insects of north Europe – a taxonomic handbook. Volume 2. Apollo Books, Stenstrup.

Litt, T., and Stebich, M. (1999). Bio- and chronostratigraphy of the lateglacial in the Eifel region, Germany. Quaternary International 61 (1), 5–16.

Livingstone, D. M., and Lotter, A. F., (1998). The relationship between air and water temperatures in lakes of the Swiss Plateau: a case study with palaeolimnological implications. Journal of Paleolimnology 19, 181–198.

Lombino, A., Atkinson, T., Brooks, S. J. (2021b). Climate reconstruction from paired oxygen-isotope analyses of chironomid larval head capsules and endogenic carbonate (Hawes Water, UK) – potential and problems. Quaternary Science Reviews, 270, 107160.

Lombino, A., Atkinson, T., Brooks, S.J. et al. (2021a). Experimental determination of the temperature dependence of oxygen-isotope fractionation between water and chitinous head capsules of chironomid larvae. Journal of Paleolimnology, 66, 117–124. doi.org/10.1007/s10933-021-00191-z

Lotter, A. F., Birks, H. J. B., Eicher, U., et al. (2000). Younger Dryas and Allerød summer temperatures at Gerzensee (Switzerland) inferred from fossil pollen and cladoceran assemblages. Palaeogeography, Palaeoclimatology, Palaeoecology, 159, 349–361.

Lotter, A. F., Birks, H. J. B., Eicher, U., et al. (2000). Younger Dryas and Allerød summer temperatures at Gerzensee (Switzerland) inferred from fossil pollen and cladoceran assemblages. Palaeogeography, Palaeoclimatology, Palaeoecology, 159, 349–361.

Lotter, A. F., Birks, H. J. B., Hofmann, W., et al. (1997). Modern diatom, cladocera, chironomid, and chrysophyte cyst assemblages as quantitative indicators for the reconstruction of past environmental conditions in the Alps. I. Climate. Journal Paleolimnology 18, 395–420.

Lotter, A. F., Eicher, U., Siegenthaler, U., et al. (1992). Late-Glacial climatic oscillations as recorded in Swiss lake-sediments. Journal of Quaternary Science, 7(3), 187–204.

Lotter, A. F., Heiri, O., Brooks, S. J., et al. (2012). Rapid summer temperature changes during Termination 1a: high- resolution multi-proxy climate reconstructions from Gerzensee (Switzerland). Quaternary Science Reviews, 36, 103-113.

Lotter, A. F., Walker, I. R., Brooks, S. J., et al. (1999). An intercontinental comparison of chironomid palaeotemperature inference models: Europe vs North America. Quaternary Science Reviews, 18(6), 717–735. doi.org/10.1016/S0277-3791(98)00044-4

Lowe, J. J., and Walker, M. J. C. (1986). Flandrian environmental history of the Island of Mull, Scotland. II . Pollen analytical data from sites in western and northern Mull. New Phytologist 103(2), 417-436.

Lowe, J. J., Birks, H. H., Brooks, S. J., et al. (1999). The chronology of palaeoenvironmental changes during the Last Glacial-Holocene transition: towards an event stratigraphy for the British Isles. Journal of the Geological Society, 156(2), 397-410.

Lowe, J. J., Rasmussen, S. O., Björck, S., et al. (2008). Synchronisation of palaeoenvironmental events in the north Atlantic region during the Last Termination: a revised protocol recommended by the INTIMATE group. Quaternary Science Reviews, 27(1), 6-17. doi.org/10.1016/j.quascirev.2007.09.016

Mackay A. P. (1979). Growth and development of larval chironomidae. Oikos, 28, 270-275.

Magny, L., Bégeot, C. Ruffaldi, P., et al. (2002). Variations paléhydrologiques de 14700 à 11000 cal BP dans le Jura et les Préalpes françaises. In: Bravard, J-P., and Magney, M. (eds.) Historie des rivières et des lacs de Lascaux à nos jours. Errance: Paris, 135-142.

Mangerud, J. (2020). The discovery of the Younger Dryas, and comments on the current meaning and usage of the term. Boreas, 50(1), 1-5.

Mangerud, J., Andersen, S.T., Berglund, et al. (1974). Quaternary stratigraphy of Norden, a proposal for terminology and classification. Boreas 3, 109-128.

Marshall, J. D., Jones, R. T., Crowley, S. F., et al. (2002). A high resolution late glacial isotopic record from Hawes Water, Northwest England. Climatic oscillations: calibration and comparison of palaeotemperature proxies. Palaeogeography, Palaeoclimatology, Palaeoecology 185, 25–40.

Marshall, J. D., Jones, R. T., Crowley, S. F., et al. (2002). A high resolution Late-Glacial isotopic record from Hawes Water, north-west England: climatic oscillations: calibration and comparison of palaeotemperature proxies. Palaeogeography, Palaeoclimatology, Palaeoecology, 185(1), 25-40.

Marshall, J. D., Lang, B., Crowley, S. F., et al. (2007). Terrestrial impact of abrupt changes in the North Atlantic thermohaline circulation: early Holocene, UK. Geology 35, 639–642

Martin-Puertas, C., Matthes, K., Brauer, A., et al. (2012). Regional atmospheric circulation shifts induced by a grand solar minimum. Nature Geoscience, 5(6), 397-401.

Marziali, L., and Rossaro, B. (2006). Thoracic horn structure in Orthocladiini pupae (Diptera: Chironomidae: Orthocladiinae). Studi Trent Scienze Naturali Acta Biologica, 82, 69-76

Massaferro, J., and Brooks, S. (2002). Response of chironomids to late quaternary environmental change in the Taitao Peninsula, southern Chile. Journal of Quaternary Science, 17(2), 101–111.

Masson-Delmotte, V., Jouzel, J., Landais, A. et al. (2005). GRIP deuterium excess reveals rapid and orbital-scale changes in Greenland moisture origin. Science, 309, 118-121.

Masson-Delmotte, V., Stenni, B., Pol, K. et al. (2010). EPICA Dome C record of glacial and interglacial intensities. Quaternary Science Reviews, 29, 113-128. doi:10.1016/j.quascirev.2009.09.030

Matthews, I. P., Birks, H. H., Bourne, A. J., et al. (2011). New age estimates and climatostratigraphic correlations for the Borrobol and Penifiler Tephras: evidence from Abernethy Forest, Scotland. Journal of Quaternary Science, 26(3), 247–252.

Mauquoy, D., van Geel, B., Blaauw, M., et al. (2002). Evidence from northwest European bogs shows Little Ice Age climatic changes driven by variations in solar activity. The Holocene 12, 1–6.

Mayle, F. E., Bell, M., Birks, H. H., et al. (1999). Climate variations in Britain during the Last Glacial–Holocene transition (15.0–11.5 Cal. ka BP): comparison with the GRIP ice-core record. Journal of the Geological Society, 156(2), 411-423.

McKenzie, J. A. and Hollander, D. J. (1993). Oxygen isotope record in recent carbonate sediments from Lake Griefen, Switzerland (1750-1986): Application of continental isotopic indicator for evaluation of changes in climate and atmospheric circulation patterns. In: Swart, P.K., Lohmann, K.C., McKenzie, J.A. et al. (eds.), Climate Change in Continental Isotopic Records. Geophysical Monographs 78, Washington, DC, American Geophysical Union, 101-112.

McKinney, C. R., McCrea, J. M., Epstein, S., et al. (1950). Improvements in mass spectrometers for the

measurement of small differences in isotope abundance ratios. Review of Scientific Instruments, 21(8), 724-730. doi:10.1063/1.1745698

McManus, J. F., Francois, R., Gherardi, J., et al. (2004). Collapse and rapid resumption of Atlantic meridional circulation linked to deglacial climate changes. Nature, 428(6985), 834–837. doi.org/10.1038/nature02494

Meese, D. A., Gow, A. J., Grootes, P., et al. (1994). The Accumulation Record from the GISP2 Core as an Indicator of Climate Change Throughout the Holocene. Science, 266(5191), 1680–1682. doi.org/10.1126/science.266.5191.1680

Merkt, J., and Müller, H. (1999). Varve chronology and palynology of the Lateglacial in North- west Germany from lacustrine sediments of Hämelsee in Lower Saxony. Quaternary International, 61(1), 41–59.

Millet, L., Rius, D., Galop, D. et al. (2012). Chironomid-based reconstruction of Lateglacial summer temperatures from the Ech palaeolake record (French western Pyrenees). Palaeogeography, Palaeoclimatology, Palaeoecology, 315–316, 86–99. doi.org/10.1016/j.palaeo.2011.11.014

Millet, L., Verneaux, V., and Magny, M. (2003) Lateglacial palaeoenvironmental reconstruction using subfossil chironomid assemblages from Lake Lautrey (Jura, France). Archiv für Hydrobiologie, 156, 405-429.

Mitchell, F., and Ryan, M. (1997). Reading the Irish Landscape, 3rd ed. Country House, Dublin.

Mitchell, G. F., Penny, L. F., Shotton, F. W., et al. (1973). A correlation of the Quaternary deposits of the British Isles. Geological Society of London, Special Report 4. Edinburgh, Scottish Press.

Mix, A. C., Bard, E., and Schneider, R. (2001). Environmental processes of the ice age: land, oceans, glaciers (EPILOG) Quaternary Science Reviews, 20(4), 627-657.

Moar, N. T. (1969). Two Pollen Diagrams from the Mainland, Orkney Islands. New Phytologist, 68(1), 201–208.

Moffa-Sanchez, P., Born, A., Hall, I. R., et al. (2014). Solar forcing of North Atlantic surface temperature and salinity over the past millennium. Nature Geoscience, 7, 275-278.

Moller Pillot, H. (2014). Chironomidae Larvae, Vol. 2: Chironomini. Leiden, The Netherlands: KNNV Publishing.

Moller Pillot, H. (2014). Chironomidae Larvae, Vol. 3: Orthocladiinae. Leiden, The Netherlands: KNNV Publishing.

Moog, O. (1995). Fauna aquatica austriaca. Abteilung für Hydrobiologie, Fischereiwirtschaft und Aquakultur der Universität für Bodenkultur, Vienna

Mook, W. G. (2006). Introduction to Isotope Hydrology. Stable and Radioactive Isotopes of Hydrogen, Oxygen and Carbon. Taylor and Francis, London

Moreno, A., Svensson, A., Brooks, S. J., et al. (2014). A compilation of Western European terrestrial records 60-8kaBP: Towards an understanding of latitudinal climatic gradients. Quaternary Science Reviews, 106, 167–185. doi.org/10.1016/j.quascirev.2014.06.030

Moreno, A., Svensson, A., Brooks, S. J., et al. (2014). A compilation of Western European terrestrial records 60–8 ka BP: towards an understanding of latitudinal climatic gradients.

Quaternary Science Reviews, 106, 167-185.

Muñoz Sobrino, C., Heiri, O., Hazekamp, M., et al. (2013). New data on the Lateglacial period of SW Europe: a high resolution multiproxy record from Laguna de la Roya (NW Iberia). Quaternary Science Reviews, 80, 58–77. doi.org/10.1016/j.quascirev.2013.08.016

Murphy, D. H., and Wilkinson, B. H. (1980). Carbonate deposition and facies distribution in a central Michigan marl lake. Sedimentology, 27(2), 123–135.

Muschitiello, F., and Wohlfarth, B. (2015b). Time-transgressive environmental shifts across Northern Europe at the onset of the Younger Dryas. Quaternary Science Reviews, 109, 49-56.

Muschitiello, F., DAndrea, W. J., Schmittner, A. et al. (2019). Deep-water circulation changes lead North Atlantic climate during deglaciation. Nature Communications, 10, 1272. doi.org/10.1038/s41467-019-09237-3

Muschitiello, F., O'Regan, M., Martens, J., et al. (2020). A new 30 000-year chronology for rapidly deposited sediments on the Lomonosov Ridge using bulk radiocarbon dating and probabilistic stratigraphic alignment. Geochronology, 2(1), 81–91. doi.org/10.5194/gchron-2-81-2020.

Muschitiello, F., Pausata, F. S. R., Watson, J. E. et al. (2015a). Fennoscandian freshwater control on Greenland hydroclimate shifts at the onset of the Younger Dryas. Nature Communications, 6, 8939. doi.org/10.1038/ncomms9939

Mykura, M. (1976). British Regional Geology: Orkney and Shetland. Edinburgh: Institute of Geological Sciences, HMSO, NERC.

Nazarova, L., Herzschuh, U., Wetterich, S. et al. (2011). Chironomid-based inference models for estimating mean July air temperature and water depth from lakes in Yakutia, northeastern Russia. Journal of Paleolimnology, 45(1), 57-71.

Nesje, A., Bakke, J., Brooks, S. J. et al. (2014). Late glacial and Holocene environmental changes inferred from sediments in Lake Myklevatnet, Nordfjord, western Norway. Vegetation History and Archaeobotany, 23(3), 229–248. doi.org/10.1007/s00334-013-0426-y

Obbink, E. A., Carlson, A. E., Klinkhammer, G. P., Obbink, E. A., Carlson, A. E., and Klinkhammer, G. P. (2010). periods Eastern North American freshwater discharge during the Bølling- Allerød warm periods. doi.org/10.1130/G30389.1

O'Connell, M., Huang, C. C., and Eicher, U. (1999). Multidisciplinary investigations, including stable-isotope studies, of thick Late-glacial sediments from Tory Hill, Co. Limerick, western Ireland. Palaeogeography, Palaeoclimatology, Palaeoecology, 147(3–4), 169–208. doi.org/10.1016/S0031-0182(98)00101-1

Oksanen, J., Blanchet F. G., Friendly, M., et al. (2017). Package vegan: community ecology package, version:2.4-4

Olander, H., Birks, H. J. B., Korhola, A. et al. (1999). An expanded calibration model for inferring lake water and air temperatures from fossil chironomid assemblages in northern Fennoscandia. The Holocene, 9, 279–94.

Oliver, D. R. (1968). Adaptations of arctic Chironomidae. Annales Zoologica Fennici, 5, 111-118

Oliver, D. R. (1971). Life history of the Chironomidae. Annual Review of Entomology, 16, 211–30.

Oliver, D. R. and Roussel, M. E. (1983). The insects and arachnids of Canada, Part II: The genera of larval midges of Canada-Diptera: Chironomidae. Agriculture Canada Publication, 1746, 1–263.

O'Neil-Munro, N. (2017). Chironomid inferred temperatures of The White bog, Co. Down, Northern Ireland: assessing landscape response to short term climatic oscillations during the Last Glacial Interstadial. MSc Thesis, Royal Holloway

O'Neil, J. R. (1986). Theoretical and experimental aspects of isotopic fractionation. Reviews in Mineralogy and Geochemistry 16, 1-40

Orendt, C. (1993). Vergleichende Untersuchungen zur Ökologie lotoraler, benthischer Chironomidae und anderer Diptera (Ceratopogonidae, Chaoboridae) in Seen des nördlichen Alpenvorlandes. Thesis, München University.

O'Sullivan, P. E. (1983). Annually laminated lake sediments and the study of Quaternary environmental changes – A review. Quaternary Science Reviews, 1(4), 245-313.

Palmer, A. P., Matthews, I. P., Candy, I., et al. (2015). The evolution of Palaeolake Flixton and the environmental context of Star Carr, NE. Yorkshire: Stratigraphy and sedimentology of the Last Glacial-Interglacial Transition (LGIT) lacustrine sequences. Proceedings of the Geologists Association, 126(1), 50–59.

Palmer, A. P., Rose, J., Lowe, J. J., et al. (2007). The pre-Holocene succession of glaciolacustrine sediments within Llangorse basin. In: Carr, S.J., Coleman, C.G., Humpage, A.J., et al. (Eds.). The Quaternary of the Brecon Beacons: Field Guide, London: Quaternary Research Association, 220-229.

Palmer, A. P., Rose, J., Lowe, J. J., et al. (2008). Annually laminated Late Pleistocene sediments from Llangorse Lake, South Wales, UK: a chronology for the pattern of ice wastage. Proceedings of the Geologists Association, 119, 245–258.

Palmer, A., Matthews, I., MacLeod, A., et al. (2021). The Late Quaternary sediment successions of Llangorse Lake, south Wales. Proceedings of the Geologists Association, 132(3), 284-296. doi.org/10.1016/j.pgeola.2021.01.004

Patton, H., Hubbard, A., Glasser, N. F., et al. (2013). The last Welsh Ice Cap: Part 1–Modelling its evolution, sensitivity and associated climate. Boreas, 42, 471–490.

Peach, B. N., and Horne, J. (1880). The glaciation of the Orkney Islands. Quarterly Journal of the Geological Society, 36(1–4), 648–663.

Pearson, F. J., Jr., and Coplen, T. B. (1978). Stable isotope studies of lakes. In: Lerman, A. (ed.), Lakes: Chemistry, Geology, Physics, New York, Springer Verlag, 325-336.

Perrin, R. M. S., Rose, J. and Davies, H. (1979). The distribution, variation and origins of pre-Devensian tills in eastern England. Philosophical Transactions of the Royal Society of London, B287, 535-570.

Petit, J. R., Jouzel, J., Raynaud, et al. (1999) Climate and atmospheric history of the past 420,000 years from the Vostock ice core, Antarctica. Nature, 399, 429-436.

Petoukhov, V., Claussen, M., Berger, A., et al. (2005). EMIC Intercomparison Project (EMIP-CO2: Comparative analysis of EMIC simulations of climate, and of equilibrium and transient responses to atmospheric CO2 doubling. Climate Dynamics, 25(4), 363–385. doi.org/10.1007/s00382-005-0042-3

Peyron O., Guiot J., Cheddadi R., et al. (1998). Climatic reconstruction in Europe for 18,000 year BP from pollen data. Quaternary Research 49, 183–196.

Peyron, O., Bégeot, C., Brewer, S., et al. (2005). Late-Glacial climatic changes in Eastern France (Lake Lautrey) from pollen, lake-levels, and chironomids. Quaternary Research, 64(2), 197–211. doi.org/10.1016/j.yqres.2005.01.006

Peyron, O., Guiot, J., Cheddadi, R, et al. (1998). Climatic reconstruction in Europe for 18,000 year BP from pollen data. Quaternary Research, 49, 183–1.

Pinder, L. C. V. (1980). Spatial distribution of Chironomidae in an English chalk stream. In: Murray, D. A., (eds.) Chironomidae: ecology, systematics, cytology and physiology. Oxford: Pergamon Press, 153–161.

Pinder, L. C. V. (1986). Biology of freshwater chironomidae. Annual review of entomology, 31, 1-23.

Pinder, L. C. V. (1995). Biology of the eggs and first-instar larvae. In: Armitage, P.D., Cranston, P.S. and Pinder, L.C., (eds.) The Chironomidae: the biology and ecology of nonbiting midges. London: Chapman and Hall, 87–106.

Pinder, L. C. V., and Reiss, F. (1983). The larvae of Chironominae (Diptera: Chironomidae) of the Holarctic region. In: Wiederholm, T. (Ed.), Chironomidae of Holarctic Region, Keys and Diagnoses (Part 1-Larvae). Entomologica Scandinavica Supplement, 293-436.

Plociennik, M., Self, A., Brooks, S. J., et al. (2011). Late-glacial and Holocene chironomid record from Lake Żabieniec, central Poland. Palaeogeography, Palaeoclimatology, Palaeoecology, 307, 150-167.

Porinchu, D. F., and Cwynar, L. C. (2002). Late-Quaternary history of midge communities and climate from a tundra site near the lower Lena River, Northeast Siberia. Journal of Paleolimnology, 27, 59–69.

Porinchu, D. F., and MacDonald, G. M. (2006). The use and application of freshwater midges (chironomidae: Insecta: Diptera) in geographical research. Progress in Physical Geography, 27(3), 378-442.

Quinlan, R., and Smol, J. P. (2001a). Chironomid-based inference models for estimating end-of-summer hypolimnetic oxygen from south-central Ontario shield lakes. Freshwater Biology, 46(11), 1529–1551. doi.org/10.1046/j.1365-2427.2001.00763.x

Quinlan, R., and Smol, J. P. (2001b). Setting minimum head capsule abundance and taxa deletion criteria in chironomid-based inference models, 26(3), 327–342.

Quinlan, R., and Smol, J. P. (2002). Regional assessment of long-term hypolimnetic oxygen changes in Ontario (Canada) shield lakes using subfossil chironomids. Journal of palaeolimnology, 27(2), 249-260.

R Core team. (2018). R: A language and environment for statistical computing. R foundation for statistical computing, Vienna, Austria. www.R-project.org

Rach, O., Brauer, A., Wilkes, H., et al. (2014). Delayed hydrological response to Greenland cooling at the onset of the Younger Dryas in western Europe. Nature Geoscience, 7, 109-112.

Rae, D. A. (1976). Aspects of glaciation in Orkney. PhD thesis, University of Liverpool.

Rasmussen, S. O., Andersen, K. K., Svensson, A. M., et al. (2006). A new Greenland ice core chronology for the last glacial termination. Journal of Geophysical Research Atmospheres, 111(6), 1–16. doi.org/10.1029/2005JD006079

Rasmussen, S. O., Bigler, M., Blockley, S. P., et al. (2014). A stratigraphic framework for abrupt climatic changes during the Last Glacial period based on three synchronized Greenland ice-core records: Refining and extending the INTIMATE event stratigraphy. Quaternary Science Reviews, 106, 14–28. doi.org/10.1016/j.quascirev.2014.09.007

Reimer P, Austin W, Bard E et al. (2020). The IntCal20 Northern Hemisphere Radiocarbon Age Calibration Curve (0–55 cal kbp). Radiocarbon 62(4), 725–757.

Reimer, P. J., Bard, E., Bayliss, A., et al. (2013). IntCal13 and Marine13 radiocarbon age calibration curves 0–50,000 years Cal. BP. Radiocarbon, 55(4), 1869-1887.

Reiss, F. (1968). Verbreitung lakustrischer Chironomiden (Diptera) des Alpengebietes. Annales Zoologici Fennici, 5, 119–125.

Renssen, H., and Bogaart, P. W. (2003). Atmospheric variability over the ∼14.7 kyr BP stadial-interstadial transition in the North Atlantic region as simulated by an AGCM. Climate Dynamics, 20(2–3), 301–313. doi.org/10.1007/s00382-002-0271-7

Renssen, H., and Isarin, R. F. B. (2001). The two major warming phases of the last deglaciation at ∼14.7 and ∼11.5 ka cal BP in Europe: Climate reconstructions and AGCM experiments. Global and Planetary Change 30(1-2), 117-153. doi.org/10.1016/S0921-8181(01)00082-0

Renssen, H., and Isarin, R. F. B. (2001). The two major warming phases of the last deglaciation at ∼14.7 and ∼11.5 ka cal BP in Europe: Climate reconstructions and AGCM experiments. Global and Planetary Change, 30(1-2), 117-153. doi.org/10.1016/S0921-8181(01)00082-0

Ricketts, R. D., and Anderson, R. F. (1998). A direct comparison between the historical record of lake level and the $\delta^{18}O$ signal in carbonate sediments from lake Turkana, Kenya. Limnology and Oceanography 43, 811–822.

Rieradevall, M., and Brooks, S. J. (2001). An identification guide to subfossil Tanypodinae larvae (Insecta: Diptera: Chironomidae) based on cephalic setation. Journal of Paleolimnology, 25, 81–99.

Rose, J. (2009). Early and Middle Pleistocene landscapes of eastern England. Proceedings of the Geologists Association, 120(1), 3–33. doi.org/10.1016/j.pgeola.2009.05.003

Rozanski, K., Araguás-Araguás, L., and Gonfiantini, R. (1992). Relation between long- term trends of oxygen-18 isotope composition of precipitation and climate. Science, 258(5084), 981-985.

Rozanski, K., Araguás-Araguás, L., and Gonfiantini, R. (1993). Isotopic patterns in modern global precipitation. In: Swart, P.K., Lohmann, K.C., McKenzie. J., et al. (eds.). Climate Change in Continental Isotopic Records, Washington DC: American Geophysical Union, 1-36.

Rozanski, K., Johnsen, S.J., Schotterer, U., et al. (1997). Reconstruction of past climates from stable isotope records of palaeoprecipitation preserved in continental archives. Hydrological sciences, 42(5), 725-745

Ruddiman, W. F., Raymo, M. E., and McIntyre, A. (1986). Matuyama 41,000-year cycles: North Atlantic Ocean and northern hemisphere ice sheets. Earth and Planetary Science Letters, 80, 117-129.

Saether, O. A. (1979). Chironomid communities as water quality indicators. Holarctic Ecology 2, 65–74.

Saether, O. A. (1983). The larvae of the Prodiamesinae (Diptera: chironomidae) of the haloarctic region – keys and diagnoses. Entomologica scandinavica supplement, 19, 141-147.

Samartin, S., Heiri, O., Vescovi, E., et al. (2012). Lateglacial and early Holocene summer temperatures in the southern Swiss Alps reconstructed using fossil chironomids. Journal of Quaternary Science, 27(3), 279–289. doi.org/10.1002/jqs.1542

Schwander, J., Eicher, U., and Ammann, B. (2000). Oxygen isotopes of lake marl at Gerzensee and Leysin (Switzerland), covering the Younger Dryas and two minor oscillations, and their correlation to the GRIP ice core. Palaeogeography, Palaeoclimatology, Palaeoecology, 159(3–4), 203–214. doi.org/10.1016/S0031-0182(00)00085-7

Schwarcz, H. (2007). Carbonate stable isotopes. In: Elias, S (Ed), Encyclopaedia Of Quaternary Science, Elsevier, Amsterdam, 291-293.

Searl, A. (1989). Diagenesis of the Gully Oolite (Lower Carboniferous) South Wales. Geological Journal, 24(4), 275-293.

Sejrup, H.P., Clark, C.D., and Hjelstuen, B.O. (2016). Rapid ice sheet retreat triggered by ice stream debuttressing: Evidence from the North Sea. Geology, 44(5), 355– 358.

Sejrup, H.P., Hjelstuen, B.O., Nygård, A., et al. (2015). Late Devensian ice-marginal features in the central North Sea - processes and chronology. Boreas, 44(1), 1–13.

Self, A. E., Brooks, S. J., Birks, H. J. B., et al. (2011). The distribution and abundance of chironomids in high-latitude Eurasian lakes with respect to temperature and continentality: Development and application of new chironomid-based climate-inference models in northern Russia. Quaternary Science Reviews, 30(9–10), 1122–1141. doi.org/10.1016/j.quascirev.2011.01.022

Seppä, H., and Birks, H. J. B. (2001). July mean temperature and annual precipitation trends during the Holocene in the Fennoscandian tree-line area: Pollen-based climate reconstructions. The Holocene, 11, 527–539.

Shemesh, A., Rosqvist, G., Rietti-Shati, M., et al. (2001). Holocene climate change in Swedish Lapland inferred from an oxygen isotope record of lacustrine biogenic silica. The Holocene 11, 447–454.

Singh, H. A., Battisti, D. S. and Bitz, C. M. A. (2014). heuristic model of dansgaard- oeschger cycles. part i: Description, results, and sensitivity studies. J. Clim. 27, 4337–4358

Sissons, J. B. (1967). Glacial stages and radiocarbon dates in Scotland. Scottish Journal of Geology, 3, 375-381.

Sissons, J. B., (1974). The Quaternary in Scotland: a review. Scottish Journal of Geology, 10, 311-337.

Słowiński, M., Zawiska, I., Ott, F., et al. (2017). Differential proxy responses to late Allerød and early Younger Dryas climatic change recorded in varved sediments of the Trzechowskie palaeolake in Northern Poland. Quaternary Science Reviews, 158, 94-106.

Smith, A. G. and Cloutman, E. W. (1988). Reconstruction of Holocene vegetation history in three dimensions at Waun-Fignen-Felen, an upland site in South Wales. Philosophical transactions of the Royal society, London (B), 322, 159-219.

Smith, D. B., Downing, R. A., Monkhouse, R.A., et al. (1976). The age of groundwater in the Chalk of the London Basin, Water Resources Research, 12, 392-403.

Steenbergen, H. A. (1993). Macrofauna-Atlas van Noord-Holland: Verspreidingskaarten en Responsies op Milieufactoren van Ongewervelde Waterdieren. Provincie Noord-Holland, Dienst Ruimte en Groen, Haarlem, The Netherlands, Basisinformatie 7.

Steffensen, J. P., Andersen, K.K., Bigler, M., et al. (2008). High-resolution Greenland ice-core data show abrupt climate change happens in few years. Science, 321(5889), 680-684.

Stocker, T. F. (1999). Abrupt climate changes: from the past to the future – a review. International Journal of Earth Sciences, 88(2), 365-374.

Strenzke, K. (1950). Systematik, Morphologie und Ökologie der terrestrischen Chironomiden. Archiv für Hydrobiologie, 18, 207–414

Stuiver, M., and Polach, H.A. (1977). Reporting of C-14 data e discussion. Radiocarbon 19, 355-363.

Sun, Y., Clemens, S. C., An, Z., et al. (2006). Astronomical timescale and palaeoclimatic implications of stacked 3.6-Myr monsoon records from the Chinese Loess Plateau. Quarernary Science Reviews, 25, 33-48.

Talbot, M. R. (1990). A review of the palaeohydrological interpretation of carbon and oxygen isotopic ratios in primary lacustrine carbonates. Chemical Geology: Isotope Geoscience Section, 80(4), 261-279.

Tallantire, P. A. (1951). Studies in the Post-Glacial History of British Vegetation, 95–107.

Tallantire, P. A. (1953a) Old Buckenham Mere Data for the study of post-glacial history: XIII. New Phytologist, 53, 131-139.

Tallantire, P. A. (1953b). Studies in the post-glacial history of British vegetation. XIII. Lopham Little Fen, a late- glacial site in central East Anglia. Journal of Ecology, 41, 361-373.

Tarasov, L., and Peltier, W.R. (2005). Arctic freshwater forcing of the Younger Dryas cold reversal. Nature, 435(7042), 662-665.

Tarkowska-Kukuryk M, and Toporowska M. (2021) Long-term responses of epiphytic midges (Diptera, Chironomidae) to emergent macrophytes removal and P concentrations in a shallow hypertrophic lake ecosystem. Science of the Total Environ. 1;750:141508. doi: 10.1016/j.scitotenv.2020.141508.

Tarkowska-Kukuryk, M. (2013). Periphytic algae as food source for grazing chironomids in a shallow phytoplankton-dominated lake. Limnologica, 43(4), 254–264. doi.org/10.1016/j.limno.2012.11.004 add in text with one above

Taylor, K.C., Mayewski, P.A., Twickler, M.S., et al. (1996). Biomass burning recorded in the GISP2 ice core: A record from eastern Canada? The Holocene 6, 1-6.

Telesiński, M. M., Ezat, M. M., Muschitiello, F., et al. (2021). Ventilation History of the Nordic Seas Deduced from Pelagic-Benthic Radiocarbon Age Offsets. Geochemistry, Geophysics, Geosystems, 22(4), 1–10. doi.org/10.1029/2020GC009132

Telford, R. (2014a). Analogue quality, reconstruction quality. [Blog] Musings on Quantitative Palaeoecology. quantpalaeo. wordpress.com/2014/05/11/analogue-quality-reconstruction- quality/ [Accessed June 2020].

Telford, R. (2014b). Beyond nearest analogue distance. [Blog] Musings on Quantitative Palaeoecology. quantpalaeo.wordpress.com/2014/ 05/17/beyond-nearest-analogue-distance/ [Accessed June 2020].

Telford, R., and Birks, H. J. B. (2009). Design and evaluation of transfer functions in spatially structured environments. Quaternary Science Reviews, 28, 1309-16.

ter Braak, C. J F., Juggins, S. (1993). Weighted Averaging Partial Least-Squares Regression (WAPLS) - an Improved Method for Reconstructing Environmental Variables from Species Assemblages. Hydrobiologia, 269, 485-502.

ter Braak, C. J. F., Juggins, S., Birks, H. J. B., et al. (1993). Weighted averaging partial least squares regression (WA-PLS): definition and comparison with other methods for species-environment calibration. In: Patil, G. P., and Rao, C. R. (eds) Multivariate Environmental Statistics. Elsevier, Amsterdam, 525–560.

Thienemann, A. (1918). Untersuchungen uber die Bezeihungen zwischen dem Sauerstoffgehalt des Wassers und der Zusammensetzung der fauna in Nord deutschen Seen. Archiv für Hydrobiologie 8, 316–46.

Thienemann, A. (1921). Seetypen. Die Naturwissenschaften, 18, 643–46.

Thienemann, A. (1922). Die beiden Chironomus arten der Tiefenfauna der norddeutschen Seen. Ein hydrobiologisches Problem. Archiv für Hydrobiologie, 13, 609–46.

Thompson, L. G., Mosley-Thompson, E., Davis, M. E., et al. (2002). Kilimanjaro Ice Core Records: Evidence of Holocene Climate change in Tropical Africa. Science, 298(5593), 589-593.

Thompson, L. G., Yao, T., Henderson, K. A., et al. (1997). Tropical climate instability: The Last Glacial Cycle from a Qinghai-Tibetan Ice Core. Science, 276(5320), 1821-1825

Thornalley, D. J. R., Elder, H., and Mccave, I. N. (2011). Reconstructing North Atlantic deglacial surface hydrography and its link to the Atlantic overturning circulation. Global and Planetary Change, 79(3-4), 163–175. doi.org/10.1016/j.gloplacha.2010.06.003

Thornalley, D. J. R., Oppo, D. W., Ortega, P., et al. (2018). Anomalously weak Labrador Sea convection and Atlantic overturning during the past 150 years. Nature, 556(7700), 227–230. doi.org/10.1038/s41586-018-0007-4.

Thornalley, D. J., McCave, I. N., and Elderfield, H. (2010). Freshwater input and abrupt deglacial climate change in the North Atlantic. Paleoceanography, 25, PA1201.

Timms, R. G. O. (2016). Developing a refined tephrostratigraphy for Scotland and constraining abrupt climatic oscillations of the Last Glacial-Interglacial Transition (ca 16-8 ka BP) using high resolution tephrochronologies. PhD thesis (unpublished).

Timms, R. G. O., Matthews, I. P., Palmer, A. P., et al. (2018). Quaternary Geochronology Toward a tephrostratigraphic framework for the British Isles: A Last Glacial to Interglacial Transition (LGIT c. 16-8 ka) case study from Crudale Meadow, Orkney. Quaternary Geochronology, 46, 28–44. doi.org/10.1016/j.quageo.2018.03.008

Titmus, G. and Badcock, R. M. (1981). A morphometric study of the effects of a mermithid parasite on its host, the Chironomid Midge Einfeldia dissidens (Walker) (Diptera). Parasitology Research, 65, 353-357.

Tokeshi, M. (1995). Production ecology. In: Armitage, P. D., Cranston, P.S. and Pinder, L.C., (eds.) The Chironomidae: the biology and ecology of non-biting midges. London: Chapman and Hall, 269–92.

Tokeshi, M. (1995). Species interactions and community structure. In: Armitage, P. D., Cranston, P. S., and Pinder, L. C. V. (eds.), The Chironomidae: The Biology and Ecology of Non-Biting Midges. Chapman and Hall, London, 297–335.

Troels-Smith, J. (1955). Characterisation of unconsolidated sediments. Geological Survey of Denmark. Series 5, 5(10), 1-73.

Turner, J. N., Holmes, N., Davis, S. R., et al. (2015). A multiproxy (micro-XRF, pollen, chironomid and stable isotope) lake sediment record for the Lateglacial to Holocene transition from Thomastown Bog, Ireland. Journal of Quaternary Science, 30(6), 514–528. doi.org/10.1002/jqs.2796

Tye, G. J. (2014) An annually resolved climate record for MIS11: Investigating landscape response to abrupt events during the closest climate analogue to the Holocene. PhD thesis (unpublished).

Urban, E. (1975). The mining fauna in four macrophytes species in Milkolajskie lake. Ekolgia Polska, 23, 417-435.

Urey, H. C. (1948). Oxygen isotopes in nature and in the laboratory. Science, 108, 489-496.

Usdowski, E., and Hoefs, J. (1990). Kinetic C-13 C-12 and O-18 O-16 effects upon dissolution and outgassing of CO2 in the system CO2–H2O. Chemical Geology, 80, 109–118.

Uutala, A. J. (1986). Paleolimnological assessment on the effects of lake acidification on Chironomidae (Diptera) assemblages in the Adirondack region of New York. PhD thesis (unpublished).

Vallenduuk, H. J., Moller Pillot, H. M. (2014). Chironomidae Larvae, Vol. 1: Tanypodinae. Leiden, The Netherlands: KNNV publishing.

van Asch, N., Heiri, O., Bohncke, S.J., et al. (2013). Climatic and environmental changes during the Weichselian Lateglacial Interstadial in the Weerterbos region, the Netherlands. Boreas, 42(1), 123-139.

van Asch, N., Kloos, M.E., Heiri, O., et al. (2012b). The younger dryas cooling in northeast Germany: summer temperature and environmental changes in the Friedländer Groβe Wiese region. Journal of Quaternary Science, 27(5), 531-543.

Van Asch, N., Lutz, A. F., Duijkers, M. C. H. (2012a). Rapid climate change during the Weichselian Lateglacial in Ireland: chironomid-inferred summer temperatures from Fiddaun, Co. Galway. Palaeogeography Palaeoclimatology Palaeoecology, 315–316, 1–11.

van Dinter, M., and Birks, H. H. (1996). Distinguishing fossil Betula nana and B. pubescens using their wingless fruits: implications for the late-glacial vegetational history of western Norway. Vegetation History and Archaeobotany, 5, 229–240.

Van Raden, U. J., Colombaroli, D., Gilli, A., et al. (2013). High-resolution late-glacial chronology for the Gerzensee lake record (Switzerland): δ18O correlation between a Gerzensee-stack and NGRIP. Palaeogeography, Palaeoclimatology, Palaeoecology, 391, 13–24. doi.org/10.1016/j.palaeo.2012.05.017

Velle, G., Brodersen, K. P., Birks, H. J B , et al. (2010). Midges as quantitative temperature indicator species: lessons for palaeoecology. The Holocene, 20, 989-1002.

Verbruggen, F., Heiri, O., Reichart, G. J., et al. (2011). Stable oxygen isotopes in chironomid and cladoceran remains as indicators for lake-water $\delta^{18}O$, 56(6), 2071–2079. doi.org/10.4319/lo.2011.56.6.2071

Verbruggen, F., Heiri, O., Reichart, G., et al. (2010). Chironomid $\delta^{18}O$ as a proxy for past lake water $\delta^{18}O$: a Lateglacial record from Rotsee. Quaternary Science Reviews, 29(17–18), 2271–2279. doi.org/10.1016/j.quascirev.2010.05.030

Verrechia, E. P. (2007). Lacustrine and palustrine geochemical sediments. In: Nash, D. J., McLaren, S. J., (eds.) Geochemical Sediments and Landscape. Blackwell Publishing. Oxford, 298–329.

Vinther, B. M., and Johnsen, S. J. (2007). Greenland stable isotopes. In: Elias, S. A. (2007). Encyclopaedia of Quaternary science. Elsevier, 403-409.

von Grafenstein, U., Erlenkeuser, H., Brauer, A., et al. (1999b). A mid-European decadal isotope-climate record from 15,500 to 5000 years BP. Science, 284, 1654–1657.

von Grafenstein, U., Erlenkeuser, H., Trimborn, P. (1999a). Oxygen and carbon isotopes in modern fresh-water ostracod valves: assessing vital offsets and autecological effects of interest for palaeoclimate studies. Palaeogeography, Palaeoclimatology, Palaeoecology 148, 133–152.

Von Grafenstein, U., Erlernkeuser, H., and Trimborn, P. (1999). Oxygen and carbon isotopes in modem fresh-water ostracod valves: Assessing vital offsets and autecological effects of interest for palaeoclimate studies. Palaeogeography, Palaeoclimatology, Palaeoecology, 148(1–3), 133–152. doi.org/10.1016/S0031-0182(98)00180-1

Wade, P. M. (1999). The impact of human activity on the aquatic macroflora of Llangorse Lake, South Wales. Aquatic Conservation: Marine and Freshwater Ecosystems, 9(5), 441–459.

Walker, I. R. (1987). Chironomidae (Diptera) in paleoecology. Quaternary Science Reviews, 6, 29–40.

Walker, I. R. (2001). Midges: Chironomidae and related Diptera. In: Smol, J. P., Birks, H. J. B., and Last, W. M. (eds.) Tracking Environmental Change Using Lake Sediments. Zoological Indicators, Developments in Paleoenvironmental Research, Dordrecht: Kluwer, 4, 43–66.

Walker, I. R. (2007) Chironomid records. In: Elias, S (Ed), Encyclopaedia Of Quaternary Science, Elsevier, Amsterdam,355-360.

Walker, I. R., (1991) Modern assemblages of arctic and alpine Chironomidae as analogues for Lateglacial communities. Hydrobiologia, 214, 223–227.

Walker, I. R., and Cwynar, L. C. (2006). Midges and palaeotemperature reconstruction – the North American experience. Quaternary Science Reviews, 25, 1911–1925.

Walker, I. R., and MacDonald, G. M. (1995). Distributions of Chironomidae (Insecta: Diptera) and other freshwater midges with respect to treeline, Northwest Territories, Canada. Arctic and Alpine Research, 27, 258–63.

Walker, I. R., and Mathewes, R. W. (1989). Early postglacial chironomid succession in southwestern British Columbia, Canada, and its paleoenvironmental significance. Journal of Paleolimnology, 2, 1–14.

Walker, I. R., and Mathewes, R. W., (1987). Chironomidae (Diptera) and postglacial climate at Marion Lake, British Columbia, Canada. Quaternary Research 27, 89–102.

Walker, I. R., Oliver, D. R., Dillon, M. E., The larva and habitat of Parakiefferiella nigra Brundin (Diptera: Chironomidae). Netherlands Journal of Aquatic Ecology, 26 (2-4), 527–531.

Walker, I. R., Smol, J. P., Engstrom, D. R. et al. (1991). An assessment of Chironomidae as quantitative

indicators of past climate change. Canadian Journal of Fisheries and Aquatic Sciences, 48, 975–87.

Walker, I.R., and Paterson, C.G. (1983). Post-glacial chironomid succession in two small, humic lakes in the New Brunswick–Nova Scotia (Canada)border area. Freshwater Invertebrate Biology, 2, 61–73.

Walker, I.R., Smol, J. P., Engstrom, D. R. et al. (1992). Aquatic invertebrates, climate, scale, and statistical hypothesis testing: a response to Hann, Warner, and Warwick. Canadian Journal of Fisheries and Aquatic Sciences, 49, 1276–1280

Walker, M. (1975). Late Glacial and Early Postglacial environmental history of the central Grampian Highlands, Scotland. Journal of Biogeography, 2(4), 265–284.

Walker, M. J. C. (1982). The Late-Glacial and Early Flandrian Deposits at Traeth Mawr, Brecon Beacons, South Wales. New Phytologist, 90(1), 177–194.

Walker, M. J. C. (2001). Rapid climate change during the last glacial-interglacial transition; implications for stratigraphic subdivision, correlation and dating. Global and Planetary Change, 30(1–4), 59–72. doi.org/10.1016/S0921-8181(01)00078-9

Walker, M. J. C. (2007a). Craig-y-Fro: pollen stratigraphy and dating. In: Carr, S.J., Coleman, C.G., Humpage, A.J., and Shakesby, R.A. (eds.). The Quaternary of the Brecon Beacons: Field Guide, London: Quaternary Research Association, 128– 129.

Walker, M. J. C. (2007b). Craig Cerrig-gleisiad: pollen stratigraphy and dating. In: Carr, S.J., Coleman, C.G., Humpage, A.J., and Shakesby, R.A. (eds.). The Quaternary of the Brecon Beacons: Field Guide, London: Quaternary Research Association, 142– 144.

Walker, M. J. C., and Harkness, D. D. (1990). Radiocarbon dating the Devensian Lateglacial in Britain: new evidence from Llanilid, South Wales. Journal of Quaternary Science, 5(2), 135-144.

Walker, M. J. C., Bohncke, S. J. P., Coope, G. R., et al. (1994). The Devensian/Weichselian Late-glacial in northwest Europe (Ireland, Britain, north Belgium, The Netherlands, northwest Germany). Journal of Quaternary Science, 9(2), 109-118.

Walker, M. J. C., Bohncke, S. J. P., Coope, G. R., et al. (1994). The Devensian/Weichselian Late-glacial in northwest Europe (Ireland, Britain, north Belgium, The Netherlands, northwest Germany). Journal of Quaternary Science, 9(2), 109-118.

Walker, M. J. C., Coope, G. R., Sheldrick, C., et al. (2003). Devensian Lateglacial environmental changes in Britain: a multi-proxy environmental record from Llanilid, South Wales, UK. Quaternary Science Reviews, 22(5-7), 475-520.

Walker, M. J. C., Coope, G. R., and Lowe, J. J. (1993) The Devensian (Weichselian) Lateglacial palaeoenvironmental record from Gransmoor, East Yorkshire, England. Quaternary Science Reviews, 12, 659-680.

Walker, M. J. C., Griffiths, H. I., Ringwood, V., et al. (1993). An early-Holocene pollen, mollusc and ostracod sequence from lake marl at Llangorse Lake, South Wales, UK. The Holocene, 3(2), 138–149. doi.org/10.1177/095968369300300205

Walker, M., and Lowe, J. (2017). Lateglacial environmental change in Scotland. Earth and Environmental Science Transactions of the Royal Society of Edinburgh, 110(1-2), 173-198. doi.org/10.1017/S1755691017000184

Walkley, A., and Black, I. A. (1934). An examination of the Degtjareff method for determining soil

organic matter, and a proposed modification of the chromic acid titration method. Soil Science, 37, 29-38.

Wallén, C. C. (eds.) (1970). World Survey of Climatology. Volume 5: Climates of Northern and Western Europe. Elsevier, Amsterdam.

Walshe, B M., (1948). The Oxygen Requirements and Thermal Resistance of Chironomid Larvae from Flowing And From Still Waters. Journal of Experimental Biology, 25(1), 35–44. doi: doi.org/10.1242/jeb.25.1.35

Watson, J. E., Brooks, S. J., Whitehouse, N. J., et al. (2010). Chironomid-inferred late-glacial summer air temperatures from Lough Nadourcan, Co. Donegal, Ireland. Journal of Quaternary Science, 25(8), 1200- 1210.

West, R. G. (1991). On the origin of Grunty Fen and other landforms in southern Fenland, Cambridgeshire. Geological Magazine, 128(3), 257-262.

Wetzel, R. G. (1975). Limnology. W.B. Saunders Co, 743

Whittington, G., Edwards, K. J., Zanchetta, G., et al. (2015). Lateglacial and early Holocene climates of the Atlantic margins of Europe: Stable isotope, mollusc and pollen records from Orkney, Scotland. Quaternary Science Reviews, 122, 112–130. doi.org/10.1016/j.quascirev.2015.05.026

Whittington, G., Fallick, A. E., and Edwards, K. J. (1996). Stable oxygen isotope and pollen records from eastern Scotland and a consideration of Late-Glacial and early Holocene climate change for Europe. Journal of Quaternary Science, 11(4), 327- 340.

Wiederholme, T. (eds). (1983). Chironomidae of the Holarctic region. Keys and Diagnoses. Part I. Larvae: Entomologica Scandinavia, Supplement 19, 1–457

Williams, J. W., Grimm, E. C., Blois, J. L., et al. (2018). The Neotoma Paleoecology Database, a multiproxy, international, community-curated data resource. Quaternary Research (United States), 89(1), 156–177. doi.org/10.1017/qua.2017.105

Williams, N., Westgate, J., Williams, D., et al. (1981). Invertebrate Fossils (Insecta: Trichoptera, Diptera, Coleoptera) from the Pleistocene Scarborough Formation at Toronto, Ontario, and their paleoenvironmental Significance. Quaternary Research, 16(2), 146-166. doi:10.1016/0033-5894(81)90042-9

Wohlfarth, B., Muschitiello, F., L. Greenwood, S., et al. (2017). Hässeldala – a key site for Last Termination climate events in northern Europe. Boreas, 46(2), 143–161. doi.org/10.1111/bor.12207

Woodward, C. A. and Shulmeister, J. (2006). New Zealand chironomids as proxies for human-induced and natural environmental change: Transfer functions for temperature and lake production (chlorophyll a). Journal of Paleolimnology, 36(4), 407-429.

Wooller, M. J., Francis, D., Fogel, M. E., et al. (2004). Quantitative paleotemperature estimates from d18O in chironomid head capsules from arctic lake sediments. Journal of Paleolimnology, 31, 267–274.

Wright, H. E. Jr. (1984). Sensitivity and response time of natural systems to climatic change in the Late Quaternary. Quaternary Research Reviews, 3, 91-131.

Yu, Z. (2007). Rapid response of forested vegetation to multiple climatic oscillations during the last deglaciation in the northeastern United States. Quaternary Research 67(2), 297–303.

Yu, Z., and Eicher, U. (1998). Abrupt climate oscillations during the last deglaciation in central North America. Science 282(5397), 2235–2238.

Zhang, E., Jones, R., Bedford, A. et al. (2007). A chironomid-based salinity inference model from lakes on the Tibetan Plateau. Journal of Paleolimnology, 38(4), 477-491.

Zinchenko, T. D. (2002). Chironomids of surface waters in the mid- and lower Volga basin (Samara district). Ecological and Faunal review. Samara: IEVB RAN, 74-85.